



---

seit 1558

Friedrich-Schiller-Universität Jena

---

Chemisch-Geowissenschaftliche Fakultät

# **Poly(2-oxazoline)-based materials for biomedical applications**

Dissertation  
(kumulativ)

zur Erlangung des akademischen Grades  
doctor rerum naturalium (Dr. rer. nat.)

vorgelegt dem Rat der Chemisch-Geowissenschaftlichen  
Fakultät der Friedrich-Schiller-Universität Jena

von Diplom-Chemiker Matthias Hartlieb  
geboren am 22.05.1986 in Gera

**Gutachter:**

1. Prof. Dr. Ulrich S. Schubert, Friedrich-Schiller-Universität Jena
2. Jun. Prof. Dr. Felix H. Schacher, Friedrich-Schiller-Universität Jena
3. Prof. Dr. Dr. Lorenz Meinel, Julius-Maximilians-Universität Würzburg

Tag der öffentlichen Verteidigung: 03.06.2015





## Table of contents

Table of contents.....	1
Documentation of authorship.....	2
1. Introduction.....	8
2. Covalently cross-linked poly(2-oxazoline)s – Hydrogels and self-assembled structures ...	13
3. Amine containing poly(2-oxazoline)s.....	16
4. Functional materials based on poly(2-oxazoline)s .....	23
4.1. Chemical hydrogels.....	23
4.2. Covalent poly(2-oxazoline) based surface coatings .....	28
4.3. Poly(2-oxazoline) based nanogels .....	33
5. Biomedical applications of poly(2-oxazoline) materials .....	42
5.1. DNA detection using hydrogels and coatings.....	42
5.2. Drug delivery using poly(2-oxazoline)-based nanogels .....	51
6. Summary .....	58
7. Zusammenfassung.....	61
8. References .....	64
List of abbreviations .....	68
Curriculum vitae.....	70
Publication list.....	71
Acknowledgement / Danksagung .....	74
Declaration of authorship / Selbstständigkeitserklärung.....	77
Publications P1 to P8.....	78

## Documentation of authorship

This section contains a list of the individual authors contribution to the publications reprinted in this thesis.

M. Hartlieb, <sup>1</sup> K. Kempe, <sup>2</sup> U. S. Schubert, <sup>3</sup> “Covalently cross-linked poly(2-oxazoline) materials for biomedical applications – from hydrogels to self-assembled and templated structures”, <i>J. Mater. Chem. B</i> <b>2015</b> , 3, 526-538.				
Author	1	2	3	
Development of concept	×	×		
Preparation of the manuscript	×	×		
Correction of the manuscript				×
Supervision of M. Hartlieb				×
Proposed publication equivalent	0.5			

M. Hartlieb, <sup>1</sup> D. Pretzel, <sup>2</sup> K. Kempe, <sup>3</sup> C. Fritzsche, <sup>4</sup> R. M. Paulus, <sup>5</sup> M. Gottschaldt, <sup>6</sup> U. S. Schubert, <sup>7</sup> “Cationic poly(2-oxazoline) hydrogels for reversible DNA binding”, <i>Soft Matter</i> <b>2013</b> , 9, 4693-4704.							
Author	1	2	3	4	5	6	7
Polymer and material synthesis	×						
Polymer and material characterization	×		×		×		
DNA binding and release studies	×	×		×			
Development of concept	×	×					×
Preparation of the manuscript	×	×					
Correction of the manuscript			×	×	×	×	×
Supervision of M. Hartlieb						×	×
Proposed publication equivalent	1.0						

## Documentation of authorship

M. Hartlieb,<sup>1</sup> D. Pretzel,<sup>2</sup> C. Englert,<sup>3</sup> M. Hentschel,<sup>4</sup> K. Kempe,<sup>5</sup> M. Gottschaldt,<sup>6</sup> U. S. Schubert,<sup>7</sup> “Matrix supported poly(2-oxazoline)-based hydrogels for DNA catch and release”, *Biomacromolecules* **2014**, *15*, 1970-1978.

Author	1	2	3	4	5	6	7
Polymer and material synthesis	×						
Polymer and material characterization	×						
DNA binding and release studies	×	×	×				
PCR studies				×			
Development of concept	×	×					×
Preparation of the manuscript	×	×					
Correction of the manuscript			×	×	×	×	×
Supervision of M. Hartlieb					×		×
Proposed publication equivalent	1.0						

M. Hartlieb,<sup>1</sup> D. Pretzel,<sup>2</sup> M. Wagner,<sup>3</sup> S. Hoepfener,<sup>4</sup> P. Bellstedt,<sup>5</sup> M. Görlach,<sup>6</sup> C. Englert,<sup>7</sup> K. Kempe,<sup>8</sup> U. S. Schubert,<sup>9</sup> “Core cross-linked nanogels based on the self-assembly of double hydrophilic poly(2-oxazoline) block copolymers”, *J. Mater. Chem. B.* **2015**, *3*, 1748-1759.

Author	1	2	3	4	5	6	7	8	9
Polymer and material synthesis	×								
Polymer and material characterization	×		×	×	×	×	×		
Biological investigations		×							
Development of concept	×	×						×	
Preparation of the manuscript	×	×							
Correction of the manuscript			×	×	×	×	×	×	×
Supervision of M. Hartlieb								×	×
Proposed publication equivalent	1.0								

## Documentation of authorship

**P5** C. Englert,<sup>1</sup> L. Tauhardt,<sup>2</sup> M. Hartlieb,<sup>3</sup> K. Kempe,<sup>4</sup> M. Gottschaldt,<sup>5</sup> U. S. Schubert,<sup>6</sup> “Linear poly(ethylene imine)-based hydrogels for effective binding and release of DNA”, *Biomacromolecules* **2014**, *15*, 1124-1131.

Author	1	2	3	4	5	6
Polymer and material synthesis	×	×				
Polymer and material characterization	×	×				
DNA binding and release	×		×			
Development of concept	×	×	×	×	×	
Preparation of the manuscript	×					
Correction of the manuscript		×	×	×	×	×
Supervision of M. Hartlieb					×	×
Proposed publication equivalent			0.25			

**P6** M. N. Leiske,<sup>1,‡</sup> M. Hartlieb,<sup>2,‡</sup> C. Paulenz,<sup>3</sup> D. Pretzel,<sup>4</sup> M. Hentschel,<sup>5</sup> C. Englert,<sup>6</sup> M. Gottschaldt,<sup>7</sup> U. S. Schubert,<sup>8</sup> “Lab in a tube: Purification, amplification and detection of DNA using poly(2-oxazoline) multilayers”, *Adv. Funct. Mater.*, in press.

<sup>‡</sup> Authors contributed equally.

Author	1	2	3	4	5	6	7	8
Polymer and material synthesis	×							
Polymer and material characterization	×	×		×				
DNA binding and release	×			×				
PCR experiments	×		×		×			
Development of concept	×	×		×		×	×	
Preparation of the manuscript		×						
Correction of the manuscript	×		×	×	×		×	×
Supervision of M. Hartlieb								×
Proposed publication equivalent		1.0						

## Documentation of authorship

**P7** L. Tauhardt,<sup>1</sup> M. Frant,<sup>2</sup> D. Pretzel,<sup>3</sup> M. Hartlieb,<sup>4</sup> C. Bucher,<sup>5</sup> G. Hildebrand,<sup>6</sup> B. Schröter,<sup>7</sup> C. Weber,<sup>8</sup> K. Kempe,<sup>9</sup> M. Gottschaldt,<sup>10</sup> K. Liefeth,<sup>11</sup> U. S. Schubert,<sup>12</sup> "Amine end-functionalized poly(2-ethyl-2-oxazoline) as promising coating material for antifouling applications", *J. Mater. Chem. B* **2014**, *2*, 4883-4893.

Author	1	2	3	4	5	6	7	8	9	10	11	12
Polymer and material synthesis	×			×	×							
Polymer and material characterization	×		×			×	×					
Bioadhesion and microscopy studies		×										
Development of concept	×							×	×			
Preparation of the manuscript	×	×										
Correction of the manuscript			×	×	×	×	×	×	×	×	×	×
Supervision of L. Tauhardt												×
Supervision of M. Hartlieb												×
Proposed publication equivalent				0.25								

**P8** M. Hartlieb,<sup>1</sup> T. Buś,<sup>2</sup> J. Kübel,<sup>3</sup> D. Pretzel,<sup>4</sup> S. Hoepfner,<sup>5</sup> K. Kempe,<sup>6</sup> B. Dietzek,<sup>7</sup> U. S. Schubert,<sup>8</sup> "Nanogels based on double hydrophilic Poly(2-oxazoline) for doxorubicin delivery", in preparation.

Author	1	2	3	4	5	6	7	8
Polymer and material synthesis	×							
Polymer and material characterization	×		×		×			
Biological investigations		×		×				
Development of concept	×							
Preparation of the manuscript	×							
Correction of the manuscript		×	×	×	×	×	×	×
Supervision of M. Hartlieb							×	×
Proposed publication equivalent	1.0							

## **Erklärung zu den Eigenanteilen des Promovenden sowie der weiteren Doktoranden/Doktorandinnen als Koautoren an Publikationen und Zweitpublikationsrechten bei einer kumulativen Dissertation**

**Für alle in dieser kumulativen Dissertation verwendeten Manuskripte liegen die notwendigen Genehmigungen der Verlage („Reprint permissions“) für die Zweitpublikation vor.**

**Die Co-Autoren der in dieser kumulativen Dissertation verwendeten Manuskripte sind sowohl über die Nutzung als auch über die oben angegebenen Eigenanteile informiert und stimmen dem zu.**

**Die Anteile der Co-Autoren an den Publikationen sind in den vorausgehenden Tabellen aufgeführt.**

**Ich bin mit der Abfassung der Dissertation als publikationsbasiert, d.h. kumulativ, einverstanden und bestätige die vorstehenden Angaben. Eine entsprechend begründete Befürwortung mit Angabe des wissenschaftlichen Anteils des Doktoranden an den verwendeten Publikationen werde ich parallel an den Rat der Fakultät der Chemisch-Geowissenschaftlichen Fakultät richten.**

Prof. Dr. Ulrich S. Schubert                      07.06.2015                      Jena \_\_\_\_\_

Matthias Hartlieb                                      07.06.2015                      Jena \_\_\_\_\_

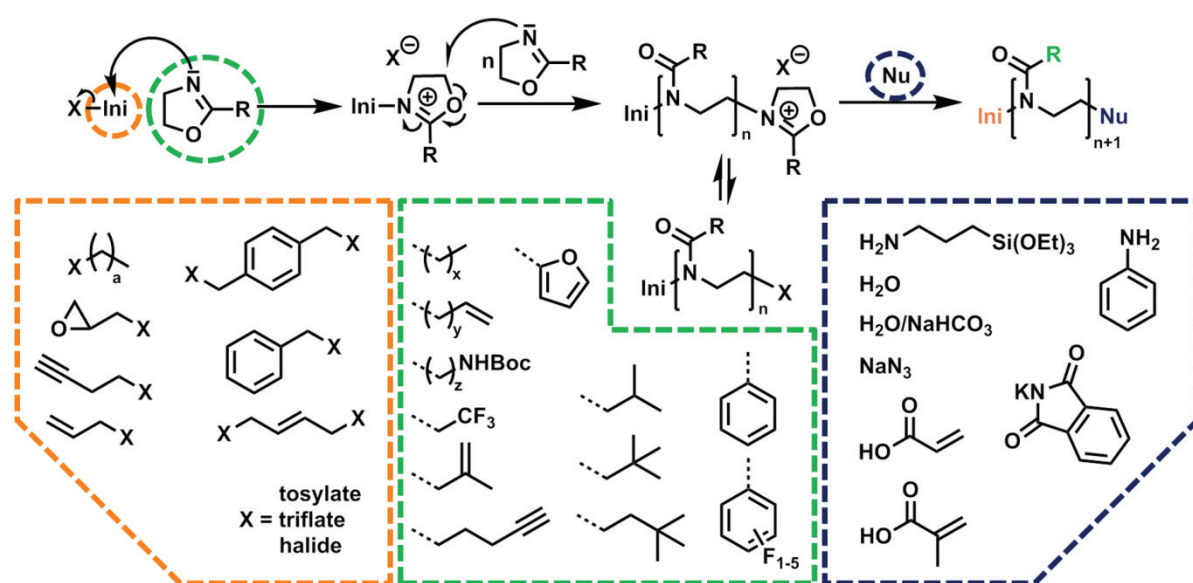




## 1. Introduction

Biocompatible polymers comprising adjustable properties are the basis for the design of smart, functional materials and are of paramount interest for the production of biomedical systems.<sup>[1]</sup> While non-toxicity, and in most cases hydrophilicity are basic requirements for macromolecular materials in this context, the possibility to accurately install functional groups while maintaining a high degree of control over the polymerization process is likewise essential. Research in nanomedicine, tissue engineering, anti-fouling or other polymer related fields is based on the generation of reproducible results and the extrapolation of structure property relationships, both relying on an accurate control over polymeric architecture and composition.<sup>[2]</sup> Living and controlled polymerization techniques such as anionic,<sup>[3]</sup> cationic,<sup>[4]</sup> as well as controlled radical polymerization techniques<sup>[5-7]</sup> fulfill these requirements and were valuable tools for researchers in the last decades.

One particularly fascinating method is the cationic ring-opening polymerization (CROP) of 2-oxazolines. The origin of this technique dates back to 1966, when it was developed independently by four different research groups.<sup>[8-11]</sup> The major drawback of the initial method was the long reaction time of hours or even days. In 2004, the combination of CROP and microwave-assisted technology lead to a tremendous acceleration of the process.<sup>[12-13]</sup> Besides an excellent control over length and dispersity of the final product, the large variety of functional groups, which can potentially be installed altering starting-, end-, and side groups is one major advantage of the CROP (Scheme 1.1).



**Scheme 1.1:** The mechanism of the cationic ring-opening polymerization of 2-oxazolines and an overview of various available initiators, monomers and end-capping agents.

## 1. Introduction

---

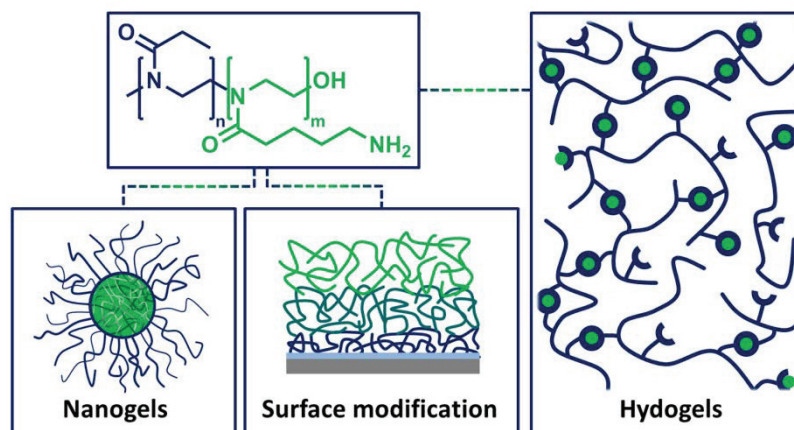
Regarding the polymer properties, side group functionalization is of utmost importance. The most commonly applied 2-oxazolines exhibit short alkyl side chains in 2-position of the monomer. By altering the length of these substituents, the solubility and crystallinity of poly(2-oxazoline)s (POx) can be fine-tuned precisely. Short substituents such as methyl or ethyl groups lead to polymers, which are readily water soluble, and even possess a stealth effect similar to poly(ethylene glycol) (PEG).<sup>[14-15]</sup> An increased length of the alkyl substituent (ethyl/propyl) results in POx having a lower critical solution temperature (LCST) behavior in a temperature range relevant for biological applications,<sup>[16]</sup> whereas longer alkyl chains, as well as aromatic substituents, produce water insoluble macromolecules.<sup>[17]</sup> However, solubility is not the only parameter worth of investigation. The use of monomers bearing functional groups offers the possibility to perform post-polymerization modifications and attach, *e.g.*, dyes or molecules, which specifically interact with biological systems. Additionally, cross-linking reactions or the attachment of polymers to substrates can be accomplished exploiting these modifications.

Cross-linking, resulting in hydrogels or nanogels, plays a tremendous role in the fabrication of biomaterials. For the synthesis of water swellable networks, the reaction, which generates the interconnection, is an important tool to influence the final material properties like mesh size (and consequently the degree of swelling), mechanical characteristics and the stability of the gel.<sup>[18]</sup> In particular, for the production of smart, functional biomaterials, cross-linking has to be specific to not interfere with functionalities or moieties, which have to be present in the final network. The covalent cross-linking of POx, producing hydrogels and nanogels, is discussed in detail in Chapter 2.

In order to achieve a likewise specific and effective cross-linking reaction, the precursor polymer needs to be decorated with a defined amount of functional groups with a known distribution over the macromolecule. Amine groups represent a highly interesting functionality in a biological context. They can be addressed by the use of epoxides, aldehydes, activated acids and other reactants to form reversible and irreversible connections. Furthermore, the positive charge of amines in an aqueous environment offers the possibility to control the charge of cross-linked structures. This approach is particularly valuable for the production of materials, which should interact with biological systems. DNA as a polyanion has a high affinity to positive charges as shown by the formation of polyplexes with poly(ethylene imine) (PEI).<sup>[19]</sup> Also, the cellular uptake of nano-scaled objects is highly dependent on their zeta potential.<sup>[20]</sup> In both cases an accurate control over the amount of amine substituents is required. To create amine containing POx it is necessary to protect the amine group during synthesis since otherwise, its nucleophilicity would interfere with the CROP.<sup>[21]</sup> The synthesis of a 2-oxazoline monomer having a protected amine group in the side chain and the kinetic of its polymerization is described in Chapter 3. Furthermore, a second way to amine containing POx starting from linear PEI and subsequent substitution of a defined fraction of the secondary amines is evaluated.

## 1. Introduction

The polymers synthesized by these methods are to be used in biomedical applications and, therefore, have to be processed into different material types to match specific requirements. The production of hydrogels, surface coatings, as well as nanogels by the utilization of covalent cross-linking is the subject of Chapter 4. An overview of the produced material types is depicted in Scheme 1.2.



**Scheme 1.2:** Schematic representation of different material types derived from amine containing POx.

The most basic materials, which can be produced by the covalent cross-linking of functional polymers are hydrogels. The hydrophilic and biocompatible character of such networks renders them as an ideal matrix for biomedical systems.<sup>[22]</sup> Chapter 4.1 describes the synthesis of POx-hydrogels by epoxide mediated cross-linking. The properties of the resulting gels are investigated and the mechanical stability of the material is further improved by the combination with porous polypropylene substrates generating matrix-supported hydrogels. Furthermore, the synthesis of hydrophilic networks by the use of thiol-ene chemistry is described.

While the three dimensional structure of hydrogels represents an advantageous feature for several applications, where large surface areas are required, it can also be unfavorable. Although these networks, depending on the material properties, are permeable to substances up to a specific size, diffusion is the constraining element in this context. This effect is beneficial for the sustained release of molecules in drug delivery applications.<sup>[23]</sup> However, for separation or detection processes in bioanalytical applications, a rapid binding and release of the desired substances is necessary. Covalent polymer multilayers on surfaces are able to accomplish this task while maintaining the hydrophilic nature of a hydrogel. If applied in a layer-by-layer (LbL) process, the thickness and, hence, the properties of these coatings can be adjusted precisely. Chapter 4.2 deals with the deposition of amine containing POx on activated substrates to create multilayers. The LbL deposition is investigated in detail, and the transition from a flat, surface bond polymer film to a hydrogel-like coating is studied.

## 1. Introduction

---

Nanogels represent another material type, which has been investigated intensively, mostly in a nanomedicine context.<sup>[24]</sup> They are water-swelling nanoscopic structures, stabilized by covalent bonds, or, in other terms, hydrogels in a nanometer size range. While it is possible to create such systems by the grinding of macroscopic gels,<sup>[25]</sup> a bottom-up approach is favorable, due to the improved degree of control. The most frequently used method comprises the self-assembly of block copolymers by exploiting the differences in solubility between the segments of the macromolecule. A phase separation on a nanometer scale can be achieved yielding micellar or vesicular structures.<sup>[26]</sup> A covalent cross-linking of either core or shell results in nanogels which have, in contrast to the precursor assembly, an improved stability, in particular in diluted solutions. Particularly in the field of drug delivery, this permanency displays a major advantage since it prevents a premature disassembly. The synthesis of micellar, as well as vesicular nanogels from amine containing block copolymers and the adjustment of their properties is described in Chapter 4.3. Additionally, the loading of the structures with dyes, as well as therapeutic agents, is discussed.

Chapter 5 focusses on the application of the materials described so far. The first part is of bioanalytical nature and deals with pathogen detection and the upstream purification and amplification of genetic material. A reliable and time-saving point of care diagnostics is of major importance regarding the control of new diseases in a globalized world.<sup>[27]</sup> However, detection displays only the last step of this approach. While the identification of DNA serves to detect different pathogens, the extraction and amplification from biological samples is a likewise challenging task. As already stated, the anionic nature of DNA leads to a strong interaction with positively charged materials, as provided by amine groups. For this purpose, amine containing polymers and networks derived from 2-oxazolines are investigated regarding their ability to reversibly bind DNA. By altering the properties of the system, the affinity to DNA can be adjusted. The focus of Chapter 5.1 lays in the generation of DNA samples, pure enough to be amplified in a polymerase chain reaction (PCR) using the materials described in Chapter 4.1. The principle is transferred to surface bound POx multilayers (Chapter 4.2), which serve as a two dimensional analogue of those networks. Using specific coatings, it is possible to design a system combining purification, amplification and detection using only a single POx coated reaction vessel.

The second part of Chapter 5 is dedicated to the use of nanoscopic drug carriers for the treatment of cancer in the human body. The poor tissue specificity of many cytostatic anti-cancer drugs is a serious issue in patient treatment since it leads to severe side effects.<sup>[28]</sup> The incorporation of therapeutics into nanoscopic carriers is one way to foreclose this lack of precision.<sup>[29]</sup> The passive targeting provided by nano-scaled objects, which accumulate in leaky tumor tissue (also known as the enhanced permeability and retention (EPR) effect), is able to improve the efficiency of cytostatic therapeutics significantly.<sup>[30]</sup> The covalent attachment of the

## 1. Introduction

---

drug to nanogels displays a further advantage since it prevents premature disassembly and a leakage of the drug into the blood stream.<sup>[31]</sup> The interaction of POx nanogels, loaded with dyes or drug molecules with cells, is subject of Chapter 5.2. The toxicity and cellular uptake behavior of labeled systems is investigated in detail. Furthermore, nanogels loaded with the drug doxorubicin (Dox) are studied regarding their cytotoxicity and uptake mechanism.

The aim of this thesis is to create functional polymer-based systems for the use in biomedical applications. Hydrogels, as well as surface coatings based on cationic polymers should be optimized regarding their affinity to genetic material and, in the end, to separate it from biological samples, which enables amplification and detection. Furthermore, nanogels from functional POx should be investigated in respect to their interaction with cells and be used for the delivery of Dox in cancer treatment.

### 2. Covalently cross-linked poly(2-oxazoline)s – Hydrogels and self-assembled structures

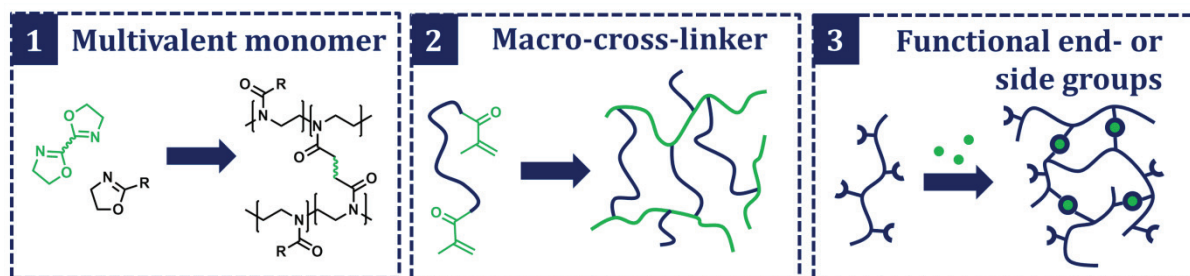
Parts of this chapter have been published in: **P1**) M. Hartlieb, K. Kempe, U. S. Schubert, *J. Mater. Chem. B* **2015**, *3*, 526-538.

Hydrogels are a material highly related to nature since cellular tissue itself can be considered as a gel.<sup>[32]</sup> It is even hypothesized that hydrogels played a key role in the origin of life due to the limited and partially directed diffusion inside such networks.<sup>[33]</sup> Since their first scientific description in the 1960s, hydrogels are a highly application related material type. The development of first synthetic gels by Otto Wichterle and Drahoslav Lím was a result of the search for new biocompatible soft materials in ophthalmology,<sup>[34]</sup> and soon after, water swellable polymer networks were produced for agricultural applications. Today, personal care is the most common field for a commercial utilization of hydrogels.<sup>[35]</sup> However, many other (research) fields such as wound dressings,<sup>[36-37]</sup> super absorbers in construction industry,<sup>[38-39]</sup> scaffolds for tissue engineering,<sup>[22]</sup> matrices for separation problems,<sup>[40]</sup> drug delivery devices<sup>[41]</sup> and sensors<sup>[42]</sup> deal with this highly versatile class of material.

To define, which properties a soft matter has to possess to be regarded as a gel, the mechanical behavior is of outstanding interest. A gel is a mixture of at least two phases with an elastic modulus higher than its viscous modulus, in other terms a solid matter, which consists of a continuous (polymer) matrix swollen in a solvent. The interconnection between the network components allows a major classification of hydrogels. A covalent cross-linking leads to the formation of chemical gels, while networks based on secondary interactions such as hydrogen bonds, ionic interactions or van-der-Waals interactions are labeled as physical gels. Since scaffolds applied in biomedical systems, *e.g.* in drug delivery or bioanalytics, require a certain degree of stability against degradation, the focus of this thesis are chemical hydrogels and nanogels.

Poly(2-oxazoline)s (POx) display an ideal starting material for the synthesis of chemical gels due to the good water solubility and biocompatibility of derivatives such as poly(2-methyl-2-oxazoline) (PMeOx) or poly(2-ethyl-2-oxazoline) (PEtOx) and the manifold functionalization possibilities. In general, POx-based hydrogels can be subdivided into three major classes (Scheme 2.1): 1) Hydrogels that are obtained in a one-step reaction using *bis*-functional monomers, 2) networks prepared *via* the macromonomer method using  $\alpha,\omega$ -functionalized POx bearing polymerizable groups, and 3) hydrogels, which are fabricated from POx with different side- and end-group functionalities and multifunctional cross-linkers.





**Scheme 2.1:** Different synthetic strategies leading to POx derived chemical cross-linked networks. 1) *Bis*-functional monomers, 2) macro monomer method and 3) side group functionalization.

The first POx-based hydrogels produced by the use of *bis*-functional 2-oxazolines were reported in 1989 by the group of Saegusa.<sup>[43]</sup> One advantage of this method is the production of gels in a one-pot process. Using distinct monomers or monomer combinations, as well as a varying cross-linker content, the swelling abilities can be fine-tuned. However, systems derived by this approach are difficult to investigate since they are synthesized from monomeric compounds directly. A statement about chain length, degree of cross-linking and a kinetic of the linking process is hardly possible or requires intensive studies.<sup>[44]</sup> Nevertheless, the versatility of this method was demonstrated recently by Schenk and coworkers, producing a hydrogel with a defined hydrophilicity, reactive groups, as well as a fluorescence label.<sup>[45]</sup> The system was investigated for cancer drug delivery applications.

A second strategy, which leads to covalently stabilized POx networks, is the so called macromonomer method. The introduction of polymerizable groups such as (meth)acrylic units results in  $\alpha$ -, and/or  $\omega$ -end-functionalized POx, which can be used as macromonomer or macro-cross-linker, respectively. The method was introduced by Uyama and coworkers in 1992 using an 2-(*iso*-propyl)-2-oxazoline based macromonomer to obtain thermo-responsive networks.<sup>[46]</sup> POx macromonomers can easily be combined with monomers used in radical polymerization processes. There are several possibilities of installing one or two polymerizable groups on the chain ends of a POx macromolecule. Most prominently, the end capping using methacrylic acid is utilized but also styrene based end groups are described.<sup>[47]</sup> A drawback of the approach is the limitation of the amount of polymerizable groups by the number of chain ends. To achieve higher degrees of functionalization the polymer architecture has to grow more complex, resulting in a diminished control over the polymerization process.

The third way of producing covalently stabilized POX networks is the gelation using side group functionalization. Generally, the introduction of functional groups into POx is possible *via* two ways: 1) The partially hydrolysis of the polymer generating secondary amines (and subsequent functionalization) or, 2) the use of functional monomers. While the first way is more versatile since the functionality generated has not to be tolerated by the polymerization process it is also less controlled. The degree of hydrolysis itself can be tuned rather well, however the following

## 2. Covalently cross-linked poly(2-oxazoline)s – Hydrogels and self-assembled structures

---

steps are polymer analogue reactions, which can limit the efficiency. Moreover, only a statistical distribution of functional groups within the macromolecule can be achieved. Utilizing the second strategy, also block or gradient copolymers can be synthesized. However, nucleophilic functionalities can only be introduced when they are protected during polymerization. The cross-linking of these polymers can be achieved applying simple processes, including the reaction of *iso*-cyanates with amines<sup>[48]</sup> or the radical thiol-ene-addition.<sup>[49-50]</sup> Also, reversible connections can be formed, *e.g.* by Diels alder reactions<sup>[51]</sup> or photo cross-linking.<sup>[52]</sup>

Besides macroscopic structures as described so far, also microscopic or nanoscopic assemblies can benefit from a covalent interconnection. In (nano) medical, pharmaceutical and diagnostic applications, micelles are highly interesting and promising materials.<sup>[53-54]</sup> The self-assembly of amphiphilic block or graft copolymers has been studied intensively during the last decades.<sup>[55]</sup> In water, the hydrophobic part self-assembles and forms the core of the micelles while the hydrophilic part constitutes the shell. The core compartments can be applied for the encapsulation of hydrophobic cargo, which is protected by the hydrophilic shell.<sup>[56]</sup> The latter also provides colloidal stability and, depending on the materials used, can lower or prevent unspecific adsorption of proteins, which is of high importance when applied as drug carrier for intravenous applications.<sup>[57]</sup> However, micelles exhibit a critical micelle concentration, *i.e.* they are in equilibrium with non-associated polymer chains, which can be shifted towards the latter upon high dilution.<sup>[58]</sup> This fact needs to be considered, in particular, for intravenous injections of such systems. Thus, to prevent disassembly of the micelles they need to be stabilized. This is typically achieved by chemical cross-linking of the core and shell, respectively.<sup>[59]</sup> During the last decades numerous studies described the self-assembly of diblock and triblock (ter)poly(2-oxazoline)s.<sup>[60]</sup> However, only a limited number of reports demonstrated the fabrication of cross-linked POx micelles. Most of the approaches comprise the immobilization of the assembly by radiation cross-linking (UV-light<sup>[61]</sup> or electron beam<sup>[62]</sup>). However, only one systems using a reversible linker (disulfide bridge) is reported.<sup>[25]</sup>



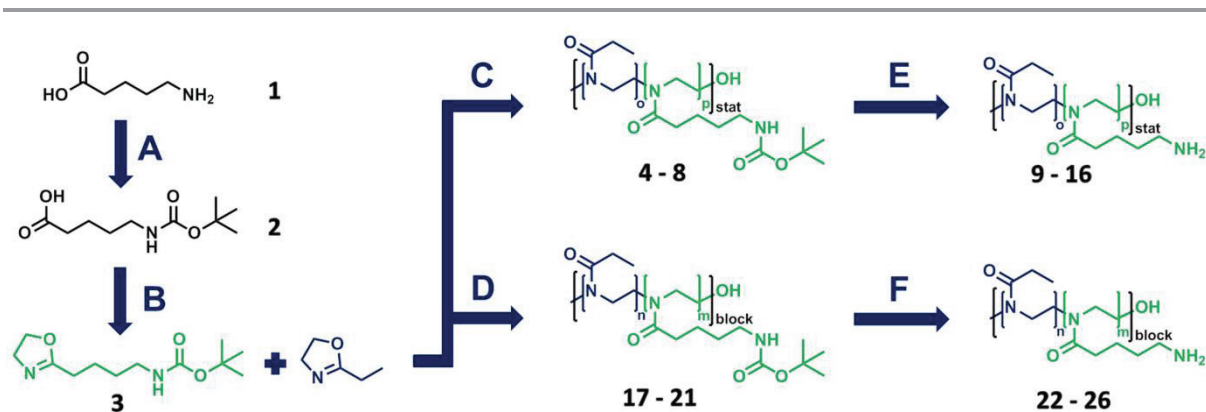
### 3. Amine containing poly(2-oxazoline)s

Parts of this chapter have been published in: **P2)** M. Hartlieb, D. Pretzel, K. Kempe, C. Fritzsche, R. M. Paulus, M. Gottschaldt, U. S. Schubert, *Soft Matter* **2013**, *9*, 4693-4704; **P3)** M. Hartlieb, D. Pretzel, C. Englert, M. Hentschel, K. Kempe, M. Gottschaldt, U. S. Schubert *Biomacromolecules* **2014**, *15*, 1970-1978; **P4)** M. Hartlieb, D. Pretzel, M. Wagner, S. Hoepfner, P. Bellstedt, M. Görlach, C. Englert, K. Kempe, U. S. Schubert, *J. Mater. Chem. B.* **2015**, *3*, 1748-1759; **P5)** C. Englert, L. Tauhardt, M. Hartlieb, K. Kempe, M. Gottschaldt, U. S. Schubert, *Biomacromolecules* **2014**, *15*, 1124-1131; **P6)** M. Leiske, M. Hartlieb, C. Paulenz, D. Pretzel, M. Hentschel, C. Englert, M. Gottschaldt, U. S. Schubert, *Adv. Funct. Mater.*, in press; **P8)** M. Hartlieb, T. Buś, J. Kübel, D. Pretzel, S. Hoepfner, K. Kempe, B. Dietzek, U. S. Schubert, in preparation.

The amine group displays an important and versatile functionality in biochemistry. Its ability to form physical bonds like hydrogen bonds or ionic clusters is of paramount importance for the base pairing of DNA<sup>[63]</sup> or the folding of proteins.<sup>[64]</sup> Moreover, the reaction of amines with carboxylic acids is the key-step in peptide synthesis.<sup>[65]</sup> However, not only nature uses the potential of this functional group. In organic synthesis, many reactions can be accomplished using amines as starting material, *e.g.* the ring-opening of epoxides, the addition to *iso*-(thio)cyanates, the imine or en-amine formation with aldehydes or ketones or the amidation using activated acids.<sup>[66]</sup> The combination of this functionality with the cationic ring-opening polymerization (CROP) of 2-oxazolines is the subject of this chapter.

In general, amine groups are incompatible with the polymerization of oxazolines since the nucleophilic character of the free electron pair of the nitrogen would terminate the living cationic chain-end of the polymer.<sup>[47]</sup> Therefore, a protection group has to be introduced in order to produce polymerizable monomers. The pathway leading to a *tert*-butyloxycarbonyl (Boc)-protected amine bearing 2-oxazoline (BocOx, **3**) is depicted in Scheme 3.1. However, despite the protection group, the monomer cannot be used in a CROP directly since the amide group is still able to react with small electrophilic compounds such as the methyl cation, which is typically used as an initiating species. For this reason, a two-step initiation process was utilized. First, methyl tosylate was mixed with three equivalence of 2-ethyl-2-oxazoline (EtOx) and heated to 140 °C to produce an EtOx oligomer. The active species of this short EtOx chain, the oxazolinium group located at the chain end, comprises a significantly larger steric demand compared to the methyl cation. Consequently, BocOx can be added and polymerized in a second step.

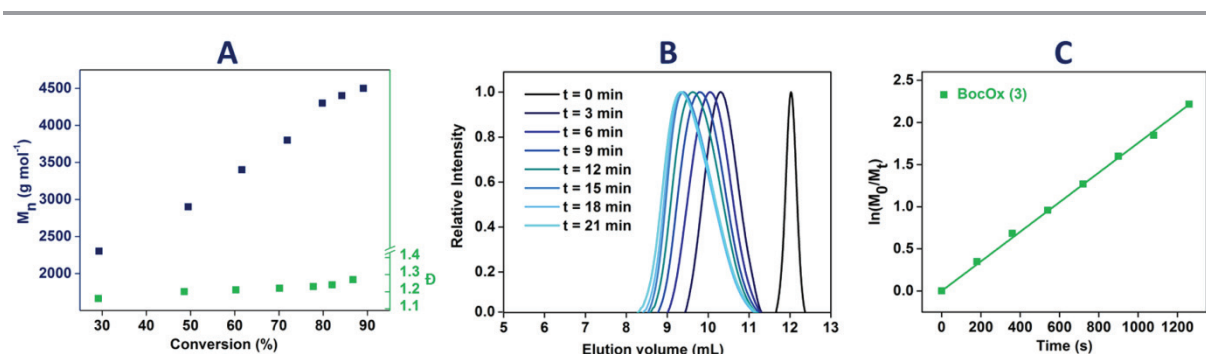
### 3. Amine containing poly(2-oxazolines)s



Scheme 3.1: Schematic representation of the synthesis of BocOx (**3**) and the subsequent polymerization and deprotection to yield statistical copolymers (**9** to **16**) as well as block copolymers (**19** to **23**). A) diBoc, dioxane/water, NaOH; B) i. ethylchloroformiat, chlorethylamine, triethylamine, DMF, ii. DMF,  $\text{K}_2\text{CO}_3$ , 60 °C; C) and D)  $\mu$ W, 140 °C, acetonitrile; E) and F) trifluoro acetic acid,  $\text{CH}_2\text{Cl}_2$ , 60 °C, Amberlyst A21.

To produce defined macromolecules, the polymerization kinetic of the monomeric compounds is of outstanding interest. It provides information about the control of the process and the velocity of the incorporation of a monomer into a polymer, which is important for the polymeric architecture. For this reason, a kinetic investigation of the polymerization of BocOx was performed using the described initiation method (Figure 3.1). The linear slope of the log plot (Figure 3.1C) was the first indication for a living polymerization process. Narrow  $\mathcal{D}$  values and mono-modal size exclusion chromatography (SEC) traces (Figure 3.1B) supported this presumption. Finally, the linear increase of the molar mass with the conversion (Figure 3.1A) proves the pseudo first order kinetic and, hence, the constancy of the concentration of the active species during the process, which is a prerequisite for a living polymerization.

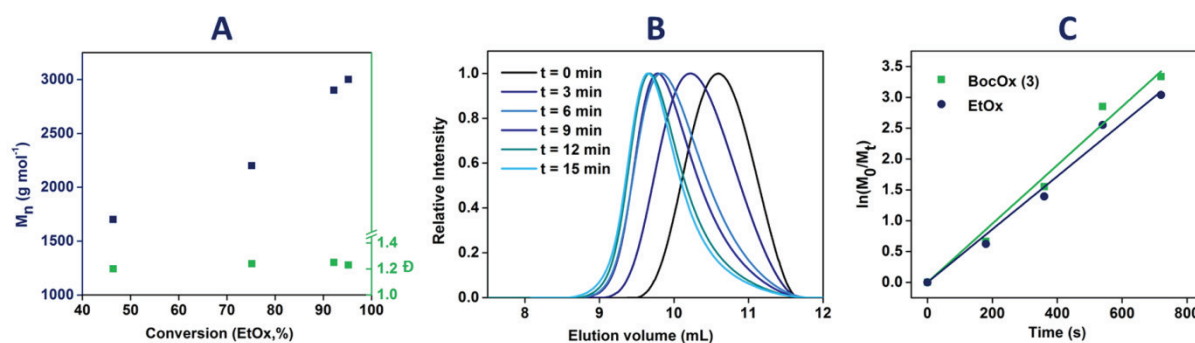
While the possibility to process BocOx without a comonomer enables the production of homopolymers, the combination with other 2-oxazolines is likewise important. It is necessary to compare the reaction velocities of comonomers to make a statement on the architecture of the final polymeric structure.



**Figure 3.1:** Kinetic investigation of the homo-polymerization of BocOx (**3**) at 140 °C in acetonitrile. A) Molar mass and  $\mathcal{D}$  as a function of conversion; B) SEC traces of kinetic samples; C) log plot.

### 3. Amine containing poly(2-oxazolines)s

In the case of diverging rate constants, the production of gradient- and in extreme cases also block-like structures is possible. Therefore, an investigation of the kinetic of BocOx and EtOx in a copolymerization was performed (Figure 3.2). Regarding molar mass increase and  $\bar{D}$  values, the process is equally controlled as observed for the homopolymerization. The similar slopes of the pseudo first order kinetic plots (Figure 3.2C) demonstrated similar reactivities of both monomers and similar incorporation of BocOx and EtOx into the final polymer structure.



**Figure 3.2:** Kinetic investigation of the copolymerization of BocOx (3) in combination with EtOx at 140 °C in acetonitrile. A) Molar mass and  $\bar{D}$  as a function of conversion; B) SEC traces of kinetic samples; C) log plot.

For later applications of amine containing POx, the content of functional groups per polymer chains represents an important factor. To investigate the influence of this parameter, a small library of statistical copolymers was synthesized (Table 3.1). While the overall degree of polymerization (DP) was kept constant at around 50 repeating units, the amine content was varied from 10 to 33%. Narrow dispersities proved the control over the polymerization.

**Table 3.1:** Analytical data of protected and deprotected amine containing POx with a statistical distribution of the comonomers.

Sample	Composition	NMR			SEC (CHCl <sub>3</sub> )		SEC (DMAc)		BocOx/AmOx (%)
		M <sub>n</sub> (g mol <sup>-1</sup> )	M <sub>n</sub> (g mol <sup>-1</sup> )	$\bar{D}$	M <sub>n</sub> (g mol <sup>-1</sup> )	$\bar{D}$	M <sub>n</sub> (g mol <sup>-1</sup> )	$\bar{D}$	
4	P(EtOx <sub>43</sub> -stat-BocOx <sub>5</sub> )	5,500	5,400	1.08					10
5	P(EtOx <sub>39</sub> -stat-PBocOx <sub>7</sub> )	5,500	5,200	1.14					15
6	P(EtOx <sub>32</sub> -stat-PBocOx <sub>9</sub> )	5,400	4,400	1.20					22
7	P(EtOx <sub>38</sub> -stat-PBocOx <sub>15</sub> )	7,400	4,600	1.17					27
8	P(EtOx <sub>32</sub> -stat-PBocOx <sub>16</sub> )	7,000	5,400	1.17					33
9	P(EtOx <sub>43</sub> -stat-PAmOx <sub>5</sub> )	5,000					8,100	1.26	10
10	P(EtOx <sub>39</sub> -stat-PAmOx <sub>7</sub> )	5,700					8,200	1.24	15
11	P(EtOx <sub>32</sub> -stat-PAmOx <sub>9</sub> )	4,500					8,700	1.25	22
12	P(EtOx <sub>38</sub> -stat-PAmOx <sub>15</sub> )	5,900					9,500	1.23	27
13	P(EtOx <sub>32</sub> -stat-PAmOx <sub>16</sub> )	5,400					9,400	1.24	33

### 3. Amine containing poly(2-oxazolines)s

After deprotection using trifluoro acetic acid (TFA), the molar masses obtained by SEC measurements increase, which is attributed to the use of poly(styrene) (PS) as a calibration standard. The cationic nature of P(EtOx-*stat*-AmOx) results in a changed column interaction compared to the Boc-protected polymers and, hence, in non-representative molar masses. The ability to detect polymers after processing into functional materials is an important requirement for production of applicable systems. Hence, a labeling of amine containing POx was conducted using a fluorescein-NHS ester and a Rhodamine B *iso*-thiocyanate (Table 3.2).

**Table 3.2:** Characteristics of fluorescence labeled amine containing POx polymers.

Sample	Composition	Dye	SEC (DMAc)		Degree of func.	Abs. Max.	Em. Max.
			$M_n$ (g mol <sup>-1</sup> )	$\bar{D}$	(%)	(nm)	(nm)
14	P(EtOx <sub>37</sub> - <i>stat</i> -AmOx <sub>9</sub> )	-	9,300	1.13	-	-	-
15	P(EtOx <sub>37</sub> - <i>stat</i> -AmOx <sub>8</sub> - <i>stat</i> -FAmOx <sub>1</sub> )	Fluorescein	11,000	1.16	78	485	530
16	P(EtOx <sub>37</sub> - <i>stat</i> -AmOx <sub>8</sub> - <i>stat</i> -RAmOx <sub>1</sub> )	Rhodamine B	12,000	1.19	5	555	590

The success of the reactions was investigated *via* SEC measurements by comparing the RI and the UV/Vis signals. An overlap of the curves and the absence of a UV signal in low molar mass regions proved the successful labeling and purity of the polymers. The amount of attached dye was verified by NMR measurements resulting in labeling efficiencies of 78 and 5%, respectively. UV/Vis spectra verified the expected absorption and emission maxima for both polymers.

As already discussed in Chapter 2, nanogels based on cross-linked micellar structures represent a highly promising material type for drug delivery applications. The basis for such assemblies are block copolymers, which exhibit a difference in solubility between the segments. Using the information acquired by the kinetic investigations of BocOx, it was possible to synthesize block copolymers of EtOx and BocOx (Table 3.3). The total DP of the polymers was kept constant at 100 with varying block ratios. The experimental block ratios were calculated from the <sup>1</sup>H NMR spectra. SEC measurements of protected polymers showed  $M_n$  values around 10,000 g mol<sup>-1</sup> and low dispersity values. After deprotection, SEC measurements of the block revealed an increase in  $M_n$  and  $\bar{D}$ . However, due to the lack of cationic SEC standards a precise determination of both values is hardly possible. To gain further information about the size distribution of the cationic P(EtOx-*b*-AmOx) copolymers, asymmetric flow field-flow fractionation (AF4) investigations were performed. The obtained molar masses fit well with the expected values based on the monomer-to-initiator ratio and the  $M_n$  values derived from the <sup>1</sup>H NMR experiments.

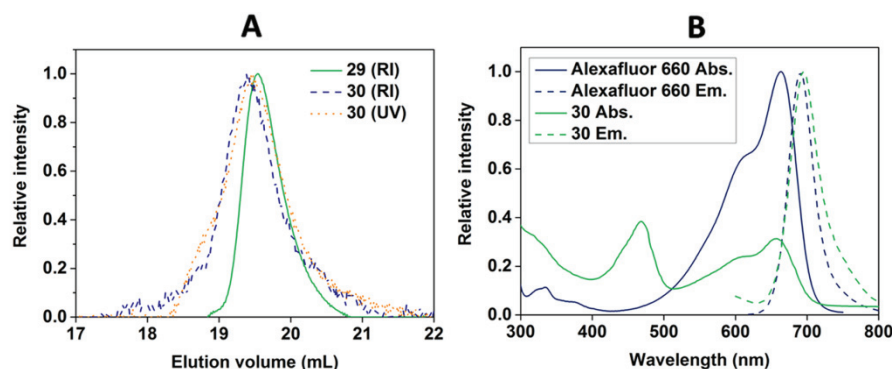
### 3. Amine containing poly(2-oxazolines)s

**Table 3.3:** Analytical data of protected and deprotected amine containing POx block-copolymers.

Sample	Composition	NMR	SEC (CHCl <sub>3</sub> )		SEC (DMAc)		AF4		Comonomer (%)
		M <sub>n</sub> (g mol <sup>-1</sup> )	M <sub>n</sub> (g mol <sup>-1</sup> )	Đ	M <sub>n</sub> (g mol <sup>-1</sup> )	Đ	M <sub>n</sub> (g mol <sup>-1</sup> )	Đ	
17	P(EtOx <sub>112</sub> - <i>b</i> -BocOx <sub>6</sub> )	12,600	7,700	1.18					5
18	P(EtOx <sub>92</sub> - <i>b</i> -BocOx <sub>10</sub> )	11,600	7,400	1.16					10
19	P(EtOx <sub>85</sub> - <i>b</i> -BocOx <sub>15</sub> )	12,100	8,900	1.20					15
20	P(EtOx <sub>84</sub> - <i>b</i> -BocOx <sub>20</sub> )	13,200	8,900	1.17					20
21	P(EtOx <sub>70</sub> - <i>b</i> -BocOx <sub>22</sub> )	12,300	7,600	1.18					22
22	P(EtOx <sub>113</sub> - <i>b</i> -AmOx <sub>5</sub> )	12,000			14,500	1.34	11,700	1.10	5
23	P(EtOx <sub>92</sub> - <i>b</i> -AmOx <sub>10</sub> )	10,600			16,800	1.23	9,200	1.14	10
24	P(EtOx <sub>72</sub> - <i>b</i> -AmOx <sub>18</sub> )	9,700			16,100	1.22	13,300	1.10	18
25	P(EtOx <sub>82</sub> - <i>b</i> -AmOx <sub>23</sub> )	11,400			18,100	1.23	13,600	1.09	22
26	P(EtOx <sub>64</sub> - <i>b</i> -AmOx <sub>26</sub> )	10,100			15,600	1.30	12,500	1.26	29
27	P(EtOx <sub>104</sub> )	10,300	9,900	1.11	20,600	1.17			0
28	P(EtOx <sub>98</sub> - <i>b</i> -BocOx <sub>32</sub> )	17,500	8,200	1.07					25
29	P(EtOx <sub>98</sub> - <i>b</i> -AmOx <sub>32</sub> )	14,200			13,900	1.11			25
30	P(EtOx <sub>98</sub> - <i>b</i> -[AmOx <sub>31</sub> - <i>stat</i> -FOx <sub>1</sub> ])	15,300			14,100	1.12			25

Since the determination was carried out using a multi-angle laser light scattering detector (MALLS) to obtain absolute molar mass values, the AF4 results are more reliable than the data derived from SEC measurements without available cationic calibration standards. Again, small Đ values indicate narrow size distributions of the block copolymers.

Polymer **29** was labeled using an Alexafluor 660-NHS ester® (**30**). The success of the dye attachment was proven by SEC measurements comparing the UV and the RI signal as described before (Figure 3.3A). The absorption spectrum of the polymer conjugated dye possesses an additional peak at 480 nm as compared to the pure fluorophor (Figure 3.3B).

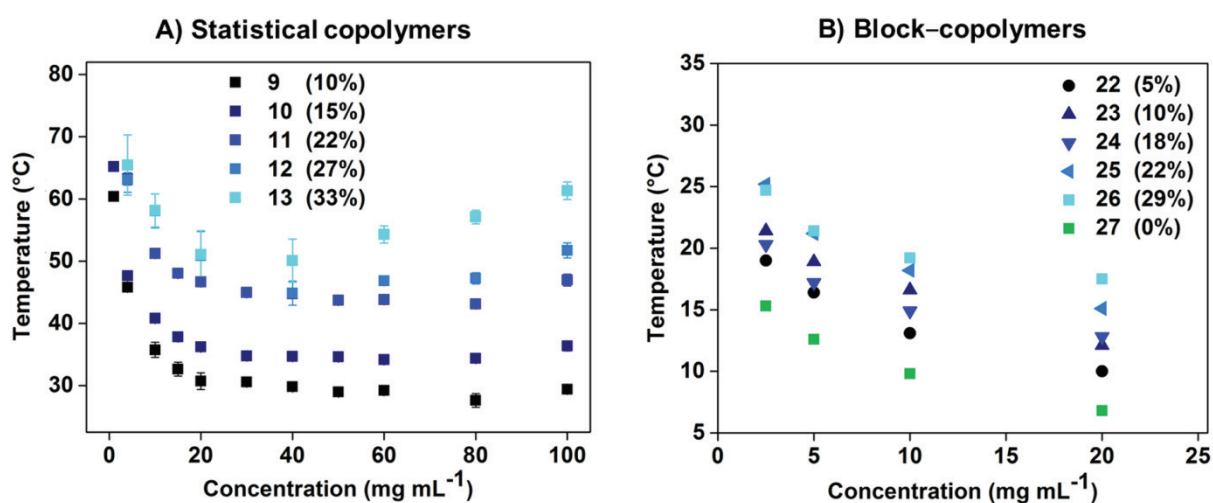


**Figure 3.3:** SEC traces of the polymers **29** and **30** in CHCl<sub>3</sub> (A) and DMAc (B) and absorbance as well as emission spectra of the dye (Alexafluor 660®) conjugated polymer.

### 3. Amine containing poly(2-oxazolines)s

However, the emission spectrum of the labeled polymer exhibits the same maximum at roughly 700 nm enabling a detection of the block copolymer by its fluorescence.

Statistical as well as block copolymers were investigated regarding their lower critical solution temperature (LCST) behavior in aqueous NaOH solution. At high pH values, the amine groups of P(AmOx) are uncharged and, hence, exhibit an increased hydrophobicity. Furthermore, the epoxide mediated cross-linking reaction, which was used for the formation of hydrogels, is carried out at a pH value of 13 (Chapter 4.1). The cloud-point curves obtained *via* turbidity measurements are depicted in Figure 3.4.



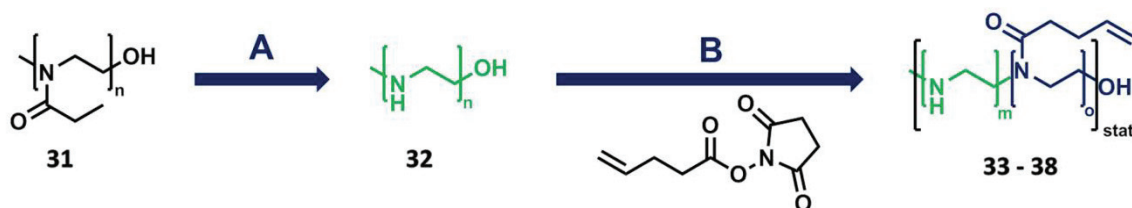
**Figure 3.4:** Cloud points of statistical (A) and block copolymers (B) at a pH value of 13 (5 wt% aqueous NaOH).

For a statistical distribution of the comonomer as well as for block copolymers, a temperature dependent phase separation is observed. The LCST of all systems decreases with decreasing AmOx content indicating that the amine containing comonomer is not responsible for the phase transition. This assumption is proven by the cloud-point of a P(EtOx) homopolymer with a comparable length (27), which phase separates at even lower temperatures. This leads to the conclusion that P(EtOx) is the responsive segment, which can be explained by a chaotropic influence of the high hydroxyl ion concentrations in solution lowering the LCST.<sup>[67-68]</sup>

A second pathway leading to amine containing POx was evaluated *via* the hydrolysis and subsequent functionalization of P(EtOx). The acidic hydrolysis of a commercial P(EtOx)<sub>500</sub> was performed in a microwave-assisted process yielding linear PEI (IPEI) with a degree of hydrolysis above 99% (Figure 3.5). In a second step, a defined amount of secondary amines was subjected to amidation *via* the use of a NHS-activated acid (Table 3.4). The result is a double bond functionalized 2-oxazoline (ButEnOx) repeating unit, which can, subsequently be utilized for cross-linking reactions while the amine groups remain intact.



### 3. Amine containing poly(2-oxazolines)s



**Figure 3.5:** Schematic representation of the synthesis of P(EI-*stat*-ButenOx) by the hydrolysis of P(EtOx) to yield linear PEI and subsequent functionalization using an NHS activated acid. A) HCl (6 mol L<sup>-1</sup>),  $\mu$ W, 130 °C, 60 min; B) 4-*N,N*-dimethylamino-pyridine, pyridine, 80 °C, 20 h.

The success of the reactions, as well as the composition of the resulting copolymers could be determined *via* <sup>1</sup>H NMR spectroscopy. Characterization by SEC revealed the formation of polymers with dispersities between 1.35 and 1.64. The molar masses obtained by SEC differ from the values calculated from <sup>1</sup>H NMR, which are based on the molar mass data of the P(EtOx) precursor provided by the supplier. The low molar mass values measured by SEC can be explained considering the different hydrodynamic volumes of the copolymers and the used PS calibration standard.

**Table 3.4:** Characterization data of P(EI-*stat*-ButEnOx).

Sample	Composition	PEI	NMR	SEC (DMAc)	
		(%)	M <sub>n</sub> (g mol <sup>-1</sup> )	M <sub>n</sub> (g mol <sup>-1</sup> )	Đ
31	P(EtOx) <sub>500</sub>	0	50,000	50,000	2.0
32	P(EI) <sub>500</sub>	100	21,500	n. d.*	n. d.*
33	P(EI <sub>355</sub> - <i>stat</i> -ButEnOx <sub>145</sub> )	71	33,400	9,400	1.35
34	P(EI <sub>310</sub> - <i>stat</i> -ButEnOx <sub>190</sub> )	62	37,100	9,900	1.37
35	P(EI <sub>255</sub> - <i>stat</i> -ButEnOx <sub>255</sub> )	50	42,800	10,700	1.44
36	P(EI <sub>220</sub> - <i>stat</i> -ButEnOx <sub>280</sub> )	44	44,500	13,700	1.38
37	P(EI <sub>130</sub> - <i>stat</i> -ButEnOx <sub>370</sub> )	26	51,800	14,800	1.64
38	P(EI <sub>25</sub> - <i>stat</i> -ButEnOx <sub>475</sub> )	5	60,500	14,400	1.48

### 4. Functional materials based on poly(2-oxazoline)s

As already addressed in Chapter 2, covalently cross-linked structures possess several advantages and unique properties, qualifying them for a range of (biomedical) applications. Within this chapter different types of networks derived from the polymeric materials described in Chapter 3 will be presented. The synthesis and properties of hydrogels, as well as covalent surface coatings will be discussed. Moreover, the synthesis of nanogels from block copolymers for the drug delivery will be described.

#### 4.1. Chemical hydrogels

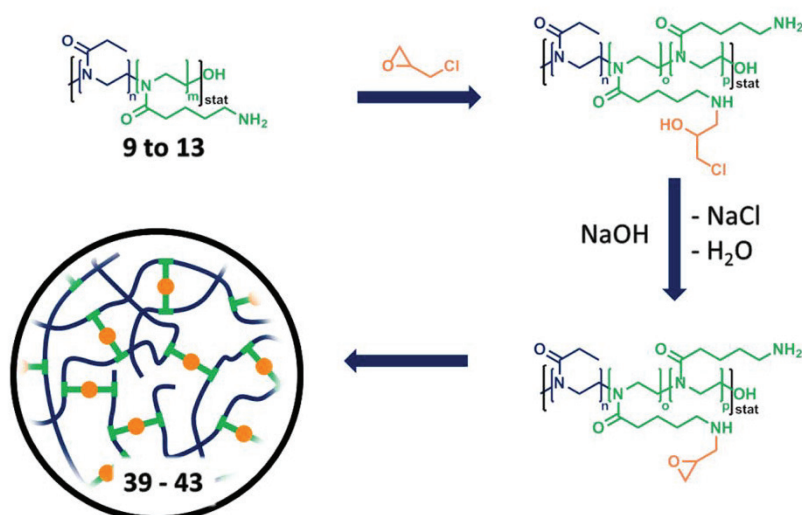
Parts of this chapter have been published in: **P2)** M. Hartlieb, D. Pretzel, K. Kempe, C. Fritzsche, R. M. Paulus, M. Gottschaldt, U. S. Schubert, *Soft Matter* **2013**, *9*, 4693-4704; **P3)** M. Hartlieb, D. Pretzel, C. Englert, M. Hentschel, K. Kempe, M. Gottschaldt, U. S. Schubert *Biomacromolecules* **2014**, *15*, 1970-1978; **P5)** C. Englert, L. Tauhardt, M. Hartlieb, K. Kempe, M. Gottschaldt, U. S. Schubert, *Biomacromolecules* **2014**, *15*, 1124-1131.

Hydrogels are the result of the cross-linking of polymers, homogeneously distributed within a solvent. While the precursor polymer has a large influence on the properties of the final network, also the cross-linking process itself can contribute to the network characteristics. Most prominently, the pore size and, consequently, the swelling degree of the hydrogel can be determined by the degree of cross-linking since gels with a denser network structure are not able to incorporate as much water as more loosely bound networks are capable of.<sup>[69]</sup>

To produce hydrogels from the polymers described in Chapter 3, the amine groups of POx had to be addressed. The applied reaction had to be specific regarding amines in order to leave other potentially functionalities untouched. Moreover, the positive charge generated by the amine groups is required in the final gels since it should trigger the ionic interaction with DNA. Consequently, the cross-linking had to produce secondary or tertiary amines which still possess the possibility of quaternization. A last important requirement is the stability of the structure. A reaction which is (under physiological conditions) irreversible needs to be applied to ensure the absence of network degradation during planned applications. Epoxides are the ideal building block to fulfil the mentioned prerequisites. The ring opening of the epoxide ring by amines leads to the formation of secondary (and after a second reaction tertiary) amines, which are stable and possess a potentially positive charge. For the production of hydrogels, statistical copolymers from EtOx and AmOx (**9** to **13**, Table 4.1) were cross-linked using epichlorohydrine (ECH) (Scheme 4.1).



## 4.1. Chemical hydrogels



**Scheme 4.1:** Schematic representation of the synthesis of hydrogels from P(EtOx-*stat*-AmOx) by the reaction with epichlorohydrin under basic conditions at 50 °C.

The linker reacts with primary and secondary amines by ring opening of the epoxide resulting in the formation of a hydroxyl group. By the elimination of hydrochloric acid from this structure, a second epoxide ring can be formed, able to react with an additional functionality. For this reason, the reaction needs to be performed under basic conditions (5 wt% NaOH) to eliminate the acid from the equilibrium.

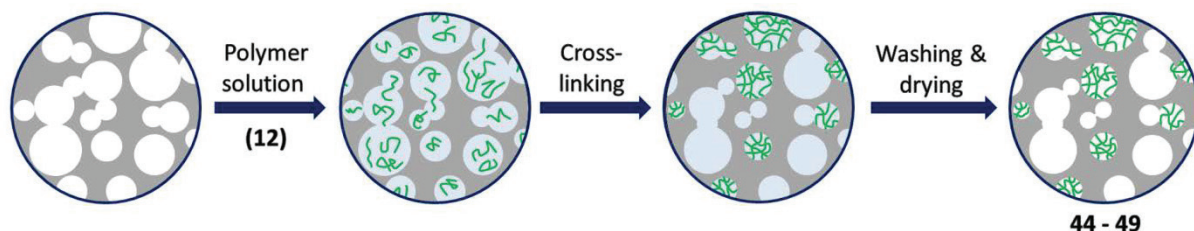
In order to investigate the influence of the amine content of the polymers on the gel properties, five networks were produced using different precursor materials. For reasons of comparability, the stoichiometry of the cross-linker was kept constant, applying five equivalence of ECH per polymer chain (Table 4.1). The gelled polymer fraction, indicating how much of the initial precursor was introduced into the gel, was determined by weighing. The swelling degrees were measured according to literature by centrifugation of the swollen sample for 10 min at 3,000 rpm.<sup>[70]</sup> No clear correlation of the swelling degree with the ratio between the two monomers is visible, although a strong dependency on the gelled polymer fraction was observed. With increasing amount of cross-linking, more polymer chains are incorporated into the scaffold, while the stiffness of the network increases. Therefore, an increased gelled polymer fraction indicates a more efficient cross-linking, which leads to lower swelling degrees, because the balance of the Gibbs free energy of mixing and the Gibbs free energy associated with the elastic nature of the polymer network is changed.<sup>[71]</sup> A drawback of the networks produced is their limited mechanical stability. In particular in the swollen state, the structures break easily, preventing an application in the purification of DNA. To circumvent this issue while maintaining swelling ability and permeability, the combination of hydrogels with porous polypropylene (PP) substrates to form matrix supported hydrogels was investigated.

## 4.1. Chemical hydrogels

**Table 4.1:** Composition and characterization of hydrogels produced from P(EtOx-*stat*-AmOx) by the reaction with epichlorohydrine under basic conditions.

Sample	Precursor	ECH ( $\mu\text{L}$ )	Ratio ( $\text{NH}_2\text{:ECH}$ )	Swelling degree (%)	Gelated polymer fraction (%)
39	P(EtOx <sub>43</sub> - <i>stat</i> -PAmOx <sub>5</sub> ) ( <b>9</b> )	3.92	5:5	97.4 +/- 0.2	34
40	P(EtOx <sub>39</sub> - <i>stat</i> -PAmOx <sub>7</sub> ) ( <b>10</b> )	3.92	7:5	94.6 +/- 0.7	45
41	P(EtOx <sub>32</sub> - <i>stat</i> -PAmOx <sub>9</sub> ) ( <b>11</b> )	4.31	9:5	91.1 +/- 0.3	49
42	P(EtOx <sub>38</sub> - <i>stat</i> -PAmOx <sub>15</sub> ) ( <b>12</b> )	3.33	15:5	95.7 +/- 0.1	42
43	P(EtOx <sub>32</sub> - <i>stat</i> -PAmOx <sub>16</sub> ) ( <b>13</b> )	3.73	16:5	97.7 +/- 0.4	32

In such composite materials the hydrogel is located within the pores of the PP matrix which stabilizes the system (Scheme 4.2). The general approach comprises the swelling of PP substrates in a solution of polymer (**12**) and cross-linker. After heating at 60 °C for 30 min, the PP substrates were separated from the residual gel, washed and dried to yield matrix supported hydrogels. The degree of cross-linking was varied, aiming for 33, 66 or 100% of linking density, respectively (Table 4.2). For this calculation it was assumed that each amine group reacts only once, applying one equivalent of ECH for every amine group at 100%. Since also secondary amines are able to ring open epoxides, the resulting networks contain primary, secondary, as well as tertiary amine groups. The water uptake of matrix supported hydrogels was determined by a thermo-gravimetric analysis (TGA) due to the low gel fraction of the composites. This method measures the change of the sample weight at 90% of relative humidity with an increased accuracy compared to conventional swelling experiments (Figure 4.1A). It has to be noted that the values derived from this method are not comparable with the swelling degrees obtained by water uptake from aqueous solution. However, the observed trend obtained by comparison of the different substrates resembles the same network parameter. Measurements of pure gels, obtained as a residue during the synthesis of matrix-supported systems, revealed a decrease of swelling with an increasing cross-linker content, which resembles the expected behavior. Furthermore, gel fractions between 5 and 10% were obtained for all structures.



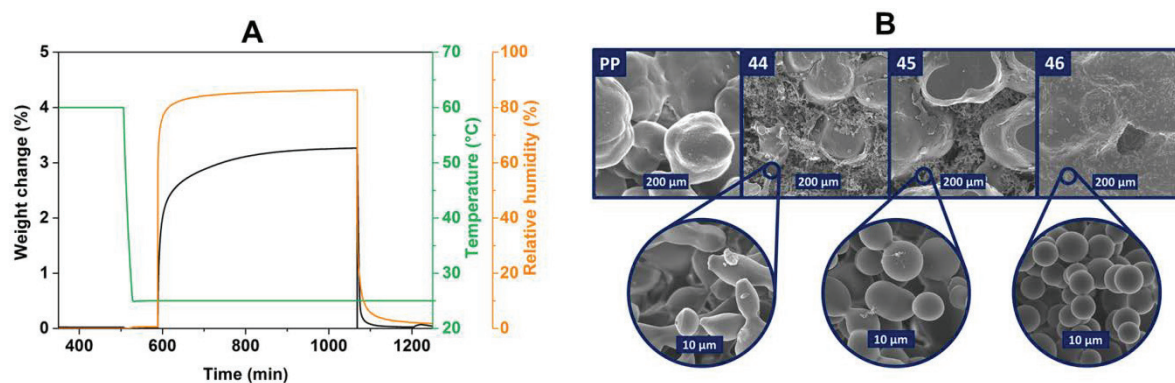
**Scheme 4.2:** Synthesis of matrix supported hydrogels based on the cross-linking of P(EtOx-*stat*-AmOx) using ECH within the pores of a PP filter substrate.

## 4.1. Chemical hydrogels

**Table 4.2:** Overview of the synthesized composite materials and hydrogels. Polymer **12** was used for the gelation of the hydrophilic component. \* Water uptake from humid (90%) air.

Sample	Substrate	Degree of cross-linking (%)	Water uptake* (%)	Gel component (wt%)
44	PP	33	3.3	5
45	PP	66	4.5	7.3
46	PP	100	3.3	6.2
47	-	33	66.5	100
48	-	66	61.5	100
49	-	100	53	100
PP	-	-	0	0

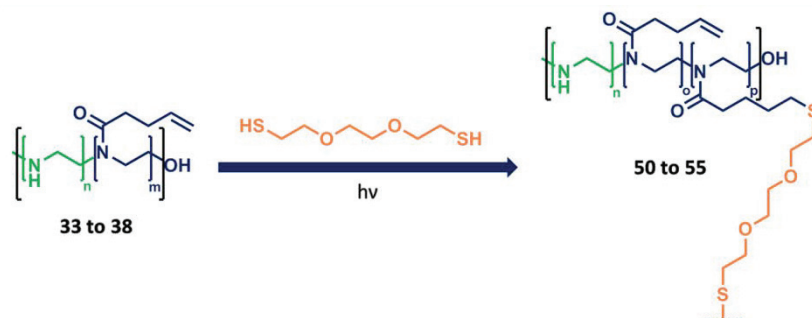
In addition, scanning electron microscopy (SEM) images show that the gel is not covering the whole space within the porous PP matrix, but is present as beads in a micrometer range (Figure 4.1B). At higher degrees of cross-linking, these structures become more defined in shape as shown by the almost perfect microspheres in system **46**. As described in Chapter 3, all statistical polymers possess a cloud-point temperature under the conditions of the gelation. This leads to the phase separation of the solution into bi-phasic systems due to a miscibility gap in the phase diagram.<sup>[72-73]</sup> The result, however, is not the precipitation of the polymer from solution but the separation into a phase with a high and a low polymer concentration, respectively.<sup>[16]</sup> Due to the concentration range of the solution, the phase with the increased concentration is present as an emulsion within the other phase, which is the reason for the increase in turbidity for such systems. The cross-linking, though it effects both phases, will only form gels from the phases with the higher concentration, because in the surrounding solution the amount of polymer is too low to form a network. The resulting hydrogel beads can be seen in the SEM pictures.



**Figure 4.1:** Characterization of matrix supported hydrogels by A) determination of the water uptake from humid air by TGA, and B) scanning electron microscopy (SEM) pictures of the gels.

## 4.1. Chemical hydrogels

One disadvantage of using the amine group for the cross-linking of polymers is, regarding the interaction with DNA, the unknown content of primary, secondary or tertiary amines, respectively. For this reason, also P(EI-*stat*-ButEnOx) copolymers (**33** to **38**) were utilized to produce hydrogels. This was accomplished using a di-thiol cross-linker, which is able to undergo an addition to the double bond present in the polymer side chain (Scheme 4.3).



**Scheme 4.3:** Hydrogel formation by radical thiol-ene addition of a di-thiol cross-linker to P(EI-*stat*-ButEnOx).

This radical thiol-ene process results in the formation of networks without interfering with the PEI subunit of the precursor polymer. Consequently, the PEI amount in the final gel structure is equal to the PEI content in the copolymers. The formed hydrogels revealed a water uptake up to a multitude of their own mass from the liquid phase (Table 4.3). The ability of the formed networks to absorb water is ascribed to the hydrophilic parts of the cross-linker and the 2-oxazoline units. But also the IPEI segments have hygroscopic properties and can exhibit different hydrated states.<sup>[74-76]</sup> As a reference, pure IPEI (which is insoluble in cold water and forms physical gels) was investigated regarding its swelling value ( $Q_{eq} = 44\%$ ). A maximum of the swelling degree of the investigated hydrogels was reached for a PEI content of 50%. This behavior can be explained by two competing trends. Starting from pure IPEI as reference, a decreasing PEI content, accompanied with an increasing amount of water soluble gel components, leads to higher swelling values.

**Table 4.3:** Composition and characteristics of hydrogels derived from (EI-*stat*-ButEnOx).

Sample	Precursor	PEI content (%)	Swelling degree (%)
32	-	100	44
50	P(EI <sub>355</sub> - <i>stat</i> -ButEnOx <sub>145</sub> ) ( <b>33</b> )	71	61
51	P(EI <sub>310</sub> - <i>stat</i> -ButEnOx <sub>190</sub> ) ( <b>34</b> )	62	60
52	P(EI <sub>255</sub> - <i>stat</i> -ButEnOx <sub>255</sub> ) ( <b>35</b> )	50	74
53	P(EI <sub>220</sub> - <i>stat</i> -ButEnOx <sub>280</sub> ) ( <b>36</b> )	44	47
54	P(EI <sub>130</sub> - <i>stat</i> -ButEnOx <sub>370</sub> ) ( <b>37</b> )	36	46
55	P(EI <sub>25</sub> - <i>stat</i> -ButEnOx <sub>475</sub> ) ( <b>38</b> )	5	23

## 4.1. Chemical hydrogels

---

The decreasing swelling values at LPEI contents lower than 50% can be ascribed to a higher network density, caused by a higher degree of cross-linking for these polymers. The increased linking density and the associated decrease of the degrees of freedom of the polymer chains limit the amount of water, which can be incorporated within the polymer network. This causes the low swelling of the 5% PEI containing gel. Compared to PEtOx-containing hydrogels with similar degrees of cross-linking (**39** to **43**,  $Q_{eq} = 97$  to  $98\%$ ), the swelling values are significantly decreased, which is caused by the lower hydrophilicity of the LPEI systems.

In conclusion, various POx based hydrogels could be synthesized. All networks possess cationic groups (*i.e.* primary, secondary and tertiary amine groups) and the linking density, as well as the amount of functional groups was varied yielding systems with diverging swelling behavior.

## 4.2. Covalent poly(2-oxazoline) based surface coatings

Parts of this chapter have been published in: **P6**) M. Leiske, M. Hartlieb, C. Paulenz, D. Pretzel, M. Hentschel, C. Englert, M. Gottschaldt, U. S. Schubert, *Adv. Funct. Mater.*, in press; **P7**) L. Tauhardt, M. Frant, D. Pretzel, M. Hartlieb, C. Bucher, G. Hildebrand, B. Schröter, C. Weber, K. Kempe, M. Gottschaldt, K. Liefelth, U. S. Schubert, *J. Mater. Chem. B* **2014**, *2*, 4883-4893.

The three dimensional structure of hydrogels is an advantage for many applications like tissue engineering or the sustained release of drugs. However, processes comprising the uptake and/or release of substances from gels are dependent on the diffusion properties of the network. If a fast interaction is required, surface coatings composed of hydrophilic polymers represent a promising alternative material type.<sup>[77]</sup> They basically resemble the two dimensional equivalent of hydrogels and exhibit a film stability sufficient for most application fields when covalently immobilized. The prevention of biofilm deposition (anti-fouling) displays one area where hydrophilic polymer films can be applied as bio-passive coatings.<sup>[78]</sup> Within this chapter, the functionalization of surfaces using POx will be described resembling a counterpart to the already discussed cationic hydrogels for the targeted interaction with DNA.

There are several ways described in literature to immobilize POx on glass surfaces. The “grafting from” approach comprises the functionalization of surfaces with moieties able to initiate a CROP like tosylates<sup>[79]</sup> or triflates.<sup>[80]</sup> The “grafting to” strategy deals with the attachment of functionalities to POx, which enables an immobilization on a substrate. A prominent example is the end-capping of the living polymerization using functional siloxanes<sup>[81-83]</sup> that will couple to glass based on the formation of a self-assembling monolayer. Other possibilities for the attachment of POx are the photo-immobilization<sup>[84]</sup> or click chemistry.<sup>[85]</sup>

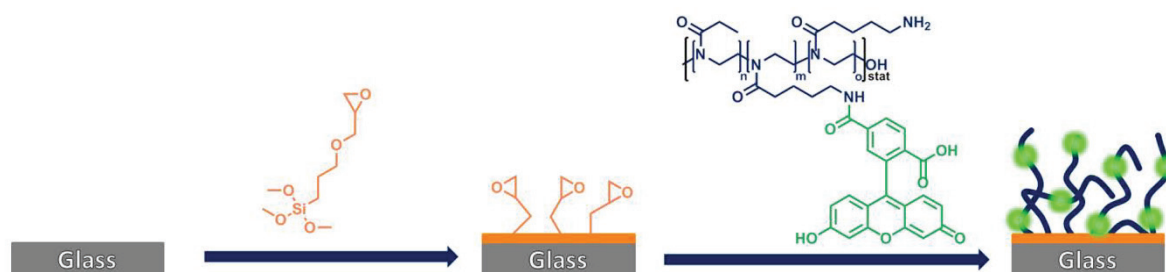


## 4.2. Covalent poly(2-oxazoline) based surface coatings

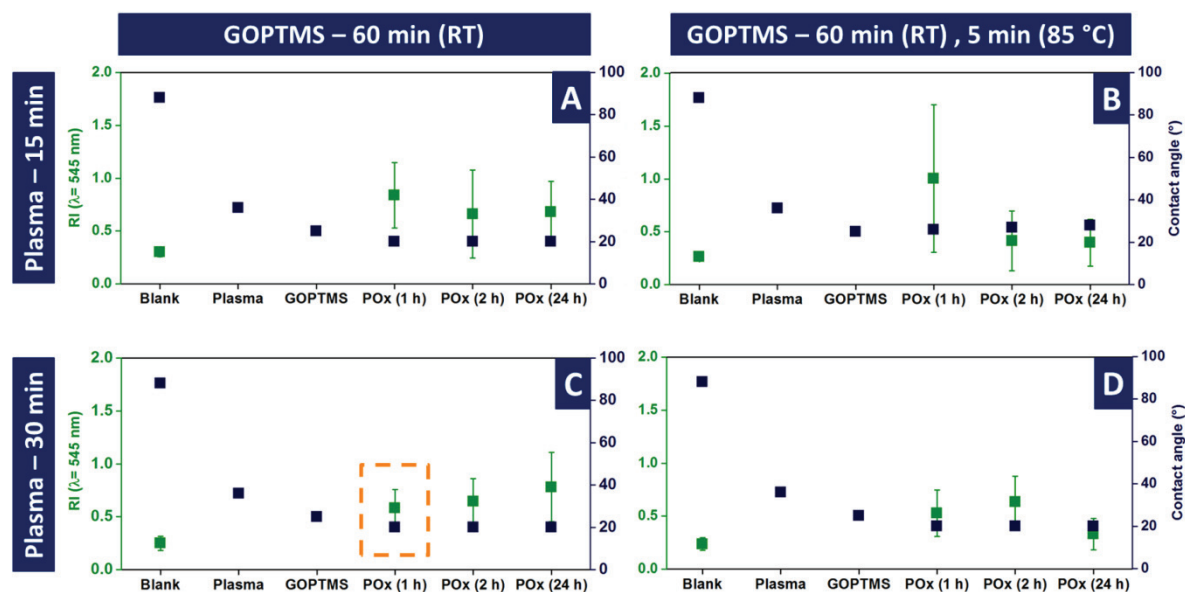
To immobilize amine containing POx, epoxide functionalized surfaces were produced. To this end, 3-glycidyloxypropyl trimethoxysilane (GOPTMS), an epoxide bearing siloxane, was used (Figure 4.2). In the presence of catalytic amounts of water, this molecule forms a siloxane monolayer on top of substrates like glass.<sup>[86]</sup> The epoxide groups expressed by this monolayer can be used to attach amine containing polymers.

A first indication of the successful immobilization of the polymer on glass was obtained by the change in surface energy as expressed by the hydrophilicity of the substrate. Contact angle (CA) measurements of water droplets deposited on the functionalized material were performed to investigate this characteristic. While pure glass exhibits a relatively high CA at around 60°, this value decreased significantly by addition of amine containing POx (**15**). The coating process with the P(EtOx) homo-polymers was further monitored by X-ray photoelectron spectroscopy (XPS) and confocal laser scanning microscopy (CLSM).

Glass and silicon display suitable substrates for the optimization of the coating procedure enabling XPS measurements. However, in view of bioanalytical applications, flexible and cheap materials are required. PP is due to low cost production and an inert character the most commonly applied support material in bioanalytics. For this reason, the surface chemistry established on glass was transferred to PP substrates. To covalently attach siloxane molecules on top of this aliphatic polymer, activation by oxidizing plasma treatment was conducted.<sup>[87]</sup> In order to evaluate suitable treatment conditions for the immobilization of preferably homogenous polymer coatings, the conditions of the plasma treatment, the GOPTMS deposition and the incubation time with the polymer were varied (Figure 4.3). CA measurements revealed that the hydrophobic character of untreated PP (CA = 88 °) decreases after activation with O<sub>2</sub> plasma (CA = 36 °), most probably due to the formation of hydroxyl groups. These oxygen functionalities react with GOPTMS to form a monolayer on the surface (CA = 25 °). After coating with polymer **16**, the hydrophilicity increases (CA < 20 °) as a result of the covalently bound macromolecules. No significant CA differences were observed with varying incubation times.



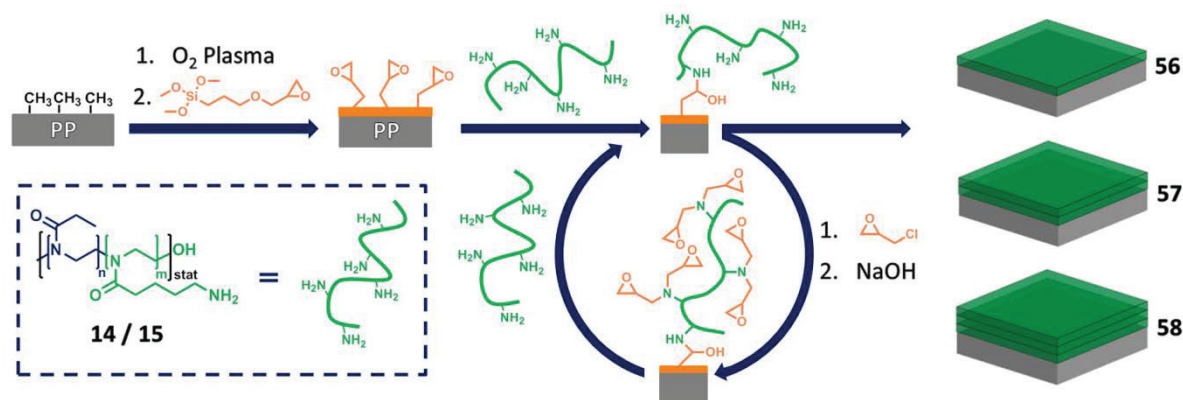
**Figure 4.2:** Schematic representation of the coating procedure applied for the covalent immobilization of fluorescently labeled P(EtOx-*stat*-AmOx) (**15**) on glass.



**Figure 4.3:** Optimization of the conditions for covalent polymer coating of PP substrates varying the plasma treatment time, the GOPTMS incubation conditions and the polymer incubation time (RI = relative intensity of fluorescence).

CLSM measurements at  $\lambda_{\text{ex}} = 543 \text{ nm}$  ( $\lambda_{\text{em}}: 560 \text{ to } 615 \text{ nm}$ ) were performed for all coated slides as well as for the blank substrates measuring an increase of fluorescence after coating with Rhodamine labeled POx (**16**). The fluorescence intensity does not change significantly by varying either coating conditions or POx incubation time. However, the film homogeneity does, which is indicated by the standard deviation of the signal. An  $\text{O}_2$  plasma treatment for 30 min and 1 h GOPTMS incubation at room temperature (RT) were chosen as the best activation and functionalization conditions, as indicated by a high mean fluorescence in combination with the most homogenous distribution of polymer on the surface within a reasonable time (Figure 4.3C). For the aimed application of DNA binding and release, the amount of amine groups and the ability to incorporate water are key parameters. Both can be varied by altering the thickness of immobilized polymer films. A straightforward method of controlling these factors is the deposition of functional material in a layer-by-layer (LbL) approach. The general procedure is depicted in Scheme 4.4. The first layer is attached by the already described method comprising surface activation, epoxide monolayer deposition and polymer immobilization. To add additional layers, the amine groups of the POx were functionalized by epichlorohydrin (ECH), which was also used to produce hydrogels. After treatment with sodium hydroxide and thoroughly washing, a second polymer layer was attached which, again, has excessive amine groups for further functionalization. This cycle can be repeated until the desired numbers of coatings are immobilized on the substrate. Within this study films composed of up to three bilayers were produced.

## 4.2. Covalent poly(2-oxazoline) based surface coatings



**Scheme 4.4:** Schematic representation of the deposition of amine containing POx in an LbL approach using ECH as a cross-linker.

A first indication of a successful layer deposition was obtained by CA measurements (Table 4.4). The blank PP substrate showed high CA values due to the hydrophobicity of the material. Plasma activation, as well as GOPTMS deposition, reduces the CA significantly, indicating an effective functionalization. Upon the attachment of POx, the CA decreases below 20°, which represents the minimum measurable CA. The activation using ECH cross-linker yields CA values above 50° that decreased again below 20° upon the addition of another POx layer.

This behavior of surface energy changes is in very good agreement with the successful deposition of POx in an LbL approach. Moreover, thermo-gravimetric analysis (TGA) revealed a linear mass increase per POx layer. Further analysis of the POx coating was conducted using reflectometric interference spectroscopy (RIFS) measurements. This method determines the thickness of layers on glass substrates having a reflective Ta<sub>2</sub>O<sub>5</sub> layer on the opposite site of the coating by measuring the peak shift of light reflected by the polymer layers.<sup>[88]</sup> Therefore, glass slides were coated applying the conditions used for PP and analyzed accordingly. During measurements, a water flow was channeled over the POx surface continuously to generate information about swollen layers.

**Table 4.4:** Analytical data of multilayer POx coatings.

Sample	Coating step	CA (°)	POx amount by TGA (wt%)	Layer thickness (on glass, nm)
-	Blank	100	-	0.0
-	O <sub>2</sub> plasma	80	-	0.6
-	GOPTMS	48	-	0.8
56	1st POx layer	< 20	0.7	3.5
-	ECH	57	-	-
57	2nd POx layer	< 20	1.3	28.4
-	ECH	72	-	-
58	3rd POx layer	< 20	1.8	109.4

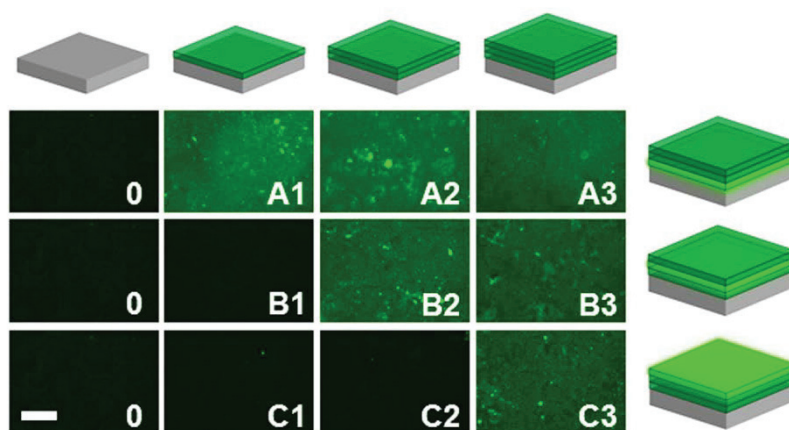


## 4.2. Covalent poly(2-oxazoline) based surface coatings

The exponential increase of the layer thickness is, at first sight, inconsistent with the information obtained from TGA. A varying cross-linking density of individual layers could be an explanation for this discrepancy. The first layer is attached to the substrate *via* the reaction with epoxide groups directly on the surface, generating a flat film of polymer chains.

With every additional layer, the mobility of the epoxide binding sites increases generating more loosely bound and mobile POx layers that are able to incorporate more water into the polymeric matrix, describing the transition from a surface coating to a hydrogel. As another qualitative proof of the LbL deposition, fluorescence analyses were performed using polymer **15**. All investigated PP slides were coated with three POx layers, however fluorescently labeled POx was only used in the first, second and third coating step, respectively. For the respective other two layers, polymer **14** was utilized. In this way, samples with one fluorescently labeled POx layer and two unlabeled layers were obtained. Every coating step was investigated using CLSM measurements (Figure 4.4). The images illustrate the control over the layer deposition by the applied method. A significant increase in fluorescence upon coating with polymer **15** shows the successful immobilization of the material (*e.g.* A1). The fluorescence signal remains relatively constant upon the addition of further layers (*e.g.* A2 and A3) proving the LbL structures on the surfaces.

In conclusion, the covalent attachment of amine containing POx on glass as well as PP was investigated and optimized by the use of CA, XPS, TGA and fluorescence measurements. The thickness and swelling of the obtained polymer films was tuned by the polymer deposition using an LbL approach, and the resulting multilayer POx films were analyzed in detail.



**Figure 4.4:** CLSM pictures of fluorescently labeled POx multilayers. Polymer **15** was used for the first (A), second (B) or third (C) polymer layer and polymer **14** for the residual layers. Pictures were captured of blank PP (0), and after the first (1), second (2), as well as third (3) coating step at a wavelength between 505 and 530 nm. Scale bar: 200  $\mu\text{m}$ .

#### 4.3. Poly(2-oxazoline) based nanogels

Parts of this chapter have been published in: **P4)** M. Hartlieb, D. Pretzel, M. Wagner, S. Hoeppener, P. Bellstedt, M. Görlach, C. Englert, K. Kempe, U. S. Schubert, *J. Mater. Chem. B.* **2015**, *3*, 1748-1759; **P8)** M. Hartlieb, T. Buś, J. Kübel, D. Pretzel, S. Hoeppener, K. Kempe, B. Dietzek, U. S. Schubert, in preparation.

While Chapters 4.1 and 4.2 aimed for the production of insoluble materials for the interaction with DNA, this chapter is dedicated to the synthesis of POx nanogels for drug delivery applications. Nanogels are covalently cross-linked structures in a nanometer size range which combine beneficial properties of hydrogels (tissue like structure, biocompatibility, stimuli responsiveness)<sup>[89]</sup> with the solubility properties of nano-assemblies, like nanoparticles or micelles. There are several ways for the production of such structures like the use of inverse emulsions<sup>[90]</sup> or *via* polymerization induced phase separation.<sup>[91]</sup> One particularly elegant way is the cross-linking of self-assembled structures like micelles or vesicles which are derived from block copolymers. The underlying principle is the nano-phase separation based on the solubility differences between two or more blocks of a macromolecule.<sup>[92]</sup> Within a selective solvent which will dissolve one segment of the polymer but not the other, the poorly soluble block will collapse in order to minimize its exposure to the solvent while the soluble block will extend into solution.<sup>[93]</sup> Depending on the length and the volume of the segments, the structure of assembly differs between cylindrical micellar or vesicular shapes.<sup>[94]</sup> One disadvantage of such materials is the equilibrium between assembly and unimer (polymer). Below the critical micelle concentration (CMC), only unimers are present.<sup>[92]</sup> Although the CMC of polymeric assemblies is low compared to liposomes, it still represents a disadvantage.<sup>[95]</sup> Systems applied in nanomedicine usually face a strong dilution upon administration into the blood system of a patient, which should not lead to disassembly. Cross-linking is the most prominent way to overcome this drawback.<sup>[31]</sup> POx-based micellar structures were investigated thoroughly over the past decades.<sup>[96-102]</sup> However, up to date, only a limited number of reports described the synthesis of cross-linked POx aggregates. The type of cross-linking reaction is of central interest for designing drug delivery systems with sufficient stability and the ability to release their cargo on demand.<sup>[103]</sup> Covalently cross-linked POx micelles stabilized by thiol-yne chemistry,<sup>[104-105]</sup> epoxide-amine addition,<sup>[106]</sup> UV mediated cross-linking<sup>[61, 107]</sup> as well as electron beam irradiation<sup>[62, 108]</sup> are described. However, only one system using a reversible linker (disulfide bridge) is reported.<sup>[25]</sup>

To fabricate nano-phase-separated systems from amine containing POx, cationic block copolymers (**22** to **26**) were utilized. While the EtOx block exhibits a good solubility in water as well as polar organic solvents, the cationically charged amine containing block is only soluble in

### 4.3. Poly(2-oxazoline) based nanogels

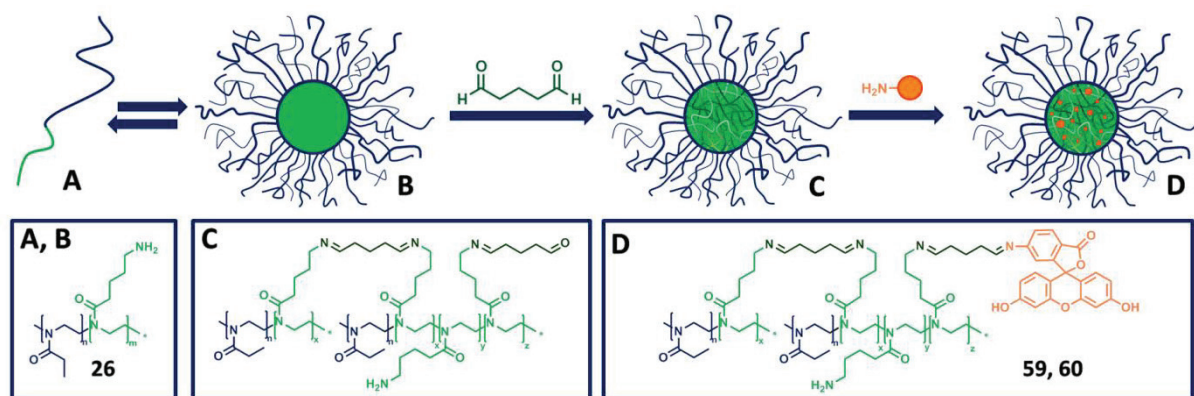
water or DMAc. For this reason, different organic solvents were investigated regarding their ability to induce a phase segregation using dynamic light scattering (DLS) (Table 4.5). As expected, pure PEOx showed no aggregation. However, all block copolymers formed structures in the range between 4 and 112 nm depending on the solvent and the composition. Surprisingly, the ratio between the two blocks did not influence the size of the aggregates as strong as the polarity of the solvent. All samples assembled in CHCl<sub>3</sub> formed structures with radii between 4 and 17 nm, which can be addressed to objects with a micellar character. In *i*PrOH, size distributions between 68 and 105 nm were detected, which indicates the formation of vesicular assemblies. The use of MeOH led to structures with even larger radii (77 to 113 nm). A possible explanation for this trend is a swelling of the selective block in dependence of the polarity of the solvent. While the amine group has a potentially cationic charge, the side chain and the backbone of the block can be readily solubilized by organic solvents resulting in a gel-like core instead of a complete collapse of the AmOx segment. When the polarity of the applied solvent increases, swelling should equally increase, resulting in a higher steric demand of the selective block, while the hydrophilic PEOx block reveals a similar solubilization in all used solvents. Thus, the transition from a micellar to a vesicular structure might be attributed to the change in the ratio between the volume of the two segments.<sup>[94]</sup>

To transfer these structures into aqueous systems, the core of the agglomerates has to be cross-linked since both polymer blocks are readily water soluble. For this purpose, two samples, which showed the most uniform size distribution in organic solvents, were chosen (highlighted in Table 4.5) and cross-linked with glutaraldehyde (GA) (Scheme 4.5). As a *bis*-aldehyde, GA is able to form imine bonds with the amine groups present in the core and, consequently, lock the structure of the assemblies. However, a direct transfer of the micelles into water yielded only hydrogels, which indicates that, even though GA was added in stoichiometric amounts, a sufficient number of free amine and aldehyde groups remained to induce intercross-linking.

**Table 4.5:** DLS screening of the self-assembling behavior of block copolymers (**22** to **26**) and PEOx (**27**) in organic solvents (5 mg mL<sup>-1</sup>; size indication in radius; number plot; no size value is specified, if the number weighted plot shows only the polymer precursor). The highlighted assemblies were subjected to cross-linking.

Solvent	0% AmOx ( <b>27</b> )		5% AmOx ( <b>22</b> )		10% AmOx ( <b>23</b> )		18% AmOx ( <b>24</b> )		22% AmOx ( <b>25</b> )		29% AmOx ( <b>26</b> )	
	Size (nm)	PDI	Size (nm)	PDI	Size (nm)	PDI	Size (nm)	PDI	Size (nm)	PDI	Size (nm)	PDI
MeOH	-	-	-	-	-	-	113	0.334	83	0.646	77	0.335
<i>i</i> PrOH	-	-	71	0.550	105	0.714	99	0.561	92	0.509	68	0.111
CHCl <sub>3</sub>	-	-	4	0.360	8	0.217	16	0.256	13	0.376	17	0.048

### 4.3. Poly(2-oxazoline) based nanogels



**Scheme 4.5:** Schematic representation of the self-assembly of P(EtOx-*b*-AmOx) followed by cross-linking and quenching/loading.

As demonstrated by Lecommandoux and co-workers, the amount of cross-linked amine groups for such reactions is only about 35%, when aiming for full conversion.<sup>[109]</sup> To overcome this drawback, low molar mass amines have to be added in large excess after the cross-linking step to consume the residual aldehydes. This strategy, in turn, does not only enable the stabilization of the self-assembled structure but also allows the simultaneous incorporation of drug molecules or fluorescence labels into the system. For this reason, 6-amino fluorescein (6AF) was used to quench the cross-linking process. After this treatment the assembled structures could be transferred into aqueous solution. A first indication of successfully cross-linked structures was provided by DLS experiments, which indicated distributions in the same size range as observed in organic solvents (Table 4.6). The PDI values of the locked systems increased slightly. This might be due to an agglomeration caused by unconsumed aldehyde groups in the core. However, the values are still in a good range for synthetic nano-sized objects. The zeta potential of all cross-linked assemblies was found to be positive, indicating the presence of free amine groups. A further investigation of size and uniformity was conducted using asymmetric flow field-flow fractionation (AF4) measurements. By utilizing this technique, it is possible to separate the samples by the diffusion coefficient and to determine the hydrodynamic radius ( $R_h$ , by online DLS measurements) and the radius of gyration ( $R_g$ , by multi-angle laser light scattering (MALLS) measurements). The data depicted in Table 4.6 are similar to the values obtained by DLS measurements.

**Table 4.6.** Characterization data for cross-linked nanostructures (DLS: 5 mg mL<sup>-1</sup>, size indication in radius). Polymer **26** served as precursor for all assemblies. The content of fluorescein was determined by the absorbance at 470 nm.

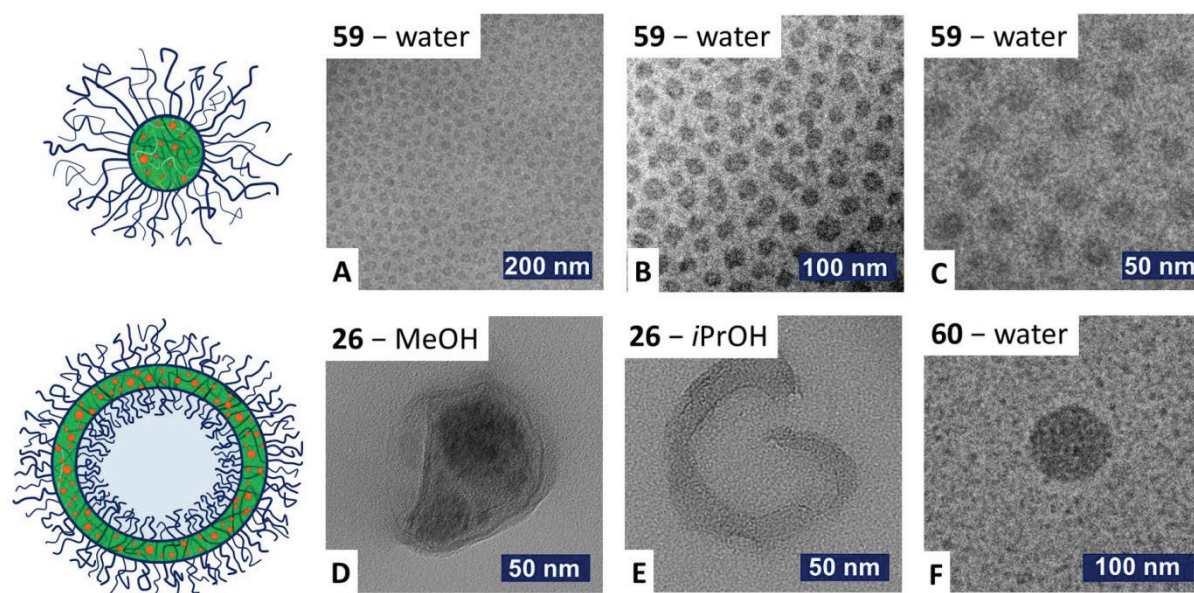
Sample	Solvent for self-assembly	Capping agent	DLS in solvent		DLS in water		$\zeta$ (mV)	AF4			Content of capping agent (wt%)
			Size (nm)	PDI	Size (nm)	PDI		$R_g$	$R_h$	$\rho$	
<b>59</b>	CHCl <sub>3</sub>	6AF	17	0.048	15	0.199	+17	-	20.0	< 0.8	29
<b>60</b>	<i>i</i> PrOH	6AF	68	0.111	50	0.179	+23	40	40.0	1.00	29



### 4.3. Poly(2-oxazoline) based nanogels

An additional information provided by this analysis is a measure of the particle shape by the comparison of both hydrodynamic radius and radius of gyration expressed in the ratio  $\rho$  ( $\rho = R_g/R_h$ ). For particles assembled in  $\text{CHCl}_3$ , the  $R_g$  value could not be determined since they were too small for detection with the MALLS detector (limit around 15 nm).<sup>[110]</sup> This indicates a  $R_g$  below 15 nm and, hence, a  $\rho$  ratio less than 0.8, which is characteristic for hard spheres and, therefore, supports the assumption of a micellar architecture of the assembled particles.<sup>[111]</sup> Larger  $\rho$ -values (around 1) as obtained for *i*PrOH derived structures indicate less dense and soft or hollow sphere structures, such as vesicles.<sup>[111]</sup> Considering the block architectures of P(EtOx-*b*-AmOx) and the fact that a fully stretched polymer chain length (32 nm) is shorter than the radius of the assemblies, a vesicular morphology of these samples is most likely. Based on this assumption, the larger nanostructures will henceforth be addressed as vesicles.

To visualize the proposed structures, cryo transmission electron microscopy (cryoTEM) measurements were performed. Samples in aqueous media, as well as non-cross-linked polymers were investigated (Figure 4.5). The non-cross-linked systems could be examined only in the dried state as vitrification of the solutions was not successful. However, the remaining polymer shells of collapsed vesicular systems were found in samples derived from MeOH and *i*PrOH (Figure 4.5D and F). CryoTEM images of the chloroform assembled and cross-linked micelles show uniform nano-objects, which are arranged in a regular pattern (Figure 4.5A-C). For both, micelles and vesicles, the radii of structures visible in the TEM images are in good agreement with the values obtained by DLS and AF4 measurements.

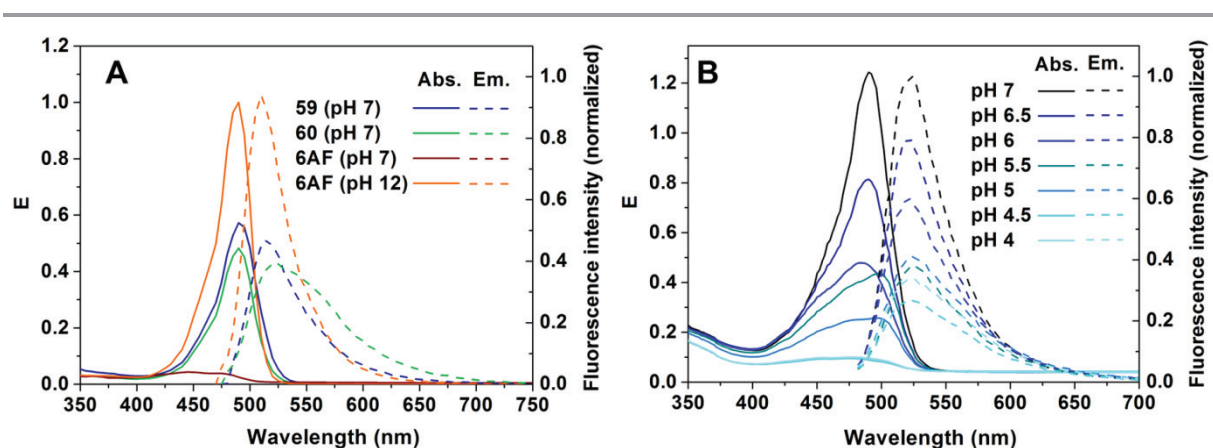


**Figure 4.5:** TEM images of the dried structures assembled in methanol and *i*PrOH, and cryoTEM images of self-assembled as well as cross-linked structures in water.

### 4.3. Poly(2-oxazoline) based nanogels

The amount of covalently bound dye was determined using its absorption and fluorescence properties. The absorption and emission spectra of 6AF-containing samples were measured in water at a pH value of 7 in order to compare the data to pure 6AF, which was measured in the presence of a 100-fold excess of GA to ensure a quantitative conversion to the imine form (Figure 4.6). While 6AF shows the typical absorption and emission spectra of the lacton derivative at a pH value of 7 (low absorption, maximum at 440 nm), both, micelles as well as vesicles, absorb and emit similar to the ring-opened di-anionic carboxy isomer state of the dye (Figure 4.6A). This behavior seems best explained by the high density of amine groups in the core of the assemblies leading to a locally increased pH value which, in turn, causes the formation of the di-anionic species characterized by a strong absorption at 490 nm.<sup>[112]</sup> A closer look at the photochemical behavior of the nano-assemblies shows that even at a pH value of 4 a significant fluorescence can be observed, indicating a basic microenvironment within the core of the nanostructures (Figure 4.6B). A direct comparison with pure 6AF is not possible due to the diminished solubility of the dye in this pH range. However, for the labeling of the nanostructures, this effect is advantageous as the micelles or vesicles, respectively, show a high fluorescence intensity even at low pH values as for instance present in the lysosomal compartment of cells which enables a detection of intact nanostructures within cells while the free dye will not interfere.

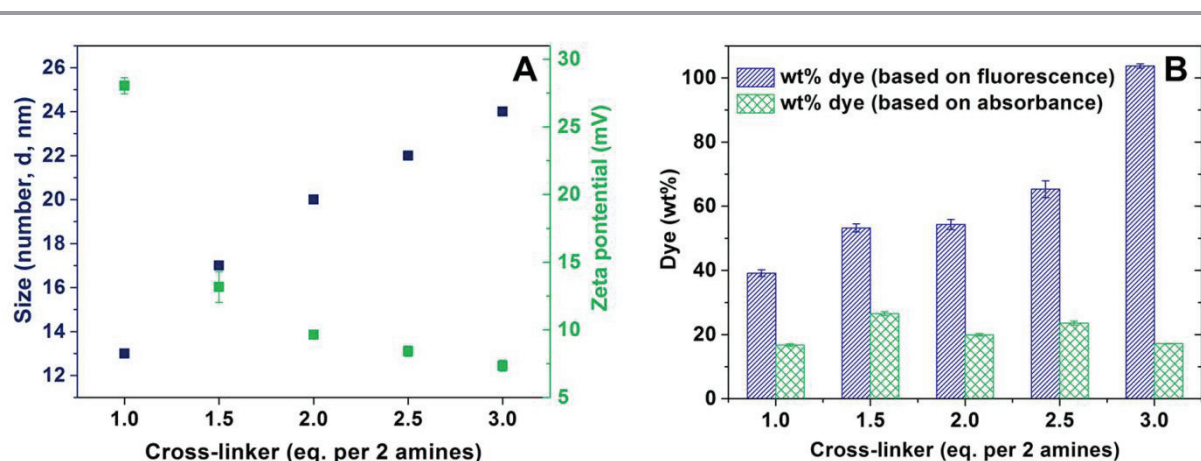
The amount of incorporated 6AF was determined at a pH value of 12 and found to be 29 wt% of dye per total mass for the micelles, as well as for the vesicles. This is equivalent to 12 6AF molecules per polymer chain, which complies with the conversion of amine groups by GA in similar systems (~35%).<sup>[109]</sup> An equal loading for both nanoarchitectures was expected as the chemical composition of both systems should be identical, while only the shape varies.



**Figure 4.6:** A) Absorption and fluorescence spectra of 6AF (pH dependent) and dye quenched nanostructures (**59**, **60**); B) pH dependent absorbance and fluorescence of compound **60** ( $0.05 \text{ mg mL}^{-1}$ ).

### 4.3. Poly(2-oxazoline) based nanogels

For the application of nanogels in drug delivery, the zeta potential is of paramount importance since it strongly influences the interaction with cell membranes.<sup>[113]</sup> Positively charged nanoparticles are taken up faster by cells compared to neutral, or slightly negatively charged carriers. The enhanced permeability and retention (EPR) effect, which was discussed in Chapter 1, describes the accumulation of nano-sized objects within tumorous tissue, however, only if their circulation times are sufficiently long. For this reason, the possibility to tune the surface charge of the presented nanogels would be highly beneficial for later applications. One possible way to influence this property is the variation of the cross-linker amount during gelation. The formed imine is, compared to amine groups, less basic, and, hence, the nucleophilic addition of a proton is less favorable. Therefore, an increase of the cross-linking density of the nanogels should result in a reduced surface charge. To confirm this assumption, polymer **29** was used to produce micellar assemblies in  $\text{CHCl}_3$ , which were subsequently cross-linked using different contents of GA and were quenched using 6AF. The amount of cross-linker was varied between one and three equivalents regarding the amount of amine groups (one GA per two amine groups) (Table 4.7). Size and zeta potential of the resulting assemblies were investigated using a Zetasizer (Figure 4.7A). As expected, the positive charge of the nano-assemblies decreased with an increasing amount of cross-linker since more amine groups are converted to imines, having a less basic character compared to the starting material. The decrease is of exponential nature having a minimum value above +5 mV. A second effect observed is the increase in size of the micelles formed. This is on the first sight contra intuitive since a higher degree of cross-linking should lead to a more dense core structure and, henceforth, to smaller agglomerates.



**Figure 4.7:** Variation of the cross-linker content of micellar POx nanogels. A) Size (determined by DLS,  $5 \text{ mg mL}^{-1}$ ) and zeta potential of the resulting assemblies. B) Amount of immobilized dye with the nanogels as determined by absorbance or fluorescence of 6AF.

### 4.3. Poly(2-oxazoline) based nanogels

**Table 4.7:** Variation of cross-linker degree for the formation of micellar nanogels and loading with Dox. Polymer **29** was used as a precursor for the assembly in CHCl<sub>3</sub> (DLS: 5 mg mL<sup>-1</sup>, size indication in diameter; Fluorescence: 6AF loading determined by the absorbance at 440 nm, Dox loading determined by the absorbance at 485 nm).

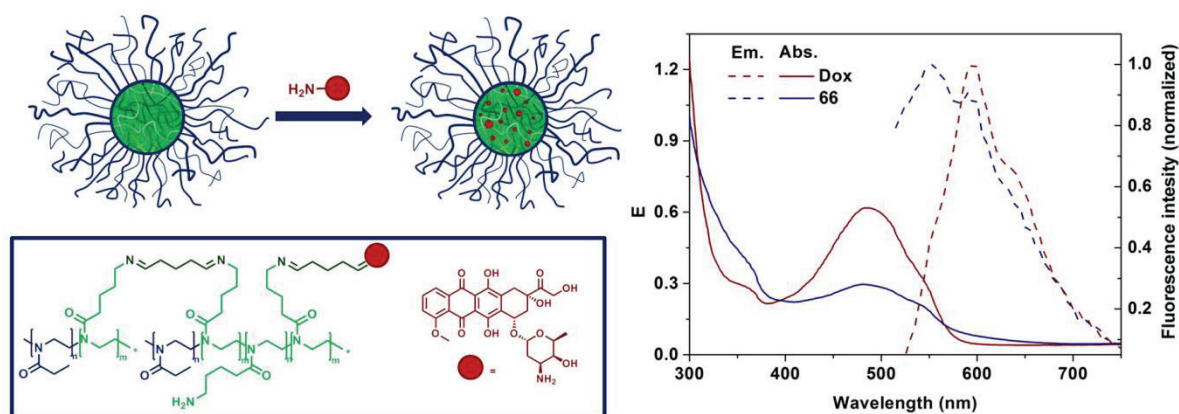
Sample	Precursor polymer	Cross-linker (eq. per 2 amines)	Capping agent	Size (nm, d)	$\zeta$ (mV)	Content of capping agent (wt%)
61	29	1	6AF	13	28	17
62	29	1.5	6AF	17	13	27
63	29	2	6AF	20	10	20
64	29	2.5	6AF	22	8	24
65	29	3	6AF	24	7	17
66	29	3	Dox	13	18	5
67	30	3	Dox	5	25	6

However, an increase in the amount of cross-linker is also accompanied by the input of water into the system. GA is applied as a 70 wt% aqueous solution and produces water upon the formation of a Schiff's base. The water will accumulate in the hydrophilic part of the phase segregated system, which is, in fact, the core of the micelle. This process could lead to a swelling of the nanostructure prior and during cross-linking, producing larger nanogels. The increase in fluorescence as depicted in Figure 4.7B was found to be the result of a quenching of non-radiative decay.

While 6AF helped to understand the basic structure of the micelles and vesicle, it does not serve any pharmaceutical purpose. Therefore, in order to produce drug delivery systems, an amine containing drug is aimed to be incorporated within the core of the nano-assemblies. For this reason, Doxorubicin (Dox), a potent anti-cancer drug was incorporated as described before (Scheme 4.6; Table 4.7). Three equivalence of cross-linker were chosen to produce these materials to aim for micelles with a preferably low zeta potential. The resulting diminished interaction with tissue and blood components should lead to an optimal exploitation of the EPR effect as described in Chapter 1. However, the zeta potential for the obtained nanostructure was significantly higher (+18 mV) compared to the 6AF-quenched sample (+7 mV). This can be explained by the di-anionic character of 6AF within the basic environment of the micellar core. The negative charge of the loading is presumably able to partially compensate the positive charge of amines and imines, which is not possible in case of Dox loading. Also the size of Dox loaded micelles is smaller than it would be expected from the 6AF equivalent (**65**).



### 4.3. Poly(2-oxazoline) based nanogels

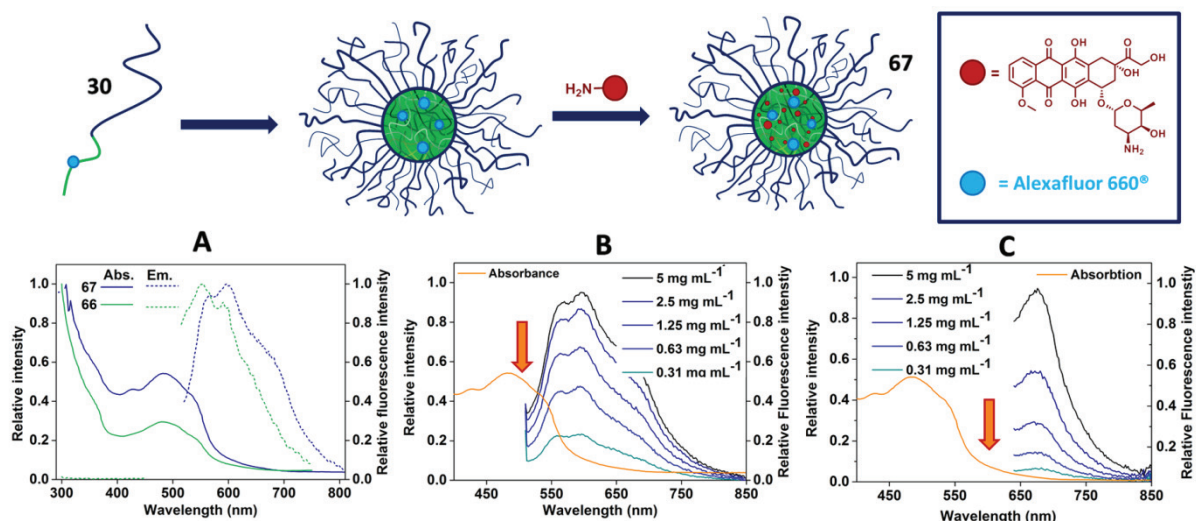


**Figure 4.9:** Covalent loading of micellar nanogels with Dox and the absorption and fluorescence spectra of the Dox and sample **66**.

This finding could be explained by the presence of keto groups within the structure of Dox, which could further cross-link the core and shrink the size of the micelles while quenching. While the absorption spectrum (Figure 4.9) is similar to the one of the pure drug, the fluorescence signal is significantly broader which, again, could be the result of the changed microenvironment within the micellar core. The fluorescence of Dox is known to be pH dependent,<sup>[114]</sup> and the alkaline core of the micelles has a similar influence on the drug as on 6AF as demonstrated before.

To be able to follow the fate of drug and carrier within cells separated from the fluorescence of Dox, polymers labeled with Alexafluor 660<sup>®</sup> were utilized for the production of micelles (sample **67**). The loading was conducted using an excess of Dox as described for micelle **66** and the immobilized drug amount was found to be similar (6 wt%). While the absorption spectrum does not differ significantly from the spectrum of micelle **66**, the fluorescence emission exhibits a broad shoulder at higher wavelengths (Figure 4.10A). When the excitation wavelength is varied from 480 nm (Figure 4.10B) to 600 nm (Figure 4.10C), the emission of the bound dye can be isolated. The fluorescence maximum is blue shifted compared to the free dye, which could be attributed to the microenvironment within the nanogel.

### 4.3. Poly(2-oxazoline) based nanogels



**Figure 4.10:** Synthesis of Dox containing micelles using Alexafluor 660<sup>®</sup> labeled polymer. A) Comparison of absorption and emission spectra of Dox micelles with and without further labeling; B and C) concentration dependent emission of micelle **67** at an excitation wavelength of 480 nm (B) and 600 nm (C).

In summary, the self-assembly of double hydrophilic POx block copolymers in organic medium was demonstrated. The structures could be locked by chemical cross-linking which has also a direct influence on the zeta potential of the micelles. Loading, as well as labeling was achieved using a fluorescein derivative or Dox as anti-cancer drug, respectively. The investigation of the presented systems with cells will be the subject of Chapter 5.2.

### 5. Biomedical applications of poly(2-oxazoline) materials

Poly(2-oxazoline)s (POx) represents a promising polymer class regarding potential biological and biomedical applications. This is due to the biocompatibility and the stealth properties of certain POx, which can be utilized for drug delivery or anti-fouling applications or the manifold functionalization possibilities of this polymer family. The materials described within this thesis are used for two separate purposes. The first application is the detection of genetic material from biological samples which will be the subject of Chapter 5.1. Here, the cationic nature of polymers, hydrogels and surface coatings are used to specifically interact with the poly-anionic DNA. Chapter 5.2 focusses on the interaction of nanoscopic assemblies such as micelles and vesicles with cells regarding toxicity, uptake, co-localization, and drug delivery.

#### 5.1. DNA detection using hydrogels and coatings

Parts of this chapter have been published in: **P2)** M. Hartlieb, D. Pretzel, K. Kempe, C. Fritzsche, R. M. Paulus, M. Gottschaldt, U. S. Schubert, *Soft Matter* **2013**, *9*, 4693-4704; **P3)** M. Hartlieb, D. Pretzel, C. Englert, M. Hentschel, K. Kempe, M. Gottschaldt, U. S. Schubert *Biomacromolecules* **2014**, *15*, 1970-1978; **P5)** C. Englert, L. Tauhardt, M. Hartlieb, K. Kempe, M. Gottschaldt, U. S. Schubert, *Biomacromolecules* **2014**, *15*, 1124-1131; **P6)** M. Leiske, M. Hartlieb, C. Paulenz, D. Pretzel, M. Hentschel, C. Englert, M. Gottschaldt, U. S. Schubert, *Adv. Funct. Mater.*, in press.

A reliable and time saving point-of-care diagnostic is one of the most important targets of today's bioanalytical science.<sup>[115-117]</sup> The optimal method would comprise an analysis of sample material directly on the spot, however, operating with the same accuracy as current laboratory tests.<sup>[118]</sup> Moreover, cost efficiency is a major requirement in this context, rendering the design of new bioanalytical devices a highly challenging task.<sup>[119]</sup> The detection of diseases based on bacterial, fungal or viral infections can be accomplished by the investigation of the pathogens nucleic acid profiles,<sup>[120-121]</sup> providing the opportunity of a fast determination and a targeted medication.<sup>[122]</sup> The recognition of the genetic material can be accomplished *via* various methods<sup>[123]</sup> including specialized DNA assays based on microchip systems.<sup>[124]</sup>

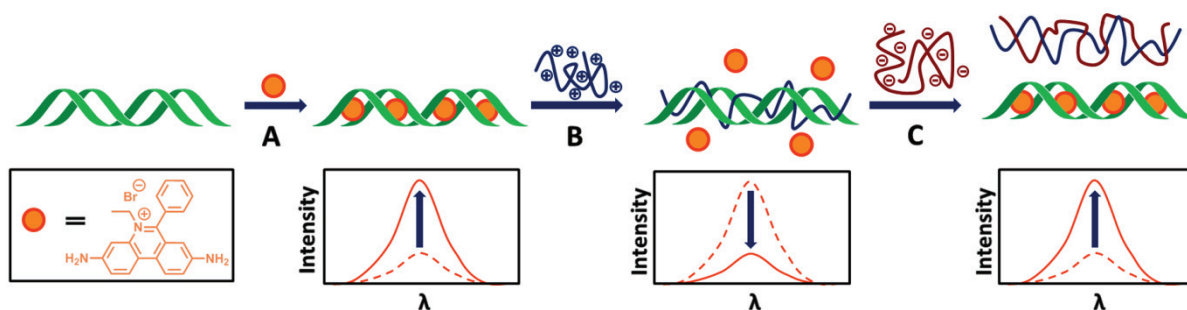
However, due to low amounts of genetic material in biological samples, amplification prior to detection is indispensable.<sup>[125]</sup> *Via* polymerase chain reaction (PCR), a few copies of a specific sequence of genetic material can be amplified by the naturally thermo-stable enzyme polymerase,<sup>[126-128]</sup> using specifically synthesized oligonucleotides (primers) for the gene-of-interest.<sup>[129]</sup> However, the PCR process is limited by the purity of the bioanalytical samples, as well as by the template DNA amount.<sup>[130]</sup>

## 5.1. DNA detection using hydrogels and coatings

Cellular components, remaining from cell lysis or other impurities, can interfere with the process and lead to non-exponential amplification or even a complete inhibition. Therefore, pure polynucleotide solutions with a high concentration are preferable. Polymer-based hydrogels offer a great opportunity for a reversible DNA binding and release.<sup>[131]</sup> Because of their high water content and the resulting permeability of the three-dimensional matrix, as well as the adjustable functionalities and a high surface to volume ratio, hydrogels represent attractive candidates for DNA immobilization.

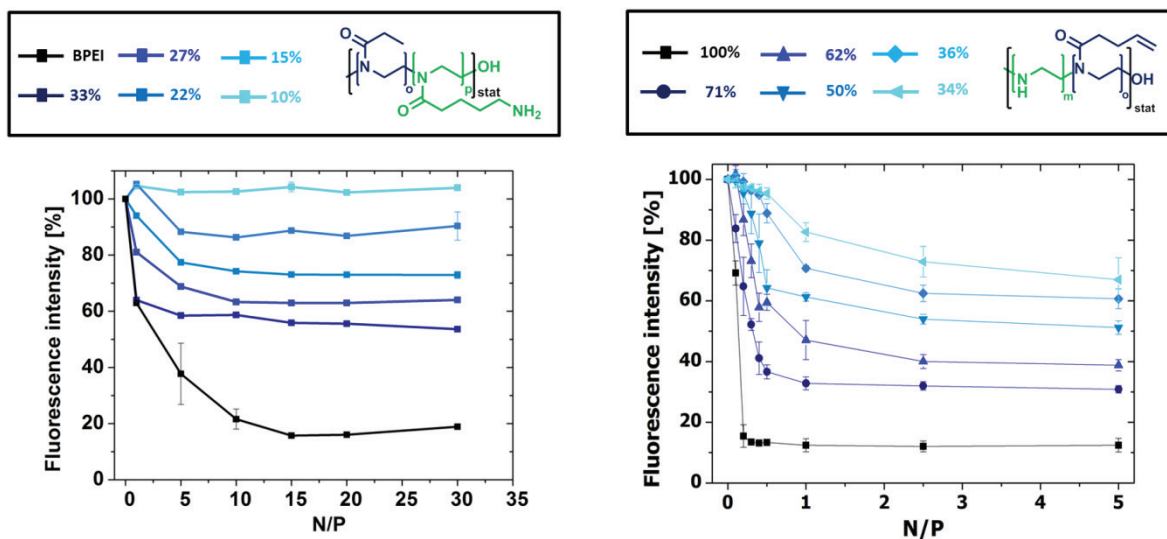
The materials described in Chapters 3 and 4 were utilized to generate such pure DNA solutions from biological samples. The interaction between the positively charged amine groups of the polymers or gels with the negative net charge of the DNA should lead to non-covalent interactions between both components. In an ideal case, this ionic interactions can be cleaved after washing processes to produce pure DNA eluates able to be amplified by PCR. The first step on the way to such an application is the investigation of the affinity of DNA to the polymers which serve as a precursor for the gels and coatings. A straightforward way to quantify this interaction is the ethidium bromide assay (EBA). The principle comprises the intercalation of a fluorescent dye (ethidium bromide (EB)) into the double helix of DNA (Scheme 5.1).<sup>[132-134]</sup>

Figure 5.1 illustrates the interaction of the cationic statistical copolymers presented in Chapter 3 with DNA. At high N/P (nitrogen/phosphate) ratios, the polycation is present in excess, which should lead to a quenching of the fluorescence since EB is displaced from the DNA helix. This decrease reaches a plateau dependent on the degree of interaction between the polycation and the genetic material. The stronger the connection between both components, the more dye is displaced from the double helix and, hence, the lower the fluorescence intensity. This behavior can be observed for POx, as well as for poly(ethylenimine) PEI based systems. Pure PEI served as a reference in both cases, however branched PEI (bPEI) was used for EBA with cationic POx while linear PEI (lPEI) was utilized for PEI based polycations.



**Scheme 5.1:** Schematic representation of the ethidium bromide assay measuring the strength of interaction between DNA and a cationic polymer sample. A) Addition of EB to DNA strands leads to intercalation and an increase in fluorescence intensity; B) a cationic samples binds to DNA and replaces EB which decreases the fluorescence; C) the addition of a competing polyanion (heparin) breaks the DNA-polycation connection and the fluorescence of EB is again increased by intercalation.

## 5.1. DNA detection using hydrogels and coatings



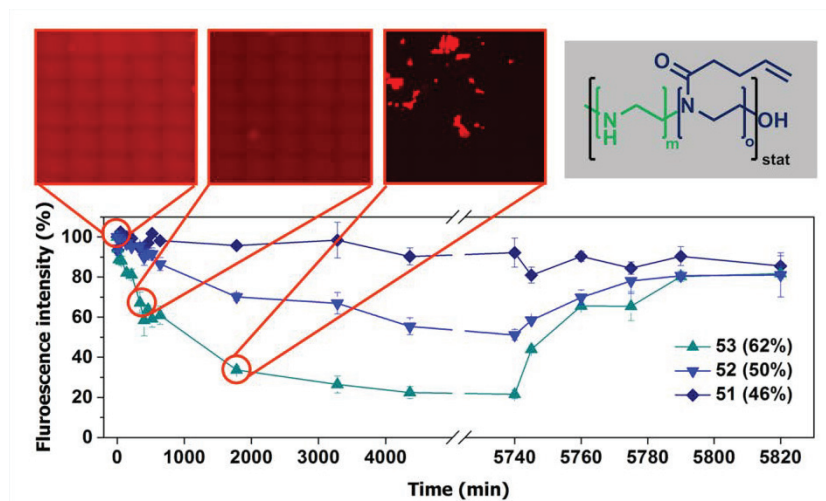
**Figure 5.1:** EBA of P(EtOx-*stat*-AmOx) and P(EI-*stat*-ButEnOx) as a function of the ratio between nitrogen and phosphate (N/P). bPEI was used as a reference for POx-based systems and lPEI as a reference for PEI-based polymers.

Regarding the minimum fluorescence, both systems were in the same range when polymers with similar amine contents are compared. Furthermore, an increasing content of positively charged comonomer leads to a lower minimum in fluorescence, which indicates a higher efficiency of the interconnection. For the PEI derived systems, however, the plateau was reached at much lower N/P ratios compared to the POx-based systems, indicating an increased efficiency in polyplex formation for these materials.

While these first results were promising regarding the interaction of the presented cationic polymers with DNA, the non-cross-linked macromolecules cannot be used to purify genetic material since the separation of polyplexes from solution would be time consuming and labor-intensive. As a consequence, hydrogels produced from the cationic polymer precursors were subjected to similar investigations. Since the DNA binding substrate was now a gel, the fluorescence of EB had to be measured from the supernatant. For comparison reasons, the N/P value was equal for all hydrogel samples within one test series. The volume of the solution was not adjusted to the swelling degree to ensure that the dilution of DNA/EB stock solution was identical for each well. The fluorescence intensity was measured as a function of time. For hydrogel samples, also the release of DNA from the network using a competing polyanion (heparin) was investigated to demonstrate the reversibility of the attachment. First, PEI based hydrogels were investigated using this method. The binding of DNA to the gels, as expressed by a decrease of the EB fluorescence, is shown in Figure 5.2. The minimum intensity reached by the material is dependent on the content of amine groups as also found for the precursor polymers. However, the time (4 days) required to reach an equilibrium is rather long.



## 5.1. DNA detection using hydrogels and coatings



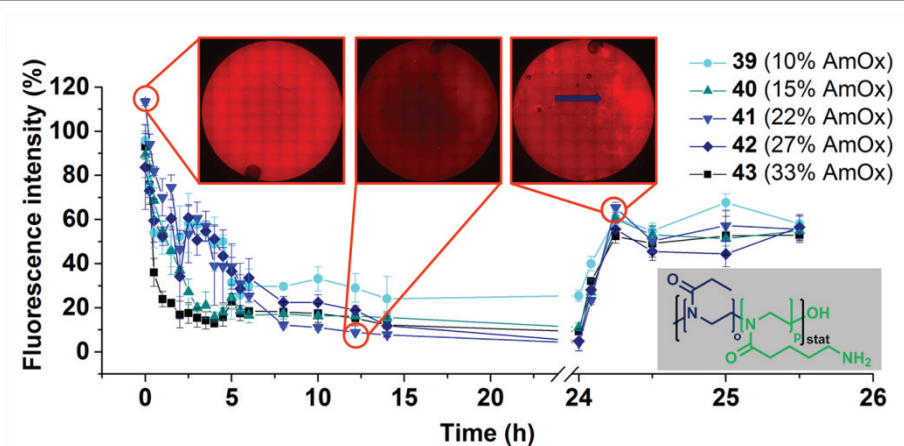
**Figure 5.2:** DNA binding and release by EBA of PEI derived hydrogels (50 to 55) and microscopy investigation of the gels in the presence of DNA and EB. Release was performed by adding heparin ( $6 \text{ mg mL}^{-1}$ ) at  $90^\circ\text{C}$ .

A release could only be accomplished by the addition of heparin and elevated temperature ( $90^\circ\text{C}$ ), which indicates a strong interaction between gel and DNA.

A similar investigation was performed for the POx derived hydrogels (Figure 5.3). In contrast to the PEI gels, all samples adsorbed a significant amount of DNA and, except the gel with only 10% AmOx, resulted up in similar minimum values. The content of positively charged groups, however, had an influence on the velocity of the uptake. While gel 36 was saturated after more than 5 h, gel 40 reached the plateau after approximately 2 h. This uptake was significantly accelerated compared to PEI gels. This can be assigned to the higher water content within the networks, which leads to a higher mobility of DNA within the matrix. The release, as induced by the addition of heparin at room temperature, required only 30 min, though the initial fluorescence intensity could not be fully restored. While only the fluorescence of the supernatant could be quantified, the fluorescence microscopic pictures revealed that the region of the well where the hydrogel was located (arrow in Figure 5.3) still had a high fluorescence intensity which was not pronounced before the addition of heparin. This behavior can be explained by the displacement of the DNA from the gel by heparin, which leads to the new intercalation of EB. However, the limited diffusion within the gel prohibits a fast release into solution. Therefore, also a diffusion control of the adsorption process can be assumed.

While these results demonstrate the functionality of the material, it becomes evident that for an application the gels, particularly in the swollen state, do not possess the mechanical properties that are required to easily separate them from solution.

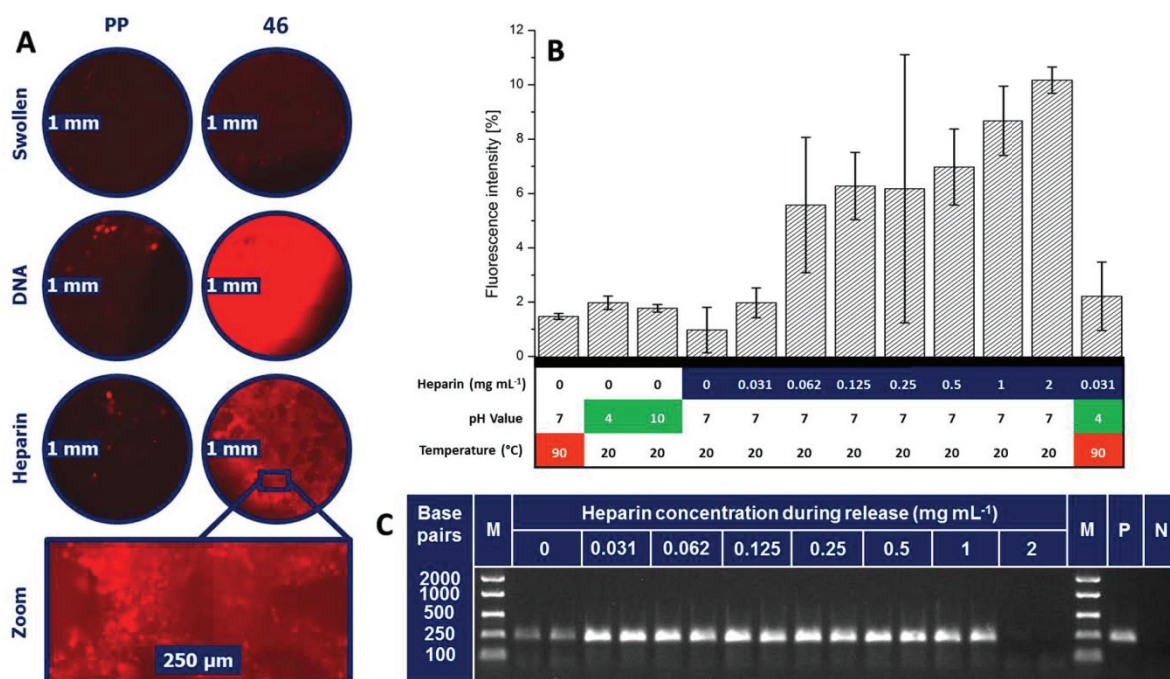
## 5.1. DNA detection using hydrogels and coatings



**Figure 5.3:** DNA binding and release by EBA of POx derived hydrogels (39 to 43) and microscopically investigation of the gels in presence of DNA and EB. After 24 h heparin ( $60 \text{ mg mL}^{-1}$ ).

To overcome this drawback, matrix-supported hydrogels were used, having the additional advantage of a porous and bead-like microstructure and a resulting large surface area. This property could be of advantage regarding the diffusion-based time limitation of the binding and release processes. To directly access information about the fate of DNA in presence of the systems, the detection method was changed. Instead of EB as free dye, Cyanine 5 (Cy5) was covalently attached to DNA. The localization of this directly labeled sample can be tracked by the fluorescence of the dye (Figure 5.4A). Matrix supported hydrogels were compared to a bare PP matrix, which served as the support structure. While the initial substrates revealed no significant fluorescence, addition of Cy5 labeled DNA and subsequent washing resulted in a bright fluorescence of the gel structure as compared to the PP matrix. Upon the addition of heparin, a significant amount of DNA was released again. In the microscopy pictures it becomes evident that the gel beads are responsible for the DNA uptake. Various conditions were examined for the release of DNA. The most promising results were observed for samples treated with up to  $2 \text{ mg mL}^{-1}$  heparin (Figure 5.4B). The eluates were subjected to PCR in order to prove the suitability of the method. Surprisingly, samples released by the use of up to  $1 \text{ mg mL}^{-1}$  heparin could successfully be amplified while eluates produced by the use of  $2 \text{ mg mL}^{-1}$  yielded no amplified DNA (amplicon). This can be explained by the polyanionic nature of heparin which leads to a high affinity towards the cationic hydrogel which is also the driving force for the replacement. If the amount of releasing agent is sufficiently low, most of the heparin will bind to the hydrogel and the released DNA can be amplified by a PCR.

The presented hydrogel systems represent promising materials regarding the catch and release of DNA for the purpose of purification. However, diffusion of DNA within the networks remains a time limiting factor and even though heparin free samples can be produced, the amount of polyanion has to be chosen carefully.

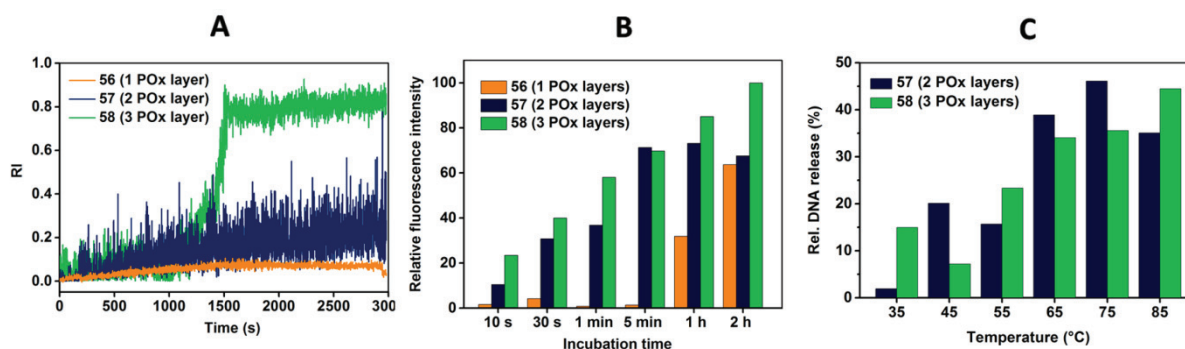


**Figure 5.4:** DNA uptake and release of matrix supported hydrogels. A) DNA binding and release by fluorescence microscopy, B) quantification of DNA release in dependence on temperature, pH value and heparin concentration, as well as C) gel electrophoresis of PCR products from release eluates.

The last part of this chapter is dedicated to the use of surface bound hydrogel multilayers for DNA catch and release experiments. The materials described in Chapter 4.2 will be investigated regarding their interaction with genetic material. First measurements were conducted by reflectometric interference spectroscopy (RIFS) of POx multilayers on glass (Figure 5.5A). As described in Chapter 4.2 the method generates information about the thickness of a swollen polymer deposit on a special glass substrate. To access information about the interaction with genetic material, a DNA solution was channelled over the POx layers. In a second channel pure water was used to swell the layers and the difference between both values gave an indication of DNA absorption. The results suggest a negligible binding for POx monolayers while two- and three-layered systems show a pronounced uptake. However, RIFS only yields an indirect measure of the DNA adsorption since the increase in layer thickness is also dependent on the ability of POx multilayers to swell in the presence of varying ion concentrations. For this reason, additional investigations using Cy5-labeled DNA were performed (Figure 5.5B and C). The time required for the DNA uptake was investigated by confocal laser scanning microscopy (CLSM) measurements of layers, which were treated with a DNA solution for a defined time. For POx monolayers, the adsorption of DNA is rather slow, showing decent values after 1 h of incubation. For di- and tri-layers, however a pronounced uptake is detectable even after 10 s of treatment. For two POx layers, saturation is reached after 5 min while the three-layered system has not reached a plateau after 2 h.



## 5.1. DNA detection using hydrogels and coatings

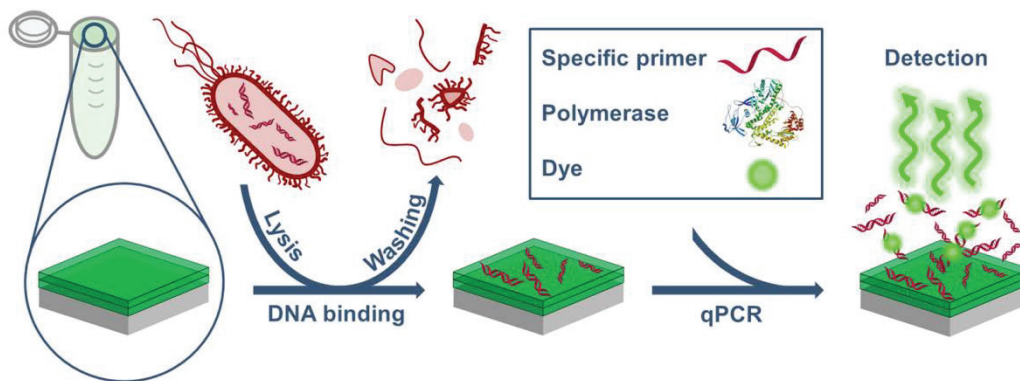


**Figure 5.5:** DNA binding and release of POx multilayers on glass or PP. A) RIFS measurements of POx layers in the presence of DNA containing solution, B) DNA binding of POx layers on PP as quantified by CLSM investigations of samples treated with Cy5 labeled DNA and C) DNA release by CLSM of POx layers treated at different temperatures.

To study the release properties of the materials, samples treated with DNA for 1 h were placed in pure water at varying temperatures, and the amount of released DNA was determined by CLSM as percent of the initially bound DNA amount (Figure 5.5C). Systems having only one POx layer were not subjected to release tests since the uptake characteristic disqualifies the material for a potential later application. POx di- as well as tri-layers revealed a release of up to 40% above a temperature of 65 °C. It should be noted that no heparin is required for this process. The detachment of genetic material is solely a result of the increased temperature, which is promising for a subsequent PCR.

One major advantage of the presented layer-by-layer (LbL) system is the possibility of coating PP substrates enabling a larger variety in the design of analytical systems. For the shown investigations, only two-dimensional PP slides were used for polymer immobilization. For detection applications, however, it would be favorable to apply POx layers on the inside of PCR reaction vessels. For this reason, PP-tubes (RoboStrip® PP) were coated accordingly. This system enables the combination of purification, amplification and detection in one coated reaction vessel since a PCR can be performed directly after DNA binding and washing. The temperature dependent release should generate a free DNA template during the PCR, which uses temperatures up to 95 °C. Scheme 5.2 illustrates the working principle of the whole process of this “lab-in-a-tube” starting with the lysis of biological samples, which leads to an immobilization of DNA within the POx layers. To demonstrate the possibility of a DNA detection in the same step, quantitative real-time PCR (qPCR) assays were performed using coated PCR tubes. The method used intercalating fluorescence dyes to directly monitor the progress of the PCR. The amount of generated DNA can be determined after each PCR cycle. The cycle threshold ( $c_t$ ) value of the qPCR assay shows at which cycle the DNA has reached a defined concentration providing an indication about the efficiency of the process and the amount of available template.

## 5.1. DNA detection using hydrogels and coatings



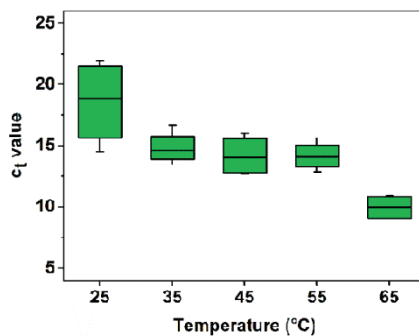
**Scheme 5.2:** Purification, amplification and detection by qPCR using a PP reaction vessel coated with POx multilayers.

The assay detects specific gene sequences, like the LacZ-Gene as *Escherichia coli* BL21 (*E. coli*) target, by the use of specific primer sequences, which only bind to the desired gene. After amplification, a positive result is reported by the melting peak of the PCR product, as detected by the use of the intercalating dyes. In the case of LacZ, the melting curve of the product should exhibit a peak around 87.5 °C. This melting-point is equivalent to the expected product of 224 base pairs (GenBank sequence accession number: AM946981.2). In first experiments, DNA from *E. coli* was extracted, bound within POx coatings for 1 h at room temperature and washed thoroughly. The DNA loaded tubes were filled with a qPCR master mix and subjected to qPCR. The results of the detection of extracted *E. coli* samples are shown in Table 5.1. Uncoated tubes with additional template served as a positive control, whereas a PCR experiment without sample DNA was used as a negative control.

**Table 5.1:** Results of *E. coli* detection from extracted DNA using the LacZ-Gene as target.

Template	Sample	Amount of DNA (ng)	Melting point (°C)	Mean c <sub>t</sub> value	Sample count
<i>E. coli</i>	Positive control	0.6	87.3	16.4	3
	Negative control	0	-	-	3
	Surface bound	n. d.	87.5	20.5	4
<i>E. coli</i> + Herring testes	Positive control	1	87.5	13.7	3
	Negative control	0	-	-	4
	Surface bound	n. d.	87.2	20	4

The qPCR result of surface bound DNA is positive for the specific *E. coli*-target and the amplicon shows the same characteristic melting point as the positive control. Also the assay is able to detect *E. coli* DNA in the presence of a background of Herring testes DNA, proving the working principle in the presence of undesired genetic material. However, for an easy and cost-effective sample analysis it is necessary to bind DNA directly from a cell lysate instead of using already purified genetic material. Consequently, the presence of other (charged) cellular components has to be tolerated.



**Figure 5.6:** Box-plot of qPCR experiments, performed in POx coated reaction vessels. The tubes were loaded with genetic material from cell lysates at different temperatures and the  $c_t$  value of the amplification was recorded.

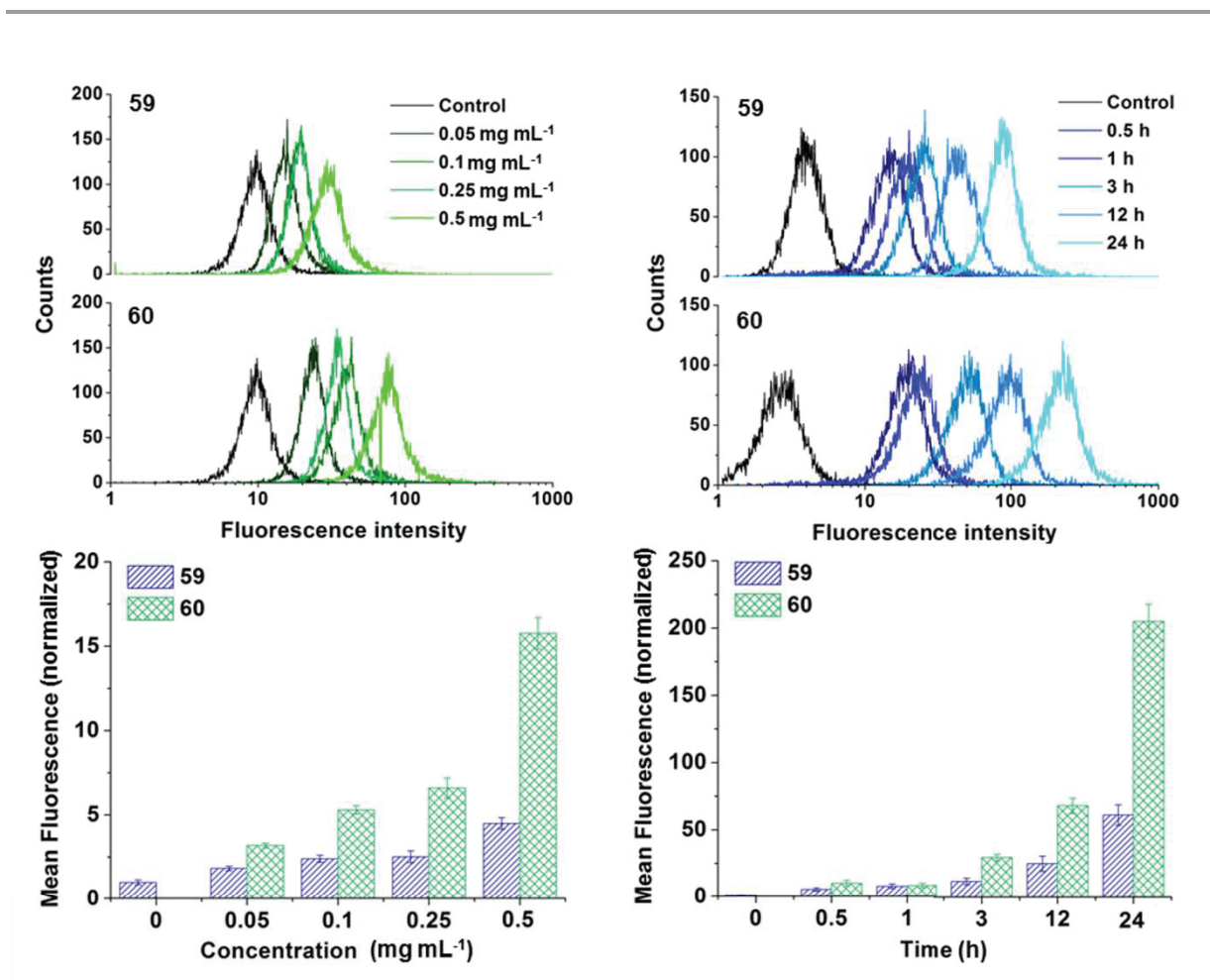
Therefore, an *E. coli* suspension ( $1.36 \times 10^9$  cfu mL<sup>-1</sup>) was incubated for 10 min at 95 °C to lyse the cells by heat induction. Aliquots of this cell lysate were filled in POx modified tubes and incubated for 1 h. To investigate the influence of temperature on the binding behavior during the incubation, the tubes were incubated at 25, 35, 45, 55 and 65 °C and the supernatant solution was removed at the specific temperature. Every incubation temperature step was tested positive for *E. coli* DNA with a melting point around 87.3 °C with no detectable melting point of the negative control. As shown in the box-plot (Figure 5.6), the  $c_t$  values of the qPCR decrease with increasing temperature, which indicates a faster amplification process. Generally, the  $c_t$  value is dependent on the amount of accessible template (a higher initial DNA concentrations leads to lower values) and the presence of inhibitors, which increase the  $c_t$  value by lowering the efficiency of the reaction. Since the amount of bound DNA is not increasing at higher temperatures (Figure 5.5C), the latter reason is presumably responsible for the faster amplification. A further indication is given by a narrowing of the value distribution at higher temperatures. To explain this behavior, the complex composition of the cell lysate can be accounted. While DNA has a high density of negative charge, also other cell components have potentially negative charges and can interact with the POx layers. The presence of these compounds leads to a disturbance or inhibition of the PCR process resulting in high  $c_t$  values. However, the binding affinity of negatively charged material decreases with increasing temperature, as already demonstrated by temperature dependent release studies (Figure 5C). It is likely that these compounds are released from the POx layers at lower temperatures than the DNA with its multiple negative charges. At 65 °C, the majorities of contaminants are unbound in solution and can be washed away, while a considerable amount of genetic material is still adsorbed to the polymer layers, accessible for a subsequent amplification. The performed experiments demonstrate the suitability of POx modified surfaces for a qPCR detection of DNA. Due to the compatibility of the modified PP surface with the qPCR process, a combination of sample purification and detection in a single tube or cavity is possible rendering the lab-in-a-tube approach a highly promising analytical tool for pathogen detection.

### 5.2. Drug delivery using poly(2-oxazoline)-based nanogels

Parts of this chapter have been published in: **P4**) M. Hartlieb, D. Pretzel, M. Wagner, S. Hoepfner, P. Bellstedt, M. Görlach, C. Englert, K. Kempe, U. S. Schubert, *J. Mater. Chem. B* **2015**, *3*, 1748-1759; **P8**) M. Hartlieb, T. Buś, J. Kübel, D. Pretzel, S. Hoepfner, K. Kempe, B. Dietzek, U. S. Schubert, in preparation.

As addressed in Chapter 4.3, the covalent cross-linking of nanoscopic structures to form nanogels represents a promising approach to overcome drawbacks of conventional drug delivery systems such as liposomes or polymeric micelles. The chemical interconnection of the aggregates prevents a premature disassembly and, when the drug is attached in a similar manner, a leakage of the therapeutic agent.<sup>[31]</sup> Further advantages are the solubilization of the cargo and its protection against degradation.<sup>[56]</sup> In the case of cancer drug delivery, *i.e.* the administration of cytostatic drugs such as *cis*-platin or Doxorubicin (Dox), tissue specificity plays an important role since most side effects can be ascribed to the interaction with healthy tissue. This issue can be addressed applying passive or/and active targeting strategies. Passive tissue specificity can be generated by the enhanced permeability and retention (EPR) effect.<sup>[30]</sup> If a drug carrier has a sufficiently long circulation time within the blood stream, the leaky architecture of tumorous tissue will cause an accumulation of objects between 10 and 150 nm. Within this chapter, the cross-linked micelles and vesicles described in Chapter 4.3 will be investigated regarding their interaction with cells.

The cellular uptake displays one important variable which was studied by flow cytometry (FC) in dependence on concentration and time. For this purpose, cells were incubated either with different concentrations of the materials (**59** and **60**) for 24 h at 37 °C or with the same concentration (0.5 mg mL<sup>-1</sup>) for different times. The fluorescence intensity distributions (histogram plots in Figure 5.7) clearly display a concentration-dependent right-shift to higher fluorescence intensity for both, the micellar and vesicular structures indicating a concentration-dependent uptake. Interestingly, the increase in fluorescence intensity was more pronounced for the vesicle samples, suggesting an increased cellular accumulation/association as compared to micelles. This becomes evident in quantitative terms when the mean fluorescence intensities (MFI) of the cell populations are evaluated as depicted in the bar charts (Figure 5.7). An up to three-fold higher uptake of the vesicles was obtained as compared to micelles with the same concentration. These results were also confirmed by fluorescence microscopic observations of the treated cell populations. For the time-dependent uptake, trends similar to the concentration-dependent internalization were observed. The cellular accumulation of material proceeds over time for both the micelles and vesicles without reaching a plateau after 24 h.



**Figure 5.7:** Flow cytometry investigation on the time and concentration dependent uptake of 6AF containing micelles/vesicles by L929 mouse fibroblasts at 37 °C. For the time dependent uptake experiments, cells were incubated between 0.5 and 24 h with micelles (59)/vesicles (60) with a concentration of 0.5 mg mL<sup>-1</sup>, whereas the concentration dependent uptake was investigated over an incubation time of 24 h using micelle/vesicle concentrations in the range between 0.05 and 0.5 mg mL<sup>-1</sup>. Cells incubated only with culture medium served as control. The data are expressed as mean  $\pm$  SD of triplicates.

Additionally, the cellular uptake of the vesicular formulation exceeds the internalization rate of the micelles by a factor of three and, again, supports the interpretation of a higher cellular internalization of the vesicles. The different cellular internalization efficiencies could be caused by the cellular uptake mechanism. It is known that very large particles enter cells by phagocytosis, whereas, in the case of nanoparticles, most internalization occurs *via* various endocytotic pathways, which can be different with regard to the nature of the surface and the structural properties of nanoparticles (*e.g.* clathrin or caveolin dependent pathways).<sup>[135]</sup> Depending on the particular pathway and also its energy dependent or independent nature, different internalization rates are achieved<sup>[136]</sup> – this could also impact the uptake efficiency of the presented micelles and vesicles.

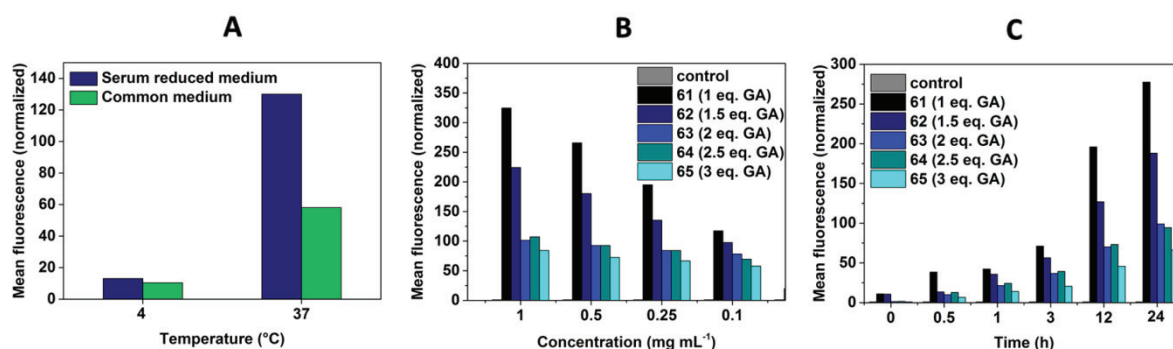
To verify an endocytotic uptake, incubation was performed at 4 °C where endocytosis, which is known to be energy dependent, is highly diminished.<sup>[137]</sup> A similar uptake efficiency at 4 °C



## 5.2. Drug delivery using poly(2-oxazoline)-based nanogels

would indicate a diffusion of micelles through the membrane of cells. The measurements were conducted within medium containing high and low amounts of serum to further investigate the dependence of the uptake on the interaction of micelles with proteins and other medium components. The uptake of compound **61** was quantified by FC as described before (Figure 5.8A). The highly diminished internalization of fluorescently labeled micelles at 4 °C indicates a primarily endocytotic uptake. However, the presence of a measurable fluorescence signal of cells cultivated at 4 °C reveals that the micelles are also able to penetrate the cell membrane in a minor extend which is attributed to their small size and cationic nature.<sup>[138]</sup> The presence of serum also influences the uptake efficiency which indicates an interaction of the nanostructures with serum components and a resulting decrease in uptake efficiency. This can be attributed to the formation of a protein corona, which leads to a further shielding of the micelles from cellular interaction.<sup>[139]</sup>

To evaluate the influence of the content of cross-linker and the resulting decreased positive charge, samples **61** to **65** were also subjected to FC investigations (Figure 5.8B and C). The decrease in mean fluorescence with increasing cross-linking degree within the series of micelles clearly shows the influence of the zeta potential on the internalization. This effect can be observed at all concentrations investigated. Also the time dependent uptake study visualizes this behavior of the nanoscopic structures. The difference in the fluorescence intensity of the different micelles was already considered for the calculation of the values. This investigation shows that the uptake, which displays a crucial factor for the utilization of the EPR effect, can be fine-tuned for the presented nanogels.



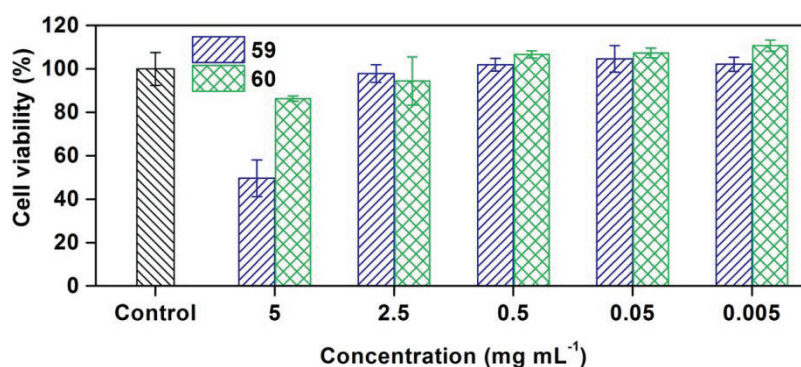
**Figure 5.8:** Flow cytometry investigation on the temperature, time and concentration dependent uptake of 6AF containing micelles (**61** to **65**) by L929 mouse fibroblasts. A) Energy dependency of the uptake of micelle **61** at 37 °C or 4 °C respectively in OptiMEM (serum reduced cell culture medium) or in R10 (containing 10% fetal calve serum) after 4 h as well as B) and C) cellular internalization of micelles **61** to **65** in dependency of the concentration (B) or the time (C) at 37 °C.

## 5.2. Drug delivery using poly(2-oxazoline)-based nanogels

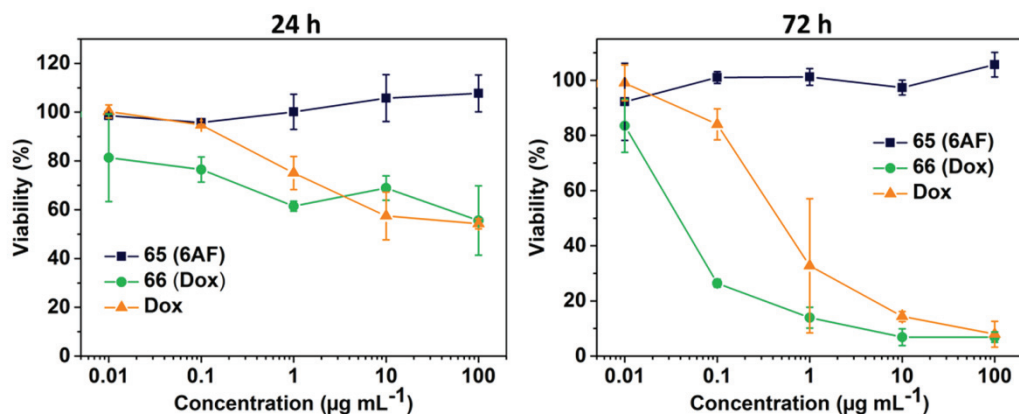
A second important parameter for the design of drug delivery systems is the cytotoxicity. In an ideal case, the carrier itself or its degradation products do not induce toxicity. Hence, adverse effects on the cellular metabolism upon incubation with 6AF labeled micelles (**59**) and vesicles (**60**) were evaluated using the established L929 cell line, which is characterized and documented by its sensitivity towards cytotoxic agents.<sup>[140]</sup> The *in vitro* cytotoxicity experiments were performed *via* a XTT assay.

After 24 h incubation with different micelle/vesicle concentrations the metabolic activity of the treated cells was found to be at the level of the untreated controls, with the exception that only the highest concentration of micelles ( $5 \text{ mg mL}^{-1}$ ) led to a significant reduction of cell viability (50%). Interestingly, the vesicular structures did not show any cytotoxic potential even at the highest concentration (Figure 5.9). One possible explanation for this behavior could be related to the size of the vesicles. The larger diameter of the structures in comparison to micelles leads to a smaller surface/volume ratio. However, the micelle concentrations which did not show an overt toxicity effect were more than adequate for potential applications which confirms the low cytotoxicity generally observed for PEtOx-based materials.<sup>[2]</sup>

An additional property, which can be evaluated by cytotoxicity investigations, is the general suitability of the system to deliver a cytotoxic drug (in this case Dox) to cells. Since the drug is immobilized covalently, a release by a cleavage of the imine bond is necessary to ensure its activity. The cytotoxicity of Dox relies on the intercalation of the molecule within the DNA double strands inhibiting the process of gene replication.<sup>[141]</sup> As a consequence, the molecule needs to enter the cell core to have an effect. This can be evaluated indirectly by the cytotoxicity of Dox conjugated micelles (**66**) compared to free Dox and 6AF loaded micelles (**61**) (Figure 5.10).



**Figure 5.9:** Cell viability of L929 mouse fibroblasts after incubation with micelles (**59**)/vesicles (**60**) up to  $5 \text{ mg mL}^{-1}$  for 24 h.

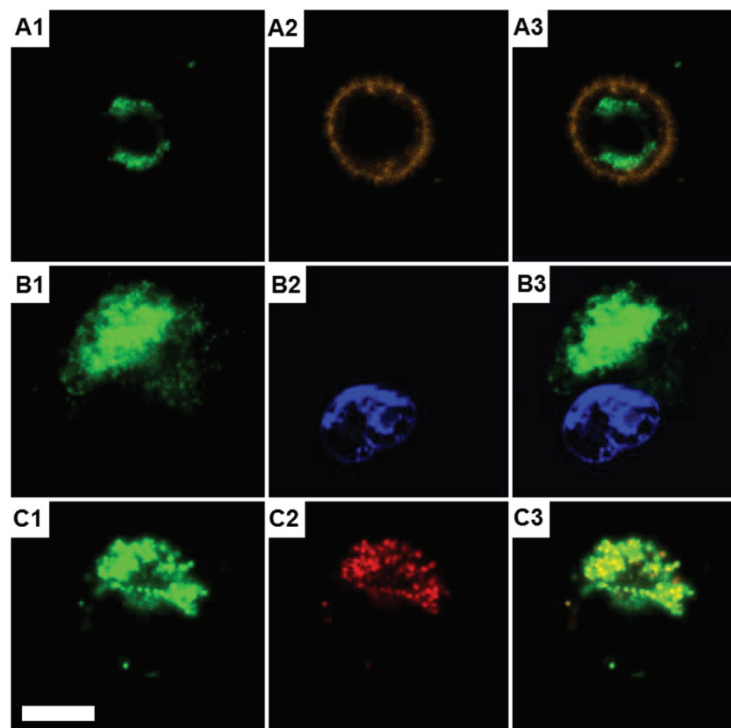


**Figure 5.10:** Cell viability of L929 mouse fibroblasts after incubation with Dox/6AF loaded micelles (**65**)/Dox loaded micelles (**66**) 24 h or 72 h respectively. Concentration indication refers to Dox (free or as bound cargo). 6AF loaded micelles were added in the same concentration as Dox loaded micelles.

The concentrations in Figure 5.10 refer to the amount of Dox within the sample. The concentration of micelles was adjusted accordingly to contain the same amount of Dox as the solution containing the free drug, respectively. The 6AF loaded nanostructures (**65**) were applied in the same concentration as their Dox containing equivalents (**66**). The low viability values obtained for cells treated with Dox containing micelles show that the drug is indeed interfering with the cell metabolism. The toxicity is even more pronounced compared to the free Dox while 6AF loaded structures show no toxic effect under these conditions.

The cellular internalization and intracellular localization of micelles and vesicles in L929 cells was elucidated by confocal laser scanning microscopy (CLSM), which enables a z-sectioning of the samples. A representative distribution of 6AF loaded vesicles in the context of cellular structures in detached cells is presented in Figure 5.11. The CLSM images suggest an intracellular localization of the vesicles, since the green fluorescence from the 6AF labeled structures is exclusively detectable within the stained cell membrane (Figure 5.11: A1 to A3). Additionally, no vesicles were observed within the nuclear compartment. They were rather associated with distinct outer nuclear membrane regions (Figure 6: B1 to B3). Hypothesizing that internalization of the vesicles/micelles proceeds *via* endocytotic pathways, an appearance of the internalized structures in the late endosomes or lysosomes was very likely. Indeed, co-localization of stained acidic endosomes and fluorescent vesicles was observed. It should be noted that only intact nanostructures can be detected by fluorescence in an intracellular environment since the emission intensity of the free dye is strongly diminished at neutral and acidic pH values. Therefore, the co-localization studies clearly suggest an endosomal location, and, hence, an internalization by endocytosis can be assumed.



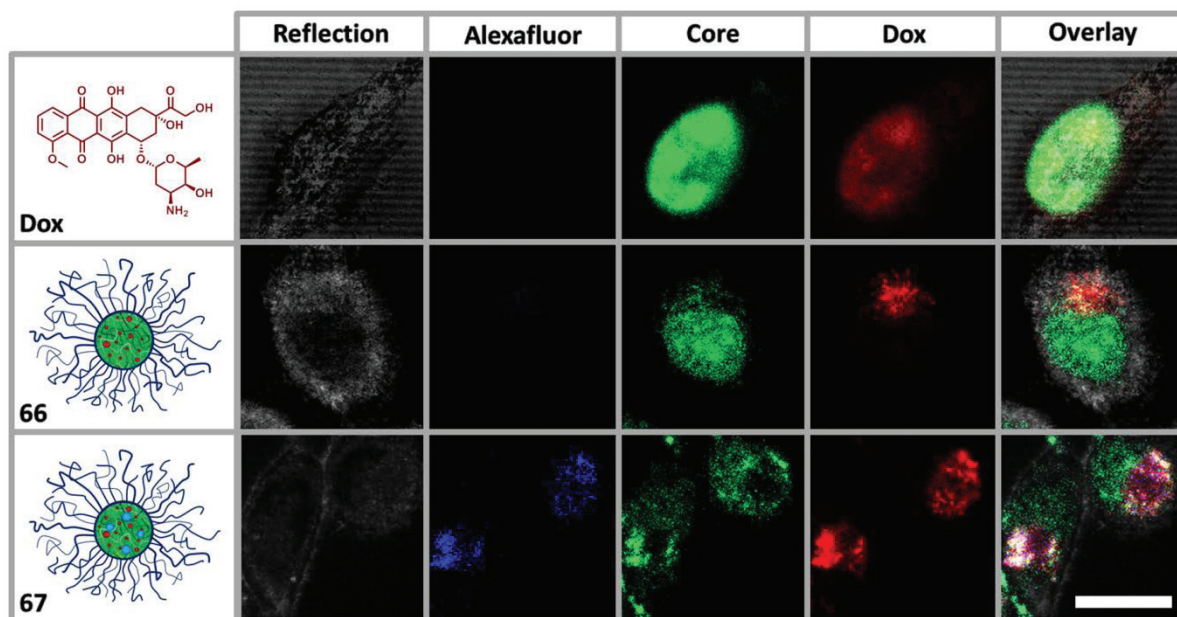


**Figure 5.11:** Representative CLSM images of detached L929 cells after 24 h incubation at 37 °C with vesicles (**60**) at a concentration of 0.1 mg mL<sup>-1</sup>. Cell membranes (A2), cell nuclei (B2), or late endosomes/lysosomes (C2) were specifically stained and correlated with the fluorescence signal of 6AF labeled vesicles (A1, B1, and C1). Superimposition of both channels (A3, B3 and C3) proves an intracellular (A3) but extra-nuclear (B3) localization of the vesicles and their apparent co-localization with endosomal structures (C3). Scale bar: 10 μm.

For further studies this behavior could be beneficial because the low pH value within these cellular compartments should lead to a disassembly of the nanostructures and might result in a release of the cargo.

To obtain information about the cellular interaction of Dox conjugated micelles besides the cytotoxicity, the co-localization of Dox, as well as the compounds **66** and **67** was investigated by CLSM (Figure 5.12). The general contour of the cells is visible in the reflection images and the nuclei were stained green. The fluorescence of Dox is depicted in red while Alexafluor® emission is displayed in blue. As evident in the first row of the graph, Dox is highly co-associated with the nucleus as expected for an intercalating cytostatic drug. For both micellar compounds, however, localization in the cytosol is indicated. The overlap of blue and red fluorescence clearly suggests the presence of (partially) intact micellar structures which is contradictory to the increased toxicity of micellar compounds compared to the free drug. The dependence of Dox fluorescence on the given microenvironment could be accounted for these findings. It is reported that the fluorescence intensity of Dox decreases upon intercalation and increases when located in micellar or liposomal systems.<sup>[141]</sup> Hence, Dox within cell nuclei could be invisible in the presence of fluorescence enhanced Dox within nanogels.

## 5.2. Drug delivery using poly(2-oxazoline)-based nanogels



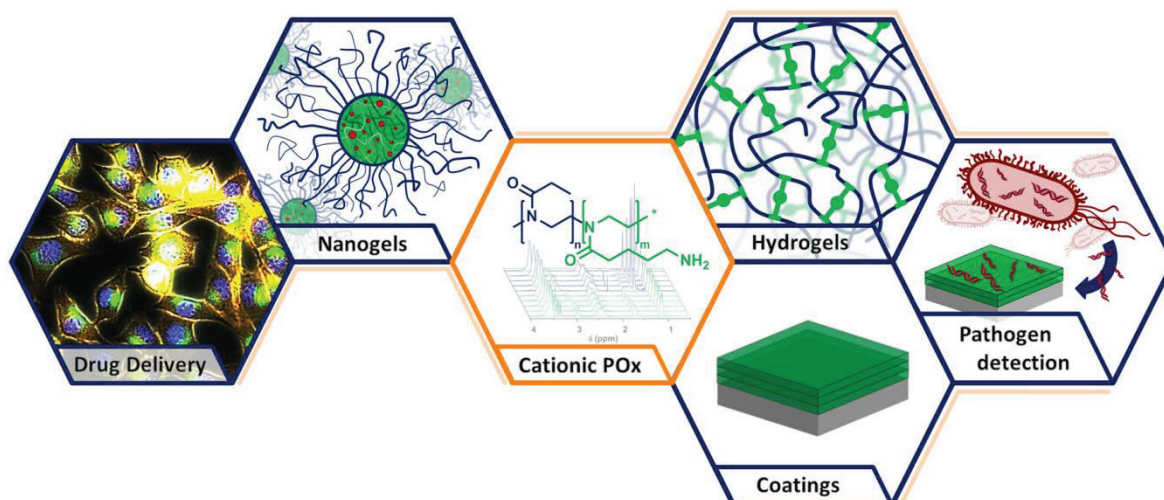
**Figure 5.12:** CLSM images of L292 mouse fibroblasts treated with either Dox, Dox conjugated micelle (**66**) or Dox conjugated micelle labeled with Alexafluor 660® (**67**) for 12 h at 37 °C using a Dox concentration of 1  $\mu\text{g mL}^{-1}$ . Cell nuclei were stained using SYTO®Green 13:  $\lambda_{\text{ex}} = 488 \text{ nm}$ ,  $\lambda_{\text{em}} = 505 \text{ to } 530$ ; Dox:  $\lambda_{\text{ex}} = 488 \text{ nm}$ ,  $\lambda_{\text{em}} = 585 \text{ to } 615 \text{ nm}$ ; Dox:  $\lambda_{\text{ex}} = 633 \text{ nm}$ ,  $\lambda_{\text{em}} = 724 \text{ to } 777 \text{ nm}$ . Scale bar: 10  $\mu\text{m}$ .

If the micelles are located within the endosome as their 6AF analogs, the acidic conditions could lead to a steady release of Dox over time. However, a detailed mechanistical investigation of the toxicity has to be the subject of further studies to confirm this assumption.

The performed investigations clearly show the potential of POx-based nanogels regarding the drug delivery of Dox. Further studies need to be conducted in order to elucidate the release and toxicity mechanism and to screen the suitability of the system *in vivo*.

## 6. Summary

The design of new, functional, biocompatible and well-defined polymeric systems is of paramount importance for the advancement of biomedical applications. Numerous research fields in life science, such as nanomedicine, tissue engineering, pathogen detection or anti-fouling require soft materials like hydrogels, nanogels or polymeric surface coatings able to fulfill specific tasks. Controlled and living polymerization techniques resulting in complex and well-defined macromolecules are used frequently for the preparation of smart and functional systems. The cationic ring-opening polymerization (CROP) of 2-oxazolines combines a high versatility with a fast and efficient polymerization process. Furthermore, poly(2-oxazoline) (POx) derivatives exhibiting short side chains are known to be biocompatible and possess a stealth effect similar to poly(ethylene glycol). The present thesis deals with the synthesis of amine containing and, henceforth, cationic POx of different architectures and their processing into hydrogels, nanogels and surface coatings. These materials were utilized for either pathogen detection or the delivery of cancer therapeutics (Figure 6.1).



**Figure 6.1:** Covalent cross-linking of cationic POx resulting in gels and coatings, which display promising materials in the detection of pathogens by DNA interaction or the delivery of cytostatic drugs for cancer treatment.

Amine groups can be utilized for a multitude of reactions and can possess a positive charge in aqueous solution. However, they are not compatible with the polymerization conditions of the cationic ring-opening polymerization (CROP) of 2-oxazolines. For this reason, a protected, amine bearing 2-oxazoline (BocOx) was synthesized and investigated regarding its polymerization kinetics in a homo polymerization, as well as in combination with 2-ethyl-2-oxazoline (EtOx) revealing the possibility of a living copolymerization. Deprotection of the polymers lead to amine containing POx (PAmOx), enabling manifold functionalization possibilities. Two small

## 6. Summary

---

polymer libraries of statistical copolymers (P(EtOx-*stat*-AmOx)) and block copolymers (P(EtOx-*b*-AmOx)) were produced and characterized in detail. The amine groups were utilized for the attachment of fluorescent dyes enabling a later detection of the material. Furthermore, poly(ethylene imine) (PEI) was used to create P(EI-*stat*-POx) copolymers to study the influence of the secondary amine groups of PEI.

The processing of P(EtOx-*stat*-AmOx) and P(EI-*stat*-Ox) by covalent cross-linking in solution was performed to yield hydrogels, which were analyzed regarding their swelling degree. Moreover, cross-linking in the presence of a microporous poly(propylene) (PP) substrate was conducted resulting in the formation of matrix supported hydrogels exhibiting an increased mechanical stability and a bead-like microstructure of the gel component.

P(EtOx-*stat*-AmOx) was further utilized for the production of gel-like surface coatings using glass, as well as PP as substrates. Covalent immobilization of the polymers on activated surfaces resulted in monolayers, which could be used to further attach amine containing POx in a layer-by-layer approach applying cross-linker and polymer in an alternating manner. The materials generated showed an increasing gel character with each additional layer, as expressed by an augmented swelling. The use of fluorescently labeled polymers enables detection and quantification of the deposited material and the utilization of PP as a scaffold provide a high versatility in substrate geometry and flexibility.

A third material class, which was fabricated, were nanogels. The self-assembly of block copolymers in organic solvents was investigated and the resulting micellar and vesicular structures were cross-linked to yield water stable nanoscopic gels. The loading of the structures with either fluorescein (as a label) or doxorubicin (Dox) (as a highly potent cytostatic) was accomplished in a covalent way. It could be shown that the degree of cross-linking has a direct influence on the size and charge density of the nanostructures. The core was found to have an alkaline microenvironment, which amplifies the fluorescence of the bound dyes by the quenching of non-radiative decay pathways.

One potential application field for amine containing polymers and gels is the purification and detection of DNA from biological samples. For this reason, P(EtOx-*stat*-AmOx), as well as P(EI-*stat*-Ox) were investigated regarding their ability to bind genetic material using the ethidium bromide (EB) assay. The affinity of the polymer types to DNA was found to be dependent on the amine content. Utilizing a similar procedure, the DNA binding and release of hydrogels was investigated. PEI containing structures generally exhibited a higher binding strength while genetic material bound in P(EtOx-*stat*-AmOx)-based systems could be released by the addition of heparin at room temperature. By fine tuning the detachment procedure, heparin free samples could be generated able to be amplified in a polymerase chain reaction (PCR). Furthermore, surface bound POx multilayers were investigated in terms of DNA interaction. A polymer double layer was found to be perfectly suitable to bind genetic material from solution and release it

## 6. Summary

---

again upon temperature increase. Using this system, DNA could be extracted directly from biological samples. Moreover, by applying coatings on the surface of the PCR reaction vessels a direct amplification and detection by quantitative real-time PCR could be accomplished. This “lab-in-a-tube” system enables the detection of pathogen DNA directly from a biological sample without laborious working steps and with a minimum of material consumption.

A second potential application examined within this thesis was the drug delivery of anti-cancer drugs. For this reason nanogels were investigated regarding their interaction with cells in terms of cytotoxicity, cellular uptake and co-localization with cellular compartments. The nanostructures were taken up by endocytosis and revealed a good biocompatibility when only loaded with a fluorescent dye. Dox loaded micelles exhibited an increased toxicity compared to the pure drug and co-localization studies suggest a diverging behavior of nanogel associated Dox as compared to the pure drug.

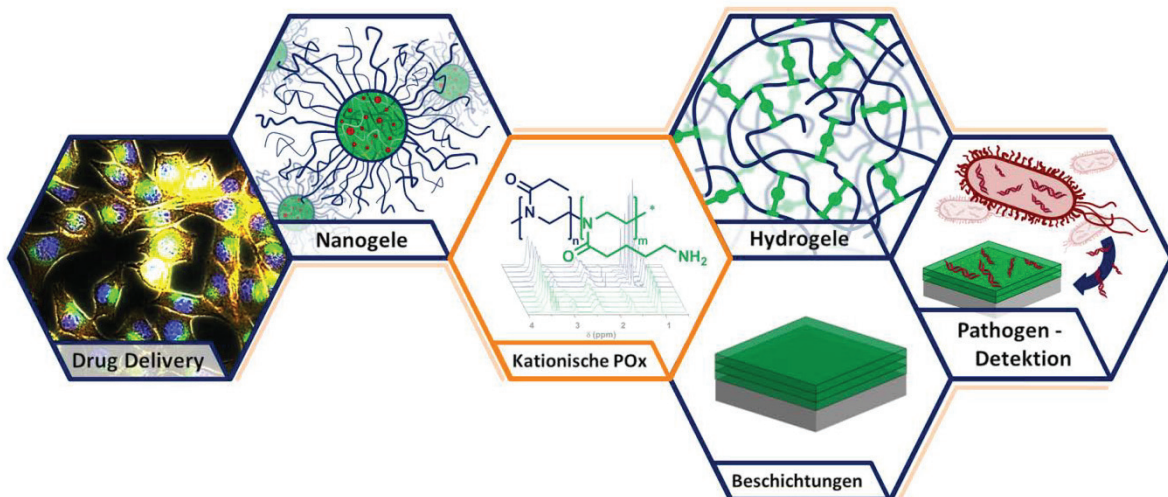
In summary, the combination of POx and amine groups results in highly versatile systems, which can be processed into various functional materials. The specific interaction of these cationic structures with DNA led to the development of a new detection system for DNA directly from biological samples. The utilization of nanogels for potential cancer drug delivery applications shows first auspicious results rendering further *in vitro* and *in vivo* studies highly promising.



## 7. Zusammenfassung

Die Entwicklung neuer, funktionaler, biokompatibler, sowie hoch definierter Polymersysteme ist eine Grundvoraussetzung für die weitere Verbesserung von Anwendungen im biomedizinischen Bereich. Eine Vielzahl an Forschungsgebieten im Bereich der Lebenswissenschaften wie z.B. Nanomedizin, Gewebekonstruktion, Pathogen-Detektion, oder Antifouling benötigen weiche Materialien wie Hydrogele, Nanogele oder polymerbasierte Oberflächenbeschichtungen, die in der Lage sind spezielle Aufgaben zu erfüllen. Kontrollierte und lebende Polymerisationsmethoden, welche zu hoch definierten und komplexen Makromolekülen führen, werden häufig für die Produktion von intelligenten, funktionalen Systemen eingesetzt. Die kationische Ringöffnungspolymerisation (CROP) von 2-Oxazolinen vereint eine große Vielseitigkeit mit einem schnellen und effizienten Polymerisationsprozess. Zudem sind Poly(2-oxazolin) (POx)-Derivate mit kurzen Seitenketten für ihre Biokompatibilität bekannt und besitzen einen „stealth effect“ ähnlich dem des Poly(ethylenglykol)s.

Das Ziel dieser Arbeit war die Synthese Amin-haltiger und somit kationischer POx in verschiedenen Polymerarchitekturen und deren Verarbeitung zu Hydrogelen, Nanogelen und Oberflächenbeschichtungen. Diese Materialien wurden für die Detektion von Pathogenen oder die Wirkstoffverabreichung von Krebsmedikamenten verwendet (Abbildung 7.1).



**Abbildung 7.1:** Die kovalente Vernetzung kationischer POx führt zu Gelen und Oberflächenbeschichtungen, welche vielversprechende Eigenschaften bezüglich der Pathogendetektion durch DNA Interaktion, sowie der Krebsbehandlung mittels der gezielten Verabreichung von Arzneimitteln aufweisen.

Amingruppen können für eine Vielzahl chemischer Reaktionen verwendet werden und im wässrigen Milieu positiv geladen sein. Sie sind jedoch nicht kompatibel mit der CROP von 2-Oxazolinen. Aus diesem Grund wurde ein geschütztes, aminhaltiges 2-Oxazolinmonomer

## 7. Zusammenfassung

---

(BocOx) hergestellt und bezüglich seiner Polymerisationskinetik untersucht. Sowohl in einer Homopolymerisation als auch in Kombination mit 2-Ethyl-2-oxazolin (EtOx) war eine lebende Polymerisation möglich. Durch die Entschützung der resultierenden Polymere wurden aminhaltige POx (PAmOx) erhalten. Es wurden zwei kleine Polymerbibliotheken bestehend aus statistischen, sowie Block-copolymeren hergestellt und charakterisiert. Die Amingruppen wurden unter anderem für das Anbringen von Fluoreszenzfarbstoffen verwendet, um eine spätere Detektion zu ermöglichen. Um den Einfluss von sekundären Amingruppen zu untersuchen wurden zudem statistische Copolymere aus Polyethylenimin (PEI) und POx P(EI-*stat*-Ox) synthetisiert.

Die kovalente Vernetzung von P(EtOx-*stat*-AmOx) und P(EI-*stat*-Ox) im wässrigen Milieu führte zur Bildung von Hydrogelen, welche bezüglich ihres Quellverhaltens hin untersucht wurden. Die Vernetzung wurde weiterhin in Gegenwart von mikroporösen Polypropylen (PP)-Substraten durchgeführt, was zur Entstehung von Matrix-unterstützten Hydrogelen führte, welche eine erhöhte mechanischer Stabilität und eine perlenförmige Mikrostruktur der Gelkomponente aufwiesen.

P(EtOx-*stat*-AmOx) wurden ferner für die Herstellung von gelartigen Oberflächenbeschichtungen auf Glas und PP verwendet. Die kovalente Immobilisierung der Polymere auf aktivierten Oberflächen resultierte in der Ausbildung von Monolagen, welche durch abwechselnde Behandlung mit Vernetzer und Polymer mit zusätzlichen Schichten versehen werden konnten. Mit zunehmender Schichtanzahl wiesen die Materialien einen steigenden Hydrogelcharakter auf, was durch ein vermehrtes Quellen festgestellt werden konnte. Die Markierung der Polymere mit Fluoreszenzfarbstoffen erlaubte die Quantifizierung des abgelagerten Materials und die Verwendung von PP eröffnet eine Vielzahl von möglichen Substratgeometrien.

Nanogele bildeten eine dritte Materialklasse, die aus kationischen POx hergestellt wurde. Die Selbstassemblierung von Block-copolymeren im organischen Medium wurde untersucht und die resultierenden mizellaren sowie vesikularen Strukturen wurden vernetzt, um wasserstabile Nanogele zu erhalten. Eine Beladung dieser Strukturen mit entweder Fluoreszein (als Farbstoff) oder Doxorubicin (Dox, als hochwirksames Zytostatika) wurde durch kovalente Anbindung erreicht. Es konnte gezeigt werden, dass der Grad der Quervernetzung einen direkten Einfluss auf Größe und Ladungsdichte der Nanostrukturen hat. Der Kern der Mizellen wies ein basisches Mikromilieu auf, das die Fluoreszenz von gebundenen Farbstoffen durch die Unterbindung von nicht strahlenden Zerfallsprozessen verstärkt.

Die Aufreinigung und Detektion von DNA aus biologischen Proben stellt ein potentielles Anwendungsfeld von kationischen Polymeren und Gelen dar. Aus diesem Grund wurden P(EtOx-*stat*-AmOx) sowie P(EI-*stat*-Ox) mit Hilfe des Ethidiumbromidassays hinsichtlich ihrer Interaktion mit genetischem Material untersucht. Es konnte eine Abhängigkeit der DNA Affinität



## 7. Zusammenfassung

---

vom Gehalt an Amingruppen festgestellt werden. Mit einem ähnlichen Verfahren wurde die Bindung und Freisetzung von DNA in Hydrogelen untersucht. Netzwerke, die PEI-Komponenten enthielten, zeigten generell eine höhere DNA Affinität, während genetisches Material, welches in P(EtOx-*stat*-AmOx) basierten Systeme gebunden wurde, bei Raumtemperatur durch die Verwendung von Heparin freigesetzt werden konnte. Durch die Feinabstimmung des Freisetzungsprozesses konnten heparinfreie Eluate erzeugt werden, welche mittels Polymerase Kettenreaktion (PCR) vervielfältigt werden konnten. Weiterhin wurden oberflächengebundene POx-Multilagen hinsichtlich ihrer Interaktion mit DNA untersucht. Eine Polymer-Doppelschicht war in der Lage, DNA aus wässriger Lösung zu binden und diese bei Temperaturerhöhung wieder freizugeben. Mit diesem System konnte genetisches Material direkt aus biologischen Proben extrahiert werden. Zudem konnte durch das Anbringen einer Beschichtung an der Innenseite von PCR-Reaktionsgefäßen eine direkte Vervielfältigung sowie Detektion durch quantitative Echtzeit-PCR erreicht werden. Dieses „Lab-in-a-tube“-System ermöglicht die Detektion von Pathogen DNA direkt aus biologischen Proben ohne aufwändige Arbeitsschritte und mit einem Minimum an Materialverbrauch.

Eine zweite, in dieser Arbeit untersuchte potentielle Anwendung war das gezielte Verabreichen von Krebsmedikamenten (Drug Delivery). Zu diesem Zweck wurden Nanogele mittels Untersuchung der Toxizität, der zellulären Aufnahme und der Colokalisation mit Zellbestandteilen hinsichtlich ihrer Interaktion mit Zellen analysiert. Es konnte eine Aufnahme durch Endozytose und eine gute Bioverträglichkeit von Farbstoff-beladenen Strukturen festgestellt werden. Mizellen, die Dox enthielten, zeigten eine erhöhte Toxizität gegenüber dem reinen Medikament, und Colokalisationsuntersuchungen zeigten ein unterschiedliches intrazelluläres Verhalten von Nanogel assoziiertem Dox und freiem Pharmazeutikum.

Zusammenfassend bietet die Kombination aus POx und Amingruppen vielfältige Möglichkeiten zur Herstellung verschiedener funktioneller Materialien. Die spezifische Wechselwirkung kationischer Strukturen mit DNA führte zur Entwicklung eines neuen Detektionssystem für DNA direkt aus biologischen Probenmaterialien. Die Verwendung von Nanogelen im Bereich der gezielten Verabreichung von Arzneimitteln zeigte erste vielversprechende Ergebnisse, und eine weitere *in vitro* sowie *in vivo* Untersuchung dieser Systeme stellt sich als aussichtvoll dar.

## 8. References

- [1] H. Jin, W. Huang, X. Zhu, Y. Zhou, D. Yan, *Chem. Soc. Rev.* **2012**, *41*, 5986-5997.
- [2] R. Luxenhofer, G. Sahay, A. Schulz, D. Alakhova, T. K. Bronich, R. Jordan, A. V. Kabanov, *J. Control. Release* **2011**, *153*, 73-82.
- [3] C. Mangold, F. Wurm, H. Frey, *Polym. Chem.* **2012**, *3*, 1714-1721.
- [4] S. Aoshima, S. Kanaoka, *Chem. Rev.* **2009**, *109*, 5245-5287.
- [5] D. J. Keddie, *Chem. Soc. Rev.* **2014**, *43*, 496-505.
- [6] W. Hadasha, B. Klumperman, *Polym. Int.* **2014**, *63*, 824-834.
- [7] J. Nicolas, Y. Guillaneuf, C. Lefay, D. Bertin, D. Gignes, B. Charleux, *Prog. Polym. Sci.* **2013**, *38*, 63-235.
- [8] T. Kagiya, S. Narisawa, T. Maeda, K. Fukui, *J. Polym. Sci. B: Polym. Lett.* **1966**, *4*, 441-445.
- [9] W. Seeliger, E. Aufderhaar, W. Diepers, R. Feinauer, R. Nehring, W. Thier, H. Hellmann, *Angew. Chem.* **1966**, *78*, 913-927.
- [10] D. A. Tomalia, D. P. Sheetz, *J. Polym. Sci., Part A: Polym. Chem.* **1966**, *4*, 2253-2265.
- [11] T. G. Bassiri, A. Levy, M. Litt, *J. Polym. Sci. B: Polym. Lett.* **1967**, *5*, 871-879.
- [12] F. Wiesbrock, R. Hoogenboom, C. H. Abeln, U. S. Schubert, *Macromol. Rapid Commun.* **2004**, *25*, 1895-1899.
- [13] K. Kempe, C. R. Becer, U. S. Schubert, *Macromolecules* **2011**, *44*, 5825-5842.
- [14] M. C. Woodle, C. M. Engbers, S. Zalipsky, *Bioconjugate Chem.* **1994**, *5*, 493-496.
- [15] S. Zalipsky, C. B. Hansen, J. M. Oaks, T. M. Allen, *J. Pharm. Sci.* **1996**, *85*, 133-137.
- [16] C. Weber, R. Hoogenboom, U. S. Schubert, *Prog. Polym. Sci.* **2012**, *37*, 686-714.
- [17] R. Luxenhofer, Y. Han, A. Schulz, J. Tong, Z. He, A. V. Kabanov, R. Jordan, *Macromol. Rapid Commun.* **2012**, 1613-1631.
- [18] P. Calvert, *Adv. Mater.* **2009**, *21*, 743-756.
- [19] M. Jäger, S. Schubert, S. Ochrimenko, D. Fischer, U. S. Schubert, *Chem. Soc. Rev.* **2012**, *41*, 4755-4767.
- [20] K. Kobayashi, J. Wei, R. Iida, K. Ijiro, K. Niikura, *Polym. J.* **2014**, *46*, 460-468.
- [21] S. Cesana, J. Auernheimer, R. Jordan, H. Kessler, O. Nuyken, *Macromol. Chem. Phys.* **2006**, *207*, 183-192.
- [22] J. Zhu, R. E. Marchant, *Expert Rev. Med. Devices* **2011**, *8*, 607-626.
- [23] A. K. Bajpai, S. K. Shukla, S. Bhanu, S. Kankane, *Prog. Polym. Sci.* **2008**, *33*, 1088-1118.
- [24] P. Baipaywad, N. Udumluck, S.-G. Pyo, H. H. Park, H. Park, *J. Nanosci. Nanotechnol.* **2014**, *14*, 7363-7373.
- [25] C. Legros, M.-C. De Pauw-Gillet, K. C. Tam, S. Lecommandoux, D. Taton, *Polym. Chem.* **2013**, *4*, 4801-4808.
- [26] R. Hoogenboom, H. Schlaad, *Polymers* **2011**, *3*, 467-488.
- [27] H. D. de Paz, P. Brotons, C. Muñoz-Almagro, *Expert Rev. Mol. Diagn.* **2014**, *14*, 827-843.
- [28] S.-S. Feng, S. Chien, *Chem. Eng. Sci.* **2003**, *58*, 4087-4114.
- [29] A. T. Press, A. Traeger, C. Pietsch, A. Mosig, M. Wagner, M. G. Clemens, N. Jbeily, N. Koch, M. Gottschaldt, N. Bézière, V. Ermolayev, V. Ntziachristos, J. Popp, M. M. Kessels, B. Qualmann, U. S. Schubert, M. Bauer, *Nat. Commun.* **2014**, *5*, 5565 (1-13).
- [30] H. Maeda, K. Greish, J. Fang, in *Polymer Therapeutics II, Vol. 193* (Eds.: R. Satchi-Fainaro, R. Duncan), Springer Berlin Heidelberg, **2006**, pp. 103-121.
- [31] M. Talelli, C. J. F. Rijcken, W. E. Hennink, T. Lammers, *Curr. Opin. Solid State Mater. Sci.* **2012**, *16*, 302-309.
- [32] D. R. Coombe, *Immunol. Cell Biol.* **2002**, *80*, 506-506.
- [33] J. T. Trevors, G. H. Pollack, *Prog. Biophys. Mol. Biol.* **2005**, *89*, 1-8.
- [34] O. Wichterle, D. Lím, *Nature* **1960**, *18*, 117-118.
- [35] F. L. Buchholz, *J. Chem. Educ.* **1996**, *73*, 512-515.

## 8. References

- [36] K. Skórkowska-Telichowska, M. Czemplik, A. Kulma, J. Szopa, *J. Am. Acad. Dermatol.* **2013**, *68*, e117-e126.
- [37] S. Thirumaleshwar, P. K. Kulkarni, D. V. Gowda, *Curr. Drug Ther.* **2012**, *7*, 212-218.
- [38] F. L. Buchholz, N. A. Peppas, *Superabsorbent Polymers: Science and Technology*, Amer. Chemical. Soc., Washington, DC, **1994**.
- [39] M. J. Zohuriaan-Mehr, H. Omidian, S. Doroudiani, K. Kabiri, *J. Mater. Sci.* **2010**, *45*, 5711-5735.
- [40] J. J. Simhadri, H. A. Stretz, M. Oyanader, P. E. Arce, *Ind. Eng. Chem. Res.* **2010**, *49*, 11866-11877.
- [41] A. Vashist, A. Vashist, Y. K. Gupta, S. Ahmad, *J. Mater. Chem. B* **2014**, *2*, 147-166.
- [42] D. Buenger, F. Topuz, J. Groll, *Prog. Polym. Sci.* **2012**, *37*, 1678-1719.
- [43] Y. Chujo, K. Sada, K. Matsumoto, T. Saegusa, *Polym. Bull.* **1989**, *21*, 353-356.
- [44] Y. Chujo, K. Sada, K. Matsumoto, T. Saegusa, *Macromolecules* **1990**, *23*, 1234-1237.
- [45] V. Schenk, E. Rossegger, C. Ebner, F. Bangerl, K. Reichmann, B. Hoffmann, M. Höpfner, F. Wiesbrock, *Polymers* **2014**, *6*, 264-279.
- [46] H. Uyama, S. Kobayashi, *Chem. Lett.* **1992**, *9*, 1643-1646.
- [47] J. C. Rueda, H. Komber, J. C. Cedrón, B. Voit, G. Shevtsova, *Macromol. Chem. Phys.* **2003**, *204*, 947-953.
- [48] Y. Chujo, K. Sada, T. Kawasaki, T. Saegusa, *Polym. J.* **1992**, *24*, 1301-1306.
- [49] B. L. Farrugia, K. Kempe, U. S. Schubert, R. Hoogenboom, T. R. Dargaville, *Biomacromolecules* **2013**, *14* 2724-2732.
- [50] T. R. Dargaville, B. G. Hollier, A. Shokoohtmand, R. Hoogenboom, *Cell Adhes. Migr.* **2014**, *8*, 88-93.
- [51] Y. Chujo, K. Sada, T. Saegusa, *Macromolecules* **1990**, *23*, 2636-2641.
- [52] Y. Chujo, K. Sada, R. Nomura, A. Naka, T. Saegusa, *Macromolecules* **1993**, *26*, 5611-5614.
- [53] H. Sun, F. Meng, R. Cheng, C. Deng, Z. Zhong, *Antioxid. Redox Signaling* **2013**, *21*, 755-767.
- [54] M. Narvekar, H. Xue, J. Eoh, H. Wong, *AAPS PharmSciTech* **2014**, *15*, 822-833.
- [55] K. Miyata, R. J. Christie, K. Kataoka, *Reactive and Functional Polymers* **2011**, *71*, 227-234.
- [56] C. Kiparissides, O. Kammona, *Can. J. Chem. Eng.* **2013**, *91*, 638-651.
- [57] C. Deng, Y. Jiang, R. Cheng, F. Meng, Z. Zhong, *Nano Today* **2012**, *7*, 467-480.
- [58] C. Oerlemans, W. Bult, M. Bos, G. Storm, J. F. Nijssen, W. Hennink, *Pharm. Res.* **2010**, *27*, 2569-2589.
- [59] C. F. van Nostrum, *Soft Matter* **2011**, *7*, 3246-3259.
- [60] C. Guerrero-Sanchez, D. Wouters, S. Hoepfener, R. Hoogenboom, U. S. Schubert, *Soft Matter* **2011**, *7*, 3827-3831.
- [61] H. Huang, R. Hoogenboom, M. A. M. Leenen, P. Guillet, A. M. Jonas, U. S. Schubert, J.-F. Gohy, *J. Am. Chem. Soc.* **2006**, *128*, 3784-3788.
- [62] S. Zschoche, J. Rueda, V. Boyko, F. Krahl, K.-F. Arndt, B. Voit, *Macromol. Chem. Phys.* **2010**, *211*, 1035-1042.
- [63] H. Clausen-Schaumann, M. Rief, C. Tolksdorf, H. E. Gaub, *Biophys. J.* **2000**, *78*, 1997-2007.
- [64] K. A. Dill, *Biochemistry* **1990**, *29*, 7133-7155.
- [65] W. Tang, M. L. Becker, *Chem. Soc. Rev.* **2014**, *43*, 7013-7039.
- [66] M. B. Smith, *March's Advanced Organic Chemistry: Reactions, Mechanisms, and Structure*, 7 ed., Wiley, New York, **2013**.
- [67] M. M. Bloksma, D. J. Bakker, C. Weber, R. Hoogenboom, U. S. Schubert, *Macromol. Rapid Commun.* **2010**, *31*, 724-728.
- [68] F. E. Bailey, R. W. Callard, *J. Appl. Polym. Sci.* **1959**, *1*, 56-62.
- [69] B. Adnadjevi, J. Jovanovi, *Int. J. Polym. Sci.* **2011**, *2011*, 14.
- [70] A. Koschella, M. Hartlieb, T. Heinze, *Carbohydr. Polym.* **2011**, *86*, 154-161.
- [71] M. E. Byrne, K. Park, N. A. Peppas, *Adv. Drug Deliv. Rev.* **2002**, *54*, 149-161.
- [72] R. Koningsveld, A. J. Staverman, *J. Polym. Sci., Part A-2* **1968**, *6*, 305-323.
- [73] R. Koningsveld, A. J. Staverman, *J. Polym. Sci., Part A-2* **1968**, *6*, 325-347.
- [74] Y. Chatani, H. Tadokoro, T. Saegusa, H. Ikeda, *Macromolecules* **1981**, *14*, 315-321.
- [75] Y. Chatani, T. Kobatake, H. Tadokoro, R. Tanaka, *Macromolecules* **1982**, *15*, 170-176.
- [76] Y. Chatani, T. Kobatake, H. Tadokoro, *Macromolecules* **1983**, *16*, 199-204.

## 8. References

- [77] M. Islam, Y. Gao, X. Li, Q. Zhang, M. Wei, M. Serpe, *Chin. Sci. Bull.* **2014**, *59*, 4237-4255.
- [78] L. Tauhardt, K. Kempe, M. Gottschaldt, U. S. Schubert, *Chem. Soc. Rev.* **2013**, *42*, 7998-8011.
- [79] T. Lehmann, J. Rühle, *Macromol. Symp.* **1999**, *142*, 1-12.
- [80] K. Yoshinaga, Y. Hidaka, *Polym. J.* **1994**, *26*, 1070-1079.
- [81] Y. Chujo, E. Ihara, H. Ihara, T. Saegusa, *Macromolecules* **1989**, *22*, 2040-2043.
- [82] R. Jordan, K. Martin, H. J. Räder, K. K. Unger, *Macromolecules* **2001**, *34*, 8858-8865.
- [83] F. Rehfeldt, M. Tanaka, L. Pagnoni, R. Jordan, *Langmuir* **2002**, *18*, 4908-4914.
- [84] N. Adden, A. Hoffmann, G. Gross, H. Windhagen, F. Thorey, H. Menzel, *J. Biomater. Sci., Polym. Ed.* **2007**, *18*, 303-316.
- [85] C. Haensch, T. Erdmenger, M. W. M. Fijten, S. Hoepfener, U. S. Schubert, *Langmuir* **2009**, *25*, 8019-8024.
- [86] T. Druzhinina, S. Hoepfener, N. Herzer, U. S. Schubert, *J. Mater. Chem.* **2011**, *21*, 8532-8536.
- [87] K. T. Lee, J. M. Goddard, J. H. Hotchkiss, *Packag. Technol. Sci.* **2009**, *22*, 139-150.
- [88] O. Birkert, G. Gauglitz, *Anal. Bioanal. Chem.* **2002**, *372*, 141-147.
- [89] G. Liu, *Z. An. Polym. Chem.* **2014**, *5*, 1559-1565.
- [90] S. E. Averick, E. Paredes, A. Irastorza, A. R. Shrivats, A. Srinivasan, D. J. Siegwart, A. J. Magenau, H. Y. Cho, E. Hsu, A. A. Averick, J. Kim, S. Liu, J. O. Hollinger, S. R. Das, K. Matyjaszewski, *Biomacromolecules* **2012**, *13*, 3445-3449.
- [91] W. Chen, M. Zheng, F. Meng, R. Cheng, C. Deng, J. Feijen, Z. Zhong, *Biomacromolecules* **2013**, *14*, 1214-1222.
- [92] G. Riess, *Prog. Polym. Sci.* **2003**, *28*, 1107-1170.
- [93] W. Ian, L. GuoJun, *Sci. China: Life Sci.* **2013**, 1-27.
- [94] J. N. Israelachvili, D. J. Mitchell, B. W. Ninham, *J. Chem. Soc., Faraday Trans. 2* **1976**, *72*, 1525-1568.
- [95] H. Ding, X. Wang, S. Zhang, X. Liu, *J. Nanopart. Res.* **2012**, *14*, 1-13.
- [96] P. Persigehl, R. Jordan, O. Nuyken, *Macromolecules* **2000**, *33*, 6977-6981.
- [97] R. Hoogenboom, M. M. Leenen, H. Huang, C.-A. Fustin, J.-F. Gohy, U. Schubert, *Colloid Polym. Sci.* **2006**, *284*, 1313-1318.
- [98] U. Mansfeld, S. Hoepfener, K. Kempe, J.-M. Schumers, J.-F. Gohy, U. S. Schubert, *Soft Matter* **2013**, *9*, 5966-5974.
- [99] R. Takahashi, T. Sato, K. Terao, X.-P. Qiu, F. M. Winnik, *Macromolecules* **2012**, *45*, 6111-6119.
- [100] R. Obeid, E. Maltseva, A. F. Thünemann, F. Tanaka, F. M. Winnik, *Macromolecules* **2009**, *42*, 2204-2214.
- [101] T. B. Bonn , K. L dtke, R. Jordan, C. M. Papadakis, *Macromol. Chem. Phys.* **2007**, *208*, 1402-1408.
- [102] R. Ivanova, T. Komenda, T. B. Bonn , K. L dtke, K. Mortensen, P. K. Pranzas, R. Jordan, C. M. Papadakis, *Macromol. Chem. Phys.* **2008**, *209*, 2248-2258.
- [103] R. K. O'Reilly, C. J. Hawker, K. L. Wooley, *Chem. Soc. Rev.* **2006**, *35*, 1068-1083.
- [104] N. t. Brummelhuis, H. Schlaad, *Polym. Chem.* **2011**, *2*, 1180-1184.
- [105] N. Engelhardt, A. Ernst, A.-L. Kampmann, R. Weberskirch, *Macromol. Chem. Phys.* **2013**, *214*, 2783-2791.
- [106] C. Legros, A.-L. Wirotius, M.-C. De Pauw-Gillet, K. C. Tam, D. Taton, S. Lecommandoux, *Biomacromolecules* **2014**, *16*, 183-191.
- [107] Y. Liu, Y. Wang, Y. Wang, J. Lu, V. Pi n n, M. Weck, *J. Am. Chem. Soc.* **2011**, *133*, 14260-14263.
- [108] S. Zschoche, J. C. Rueda, M. Binner, H. Komber, A. Janke, K.-F. Arndt, S. Lehmann, B. Voit, *Macromol. Chem. Phys.* **2012**, *213*, 215-226.
- [109] J. Rodr guez-Hern ndez, J. Babin, B. Zappone, S. Lecommandoux, *Biomacromolecules* **2005**, *6*, 2213-2220.
- [110] M. Wagner, S. Holzschuh, A. Traeger, A. Fahr, U. S. Schubert, *Anal. Chem.* **2014**, *86*, 5201-5210.



## 8. References

---

- [111] W. Burchard, in *Branched Polymers II, Vol. 143* (Ed.: J. Roovers), Springer Berlin Heidelberg, **1999**, pp. 113-194.
- [112] R. Sjöback, J. Nygren, M. Kubista, *Spectrochim. Acta, Part A* **1995**, *51*, L7-L21.
- [113] A. Verma, F. Stellacci, *Small* **2010**, *6*, 12-21.
- [114] K. K. Karukstis, E. H. Z. Thompson, J. A. Whiles, R. J. Rosenfeld, *Biophys. Chem.* **1998**, *73*, 249-263.
- [115] A. Moody, *Clin. Microbiol. Rev.* **2002**, *15*, 66-78.
- [116] B. C. Ross, L. Marino, F. Oppedisano, R. Edwards, R. M. Robins-Browne, P. D. Johnson, *J. Clin. Microbiol.* **1997**, *35*, 1696-1700.
- [117] A. J. Herring, N. F. Inglis, C. K. Ojeh, D. R. Snodgrass, J. D. Menzies, *J. Clin. Microbiol.* **1982**, *16*, 473-477.
- [118] M. Bally, M. Graule, F. Parra, G. Larson, F. Höök, *Biointerphases* **2013**, *8*, 1-9.
- [119] P. L. Kole, G. Venkatesh, J. Kotecha, R. Sheshala, *Biomed. Chromatogr.* **2011**, *25*, 199-217.
- [120] K. Zro, S. Azelmat, Y. Bendouro, J. H. Kuhn, E. El Fahime, M. M. Ennaji, *J. Virol. Methods* **2014**, *204*, 38-43.
- [121] N. C. Engleberg, B. I. Eisenstein, *Annu. Rev. Med.* **1992**, *43*, 147-155.
- [122] M. Neely, R. Jelliffe, *J. Clin. Pharmacol.* **2008**, *48*, 1081-1091.
- [123] A. Sassolas, B. D. Leca-Bouvier, L. J. Blum, *Chem. Rev.* **2007**, *108*, 109-139.
- [124] L. Schwenkbier, S. König, S. Wagner, S. Pollok, J. Weber, M. Hentschel, J. Popp, S. Werres, K. Weber, *Microchim. Acta* **2014**, *181*, 1669-1679.
- [125] N. Wellinghausen, C. Frost, R. Marre, *Appl. Environ. Microbiol.* **2001**, *67*, 3985-3993.
- [126] M. A. Innis, K. B. Myambo, D. H. Gelfand, M. A. Brow, *Proc. Natl. Acad. Sci.* **1988**, *85*, 9436-9440.
- [127] R. Saiki, D. Gelfand, S. Stoffel, S. Scharf, R. Higuchi, G. Horn, K. Mullis, H. Erlich, *Science* **1988**, *239*, 487-491.
- [128] A. M. Wang, M. V. Doyle, D. F. Mark, *Proc. Natl. Acad. Sci.* **1989**, *86*, 9717-9721.
- [129] K. B. Mullis, H. A. Erlich, N. Arnheim, G. T. Horn, R. K. Saiki, S. J. Scharf, US4683195 A, **1987**.
- [130] J. Ning, J. Liebich, M. Kästner, J. Zhou, A. Schäffer, P. Buraue, *Appl. Microbiol. Biotechnol.* **2009**, *82*, 983-993.
- [131] M. Hartlieb, D. Pretzel, K. Kempe, C. Fritzsche, R. M. Paulus, M. Gottschaldt, U. S. Schubert, *Soft Matter* **2013**, *9*, 4693-4704.
- [132] J. B. Lepecq, C. Paoletti, *J. Mol. Biol.* **1967**, *27*, 87-106.
- [133] H. M. Sobell, C.-C. Tsai, S. C. Jain, S. G. Gilbert, *J. Mol. Biol.* **1977**, *114*, 333-365.
- [134] B. C. Baguley, E. M. Falkenhaus, *Nucleic Acids Res.* **1978**, *5*, 161-171.
- [135] S. Xiang, H. Tong, Q. Shi, J. C. Fernandes, T. Jin, K. Dai, X. Zhang, *J. Control. Release* **2012**, *158*, 371-378.
- [136] S. Lerch, M. Dass, A. Musyanovych, K. Landfester, V. Mailänder, *Eur. J. Pharm. Biopharm.* **2013**, *84*, 265-274.
- [137] R. M. Steinman, I. S. Mellman, W. A. Muller, Z. A. Cohn, *J. Cell Biol.* **1983**, *96*, 1-27.
- [138] P. R. Leroueil, S. Hong, A. Mecke, J. R. Baker, B. G. Orr, M. M. Banaszak Holl, *Acc. Chem. Res.* **2007**, *40*, 335-342.
- [139] A. Lesniak, F. Fenaroli, M. P. Monopoli, C. Åberg, K. A. Dawson, A. Salvati, *ACS Nano* **2012**, *6*, 5845-5857.
- [140] T. Tsuchiya, *J. Biomater. Appl.* **1994**, *9*, 138-157.
- [141] P. Mohan, N. Rapoport, *Mol. Pharm.* **2010**, *7*, 1959-1973.

## List of abbreviations

AF4	-	Asymmetric flow field-flow fractionation
Boc	-	<i>tert</i> -Butyloxycarbonyl
BocOx	-	2-(4-(( <i>tert</i> -Butoxycarbonyl)amino)butyl)-2-oxazoline
BPEI	-	Branched poly(ethylene imine)
ButenOx	-	2-(But-3-en-1-yl)-4,5-dihydrooxazole
CA	-	Contact angle
CLSM	-	Confocal laser scanning microscopy
CMC	-	Critical micelle concentration
CROP	-	Cationic ring-opening polymerization
cryoTEM	-	Cryo transmission electron microscopy
$c_t$	-	Cycle threshold
Cy5	-	Cyanine 5
DLS	-	Dynamic light scattering
Dox	-	Doxorubicin
EB	-	Ethidium bromide
EBA	-	Ethidium bromide assay
ECH	-	Epichlorohydrine
<i>E. coli</i>	-	<i>Escherichia coli</i>
EPR	-	Enhanced permeability and retention
EtOx	-	2-Ethyl-2-oxazoline
GA	-	Glutaraldehyde
GOPTMS	-	3-Glycidyloxypropyl trimethoxysilane
LbL	-	Layer-by-layer
LCST	-	Lower critical solution temperature
IPEI	-	Linear poly(ethylene imine)
MALLS	-	Multi-angle light scattering
PCR	-	Polymerase chain reaction
PAmOx	-	Poly(2-(4-aminobutyl)-2-oxazoline)
PEG	-	Poly(ethylene glycole)
PEI	-	Poly(ethylene imine)
PEtOx	-	Poly(2-ethyl-2-oxazline)
PMeOx	-	Poly(2-methyl-2-oxazoline)
POx	-	Poly(2-oxazoline)

## List of abbreviations

---

PP	-	Poly(propylene)
PS	-	Poly(styrene)
qPCR	-	Quantitative real-time polymerase chain reaction
RIFS	-	Reflectometric interference spectroscopy
SEC	-	Size exclusion chromatography
SEM	-	Scanning electron microscopy
TFA	-	Trifluoro acetic acid
TGA	-	Thermo-gravimetric analysis
XPS	-	X-ray photoelectron spectroscopy



## Curriculum vitae



22/05/1986	Born in Gera, Germany
1992 - 1996	Public-Elementary School, Unterweißbach
1996 - 2004	Friedrich-Fröbel-Gymnasium, Bad Blankenburg Degree: General qualification for university entrance
2000	Internship at the TITK (Thuringian Institute of Textile and Plastics Research e.V.) Rudolstadt
2004 - 2005	Alternative civilian Service (City of Rudolstadt)
2005 - 2010	Student of Chemistry (MSc), Friedrich Schiller University Jena
2009	Student assistant at the group of Prof. Dr. Thomas Heinze, FSU Jena
2010-2011	Diploma thesis at the Friedrich Schiller University Jena in the group of Prof. Dr. Ulrich S. Schubert, Title: "Functional hydrogels from poly(2-oxazoline)s for bioapplications"
2011	Research assistant in the group of Prof. Dr. Ulrich S. Schubert, FSU Jena
Since 2011	PhD student at the Laboratory of Organic and Macromolecular Chemistry (IOMC) at the Friedrich Schiller University Jena in the group of Prof. Dr. Ulrich S. Schubert; Thesis: "Poly(2-oxazoline)-based materials for biomedical applications"
2012	STIFT Award for "excellent application oriented thesis at thuringian universities"

## Publication list

### Peer-reviewed publications

D. Pretzel, B. Sandmann, M. Hartlieb, J. Vitz, S. Hölzer, N. Fritz, N. Moszner, U. S. Schubert, "Biological evaluation of 1,2,3-triazole based polymers for potential applications as hard tissue material", *J. Polym. Sci. Part A: Polym. Chem.* **2015**, DOI: 10.1002/pola.27676.

M. N. Leiske,<sup>‡</sup> M. Hartlieb,<sup>‡</sup> C Paulenz, D. Pretzel, M. Hentschel, C. Englert, M. Gottschaldt, U. S. Schubert, "Lab in a tube: Purification, amplification and detection of DNA using poly(2-oxazoline) multilayers", *Adv. Funct. Mater.*, in press.

M. Hartlieb, D. Pretzel, M. Wagner, S. Hoepfener, P. Bellstedt, M. Görlach, C. Englert, K. Kempe, U. S. Schubert, "Core cross-linked nanogels based on the self-assembly of double hydrophilic poly(2-oxazoline) block copolymers", *J. Mater. Chem. B* **2015**, 3, 1748-1759.

M. Hartlieb, K. Kempe, U. S. Schubert, "Covalently cross-linked poly(2-oxazoline) materials for biomedical applications – from hydrogels to self-assembled and templated structures", *J. Mater. Chem. B* **2015**, 3, 526-538.

M. Hartlieb, S. Schubert, K. Kempe, N. Windhab, U. S. Schubert, "Stabilization of Factor VIII by poly(2-oxazoline) hydrogels", *J. Polym. Sci., Part A: Polym. Chem.* **2015**, 53, 10-14.

M. Hartlieb, D. Pretzel, C. Englert, M. Hentschel, K. Kempe, M. Gottschaldt, U. S. Schubert, "Matrix supported poly(2-oxazoline)-based hydrogels for DNA catch and Release", *Biomacromolecules* **2014**, 15, 1970-1978.

C. Englert, L. Tauhardt, M. Hartlieb, K. Kempe, M. Gottschaldt, U. S. Schubert, "Linear poly(ethylene imine)-based hydrogels for effective binding and release of DNA", *Biomacromolecules* **2014**, 15, 1124-1131.

L. Tauhardt, M. Frant, D. Pretzel, M. Hartlieb, C. Bucher, G. Hildebrand, B. Schroter, C. Weber, K. Kempe, M. Gottschaldt, K. Liefelth, U. S. Schubert, "Amine end-functionalized poly(2-ethyl-2-oxazoline) as promising coating material for antifouling applications", *J. Mater. Chem. B* **2014**, 15, 1970-1978.

M. Hartlieb, D. Pretzel, K. Kempe, C. Fritzsche, R. M. Paulus, M. Gottschaldt, U. S. Schubert, „Cationic poly(2-oxazoline) hydrogels for reversible DNA binding“, *Soft Matter* **2013**, 9, 4693-4704.

A. Koschella, M. Hartlieb, T. Heinze, “A “click-chemistry” approach to cellulose-based hydrogels“, *Carbohydr. Polym.* **2011**, 86, 154-161.

### Manuscripts in preparation

M. Hartlieb, T. Buś, J. Kübel, D. Pretzel, S. Hoepfener, K. Kempe, B. Dietzek, U. S. Schubert, „Nanogels based on double hydrophilic poly(2-oxazoline) for doxorubicin delivery“, in preparation.

### Non-peer-reviewed conference proceedings

M. Hartlieb, D. Pretzel, K. Kempe, C. Fritzsche, R. Paulus, M. Gottschaldt, U. S. Schubert, “Cationic poly(2-oxazoline) hydrogels for reversible DNA binding” *246th ACS National Meeting & Exposition*, **2013**, 300-302

M. Jaeger, M. Hartlieb, U. S. Schubert, “Synthesis and characterization of functionalized benzocycloctynes via intramolecular Pd-catalyzed C-C coupling reactions” *242nd ACS National Meeting & Exposition*, **2011**, 224-226.

### Oral presentations

“Amine containing poly(2-oxazoline) hydrogels for reversible DNA immobilization” *Euro BioMat* **2013**, Weimar, Germany.

“Poly(2-oxazoline) based hydrogels for DNA catch and release” *JCF Frühjahrsymposium* **2014**, Jena, Germany.

### Poster presentation

L. Tauhardt, D. Pretzel,<sup>§</sup> M. Hartlieb, C. Bücher, G. Hildebrand, M. Frant, K. Liefelth, M. Gottschaldt, U. S. Schubert “Poly(2-ethyl-2-oxazoline) based polymers for the prevention of biofilm formation” *246th ACS National Meeting & Exposition, 2013*, Indianapolis, United States.

M. Hartlieb, D. Pretzel<sup>§</sup>, C. Fritzsche, K. Kempe, M. Gottschaldt, U. S. Schubert, “Amine containing Poly(2-oxazoline) hydrogels and interpenetrating networks for DNA binding” *246th ACS National Meeting & Exposition, 2013*, Indianapolis, United States.

M. Hartlieb, S. Schubert, K. Kempe, N. Windhab, U. S. Schubert “Poly (2-oxazoline) hydrogels” *Smart polymers 2012*, Mainz, Germany.

‡ Equal contribution

§ Presenter

## Acknowledgement / Danksagung

At last, I want to thank all the people who supported me over all the years and worked hard to make all this possible.

At first, I want to express my deep gratitude to my scientific supervisor **Prof. Dr. Ulrich S. Schubert**. Thank you, Uli for all the support and the trust in my work over the years. I loved working in such an interdisciplinary, international and incredibly well equipped group. It is really fantastic what you developed in Jena and I am eager to see where it goes in the future.

Furthermore, I want to thank **Dr. Kristian Kempe** for his continuous support and supervision over the years. Kristian, I cannot emphasize enough how much you helped me, also after you moved to Australia and later UK. Whenever I needed some help, discussion, assurance, or only some nice words you were available.

I would also like to thank **Bundesministerium für Bildung und Forschung** for Funding (project: BASIS, 03WKCB01C).

In the following I want to acknowledge all the coworkers within or outside the Schubert group who supported me and cooperated with me over the years. Firstly, I want to thank **Meike Leiske**, my first (and up to now only) master student. Thank you, Meike for all the help and work you did in the lab and being such an enthusiastic student. I am keen to see what you will accomplish in the future.

I'd like to thank **Dr. Michael Gottschaldt**, **Dr. Christine Weber** for all the discussions and the support. Furthermore, a big thanks to the bio-people. Most of all **Dr. David Pretzel** for a lot of discussions and all the cool projects we did together. But also **Carolin Fritzsche** and **Tanja Buš** for all the assays and experiments, as well as **Alexandra Rinkenauer** and **Dr. Anja Träger** for a lot of discussions. Alex, too bad that the things we planned together never worked out.

I'd also like to thank **Dr. Michael Wagner** for many DLS and AF4 measurements and explaining what the meanings behind these things are. Furthermore, I would like to thank **Dr. Stephanie Schubert** and **Christoph Englert** for help and discussion in many situations. My thanks also go to **Jun. Prof. Felix H. Schacher** for a lot of helpful discussions over the years and much support with proposals.

I also want to acknowledge our cooperation partners from Analytik Jena AG: **Martin Hentschel** and **Christian Paulenz**. Thank you both for all the work during the BASIS project and beyond. It was a pleasure to work with you and I hope we will maintain contact in the future.

For all surface related work which was done within the BASIS project I'd like to thank **Dr. Lutz Tauhardt**, **Alexander Meier** and of course also David for these countless coatings, characterizations and discussions (BASIS-\*fistbump\* ☺). In this context, I also want to

acknowledge all the people from the **Institut für Bioprozess- und Analysenmesstechnik e.V.** in Heiligenstadt who were involved in the project for this nice partnership, as there are: **Prof. Dr. Klaus Liefelth, Dr. Gerhardt Hildebrandt, Dr. Marion Frandt, Christian Bücher** and **Dr. Bernd Schröter** from the physics department of the FSU for the XPS measurements.

Furthermore, I'd like to thank the solid state NMR crew from the FLI, **Dr. Matthias Görlach** and **Dr. Peter Bellstedt** for the nice and successful cooperation. Matthias, also thanks for sharing your incredibly elaborated English with me which lead to many nice phrasings in our paper☺.

From the IPHT Jena I want to acknowledge **Joachim Kübel** and **Prof. Dr. Benajmin Dietzek** for the Fluorescence lifetime measurements.

There are of course a lot of people working in "the background", keeping all the devices running, measuring a lot of samples and supplying the group with all necessary items. Big thanks go to all the MS people (**Sarah Crotty, Dr. Ezra Altuntas, Dr. Anja Baumgärtel and Anett Urbanek**), the SEC team (**Dr. Grit Festag, Nicole Fritz**), the NMR people (**Dr. Wolfgang Günther, Gabriele Sentis**), the SEM/TEM people (**Dr. Stephanie Höppener, Steffi Stumpf**) and **Renzo Paulus** as well as **Dr. Jürgen Vitz** for the thermal analysis. Thank you all very much for keeping everything running and countless measurements.

As for the supplies I'd like to thank a lot **Dr. Uwe Köhn** and **Sandra Köhn** for ordering, and making sure that all the cupboards are full if someone needs something.

Another important part of such a big group is the people caring about finances and administration. In this regard, I want to thank **Tanja Wagner, Simone Burchardt** and **Sylvia Braunsdorf**, as well as **Doreen Küchler** and **Jeanette Frommhold**.

Finally (in terms of work), no chemist would be complete without proper lab-mates. Thanks to **Tobias Rudolph, Ulrike Freier, Christoph Hörenz, Dr. Antje Vollrath, Dr. Christian Pietsch** and **Dr. Katrin Knop** back in TO and to **Dr. Lutz Tauhardt, Meike Leiske, Martin Reifahrt, Turgay Yldirim** and **Anne-Kristin Trützscher**. Lutz, without your help I would probably still unpack glassware and write excel sheets ;-). Also, thanks to all the students who did practical courses and contributed to my work (**Franziska Eberl, Sarina Massman** and **Fabian Sobotta**).

In this context, I also want to thank all the office "inmates" for fun, distraction, help, coffee,... so like the things that matter. Let's start with the original office crew in TO (**Aydin Can, Renzo Paulus, Dr. Jürgen Vitz**, a bit later **Stefan Hölzer** and for the last weeks **Tobias Janoschka**) and conclude with the "new" people in ZAF (**Dr. David Pretzel, Christoph Englert, Tobias Majdanski, Dr. Justyna Czaplewska, Michael Pröhl** and **Meike Leiske**). Thank you all for a great time! Special thanks goes to Stefan who helped me a lot with image processing and related questions.

As much as work related help matters in terms of success (and survival) as much value has friendship and support far from work.



In this regard I want to say thank you to the “original” TO-crew (**Dr. Kristian Kempe, Dr. Antje Vollrath, Andreas Krieg, Dr. Christian Pietsch, Dr. Sebastian Wünscher, Dr. Katrin Knop, Dr. Anke Teichler, Dr. Markus Barthel Sofia Ochrimenko, Alexandra Rinkenauer, Dr. Thorsten Walter, Dr. Anja Baumgärtel**). You all made my first years in the Schubert group an incredible exciting and funny experience. I still like to think of our “Klassenfahrt” in the snow of the Thuringia forest ☺.

Another important group of people I would like to thank is the “Kochrunde” consistent of **Joachim Kübel, Martin Elstner, Roman Goy, Dr. Frank Theil** and **Daniel Heine**. Thank you guys for all the culinary experiences of our *bi*-weekly meetings, for the fun and also for help with work related topics. It is nice to see that we are all now finishing our PhD (in a rather successful way!) and I hope we will still manage to stay in contact and meet, as we did after lectures ended. Within the last years I spend a lot of time with **Sebastian, Antje, Renzo, Andreas, Sofia, Anke** and **Stefan**. Thank you all for your friendship the nice time we spent together and all the support. Whenever I came along with a problem you guys helped me solving.

I also want to acknowledge my childhood friends from Rudolstadt (**Adrian Röttig, Christian Förster, Phillipp Wöllner, Christina Müller, Andre Hilla, Enrico Heise, Martin Melcher** and **Michael Unsinn**). I know we don't see each other much these days, but when we meet its always legendary ;-).

I also want to thank my parents, **Andreas** and **Hannelore Hartlieb**, as well as my siblings **Jan** and **Karsten Hartlieb**, and **Claudia Stehr** for their continuous support in whatever situation of life and last but not least my soon-to-be wife **Karolin Kempfert**. Without you I certainly would have failed or lost confidence multiple times on my way.

## **Declaration of authorship / Selbstständigkeitserklärung**

Hiermit erkläre ich, dass ich die vorliegende Arbeit selbständig angefertigt, nicht anderweitig zu Prüfungszwecken vorgelegt und keine anderen als die angegebenen Hilfsmittel verwendet habe. Sämtliche wissentlich verwendete Textausschnitte, Zitate oder Inhalte anderer Verfasser wurden ausdrücklich als solche gekennzeichnet.

I hereby certify that the work disclosed here is, to the best of my knowledge, original and the result of my own investigations, except as acknowledged, and has not been submitted, either in part or whole, for a degree at this or any other university.

Jena, den 07.06.2015

---

Matthias Hartlieb

## Publications P1 to P8

**P1:** Reprinted by permission of Royal Society of Chemistry.

**P2:** Reprinted by permission of Royal Society of Chemistry.

**P3:** Reprinted by permission of the American Chemical Society. Copyright 2015

**P4:** Reprinted by permission of Royal Society of Chemistry.

**P5:** Reprinted by permission of the American Chemical Society. Copyright 2015

**P6:** Reprinted by permission of Wiley VCH.

**P7:** Reprinted by permission of Royal Society of Chemistry.

**P8:** Reprinted by permission of M. Hartlieb, T. Bús, J. Kübel, D. Pretzel, S. Hoepfener, K. Kempe, B. Dietzek, and U. S. Schubert.

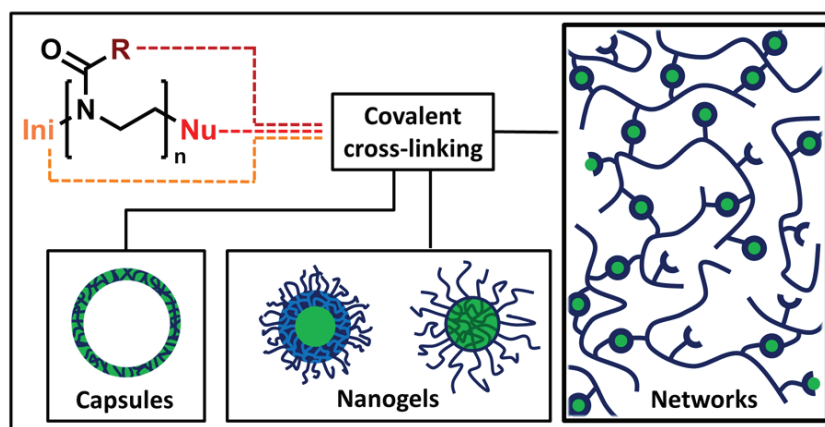


## Publication 1

### Covalently cross-linked poly(2-oxazoline) materials for biomedical applications – from hydrogels to self-assembled and templated structures

M. Hartlieb, K. Kempe, U. S. Schubert

*J. Mater. Chem. B* **2015**, *3*, 526-538





Cite this: *J. Mater. Chem. B*, 2015, 3, 526

## Covalently cross-linked poly(2-oxazoline) materials for biomedical applications – from hydrogels to self-assembled and templated structures

Matthias Hartlieb,<sup>ab</sup> Kristian Kempe<sup>†ab</sup> and Ulrich S. Schubert<sup>\*ab</sup>

Covalently cross-linked polymeric materials play an important role in life science. Hydrogels produced from multifunctional polymers can be utilized in numerous (bio)applications, such as drug delivery, tissue engineering and (bio)sensing. Also nano-/micro-scale assemblies benefit from a covalent linkage for instance to prevent premature disassembly or to generate a passive tissue specificity when used as a drug delivery agent. In both cases there is a need for biocompatible polymers with manifold (orthogonal) functionalization possibilities. By using the cationic ring-opening polymerization of 2-oxazolines it is possible to accomplish both tasks. In this review we summarize covalently cross-linked structures consisting of poly(2-oxazoline)s including three dimensional scaffolds, micellar systems as well as multilayer capsules. We focus on the cross-linking chemistry and the impact of the addressed systems regarding biological application.

Received 8th October 2014  
Accepted 16th November 2014

DOI: 10.1039/c4tb01660b

[www.rsc.org/MaterialsB](http://www.rsc.org/MaterialsB)

<sup>a</sup>Laboratory of Organic and Macromolecular Chemistry (IOMC), Friedrich Schiller University Jena, Humboldtstrasse 10, 07743, Jena, Germany. E-mail: [ulrich.schubert@uni-jena.de](mailto:ulrich.schubert@uni-jena.de)

<sup>b</sup>Jena Center for Soft Matter (JCSM), Friedrich Schiller University Jena, Philosophenweg 7, 07743, Jena, Germany

<sup>†</sup> Current address: Department of Chemistry, University of Warwick, Gibbet Hill Road, Coventry, CV4 7AL, UK.

### 1. Introduction

Biocompatible polymers are of paramount importance for the preparation of (smart) polymeric scaffolds, assemblies and coatings for biomedical applications.<sup>1</sup> However, besides biocompatibility, such macromolecular systems need to fulfil



Matthias Hartlieb was born in 1986 in Gera. He studied chemistry at the Friedrich-Schiller-University Jena where he received his diploma in 2011. His diploma thesis was awarded with the STIFT award for “excellent application oriented thesis at Thuringian universities” in 2012. He is currently working on his PhD thesis in the group of Prof. Ulrich S. Schubert at the Friedrich Schiller Univer-

sity Jena. His research focusses on the synthesis of functional polymers and the preparation of hydrogels and nanogels for application in the biomedical field.



Kristian Kempe studied chemistry at the Friedrich Schiller University Jena. In 2010 he was a visiting researcher in the group of Prof. Craig J. Hawker (University of California, Santa Barbara) and completed his PhD in 2011 under the supervision of Prof. Ulrich S. Schubert (Friedrich Schiller University Jena). In 2012 he received an Alexander von Humboldt-fellowship to conduct research in the

groups of Prof. Frank Caruso (The University of Melbourne) as well as Prof. David M. Haddleton and Prof. Thomas P. Davis (Monash University). Since mid-2014 he has held a Senior Researcher position in the group of Prof. David M. Haddleton (University of Warwick). His research interests include the preparation of functional macromolecules, poly(2-oxazoline)s, efficient polymer modification reactions and the design of functional particle systems and hydrogels for applications in nanomedicine and materials science.

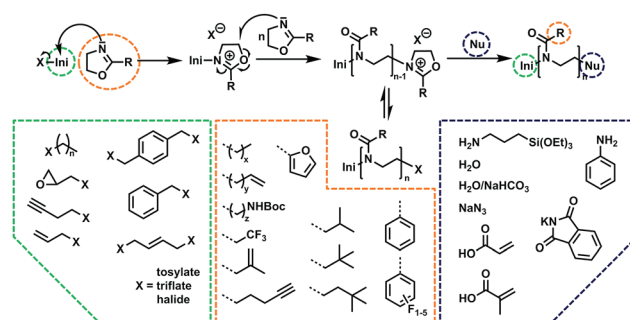


## Review

other criteria in order to become suitable candidates for the specified tasks, such as having no unspecific interaction with biological materials (anti/low-fouling), stability within the human body, and in the case of drug carriers a high loading capacity and release on demand. Also, in order to cross-link, label or load the material covalently, a high degree of (orthogonal) functionality is a huge necessity. As a consequence of these high demands, the search for new biocompatible and multifunctional polymers has been the subject of ongoing intensive research.

A highly interesting polymer class in this context is poly(2-oxazoline)s (POx), which are considered to be pseudo-peptides, showing structural similarities to naturally occurring polypeptides.<sup>2,3</sup> In particular, the water soluble (co)polymers based on 2-methyl-2-oxazoline (MeOx) and 2-ethyl-2-oxazoline (EtOx) have attracted significant attention due to their high biocompatibility,<sup>4</sup> antifouling properties<sup>5</sup> and similarities to poly(ethylene glycol).<sup>6</sup> The origin of POx dates back to 1966 when the cationic ring-opening polymerization (CROP) of 2-oxazolines was discovered by four research groups.<sup>7–10</sup> The main drawback of the original method was the long polymerization times of hours or even days. Decades later, in 2004, the combination of CROP and microwave technology led to a significant acceleration of the process, which resulted in a renaissance of this potent polymer class.<sup>11,12</sup>

The main advantages of the CROP of 2-oxazolines in terms of synthesis are the high degree of polymerization control, the resulting well-defined polymeric structures,<sup>13</sup> and the large variety of end- and side-group functionalities, which can be introduced using appropriate initiators/terminating agents and monomers, respectively.<sup>14</sup> The modularity of this polymer class enables the synthesis of highly functional materials with tailor-made properties. Scheme 1 illustrates the mechanism of the polymerization and summarizes reported initiators, monomers and terminating agents.



Scheme 1 Mechanism of the cationic ring-opening polymerization and possible ways of altering the functionalization of the resulting polymers.

Typical initiators for CROP consist of an organic moiety with an attached leaving group, which acts as the counter ion for the oxazolinium species during polymerization. The most commonly used initiators are tosylates or triflates of small aliphatic molecules but also alkyl halides are frequently applied. Altering the nature of the initiator leads to POx with functional  $\alpha$ -end groups. A change of the counter ion, however, has an influence on the velocity and control of the polymerization.<sup>15</sup> A second potential way to introduce functionalities is by end-capping the living polymer chain with nucleophiles, including amines,<sup>16</sup> azides<sup>17</sup> or acids.<sup>18</sup> Since most carboxylic acids will form an ester bond with the active chain end (when activated with an amine base) a wide variety of structures is accessible. The third possibility is the variation of the monomer substitution in the 2-position. While this group does not influence the polymerization directly if its nucleophilicity is low enough, functional groups, such as alkynes and alkenes<sup>19</sup> or (protected) amine groups<sup>20</sup> can be attached to the polymeric structure. The assortment of suitable monomers is not as manifold as that of possible end-capping agents, however, this functionalization offers a higher degree of freedom in the generation of functional polymers. The combination of several (functional) monomers in the variation of the architectures leads to multiplicity of possible structures. Also, the amount of functional groups per polymer chain is only limited by the degree of polymerization.

In this review we aim to provide an overview of functionalization/modification strategies, which are employed to prepare covalently cross-linked POx materials with potential for biomedical applications. The materials reported consist of polymer chains, which are interconnected by chemical cross-linkers. The main part of this review is concerned with covalently stabilized hydrogels and cross-linked self-assembled micelles. Furthermore, as recently introduced, a short paragraph will highlight the potential of POx for the fabrication of hydrogel capsules obtained by the layer-by-layer (LbL) technique. Our aim is to provide a review of the research happening in this particular field with an overview of the building blocks and strategies, which have been used to create POx-based covalently cross-linked hydrogels, micelles and capsules.



*Ulrich S. Schubert studied chemistry in Frankfurt and Bayreuth and the Virginia Commonwealth University, Richmond (USA). His PhD studies were performed at the Universities of Bayreuth and South Florida/Tampa (USA). After postdoctoral training with Jean-Marie Lehn at the University in Strasbourg (France), he moved to the TU München and obtained his habilitation in 1999. From 1999 to 2000 he was Professor at*

*the Center for NanoScience, University of Munich, and from 2000 to 2007 Full-Professor at TU Eindhoven (The Netherlands). Currently he holds a chair at the Friedrich Schiller University Jena with research interest in nanoparticle systems as sensor and drug delivery devices, supramolecular chemistry, inkjet printing of polymers, polymers for energy applications, and self-healing materials.*

## 2. Poly(2-oxazoline) hydrogels

Hydrogels are a widely spread material in nature since cellular tissue itself can be considered as a gel.<sup>21</sup> It is even hypothesized that hydrogels play a key role in the origin of life due to the limited and partially directed diffusion inside such networks.<sup>22</sup>

The first description of an artificial polymeric hydrogel was made in 1960 by Otto Wichterle and Drahoslav Lím who sought for a material with properties suitable for the production of new contact lenses.<sup>23</sup> The material was expected to be soft, water swellable, permeable to metabolites and inert to biological processes. Nowadays, artificial hydrogels have gained importance in many sectors of life science and daily life such as contact lenses,<sup>24</sup> wound dressing,<sup>25,26</sup> super absorbers (diapers, packaging, construction industry),<sup>27,28</sup> scaffolds for tissue engineering,<sup>29</sup> matrices for separation problems,<sup>30</sup> drug delivery devices<sup>31</sup> and sensors.<sup>32</sup>

To define which properties a soft matter has to possess to be labelled as a gel, the mechanical behavior is of outstanding interest. A gel is a mixture of at least two phases with an elastic modulus higher than its viscous modulus, in other terms a solid matter which consists of a continuous matrix swollen in a solvent. In the case of hydrogels this solvent is, of course, water. Polymeric gels are networks of cross-linked macromolecules, which can be obtained either by the formation of covalent connections (chemical gels) or secondary interactions (physical gels).

Physical POx gels, which are polymer networks cross-linked in a non-covalent way, applying secondary interactions, including hydrogen bonding, hydrophobic interactions, metal complexation or ionic interactions, are not considered in this review. However, an excellent overview is provided in a previous review by Wiesbrock and coworkers.<sup>33</sup>

In general, chemical cross-linked POx-based hydrogels can be subdivided into three major classes (Scheme 2): (1) hydrogels that are obtained in a one-step reaction using bis-functional monomers, (2) networks prepared *via* the macro-monomer method using  $(\alpha,\omega)$ -functionalized POx bearing polymerizable groups, and (3) hydrogels which are fabricated from POx with different side- and end-group functionalities and multifunctional cross-linkers.

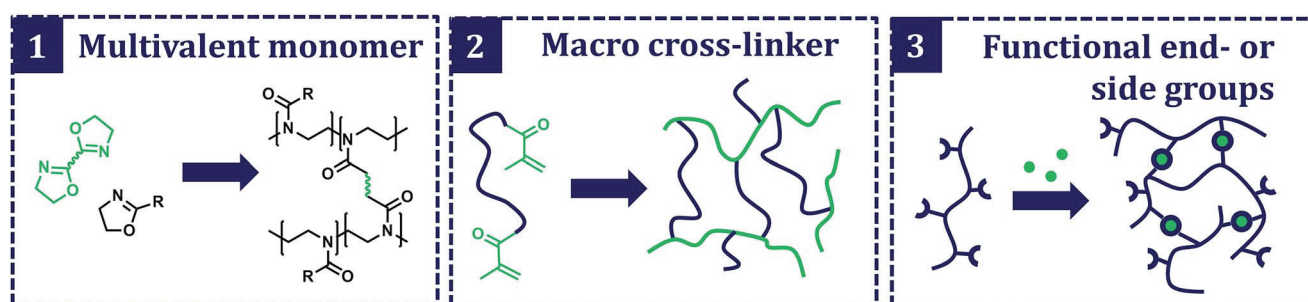
In the following sections, these three classes will be presented in detail starting with the use of bis-functional oxazolines.

### Hydrogels by CROP including multivalent monomers

The first synthesis of POx based hydrogels was reported in 1989 by the group of Takeo Saegusa.<sup>34</sup> The authors copolymerized MeOx with different 2-alkyl-2-oxazolines (*n*-butyl, *n*-octyl, *n*-dodecanyl), and an aliphatic bis-2-oxazoline. Five equivalents of the latter cross-linker per polymer chain (DP ~ 100) were sufficient to form stable gel structures. The variation of the comonomer enabled the tuning of the hydrophilicity of the resulting amphigels as determined by swelling in water and different organic solvents. While up to this point the gels were only characterized by the determination of the swelling values and detection of the absence of monomers after polymerization by gas chromatography, the reaction kinetics of the monomer mixture and the mechanism of gelation were reported later on.<sup>35</sup> The conversions of both monomers were analysed based on the reaction time revealing a much faster reaction rate of the cross-linker in comparison to MeOx. Furthermore, POx hydrogels were hydrolyzed resulting in linear PEI with relatively narrow molar mass distributions (PDI = 1.02), which indicated that the control of the polymerization is not lost even when cross-linkers are added. However, the difference in the reaction rate between the monomer and cross-linker led to gradient-like copolymers, which are unfavorable for the production of homogeneous networks.

Kelly *et al.* produced hydrogels using a new bis-oxazoline linked by a benzylic spacer.<sup>36</sup> The authors synthesized a 32-membered hydrogel library using different monomer (EtOx, 2-phenyl-2-oxazoline) to cross-linker ratios. The swelling in water, ethanol and dichloromethane was investigated based on the composition of the network. Small molecules like Eosin Y could be either covalently bound to the gel or entrapped by diffusion and, later on, released by a solvent change. A possible use as a sensor or drug delivery system was proposed and the performed cytotoxicity tests supported this claim by a proof of the biocompatibility.

A similar benzyl based bis-oxazoline was used by our group in 2014 to produce POx hydrogels in a one-pot reaction utilizing microwave-assisted reaction conditions.<sup>37</sup> The networks, mainly consisting of PEtOx, were investigated for their ability to



Scheme 2 Different synthetic strategies leading to POx derived chemical cross-linked networks. (1) Bis-functional monomers, (2) macro-monomer method and (3) side-/end-group functionalization.

stabilize the highly labile coagulation Factor FVIII in aqueous solution revealing a significant increase of the half life time of the protein by incorporation within the gels.

Schenk and co-workers reported the synthesis of networks consisting of EtOx, 2-nonyl-2-oxazoline (NonOx), and 2-(dec-9-enyl)-2-oxazoline (DecEnOx) as a functional handle connected by an aliphatic bis-2-oxazoline (Scheme 3).<sup>38</sup> Labelling was accomplished by end-capping using a fluorescein derivative. The swelling of the gels could be controlled by varying the composition between the hydrophilic and hydrophobic monomers and a change in the degree of cross-linking.

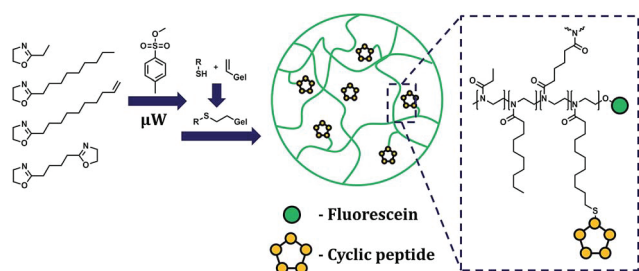
After grinding the gels to particles with a diameter larger than 1  $\mu\text{m}$ , the functional DecEnOx was used to attach an RGD-peptide sequence to the networks *via* thiol-ene chemistry. The particles were incubated with cancer and non-cancer cells showing a high affinity of attachment to cancerous cells, making this system a potential drug carrier for cancer treatment.

In 2003 Rueda *et al.* used multivalent initiators consisting of copolymers of methyl methacrylate (MMA) and chloromethyl styrene to form gel structures.<sup>39</sup> CROP was carried out in the presence of an aliphatic bis-oxazoline. This approach allows reduction of the ratio of the cross-linker to initiator to below 1, still forming stable structures with rigid hydrophobic domains. Two years later the same authors described the incorporation of a second, hydrophobic monomer (NonOx) to alter the hydrophilicity of the networks as determined by swelling experiments in different solvents.<sup>40</sup> An overview of POx gels produced using bis-functional oxazolines is given in Table 1.

### Hydrogels from POx macro-monomers

The second strategy, which leads to covalently stabilized POx networks, is the so-called macro-monomer method. The introduction of polymerizable groups such as (meth)acrylic units results in  $\alpha$ -, and/or  $\omega$ -end functionalized POx, which can be used as a macro-monomer and cross-linker in a second polymerization reaction, respectively. Gels produced by this method are summarized in Table 2.

The first example of a hydrogel produced using this technique was described in 1992 by Uyama *et al.*<sup>41</sup> The use of 2-isopropyl-oxazoline (iPrOx) resulted in polymers which possess a cloud point behavior in aqueous solution at 36  $^{\circ}\text{C}$ . To create



Scheme 3 Hydrogels containing hydrophilic and hydrophobic monomers, peptide functionalization and dye labelling (reproduced from Schenk *et al.*<sup>38</sup>).

Table 1 POx-hydrogels produced by the polymerization of multivalent monomers

Year	Author	Cross-linker	Monomers
1989	Chujo <i>et al.</i> <sup>34</sup>		
1990	Chujo <i>et al.</i> <sup>35</sup>		
2003	Rueda <i>et al.</i> <sup>39</sup>		
2005	Rueda <i>et al.</i> <sup>40</sup>		
2011	Kelly <i>et al.</i> <sup>36</sup>		
2014	Schenk <i>et al.</i> <sup>38</sup>		
2014	Hartlieb <i>et al.</i> <sup>37</sup>		

macro-monomers, the living polymer chains were end-capped with a primary amine bearing a styryl moiety, established by Kobayashi *et al.*<sup>42</sup> This mono-functional macro-monomer and ethyleneglycol bis-methacrylate were polymerized to yield hydrogels with a temperature dependent swelling degree (20 to 40  $^{\circ}\text{C}$ ).<sup>41</sup>

While in this first publication, the POx-based networks were cross-linked by a bifunctional PEG, the synthesis of hydrogels entirely consisting of POx was reported in 1997 by Christova and co-workers.<sup>43</sup> 1,4-Dibromo-2-butene was used as a bis-functional initiator to synthesize telechelic POx with acrylic acid end-groups. In a second step, the macro-cross-linker was polymerized in a free radical process initiated by either UV light or thermal activation. This concept was used to fabricate segmented polymer networks with methyl methacrylate (MMA) as the co-monomer.<sup>44</sup> Using thermal analysis, the morphology of the created systems was investigated with the conclusion that the gels resemble immobilized non-equilibrium systems, which would phase separate into a PMMA and a POx phase if not cross-linked.

Further work on these systems was conducted in 2003 to create thermo-responsive POx networks.<sup>45</sup> PETox-based macro-cross-linkers were copolymerized with different acrylic monomers, namely MMA, 2-hydroxypropyl acrylate (HPA), and 2-hydroxyethyl methacrylate (HEMA). A phase transition of the networks took place at temperatures between 46 and 56  $^{\circ}\text{C}$  depending on the co-monomer and composition. Repetitive swelling and deswelling proved the reversibility of this stimuli responsiveness. 10 years later this concept was used to create hydrogels, which were able to release ibuprofen in a controlled way over different time periods.<sup>46</sup> The combination of POx with either HPA or HEMA resulted in gels with a temperature dependent water uptake. All reported structures doubled their swelling degree upon heating from 20 to 37  $^{\circ}\text{C}$ . Up to 77 wt% Ibuprofen was incorporated into the networks by swelling in an



Table 2 POx hydrogels synthesized by the macro-monomer method

Year	Author	Network components
1992	Uyama <i>et al.</i> <sup>41</sup>	
1997	Christova <i>et al.</i> <sup>43</sup>	
2002	Christova <i>et al.</i> <sup>44</sup>	
2002	Wang <i>et al.</i> <sup>47</sup>	
2003	Christova <i>et al.</i> <sup>45</sup>	
2003	Rueda <i>et al.</i> <sup>48</sup>	
2004	Kim <i>et al.</i> <sup>55</sup>	
2006	David <i>et al.</i> <sup>50,56</sup>	
2006	Kim <i>et al.</i> <sup>54</sup>	
2008	David <i>et al.</i> <sup>49,51</sup>	
2013	Kostova <i>et al.</i> <sup>46</sup>	

Table 2 (Contd.)

Year	Author	Network components
2014	Rueda <i>et al.</i> <sup>52</sup>	
2014	Zhu <i>et al.</i> <sup>53</sup>	

ethanol solution of the drug. The *in vitro* release of the molecule could be delayed significantly (40 to 100% within 15 h) and was dependent on the gel composition.

The combination of POx with poly(lactic acid) (PLA) was demonstrated by Wang *et al.*<sup>47</sup> The structure of the oxazoline based component was similar to the ones presented by Christova earlier, except that EtOx was the only monomer used and the polymerizable end-groups were introduced in a post polymerization reaction by esterification of the terminal hydroxyl groups. The second macro-cross-linker was obtained from a tri-functional initiator (glycerol), which was used to polymerize D,L-lactide with terminal OH-groups which were also converted into polymerizable groups by esterification with methacrylic acid. Radical polymerization of a 30 wt% polymer solution with varying contents of the POx macro-cross-linker resulted in hydrogels with temperature (transition between 20 and 40 °C) and pH value (5 to 10) responsive swelling. The latter was ascribed to the quaternization of the amide function of the POx, however, this assumption was not proven.

Rueda *et al.* demonstrated the synthesis of PMeOx cross-linkers bearing styrenic end-groups.<sup>48</sup> To produce  $\alpha,\omega$ -functionalized POx the authors did not use a bis-functional initiator but initiated the polymerization with iodomethyl styrene and introduced the second styrene group by end-capping with a styrene modified piperazine. This cross-linker was subsequently homo- or copolymerized with *N*-vinyl pyrrolidone (NVP) to yield non-ionic polymer networks. The swelling of these gels in water and organic solvents (methanol, DMF, chloroform) was studied and the structure of the hydrogels was confirmed using solid-state NMR spectroscopy.

The combination of POx macro-monomers with thermo-responsive *N*-isopropylacrylamide (NiPAAm) was demonstrated by David and co-workers in 2008.<sup>49</sup> Two different cross-linkers derived from POx were used to obtain networks: unsaturated polyester type structure<sup>50</sup> and a bis-functional POx with cinnamic acid as polymerizable end-groups, which was described before by the same group.<sup>51</sup> A further variation was conducted

by applying a precipitation polymerization method to generate microgels in the size range of 30 to 200 nm. These colloidal particles aggregated during drying to form porous gel structures with channels of 5 to 10  $\mu\text{m}$  diameter. Depending on the composition of the networks, a shrinkage upon heating was detected in the range from 28 to 38  $^{\circ}\text{C}$ . This behavior was utilized to release bovine serum albumin (BSA) as a model drug when heating the loaded gels from 10 to 37  $^{\circ}\text{C}$ .

The combination of POx with NiPAAM was also described by Rueda *et al.* in 2014.<sup>52</sup> Macro-monomers consisting of MeOx and a methoxy carbonyl substituted 2-oxazoline were synthesized using iodomethyl styrene as the initiator. Subsequent hydrolysis yielded carboxy functionalized macro-monomers, which were polymerized with NiPAAM and a bis-acrylic cross-linker *via* radical polymerization. The swelling of these systems was shown to be dependent on the temperature (due to the LCST behavior of the NiPAAM component) and on the pH range (due to the carboxylic functions of the POx segment).

The combination of PMeOx with poly(dimethyl siloxane) (PDMS) to create macro-monomers was reported by Zhu *et al.* in 2014.<sup>53</sup> PMeOx (*ca.* 1000  $\text{g mol}^{-1}$ ) was functionalized with an isocyanide group, and, in a second step, with PDMS. The left-over OH end-group of the siloxane polymer was used to introduce a methacrylic group resulting in a PMeOx-*b*-PDMS macro-monomer.

The UV induced polymerization with a second silyl type acrylic monomer and triethylene glycol dimethacrylate as a cross-linker resulted in hydrogels with different ratios of POx. Since the focus of the work was to synthesize materials for contact lenses, transmittance, mechanical properties as well as ion diffusion were investigated and found to be suitable for application in ophthalmology. Also, the material had a decreasing protein adsorption when more POx copolymer was incorporated. However, the ratio between PDMS and POx was equal for all samples which prohibits a final conclusion about the role of the two polymers regarding the antifouling properties.

To generate a further variety and alter the properties of POx derived networks it is also possible to introduce a second gel matrix which is cross-linked in a different way. Consecutive cross-linking of the two components in the presence of each other leads to a material that consists of two separate networks which intercalate on a polymer size scale, the so-called interpenetrating polymer network (IPN).<sup>57</sup>

The combination of POx with poly(vinyl alcohol) (PVA) to form such a structure was investigated in 2004 by Kim *et al.*<sup>55</sup> PEtOx macro-monomers were synthesized by initiation with a bis-functional initiator followed by end-capping with MAA. The addition of PVA to the mixture while polymerizing the POx component in a radical process and the cross-linking of the hydroxyl groups in a second step using glutaraldehyde lead to two networks with an entanglement on a polymer scale. The swelling of the resulting films was shown to be dependent on the pH of the surrounding solution (maximum swelling at pH 10), the temperature (slow decrease from 20 to 70  $^{\circ}\text{C}$ ), as well as on the content of PVA in the IPN. Unfortunately, no information regarding the length, end-capping efficiency and purity of the

POx component as well as proof of the absence of phase separation was provided. Therefore, a comparison with other reviewed systems is hardly possible.

A second example of a POx based IPN was presented by David and co-workers.<sup>56</sup> Hydrogels were prepared using a POx macro-cross-linker based on an unsaturated polyester type structure in combination with MMA or HEMA. In contrast to the previous publication these gels were purified and converted to an IPN by swelling in the corresponding OH-functionalized polysiloxane, which was cross-linked subsequently. Also poly(urethane)s were used to create semi-IPNs.

The combination of POx with polysaccharides to form IPNs was demonstrated by Kim *et al.* in the same year.<sup>54</sup> Besides the already well described EtOx based macro-cross-linker with telechelic methacrylic end groups, chitosan was used to form a second network. A mixture of the POx macro-cross-linker and chitosan was, in a first step, treated with AIBN to induce a radical polymerization of the POx component. Subsequently, the polysaccharide was cross-linked using glutaraldehyde. The degree of swelling of the IPN showed a strong dependence on the pH value. While at low pH values (2 and 4) the protonated amine groups induced a high water uptake, pH values above 7 resulted in minor swelling.

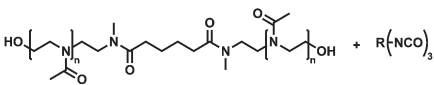
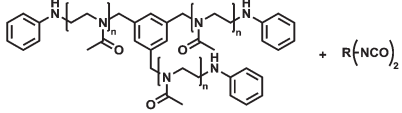
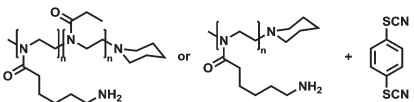
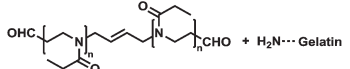
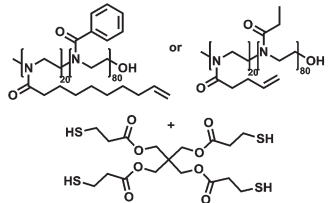
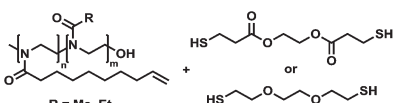
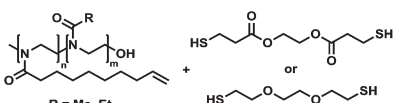
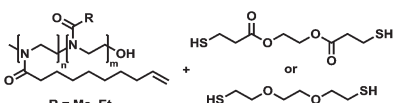
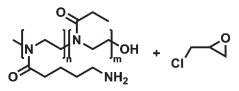
### Gels cross-linked *via* end-group functionalization

The last subchapter is dedicated to a particular end-capping strategy and the formation of hydrogels *via* radical polymerization. However, the versatility of the CROP of 2-oxazolines enables the incorporation of not only (meth)acrylic units but also other end-groups, which can allow further functionalization and polymerization, respectively. An overview of hydrogels prepared by conversion of functional side- and end-groups is presented in Table 3.

The first example of such a POx based hydrogel was given by Park and co-workers in 1991.<sup>58</sup> The authors used 2,2'-tetramethylene bis-2-oxazoline, which was described above as a cross-linker monomer for CROP, and transformed it into its bis-oxazolinium species using two equivalents of methyl tosylate, which was used to polymerize MeOx with two growing chain ends. Quenching of the polymerization led to telechelic hydroxyl-functionalized macromolecules, which were gelled by conversion with tri-functional isocyanides. The swelling degrees of these polyurethane-like hydrogels in water and organic solvents were studied intensively based on the length of the POx and on the ratio and structure of the cross-linker.

A similar approach was described one year later by Chujo *et al.*<sup>59</sup> The POx component of the networks was polymerized using a tri-functional benzylic initiator with iodide or tosylate as the leaving group. The termination with benzylamine yielded POx stars with secondary amine groups on each chain end, which were then cross-linked using bis-functional isocyanides. Unfortunately, no analytical data on the star-shaped polymers were provided. However, the degree of functionalization ranging between 0.56 and 0.82 indicates an incomplete growth of the star arms. Also the precursor polymer with the highest degree of functionalization, in contrast to the others, did not

Table 3 POx hydrogels based on end- and side-group linkage

Year	Author	Network components
1991	Park <i>et al.</i> <sup>58</sup>	
1992	Chujo <i>et al.</i> <sup>59</sup>	
2006	Cesana <i>et al.</i> <sup>61</sup>	
2008	Rathna <sup>60</sup>	
2012	Schenk <i>et al.</i> <sup>64</sup>	
2012	Dargaville <i>et al.</i> <sup>65</sup>	
2013	Farrugia <i>et al.</i> <sup>63,66</sup>	
2013	Hartlieb <i>et al.</i> <sup>20</sup>	
2014	Hartlieb <i>et al.</i> <sup>62</sup>	

form a network, which was not adequately clarified in the publication.

The conversion of terminal hydroxyl end-groups of POx to aldehyde groups was demonstrated by Rathna in 2008.<sup>60</sup> 1,4-Dibromo butane served as an initiator to synthesize PEtOx chains with  $\alpha,\omega$ -hydroxyl end-groups which were oxidized with acetic anhydride to aldehydes. Schiff-base formation with gelatine followed by reductive amination resulted in networks, which were analysed for their swelling behavior depending on the composition and the pH value (4.5 vs. 7.4). Chlorhexidine was loaded into the hydrogels as a model substance for drug delivery applications and released into aqueous medium revealing a much faster release profile at low pH values compared to neutral water.

### Gels cross-linked *via* side-group functionalization

The introduction of functional end-groups in an initiation-termination fashion is a popular approach to synthesize POx, which can be polymerized and functionalized to obtain hydrogels. However, there are also obvious limitations of this approach. If multiple polymerizable groups are required, the polymeric architecture has to become more complex and is,

therefore, hard to control. Alternatively, CROP allows incorporation of functional repeating units into the polymer using functional 2-oxazoline monomers. Thus, the degree of functionalization is only limited by the degree of polymerization. In 2006 Cesana *et al.* were the first to use such an approach for the production of hydrogels.<sup>61</sup> The authors synthesized POx with amino side chains *via* the polymerization of a Boc-protected monomer. Copolymerization with EtOx yielded statistical copolymers, which were further functionalized or cross-linked. The conversion with iso-thiocyanates was demonstrated using a fluorescein derivative. Benzyl bis-isothiocyanate was used to cross-link the polymers covalently. However the resulting networks were not studied in detail.

This work was continued by our group in 2013. A similar Boc protected monomer and the respective statistical copolymers were prepared.<sup>20</sup> Cross-linking with epichlorhydrin led to hydrogels bearing primary, secondary and tertiary amino groups, which were then used to bind genetic material and release it again upon the addition of heparin. To improve their mechanical stability the amine containing gels were incorporated into porous filter substrates.<sup>62</sup> Due to the LCST of the precursor polymers in basic aqueous solution the resulting hydrogels showed a bead-like structure with an improved surface-to-volume ratio.

It was demonstrated that this network exhibits potential for DNA purification applications. DNA was entrapped and released by heparin, and could be amplified after the release by the polymerase chain reaction.

Another method for the gelation of POx was demonstrated in 2012 by Schenk *et al.* using the thiol-ene reaction to cross-link alkenyl side-chains containing POx with a tetra functional thiol.<sup>64</sup> The system was used as a photoresist for photolithography. For this purpose, the linking process was performed in the solid state after spin coating of a polymer/thiol mixture by UV irradiation.

A similar approach was reported by Dargaville *et al.* to produce hydrogel structures.<sup>65</sup> Copolymers prepared from DecEnOx and MeOx or EtOx were cross-linked *via* a UV-induced thiol-ene reaction with difunctional thiols. Tunable water swellable networks were obtained, and MeOx-based systems were found to show increased swelling degrees compared to the EtOx-based systems. The same group used this approach to create polymer networks, which are cell compatible and can be used as material for tissue engineering.<sup>63,66</sup> To this end, the P(MeOx-*stat*-DecEnOx) copolymer was functionalized with an RGD peptide in a first step and, subsequently, cross-linked using a dithiol (Fig. 1). To decrease the toxic effect of the photoinitiator required for cross-linking, its minimum amount was determined in a kinetic study. Hydrogels with an RGD peptide enabled the attachment of human fibroblast to the hydrogel surface, whereas no peptide functionalization resulted in cell repulsion. Furthermore, cells were encapsulated inside the hydrogel by mixing them within the hydrogel precursor mixture and exposing them to UV light. RGD functionalized hydrogels improved the cell survival compared to the non-functionalized ones.



### Gels *via* hydrolyzation and functionalization of POx

A different way to introduce functional groups into the side-chain of POx is the partial or full hydrolysis to yield POx-polyethylene imine copolymers (P(Ox-*stat*-EI)) and the subsequent conversion of the secondary amines. The advantage this method bears is the high versatility since the final functional group does not interfere with the polymerization process, enabling a large variety of nucleophiles to be attached. Drawbacks are the lack of selectivity and control of the hydrolysis process producing only statistical copolymers with a degree of functionalization which is hard to predict. Also the efficiency of the functionalization reaction of the polymer analogue displays a limitation of this strategy. The hydrolysis of POx can be achieved either under acidic or basic conditions. The use of acids generally yields higher degrees of hydrolyzation up to a quantitative abstraction of the side group and can be accelerated by the use of microwave assisted synthesizing technology.<sup>67</sup> Networks synthesized using partially or fully cleaved POx are summarized in Table 4.

The first network derived from partially hydrolysed POx was introduced by Chujo *et al.* in 1989.<sup>68</sup> By varying the amount of base and the reaction time it was possible to produce polymers having 2.5 to 25% cleaved side chains. The cross-linking of these precursors was achieved using a bis-isocyanate while working in bulk. In solution (dimethyl formamide) the linking process was carried out with a bis-functional acid chloride. The resulting networks showed a water swelling behavior based on the linking density which decreased significantly in aqueous salt solutions indicating the existence of ionic groups (remaining amino functions) in the gels after gelation. Consumption of the amines by applying an excess of ethyl-isocyanide led to negation of this effect.

A second example was published one year later using Diels-Alder chemistry for the cross-linking process.<sup>69</sup> While working on a similar range of free secondary amino groups, the method of gel formation was changed. In contrast to the previous work, the consumption of the PEI units was used to create functional polymers which were subsequently cross-linked in a second step. Two POx derivatives with either furan or maleimide side chains were created and mixed in equimolar quantities. The

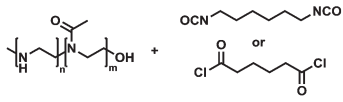
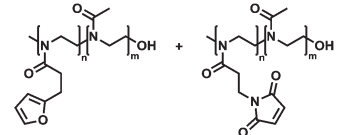
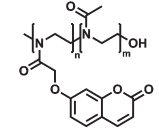

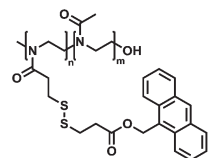
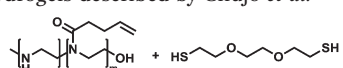
linking was achieved in bulk over seven days and it was shown that by applying retro Diels Alder conditions a full degelation of the system was possible.

A further contribution of the group of Saegusa to this particular field of POx gels was reported in the same year when coumarin was introduced as a photo-cross-linkable unit.<sup>70</sup> By using POx-*co*-PEI with up to 30% of hydrolysis the coumarin moieties were coupled *via* the reaction of an attached acid group, mediated by a carbodiimide. The photo-gelation was achieved by irradiation of the bulk polymer at >310 nm and was shown to be partially reversible by the cleavage at 253 nm with up to 60% efficiency.

In 1993 this concept was expanded to di-thiol based cross-linkers which were introduced in two separate ways.<sup>71</sup> For the first method a bis-isocyanate compound containing a S-S bridge was protected on only one side with an anthracene moiety while the other side was attached to partially hydrolyzed POx as described before. Under reductive conditions the anthracene was cleaved and the polymer gelled under the presence of oxygen in the bulk state. The second method involves the direct cross-linking using the bis-acid compound mentioned before. The formed networks could be cleaved again under reductive conditions within one day. It was also shown that the swelling of the gels decreased with the proceeding reaction time of the reduction.

The above-mentioned anthracene protected POx was also gelled photochemically using light induced photo-dimerization

Table 4 Hydrogels containing partially or fully hydrolysed POx

Year	Author	Network components
1989	Chujo <i>et al.</i> <sup>68</sup>	
1990	Chujo <i>et al.</i> <sup>69</sup>	
1990	Chujo <i>et al.</i> <sup>70</sup>	
1993	Chujo <i>et al.</i> <sup>71</sup>	
1993	Chujo <i>et al.</i> <sup>72</sup>	
1999	Zewert <i>et al.</i> <sup>73</sup>	Hydrogels described by Chujo <i>et al.</i> <sup>68,69,71</sup>
2014	Englert <i>et al.</i> <sup>74</sup>	

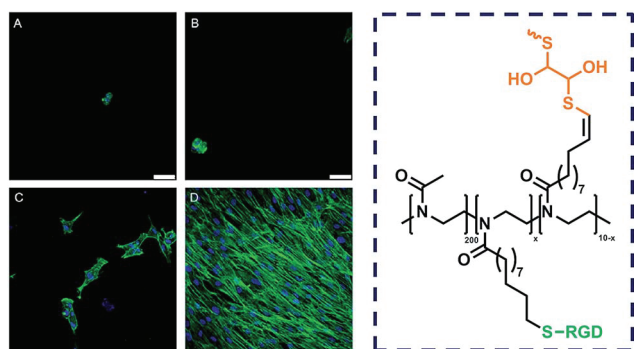


Fig. 1 Fibroblast growth in double bond containing POx networks (A) functionalized with either mercaptanol (B), an RDG- (C) or an RGD-peptide (D) (Reproduced from Farrugia *et al.*<sup>63</sup>).

of the anthracene moiety.<sup>72</sup> Also these gels were shown to be degradable under reductive conditions and the initial polymers could be isolated after the reaction with a small organic thiol.

Some of the above-mentioned systems were investigated to be used as gel electrophoresis matrices in 1999.<sup>73</sup> The authors found the Diels–Alder based gelation process most promising for application in the lab and pointed out the increased stability in comparison to conventional poly(acrylamide) gels.

The latest example of a hydrogel originating from hydrolysed POx was published by our group in 2014. Fully hydrolysed PEOx was partially reacted with an activated acid bearing a double bond to create statistical POx–PEI copolymers. Cross-linking was achieved *via* the thiol-ene reaction of the polymeric precursor with a bis-thiol under UV irradiation. The variation of the PEI content and, hence, the degree of cross-linking was used to adjust the swelling degree and the affinity to DNA. It was shown that these hydrogels were able to bind and release DNA which makes them an interesting material for the purification of genetic material from biological samples.<sup>74</sup>

### Cross-linked self-assembled structures

Micelles are highly interesting materials, *e.g.* for (nano) medical, pharmaceutical and diagnostic applications. The self-assembly of amphiphilic block- or graft-copolymers has been studied intensively during the last decades.<sup>75</sup> In water, the hydrophobic part self-assembles and forms the core of the micelles while the hydrophilic part constitutes the shell. The core compartments can be applied for the encapsulation of hydrophobic cargo, which is protected by the hydrophilic shell.<sup>76</sup> The latter also provides colloidal stability and depending on the material used can lower or prevent unspecific adsorption of proteins, which is of high importance when applied as a drug carrier.<sup>77</sup> However, micelles exhibit a critical micelle concentration, *i.e.* micelles are in equilibrium with non-associated polymer chains, which can be shifted towards the latter upon high dilution.<sup>78</sup> This fact needs to be considered, in particular, *e.g.* for intravenous injections of micellar systems. Thus, to prevent disassembly of the micelles they need to be stabilized. This is typically achieved by chemical cross-linking of the core and shell, respectively (Scheme 4).<sup>79</sup> During the last decades numerous studies described the self-assembly of diblock and triblock (ter)poly(2-oxazoline)s.<sup>80,81</sup> However, only a limited number of reports demonstrated the fabrication of cross-linked POx micelles (Table 5).

In 2006 Huang *et al.* studied the self-assembly behavior of a soy bean-based diblock POx in aqueous solution.<sup>82</sup> The micelles formed were further cross-linked by UV irradiation and exhibited reversible morphological transitions when transferred from water into acetone.

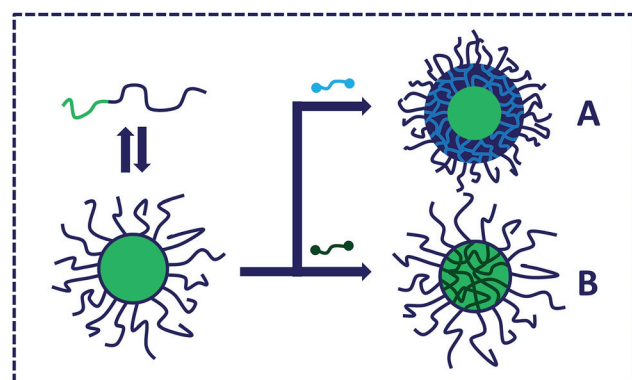
In 2010 ten Brummelhuis and Schlaad described the synthesis and self-assembly of poly(2-(3-butynyl)-2-oxazoline)-*b*-PEtOx in aqueous solution.<sup>83</sup> The authors simultaneously cross-linked and functionalized the micelles by radical thiol-ene chemistry, which resulted in the formation of stimuli-responsive micelles. The systems showed a cloud point temperature between 48 and 82 °C depending on the ionic strength and the nature of the ion.

Liu *et al.* demonstrated the application of cross-linked triblock POx micelles as a support structure for Co(III)–salen complexes and their high catalytic activity for the hydrolysis of epoxides.<sup>84</sup> The triblock copolymer was obtained by microwave-assisted CROP and consisted of 2-methyl-2-oxazoline as the hydrophilic component and a cinnamate containing monomer and methyl 3-(oxazol-2-yl)pentanoate as a cross-linkable and functionalizable block, respectively (Fig. 2). The Co(III)–salen complex was introduced in a post-polymerization fashion by deprotection and esterification of the carboxylic acid groups of the hydrophobic block. In contrast to non-cross-linked micelles, the nanogels showed a remarkable substrate selectivity, which the authors ascribed to the limited substrate permeability in case of the cross-linked micelles. Furthermore, the high stability of the micelles allowed them to be reused for eight catalytic cycles.

Zschoche *et al.* used two different graft copolymers for the synthesis of core-shell nano-gels. First, they reported the stabilization of poly(NiPAAm-*graft*-EtOx) micelle-like aggregates by electron-beam irradiation and their temperature-responsive swelling behavior.<sup>85</sup> In a later study the authors used 2-carboxyethyl-2-oxazoline to prepare the graft polymers.<sup>86</sup> The respective cross-linked micelles exhibited temperature and pH-responsive properties.

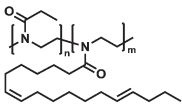
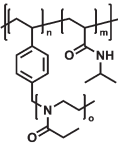
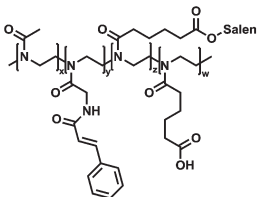
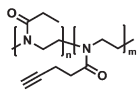
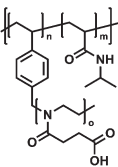
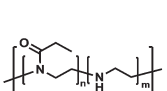
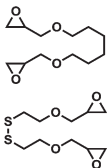
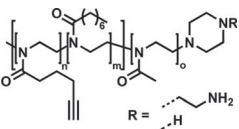
The fabrication of pH and redox-responsive nano-gels based on the functionalization of partially hydrolyzed PEOx was reported by Legros *et al.*<sup>87</sup> The nano-materials were either obtained by cross-linking of the secondary amine groups of the polymer backbone with 1,6-hexanediol di-glycidyl ether in dilute media or by an inverse emulsion process with 1,6-hydroxyethyl disulfide-bis-di-glycidyl ether as the cross-linker. The latter contains a disulfide bond, which is susceptible to redox changes. Furthermore, all nanogels prepared showed a pH-responsiveness due to the remaining secondary amine groups in the polymer.

In 2013, Engelhardt *et al.* presented a further POx nano-gel, produced from block copolymers having PMeOx as hydrophilic segment and a mixture of 2-(pent-4-ynyl)-2-oxazoline and 2-heptyl-2-oxazoline as core forming block.<sup>88</sup> The polymerization was end-capped by piperazine to introduce a secondary amine



Scheme 4 Nano-gels by self-assembly of block copolymers and subsequent cross-linking of the core (A) or the shell (B).

Table 5 Chemically cross-linked POx-based micelles and nanogels

Year	Author	Polymer precursor	Cross-linking
2006	Huang <i>et al.</i> <sup>82</sup>		UV irradiation
2010	Zschoche <i>et al.</i> <sup>85</sup>		Electron-beam irradiation
2011	Liu <i>et al.</i> <sup>84</sup>		UV irradiation
2011	ten Brummelhuis <i>et al.</i> <sup>83</sup>		Thiols, UV irradiation
2012	Zschoche <i>et al.</i> <sup>86</sup>		Electron-beam irradiation
2013	Legros <i>et al.</i> <sup>87</sup>		
2013	Engelhardt <i>et al.</i> <sup>88</sup>		UV irradiation

group at the chain-end, which was additionally converted into a primary amine by the use of hydrazine. Core-cross-linking was accomplished by UV irradiation and the nano-gels were reacted with different aromatic compounds as a proof of concept for a surface modification of the nanostructures.

### Hydrogel poly(2-oxazoline) capsules *via* templated assembly

Layer-by-layer (LbL)-templated polymer capsules have attracted increasing interest in the field of nano-medicine due to the ease in accessing smart polymeric carriers with tunable properties.<sup>89,90</sup> Physical and chemical properties can be altered by the choice of the template, the assembly conditions, and the material interactions.<sup>91</sup> Hydrogen bonding assembled films are of particular interest because, unlike electrostatically assembled films, they can be designed to be charge neutral and

responsive to biological triggers. Hydrogen bonding multilayer films are obtained by the alternate deposition of hydrogen bonding acceptors (*e.g.* poly(ethylene glycol), and poly(*N*-vinylpyrrolidone)) and donors (*e.g.* poly(methacrylic acid) (PMAA), and poly(acrylic acid)).<sup>92</sup> However, the pH range in which stable films can be formed is limited and depends on the pK<sub>a</sub> of the polymers and the interaction between the hydrogen bonding pair. To prepare (single-component) hydrogen bonding polymeric nano-/microcapsules, which are stable in the physiological range (pH 6 to 8) after template removal, the layers have to be covalently cross-linked (Scheme 5).

Recently, POx was applied for the preparation of hydrogen-bonded multilayer films with tannic acid as the hydrogen bonding donor to form two-component multilayer films, which are stable in a wide pH range.<sup>93,94</sup> Furthermore, the interaction between functional POx and PMAA was exploited for the assembly of low-fouling degradable polymer capsules. As demonstrated by Kwon *et al.* POx are excellent hydrogen bonding acceptors, and can form a hydrogen bonding pair with, *e.g.* PMAA at low pH values (pH < 5).<sup>95</sup> To create POx based capsules using this effect, linear and brush-like POx were synthesized by CROP and RAFT polymerization, respectively, and endowed with different cross-linkable moieties.<sup>96</sup> After (POx/PMAA) multilayer assembly onto silica particle templates, the films were stabilized by thiol-ene chemistry (linear POx) or copper-catalyzed azide-alkyne cycloaddition (brush-like POx) and the template was removed using hydrofluoric acid. Both linear and brush-like POx capsules exhibited low-fouling properties as demonstrated by low adsorption of two model proteins, namely bovine serum albumin (BSA) and lysozyme. The potential of (brush-like) POx capsules was further exploited for the fabrication of redox-responsive systems.<sup>97</sup> To this end, oligo(2-ethyl-2-oxazoline) methacrylate was copolymerized with glycidyl methacrylate (GMA) *via* ATRP. Pendant thiol moieties were introduced by the ring-opening reaction of the GMA repeating units with an amine-containing disulfide linker. Prior to the layering process the disulfide bonds were reduced to free thiols. Hydrogen bonding LbL assembly between the thiol-containing POx and PMAA on planar and particular supports yielded stable disulfide cross-linked multilayer films (Fig. 3). The redox-responsive capsules obtained are degradable under reducing conditions both in a simulated biological environment (pH 5.9, 5 mM glutathione) and intracellularly, where capsules were found to disintegrate into polymer fragments. Furthermore, incubation of the planar stabilized films in full human serum demonstrated the low-fouling properties of both brush-like POx films.

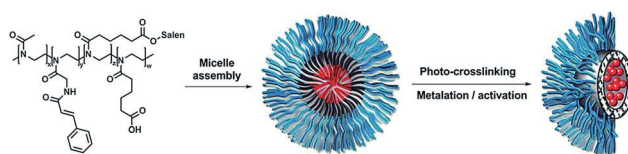
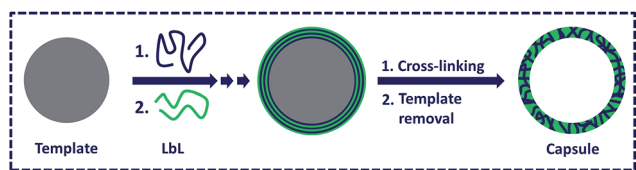


Fig. 2 Schematic representation of the synthesis of poly(2-oxazoline) shell cross-linked micelles with Co(III)-salen-functionalized cores (reproduced from Liu *et al.*<sup>84</sup>).





Scheme 5 Schematic representation of the assembly of polymeric capsules in a LbL approach with subsequent template removal.

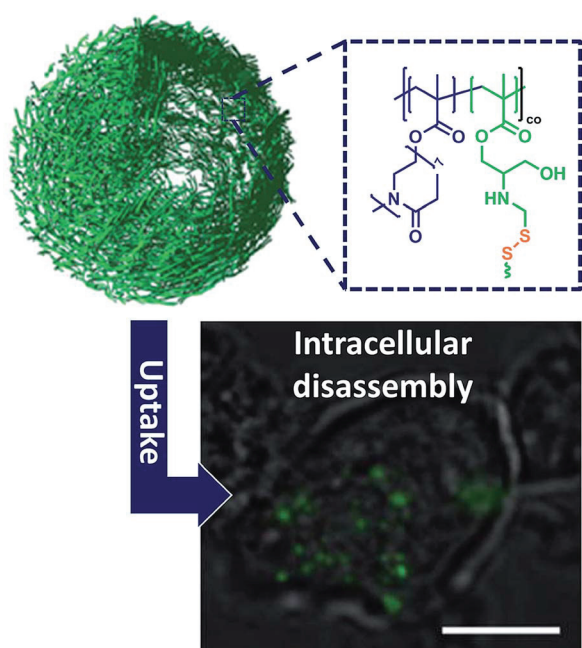


Fig. 3 Schematic representation of (brush-like) POx capsules stabilized by disulfide chemistry and their disassembly in an intracellular reducing environment (reproduced after Kempe *et al.*<sup>97</sup>). Scale bar: 10  $\mu\text{m}$ .

### 3. Conclusions

Poly(2-oxazoline)s combine beneficial biocompatibility and stealth properties with multi-functionality, which make them perfectly suitable for the fabrication of smart materials for a wide range of applications in bio-medicine. The microwave assisted cationic ring-opening polymerization of 2-substituted 2-oxazolines enables the synthesis of polymers with tailored properties due to the living character of the polymerization. The introduction of functionalities into the polymer system by selection of appropriate initiator and termination agents as well as monomers provides the polymers with further post-polymerization modification possibilities. In this review special focus is laid on the potential of POx for the preparation of covalently cross-linked systems, including hydrogels, micelles and hydrogel LbL capsules.

POx hydrogels can be prepared in numerous ways, including the utilization of multifunctional 2-oxazoline monomers and macro-monomers with polymerizable groups, as well as the cross-linking of functional end- and side-groups in efficient

modification reactions. The ease of tuning the hydrophilicity of the POx system by copolymerization of hydrophilic and hydrophobic monomers and the cross-linking density enables the adjustment of the swelling characteristics of the hydrogels, which is particularly beneficial for drug delivery or tissue engineering applications, for example for the sustained release of small molecules. Moreover, smart hydrogels, which change their degree of swelling on demand, can be produced by utilizing environmental responsive POx, containing *e.g.* iPrOx (for a temperature response) or carboxylic oxazoline (for a pH response). But also the combination with well-described non-POx systems such as PNiPAAm or PAA is realizable in a straightforward manner using the macro-monomer method. Other examples of responsive POx hydrogels are systems which cross-link and dissolve in response to light (*e.g.* anthracene dimerization), temperature (Diels–Alder chemistry), electrical current (*e.g.* throughout local pH effects) and a reductive environment (*e.g.* due to S–S bond containing cross-linkers). However, only a minor fraction of the presented reports demonstrates the potential of POx hydrogels for biological applications.

This slightly changes when it comes to nano-gels. Covalently stabilized nanostructures, such as reversibly cross-linked micelles or capsules, exhibit a tremendous potential for drug delivery applications as they can be designed to completely disassemble on demand.<sup>98</sup> In order to obtain nano-carriers, which are stable within the blood stream, a combination of covalent cross-linking and shielding against unspecific interactions using PMeOx or PETOx can be utilized. Generally, reversible cross-linking should be favoured over irreversible cross-linking as it endows the carrier with the desired release properties.

In conclusion, several excellent studies have emphasized the potential of covalently cross-linked POx systems and first reports have demonstrated their application in the drug delivery and tissue engineering area. However, further efficient cross-linking reactions should be utilized for the preparation of covalently cross-linked POx systems. More elaborate biological studies *in vitro* and *in vivo* are necessary to prove and evidence the potential of POx systems.

### Acknowledgements

We thank the Bundesministerium für Bildung und Forschung (Germany) for funding (project: BASIS, 03WKCB01C). Kristian Kempe acknowledges the Alexander von Humboldt-foundation for a Feodor-Lynen fellowship.

### References

- 1 H. Jin, W. Huang, X. Zhu, Y. Zhou and D. Yan, *Chem. Soc. Rev.*, 2012, **41**, 5986–5997.
- 2 H. Schlaad, C. Diehl, A. Gress, M. Meyer, A. L. Demirel, Y. Nur and A. Bertin, *Macromol. Rapid Commun.*, 2010, **31**, 511–525.
- 3 R. Hoogenboom and H. Schlaad, *Polymers*, 2011, **3**, 467–488.

- 4 R. Luxenhofer, G. Sahay, A. Schulz, D. Alakhova, T. K. Bronich, R. Jordan and A. V. Kabanov, *J. Controlled Release*, 2011, **153**, 73–82.
- 5 L. Tauhardt, K. Kempe, M. Gottschaldt and U. S. Schubert, *Chem. Soc. Rev.*, 2013, **42**, 7998–8011.
- 6 K. Knop, R. Hoogenboom, D. Fischer and U. S. Schubert, *Angew. Chem., Int. Ed.*, 2010, **49**, 6288–6308.
- 7 T. Kagiya, S. Narisawa, T. Maeda and K. Fukui, *J. Polym. Sci., Part B: Polym. Lett.*, 1966, **4**, 441–445.
- 8 W. Seeliger, E. Aufderhaar, W. Diepers, R. Feinauer, R. Nehring, W. Thier and H. Hellmann, *Angew. Chem.*, 1966, **78**, 913–927.
- 9 D. A. Tomalia and D. P. Sheetz, *J. Polym. Sci., Part A: Polym. Chem.*, 1966, **4**, 2253–2265.
- 10 T. G. Bassiri, A. Levy and M. Litt, *J. Polym. Sci., Part B: Polym. Lett.*, 1967, **5**, 871–879.
- 11 F. Wiesbrock, R. Hoogenboom, C. H. Abeln and U. S. Schubert, *Macromol. Rapid Commun.*, 2004, **25**, 1895–1899.
- 12 K. Kempe, C. R. Becer and U. S. Schubert, *Macromolecules*, 2011, **44**, 5825–5842.
- 13 N. Adams and U. S. Schubert, *Adv. Drug Delivery Rev.*, 2007, **59**, 1504–1520.
- 14 B. Guillermin, S. Monge, V. Lapinte and J.-J. Robin, *Macromol. Rapid Commun.*, 2012, **33**, 6000–6016.
- 15 R. Hoogenboom, in *Handbook of Ring-Opening Polymerization*, Wiley-VCH Verlag GmbH & Co. KGaA, 2009, pp. 141–164.
- 16 L. Tauhardt, M. Frant, D. Pretzel, M. Hartlieb, C. Bucher, G. Hildebrand, B. Schroter, C. Weber, K. Kempe, M. Gottschaldt, K. Liefelth and U. S. Schubert, *J. Mater. Chem. B*, 2014, **2**, 4883–4893.
- 17 K. Kempe, R. Hoogenboom, M. Jaeger and U. S. Schubert, *Macromolecules*, 2011, **44**, 6424–6432.
- 18 M. Miyamoto, K. Naka, M. Tokumizu and T. Saegusa, *Macromolecules*, 1989, **22**, 1604–1607.
- 19 K. Kempe, R. Hoogenboom and U. S. Schubert, *Macromol. Rapid Commun.*, 2011, **32**, 1484–1489.
- 20 M. Hartlieb, D. Pretzel, K. Kempe, C. Fritzsche, R. M. Paulus, M. Gottschaldt and U. S. Schubert, *Soft Matter*, 2013, **9**, 4693–4704.
- 21 D. R. Coombe, *Immunol. Cell Biol.*, 2002, **80**, 506.
- 22 J. T. Trevors and G. H. Pollack, *Prog. Biophys. Mol. Biol.*, 2005, **89**, 1–8.
- 23 O. Wichterle and D. Lim, *Nature*, 1960, **18**, 117–118.
- 24 K. Jindrich, *J. Polym. Sci., Part A: Polym. Chem.*, 2009, **47**, 5929–5946.
- 25 K. Skórkowska-Telichowska, M. Czemplik, A. Kulma and J. Szopa, *J. Am. Acad. Dermatol.*, 2013, **68**, e117–e126.
- 26 S. Thirumaleswar, P. K. Kulkarni and D. V. Gowda, *Curr. Drug Ther.*, 2012, **7**, 212–218.
- 27 F. L. Buchholz and N. A. Peppas, *Superabsorbent Polymers: Science and Technology*, Amer Chemical Soc, Washington, DC, 1994.
- 28 M. J. Zohuriaan-Mehr, H. Omidian, S. Doroudiani and K. Kabiri, *J. Mater. Sci.*, 2010, **45**, 5711–5735.
- 29 J. Zhu and R. E. Marchant, *Expert Rev. Med. Devices*, 2011, **8**, 607–626.
- 30 J. J. Simhadri, H. A. Stretz, M. Oyanader and P. E. Arce, *Ind. Eng. Chem. Res.*, 2010, **49**, 11866–11877.
- 31 A. Vashist, A. Vashist, Y. K. Gupta and S. Ahmad, *J. Mater. Chem. B*, 2014, **2**, 147–166.
- 32 D. Buenger, F. Topuz and J. Groll, *Prog. Polym. Sci.*, 2012, **37**, 1678–1719.
- 33 A. M. Kelly and F. Wiesbrock, *Macromol. Rapid Commun.*, 2012, **33**, 1632–1647.
- 34 Y. Chujo, K. Sada, K. Matsumoto and T. Saegusa, *Polym. Bull.*, 1989, **21**, 353–356.
- 35 Y. Chujo, K. Sada, K. Matsumoto and T. Saegusa, *Macromolecules*, 1990, **23**, 1234–1237.
- 36 A. M. Kelly, A. Hecke, B. Wirnsberger and F. Wiesbrock, *Macromol. Rapid Commun.*, 2011, **32**, 1815–1819.
- 37 M. Hartlieb, S. Schubert, K. Kempe, N. Windhab and U. S. Schubert, *J. Polym. Sci., Part A: Polym. Chem.*, 2015, **53**, 10–14.
- 38 V. Schenk, E. Rossegger, C. Ebner, F. Bangerl, K. Reichmann, B. Hoffmann, M. Höpfner and F. Wiesbrock, *Polymers*, 2014, **6**, 264–279.
- 39 J. Rueda, R. Suica, H. Komber and B. Voit, *Macromol. Chem. Phys.*, 2003, **204**, 954–960.
- 40 J. C. Rueda, H. Komber and B. Voit, *J. Polym. Sci., Part A: Polym. Chem.*, 2005, **43**, 122–128.
- 41 H. Uyama and S. Kobayashi, *Chem. Lett.*, 1992, **9**, 1643–1646.
- 42 S. Kobayashi, M. Kaku, S. Sawada and T. Saegusa, *Polym. Bull.*, 1985, **13**, 447–451.
- 43 D. Christova, R. Velichkova and E. J. Goethals, *Macromol. Rapid Commun.*, 1997, **18**, 1067–1073.
- 44 D. Christova, R. Velichkova, E. J. Goethals and F. E. Du Prez, *Polymer*, 2002, **43**, 4585–4590.
- 45 D. Christova, R. Velichkova, W. Loos, E. J. Goethals and F. E. Du Prez, *Polymer*, 2003, **44**, 2255–2261.
- 46 B. Kostova, K. Ivanova-Mileva, D. Rachev and D. Christova, *AAPS PharmSciTech*, 2013, **14**, 352–359.
- 47 C.-H. Wang and G.-H. Hsiue, *J. Polym. Sci., Part A: Polym. Chem.*, 2002, **40**, 1112–1121.
- 48 J. C. Rueda, H. Komber, J. C. Cedrón, B. Voit and G. Shevtsova, *Macromol. Chem. Phys.*, 2003, **204**, 947–953.
- 49 G. David, B. C. Simionescu and A.-C. Albertsson, *Biomacromolecules*, 2008, **9**, 1678–1683.
- 50 G. David, V. Alupeii and B. C. Simionescu, *Eur. Polym. J.*, 2001, **37**, 1353–1358.
- 51 G. David and A. Ioanid, *J. Appl. Polym. Sci.*, 2001, **80**, 2191–2199.
- 52 J. C. Rueda, E. Campos, H. Komber, S. Zschoche, L. Häussler and B. Voit, *Des. Monomers Polym.*, 2014, **17**, 208–216.
- 53 Z. Zhu and X. Li, *J. Appl. Polym. Sci.*, 2014, **131**, DOI: 10.1002/app.39867.
- 54 S. J. Kim, K. J. Lee, I. Y. Kim, D. I. Shin and S. I. Kim, *J. Appl. Polym. Sci.*, 2006, **99**, 1100–1103.
- 55 S. J. Kim, K. J. Lee and S. I. Kim, *J. Macromol. Sci., Part A: Pure Appl. Chem.*, 2004, **41**, 267–274.
- 56 G. David, M. Pinteala and B. C. Simionescu, *Dig. J. Nanomat. Biostr.*, 2006, **1**, 129–138.

- 57 W. Richtering and B. R. Saunders, *Soft Matter*, 2014, **10**, 3695–3702.
- 58 I.-H. Park, I.-S. Han, D.-K. Kim and T. Saegusa, *Angew. Makromol. Chem.*, 1991, **190**, 165–176.
- 59 Y. Chujo, K. Sada, T. Kawasaki and T. Saegusa, *Polym. J.*, 1992, **24**, 1301–1306.
- 60 G. Rathna, *J. Mater. Sci.: Mater. Med.*, 2008, **19**, 2351–2358.
- 61 S. Cesana, J. Auernheimer, R. Jordan, H. Kessler and O. Nuyken, *Macromol. Chem. Phys.*, 2006, **207**, 183–192.
- 62 M. Hartlieb, D. Pretzel, C. Englert, M. Hentschel, K. Kempe, M. Gottschaldt and U. S. Schubert, *Biomacromolecules*, 2014, **15**, 1970–1978.
- 63 B. L. Farrugia, K. Kempe, U. S. Schubert, R. Hoogenboom and T. R. Dargaville, *Biomacromolecules*, 2013, **14**, 2724–2732.
- 64 V. Schenk, L. Ellmaier, E. Rossegger, M. Edler, T. Griesser, G. Weidinger and F. Wiesbrock, *Macromol. Rapid Commun.*, 2012, **33**, 396–400.
- 65 T. R. Dargaville, R. Forster, B. L. Farrugia, K. Kempe, L. Voorhaar, U. S. Schubert and R. Hoogenboom, *Macromol. Rapid Commun.*, 2012, **33**, 1695–1700.
- 66 T. R. Dargaville, B. G. Hollier, A. Shokohmand and R. Hoogenboom, *Cell Adhes. Migrat.*, 2014, **8**, 0–5.
- 67 L. Tauhardt, K. Kempe, K. Knop, E. Altuntaş, M. Jäger, S. Schubert, D. Fischer and U. S. Schubert, *Macromol. Chem. Phys.*, 2011, **212**, 1918–1924.
- 68 Y. Chujo, Y. Yoshifuji, K. Sada and T. Saegusa, *Macromolecules*, 1989, **22**, 1074–1077.
- 69 Y. Chujo, K. Sada and T. Saegusa, *Macromolecules*, 1990, **23**, 2636–2641.
- 70 Y. Chujo, K. Sada and T. Saegusa, *Macromolecules*, 1990, **23**, 2693–2697.
- 71 Y. Chujo, K. Sada, A. Naka, R. Nomura and T. Saegusa, *Macromolecules*, 1993, **26**, 883–887.
- 72 Y. Chujo, K. Sada, R. Nomura, A. Naka and T. Saegusa, *Macromolecules*, 1993, **26**, 5611–5614.
- 73 T. E. Zewert and M. G. Harrington, *Electrophoresis*, 1999, **20**, 1339–1348.
- 74 C. Englert, L. Tauhardt, M. Hartlieb, K. Kempe, M. Gottschaldt and U. S. Schubert, *Biomacromolecules*, 2014, **15**, 1124–1131.
- 75 K. Miyata, R. J. Christie and K. Kataoka, *React. Funct. Polym.*, 2011, **71**, 227–234.
- 76 C. Kiparissides and O. Kammona, *Can. J. Chem. Eng.*, 2013, **91**, 638–651.
- 77 C. Deng, Y. Jiang, R. Cheng, F. Meng and Z. Zhong, *Nano Today*, 2012, **7**, 467–480.
- 78 C. Oerlemans, W. Bult, M. Bos, G. Storm, J. F. Nijssen and W. Hennink, *Pharm. Res.*, 2010, **27**, 2569–2589.
- 79 C. F. van Nostrum, *Soft Matter*, 2011, **7**, 3246–3259.
- 80 R. Luxenhofer, A. Schulz, C. Roques, S. Li, T. K. Bronich, E. V. Batrakov, R. Jordan and A. V. Kabanov, *Biomaterials*, 2010, **31**, 4972–4979.
- 81 K. Kempe, R. Hoogenboom, S. Hoepfener, C.-A. Fustin, J.-F. Gohy and U. S. Schubert, *Chem. Commun.*, 2010, **46**, 6455–6457.
- 82 H. Huang, R. Hoogenboom, M. A. M. Leenen, P. Guillet, A. M. Jonas, U. S. Schubert and J.-F. Gohy, *J. Am. Chem. Soc.*, 2006, **128**, 3784–3788.
- 83 N. t. Brummelhuis and H. Schlaad, *Polym. Chem.*, 2011, **2**, 1180–1184.
- 84 Y. Liu, Y. Wang, Y. Wang, J. Lu, V. Piñón and M. Weck, *J. Am. Chem. Soc.*, 2011, **133**, 14260–14263.
- 85 S. Zschoche, J. Rueda, V. Boyko, F. Krahl, K.-F. Arndt and B. Voit, *Macromol. Chem. Phys.*, 2010, **211**, 1035–1042.
- 86 S. Zschoche, J. C. Rueda, M. Binner, H. Komber, A. Janke, K.-F. Arndt, S. Lehmann and B. Voit, *Macromol. Chem. Phys.*, 2012, **213**, 215–226.
- 87 C. Legros, M.-C. De Pauw-Gillet, K. C. Tam, S. Lecommandoux and D. Taton, *Polym. Chem.*, 2013, **4**, 4801–4808.
- 88 N. Engelhardt, A. Ernst, A.-L. Kampmann and R. Weberskirch, *Macromol. Chem. Phys.*, 2013, **214**, 2783–2791.
- 89 S. De Koker, R. Hoogenboom and B. G. De Geest, *Chem. Soc. Rev.*, 2012, **41**, 2867–2884.
- 90 A. L. Becker, A. P. R. Johnston and F. Caruso, *Small*, 2010, **6**, 1836–1852.
- 91 J. Cui, M. P. van Koeveden, M. Müllner, K. Kempe and F. Caruso, *Adv. Colloid Interface Sci.*, 2014, **207**, 14–31.
- 92 G. K. Such, A. P. R. Johnston and F. Caruso, *Chem. Soc. Rev.*, 2011, **40**, 19–29.
- 93 A. B. da Fonseca Antunes, M. Dierendonck, G. Vancoillie, J. P. Remon, R. Hoogenboom and B. G. De Geest, *Chem. Commun.*, 2013, **49**, 9663–9665.
- 94 I. Erel, H. Schlaad and A. L. Demirel, *J. Colloid Interface Sci.*, 2011, **361**, 477–482.
- 95 I. C. Kwon, Y. H. Bae and S. W. Kim, *Nature*, 1991, **354**, 291–293.
- 96 K. Kempe, S. L. Ng, K. F. Noi, M. Müllner, S. T. Gunawan and F. Caruso, *ACS Macro Lett.*, 2013, **2**, 1069–1072.
- 97 K. Kempe, S. L. Ng, S. T. Gunawan, K. F. Noi and F. Caruso, *Adv. Funct. Mater.*, 2014, **24**, 6187–6194.
- 98 M. Talelli, C. J. F. Rijcken, W. E. Hennink and T. Lammers, *Curr. Opin. Solid State Mater. Sci.*, 2012, **16**, 302–309.

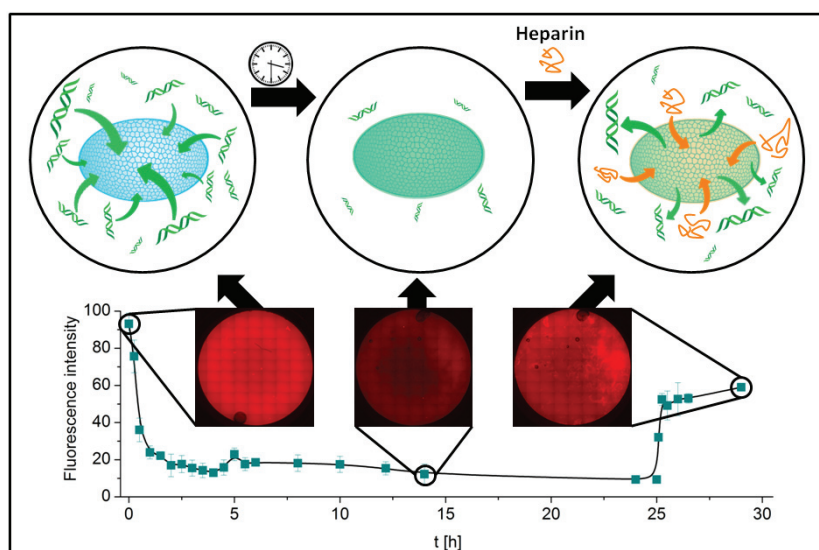


## Publication 2

### “Cationic poly(2-oxazoline) hydrogels for reversible DNA binding”

M. Hartlieb, D. Pretzel, K. Kempe, C. Fritzsche, R. M. Paulus, M. Gottschaldt, U. S. Schubert

*Soft Matter* 2013, 9, 4693-4704.



## Cationic poly(2-oxazoline) hydrogels for reversible DNA binding

Cite this: *Soft Matter*, 2013, **9**, 4693

Matthias Hartlieb,<sup>ab</sup> David Pretzel,<sup>ab</sup> Kristian Kempe,<sup>†ab</sup> Carolin Fritzsche,<sup>ab</sup> Renzo M. Paulus,<sup>ab</sup> Michael Gottschaldt<sup>ab</sup> and Ulrich S. Schubert<sup>\*ab</sup>

A new 2-oxazoline monomer with a Boc-protected amino group in the side chain (BocOx) was synthesized. Homopolymerization as well as copolymerization with 2-ethyl-2-oxazoline (EtOx) revealed a pseudo first order kinetic. A series of homopolymers was synthesized, deprotected and characterized regarding their structure and thermal properties. The copolymerization with EtOx yielded a series of water soluble polymers with varying amino contents. After deprotection it was shown by the ethidium bromide assay that these polymers were able to form complexes with DNA. Treatment with epichlorohydrin leads to the formation of hydrogels. The swelling properties of the gels were investigated and it could be demonstrated that also the polymeric scaffolds were able to immobilize DNA from aqueous solution. Furthermore, the release of the DNA was accomplished using heparin.

Received 11th January 2013  
Accepted 8th March 2013

DOI: 10.1039/c3sm00114h

[www.rsc.org/softmatter](http://www.rsc.org/softmatter)

### Introduction

DNA chips and microarrays are effective tools for life science research, for instance in modern clinical diagnostics,<sup>1</sup> genetic analysis,<sup>2</sup> drug discovery,<sup>3</sup> and pathogen detection.<sup>4</sup> These efficient analytical devices are mostly characterized by a low detection level combined with a high specificity and reproducibility as well as low costs allowing high-throughput experiments.<sup>1</sup> The basic principle of DNA chips relies on the hybridization of target DNA molecules from the sample with specific single stranded oligonucleotides attached to a 2-dimensional solid support like glass,<sup>5–7</sup> silicon wafers, gold surfaces,<sup>8</sup> or polymers such as poly(methyl methacrylate).<sup>9,10</sup>

One major drawback of two-dimensional DNA chips is the limited loading capacity of surface materials and the restricted hybridization efficiency influenced by the probe density resulting in a diminished/low test signal.<sup>11,12</sup> To overcome these issues, a challenging alternative approach is the immobilization of single stranded DNA molecules within a 3-dimensional hydrogel matrix. Thereby, a multifold increased loading capacity compared to 2D supports can be achieved.<sup>13,14</sup> The high water content of the hydrogel and the resulting rapid diffusion of target DNA within the 3D matrix predetermine such material attractive for DNA immobilization and hybridization. Hence, various reports describe methods for the

immobilization of DNA and other biomolecules within hydrogel-like structures.<sup>15–17</sup>

Beside the above described detection unit of common DNA chips and microarrays, another interesting application for DNA binding hydrogels aims at a step prior to chip analysis: the isolation of DNA from the sample. It is of particular interest for fully integrated “lab on a chip” solutions that in a single device a DNA binding/purification/enrichment phase, which releases isolated DNA on a certain stimulus, can be combined with the detection area, where specific oligonucleotides are immobilized on a 3-dimensional substrate to catch and hybridize the analyte DNA.

The extraction of DNA from living or conserved tissues, cells, virus particles, or other samples is the starting point for downstream processes including diagnostic kits.<sup>18</sup> The general steps of nucleic acid purification include cell lysis, inactivation of cellular nucleases and separation of desired nucleic acid from cell debris.<sup>19</sup> Currently, there are many specialized methods for extracting DNA, which are generally divided into solution-based (*e.g.* guanidinium thiocyanate–phenol–chloroform extraction; alkaline extraction, ethidium bromide–caesium chloride gradient centrifugation) or solid phase-based methods (mostly spin columns with matrices containing silica, nitrocellulose and polyamide or anion exchange resins *e.g.* with diethylaminoethyl cellulose groups).<sup>20–24</sup> Whereas solid-phase nucleic acid purification systems allow quick and efficient purification compared to conventional liquid phase methods<sup>25</sup> and display the current state of the art, similar limitations as described for 2-dimensional DNA chip technologies occur such as limited accessible reactive surfaces. The use of functional DNA binding hydrogels for the isolation, enrichment, purification and stimuli responsive release of these biomolecules

<sup>a</sup>Laboratory of Organic and Macromolecular Chemistry (IOMC), Friedrich Schiller University Jena, Humboldtstrasse 10, 07743, Jena, Germany. E-mail: [ulrich.schubert@uni-jena.de](mailto:ulrich.schubert@uni-jena.de)

<sup>b</sup>Jena Center for Soft Matter (JCSM), Friedrich Schiller University Jena, Philosophenweg 7, 07743, Jena, Germany

<sup>†</sup> Current address: Department of Chemical and Biomolecular Engineering, The University of Melbourne, Victoria 3010, Australia.

displays an ideal possibility to combine advantages of common liquid and solid phase extraction systems, such as a high diffusion rate, tuneable functionalities and a high reaction surface for the binding of target molecules.

For the synthesis of DNA binding hydrogels, inspiration can be found in the exploited field of non-viral gene delivery, where cationic polymers, such as poly(ethylene imine)s (PEI),<sup>26,27</sup> poly(L-lysine)s<sup>28,29</sup> and poly(methacrylate)s containing amino functionalities<sup>30–32</sup> have been extensively studied in the last few decades. Branched PEI (BPEI) has become the gold standard, due to its efficient polyplex formation.<sup>33,34</sup> The charge density and the length of the polymer backbone represent crucial factors for efficient DNA binding.<sup>35</sup> The synthesis path, which leads to linear PEI (LPEI), the acidic/basic hydrolysis of poly(2-oxazoline)s (POx)s in particular of poly(2-methyl-2-oxazoline) and poly(2-ethyl-2-oxazoline) (PEtOx),<sup>36</sup> limits the structural versatility of these gene delivery systems due to the incompatibility of most of the functional groups under these conditions. Additionally, PEI shows an unsatisfying water solubility for biological applications.<sup>37</sup>

Various reports have demonstrated the conjugation of PEI to other biochemically relevant polymers such as polyethylene glycol (PEG),<sup>9–11</sup> POxs,<sup>38</sup> and poly(caprolactone)<sup>39,40</sup> in post-polymerization reactions to overcome these issues. But also for this approach, the variety of possible end-groups for selective coupling reactions and the structural control over the PEI block are strongly limited under the hydrolysis conditions.<sup>41</sup>

However, the possibilities provided by the cationic ring opening polymerization (CROP) of 2-oxazolines are very versatile. It is possible to introduce functionalities into the polymer using functional initiators, end capping reagents and variation of the substituent at the 2-position of the monomer.<sup>42–44</sup> The living character of the reaction leads to an excellent control over the polymer length and the polydispersity index (PDI).<sup>45</sup> This variety is only limited by the requirements of the cationic polymerization, where nucleophiles can quench the propagating chain.

Cesana *et al.* reported the synthesis of cationic POx in 2006.<sup>46</sup> They used a 2-oxazoline monomer bearing a protected amino group at the 2-position to create polymers, which exhibit cationic side chains after deprotection. To the best of our knowledge, this represents the only study about cationic POxs to date. With this type of monomer it is possible to adjust the sequence, length and charge density rather easily by the CROP technique. However, the potential of this polymeric system has never been used for biochemical applications.

Moreover, (co)polymers containing amino side chains exhibit enormous potential for the design of smart hydrogels. While the synthesis of hydrogels from partially<sup>47–49</sup> or fully cleaved<sup>50–52</sup> POxs is known in the literature, the application of these systems for the reversible binding of DNA, *e.g.* for the enrichment of genes in biochip devices, has never been described to the best of our knowledge. Besides the swelling value, a basic structural requirement for such hydrogels displays the presence of amino groups in the gel matrix to interact with the DNA in solution.

This report focuses on the synthesis and detailed characterization of amino bearing POxs and their ability to bind DNA.

Furthermore, hydrogels are produced on the basis of these polymers in order to act as solid substrates for the reversible binding of DNA, which is investigated using the fluorescence of ethidium bromide (EB).

## Experimental part

### Materials and instrumentation

All chemicals and solvents were purchased from Sigma-Aldrich, Merck, Fluka, and Acros. 2-Ethyl-2-oxazoline (EtOx) and methyl tosylate (MeTos) were distilled to dryness prior to use.

The Initiator Sixty single-mode microwave synthesizer from Biotage, equipped with a noninvasive IR sensor (accuracy: 2%), was used for polymerizations under microwave irradiation. Microwave vials were heated overnight to 110 °C and allowed to cool to room temperature under an argon atmosphere before usage. All polymerizations were carried out under temperature control.

Size-exclusion chromatography (SEC) of protected polymers was performed on a Shimadzu system equipped with a SCL-10A system controller, a LC-10AD pump, a RID-10A refractive index detector and a PSS SDV column with chloroform–triethylamine (TEA)–2-propanol (94 : 4 : 2) as eluent. The column oven was set to 50 °C. SEC of the deprotected statistical copolymers was performed on a Shimadzu system with a LC-10AD pump, a RID-10A refractive index detector, a system controller SCL-10A, a degasser DGU-14A, and a CTO-10A column oven using *N,N*-dimethylacetamide with 2.1 g L<sup>-1</sup> LiCl as the eluent and the column oven set to 50 °C. Poly(styrene) (PS) samples were used as calibration standards for both solvent systems. SEC measurements in water were performed on a Jasco system equipped with a RI detector using a 0.1% aqueous solution of trifluoro acetic acid (TFA) with 0.05 mol L<sup>-1</sup> NaCl using a pullulan standard.

Proton NMR spectroscopy (<sup>1</sup>H NMR) measurements were performed at room temperature on a Bruker AC 300 and 400 MHz spectrometer, using CDCl<sub>3</sub>, MeOD or DMSO-d<sub>6</sub> as solvents. The chemical shifts are given in ppm relative to the signal from the residual non-deuterated solvent. Fourier transform infrared (FTIR) spectroscopy was performed on an Affinity-1 FT-IR from Shimadzu, using the reflection technique. Gas chromatography (GC) was performed on a GC-2010 from Shimadzu. Acetonitrile was used as an internal standard to determine the monomer conversion.

High resolution electrospray ionization (HR-ESI) mass spectrometry (MS) was performed on a micrOTOF Q-II (Bruker Daltonics) mass spectrometer equipped with an automatic syringe pump from KD Scientific for sample injection at 4.5 kV at a desolvation temperature of 180 °C. The mass spectrometer was operating in the positive ion mode. Matrix assisted laser desorption ionization (MALDI) time of flight (ToF)-MS spectra were recorded on an Ultraflex III TOF/TOF (Bruker Daltonics GmbH, Bremen, Germany). The instrument was equipped with a frequency-tripled Nd:YAG operating at a wavelength of 355 nm. Spectra were recorded in the positive reflector and in linear mode. 2,5-Dihydroxybenzoic acid was used as a matrix for the sample preparation.

Differential scanning calorimetry (DSC) was performed on a Netzsch DSC 204 F1 Phoenix under a nitrogen atmosphere with a heating rate of 20 K min<sup>-1</sup> from -100 to 200 °C. 3 Cycles were recorded for each sample. The glass transition temperature ( $T_g$ ) values are reported for the second heating run. Thermo-gravimetric analysis (TGA) was performed under a nitrogen atmosphere on a Netzsch TG 209 F1 Iris in the range from room temperature to 800 °C with a heating rate of 10 K min<sup>-1</sup>.

### 5-((*tert*-Butoxycarbonyl)amino)valeric acid<sup>53</sup> (2)

5-amino valeric acid (**1**, 5.15 g, 50.4 mmol) was dissolved in a mixture of aqueous sodium hydroxide solution (2 wt%, 100 mL) and dioxane (100 mL). Di-*tert*-butyldicarbonate (DiBoc) (11 g, 50.4 mmol) was dissolved in dioxane (50 mL) and added dropwise to the yellow solution. The reaction mixture was stirred for 20 h at room temperature and acidified using aqueous HCl (1 mol L<sup>-1</sup>) until a pH of 3 was reached. The turbid mixture was washed with dichloromethane (3 × 50 mL), the combined organic phases were washed with water (3 × 100 mL) and dried over sodium sulfate. After evaporation of the solvent and drying in a high vacuum, the product was obtained as a white crystalline solid (8.41 g, 39 mmol, 77%).

<sup>1</sup>H NMR (DMSO-*d*<sub>6</sub>, 300 MHz):  $\delta$  = 5.77 (0.3H, s, COOH), 4.60 (0.77H, s, NH), 3.10 (2H, s, CH<sub>2</sub>-CH<sub>2</sub>-N), 2.38 (2H, t, CH<sub>2</sub>-CH<sub>2</sub>-COO), 1.67 (2H, q, CH<sub>2</sub>-CH<sub>2</sub>-CH<sub>2</sub>, 7.10 Hz), 1.54 (2H, q, CH<sub>2</sub>-CH<sub>2</sub>-CH<sub>2</sub>, 6.39 Hz), 1.45 (9H, s, CH<sub>3</sub>) ppm.

HR-ESI: *m/z* calc. for C<sub>10</sub>H<sub>19</sub>NO<sub>4</sub>Na [M + Na]: 240.1206, found: 240.1243 (error: 15.4 ppm).

FTIR:  $\bar{\nu}$  (cm<sup>-1</sup>) = 3374, 2983, 2951, 2879, 1720, 1683, 1520, 1486, 1462, 1444, 1431, 1415, 1388, 1361, 1330, 1277, 1242, 1204, 1165.

### *tert*-Butyl 5-((2-chloroethyl)amino)-5-oxopentyl)carbamate (3)

To a solution of **2** (2 g, 9.21 mmol) in tetrahydrofuran (THF) (80 mL), TEA (1.276 mL, 9.21 mmol) was added and the mixture was cooled to 0 °C. After a dropwise addition of ethyl chloroformate (0.87 mL, 9.21 mmol) the reaction solution was allowed to reach room temperature and stirred for 1 h. After cooling again to 0 °C, a mixture of 2-chloroethylamine hydrochloride (1.067 g, 9.21 mmol) and TEA (1.276 mL, 9.21 mmol) in dimethylformamide (DMF) (10 mL) was added and the reaction mixture was stirred for 1.5 h.

After evaporation of the solvent, the residue was re-dissolved in dichloromethane and washed with aqueous sodium bicarbonate solution (3 × 50 mL) and brine (3 × 50 mL). The solution was dried over sodium sulfate and the solvent was evaporated. The intermediate product was obtained as a white crystalline solid (1.93 g, 6.9 mmol, 75%) and used without further purification.

<sup>1</sup>H NMR (CDCl<sub>3</sub>, 300 MHz):  $\delta$  = 6.13 (1H, s, CH<sub>2</sub>-NH-CO), 4.64 (1H, s, Boc-NH-CO), 3.61 (4H, m, CH<sub>2</sub>Cl-CH<sub>2</sub>-NH), 3.13 (2H, t, CH<sub>2</sub>-CH<sub>2</sub>-NHBoc, 6 Hz), 2.25 (2H, t, CH<sub>2</sub>-CH<sub>2</sub>-CON, 7.14 Hz), 1.68 (2H, q, CH<sub>2</sub>-CH<sub>2</sub>-CH<sub>2</sub>, 7.40 Hz), 1.52 (2H, q, CH<sub>2</sub>-CH<sub>2</sub>-CH<sub>2</sub>, 6.6 Hz), 1.44 (9H, s, CH<sub>3</sub>) ppm.

HR-ESI: *m/z* calc. for C<sub>12</sub>H<sub>23</sub>ClN<sub>2</sub>O<sub>4</sub>Na [M + Na]: 301.1289; found: 301.1318 (error: 9.6 ppm).

FTIR:  $\bar{\nu}$  (cm<sup>-1</sup>) = 3377, 3312, 3275, 2980, 2944, 1747, 1691, 1671, 1646, 1547, 1524, 1481, 1366, 1277, 1249, 1219, 1160.

### 2-(4-((*tert*-Butoxycarbonyl)amino)butyl)-2-oxazoline (BocOx) (4)

**3** (1.93 g, 6.9 mmol) was dissolved in DMF (150 mL) and potassium carbonate (1.91 g, 13.8 mmol) was added. The suspension was stirred at 70 °C for 5 h. After evaporation of the solvent, the yellow oil was dissolved in dichloromethane and washed with distilled water (3 × 100 mL). The solution was dried using sodium sulfate and the solvent was evaporated under reduced pressure. The crude product was purified by distillation (6 × 10<sup>-2</sup> mbar, 115 °C) to yield **BocOx** as a colorless viscous liquid (1 g, 4.14 mmol, 60%,  $\rho$  = 0.97 g cm<sup>-3</sup>).

<sup>1</sup>H NMR (CDCl<sub>3</sub>, 300 MHz):  $\delta$  = 4.65 (1H, s, NH), 4.21 (2H, t, CH<sub>2</sub>-oxazoline, 9.3 Hz), 3.80 (2H, t, CH<sub>2</sub>-oxazoline, 9.8 Hz), 3.12 (2H, t, CH<sub>2</sub>-CH<sub>2</sub>-NH, 6.3 Hz), 2.28 (2H, t, CH<sub>2</sub>-CH<sub>2</sub>-CON, 7.2 Hz), 1.65 (2H, q, CH<sub>2</sub>-CH<sub>2</sub>-CH<sub>2</sub>, 7.40 Hz), 1.53 (2H, q, CH<sub>2</sub>-CH<sub>2</sub>-CH<sub>2</sub>, 6.6 Hz), 1.42 (9H, s, CH<sub>3</sub>) ppm.

HR-ESI: *m/z* calc. for C<sub>12</sub>H<sub>22</sub>N<sub>2</sub>O<sub>3</sub>Na [M + Na]: 265.1523; found: 265.1534 (error: 4 ppm).

FTIR:  $\bar{\nu}$  (cm<sup>-1</sup>) = 3325, 2978, 2932, 1694, 1663, 1524, 1451, 1366, 1246, 1165.

### Kinetic studies

For kinetic investigations an *in situ* oligoinitiator was synthesized from a stock solution of EtOx, MeTos (3 : 1) and acetonitrile ([M] = 1 mol L<sup>-1</sup>) by microwave-assisted polymerization (140 °C, 90% conversion). Subsequently, BocOx (and EtOx for the copolymerization) was added to the initiator mixture. The stock solution was aliquoted into microwave vials (1 mL per vial) and heated in the microwave synthesizer (140 °C, varying reaction times). After polymerization, the conversions of the monomers were determined by GC with acetonitrile as an internal standard. The reaction rate constant  $k_p$  of the monomers was determined using eqn (1) and (2) assuming that the slope of the linear fit of  $\ln([M]_0/[M]_t) = f(t)$  complies with  $k_{\text{eff}}$ .

$$\ln M_0 - \ln M_t = k_{\text{eff}}t \quad (1)$$

$$k_{\text{eff}} = k_p[I] \quad (2)$$

### Homopolymerization of BocOx (PBocOx) (5-8)

In a microwave vial, EtOx (121  $\mu$ L, 1.2 mmol), MeTos (60.6  $\mu$ L, 0.4 mmol) and acetonitrile (2.95 mL) were mixed under inert conditions. After heating the vial in the microwave at 140 °C for 6 min, BocOx (403.7  $\mu$ L, 4 mmol) was added under an argon stream and the mixture was heated again in the microwave synthesizer (140 °C, 5 min). The polymer solution was diluted with dichloromethane (50 mL) and extracted with saturated aqueous solution of sodium bicarbonate (3 × 50 mL) and water (3 × 50 mL). Subsequently, the solution was concentrated and the polymer was precipitated in 150 mL ice-cold diethyl ether. The white precipitate was filtered and dried in a high vacuum (392 mg, 85%).



$^1\text{H}$  NMR ( $\text{CDCl}_3$ , 300 MHz):  $\delta = 5.17$  (s, 1H, NH), 3.44 (s, 4H, backbone), 3.10 (s, 2H,  $\text{CH}_2\text{-CH}_2\text{-NH}$ ), 2.35 (s, 2H,  $\text{CH}_2\text{-CH}_2\text{-CO}$ ), 1.62 (s, 2H,  $\text{CH}_2\text{-CH}_2\text{-CH}_2$ ), 1.52 (s, 2H,  $\text{CH}_2\text{-CH}_2\text{-CH}_2$ ), 1.41 (s, 9H,  $\text{CH}_3$ ) ppm.

SEC (5) (eluent:  $\text{CHCl}_3$ -i-propanol-TEA, PS-standard):  $M_n = 3700 \text{ g mol}^{-1}$ ,  $M_w = 4700 \text{ g mol}^{-1}$ , PDI = 1.25.

#### Copolymerization of EtOx and BocOx (P(EtOx-*stat*-BocOx)) (9–13)

In a microwave vial, EtOx (181.7  $\mu\text{L}$ , 1.8 mmol), MeTos (90.8  $\mu\text{L}$ , 0.600 mmol) and acetonitrile (11.5 mL) were mixed under inert conditions. After heating in the microwave at 140  $^\circ\text{C}$  for 16 min EtOx (2543  $\mu\text{L}$ , 25.2 mmol) and BocOx (749  $\mu\text{L}$ , 3 mmol) were added under an argon stream and the mixture was heated again in the microwave synthesizer (140  $^\circ\text{C}$ , 11 min). The solution was diluted with dichloromethane (100 mL) and extracted with saturated aqueous solution of sodium bicarbonate ( $3 \times 100 \text{ mL}$ ) and water ( $3 \times 100 \text{ mL}$ ). Subsequently, the solution was concentrated and the polymer was precipitated in 400 mL ice-cold diethyl ether. The white precipitate was filtered and dried in a high vacuum (2.77 g, 78%).

$^1\text{H}$  NMR ( $\text{CDCl}_3$ , 300 MHz):  $\delta = 4.99$  (s, 0.2H, NH), 3.45 (s, 4H, backbone), 3.11 (s, 0.3H,  $\text{CH}_2\text{-CH}_2\text{-NH}$  (BocOx)), 2.40 (s, 1.9H,  $\text{CH}_2$  (EtOx)), 1.92 (s, 0.3H,  $\text{CH}_2\text{-CH}_2\text{-CO}$  (BocOx)), 1.64 (s, 0.3H,  $\text{CH}_2\text{-CH}_2\text{-CH}_2$  (BocOx)), 1.53 (s, 0.3H,  $\text{CH}_2\text{-CH}_2\text{-CH}_2$  (BocOx)), 1.42 (s,  $\text{CH}_3$  (BocOx)), 1.21 (s, 1.3H,  $\text{CH}_3$  (EtOx)) ppm.

SEC (9) (eluent:  $\text{CHCl}_3$ -i-propanol-TEA, PS-standard):  $M_n = 5300 \text{ g mol}^{-1}$ ,  $M_w = 5700 \text{ g mol}^{-1}$ , PDI = 1.08.

#### Deprotection of PBocOx (PAmOx) (14–17)

PBocOx (5, 195 mg, 0.8 mmol of amino groups) was dissolved in dichloromethane (2.5 mL) and TFA (617  $\mu\text{L}$ , 8 mmol) was added subsequently. After heating at 60  $^\circ\text{C}$  for 1 h and stirring for 24 h at room temperature, the mixture was diluted with 5 mL of methanol and precipitated in 150 mL of ice-cold diethyl ether. The yellow precipitate was re-dissolved in methanol (50 mL) and stirred with Amberlyst A21 for 24 h. Subsequently, the solution was concentrated and the polymer was precipitated in ice-cold diethyl ether (150 mL), filtered, dried in a high vacuum and obtained as a yellowish powder (103 mg, 90%).

$^1\text{H}$  NMR ( $\text{D}_2\text{O}$ , 400 MHz):  $\delta = 3.51$  (s, 4H, backbone), 2.85 (s, 2H,  $\text{CH}_2\text{-CH}_2\text{-NH}_2$ ), 2.42 (2H,  $\text{CH}_2\text{-CH}_2\text{-CO}$ ), 1.65 (s, 4H,  $\text{CH}_2\text{-CH}_2\text{-CH}_2$ ) ppm.

SEC (14) (eluent: water-TFA-NaCl, pullulan-standard):  $M_n = 15\,100 \text{ g mol}^{-1}$ ,  $M_w = 18\,500 \text{ g mol}^{-1}$ , PDI = 1.23.

#### Deprotection of P(EtOx-*stat*-BocOx) (P(EtOx-*stat*-AmOx)) (18–22)

P(EtOx-*stat*-BocOx) (9, 2 g) was dissolved in TFA (5 mL) and heated at 60  $^\circ\text{C}$  for 1 h. After stirring for 24 h at room temperature, the mixture was diluted with 10 mL methanol and precipitated in 400 mL of cold diethyl ether. The yellowish precipitate was re-dissolved in methanol (200 mL) and stirred with Amberlyst A21 for 24 h. Subsequently, the solution was concentrated and the polymer was precipitated in cold diethyl ether (400 mL), filtered, dried in a high vacuum and obtained as a yellowish powder (1.58 g, 87%).

$^1\text{H}$  NMR (MeOD, 400 MHz):  $\delta = 3.52$  (s, 4H, backbone), 2.96 (0.23H, s,  $\text{CH}_2\text{-CH}_2\text{-NH}_2$ ), 2.42 (2H, s,  $\text{CH}_2$  (EtOx) +  $\text{CH}_2\text{-CH}_2\text{-CO}$  (AmOx)), 1.69 (0.41H, s,  $\text{CH}_2\text{-CH}_2\text{-CH}_2\text{-CH}_2$  (AmOx)), 1.11 (2.8H, s,  $\text{CH}_3$  (EtOx)) ppm.

SEC (18) (eluent: DMAc-LiCl, PS-standard):  $M_n = 8100 \text{ g mol}^{-1}$ ,  $M_w = 10\,200 \text{ g mol}^{-1}$ , PDI = 1.26.

#### Hydrogel synthesis (23–27)

P(EtOx-*stat*-AmOx) (18, 100 mg, 0.1 mmol  $\text{NH}_2$ -groups) was dissolved in a 5 wt% aqueous solution of sodium hydroxide. Epichlorohydrin (3.92  $\mu\text{L}$ , 0.05 mmol) was added to the reaction solution and the mixture was heated at 50  $^\circ\text{C}$  for 1 h. Gelation occurred after 10 min. The gel was washed with methanol ( $5 \times 20 \text{ mL}$ ) and water ( $2 \times 20 \text{ mL}$ ) and freeze dried at  $-35 \text{ }^\circ\text{C}$  and 0.2 mbar (55 mg, 52%).

FTIR:  $\bar{\nu}$  ( $\text{cm}^{-1}$ ) = 2978, 2936, 1628, 1466, 1420, 1373, 1315, 1238, 1196, 1126, 1061.

#### Swelling studies

The water uptake of the freeze dried hydrogel samples was measured gravimetrically using centrifuge filter tubes. The filter tube was saturated with water and the excess solvent was removed by centrifugation (3000 rpm, 10 min). The tube was weighed to yield  $m_0$ . After addition of the hydrogel sample (10 to 20 mg), the tube was weighed again ( $m_{0,\text{gel}}$ ) and the sample weight ( $m_{\text{gel}}$ ) was determined using eqn (3).

$$m_{\text{gel}} = m_{0,\text{gel}} - m_0 \quad (3)$$

After swelling of the sample in water for 24 h the filter tube was centrifuged (3000 rpm, 10 min) and weighed ( $m_{\text{wet}}$ ) to determine the mass of the swollen gel ( $m_{\text{sw}}$ ) using eqn (4).

$$m_{\text{sw}} = m_{\text{wet}} - m_0 \quad (4)$$

The swelling degree ( $Q_{\text{eq}}$ ) was calculated according to eqn (5).<sup>54</sup>

$$Q_{\text{eq}} = \frac{m_{\text{sw}} - m_{\text{gel}}}{m_{\text{sw}}} \times 100\% \quad (5)$$

The gelled polymer fraction ( $F_{\text{p}}$ ) was determined using eqn (6).<sup>54</sup>

$$F_{\text{p}} = \frac{m_{\text{th}}}{m_{\text{d}}} \times 100\% \quad (6)$$

$m_{\text{th}}$ : theoretical mass of the polymer in the gel (based on the mass of the polymer precursor and cross-linker), and  $m_{\text{d}}$ : mass of the dried sample.

#### Ethidium bromide assay (EBA) of P(EtOx-*stat*-PAmOx)

The complex formation of plasmid-DNA (pDNA, 4700 base pairs) with cationic polymers was detected by quenching of the EB fluorescence as described in the literature.<sup>55</sup>

pDNA (7.5  $\mu\text{g mL}^{-1}$ ) and EB (0.4  $\mu\text{g mL}^{-1}$ ) were dissolved in HBG-buffer (HEPES buffered glucose, pH 7) and incubated for 10 min at room temperature. 100  $\mu\text{L}$  of the pDNA-EB solution were transferred to the wells of a black 96-well plate (Nunc,

Langensfeld, Germany) containing different polymer concentrations. Fluorescence was measured after 20 min of incubation with the polymer solution using a Tecan M200 Pro fluorescence microplate reader (Crailsheim, Germany) at the following wavelengths: Ex 525 nm/Em 605 nm. An internal standard containing only pDNA and EB was used to calibrate the measurements.

### EBA of hydrogel samples and release studies

Between 0.8 and 2.25 mg of hydrogels per well (12-well plate) were used depending on the amino content of the samples to reach a nitrogen to phosphate (N/P) value of 1000 for every sample. The gels were swollen overnight in 250  $\mu\text{L}$  of HBG-buffer (pH 7). Subsequently, 1 mL of pDNA-EB solution (containing 7.5  $\mu\text{g}$  pDNA per mL and 0.4  $\mu\text{g}$  EB per mL) was added and the sample aliquots of 50  $\mu\text{L}$  for every time interval were taken. Fluorescence was measured in black 96-well plates using a Tecan M200 Pro fluorescence microplate reader.

For release studies, 1 mL of a mixture of heparin (6  $\text{mg mL}^{-1}$ , 2 eq.) and EB (0.4  $\mu\text{g mL}^{-1}$ ) in HPG-buffer (pH 7) was added to each of the swollen gel samples. For every measuring point, 50  $\mu\text{L}$  were collected and the fluorescence was determined as described above.

### Microscopic detection of hydrogel supported DNA binding and release

Approximately 0.18 mg of hydrogels per well were transferred into the cavity of a clear bottom black walled 96 well plate and the gels were swollen overnight in 50  $\mu\text{L}$  of HBG-buffer (pH 7). Next, 100  $\mu\text{L}$  of pDNA-EB (containing 7.5  $\mu\text{g}$  pDNA per mL and 0.4  $\mu\text{g}$  EB per mL) solution were added and the fluorescence signal was captured directly in the wells using a fluorescence microscope (Cell Observer Z1, Carl Zeiss, Jena, Germany) equipped with a mercury arc UV lamp and the appropriate filter combinations for excitation and detection of emission. Images of a series (11  $\times$  11 pictures per well) were captured with a 10 $\times$  objective using identical instrument settings (e.g. UV lamp power, integration time, and camera gain) and spots of the 96 well plate were addressed using an automated XY table. Control samples contained only 100  $\mu\text{L}$  of pDNA-EB (7.5  $\mu\text{g}$  pDNA per mL and 0.4  $\mu\text{g}$  EB per mL) and 50  $\mu\text{L}$  of HBG-buffer. Microscopic detection of the resulting fluorescence signal was performed at different time points (0 min, 5 min, 30 min and 120 min).

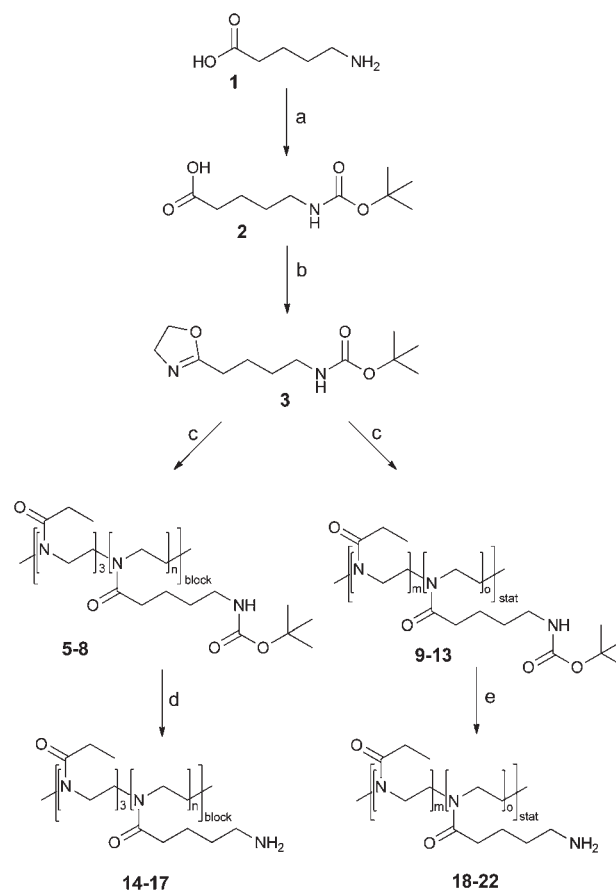
For the release of the DNA from the hydrogel, 50  $\mu\text{L}$  of heparin (60  $\text{mg mL}^{-1}$ ) were added directly to the wells and the resulting fluorescence signal was immediately analyzed microscopically as described above.

Quantification of the relative fluorescence intensity signal was performed using 8 bit, grayscale-converted images and ImageJ software. The average fluorescence intensity per pixel was obtained and the samples were normalized to the references.

## Results and discussion

### Monomer synthesis

The aim of this work was the synthesis of precursors for the production of hydrogels (Scheme 1), which possess the ability to

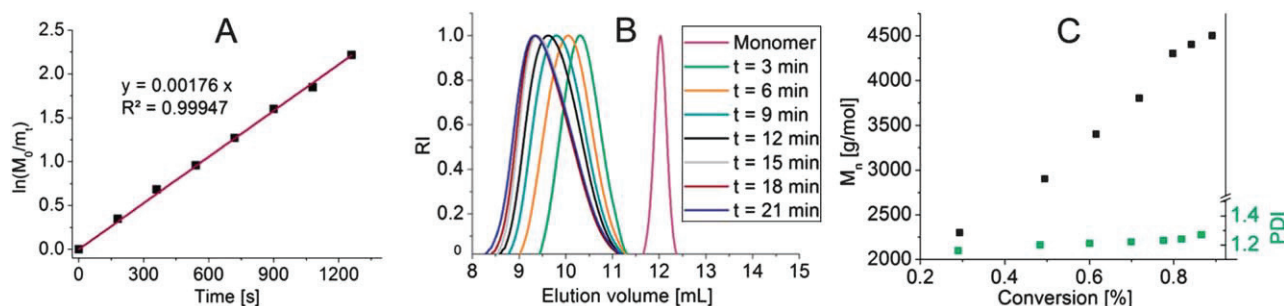


**Scheme 1** Schematic overview of the synthesis of the amino bearing 2-oxazoline monomer and its polymerization with and without a comonomer. (a) diBoc, dioxane-water, NaOH; (b) (1) ethylchloroformate, chloroethylamine, TEA, DMF, (2) DMF,  $\text{K}_2\text{CO}_3$ , 60  $^\circ\text{C}$ ; (c)  $\mu\text{W}$ , 140  $^\circ\text{C}$ , acetonitrile; (d) TFA (10 eq.), dichloromethane, 60  $^\circ\text{C}$ , Amberlyst A21 and (e) TFA, 60  $^\circ\text{C}$ , Amberlyst A21.

reversibly bind DNA. For this purpose, (POx)s suitable for cross-linking reactions and binding of DNA are necessary. Both features can be accomplished by amino groups in the side chain of the polymers. Because free amino functionalities would quench a CROP immediately, it is necessary to use a monomer with a protected amino group, which is separated from the oxazoline ring by a spacer. The distance between the amino group and the ring should be sufficiently large to ensure that the polymerization is not influenced by the functional group. In addition, it should be short enough to yield polymers with a certain hydrophilicity.

To this end, 5-amino valeric acid was chosen as a raw material for the monomer synthesis. The butoxy-carbonyl (Boc)-protection of the amino functionality was carried out according to a patent from Fino *et al.*<sup>53</sup> The amidation with chloroethylamine hydrochloride was performed in a similar fashion as reported by Cesana *et al.*<sup>46</sup> in a THF-DMF solvent mixture with ethyl chloroformate as an activation agent. The  $^1\text{H}$  NMR spectrum of the intermediate shows that 10% of the final monomer had already been formed as indicated by the appearance of the respective oxazoline ring signals. Eventually, BocOx was obtained by treatment of the intermediate mixture with potassium carbonate in DMF. The monomer was distilled to yield a product with a purity that fulfills the requirements of CROP.





**Fig. 1** Kinetic study of the homopolymerization of BocOx. (A) First-order kinetic plot, (B) SEC traces of the kinetic samples and (C)  $M_n$  against conversion plot as well as PDI values of PBocOx kinetic samples.

Cesana *et al.* reported that an initiation using small cations such as the methyl cation of the common initiators, MeTos and methyl triflate, is not suitable for this type of monomer because the cationic species will also attack the amide nitrogen of the oxazoline side chain. Preliminary tests supported these results yielding polymers with multimodal SEC traces (data not shown). Therefore, a two-step initiation was used for the polymerization of BocOx. First, the desired amount of initiator was mixed with three equivalents of EtOx in acetonitrile. This solution was heated under microwave conditions until a conversion of  $\sim 90\%$  was reached (calculated from rate constants reported in the literature<sup>56</sup>). In a second step, BocOx was introduced into the microwave vial under inert conditions and polymerized in the microwave. The EtOx-oligomer produced in step one acts as an initiator for the polymerization of the BocOx monomer and the sterical hindrance of the oxazolinium species prevents an attack at the side chain. A ratio of EtOx to MeTos of 3 : 1 was necessary to ensure that all methyl cations are consumed before the addition of BocOx. Tests with a ratio of 1 : 1 resulted in significantly higher PDI values.

### Synthesis and characterization of BocOx homopolymers

The first step to well-defined polymers by CROP is the knowledge about the reaction kinetic of the polymerization under the given conditions. Consequently, a kinetic study of the homopolymerization of BocOx was performed using the initiation method described above. The conversion of the monomer was determined by GC using the polymerization solvent (acetonitrile) as an internal standard. The resulting pseudo first-order kinetic plot is depicted in Fig. 1A. The linearity of the graph demonstrates a constant concentration of the propagating species during the polymerization, which is indicative of a living polymerization mechanism of BocOx. The polymerization rate was determined from the slope of the linear fit of the log plot using eqn (1) and (2). The  $k_p$  value was found to be  $153 \text{ L mol}^{-1} \text{ s}^{-1} \times 10^{-3}$ , which is in the same order of magnitude as EtOx in acetonitrile under the same conditions ( $105 \text{ L mol}^{-1} \text{ s}^{-1} \times 10^{-3}$ ).<sup>56</sup> The livingness of this polymerization is supported by the linear increase of the molar mass with conversion (Fig. 1C), as well as monomodal SEC curves and low PDI values ( $1.2 < \text{PDI} < 1.3$ ) (Fig. 1B and 1C).

To investigate the properties of this polymer, four homopolymers with different lengths were synthesized using the data obtained from the kinetic study (Table 1). The values for the degree of polymerization (DP) of PBocOxs were determined by  $^1\text{H}$  NMR, comparing the signal of the polymer backbone with the peaks of the initiator (tosylate) before purification. After extraction and precipitation SEC measurements revealed high PDI values for  $\text{DP} > 35$  and, therefore, a loss of control for higher DP values. Similar observations were made for PEtOx as well, however, at higher molar masses.<sup>57</sup> MALDI-ToF analysis of the polymers revealed complex spectra, which is attributed to the initiation method and the resulting formation of copolymer like systems. Surprisingly, the main distribution of the spectrum of 5 is an H-initiated PBocOx without an EtOx unit as a starting group. The thermal behavior of these polymers was investigated *via* DSC and TGA (Table 1). The  $T_g$  values of PBocOxs range between 36 and 47 °C with a dependence on the molar mass. It is known that the  $T_g$  is increasing with increasing molar mass until a plateau is reached.<sup>58</sup> For the present polymers, the rather small change of 1 °C from  $\text{DP} = 35$  to  $\text{DP} = 125$  indicated that the value of 47 °C is close to the maximum  $T_g$  for this polymer class. The thermal degradation of PBocOx was investigated by TGA under a nitrogen atmosphere. The decomposition was defined as the temperature where 5 wt% of the substance is destroyed. The difference between the degradation temperatures of the samples is most likely attributed to the uncertainty of the measurement. The differing amount of EtOx cannot be

**Table 1** Detailed characterization data for PBocOx and PAmOx. The  $M_n$  values were calculated from the  $M_w/M_n$  values of the polymerization

Sample number	Polymer	$M_n$ (calc.) [g mol <sup>-1</sup> ]	$M_n$ (SEC) [g mol <sup>-1</sup> ]	Yield [%]	$T_g$ [°C]	Thermal stability [°C]
5	PBocOx <sub>10</sub>	2000	2600	1.18	82	36
6	PBocOx <sub>25</sub>	5600	3700	1.25	85	40
7	PBocOx <sub>35</sub>	8000	6400	1.25	62	46
8	PBocOx <sub>125</sub>	30 000	10 000	1.51	77	47
14	PAmOx <sub>10</sub>	1800	15 700	1.19	90	—
15	PAmOx <sub>25</sub>	3900	21 100	1.23	96	16
16	PAmOx <sub>35</sub>	5300	32 200	1.38	95	27
17	PAmOx <sub>125</sub>	18 100	52 800	2.07	94	25

responsible for the change since PEtOx itself decomposes thermally at around 350 °C.<sup>59</sup> The degradation takes place in two steps. The first one is associated with a mass loss of 41 wt% at 250 °C and indicates that the protection group is cleaved thermally.

### Deprotection of the BocOx homopolymers

The chemical deprotection of the synthesized polymers was carried out under acidic conditions as commonly applied in the literature.<sup>60</sup> The polymers were dissolved in a 1 : 1 mixture of TFA and dichloromethane under elevated temperatures (60 °C) to yield the respective deprotected polymers (PAmOx). The resulting TFA-anion was removed with Amberlyst A21, because PAmOx is too hydroscopic for an extraction with aqueous sodium bicarbonate solution as usually applied for PEtOx. <sup>1</sup>H NMR spectroscopy proves the successful deprotection since the signal of the *tert*-butyl group has vanished in all cases (Fig. 2). SEC measurements of PAmOx were performed in water under acidic conditions. However, the standard for the measurements was pullulan which is due to its structural difference and the lack of cationic charges a poor comparison for these polymers. Thus, the obtained molar masses should be considered

deliberately, also because the length of the polymer should not have changed significantly during deprotection. The MALDI-ToF spectra of PAmOx show even more distributions than the protected polymers. A reason could be the raised laser intensity, which was necessary to desorb and ionize the polymers, together with an attributed degradation. However, the most prominent difference between peaks of the major distributions is 142 g mol<sup>-1</sup>, which is equal to the mass of AmOx. The glass transition of the polymers changed significantly after deprotection to lower values (16 to 27 °C).

The  $T_g$  of polymer **14** could not be determined because it interferes with a dip at around 0 °C, which is present in the DSC curves of all PAmOx samples. Most likely this drop-off is associated with adherent water molecules. PAmOx exhibits a high hydroscopic tendency. After some minutes under ambient conditions, the consistency of the polymers changes from a powder to a highly viscous liquid. Also TGA shows approximately 10% of water content for all polymers. The thermal stability does not change significantly in comparison to the protected samples.

### Statistical copolymerization

Because the water solubility of PAmOx was found to be unsatisfying, it was necessary to introduce a second monomer to yield polymers which combine functionality with hydrophilicity. The  $k_p$  value of BocOx already indicates the possibility of a statistical copolymerization with EtOx. Nevertheless, a kinetic study was performed to confirm this expectation. Using the same initiation method as described before, a stock solution of the initiating species was produced. A defined amount of BocOx and EtOx (1 : 4) was added and the solution was distributed over several microwave vials to investigate the conversions of both monomers depending on the reaction time by GC. The analytical data of the investigations are depicted in Fig. 3.

The copolymerization under microwave irradiation at 140 °C fulfills the characteristics for a living polymerization: linear pseudo first-order kinetics, a linear increase of the molar mass with conversion as well as narrow molar mass distributions. The calculated rate constants of the monomers ( $k_p(\text{EtOx}) = 159 \text{ (L mol}^{-1} \text{ s}^{-1}) \times 10^{-3}$ ,  $k_p(\text{BocOx}) = 175 \text{ (L mol}^{-1} \text{ s}^{-1}) \times 10^{-3}$ ) increased in comparison to the homo-polymerization.

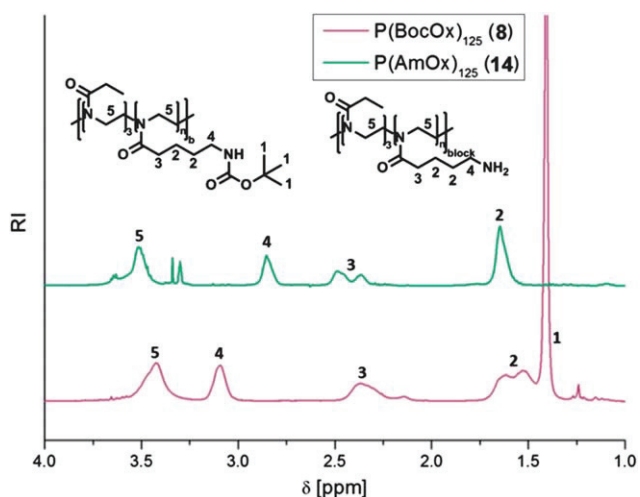


Fig. 2 Comparison of the <sup>1</sup>H NMR spectra of P(BocOx) (**8**, in CDCl<sub>3</sub>, 300 MHz) and P(AmOx) (**14**, in D<sub>2</sub>O, 400 MHz).

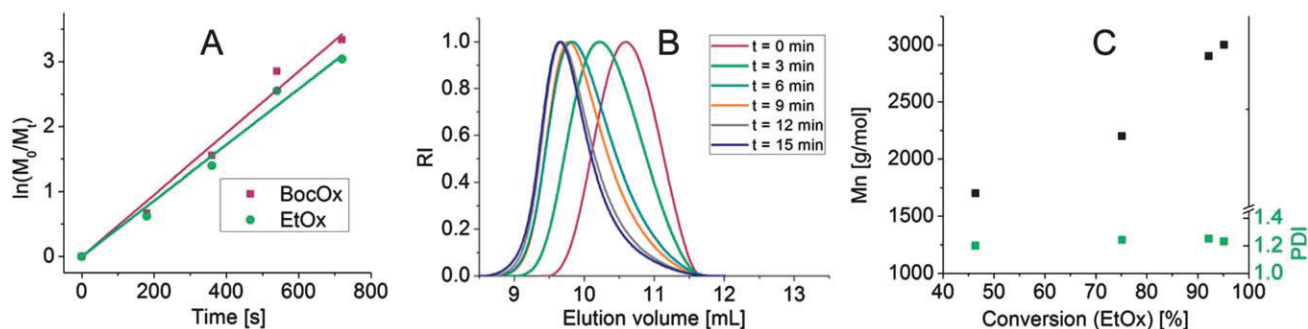


Fig. 3 Kinetic study of the statistical copolymerization of BocOx with EtOx. (A) First-order kinetic plot, (B) SEC traces of the kinetic samples and (C)  $M_n$  against conversion plot as well as PDI values of P(EtOx-*stat*-BocOx) kinetic samples.

**Table 2** Detailed characterization data for P(EtOx-*stat*-BocOx) and P(EtOx-*stat*-AmOx)

Sample number	Polymer	$M_n$ (SEC)	Yield [%]	BocOx/AmOx [%]	
		[g mol <sup>-1</sup> ]			PDI
9	P(EtOx <sub>43</sub> - <i>stat</i> -BocOx <sub>5</sub> )	5400	1.08	78	10
10	P(EtOx <sub>39</sub> - <i>stat</i> -PBocOx <sub>7</sub> )	5200	1.14	61	15
11	P(EtOx <sub>32</sub> - <i>stat</i> -PBocOx <sub>9</sub> )	4400	1.20	75	22
12	P(EtOx <sub>38</sub> - <i>stat</i> -PBocOx <sub>15</sub> )	4600	1.17	79	27
13	P(EtOx <sub>32</sub> - <i>stat</i> -PBocOx <sub>16</sub> )	5400	1.17	81	33
18	P(EtOx <sub>43</sub> - <i>stat</i> -PAmOx <sub>5</sub> )	8100	1.26	95	10
19	P(EtOx <sub>39</sub> - <i>stat</i> -PAmOx <sub>7</sub> )	8200	1.24	90	15
20	P(EtOx <sub>32</sub> - <i>stat</i> -PAmOx <sub>9</sub> )	8700	1.25	93	22
21	P(EtOx <sub>38</sub> - <i>stat</i> -PAmOx <sub>15</sub> )	9500	1.23	89	27
22	P(EtOx <sub>32</sub> - <i>stat</i> -PAmOx <sub>16</sub> )	9400	1.24	96	33

With this knowledge, it was possible to synthesize P(EtOx-*stat*-BocOx) with varying amounts of protected amino groups in the side chain. An overview of the produced polymers is provided in Table 2. It was aimed to synthesize P(EtOx-*stat*-BocOx) with a constant DP of 50 but varying amounts of BocOx between 10 and 30%. The DP, as well as the ratio between the monomers, was determined by <sup>1</sup>H NMR by comparison of the backbone signal with either the aromatic peaks of the tosylate or the integral of the protection group. SEC measurements reveal narrow PDI values and molar mass values in the expected range. The MALDI-ToF analysis of these polymers is rather complicated because of the broad variety of possible combinations of both monomers. However, it was possible to identify both types of repeating units in the spectra. The deprotection of the statistical copolymers was carried out in pure TFA since the reaction in a mixture of acid with dichloromethane yielded only a partial cleavage of the protection group. The TFA anion was removed in a similar fashion as for the homopolymers using Amberlyst A21. Quantitative deprotection was proven by <sup>1</sup>H NMR spectroscopy (Fig. 4).

Beside the disappearance of the *tert*-butyl peak, the signals of both middle CH<sub>2</sub> groups of the side chain of AmOx shift to higher ppm values and form one singlet. The SEC analysis of the copolymers was performed in DMAc (calibration against PS standard) which should enable a comparison with the protected

polymers (P(EtOx-*stat*-BocOx)). However, the measured molar mass values appear to be higher in comparison to the protected polymers, which can be attributed to the positive charges of the final polymeric material. Also for the deprotected polymers, complex MALDI-ToF spectra were obtained, in which both monomer masses could be identified.

### Hydrogel synthesis

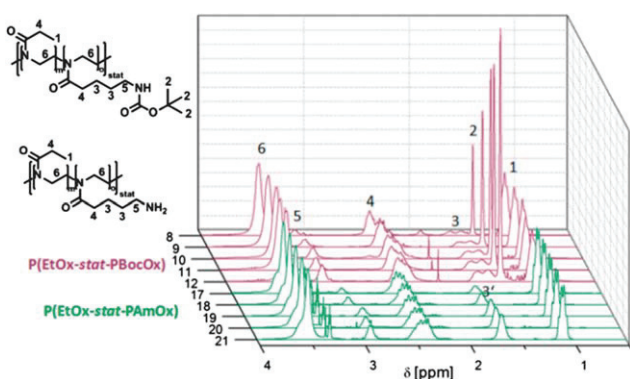
To perform DNA binding and release on solid supports it was necessary to form scaffolds out of the synthesized copolymers. For this purpose, a certain amount of the amino functionalities was consumed during the reaction with a cross-linker. However, the remaining primary amines and the secondary and tertiary amines which are formed during the process of linking should still possess the ability to bind negatively charged gene material.

Epichlorohydrin was chosen as a cross-linker. The epoxide functionality of the molecule reacts with amines under elevated temperature. After coupling to a polymer chain, a second epoxide function is formed under basic conditions, which can react with a second polymer chain (Scheme 2). The amount of cross-linker for the synthesis of hydrogels was chosen for every copolymer to consume only 5 amino functions per chain (Table 3). This value is sufficient to form a network while NH<sub>2</sub>-groups are left for the DNA interaction for most of the samples. The mixture of polymer and cross-linker in a 5 wt% sodium hydroxide solution showed no gelation after 3 h at room temperature. However, heating the sample to 50 °C for 10 min resulted in the formation of a polymer network. Subsequently the gels were washed with methanol and water to extract unlinked polymer chains, residual cross-linker and to neutralize the hydrogels.

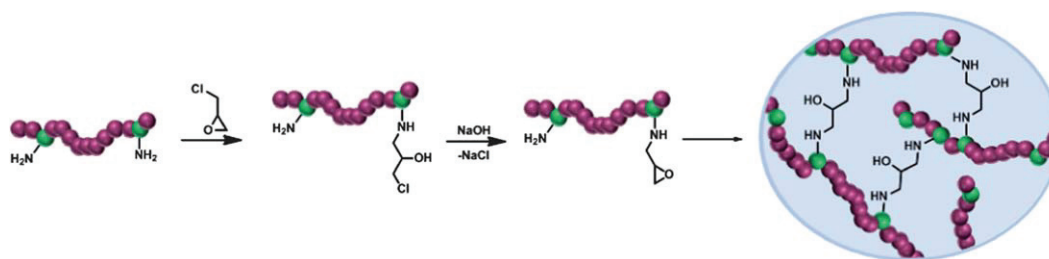
The swelling degrees were measured according to the literature by centrifugation of the swollen sample for 10 min at 3000 rpm.<sup>54</sup> The results are depicted in Table 3. No clear trend in the swelling degree with the ratio between the two monomers is visible, although a strong dependency on the gelled polymer fraction was observed. With an increasing amount of cross-linking, more polymer chains are incorporated into the scaffold, while the stiffness of the network increases. Therefore, an increased gelled polymer fraction indicates a more efficient cross-linking which leads to lower swelling degrees, because the balance of the Gibbs free energy of mixing and the Gibbs free energy associated with the elastic nature of the polymer network is changed.<sup>61</sup> However, the most outstanding property for the binding of DNA is the content of amino groups which is linearly increasing within the series of hydrogels.

### DNA-binding and release

The ability of the synthesized polymers to complex DNA in aqueous solution is crucial for the aimed application. The ethidium bromide assay offers the possibility to investigate this interaction by the measurement of the fluorescence intensity of the dye. The intensity differs depending on the environment of the ethidium bromide. The dye, incorporated into a DNA helix, shows enhanced fluorescence intensity in comparison to the

**Fig. 4** Comparison of the NMR data of P(EtOx-*stat*-BocOx) (in CDCl<sub>3</sub>) and the deprotected polymers P(EtOx-*stat*-AmOx) (in MeOD).





**Scheme 2** Schematic representation of the hydrogel synthesis using P(EtOx-*stat*-AmOx) and epichlorohydrin.

**Table 3** Overview of P(EtOx-*stat*-PAmOx) based hydrogels (per gel 100 mg of polymer were used as the starting material)

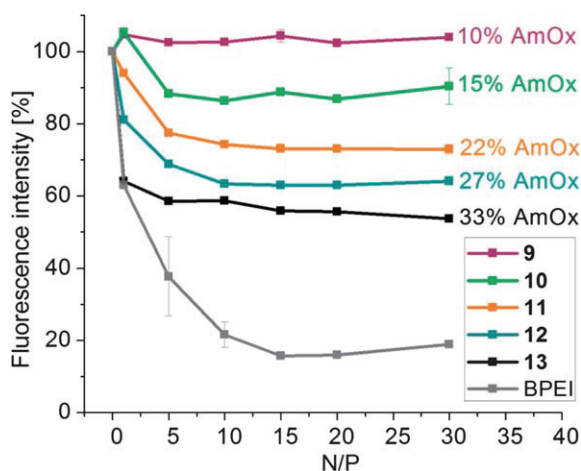
Sample number	Feed material	Epichlorohydrin [ $\mu\text{L}$ ]	Ratio ( $\text{NH}_2$ : ECH)	Swelling degree [%]	Gelated polymer fraction [%]
23	P(EtOx <sub>43</sub> - <i>stat</i> -PAmOx <sub>5</sub> )	3.92	5 : 5	97.4 $\pm$ 0.2	34
24	P(EtOx <sub>39</sub> - <i>stat</i> -PAmOx <sub>7</sub> )	3.92	7 : 5	94.6 $\pm$ 0.7	45
25	P(EtOx <sub>32</sub> - <i>stat</i> -PAmOx <sub>9</sub> )	4.31	9 : 5	91.1 $\pm$ 0.3	49
26	P(EtOx <sub>38</sub> - <i>stat</i> -PAmOx <sub>15</sub> )	3.33	15 : 5	95.7 $\pm$ 0.1	42
27	P(EtOx <sub>32</sub> - <i>stat</i> -PAmOx <sub>16</sub> )	3.73	16 : 5	97.7 $\pm$ 0.4	32

free, dissolved species. By displacement of EB with cationic species, such as polycations, the fluorescence intensity decreases and the quality of the complexation can be determined. BPEI (10 kDa) was used as a reference for the performed tests. The results of the EBA for P(EtOx-*stat*-AmOx) are depicted in Fig. 5.

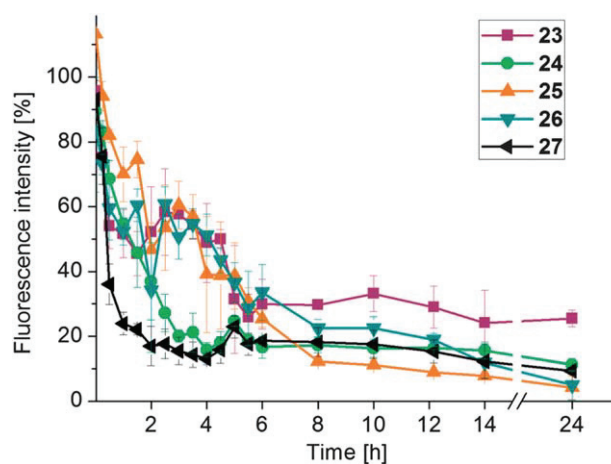
Most of the copolymers show an interaction with DNA. While a content of 10% amino bearing monomer per chain seems to be insufficient for a replacement of ethidium bromide, all other samples decrease the fluorescence intensity. Furthermore, a dependency on the strength of interaction with the amount of amino functions is clearly visible. With an increase of 5% of amino groups per chain it is possible to decrease the fluorescence intensity by around 10%. The plateau, where a further excess of positive charges is not able to replace more dye, is reached for all samples at an N/P ratio of 5. However, BPEI shows a higher complexation efficiency which can be attributed

to its higher charge density. The point of saturation of BPEI is reached at an N/P ratio of 15 in this assay. To investigate the DNA binding potential of the hydrogels, the procedure for the EBA was changed. With an insoluble substrate it is not possible to dilute a stock solution and reach relatively low concentrations as performed for the copolymers. However, for comparison reasons, the chosen N/P value of 1000 was equal for all hydrogel samples in the tests. The amount of gel varied between 0.8 and 2.25 mg per well depending on the content of amines in the scaffold. Subsequently, the hydrogel samples were swollen in a 24-well plate in 250  $\mu\text{L}$  of HBG buffer solution. The amount of buffer was not adjusted to the swelling degree to ensure that the dilution of DNA-EB stock solution is identical for each well.

After 24 h of swelling, 1 mL of the mentioned stock solution was added. For every time interval a sample of 50  $\mu\text{L}$  was taken and investigated regarding its fluorescence intensity. The results of these measurements are depicted in Fig. 6. It is clearly visible that all gel samples decrease the fluorescence intensity



**Fig. 5** EBA of P(EtOx-*stat*-AmOx) (branched polyethylene imine (BPEI) was used as positive control).



**Fig. 6** EBA of P(EtOx-*stat*-AmOx) hydrogels.

over time. A solution of EB–DNA was used as a reference for each measuring point and treated in the same way as the other samples. Therefore, the decrease of intensity cannot be attributed to a degradation of the EB–DNA complex over time. In contrast to the polymeric precursors, no clear trend concerning the percental amount of amino groups is visible, though the gel with the highest content of AmOx (27) reaches the plateau of constant fluorescence in 2 h before the other samples. Moreover, it can be observed that the fluorescence intensity reached by the gel with the lowest amount of comonomer (23) is in contrast to the other samples 10% higher. A possible explanation is that this gel is saturated with DNA at the point where the plateau is reached, while the absorbance capacity of the other gel samples is high enough to bind all DNA from the solution. The residual fluorescence signal of about 10% is attributed to the remaining fluorescence of the free dye in solution. The relatively large error bars, in particular in the region of strong changes of the intensity, are attributed to the solid substrate for DNA uptake. The long adsorption period of all gels indicates a diffusion control for the process of DNA immobilization. Differences of the surface/volume ratio lead to a large deviation between the three measurements which were performed for each gel.

For biochip applications it is necessary to absorb but also to release the DNA, using a certain stimulus. For the release studies, heparin, a polyanion with multiple negative charges per repeating unit, was used to replace the DNA in the polymeric scaffold. The heparin was dissolved in an aqueous EB solution of the same concentration as applied before. The released DNA should bind to the EB in solution and increase its fluorescence. As a standard for these measurements, an EB–DNA solution was used and defined as 100%. The concentration of DNA was equal to the amount, which should be bound in the gel if all material was adsorbed during the first assay. The results of the release studies are depicted in Fig. 7. The intensity increases rapidly after the addition of heparin and reaches a plateau at *ca.* 30 min for all samples. The fluorescence value of around 60% indicates an incomplete release. But also the dilution of the test solution by the buffer, which was still present in the swollen gel sample,

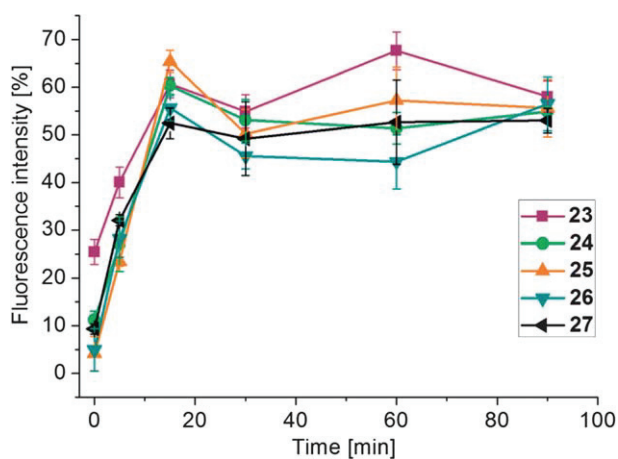


Fig. 7 Heparin induced release of DNA from P(EtOx-*stat*-AmOx) hydrogels.

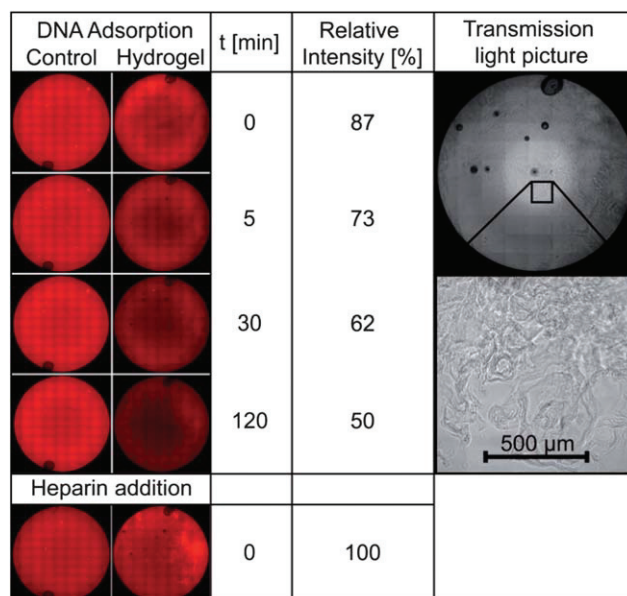


Fig. 8 Investigation of DNA binding and release using a fluorescence microscope (Gel sample 27). Left side: absorption and release of gene material in single wells (96-well plate), indicated by fluorescence (red). Right side: transmission light picture of the well with the swollen gel sample.

and a potential loss of hydrogel during the assay can be responsible for this observation.

As a final proof of the reversible absorption of DNA into P(EtOx-*stat*-AmOx) hydrogels, the process of immobilization and release was investigated using a fluorescence microscope (Fig. 8). The experiment clearly shows the decrease of fluorescence intensity of DNA–EB after the addition to the hydrogel as compared to the reference, containing a DNA–EB solution of the same concentration. The relative intensity values were calculated from the gray scale values of the samples normalized to the references. In contrast to the previous measurements, the fluorescence intensity only decreases to a value of 50%, which is related to the method. In contrast to the photometric measurements of the supernatant of P(EtOx-*stat*-AmOx) copolymers and the respective hydrogels, the microscopic study was performed with the complete sample including the hydrogel. Since the DNA, which is bound to the gel, has still free coordination sites for EB, a fluorescence signal is still detectable in the area associated with the hydrogel location. This observation was confirmed by the fact that the red fluorescence is more dominant in the boundary area of the well, where the hydrogel is mainly located, as indicated by the transmission light micrographs (Fig. 8).

The disintegration of the hydrogel-coordinated DNA turned out to be even faster than in the previous investigations. As indicated by the obtained gray scale values, a full release of DNA occurs immediately after the addition of heparin. The pictures clearly show an increased intensity in the area of the hydrogel which proves that the DNA is replaced by heparin but not diffused out of the gel (Fig. 8). This observation supports the assumption that the release of gene material from the hydrogels is diffusion controlled.

## Conclusion and outlook

In summary it was shown that amino bearing POx can be synthesized starting from an oxazoline monomer with a protected amino functionality at the 2-position (BocOx). Kinetic studies were performed for a homopolymerization and a series of polymers (PBocOx) were synthesized. The deprotected polymers (PAmOx) were characterized regarding their structure,  $T_g$  values and thermal degradation behavior. Because of a lack of water solubility of the resulting homopolymers, EtOx was used as a comonomer. Kinetic investigations revealed that both monomers possess similar polymerization rates in a copolymerization. P(EtOx-*stat*-BocOx) were synthesized with differing amounts of BocOx (10 to 33%) and deprotected subsequently. It was shown that these polymers are able to form complexes with DNA using the EB-assay. The strength of the interaction correlates directly with the amount of amino groups per polymer. P(EtOx-*stat*-AmOx)s were cross-linked using epichlorohydrin to form hydrogels. These polymeric scaffolds were investigated regarding their swelling degrees and ability to absorb DNA from aqueous solution in a similar manner as investigated for the polymer precursors. It was shown that all hydrogels possess the ability to immobilize DNA from solution. It was also possible to release DNA from the scaffolds by the addition of heparin as a polyanion. Amounts larger than 60% of the initial DNA quantity could be set free again by the replacement with heparin. The process was also investigated using a fluorescence microscope, proving the previous findings and indicating quantitative release.

Further studies will focus on the release of gene material from hydrogels by a certain stimulus. While heparin is sufficient to replace the DNA in the first tests, a release induced by temperature or pH change would be more meaningful with regard to the targeted applications. Furthermore, biochips will be equipped with the produced hydrogels by inkjet printing to check their ability for DNA enrichment also on a smaller scale.

## Acknowledgements

The authors would like to thank the Bundesministerium für Bildung und Forschung (Germany) for funding (project: BASIS, 03WKCB01C). Kristian Kempe acknowledges the Alexander von Humboldt foundation. Grateful thanks to Esra Altuntas (Friedrich Schiller University Jena) for ESI-MS, Sarah Crotty (Friedrich Schiller University Jena) for MALDI-ToF-MS measurements and Dr. Stephanie Schubert for correction of the manuscript.

## Notes and references

- 1 J. Peeters and P. Van der Spek, *Cell Biochem. Biophys.*, 2005, **43**, 149–166.
- 2 T. R. Gingeras, D. Y. Kwoh and G. R. Davis, *Nucleic Acids Res.*, 1987, **15**, 5373–5390.
- 3 J. M. Anderton, R. Tokarz, C. D. Thill, C. J. Kuhlow, C. S. Brooks, D. R. Akins, L. I. Katona and J. L. Benach, *Infect. Immun.*, 2004, **72**, 2035–2044.
- 4 C. W. Wong, T. J. Albert, V. B. Vega, J. E. Norton, D. J. Cutler, T. A. Richmond, L. W. Stanton, E. T. Liu and L. D. Miller, *Genome Res.*, 2004, **14**, 398–405.
- 5 L. G. Britcher, D. C. Kehoe, J. G. Matisons, R. S. C. Smart and A. G. Swincer, *Langmuir*, 1993, **9**, 1609–1613.
- 6 B. Joos, H. Kuster and R. Cone, *Anal. Biochem.*, 1997, **247**, 96–101.
- 7 Y.-H. Rogers, P. Jiang-Baucom, Z.-J. Huang, V. Bogdanov, S. Anderson and M. T. Boyce-Jacino, *Anal. Biochem.*, 1999, **266**, 23–30.
- 8 A. B. Steel, R. L. Levicky, T. M. Herne and M. J. Tarlov, *Biophys. J.*, 2000, **79**, 975–981.
- 9 F. Fixe, M. Dufva, P. Telleman and C. B. V. Christensen, *Nucleic Acids Res.*, 2004, **32**, e9.
- 10 E. Waddell, Y. Wang, W. Stryjewski, S. McWhorter, A. C. Henry, D. Evans, R. L. McCarley and S. A. Soper, *Anal. Chem.*, 2000, **72**, 5907–5917.
- 11 A. W. Peterson, R. J. Heaton and R. M. Georgiadis, *Nucleic Acids Res.*, 2001, **29**, 5163–5168.
- 12 J. B. Rampal, *Microarrays: Synthesis Methods*, Humana Press, Totowa, 2001.
- 13 P. Anzenbacher Jr, Y.-l. Liu and M. E. Kozelkova, *Curr. Opin. Chem. Biol.*, 2010, **14**, 693–704.
- 14 D. Guschin, G. Yershov, A. Zaslavsky, A. Gemmell, V. Shick, D. Proudnikov, P. Arenkov and A. Mirzabekov, *Anal. Biochem.*, 1997, **250**, 203–211.
- 15 O. Okay, *J. Polym. Sci., Part B: Polym. Phys.*, 2011, **49**, 551–556.
- 16 F. Kivlehan, M. Paolucci, D. Brennan, I. Ragoussis and P. Galvin, *Anal. Biochem.*, 2012, **421**, 1–8.
- 17 J. Liu, *Soft Matter*, 2011, **7**, 6757–6767.
- 18 M. Wink, *An Introduction to Molecular Biotechnology: Molecular Fundamentals, Methods and Applications in Modern Biotechnology*, Wiley-VCH, Weinheim, Germany, 2006.
- 19 K. Doyle, *The Source of Discovery: Protocols and Applications Guide*, PROMEGA, Madison, Wis, USA, 1996.
- 20 L. Buckingham and M. L. Flaws, *Molecular Diagnostics: Fundamentals, Methods, & Clinical Applications*, F. A. Davis, Philadelphia, Pa, USA, 2007.
- 21 J. Sambrook and D. Russel, *Molecular Cloning: A Laboratory Manual*, Cold Spring Harbor Laboratory Press, New York, NY, USA, 2001.
- 22 *Pierce Strong Ion Exchange Spin Columns*, Thermo Scientific, New Hampshire, NH, USA, 2007.
- 23 *QIAGEN Genomic DNA Handbook*, QIAGEN, Valencia, Calif, USA, 2001.
- 24 D. T. Gjerse, L. Hoang and D. Hornby, *RNA Purification and Analysis: Sample Preparation, Extraction, Chromatography*, Wiley-VCH, Weinheim, Germany, 2009.
- 25 K.-H. Esser, W. H. Marx and T. Lisowsky, *BioTechniques*, 2005, **39**, 270–271.
- 26 H. Pollard, J.-S. Remy, G. Loussouarn, S. Demolombe, J.-P. Behr and D. Escande, *J. Biol. Chem.*, 1998, **273**, 7507–7511.
- 27 O. Boussif, F. Lezoualc'h, M. A. Zanta, M. D. Mergny, D. Scherman, B. Demeneix and J. P. Behr, *Proc. Natl. Acad. Sci. U. S. A.*, 1995, **92**, 7297–7301.



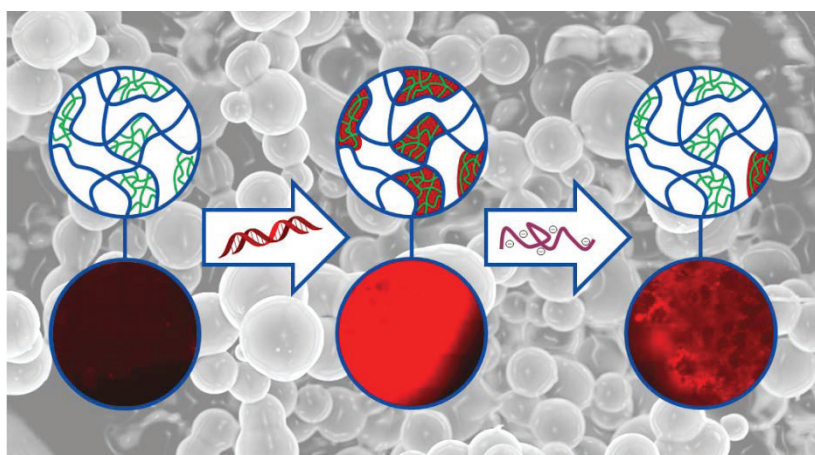
- 28 G. Y. Wu and C. H. Wu, *J. Biol. Chem.*, 1988, **263**, 14621–14624.
- 29 G. Y. Wu and C. H. Wu, *J. Biol. Chem.*, 1987, **262**, 4429–4432.
- 30 J. Luten, N. Akeroyd, A. Funhoff, M. C. Lok, H. Talsma and W. E. Hennink, *Bioconjugate Chem.*, 2006, **17**, 1077–1084.
- 31 A. M. Funhoff, C. F. van Nostrum, A. P. C. A. Janssen, M. H. A. M. Fens, D. J. A. Crommelin and W. E. Hennink, *Pharm. Res.*, 2004, **21**, 170–176.
- 32 P. van de Wetering, J.-Y. Cherng, H. Talsma and W. E. Hennink, *J. Controlled Release*, 1997, **49**, 59–69.
- 33 M. A. Mintzer and E. E. Simanek, *Chem. Rev.*, 2008, **109**, 259–302.
- 34 D. D. Dunlap, A. Maggi, M. R. Soria and L. Monaco, *Nucleic Acids Res.*, 1997, **25**, 3095–3101.
- 35 H. P. C. Van Kuringen, J. Lenoir, E. Adriaens, J. Bender, B. G. De Geest and R. Hoogenboom, *Macromol. Biosci.*, 2012, **12**, 1114–1123.
- 36 L. Tauhardt, K. Kempe, K. Knop, E. Altuntaş, M. Jäger, S. Schubert, D. Fischer and U. S. Schubert, *Macromol. Chem. Phys.*, 2011, **212**, 1918–1924.
- 37 A. Kichler, *J. Gene Med.*, 2004, **6**, 3–10.
- 38 G.-H. Hsiue, H.-Z. Chiang, C.-H. Wang and T.-M. Juang, *Bioconjugate Chem.*, 2006, **17**, 781–786.
- 39 R. Arote, T.-H. Kim, Y.-K. Kim, S.-K. Hwang, H.-L. Jiang, H.-H. Song, J.-W. Nah, M.-H. Cho and C.-S. Cho, *Biomaterials*, 2007, **28**, 735–744.
- 40 X. Shuai, T. Merdan, F. Unger, M. Wittmar and T. Kissel, *Macromolecules*, 2003, **36**, 5751–5759.
- 41 M. Jäger, S. Schubert, S. Ochrimenko, D. Fischer and U. S. Schubert, *Chem. Soc. Rev.*, 2012, **41**, 4755–4767.
- 42 B. Guillermin, S. Monge, V. Lapinte and J.-J. Robin, *Macromol. Rapid Commun.*, 2012, **33**, 6000–6016.
- 43 K. Kempe, R. Hoogenboom, M. Jaeger and U. S. Schubert, *Macromolecules*, 2011, **44**, 6424–6432.
- 44 K. Kempe, M. Lobert, R. Hoogenboom and U. S. Schubert, *J. Polym. Sci., Part A: Polym. Chem.*, 2009, **47**, 3829–3838.
- 45 N. Adams and U. S. Schubert, *Adv. Drug Delivery Rev.*, 2007, **59**, 1504–1520.
- 46 S. Cesana, J. Auernheimer, R. Jordan, H. Kessler and O. Nuyken, *Macromol. Chem. Phys.*, 2006, **207**, 183–192.
- 47 Y. Chujo, Y. Yoshifuji, K. Sada and T. Saegusa, *Macromolecules*, 1989, **22**, 1074–1077.
- 48 Y. Chujo, K. Sada and T. Saegusa, *Macromolecules*, 1990, **23**, 2636–2641.
- 49 Y. Chujo, K. Sada and T. Saegusa, *Polym. J.*, 1993, **25**, 599–608.
- 50 J.-J. Yuan and R.-H. Jin, *Langmuir*, 2005, **21**, 3136–3145.
- 51 D. Kim and K. Park, *Polymer*, 2004, **45**, 189–196.
- 52 F. Khan, R. S. Tare, R. O. C. Oreffo and M. Bradley, *Angew. Chem., Int. Ed.*, 2009, **48**, 978–982.
- 53 Fino, *et al.*, *US Pat.*, US 4476229, 1984.
- 54 A. Koschella, M. Hartlieb and T. Heinze, *Carbohydr. Polym.*, 2011, **86**, 154–161.
- 55 A. N. Zelikin, E. S. Trukhanova, D. Putnam, V. A. Izumrudov and A. A. Litmanovich, *J. Am. Chem. Soc.*, 2003, **125**, 13693–13699.
- 56 R. Hoogenboom, M. W. M. Fijten, H. M. L. Thijs, B. M. van Lankvelt and U. S. Schubert, *Des. Monomers Polym.*, 2005, **8**, 659–671.
- 57 F. Wiesbrock, R. Hoogenboom, M. A. M. Leenen, M. A. R. Meier and U. S. Schubert, *Macromolecules*, 2005, **38**, 5025–5034.
- 58 P. Claudy, J. M. Létoffé, Y. Camberlain and J. P. Pascault, *Polym. Bull.*, 1983, **9**, 208–215.
- 59 C. Weber, A. Krieg, R. M. Paulus, H. M. L. Lambermont-Thijs, C. R. Becer, R. Hoogenboom and U. S. Schubert, *Macromol. Symp.*, 2011, **308**, 17–24.
- 60 P. G. M. Wuts and T. W. Greene, *Greene's Protective Groups in Organic Synthesis*, Wiley-VCH, Weinheim, 4th edn, 2006.
- 61 M. E. Byrne, K. Park and N. A. Peppas, *Adv. Drug Delivery Rev.*, 2002, **54**, 149–161.

## Publication 3

„Matrix supported poly(2-oxazoline)-based hydrogels for DNA catch and release“

M. Hartlieb, D. Pretzel, C. Englert, M. Hentschel, K. Kempe, M. Gottschaldt, U. S. Schubert

*Biomacromolecules* **2014**, *15*, 1970-1978.



# Matrix Supported Poly(2-oxazoline)-Based Hydrogels for DNA Catch and Release

Matthias Hartlieb,<sup>†,‡</sup> David Pretzel,<sup>†,‡</sup> Christoph Englert,<sup>†,‡</sup> Martin Hentschel,<sup>§</sup> Kristian Kempe,<sup>†,‡,||</sup> Michael Gottschaldt,<sup>†,‡</sup> and Ulrich S. Schubert<sup>\*,†,‡</sup>

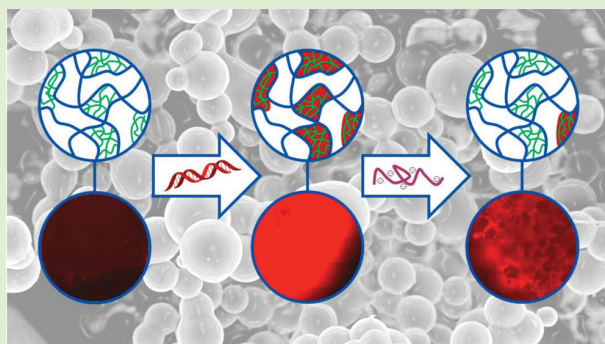
<sup>†</sup>Laboratory of Organic and Macromolecular Chemistry (IOMC), Friedrich Schiller University Jena, Humboldtstrasse 10, 07743 Jena, Germany

<sup>‡</sup>Jena Center for Soft Matter (JCSM), Friedrich Schiller University Jena, Philosophenweg 7, 07743 Jena, Germany

<sup>§</sup>Analytik Jena AG, Konrad-Zuse-Straße 1, 07745 Jena, Germany

## S Supporting Information

**ABSTRACT:** We describe the synthesis of matrix supported hydrogel structures based on amine containing poly(2-oxazoline)s and their use to bind and release genetic material for potential applications in diagnostics or pathogen detection. Amine containing poly(2-oxazoline)s were synthesized by copolymerization of 2-ethyl-2-oxazoline with a monomer bearing a *tert*-butyl oxycarbonyl (Boc) protected amine group in the 2-position and subsequent deprotection. The statistical copolymers were used to generate hydrogels and matrix supported hydrogels by cross-linking of a certain fraction of the amine groups with epichlorhydrin. Supported structures were prepared by soaking porous polyethylene (PE) or polypropylene (PP) filter materials in a copolymer/epichlorhydrin solution, which was cross-linked upon heating. Scanning electron microscopy (SEM) of the composites revealed a bead like structure of the gel phase, which could be attributed to a lower critical solution temperature (LCST) behavior of the initial polymer prior to gelation. The dependency of the LCST behavior on the content of amine groups was investigated. Swelling values and the ratio of hydrogel per composite was determined using water sorption analysis. Subsequently, the ability of the systems to absorb and release labeled DNA was tested. Uptake and stimulated release, triggered by changes in pH, temperature, and heparin concentration, were investigated using fluorescence microscopy. Polymerase chain reaction (PCR) proved the successful recovery of the DNA, demonstrating the potential of the presented system for a broad range of molecular biological applications.



## INTRODUCTION

The isolation of nucleic acids from biological samples, such as cells, tissues, and viruses, is of significant importance for DNA-based applications in modern clinical diagnostics,<sup>1</sup> genetic analysis,<sup>2</sup> drug discovery,<sup>3</sup> and pathogen detection.<sup>4</sup> To guarantee a successful and specific detection of DNA sequences in downstream processes, purification of the genetic material is the main requirement. An optimal DNA extraction system comprises the fast and efficient isolation of DNA ideally directly from complex biological samples, the avoidance of toxic reagents and inhibitory substances, and a cost-effective fabrication enabling disposable devices.<sup>5,6</sup> However, the low amount of DNA in cell/tissue extracts and its structural and chemical similarity to other cell components (size, negative charge, molecular mass, and hydrophobicity)<sup>7</sup> results in poor selectivity and considerable coelution.<sup>8</sup>

A broad diversity of DNA purification and extraction techniques have been developed in the past decades, and up to now, no universal purification method exists.<sup>9</sup> Well

established approaches are based on, e.g., phenol–chloroform extraction or CsCl/ethidium bromide density gradient centrifugation. These extraction techniques, performed in liquid phases, are time-consuming and associated with the use of toxic, hazardous reagents.<sup>10,11</sup> Solid phase extraction (SPE) techniques using mostly glass fiber, silicon dioxide, diatomaceous earth, nitrocellulose, polyamide, or anion exchange resins as solid phases have become the most common method to prepare DNA samples for genetic analysis and other biomedical techniques.<sup>12–17</sup>

In consideration of the fact that the potential of common SPE is fairly exhausted, future developments need to involve new materials. A highly promising alternative approach is the catch and release of DNA molecules within a three-dimensional hydrogel matrix. Hydrogels possess a high water content, resulting in a mobility of guest molecules by diffusion,<sup>18</sup> are

Received: November 10, 2013

Published: February 26, 2014

tunable in pore size<sup>19</sup> and chemical functionality,<sup>20</sup> and most importantly, they provide a large surface area for binding of targeted molecules. To make use of these systems for DNA purification processes, hydrogels can be endowed with, e.g., cationic functionalities, which enables electrostatic interactions with the negatively charged DNA. The advantage of this approach over SPE is the avoidance of chaotropic salt solutions and alcohols, which can contaminate the samples and, e.g., inhibit polymerase chain reactions (PCR).<sup>21</sup> In addition, hydrogels exhibit an inherent wettability enabling the efficient interaction with the DNA containing solution in contrast to the often relatively hydrophobic solid surfaces. Elution from the hydrogel can be performed either specifically, using a competitive ligand, or nonspecifically, by changing the pH, ionic strength, or polarity of the solvent depending on the matrix used and the chemical characteristics of the biomolecules.

Poly(2-oxazoline)s (POx) represent a highly promising platform for the synthesis of functional materials. The living cationic ring-opening polymerization (CROP) of 2-oxazolines, which was discovered in 1966,<sup>22–25</sup> enables the design of well-defined (co)polymers with tailored molar mass and functionalities.<sup>26</sup> The polymer properties are mainly determined by the choice of the monomer and can be further fine-tuned by the introduction of functional groups that are able to be modified in postpolymerization reactions.<sup>27,28</sup> The first examples of POx-based hydrogels were reported in 1989 by Saegusa and co-workers. The authors copolymerized conventional monomers with bis-functional oxazolines.<sup>29</sup> In the following years, their method of choice was the partial hydrolysis of POx and the subsequent esterification of the resulting poly(ethylene imine) units. Using this approach, it was possible to introduce several functionalities and to cross-link the polymers via secondary interactions<sup>30–32</sup> or covalent bonds.<sup>33–35</sup> More than one decade later, other groups continued studying POx-based networks and reported different approaches for the network synthesis, e.g., by the preparation of methacrylate functionalized POx macromonomers and their use as cross-linker in radical polymerizations.<sup>36–39</sup> The first example of amine bearing POx and their general ability to form hydrogels was reported by Cesana et al. in 2006.<sup>40</sup> In more detail, we recently studied the kinetics of a 2-oxazoline monomer with a protected amine functionality and were able to produce polymers and networks with defined compositions. Furthermore, we could show that these systems are able to reversibly bind genetic material from solution.<sup>18</sup> However, before these systems can be used in the above-mentioned applications, two problems have to be solved: (i) the lack of mechanical stability of the hydrogels (in particular relevant for common extraction protocols requiring centrifugation steps that cause considerable shear forces) and (ii) the dependence of the release process on high concentrations of heparin, which would interfere with subsequently performed PCR. To overcome the former issue, the use of a supportive inert polymer-based matrix in which the hydrogel component is localized represents a promising approach. While the (amine-containing) hydrogel network is meant to bind and release DNA, the second network introduces additional stability and protects it from mechanical degradation. The latter issue can be overcome by a change in the release stimuli, using temperature and pH changes or by a reduction of the initial heparin concentration.

In this contribution, we report on the fabrication of composite materials composed of a polyethylene (PE) or

polypropylene (PP) matrix and amine containing POx hydrogels. To gain insights into the phase conditions during formation of the POx hydrogels, the LCST behavior of the precursor polymer in dependence of the amine content was studied. The microstructure of the produced hydrogels was investigated via SEM, and the ability of the substrates to absorb water from the gas phase was determined using TGA. The potential of the material for binding and release of DNA in dependence of the heparin concentration was studied using fluorescence microscopy.

## EXPERIMENTAL SECTION

**Materials and Instrumentation.** All chemicals and solvents were purchased from Sigma-Aldrich, Merck, Fluka, and Acros. 2-Ethyl-2-oxazoline (EtOx) and methyl tosylate (MeTos) were distilled to dryness prior to use.

2-(4-((*tert*-Butoxycarbonyl)amino)butyl)-2-oxazoline (BocOx) was synthesized as described in our previous work.<sup>41</sup> Filter substrates consisting of PE (90  $\mu\text{m}$  pore size) or PP (120  $\mu\text{m}$  pore size) were purchased from Porex technologies GmbH and perforated to pills with a diameter of 7 mm and a thickness of 1.6 mm. CyS labeled DNA was provided by Analytik Jena.

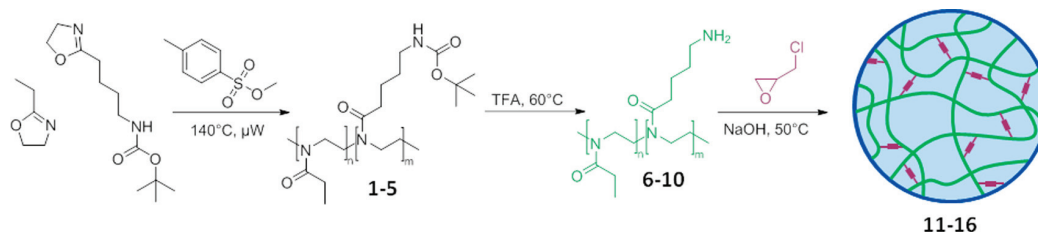
The Initiator Sixty single-mode microwave synthesizer from Biotage, equipped with a noninvasive IR sensor (accuracy 2%), was used for polymerizations under microwave irradiation. Microwave vials were heated overnight to 110 °C and allowed to cool to room temperature under argon atmosphere before usage. All polymerizations were carried out under temperature control. Size-exclusion chromatography (SEC) of protected polymers was performed on a Shimadzu system equipped with a SCL-10A system controller, a LC-10AD pump, a RID-10A refractive index detector, and a PSS SDV column with chloroform/triethylamine ( $\text{NEt}_3$ )/2-propanol (94:4:2) as eluent. The column oven was set to 50 °C. SEC of the deprotected statistical copolymers was performed on a Shimadzu system with a LC-10AD pump, a RID-10A refractive index detector, a system controller SCL-10A, a degasser DGU-14A, and a CTO-10A column oven using *N,N*-dimethylacetamide with 2.1 g/L LiCl as the eluent and the column oven set to 50 °C. Poly(styrene) (PS) samples were used as calibration standards for both solvent systems. Proton NMR spectroscopy (<sup>1</sup>H NMR) measurements were performed at room temperature on a Bruker AC 300 and 400 MHz spectrometer, using  $\text{CDCl}_3$  or MeOD as solvents. The chemical shifts are given in ppm relative to the signal from the residual nondeuterated solvent. Fourier transform infrared (FTIR) spectroscopy was performed on an Affinity-1 FT-IR from Shimadzu, using the reflection technique. Gas chromatography (GC) was performed on a GC-2010 from Shimadzu. Acetonitrile was used as an internal standard to determine the monomer conversion. Scanning electron microscopy (SEM) was measured using a field emission scanning electron microscope Gemini 1530 type LEO from Carl Zeiss AG, Germany. Investigated samples were freeze-dried matrix supported hydrogels. Cloud points were determined in a Crystal 16 from Avantium Technologies connected to a chiller (Julabo FP 40) at a wavelength of 500 nm.

**Copolymerization of EtOx and BocOx (P(EtOx-stat-BocOx)) (1–5).** In a microwave vial, EtOx (181.7  $\mu\text{L}$ , 1.8 mmol), MeTos (90.8  $\mu\text{L}$ , 0.600 mmol), and acetonitrile (11.5 mL) were mixed under inert conditions. After heating in the microwave at 140 °C for 16 min, EtOx (2543  $\mu\text{L}$ , 25.2 mmol) and BocOx (749  $\mu\text{L}$ , 3 mmol) were added under argon stream and the mixture was heated again in the microwave synthesizer (140 °C, 11 min). The solution was diluted with dichloromethane (100 mL) and extracted with saturated aqueous solution of sodium bicarbonate (3  $\times$  100 mL) and water (3  $\times$  100 mL). Subsequently, the solution was concentrated and the polymer was precipitated in 400 mL ice-cold diethyl ether. The white precipitate was filtered and dried in high vacuum (2.77 g, 78%).

<sup>1</sup>H NMR ( $\text{CDCl}_3$ , 300 MHz):  $\delta$  = 4.99 (s, 0.2 H, NH), 3.45 (s, 4 H, backbone), 3.11 (s, 0.3 H,  $\text{CH}_2\text{-CH}_2\text{-NH}$  (BocOx)), 2.40 (s, 1.9 H,  $\text{CH}_2$  (EtOx)), 1.92 (s, 0.3 H,  $\text{CH}_2\text{-CH}_2\text{-CO}$  (BocOx)), 1.64 (s, 0.3



Scheme 1. Schematic Representation of the Polymer and Hydrogel Synthesis



H, CH<sub>2</sub>–CH<sub>2</sub>–CH<sub>2</sub> (BocOx)), 1.53 (s, 0.3 H, CH<sub>2</sub>–CH<sub>2</sub>–CH<sub>2</sub> (BocOx)), 1.42 (s, CH<sub>3</sub> (BocOx)), 1.21 (s, 1.3 H, CH<sub>3</sub> (EtOx)) ppm.

SEC (9) (eluent: CHCl<sub>3</sub>/2-propanol/NEt<sub>3</sub>, PS-standard):  $M_n$  = 5300 g/mol,  $M_w$  = 5700 g/mol, PDI = 1.08.

**Deprotection of P(EtOx-stat-BocOx) (P(EtOx-stat-AmOx) (6–10).** Exemplarily, P(EtOx-stat-BocOx) (1, 2 g) was dissolved in trifluoroacetic acid (TFA) (5 mL) and heated at 60 °C for 1 h. After stirring for 24 h at room temperature, the mixture was diluted with 10 mL of methanol and precipitated in 400 mL of cold diethyl ether. The yellowish precipitate was redissolved in methanol (200 mL) and stirred with Amberlyst A21 for 24 h. Subsequently, the solution was concentrated and the polymer was precipitated in cold diethyl ether (400 mL), filtered, dried in high vacuum, and obtained as a yellowish powder (1.58 g, 87%).

<sup>1</sup>H NMR (MeOD, 400 MHz):  $\delta$  = 3.52 (s, 4 H, backbone), 2.96 (0.23 H, s, CH<sub>2</sub>–CH<sub>2</sub>–NH<sub>2</sub>), 2.42 (2 H, s, CH<sub>2</sub> (EtOx) + CH<sub>2</sub>–CH<sub>2</sub>–CO (AmOx)), 1.69 (0.41 H, s, CH<sub>2</sub>–CH<sub>2</sub>–CH<sub>2</sub>–CH<sub>2</sub> (AmOx)), 1.11 (2.8 H, s, CH<sub>3</sub> (EtOx)) ppm.

SEC (18) (eluent: DMAc/LiCl, PS-standard):  $M_n$  = 8,100 g/mol,  $M_w$  = 10,200 g/mol, PDI = 1.26.

**Investigation of the Cloud Point Behavior of P(EtOx-stat-PAmOx).** To determine the temperature responsive solubility changes of P(EtOx-stat-AmOx), the polymer was dissolved in distilled water at different concentrations ranging from 0.4 to 100 mg/mL. The solutions were heated from 2 to 100 °C under stirring with a heating rate of 1 °C/min. The turbidity of the solution was recorded as a function of the temperature. The cloud point was defined as the temperature where the solution reaches 50% of transmission. Three heating cycles were performed, and the average value was used. For one measurement point, four samples of identical concentrations were investigated in parallel.

**Synthesis of Matrix Supported (11–16) and Nonsupported Hydrogels (17–19).** In a typical experiment, the filter substrates were swollen in a 1 mL solution of 9 (200 mg, 0.034 mmol, 0.51 mmol based on amine groups) and epichlorohydrin (6.66  $\mu$ L, 0.085 mmol) in 5 wt % sodium hydroxide (NaOH) solution. After 10 min, the mixture was heated to 50 °C for 1 h. The filter substrates were separated from the residual gel, washed in water (3  $\times$  100 mL, 1 day), and freeze-dried.

**Water Uptake Measurements.** The swelling of the matrix supported hydrogels was investigated using a TGA Q5000 SA thermogravimetric analyzer from TA Instruments Eschborn, Germany. For data evaluation the “Universal Analysis Software” was used. Substrates were dried in the machine at 60 °C and 0% relative humidity until weight constancy was reached. Water uptake was performed at room temperature and 90% relative humidity. The measurement was stopped when the samples were saturated with water.

The weight fraction of hydrogel in the composite materials was determined using eq 1.

$$m_{\text{HG}}(\text{wt}\%) = \frac{Q_{\text{ges}} - Q_{\text{F}}}{Q_{\text{HG}} - Q_{\text{F}}} \times 100\% \quad (1)$$

where  $Q_{\text{ges}}$  = swelling value of the composite,  $Q_{\text{HG}}$  = swelling value of the hydrogel, and  $Q_{\text{F}}$  = swelling value of the host matrix.

**DNA Binding and Release of Composite Materials.** DNA absorption of matrix supported hydrogels was measured using labeled

DNA (Cy5) and a fluorescence microscope (Cell Observer Z1, Carl Zeiss, Jena, Germany) equipped with a mercury arc UV lamp and the appropriate filter combinations for excitation and detection of emission. Images of a series (11  $\times$  11 pictures per well) were captured with a 10 $\times$  objective using identical instrument settings (e.g., UV lamp power, integration time, and camera gain), and spots of the 96-well plate were addressed using an automated XY table.

The matrix supported gels were swollen in HBG-buffer (HEPES buffered glucose, pH 7) for 30 min and, subsequently, in a DNA solution (500  $\mu$ L, 10  $\mu$ g/mL) for 30 min. After washing with buffer solution for another 30 min, the fluorescence of the substrates was detected. The release was accomplished applying a 2 mL of a 6 mg/mL heparin solution in water for 30 min. Surface adherent water was removed before each measurement. Fluorescence pictures were taken from the buffer-swollen material after DNA binding and washing and after the release took place.

**Stimuli Responsive Release.** The temperature, pH, and heparin concentration dependency of the release process was investigated by measuring the fluorescence of the supernatant of the matrix supported hydrogel after treatment with the respective condition for 1 h. Samples were swollen in a solution of Cy5-labeled DNA (200 mL, 10 ng/mL). Subsequently, the solution was removed and the gel was washed using 200  $\mu$ L of water. Again, the water was removed and replaced with either water, buffer (pH = 4), or heparin solution of varying concentration. After 1 h, the supernatant was analyzed using the Tecan M200 Pro fluorescence microplate reader (Crailsheim, Germany) at the following wavelengths: Ex 649 nm/Em 670 nm.

**DNA Extraction and Real-Time PCR Assay.** The gDNA extraction of a laboratory isolated strain of *Escherichia coli* K12 was performed with a magnetic particle based system for fully automated isolation and purification of nucleic acids (AJ InnuPure C16). The real-time PCR assay was realized in a AJ TOptical Real-time Thermocycler and was carried out in a 20  $\mu$ L of reaction mixture with the follow compositions: DNA extract (5  $\mu$ L), 0.025 units Taq DNA polymerase (AJ innuTaq Hot-A DNA polymerase), 4 mM magnesium chloride, 1.0 mM of deoxy-nucleotriphosphate, 2.5 mM buffer, 1 $\times$  EvaGreen Fluorescent DNA Stain, and 0.5  $\mu$ M of each primer. For amplification, an initial denaturation for 2 min at 95 °C was followed by 45 cycles of 95 °C for 30 s, 57 °C for 30 s, and 72 °C for 30 s. In this study, a DNA fragment of *E. coli* LacZ was used as positive control and without DNA as negative control. The PCR products were analyzed by agarose gel electrophoresis using 2.0% agarose gel containing ethidium bromide, and the gels were viewed on a UV transilluminator (AJ Biometra UVsolo TS). Additional information about the primers can be found in the Supporting Information.

## RESULTS AND DISCUSSION

**Polymer and Hydrogel Synthesis.** The synthesis of amine containing poly(2-oxazoline)s (POx)s was carried out, as described previously (Scheme 1).<sup>41</sup> 2-Ethyl-2-oxazoline (EtOx) was copolymerized with 2-(4-((*tert*-butoxycarbonyl)amino)-butyl)-2-oxazoline (BocOx), a 2-oxazoline monomer bearing a Boc-protected amine group in the side chain. To ensure that the initiator, namely methyl tosylate (MeTos), does not attack the Boc-protected amine group of the comonomer, an



macroinitiator containing three repeating units EtOx was synthesized in the first step. The increased sterically hindrance of the oxazolinium species is expected to diminish the reaction with the functional group. The respective primary amine containing copolymers (P(EtOx-*stat*-AmOx)) were obtained after deprotection of the amine group using TFA (Table 1).

**Table 1. Selected Analytical Data of the Amine Containing POx**

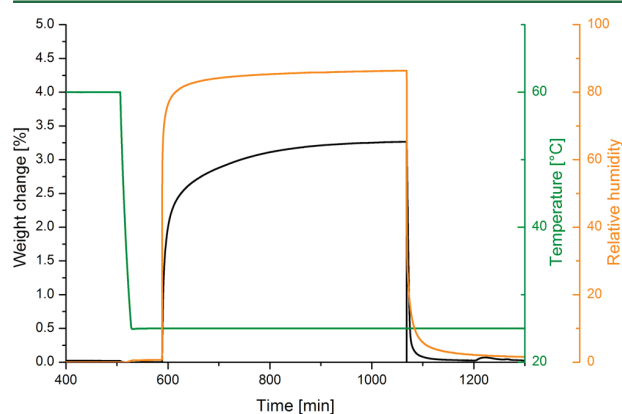
sample no.	polymer	Mn (SEC) [g/mol]	PDI	yield [%]	AmOx [%]
6	P(EtOx <sub>43</sub> - <i>stat</i> -PAmOx <sub>5</sub> )	8100	1.26	95	10
7	P(EtOx <sub>39</sub> - <i>stat</i> -PAmOx <sub>7</sub> )	8200	1.24	90	15
8	P(EtOx <sub>32</sub> - <i>stat</i> -PAmOx <sub>9</sub> )	8700	1.25	93	22
9	P(EtOx <sub>38</sub> - <i>stat</i> -PAmOx <sub>15</sub> )	9500	1.23	89	27
10	P(EtOx <sub>32</sub> - <i>stat</i> -PAmOx <sub>16</sub> )	9400	1.24	96	33

The gelation reaction was performed using epichlorhydrin (ECH) as cross-linker. Under the basic conditions applied (pH 14), ECH undergoes a ring-opening reaction with the amine groups of the copolymers. The resulting OH group and the chlorine group of ECH can reform an epoxide moiety by the elimination of hydrochloric acid. This functionality can undergo a second reaction to covalently cross-link the polymers.

**Matrix Supported Hydrogels.** For the fabrication of matrix supported hydrogels, polymer **9** was selected as it demonstrated good DNA binding capabilities.<sup>41</sup> A host network (PE or PP based porous filter substrate) was swollen in an aqueous solution of polymer (**9**), cross-linker (ECH), and sodium hydroxide for 30 min. The linker concentration was chosen to react with 33% (**11**, **14**), 66% (**12**, **15**), and 100% (**13**, **16**) of the available amine groups. Gelation occurred after 1 h at 50 °C. Subsequently, the filter substrates were separated from the supernatant gel and cleaned from surface adherent gel particles using a spatula. The composite material and the residual gels (**17–19**) were purified by washing with distilled water (3 × 5 mL per substrate, 24 h) and freeze-drying (Figure 1). Six different matrix supported gels were prepared comprising two host materials (PP and PE) with the three

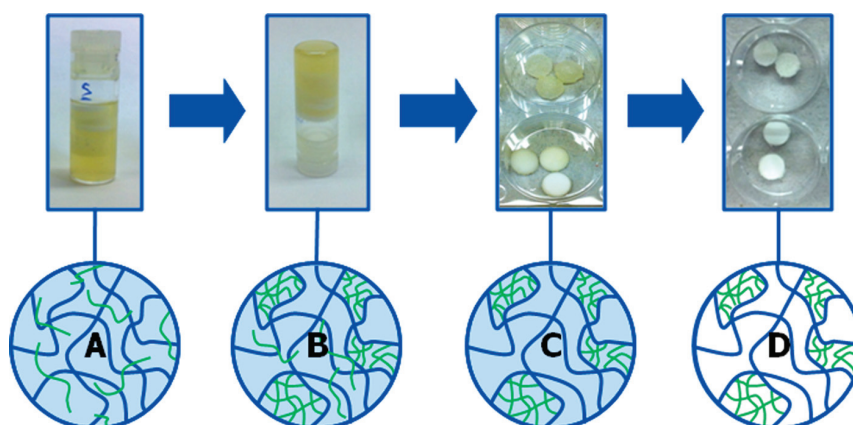
different degrees of cross-linking. The stoichiometry was calculated in assumption that every amine group reacted once with ECH resulting in a secondary amine. However, the real case is a mix of unreacted, secondary, and tertiary amines within the network.

A first evidence for the successful incorporation of the POx gel within the host matrix could be obtained by the investigation of the water uptake from the gas phase. This measurement was carried out using a special TGA setup where the sample weight can be determined in dependency of the relative humidity and temperature of the surrounding atmosphere. To exclude swelling prior to the measurement, the samples were annealed at 60 °C and 0% humidity for 2 h. After weight constancy was reached, the measurement was started by an increase of the relative humidity to 90% at room temperature. As depicted in Figure 2, the weight of the substrate increases upon this environmental change. The measurement was stopped when no further change of the sample weight could be detected.



**Figure 2.** Water uptake measurement of composite **11**.

The composition of hydrogels and matrix supported gels as well as the results of the water uptake studies are summarized in Table 2. The pure POx gels show a good swelling behavior from humid air and absorb up to 66% of their own weight of water. A trend is clearly visible; the higher the degree of cross-linking of the network, the lower the swelling value of the gel.



**Figure 1.** Synthesis of matrix supported gels from POx (green) within a host structure (blue): (A) Host material swollen in polymer solution, (B) gelled polymer within the pores of the host, (C) matrix supported gel separated from residual gel, and (D) isolated as well as freeze-dried product.

Table 2. Overview of the Synthesized Composite Materials and Hydrogels<sup>a</sup>

	11	12	13	14	15	16	17	18	19	PP	PE
substrate	PP	PP	PP	PE	PE	PE					
ratio ECH/amine (%)	33.0	66.0	100.0	33.0	66.0	100.0	33.0	66.0	100.0		
swelling value (%)	3.3	4.5	3.3	2.2	3.0	1.9	66.5	61.5	53.0	0.0	0.2
gel component (wt %)	5.0	7.3	6.2	3.0	4.6	3.2	100.0	100.0	100.0	0.0	0.0

<sup>a</sup>Polymer 9 was used for the gelation of the hydrophilic component.

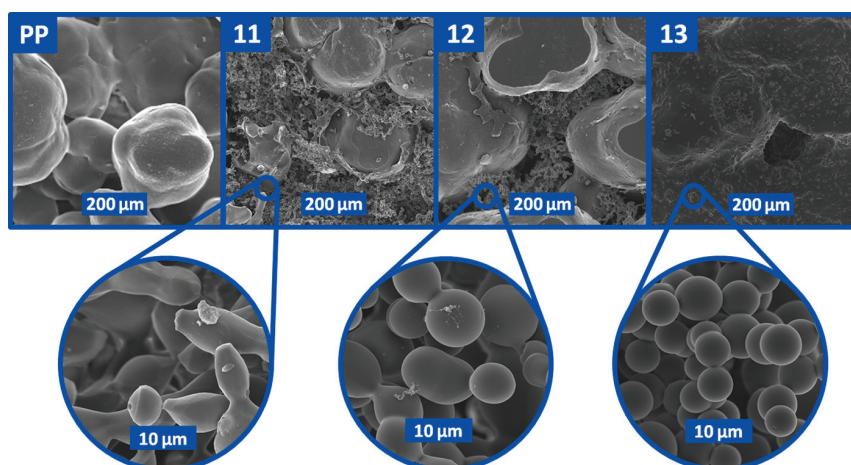


Figure 3. SEM pictures of PP-based composites. The magnified images show the appearance of hydrogel beads with a diameter of 5 to 10  $\mu\text{m}$ .

In contrast, the material based on the PE and PP host substrates only show minimal water uptake of 1.9 to 4.5%. In combination with the water uptake of the bare substrates (0.0% for PP and 0.2% for PE), this clearly indicates the presence of a second, hydrophilic component within the host matrix.

It was possible to calculate the mass of the entrapped gel from the swelling value of the composite and the water uptake of the single components. The fact that the PP-based materials contains more hydrogel is attributed to the pore size of the material which is larger than the one of PE (PP = 120  $\mu\text{m}$ , PE = 90  $\mu\text{m}$ ). Therefore, the swelling in the polymer solution prior to gelation is more efficient and results in a higher weight fraction.

A further proof of the proposed structure of the matrix supported gels could be obtained by SEM investigations (Figure 3). The large pore structure of the host material is visible in the first picture (PP). The images of the composites clearly show the existence of a second component within the host matrix consisting of a network of hydrogel beads. The bead size is similar for all different cross-linking degrees. Only the shape becomes more regular with increasing amount of linker. SEM pictures of the PE-based supported hydrogels can be found in the Supporting Information (Figure S2).

**LCST of the Copolymers.** The appearance of gel particles instead of a homogeneous network was unexpected. To understand this effect, the behavior of the polymer during the process of gelation (aqueous solution of sodium hydroxide (pH 14), 50  $^{\circ}\text{C}$ ) was investigated in more detail. Poly(2-ethyl-2-oxazoline) (PEtOx) based systems are known to exhibit lower critical solution temperature (LCST) behaviors in aqueous solution, i.e., EtOx-containing copolymers show a coil-to-globular transition at elevated temperatures.<sup>42</sup> If the polymers reported here reveal a cloud point behavior where the homogeneous solution separates into two phases with different polymer concentrations, gelation of only one phase would lead

to gel particles as observed. This phase transition can be investigated measuring the transmission of the solution in dependence of the applied temperatures because the turbidity of the solution increases by the light scattering of one phase.<sup>43</sup>

As depicted in Figure 4, all polymers exhibited cloud points in the investigated concentration range in aqueous solution

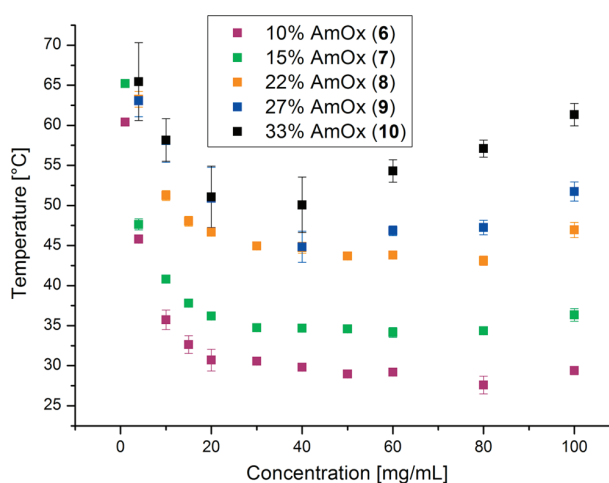


Figure 4. Concentration dependent evaluation of the cloud points of P(EtOx-stat-AmOx) at pH 14.

(pH 14). Furthermore, an influence of the polymer composition on the cloud point temperature was observed. An increased AmOx content resulted in increased cloud point temperature, with values between 25 and 65  $^{\circ}\text{C}$ . However, PEtOx itself exhibits a LCST behavior but only at higher molar masses and higher temperatures (61–69  $^{\circ}\text{C}$  for PEtOx with  $M_n$  of 20,000  $\text{g/mol}^{-1}$ ).<sup>42</sup> Therefore, the AmOx monomer seems

to have a significant effect on the thermal properties of these systems. The incorporation of 10 mol % AmOx causes a decrease of the cloud point temperature to almost as low as room temperature. A further increase of the AmOx amount should lead to a faster response and, therefore, to an even lower cloud point temperature. However, a contrary behavior was observed. This could be attributed to two competing trends. The polymer side chain exhibits two different domains: the hydrophobic alkyl chain and the hydrophilic amine group, which is not protonated at the pH values studied. While the hydrophobic domain induces the phase transition, the amine group promotes the water solubility. A stronger increase of the influence of the amine in comparison to the hydrophobic behavior of the alkyl chain could explain a rising cloud point with increasing amounts of comonomer, as observed. A different explanation could be the chaotropic influence of the high OH<sup>-</sup> concentration resulting in a lowering of the cloud point of the PEtOx part.

All investigated polymers exhibit LCSTs between 40 and 80 mg/mL under the conditions of the gelation reaction. Therefore, the polymer solution is phase separated before the gelation occurs. The cross-linking then proceeds in the phase with the high polymer concentration, forming small gel beads as visible in the SEM pictures.

This behavior is favorable for the foreseen application in several aspects. First of all, a bead-like structure provides a large surface to volume ratio, which is beneficial for the purpose of DNA capture and release because the diffusion control of the process is decreased. Moreover, the porous structure of the host material is not completely filled by the gel. This increases the ability of a sample solution to pass through the filter matrix in a given time without the need of intense force which is also beneficial for the targeted application where a sample solution should be pumped through the filter matrix on a short time scale.

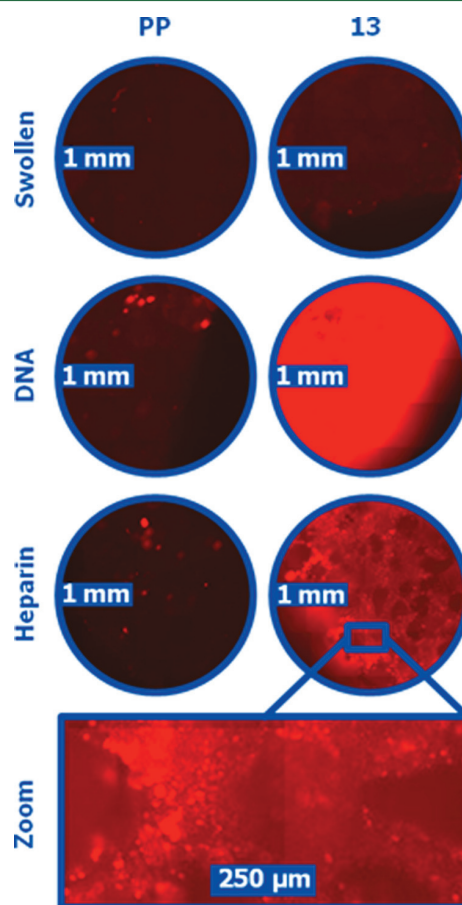
**DNA Binding and Release.** To investigate the ability of the synthesized composites to absorb and release genetic material, Cy5 (Abs, 649 nm; Em, 670 nm) labeled DNA was used. The location and concentration of this DNA derivative can be measured directly by spectroscopic and microscopic techniques tracking the fluorescence of the attached dye. In a general procedure, the matrix supported gels were swollen in HBG-buffer (HEPES buffered glucose, pH 7, 2 mL) for 30 min. Afterward, the samples were transferred into a DNA solution for 30 min. The prior swelling limits the penetration of the gel by DNA to passive diffusion. Subsequently, the gels were cleaned from adhered liquid and washed in buffer solution for another 30 min to exclude the detection of DNA which is not bound (Figure 5).

The samples were investigated using fluorescence microscopy. The results of the measurements for the PP-based composites are depicted in Figure 6 (uptake and release studies



**Figure 5.** Schematic representation of the DNA uptake and release by the composite materials. (A) Uptake of fluorescently labeled DNA by the hydrogel component and (B) release of DNA by the addition of heparin.

of all other supported hydrogels can be found in the Supporting Information, Figure S3).



**Figure 6.** DNA uptake and release of PP-based composite 13.

The first row shows fluorescence images of the samples which were swollen in buffer solution. The slightly increased intensity of the red color in comparison to the initial PP material resembles the autofluorescence of the hydrogel which is bound to the substrate. After the addition of DNA and a washing step, a bright fluorescence of the composite is visible while the bare PP matrix shows only some bright spots which are attributed to the encapsulation of DNA solution droplets within the pores of the material. Treatment of the filters with heparin solution (6 mg/mL) for 30 min caused a fraction of the bound DNA to be released again as depicted in the last row. Heparin is a polyanion able to replace genetic material in electrostatic complexes. In the enlargement of the picture, the microstructure of the hydrogel beads is clearly visible and provides a further proof that the POx hydrogel is responsible for the binding of DNA because only the beads light up under the fluorescence microscope.

While the release using heparin is an efficient method to regain the bound DNA, it has also drawbacks. The most prominent one is that heparin acts as an inhibitor in a PCR. Therefore, other stimuli for the release of DNA from the gels were tested. The most obvious trigger for this purpose is a change of the temperature. To investigate this influence, the DNA loaded substrates (13) were placed in water (500 μL) and heated to a specific temperature between 30 and 90 °C.



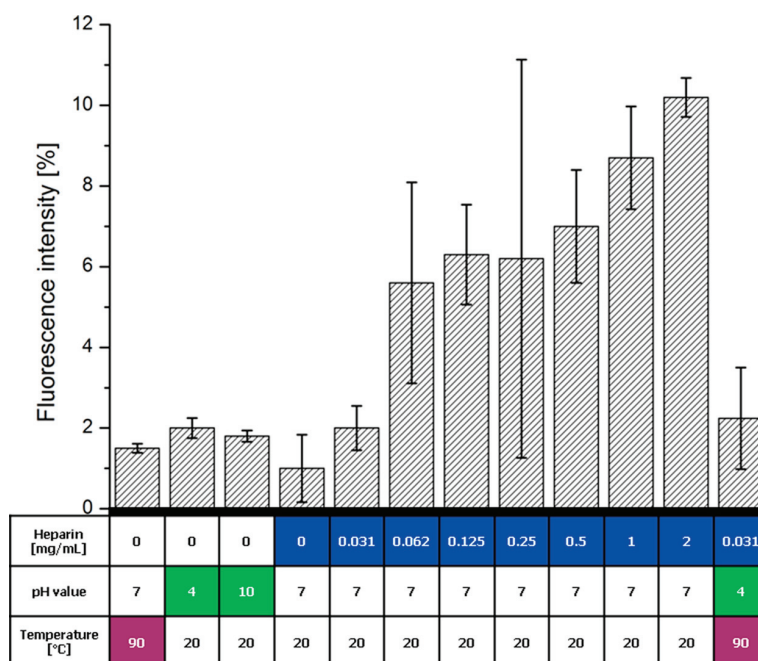


Figure 7. Release studies of the composites varying the temperature, pH value, and heparin concentration.

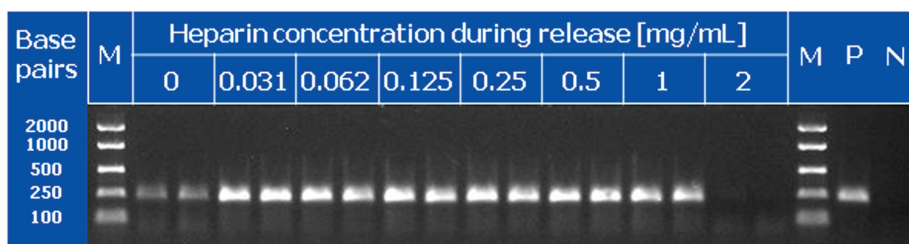


Figure 8. Agarose gel of the heparin released DNA samples after PCR and electrophoresis (M = DNA ladder standard, P = positive control, N = negative control).

After 1 h, the supernatant was transferred into a well plate and the fluorescence was measured using a plate reader. The data were related to reference samples which were treated with the same temperature program but without the presence of a composite. Unfortunately, no release could be detected up to a temperature of 80 °C. At 90 °C, about 1.5% of the labeled DNA was detected in the supernatant (Figure 7). Also a change of pH to lower or higher values did not lead to a sufficient release.

Another possibility to minimize the heparin concentration in the final DNA solution is the variation of the initial heparin amount added to the composite. The DNA is set free from the gel by a replacement with heparin, which blocks the cationic binding site of the network. Because of its higher charge density, heparin has a higher affinity to the gel than the genetic material. If the concentration of heparin is low enough for a complete absorption into the gel but high enough for a partially replacement of DNA, the resulting sample solution would be suitable for a PCR. An increase of the heparin concentration resulted, as expected, in a higher DNA release, although this enhancement is not linearly increasing with the concentration of polyanion. Also, a combination of the three triggers did not result in an increased release of DNA.

**PCR Results.** To prove the suitability of the presented system for the aimed application, DNA fragments released by heparin were amplified in a real-time PCR process. For this purpose, the three different samples, which were released for each concentration, were pooled and an aliquot was subsequently subjected to PCR. The amplification curves are depicted in the Supporting Information (Figure S4). Additionally, the resulting PCR products were analyzed using conventional agarose gel electrophoresis (Figure 8). The size of the sample products and the positive control matches with the theoretical value of the gene aimed at (LacZ; approximately 228 base pairs). Exclusively, the DNA sample, which was released using 2 mg/mL heparin, was not amplified in the PCR. This is most probably attributed to the inhibitory effect of the higher heparin content. It seems reasonable that in all other cases the heparin concentration is sufficiently low (0.031 to 1 mg/mL) that the majority of the heparin added to the DNA loaded hydrogel is entrapped within the polymer network and hence does not interfere with the subsequent PCR. This assumption is supported by the fact that already very low heparin concentrations around 0.02 mg/mL inhibit the amplification of genetic material in the reported protocol (Supporting Information, Figure S5). For a heparin concentration of 2 mg/mL, the gel sample is saturated with anionic material and hence

further excess of heparin cannot be held back. Therefore, no PCR product could be obtained. Having in mind that the DNA release using 1 mg/mL is almost as high as with 2 mg/mL (Figure 7), this effect is negligible for the PCR application presented here.

## CONCLUSION AND OUTLOOK

In summary, we demonstrated the successful combination of functional POx hydrogels and polymeric filter substrates. The presence of a gel component within the host material could be proven by an increased water uptake and scanning electron microscopy studies. Furthermore, the amount of incorporated gel could be determined indirectly by the swelling values.

The cloud point behavior of the precursor polymer was investigated to gain insights of the state of dissolution during the hydrogel synthesis. All polymers showed LCST behavior in dependency of the amount of amine containing comonomer in aqueous solution (pH 14). The phase separation of the polymer solution at the conditions of the gelation resulted in the formation of hydrogels with bead-like microstructure as detected by SEM.

It was shown that the composites are able to absorb DNA from solution and that the release was accomplished via a replacement of the genetic material by heparin. Furthermore, the influence of the heparin concentration was examined. PCR studies demonstrated that recovered DNA, which was released with heparin concentrations up to 1 mg/mL, was still intact and could be amplified. Moreover, temperature and pH value were investigated as stimuli for the release of DNA from the hydrogels. However, both resulted in low amounts of free DNA.

Because the release of genetic material from all the hydrogels synthesized so far is rather restricted, further studies will focus on different release stimuli, as well as systems which are able to immobilize DNA on surfaces without the absorption into a three-dimensional substrate. Using this approach, it could be possible to perform a PCR directly on the surface to accumulate DNA copies in the surrounding solution without any need for a DNA release.

## ASSOCIATED CONTENT

### Supporting Information

PCR primer information, SEM pictures, as well as DNA catch and release studies of all produced composite materials. PCR amplification curves, PCR inhibiting properties of heparin. This material is available free of charge via the Internet at <http://pubs.acs.org>.

## AUTHOR INFORMATION

### Corresponding Author

\*E-mail: [Ulrich.Schubert@uni-jena.de](mailto:Ulrich.Schubert@uni-jena.de).

### Present Address

<sup>†</sup>For K.K.: Department of Chemical and Biomolecular Engineering, The University of Melbourne, Victoria 3010, Australia.

### Notes

The authors declare no competing financial interest.

## ACKNOWLEDGMENTS

We thank the Bundesministerium für Bildung und Forschung (Germany) for funding (project: BASIS, 03WKCB01C). Kristian Kempe acknowledges the Alexander von Humboldt

Foundation. Grateful thanks to Steffi Stumpf for SEM investigations, Jürgen Vitz for TGA analysis, and Christine Weber for helpful discussions.

## ABBREVIATIONS USED

Boc, *tert*-butyl oxycarbonyl; BocOx, 2-(4-((*tert*-butoxycarbonyl)amino)butyl)-2-oxazoline; CROP, cationic ring-opening polymerization; EtOx, ethyl-2-oxazoline; FTIR, Fourier transform infrared; GC, gas chromatography; <sup>1</sup>H NMR, proton NMR spectroscopy; LCST, lower critical solution temperature; MeTos, methyl tosylate; NaOH, sodium hydroxide; NEt<sub>3</sub>, triethylamine; PCR, polymerase chain reactions; PE, polyethylene; PP, polypropylene; POx, poly(2-oxazoline)s; PS, poly(styrene); SEC, size-exclusion chromatography; SEM, scanning electron microscopy; SPE, solid phase extraction

## REFERENCES

- (1) Peeters, J.; Van der Spek, P. *Cell Biochem. Biophys.* **2005**, *43*, 149–166.
- (2) Gingeras, T. R.; Kwok, D. Y.; Davis, G. R. *Nucleic Acids Res.* **1987**, *15*, 5373–5390.
- (3) Anderton, J. M.; Tokarz, R.; Thill, C. D.; Kuhlow, C. J.; Brooks, C. S.; Akins, D. R.; Katona, L. L.; Benach, J. L. *Infect. Immun.* **2004**, *72*, 2035–2044.
- (4) Wong, C. W.; Albert, T. J.; Vega, V. B.; Norton, J. E.; Cutler, D. J.; Richmond, T. A.; Stanton, L. W.; Liu, E. T.; Miller, L. D. *Genome Res.* **2004**, *14*, 398–405.
- (5) Reedy, C. R.; Price, C. W.; Sniogowski, J.; Ferrance, J. P.; Begley, M.; Landers, J. P. *Lab Chip* **2011**, *11*, 1603–1611.
- (6) Boom, R.; Sol, C. J. A.; Salimans, M. M. M.; Jansen, C. L.; Wertheimvanden, P. M. E.; Vandernoordaa, J. *J. Clin. Microbiol.* **1990**, *28*, 495–503.
- (7) Stadler, J.; Lemmens, R.; Nyhammar, T. *J. Gene Med.* **2004**, *6*, 54–S66.
- (8) Diogo, M. M.; Queiroz, J. A.; Prazeres, D. M. F. *J. Chromatogr., A* **2005**, *1069*, 3–22.
- (9) Ghanem, A.; Healey, R.; Adly, F. G. *Anal. Chim. Acta* **2013**, *760*, 1–15.
- (10) Buckingham, L.; Flaws, M. L., *Molecular Diagnostics: Fundamentals, Methods, and Clinical Applications*; F. A. Davis: Philadelphia, PA, 2007.
- (11) Sambrook, J.; Russel, D., *Molecular Cloning: A Laboratory Manual*; Cold Spring Harbor Laboratory Press: New York, 2001; Vol. 3.
- (12) *Pierce Strong Ion Exchange Spin Columns*; Thermo Scientific: Hudson, NH, 2007.
- (13) *QIAGEN Genomic DNA Handbook*; QIAGEN: Valencia, CA, 2001.
- (14) Gjerse, D. T.; Hoang, L.; Hornby, D., *RNA Purification and Analysis: Sample Preparation, Extraction, Chromatography*; Wiley-VCH: Weinheim, Germany, 2009.
- (15) Esser, K.-H.; Marx, W. H.; Lisowsky, T. *BioTechniques* **2005**, *39*, 270–271.
- (16) Chen, C. W.; Thomas, C. A., Jr. *Anal. Biochem.* **1980**, *101*, 339–341.
- (17) Carter, M. J.; Milton, I. D. *Nucleic Acids Res.* **1993**, *21*, 1044.
- (18) Wiesbrock, F.; Hoogenboom, R.; Leenen, M. A. M.; Meier, M. A. R.; Schubert, U. S. *Macromolecules* **2005**, *38*, 5025–5034.
- (19) Koschella, A.; Hartlieb, M.; Heinze, T. *Carbohydr. Polym.* **2011**, *86*, 154–161.
- (20) Hoogenboom, R.; Fijten, M. W. M.; Thijs, H. M. L.; van Lankvelt, B. M.; Schubert, U. S. *Des. Monomers Polym.* **2005**, *8*, 659–671.
- (21) Nakagawa, T.; Tanaka, T.; Niwa, D.; Osaka, T.; Takeyama, H.; Matsunaga, T. *J. Biotechnol.* **2005**, *116*, 105–111.
- (22) Tomalia, D. A.; Sheetz, D. P. *J. Polym. Sci., Part A: Polym. Chem.* **1966**, *4*, 2253–2265.



- (23) Seeliger, W.; Aufderhaar, E.; Diepers, W.; Feinauer, R.; Nehring, R.; Thier, W.; Hellmann, H. *Angew. Chem.* **1966**, *78*, 913–927.
- (24) Kagiya, T.; Narisawa, S.; Maeda, T.; Fukui, K. *J. Polym. Sci., Part B: Polym. Lett.* **1966**, *4*, 441–445.
- (25) Bassiri, T. G.; Levy, A.; Litt, M. *J. Polym. Sci., Part B: Polym. Lett.* **1967**, *5*, 871–879.
- (26) Adams, N.; Schubert, U. S. *Adv. Drug Delivery Rev.* **2007**, *59*, 1504–1520.
- (27) Guillerm, B.; Monge, S.; Lapinte, V.; Robin, J.-J. *Macromol. Rapid Commun.* **2012**, *33*, 6000–6016.
- (28) Kempe, K.; Hoogenboom, R.; Jaeger, M.; Schubert, U. S. *Macromolecules* **2011**, *44*, 6424–6432.
- (29) Chujo, Y.; Sada, K.; Matsumoto, K.; Saegusa, T. *Polym. Bull.* **1989**, *21*, 353–356.
- (30) Chujo, Y.; Sada, K.; Saegusa, T. *Macromolecules* **1993**, *26*, 6315–6315.
- (31) Chujo, Y.; Sada, K.; Saegusa, T. *Macromolecules* **1993**, *26*, 6320–6323.
- (32) Chujo, Y.; Sada, K.; Saegusa, T. *Polym. J.* **1993**, *25*, 599–608.
- (33) Chujo, Y.; Yoshifujii, Y.; Sada, K.; Saegusa, T. *Macromolecules* **1989**, *22*, 1074–1077.
- (34) Chujo, Y.; Sada, K.; Saegusa, T. *Macromolecules* **1990**, *23*, 2636–2641.
- (35) Chujo, Y.; Sada, K.; Naka, A.; Nomura, R.; Saegusa, T. *Macromolecules* **1993**, *26*, 883–887.
- (36) Christova, D.; Velichkova, R.; Goethals, E. J.; Du Prez, F. E. *Polymer* **2002**, *43*, 4585–4590.
- (37) Christova, D.; Velichkova, R.; Loos, W.; Goethals, E. J.; Prez, F. D. *Polymer* **2003**, *44*, 2255–2261.
- (38) Rueda, J. C.; Komber, H.; Cedrón, J. C.; Voit, B.; Shevtsova, G. *Macromol. Chem. Phys.* **2003**, *204*, 947–953.
- (39) Rueda, J.; Suica, R.; Komber, H.; Voit, B. *Macromol. Chem. Phys.* **2003**, *204*, 954–960.
- (40) Cesana, S.; Auernheimer, J.; Jordan, R.; Kessler, H.; Nuyken, O. *Macromol. Chem. Phys.* **2006**, *207*, 183–192.
- (41) Hartlieb, M.; Pretzel, D.; Kempe, K.; Fritzsche, C.; Paulus, R. M.; Gottschaldt, M.; Schubert, U. S. *Soft Matter* **2013**, *9*, 4693–4704.
- (42) Weber, C.; Hoogenboom, R.; Schubert, U. S. *Prog. Polym. Sci.* **2012**, *37*, 686–714.
- (43) Weber, C.; Becer, C. R.; Hoogenboom, R.; Schubert, U. S. *Macromolecules* **2009**, *42*, 2965–2971.

# Supporting Information

## Matrix supported poly(2-oxazoline)-based hydrogels for DNA catch and release

*Matthias Hartlieb<sup>a,b</sup>, David Pretzel<sup>a,b</sup>, Christoph Englert<sup>a,b</sup>, Martin Hentschel<sup>c</sup>, Kristian  
Kempe<sup>a,b,†</sup>, Michael Gottschaldt<sup>a,b</sup>, Ulrich S. Schubert<sup>a,b,\*</sup>*

<sup>a</sup> Laboratory of Organic and Macromolecular Chemistry (IOMC), Friedrich Schiller  
University Jena, Humboldtstrasse 10, 07743, Jena, Germany

<sup>b</sup> Jena Center for Soft Matter (JCSM), Friedrich Schiller University Jena,  
Philosophenweg 7, 07743, Jena, Germany

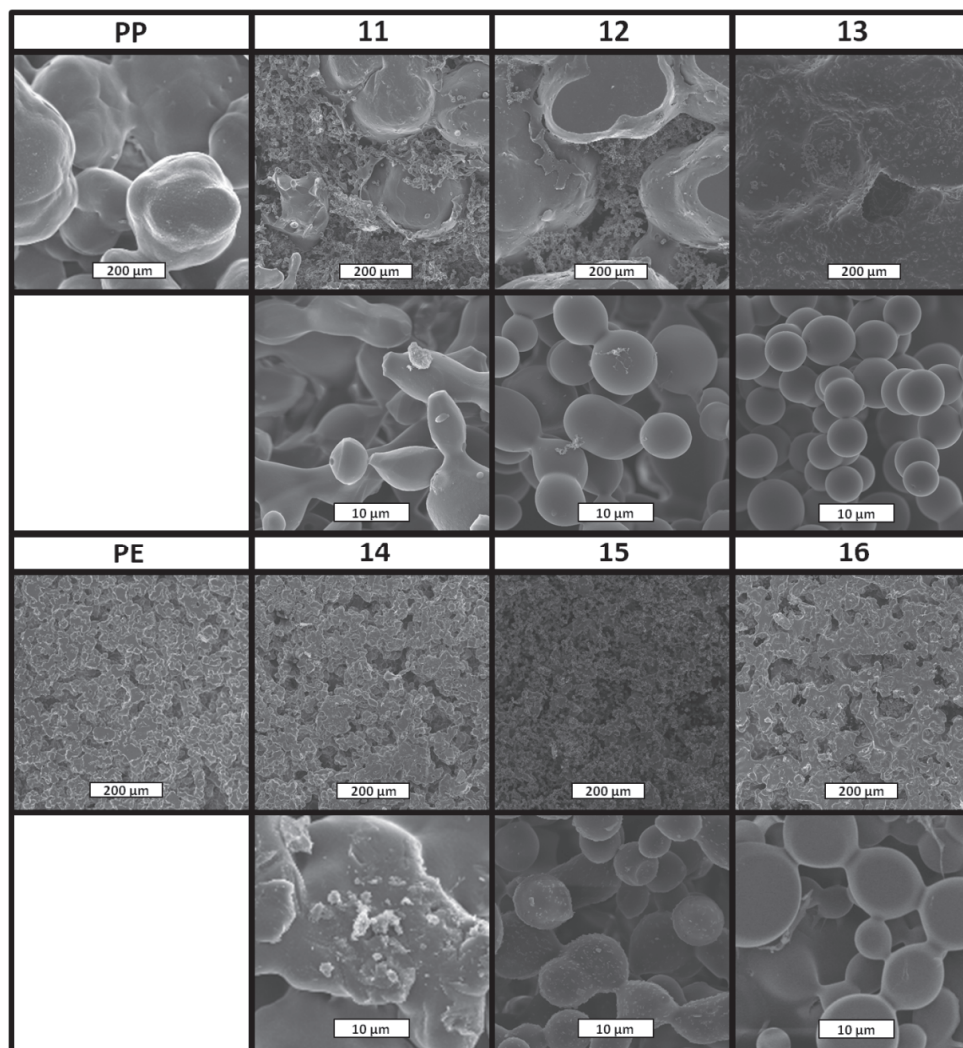
<sup>c</sup> Analytik Jena AG, Konrad-Zuse-Straße 1, 07745 Jena, Germany

† Current address: Department of Chemical and Biomolecular Engineering, The  
University of Melbourne, Victoria 3010, Australia

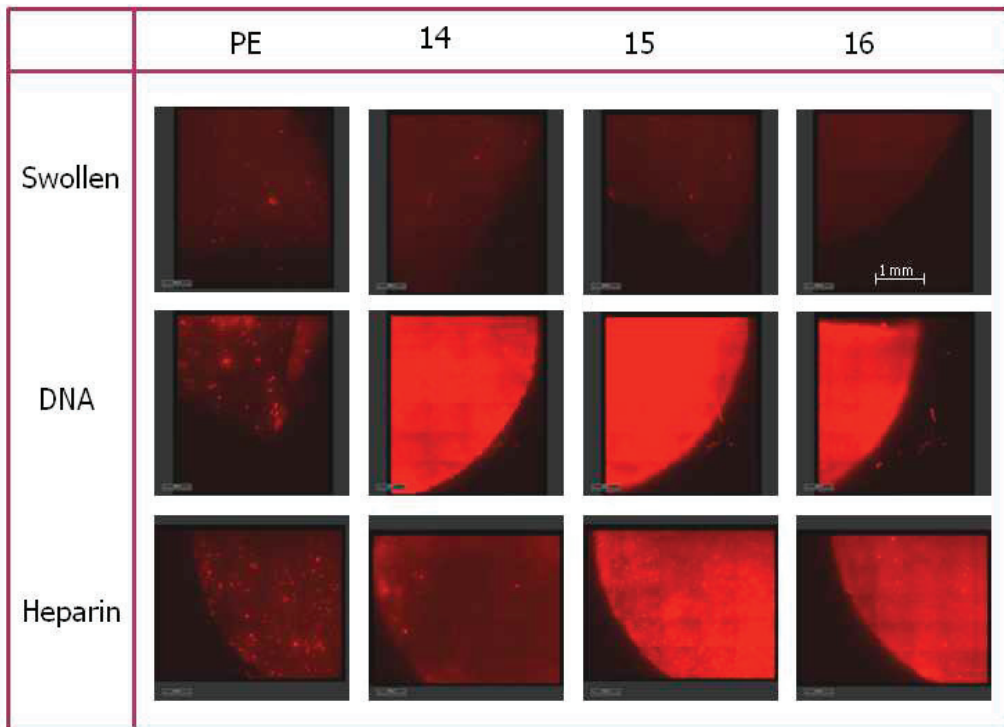
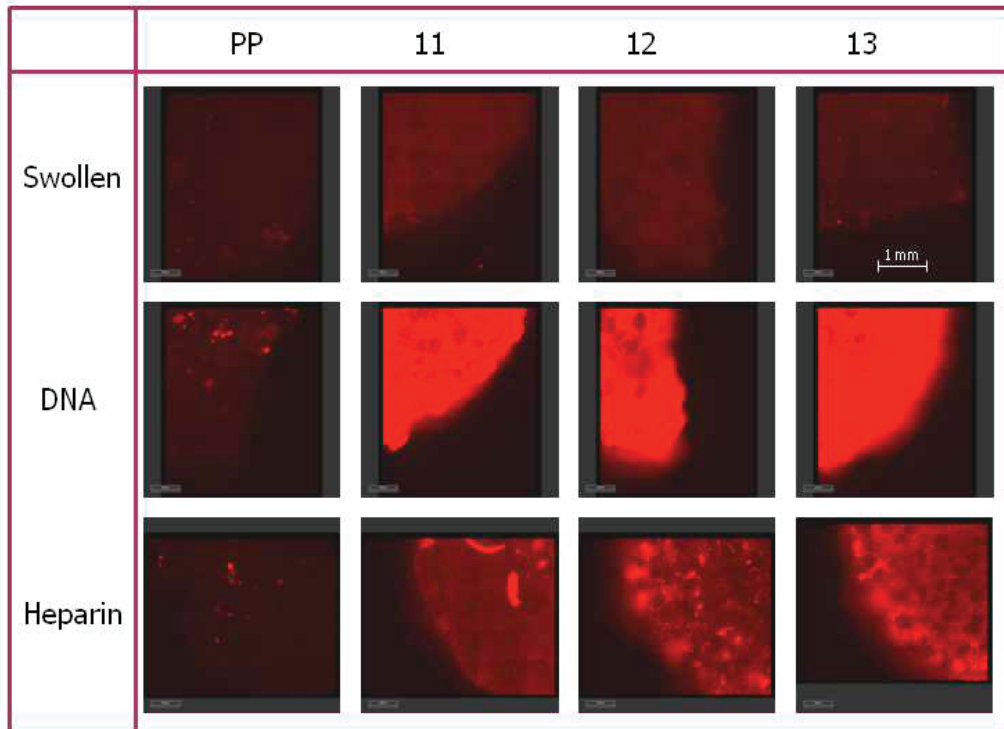
**S1. Primers for qPCR amplification of *Escherichia coli* K12**

Target	Sequence	Product size [bp]	Label
LacZ	5'-CTG GCG TAA TAG CGA AGA AG-3' (20)	228	biotin
LacZ	5'-GGA TTG ACC GTA ATG GGA TAG (21)	228	Cy5

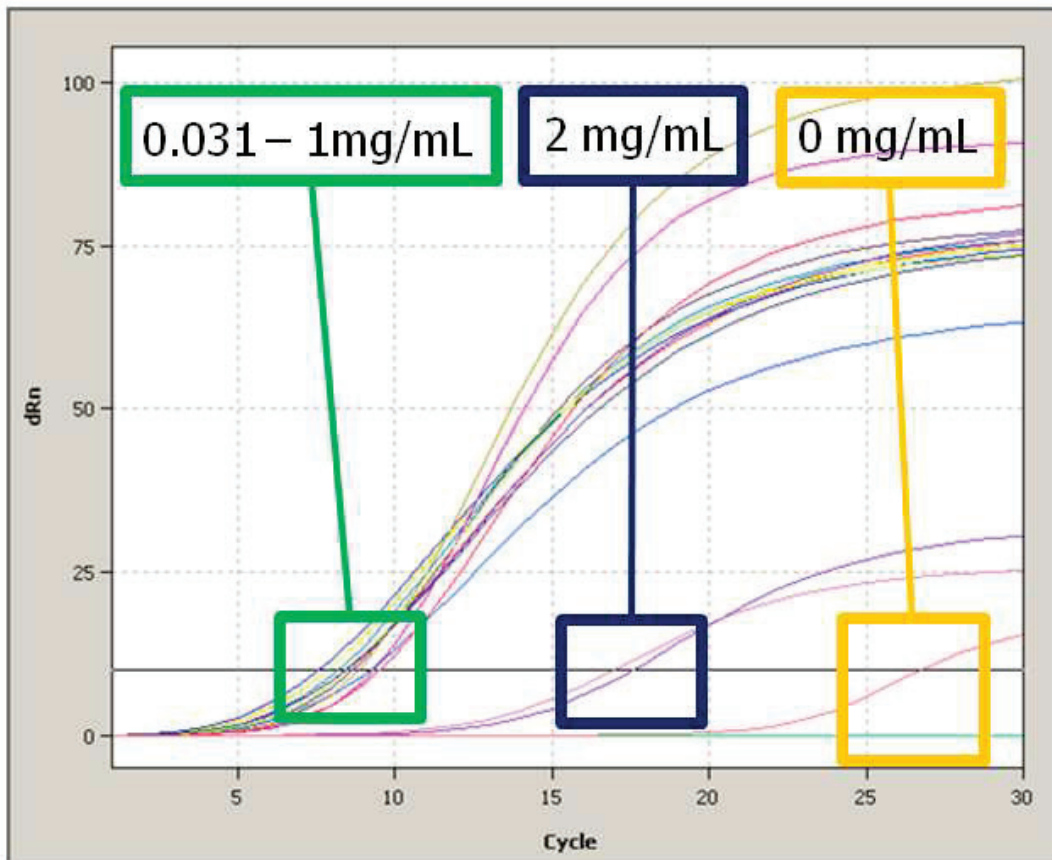
**S2. SEM pictures of PP and PE substrates and supported hydrogels.**



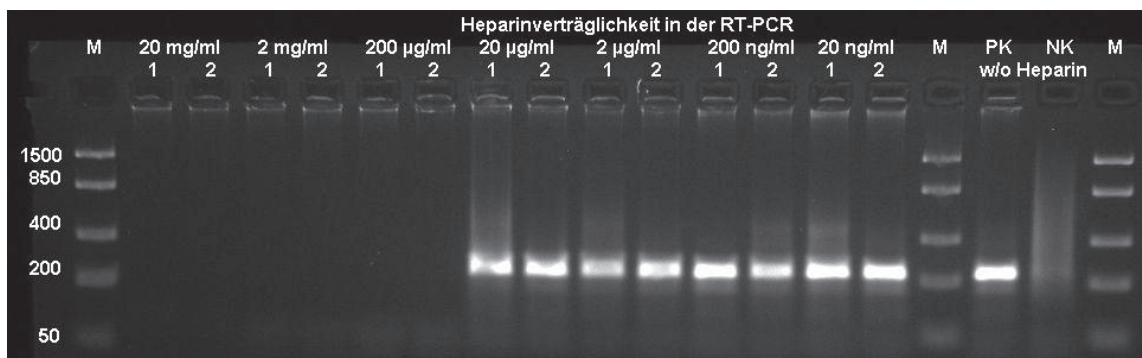
**S3. DNA catch and release of all produced supported hydrogels.**



**S4. PCR amplification curves.**



**S5. PCR inhibiting properties of heparin for the evaluated system.**



Heparin concentrations down to 20 µg/mL disturb the PCR process.

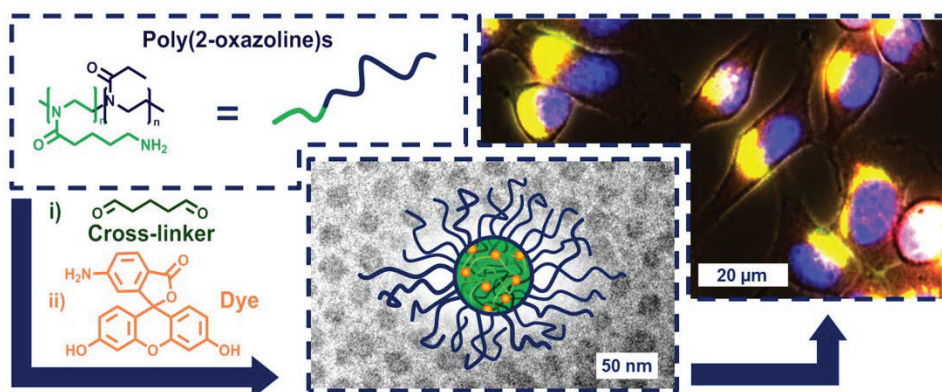


## Publication 4

„Core cross-linked nanogels based on the self-assembly of double hydrophilic poly(2-oxazoline) block copolymers“

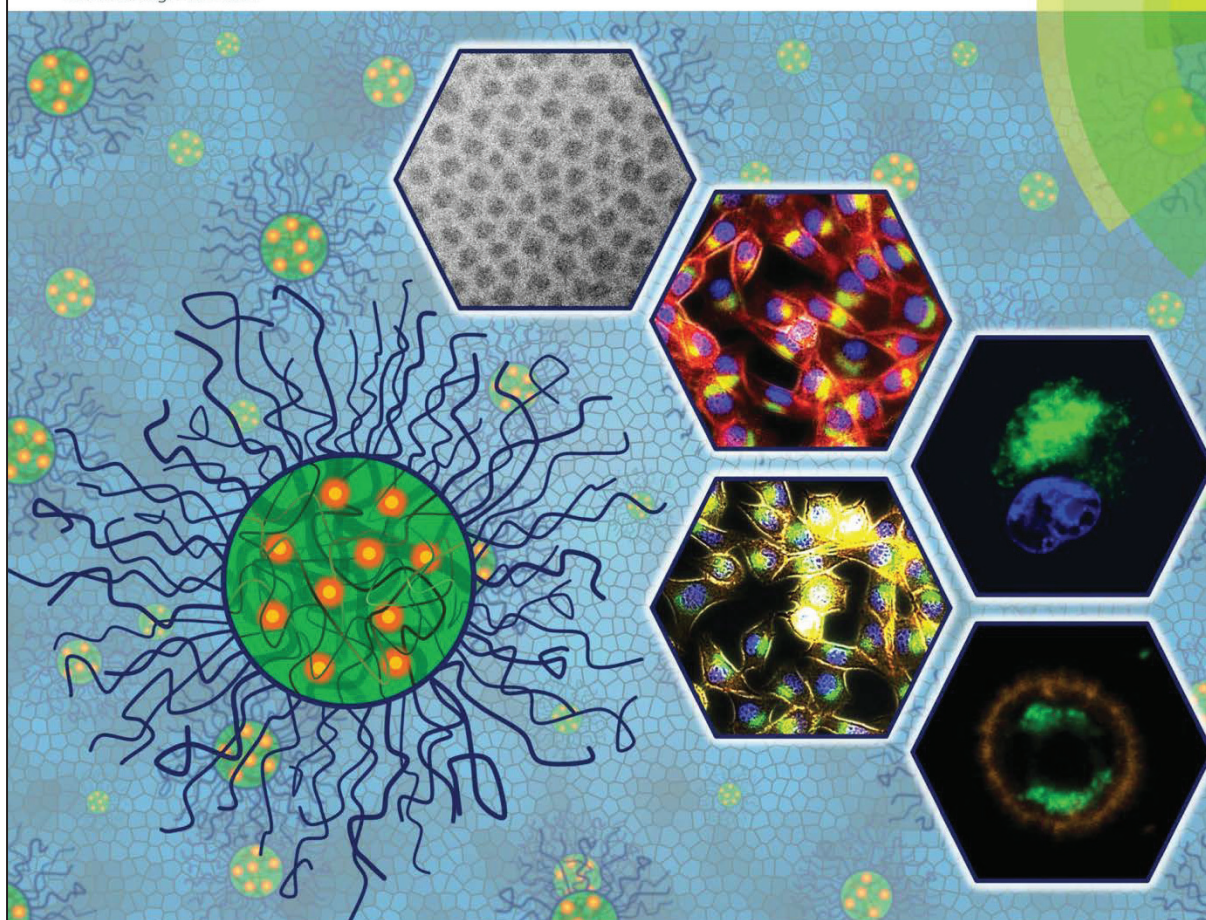
M. Hartlieb, D. Pretzel, M. Wagner, S. Höppener, P. Bellstedt, M. Görlach, C. Englert, K. Kempe,  
U. S. Schubert

*J. Mater. Chem. B.* **2015**, *3*, 1748-1759.



# Journal of Materials Chemistry B

Materials for biology and medicine  
[www.rsc.org/MaterialsB](http://www.rsc.org/MaterialsB)



ISSN 2050-750X



PAPER

Ulrich S. Schubert *et al.*

Core cross-linked nanogels based on the self-assembly of double hydrophilic poly(2-oxazoline) block copolymers



Cite this: DOI: 10.1039/c4tb02069c

## Core cross-linked nanogels based on the self-assembly of double hydrophilic poly(2-oxazoline) block copolymers†

Matthias Hartlieb,<sup>ab</sup> David Pretzel,<sup>ab</sup> Michael Wagner,<sup>ab</sup> Stephanie Hoepfner,<sup>ab</sup> Peter Bellstedt,<sup>c</sup> Matthias Görlach,<sup>c</sup> Christoph Englert,<sup>ab</sup> Kristian Kempe<sup>‡ab</sup> and Ulrich S. Schubert<sup>\*ab</sup>

The synthesis of poly(2-oxazoline)-based block copolymers consisting of a cationic and a hydrophilic segment is described. The self-assembly of these macromolecules in organic solvents results in the formation of micelles and vesicles, respectively, depending on the solvent used. To transfer the systems into water, cross-linking using glutaraldehyde was applied, followed by the consumption of excessive aldehyde functions by either diethylamine or 6-aminofluorescein (6AF). The cross-linked assemblies were analyzed regarding their size and shape by electron microscopy and light scattering methods, as well as for their chemical composition by solid state NMR spectroscopy. 6AF associated samples were examined with respect to their absorption and fluorescence behavior in aqueous environment, revealing an alkaline microenvironment within the presented nanostructures. The toxicity of the systems against mouse fibroblast cell line L929 was examined by the XTT assay and was found to be insignificant for concentrations of up to 2.5 mg mL<sup>-1</sup>. Flow cytometry and fluorescence microscopy analysis revealed an efficient concentration and time dependent cellular uptake of the nanogels.

Received 15th December 2014  
Accepted 13th January 2015

DOI: 10.1039/c4tb02069c

www.rsc.org/MaterialsB

## Introduction

The term nanomedicine refers to the use of nanoscopic objects in medical applications like drug delivery and has received considerable attention in recent years.<sup>1,2</sup> The utilization of drug carriers, such as liposomes, polymeric micelles, vesicles, nanoparticles, and dendrimers offers numerous advantages. Besides potential control over pharmacokinetics and toxicity, the solubilization and protection of the drug is of paramount interest. In particular, polymeric micelles are frequently studied for the administration of hydrophobic compounds.<sup>3</sup> Such

micelles are formed *via* the aqueous self-assembly of block copolymers consisting of hydrophilic and hydrophobic segments.<sup>4</sup> While the hydrophilic shell reduces non-specific interactions with tissue and blood components, the hydrophobic core contains and protects the therapeutic and/or diagnostic molecule. The critical micelle concentration (CMC) of polymeric micelles is rather low (10<sup>-6</sup> to 10<sup>-7</sup> mol L<sup>-1</sup>) as compared to surfactant based nanocarriers (10<sup>-3</sup> to 10<sup>-4</sup> mol L<sup>-1</sup>).<sup>5</sup> However, even above their CMC a component exchange or a disassembly is possible. As a consequence, Lammers and co-workers have recently proposed that cross-linking of such systems and covalent attachment of the cargo are paramount prerequisites for their successful application.<sup>6</sup> Nanogels are covalently cross-linked structures in the nanometer size range and combine beneficial properties of hydrogels (*e.g.* tissue-like structure, biocompatibility, and stimuli responsiveness)<sup>1</sup> with the solubility properties of nano-assemblies, such as nanoparticles or micelles. There are several ways for the production of these structures such as the use of inverse emulsions<sup>7</sup> or *via* polymerization induced phase separation, respectively.<sup>8</sup> One particularly elegant way is the cross-linking of self-assembled structures.

In this context, type and properties of the polymeric material serving as precursor for nanogels are highly important. Besides a well-controlled polymerization process as a prerequisite to yield highly defined block copolymers, the biocompatibility and functionality of the resulting polymers is of outstanding interest.

<sup>a</sup>Laboratory of Organic and Macromolecular Chemistry (IOMC), Friedrich Schiller University Jena, Humboldtstrasse 10, 07743, Jena, Germany. E-mail: ulrich.schubert@uni-jena.de

<sup>b</sup>Jena Center for Soft Matter (JCSM), Friedrich Schiller University Jena, Philosophenweg 7, 07743, Jena, Germany

<sup>c</sup>Biomolecular NMR Spectroscopy, Leibniz Institute for Age Research – Fritz Lipmann Institute, Beutenbergstr. 11, 07745 Jena, Germany

† Electronic supplementary information (ESI) available: Materials and instrumentation; NMR and SEC plots of polymers (Fig. S1 and S2); cloud-points of P(EtOx-*b*-AmOx) (Fig. S3); AF4 data of polymers (Table S1); DLS plots for nanostructures in organic solvent (Fig. S4) and water (Fig. S5); AF4 plots of cross-linked structures (Fig. S6); NMR of assembled structures (Fig. S7); solid state NMR of 6AF (Fig. S8); epifluorescence pictures of cells for FC analysis (Fig. S9); co-localization studies of micelles using epifluorescence (Fig. S10) and CLSM (Fig. S11). See DOI: 10.1039/c4tb02069c

‡ Current address: Department of Chemistry, University of Warwick, Gibbet Hill Road, Coventry, CV4 7AL, UK.



Poly(2-oxazoline)s (POx) represent a promising class of materials for biomedical applications. Such as poly(ethylene glycol) (PEG), poly(2-methyl oxazoline) (PMeOx) and poly(2-ethyl-2-oxazoline) (PEtOx) are highly soluble in water and organic solvents, biocompatible<sup>9,10</sup> and exhibit stealth properties.<sup>11,12</sup>

The cationic ring-opening polymerization (CROP) of 2-oxazolines provides access to multifunctional polymers with a wide range of possible structural variations, using different functional initiators, terminating agents and functional monomers.<sup>13</sup> This versatility, in combination with the possibility to combine different monomers in distinct architectures, including statistical, gradient or block copolymers, renders the CROP of 2-oxazolines a powerful toolbox to produce functional polymers for biological applications.<sup>14</sup>

POx-based micellar structures were investigated thoroughly over the past decades.<sup>15–21</sup> This includes also studies on the incorporation of anti-cancer drugs.<sup>22–24</sup> However, up to date only a limited number of reports are available on the synthesis and potential of cross-linked POx aggregates. The type of cross-linking reaction is of central interest for designing drug delivery systems with sufficient stability and the ability to release their cargo on demand.<sup>25</sup> Covalently cross-linked POx micelles, stabilized by thiol-yne chemistry,<sup>26,27</sup> epoxide-amine cross-linking,<sup>28</sup> UV mediated cross-linking<sup>29,30</sup> as well as electron beam irradiation<sup>31,32</sup> have been described. To the best of our knowledge only one reversible system using a disulfide bond linker, is reported so far.<sup>33</sup>

Herein, we describe the synthesis of double hydrophilic POx-based block copolymers including a neutral (PEtOx) as well as a cationic (PAmOx) block and their self-assembly in organic solvents. The polymerization of 2-oxazolines carrying a protected amine group was first introduced by Cesana *et al.*<sup>34</sup> and is

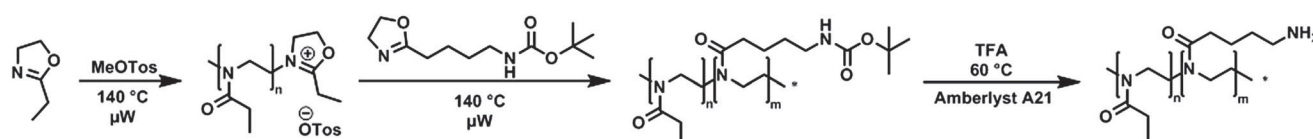
continuously developed.<sup>35</sup> The self-assembly of the polymers in organic solvents is investigated and the structures are cross-linked by Schiff-base chemistry and covalently loaded with 6-amino fluorescein as a model compound. This connection is known to be reversible<sup>36</sup> enabling a later disassembly. The nanogels were characterized intensively and their interaction with cells was investigated. They exhibit low toxicity and an endosomal localization.

## Results and discussion

### Polymer synthesis

In this study we describe the synthesis of block copoly(2-oxazoline)s and their self-assembly into nano-scaled objects. The block copolymer P(EtOx-*b*-AmOx) consists of a hydrophilic (EtOx) and a hydrophilic/cationic segment (AmOx). While PEtOx is known to be biocompatible<sup>37,38</sup> and soluble in a wide range of solvents, including water, the second block is (after deprotection) cationically charged due to the primary amine groups in the side chain and, therefore, lacks solubility in organic solvents.

The synthesis of P(EtOx-*b*-AmOx) is depicted in Scheme 1. The polymerization of EtOx, which constitutes the first block, was initiated by methyl tosylate (MeOTos) at 140 °C under microwave irradiation (see ref. 39 for optimized polymerization conditions). After close to full conversion ( $\ln([M]_0/[M]_t) = 4$ ) of the first monomer, the living polymer was chain extended with 2-(4-((*tert*-butoxycarbonyl)amino)butyl)-2-oxazoline (BocOx), the Boc-protected precursor of the cationic AmOx segment, which was deprotected after termination of the polymerization using trifluoroacetic acid (TFA) and Amberlyst A21 solid phase catalyst to remove trifluoroacetate salts. By changing initiator-to-monomer ratios and polymerization times, block copolymers of



Scheme 1 Schematic representation of the synthesis of amphiphilic block copolymers (P(EtOx-*b*-AmOx)).

Table 1 Analytical data and composition of the prepared block copolymers

Sample	Composition	NMR			SEC (CHCl <sub>3</sub> )		SEC (DMAc)		AF4		Co-monomer [%]
		$M_n$ [g mol <sup>-1</sup> ]	$M_n$ [g mol <sup>-1</sup> ]	$D$	$M_n$ [g mol <sup>-1</sup> ]	$D$	$M_n$ [g mol <sup>-1</sup> ]	$D$	$M_n$ [g mol <sup>-1</sup> ]	$D$	
1	P(EtOx <sub>104</sub> )	10 300	9900	1.11	20 600	1.17					0
2	P(EtOx <sub>112</sub> - <i>b</i> -BocOx <sub>6</sub> )	12 600	7700	1.18							5
3	P(EtOx <sub>92</sub> - <i>b</i> -BocOx <sub>10</sub> )	11 600	7400	1.16							10
4	P(EtOx <sub>85</sub> - <i>b</i> -BocOx <sub>15</sub> )	12 100	8900	1.20							15
5	P(EtOx <sub>84</sub> - <i>b</i> -BocOx <sub>20</sub> )	13 200	8900	1.17							20
6	P(EtOx <sub>70</sub> - <i>b</i> -BocOx <sub>22</sub> )	12 300	7600	1.18							22
7	P(EtOx <sub>113</sub> - <i>b</i> -AmOx <sub>5</sub> )	12 000			14 500	1.34	11 700	1.10			5
8	P(EtOx <sub>92</sub> - <i>b</i> -AmOx <sub>10</sub> )	10 600			16 800	1.23	9200	1.14			10
9	P(EtOx <sub>72</sub> - <i>b</i> -AmOx <sub>18</sub> )	9700			16 100	1.22	13 300	1.10			18
10	P(EtOx <sub>82</sub> - <i>b</i> -AmOx <sub>23</sub> )	11 400			18 100	1.23	13 600	1.09			22
11	P(EtOx <sub>64</sub> - <i>b</i> -AmOx <sub>26</sub> )	10 100			15 600	1.30	12 500	1.26			29

different compositions were prepared, as summarized in Table 1. To investigate the length of the polymer chains,  $^1\text{H}$  NMR investigations were conducted directly after polymerization and the integral of the initiator tosylate peaks was compared to the integral of the polymer backbone revealing total degree of polymerization (DP) values of around 100 for all macromolecules. The block ratios were calculated from the  $^1\text{H}$  NMR spectra before and after deprotection, respectively (ESI: Fig. S1 and S2†). The difference in the calculated values can be explained by the overlap of solvent peaks with the EtOx- $\text{CH}_3$ -group for polymers 2 to 6, limiting the accuracy of the determination. After deprotection, these solvent peaks disappear and, thus, we refer in the following to the values obtained from the deprotected polymers. Size exclusion chromatography (SEC) measurements of protected polymers indicated  $M_n$  values around  $10\,000\text{ g mol}^{-1}$ . Low dispersity ( $D$ ) values prove a narrow molar mass distribution of the synthesized block copolymers. After deprotection, SEC measurements of the block copolymers were performed in *N,N*-dimethyl acetamide (DMAc), a non-selective solvent for both blocks, showing an increase in  $M_n$  and  $D$ . However, due to the lack of cationic SEC standards a precise determination of  $M_n$  and  $D$  is hardly possible. The comparison of the SEC derived  $M_n$  and  $D$  values of the PEtOx homopolymer (which increases when changing the solvent to DMAc) indicated a similar size and uniformity of the protected and the deprotected polymers.

As a consequence, to gain further information about the size distribution of the cationic P(EtOx-*b*-AmOx) copolymers, asymmetric flow field-flow fractionation (AF4) investigations were performed. The measurements were carried out at a low pH value (3.5) to ensure a neutral or cationic charge of the membrane resulting in an electrostatic repulsion of the cationic samples to reduce adsorption phenomena. The obtained size values fit well with the expected values based on the monomer-to-initiator ratio and the  $M_n$  values derived from the  $^1\text{H}$  NMR experiments. Since the determination of the molar masses was carried out using a multi-angle laser light scattering detector (MALLS) to obtain absolute molar mass values, the AF4 results are more reliable than the data derived from SEC measurements without available cationic calibration standards. Again, small  $D$  values indicate narrow size distributions of the block copolymers. Nevertheless, the molar masses obtained by AF4 might be slightly overestimated as most probably some low molar mass fractions are washed out through the membrane (nominal cut-off  $10\,000\text{ g mol}^{-1}$ ). This is supported by a recovery rate of around 75 to 85% (ESI: Table S1†).

### Self-assembly, cross-linking and labeling of block copolymers

Since the LCST behavior of the polymers in aqueous solution could not be utilized for a self-assembly (ESI Fig. S3†) of P(EtOx-*b*-AmOx), the low solubility of the cationic block in organic solvents was exploited. First, the self-assembling behavior of P(EtOx-*b*-AmOx) (7–11) was screened in three organic solvents (MeOH, *i*PrOH and  $\text{CHCl}_3$ ) using dynamic light scattering (ESI: Fig. S4†). The results of these measurements are summarized in Table 2. As expected, pure PEtOx showed no aggregation in these solvents. All block copolymers however formed structures in the range between 4 and 112 nm depending on the solvent and the composition. Surprisingly, the ratio between the two blocks did not influence the size of the aggregates as much as the polarity of the solvents used. All samples assembled in  $\text{CHCl}_3$  formed structures with radii between 4 and 17 nm.

In *i*PrOH, size distributions between 68 and 105 nm were detected, and MeOH led to structures with even larger radii (77 to 113 nm). In dependence on the solvent and block ratio, most of the samples show rather high polydispersity indices, which can be traced back to the formation of a small fraction of aggregates. Therefore, only samples with low PDI values indicating narrow size distributions are selected for further experiments.

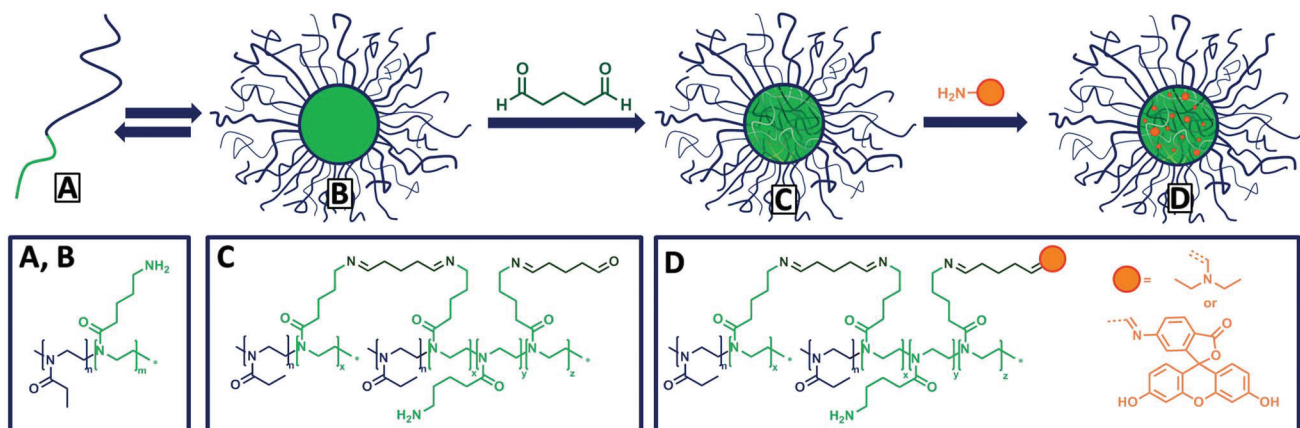
To transfer these structures into aqueous solution, the core of the agglomerates has to be cross-linked, as both polymer blocks are readily water soluble. For this purpose, two samples, exhibiting the most uniform size distribution in organic solvents were chosen (labeled with <sup>a</sup> in Table 2) and cross-linked with glutaraldehyde (GA) (Scheme 2). As a *bis*-aldehyde, GA is able to form imine bonds with the amine groups present in the core and, consequently, lock the structure of the assemblies. However, a direct transfer of the micelles into water yielded only hydrogels, which indicated that even though GA was added in stoichiometric amounts, a sufficient number of free amine and aldehyde groups remained to cross-link the colloidal structures among each other. As demonstrated by Lecommandoux and co-workers, the amount of cross-linked amine groups for such reactions is only about 35%, when aiming for a full conversion.<sup>40</sup> To overcome this drawback, low molar mass amines have to be added in large excess after the cross-linking step to consume the residual aldehydes. This strategy, in turn, does not only enable the stabilization of the self-assembled structure, but also allows the simultaneous incorporation of drug molecules or fluorescence labels into the system. Here, diethylamine

**Table 2** DLS screening of the self-assembling behavior of the block copolymers in organic solvents ( $5\text{ mg mL}^{-1}$ ; size indication in radius; number plot; no size value is specified, if the number weighted plot shows only the polymer precursor)

Solvent	0% AmOx (1)		5% AmOx (7)		10% AmOx (8)		18% AmOx (9)		22% AmOx (10)		29% AmOx (11)	
	$R_h$ [nm]	PDI	$R_h$ [nm]	PDI	$R_h$ [nm]	PDI	$R_h$ [nm]	PDI	$R_h$ [nm]	PDI	$R_h$ [nm]	PDI
MeOH	—	—	—	—	—	—	113	0.334	83	0.646	77	0.335
<i>i</i> PrOH	—	—	71	0.550	105	0.714	99	0.561	92	0.509	68 <sup>a</sup>	0.111
$\text{CHCl}_3$	—	—	4	0.360	8	0.217	16	0.256	13	0.376	17 <sup>a</sup>	0.048

<sup>a</sup> Samples selected for further cross-linking.





Scheme 2 Schematic representation of the self-assembly of P(EtOx-*b*-AmOx) followed by cross-linking and quenching/loading.

(DEA) and 6-amino fluorescein (6AF), respectively, were used as model substances to quench the cross-linking process. After this treatment the assembled structures could be transferred into aqueous solution, successfully.

#### Characterization of self-assembled structures by light scattering and electron microscopy

To purify the systems from unbound amine or cross-linker molecules, the crude products were precipitated in diethyl ether and dialyzed in a water-methanol mixture (4 : 1), where methanol acted as a solubility mediator for 6AF, which is barely soluble in water. A first indication of successfully cross-linked structures was provided by DLS experiments, which indicated distributions in the same size range as observed in organic solvents (Table 3, ESI: Fig. S5<sup>†</sup>). The PDI values of the locked systems increased slightly, which suggests an agglomeration caused by unconsumed aldehyde groups in the core.

However, the values are still in a good range for synthetic nano-sized objects. The zeta potential of all cross-linked assemblies was found to be positive, indicating the presence of free amine groups in the colloid.

A further investigation of size and uniformity was conducted using asymmetric flow field-flow fractionation measurements. Utilizing this technique it is possible to separate the samples by the diffusion coefficient and to determine the hydrodynamic radius ( $R_h$ , by online DLS measurements) and the radius of gyration ( $R_g$ , by multi-angle laser light scattering (MALLS)

measurements). The data depicted in Table 3 (Graphs in ESI: Fig. S6<sup>†</sup>) are similar to the values obtained by DLS measurements. For samples originating from *i*PrOH the obtained AF4-DLS values are significantly smaller than the collected sizes from the DLS measurements, which can be attributed to the AF4 separation technique. While DLS investigations provide a radius comprising also small fractions of aggregates, after separation by AF4 single colloidal structures are examined. An additional information provided by this analysis is an indication of the particle shape by the comparison of both, hydrodynamic radius and radius of gyration, expressed in the ratio  $\rho$  ( $\rho = R_g/R_h$ ). For particles assembled in  $\text{CHCl}_3$ , the  $R_g$  value could not be determined since they were too small for detection *via* the MALLS detector (limit around 15 nm).<sup>41</sup> This indicates a  $R_g$  below 15 nm and, hence, a  $\rho$  ratio less than 0.8, which is characteristic for hard spheres and, therefore, indicated a compact structure like a micellar architecture of the assembled particles.<sup>42</sup> Larger ratios (around 1) as obtained for *i*PrOH derived structures are usually attributed to less dense and soft structures, which might indicate vesicles.<sup>42</sup> A possible explanation for this trend is a swelling of the selective block induced by the different polarity of the solvents used. While the amine group has a potentially cationic charge, the side chain and the backbone of the block can be readily solubilized by organic solvents resulting in a gel-like core instead of a complete collapse of the AmOx segment. Upon increase of polarity of the applied solvent, swelling should concomitantly increase, resulting in a higher steric demand of the selective block, while

Table 3 Characterization data for cross-linked nanostructures (DLS: 5 mg mL<sup>-1</sup>, size indication in radius). Polymer 11 served as precursor for all assemblies. The content of fluorescein was determined by the absorbance at 470 nm

Sample	Solvent for self-assembly	Capping agent	DLS in solvent		DLS in water			AF4			Content of capping agent (wt%)
			Size, $R_h$ [nm]	PDI	Size, $R_h$ [nm]	PDI	$\zeta$ [mV]	$R_g$	$R_h$	$\rho$	
12	$\text{CHCl}_3$	DEA	17	0.048	17	0.093	+7	—	19	<0.8	N. d.
13		6AF			15	0.199	+17	—	20.0	<0.8	29
14	<i>i</i> PrOH	DEA	68	0.111	59	0.246	+17	41	37	1.11	N. d.
15		6AF			50	0.179	+23	40	40.0	1.00	29

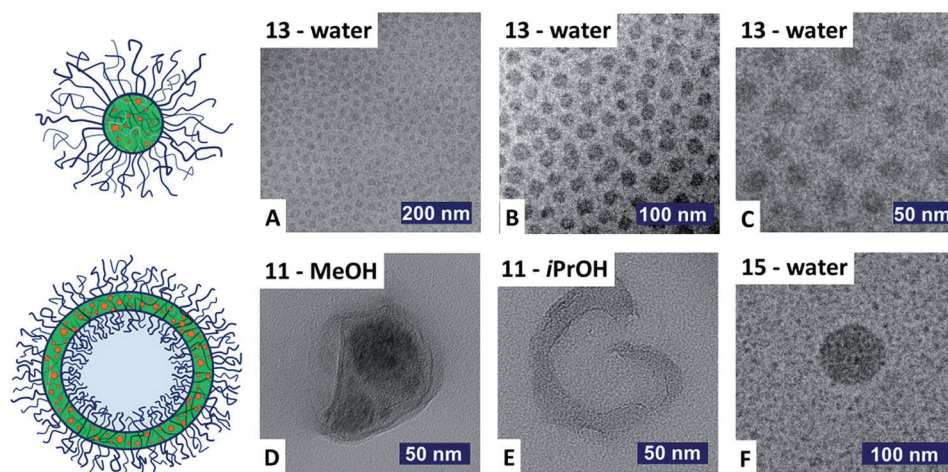


Fig. 1 TEM images of the dried structures assembled in methanol (D) and *i*PrOH (E), and cryoTEM images of self-assembled as well as cross-linked structures (A–C and F).

the hydrophilic PEtOx block reveals a similar solubilization in all solvents used. Thus, the transition from a micellar to a vesicular structure might be attributed to the change in the ratio between the volume of the two segments.<sup>43</sup> Considering the block architectures of P(EtOx-*b*-AmOx) and the fact that a fully stretched polymer chain is with roughly 32 nm length (calculated from the bond length; C–C = 154 pm, C–N = 135 pm under consideration of the bond angles) shorter than the radius of the assemblies, support a vesicular morphology of these samples.

To further investigate the proposed structures, (cryo) transmission electron microscopy (cryoTEM) measurements were performed. Samples in aqueous media (Fig. 1A–C and F) as well as non-cross-linked polymers in organic solvents were investigated (Fig. 1D and E). The non-cross-linked polymers could be examined only in the dried state as vitrification of the solutions was not successful. However, structures found in samples derived from MeOH and *i*PrOH (Fig. 1D and E) might originate from the collapse of a vesicle shell, supporting the assumption of a vesicular architecture. The cryoTEM picture of the cross-linked equivalent (Fig. 1F) does not show a hollow sphere which could be attributed to hydrophilicity of the nanogel. The swelling of the structure in water reduces the contrast of the picture compared to TEM investigations in organic solvents. Based on the combined investigations the larger nanostructures will henceforth be referred to as vesicles. Nevertheless, we are aware, that this interpretation of AF4 and TEM data has to be treated with caution and that the hypothesis of a vesicular nanostructure is not fully proven.

#### Determination of 6AF loading and release

For samples which were loaded with 6AF, the amount of covalently bound dye was determined using its absorption and fluorescence properties. The absorption and emission spectra of 6AF-containing samples were measured in water at a pH value of 7 in order to compare the data to pure 6AF, which was measured in the presence of a 100-fold excess of GA to ensure a

quantitative conversion to the imine form (Fig. 2). While 6AF shows the typical absorption and emission spectra of the lacton derivative at a pH value of 7 (low absorption, maximum at 440 nm), both, micelles as well as vesicles absorb and emit similar to the ring-opened di-anionic carboxy isomer state of the dye (Fig. 2A). This behavior seems best explained by the high density of amine groups in the core of the assemblies leading to a locally increased pH value, which, in turn, causes the formation of the di-anionic species characterized by a strong absorption at 490 nm.<sup>44</sup> A closer look at the photochemical behavior of the nano-assemblies shows that even at a pH value of 4 still a significant amount of 6AF emits indicating an alkaline microenvironment within the core of the nanostructures.

To determine the amount of loaded dye, samples were investigated in aqueous NaOH solution (0.1 mol L<sup>-1</sup>) to ensure the quantitative presence of the carboxy-form of fluorescein in the 6AF calibration. For a better comparison with the bound dye, a 100-fold excess of GA was added to the free 6AF generating the imine derivative *in situ* as described before. Both, absorption as well as fluorescence spectra showed equal maxima and shape for the samples as well as calibration. The amount of incorporated 6AF was found to be 29 wt% of dye per total mass for the micelles, as well as for the vesicles. This is equivalent to 12 6AF molecules per polymer chain, which complies with the conversion of amine groups by GA in similar systems (~35%).<sup>40</sup> An equal loading for both nano-architectures was expected as the chemical composition of both systems should be identical, while only the shape varies.

#### Liquid and solid state (ss) NMR spectroscopy

While light scattering and electron microscopy experiments shed light on size and shape of the assemblies, they do not provide insights into their chemical composition. Liquid and solid state NMR spectroscopy were employed for a more detailed characterization. Both, micelles and vesicles yield non-turbid solutions in solvents such as water or chloroform. In the liquid state <sup>1</sup>H NMR spectra of non-cross-linked polymers in

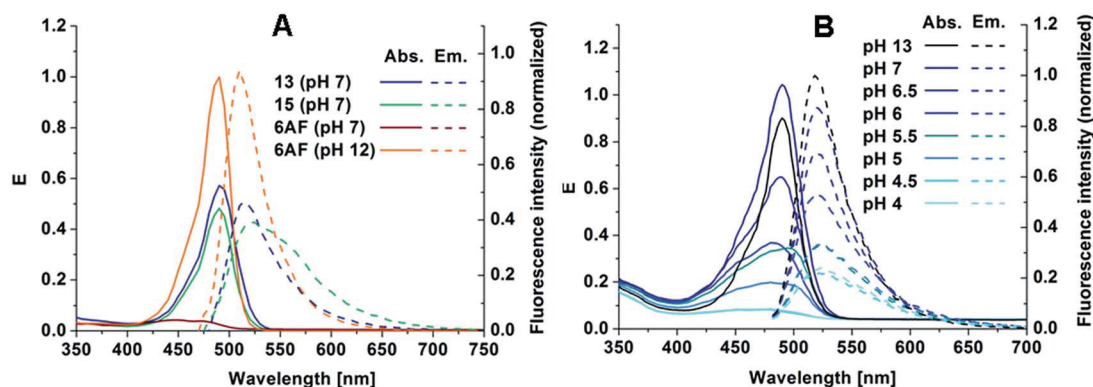


Fig. 2 (A) Absorption and fluorescence spectra of 6AF (pH dependent) and dye quenched nanostructures; (B) pH dependent absorbance and fluorescence of compound 15 ( $0.05 \text{ mg mL}^{-1}$ ).

$\text{CHCl}_3$  (ESI: Fig. S7<sup>†</sup>) solely signals of the PEtOx block are visible, probably as they represent highly mobile groups once in contact with the solvent. In contrast, cross-linking of the core is likely to physically link the mobility of individual core components to the overall rotational correlation time of the vesicle/micelle, thereby increasing the relaxation rate of the core components significantly and, hence, leading to an absence of signals attributable to the AmOx side chain, GA and DEA or 6AF, respectively.

To qualitatively assess the cross-linked system, natural abundance CP MAS solid state  $^{13}\text{C}$  NMR spectroscopy was employed (Fig. 3). We assigned the prominent signals to the carbonyl functions (A), the backbone (D), and to the side groups (F) and (H), respectively of the abundant PEtOx units. Furthermore, the resonance (E) detectable at  $\sim 30$  ppm represents two methylene groups of the AmOx side chain. The presence of the AmOx part is also supported by a resonance at 60 ppm (C). The shoulder at 20 ppm (G) is attributed to the outer methylene groups of the AmOx spacer and the GA methylenes. The GA gives in addition rise to a broad resonance at  $\sim 160$  ppm (B)

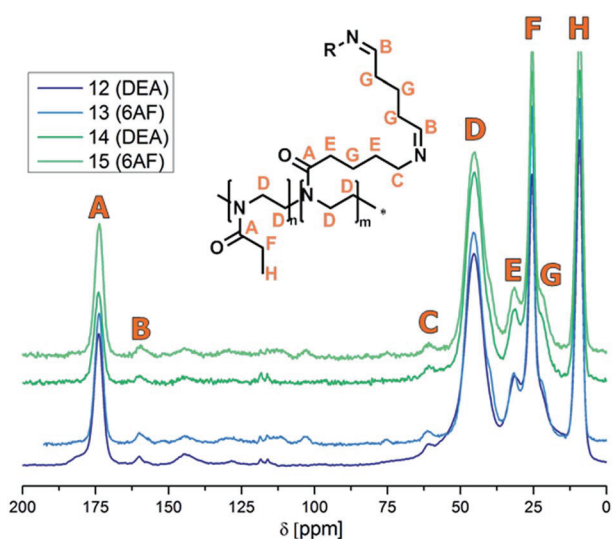


Fig. 3 Solid state  $^{13}\text{C}$  NMR spectra of cross-linked micelles (samples 12 and 13) and vesicles (samples 14 and 15).

assigned to its  $\text{C}=\text{N}$  bond. It should also be noted that the GA groups are the least abundant ones in the cross-linked system. Taken together, these tentative assignments are compatible with the relative abundance, and hence, the observed relative intensities of the respective chemical groups. However, a bona fide quantitative assessment *via* integration of signals of the individual chemical groups, as typically performed in liquid state NMR, is not reliable due to the non-uniform efficiency of the cross-polarization transfer (CP) step in the ssNMR experiment and the significant line broadening observed which, in turn, preclude to identify individual groups. In addition, the comparably low intensities of the broad signals (B) and (C), suggest an under-representation of the core, which might be due to a conformational heterogeneity with concomitant line broadening in the cross-linked region. Likewise, signals for the 6AF are of an intensity lower than expected from the quantitative fluorescence analysis (Table 3). To assign resonances arising from the 6AF moiety, we compared commercial microcrystalline 6AF with amorphous and with KOH treated, ring-opened 6AF (ESI: Fig. S8<sup>†</sup>). From this comparison, we concluded that the signals detectable at 155 ppm, at 120 to 100 ppm and a shifted signal at 75 ppm arise from 6AF. Notably, already the conversion of microcrystalline into amorphous 6AF, produced by dissolving in MeOH, flash-freezing and lyophilisation, caused a severe line broadening in the ssNMR spectra of some of the 6AF resonances and other lines become virtually undetectable. This clearly indicates that a certain degree of conformational heterogeneity ('amorphousness') of the 6AF moiety causes severe line-broadening or in-detectability of some groups in the ssNMR spectra. In summary, we interpret the low intensity signal pattern of the 6AF moiety as resulting from differences in the CP transfer efficiency, severe line broadening and the mainly ring-open form (see Fluorescence experiments) and a residual proportion of amorphous 6AF, the latter giving rise to the signals at 155, 100 to 120 and 80 ppm, respectively.

### Biocompatibility of self-assembled structures

The evaluation of the biocompatibility is one of the first steps to assess the applicability of the micellar/vesicular structures presented herein for potential biomedical applications. Hence,



adverse effects on the cellular metabolism upon incubation with 6AF labeled micelles (sample 13) and vesicles (sample 15) were evaluated using the established L929 cell line, which is characterized and documented by its sensitivity towards cytotoxic agents.<sup>45</sup>

The *in vitro* cytotoxicity experiments were performed *via* a XTT assay according to the German standard institution guideline DIN ISO 10993-5 as a reference for biomaterial testing. After 24 h of incubation with different micelle/vesicle concentrations (0.005, 0.05, 0.5, 2.5 and 5 mg mL<sup>-1</sup>) the metabolic activity of the treated cells was found to be at the level of the untreated controls, with the exception that only the highest concentration of micelles (5 mg mL<sup>-1</sup>) led to a significant reduction of cell viability (50%). Interestingly, the vesicular structures did not show any cytotoxic potential even at the highest concentration (Fig. 4 top). One possible explanation for this behavior could be related to the size of the vesicles. The larger diameter of the structures in comparison to micelles leads to a smaller surface/volume ratio. Furthermore, related to the vesicular architecture, half of the surface faces the inside of the nano-assembly. However, the micelle concentrations which did not show an overt toxicity effect were more than adequate for potential applications.

Microscopic assessment of the proportion of live and dead cells confirmed the findings from the XTT assay – the membrane integrity of viable cells was proven by the exclusion of red fluorescent propidium iodide (PI) from cell nuclei indicating their excellent viability (Fig. 4 bottom panel; B3). In

addition, the microscopic investigations provided first hints for a cellular internalization of the fluorescein containing micelles (Fig. 4, B5).

In the case of the highest micelle concentration, images revealed a disintegration of the cell membrane (PI positive cell nuclei) accompanied by a reduced intracellular localization of micelles, which might be caused by a diffusion of the micelles through the leaky membrane out of the dead cells (Fig. 4, A3 and A4). These results confirm the low cytotoxicity generally observed for PEtOx-based materials with different molar masses and PEtOx-containing block copolymers, which were evaluated before.<sup>9</sup>

### Flow cytometric (FC) investigations on time and concentration dependent uptake

The time and concentration dependent uptake of the fluorescein containing micelles/vesicles was quantified by FC measurements. For this purpose, cells were incubated either with different concentrations (0.05, 0.1, 0.25, and 0.5 mg mL<sup>-1</sup>) of the materials for 24 h at 37 °C or with one concentration (0.5 mg mL<sup>-1</sup>) for different time scales (0.5, 1, 3, 12, and, 24 h; 37 °C). Following the incubation, the excess of micelle/vesicle material was removed by washing with PBS. Subsequently, the cells were trypsinized and subjected to FC analysis.

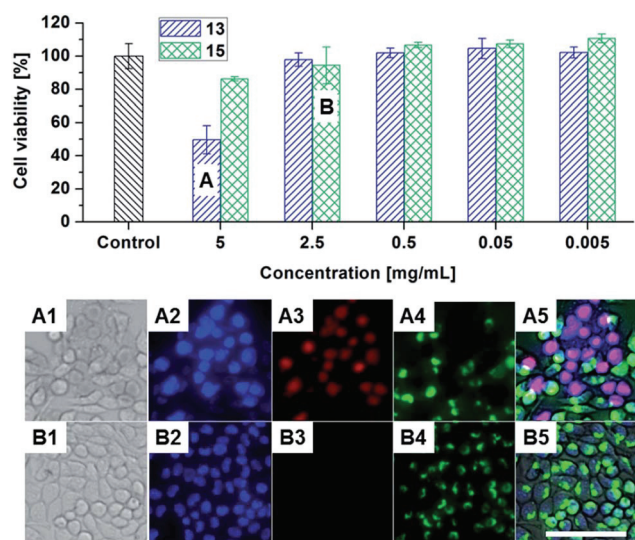


Fig. 4 (Top) Cell viability of L929 mouse fibroblasts after incubation with micelles (13)/vesicles (15) up to 5 mg mL<sup>-1</sup> for 24 hours. (Bottom) Representative bright field and fluorescence microscopy images of Hoechst 33342/PI stained L929 mouse fibroblast cells cultured for 24 h in the presence of sample 13 (A1–A5; 5 mg mL<sup>-1</sup>) and sample 15 (B1–B5; 0.5 mg mL<sup>-1</sup>). Blue fluorescent Hoechst dye labels nuclei of all cells present (A2 and B2), while red fluorescent PI signals (A3 and B3) indicate nuclei of dead cells. Green fluorescence originates from the dye containing nanostructures (A4 and B4). Additionally, image superimpositions for all four channels are displayed (A5 and B5). Scale bar: 100  $\mu$ m.

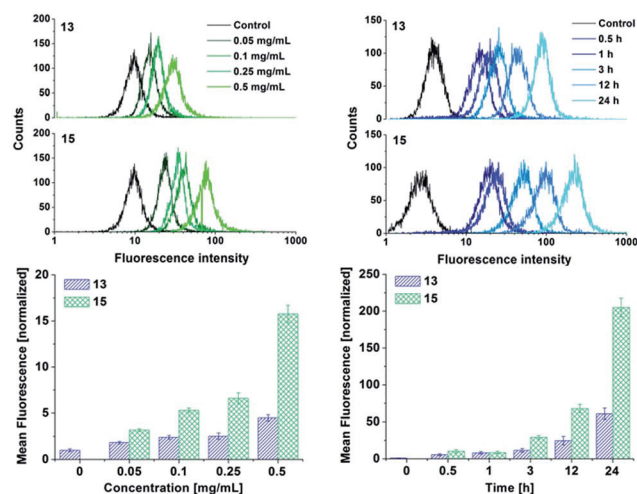


Fig. 5 Flow cytometry investigation on the time and concentration dependent uptake of 6AF containing micelles/vesicles by L929 mouse fibroblasts at 37 °C. For time dependent uptake cells were incubated between 0.5 and 24 h with micelles (13)/vesicles (15) with a concentration of 0.5 mg mL<sup>-1</sup>, whereas the concentration dependent uptake was investigated over an incubation time of 24 h using micelle/vesicle concentrations in the range between 0.05 and 0.5 mg mL<sup>-1</sup>. Cells incubated only with culture medium served as control. For histogram plots the fluorescence intensity on the x-axis is plotted against the number of events on the y-axis. A shift of the histogram toward the right side demonstrates an increasing amount of dye containing micelles/vesicles associated to the cells. The bar charts depict the results for the corresponding normalized mean fluorescence intensities, obtained from flow cytometry of the analyzed cell populations. The data are expressed as mean  $\pm$  SD of triplicates.

The fluorescence intensity distributions (histogram plots in Fig. 5) clearly display a concentration-dependent right-shift to higher fluorescence intensity for both, the micellar and vesicular structures indicating a concentration-dependent uptake.

Interestingly, the increase in fluorescence intensity was more pronounced for the vesicle samples, suggesting an increased cellular accumulation/association as compared to micelles.

This becomes evident in quantitative terms when the mean fluorescence intensities (MFI) of the cell populations are evaluated as depicted in the bar charts (Fig. 5). An up to three-fold uptake of the vesicles was obtained as compared to micelles with the same concentration. These results were also confirmed by fluorescence microscopic observations of the treated cell populations (ESI: Fig. S9†). Interestingly, the proportion of “positive cells” having associated micelles or vesicles did not only increase at higher material concentrations but was also higher for vesicular compared to micellar samples, e.g. at 0.05 mg mL<sup>-1</sup> 83 to 13% and at 0.5 mg mL<sup>-1</sup> 98 to 88% (data not shown).

For the time-dependent uptake trends similar to the concentration-dependent internalization were observed. The cellular accumulation of material proceeds over time for both the micelles and vesicles without reaching a plateau after 24 h. Additionally, the cellular uptake of the vesicular formulation exceeds the internalization rate of the micelles by a factor of 3 and, again, supports the interpretation of a higher cellular internalization of the vesicles. It should be noted that the initially conducted fluorescence measurements of the micelle and vesicle suspensions at equivalent concentrations (weight/volume) demonstrated that both show similar fluorescence values (Fig. 3). Therefore, the observed increase in cell associated fluorescence can clearly be attributed to an enhanced vesicle uptake.

The different cellular internalization efficiencies could be caused by the cellular uptake mechanism. It is known that very large particles enter cells by phagocytosis, whereas, in the case

of nanoparticles, most internalization occurs *via* various endocytotic pathways, which can be different with regard to the nature of the surface and the structural properties of nanoparticles (e.g. clathrin or caveolin dependent pathways).<sup>46</sup> Depending on the particular pathway and also its energy dependent or independent nature, different internalization rates are achieved<sup>47</sup> – this could also impact the uptake efficiency of the presented micelles and vesicles. To elucidate these phenomena further investigations are required, e.g. by assessing or blocking certain uptake pathways using specific inhibitors.

### Internalization and co-localization with cellular compartments

The cellular internalization and intracellular localization of micelles and vesicles in L929 cells was further elucidated by epifluorescence and confocal laser scanning microscopy (CLSM) investigations. For this purpose, the cells were incubated for 24 h with 0.5 mg mL<sup>-1</sup> of the respective substance at 37 °C and, in order to assign the localization of the fluorescent micelles/vesicles to cellular compartments, the living adherent or suspended cells were stained with specific dyes for the cell plasma membrane (Cell Mask Orange), the nuclei (Hoechst 33342 or SytoRed59) or the acidic late endosomes and lysosomes (LysoTracker), respectively.

A representative distribution of fluorescent vesicles in the context of cellular structures in adherent cells is presented in Fig. 6. The epifluorescence images suggest an intracellular localization of the vesicles, since no green fluorescent signal (from the 6AF labeled structures) is detectable at the outer cell membrane, which would be the case when vesicles are adsorbed to, but not transported through the membrane (Fig. 6: A2, A3 and A5). Additionally, no vesicles were observed within the nuclear compartment: They were rather associated with distinct outer nuclear membrane regions (Fig. 6: A5).

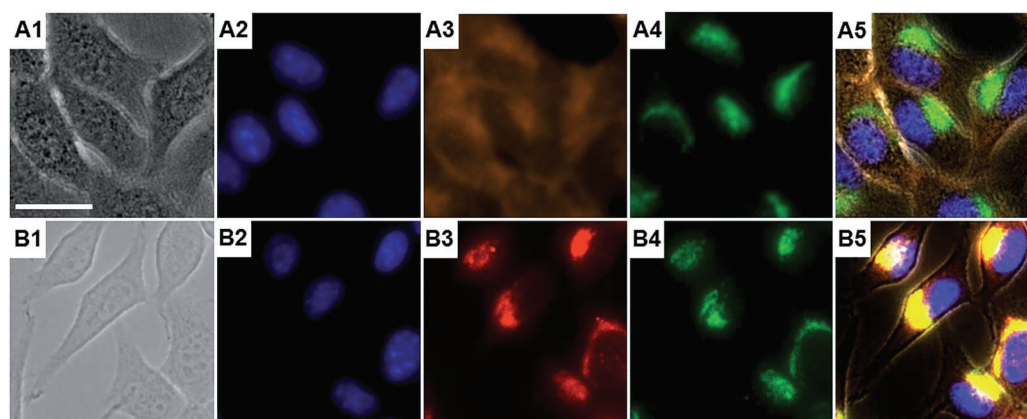


Fig. 6 Representative bright field (A1 and B1) and epifluorescence images of adherent L929 cells after 24 h incubation at 37 °C with vesicles (15) at a concentration of 0.1 mg mL<sup>-1</sup>. Cell nuclei (A2 and B2), cell membranes (A3) or late endosomes/lysosomes (B3) were specifically stained and their fluorescence signal was captured in addition to the fluorescence signal originating from the internalized 6AF labeled vesicles (A4 and B4). Co-localization was examined by superimposing all four channels (A5 and B5). Identical results were obtained for micelles (ESI: Fig. S10†). Scale bar: 20 μm.



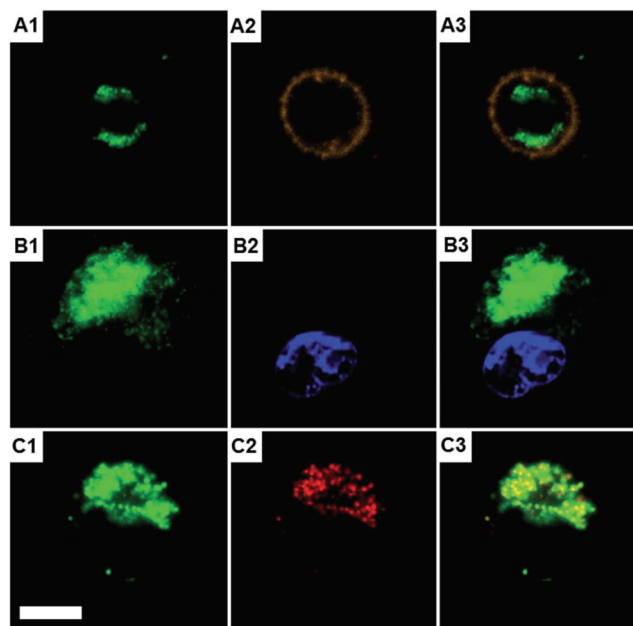


Fig. 7 Representative CLSM images of detached L929 cells after 24 h incubation at 37 °C with vesicles (15) at a concentration of 0.1 mg mL<sup>-1</sup>. Cell membranes (A2), cell nuclei (B2), or late endosomes/lysosomes (C2) were specifically stained and correlated with the fluorescence signal of 6AF labeled vesicles (A1, B1, and C1). Superimposition of both channels (A3, B3 and C3) proves an intracellular (A3) but extra-nuclear (B3) localization of the vesicles and their apparent co-localization with endosomal structures (C3). Identical results were obtained for micelles (ESI: Fig. S11†). Scale bar: 10 μm.

Hypothesizing that internalization of the vesicles/micelles proceeds *via* endocytotic pathways, an appearance of the internalized structures in the late endosomes or lysosomes was very likely. Indeed, co-localization of stained acidic endosomes and fluorescent vesicles was observed (Fig. 6: B2, B3 and B5). CLSM investigations on cells treated as mentioned above but additionally detached after incubation and subjected to microscopic analysis with precise optical z-sectioning through the cell body confirmed an extra-nuclear presence and the complete internalization of the vesicles into the lysosomal compartment (Fig. 7: A1 to C3).

Identical results for internalization and lysosomal localization were obtained for the micellar forms suggesting similar endocytotic uptake and distribution mechanisms for both, vesicles and micelles. It should be noted that only intact nanostructures can be detected by fluorescence in an intracellular environment since the emission intensity of the free dye is strongly diminished at neutral and acidic pH values (Fig. 2). Therefore, the co-localization studies clearly suggest an endosomal location and, hence, a internalization by endocytosis can be assumed. For further studies this behavior could be beneficial because the low pH value within these cellular compartments should lead to a disassembly of the nanostructures and might result in a release of the cargo. With the presented loading, however, no pH dependent release can be investigated due to the low solubility of the dye at neutral and acidic pH values.

## Conclusion

In this contribution we describe the synthesis of block copolymers with a neutral hydrophilic (EtOx) and a cationic hydrophilic (AmOx) segment as well as the self-assembling behaviour of the system into micelles and vesicles in organic solvents.

Glutaraldehyde mediated cross-linking resulted in the formation of nanogels, which were covalently loaded with 6-amino fluorescein. A detailed characterization of these nanostructures led to the conclusion that formation of either micellar or vesicular structures, respectively, is significantly dependent upon the nature of the solvent used for assembly. The presented nanogels exhibit a good biocompatibility for concentrations of up to 5 mg mL<sup>-1</sup> and reveal a concentration and time dependent uptake by cells, presumably by endocytosis, as investigated by co-localization studies.

Further studies will focus on the immobilization of drugs like cytostatica and the investigation of the release of these compounds. Moreover, a variation of the zeta potential by changing the degree of cross-linking will be studied in order to control the interaction with cells and the rate of the uptake.

## Experimental section

Information about materials and instrumentation can be found in the ESI.†

### Block copolymers of 2-ethyl-2-oxazoline (EtOx) and 2-(4-((*tert*-butoxycarbonyl)amino)butyl)-2-oxazoline (BocOx) (P(EtOx-*b*-BocOx)), (2–6)

In a microwave vial, EtOx (606 μL, 6 mmol), MeOTos (12.1 μL, 0.08 mmol) and acetonitrile (2.9 mL) were mixed under inert conditions. After heating in the microwave synthesizer at 140 °C for 28 min, a solution of BocOx (500 μL, 2 mmol) in acetonitrile (1.5 mL) was added through a syringe and the mixture was heated again in the microwave synthesizer (140 °C, 22 min). The solution was precipitated in cold (–80 °C) diethyl ether. The white precipitate was filtered and dried in high vacuum (994 mg, 92%).

<sup>1</sup>H NMR (CDCl<sub>3</sub>, 300 MHz) (6): δ = 7.67, (d, 8.1 Hz, 0.018H, tosylate), 7.14 (d, 8.21 Hz, 0.018H, tosylate), 3.46 (s, 4H, backbone), 3.10 (s, 0.5H, CH<sub>2</sub>–CH<sub>2</sub>–NH (BocOx)), 2.50–2.15 (m, 1.96H, CH<sub>2</sub> (EtOx)/CH<sub>2</sub>–CH<sub>2</sub>–NH(Boc)), 1.62 (s, 0.46H, CH<sub>2</sub>–CH<sub>2</sub>–CH<sub>2</sub> (BocOx)), 1.52 (s, 0.46H, CH<sub>2</sub>–CH<sub>2</sub>–CH<sub>2</sub> (BocOx)), 1.42 (s, 2.1H, CH<sub>3</sub> (BocOx)), 1.21 (s, 2.1H, CH<sub>3</sub> (EtOx)) ppm.

Size exclusion chromatography (SEC) (6) (eluent: CHCl<sub>3</sub>/*iso*-propanol/NEt<sub>3</sub>, PS-standard): *M*<sub>n</sub> = 7.600 g mol<sup>-1</sup>, *M*<sub>w</sub> = 9.000 g mol<sup>-1</sup>, *D* = 1.18.

### Deprotection of P(EtOx-*b*-BocOx) P(EtOx-*b*-AmOx), (7–11)

Exemplarily, P(EtOx-*b*-BocOx) (6, 500 mg) was dissolved in TFA (5 mL) and heated to 60 °C for 1 h. After stirring for 12 h at room temperature, the mixture was diluted with 10 mL methanol and precipitated in 200 mL of cold (–80 °C) diethyl ether. The precipitate was re-dissolved in methanol (100 mL) and stirred with Amberlyst A21 for 48 h. Subsequently, the solvent was

removed, the polymer was dissolved in de-ionized water and freeze dried ( $-80\text{ }^{\circ}\text{C}$ ,  $0.003\text{ mbar}$ ). The polymer was obtained as white powder (456 mg, 91%).

$^1\text{H NMR}$  ( $N,N$ -dimethyl formamide (DMF)- $D_7$ , 300 MHz) (**11**):  $\delta = 5.37$  (s, 1.7H,  $\text{NH}_2$ ), 3.69 (s, 4H, backbone), 3.23 (s, 0.55H,  $\text{CH}_2\text{-CH}_2\text{-NH}_2$ ), 2.78–2.45 (m, 2.1H,  $\text{CH}_2$  (EtOx)/ $\text{CH}_2\text{-CH}_2\text{-CO}$  (AmOx)), 2.06–1.72 (m, 1.1H,  $\text{CH}_2\text{-CH}_2\text{-CH}_2\text{-CH}_2$  (AmOx)), 1.2 (s, 2.5H,  $\text{CH}_3$  (EtOx)) ppm.

SEC (**11**) (eluent: DMAc/LiCl, PS-standard):  $M_n = 15\ 600\text{ g mol}^{-1}$ ,  $M_w = 20\ 300\text{ g mol}^{-1}$ ,  $D = 1.30$ .

### Determination of cloud point behavior in aqueous sodium hydroxide solution

To investigate the cloud point behavior, P(EtOx-*b*-AmOx) was dissolved in an aqueous solution of sodium hydroxide (5 wt%) in concentrations varying from 2.5 to 20 mg  $\text{mL}^{-1}$ . The turbidity was recorded as a function of the temperature, which was modulated between 2 and 98  $^{\circ}\text{C}$  in three cycles (1  $^{\circ}\text{C min}^{-1}$ ). The cloud point was determined at 50% transmission. Cloud points were measured in a Crystal 16 from Avantium Technologies connected to a chiller (Julabo FP 40) at a wavelength of 500 nm.

### Self-assembly and cross-linking

To create nanostructures, the block copolymer (**11**, 150 mg, 0.015 mmol, 0.39 mmol of amine) was dissolved in the respective solvent (MeOH, *i*PrOH or  $\text{CHCl}_3$ , 5 mg  $\text{mL}^{-1}$ ) and stirred for 3 h. Subsequently, glutaraldehyde (19.5 mg, 0.195 mmol, 0.5 eq. per amine) was added and the solution was stirred for another 3 h. With proceeding reaction time the color of the solution changed from colorless to yellow. To quench the excess aldehyde function, diethylamine or 6-amino fluorescein was added, respectively, and stirred for 12 h. Subsequently, the amount of solvent was reduced under an argon stream and the residual was precipitated in 100 mL cold diethyl ether ( $-80\text{ }^{\circ}\text{C}$ ). To purify the self-assembled structures from residual amine and cross-linker, dialysis in MeOH-water (1 : 4) was applied using a membrane with a molar mass cut off of 3500  $\text{g mol}^{-1}$  (Roth Zellutrans). After the extraction was finished, the dialysis medium was changed to pure water and the aqueous solution was freeze dried to yield an orange powder (140 mg). The size distribution of all intermediate steps was examined by dynamic light scattering (DLS) measurements.

### Determination of dye loading content by absorbance/fluorescence

The absorbance/fluorescence of nanostructures was investigated under alkaline conditions (1 mol  $\text{L}^{-1}$  NaOH in water) in diluted solution (0.1, 0.05 and 0.025 mg  $\text{mL}^{-1}$ ). The absorbance was determined at a wavelength of 490 nm and compared to a dilution series of 6AF in the same aqueous NaOH solution. To the 6AF stock solution a 100 fold excess of glutaraldehyde was added to ensure that only the imine species of 6AF is present. Emission was detected at an excitation wavelength of 450 nm. Micellar samples as well as 6AF calibration exhibit an emission maximum at 510 nm. All measurements were carried out in a 96

well-plate format with 200  $\mu\text{L}$  per well and double determination for each measuring point. The read out was accomplished using a Tecan M200 Pro fluorescence micro plate reader (Crailsheim, Germany). DEA loaded nanostructures served as a reference for all measurements.

### Cytotoxicity assay

For the cytotoxicity screening, the mouse fibroblast cell line L929 was purchased from a commercial cell bank (Cell line service, Eppelheim, Germany). The cells were routinely cultured as follows: cell culture media Dulbecco's modified eagle's medium (DMEM) was supplemented with 10% fetal calf serum, 100 U  $\text{mL}^{-1}$  penicillin, and 100  $\mu\text{g mL}^{-1}$  streptomycin (all components from Biochrom, Berlin, Germany) at 37  $^{\circ}\text{C}$  in a humidified atmosphere with 5% (v/v)  $\text{CO}_2$ . The cytotoxicity was determined using a XTT assay following the ISO/EN 10993 part 5 protocol: cells were seeded in 96-well plates at a density of  $1 \times 10^4$  cells per well and grown as monolayer cultures for 24 h. The cells were subsequently incubated separately with different concentrations of the micelles and vesicles (from 0.005 to 5 mg  $\text{mL}^{-1}$ ) for 24 h. Control cells were incubated with fresh culture medium. After incubation, the cells were washed once with PBS and a mixture of 100  $\mu\text{L}$  fresh medium and 50  $\mu\text{L}$  of a XTT solution, prepared according to the manufacturer's instructions, were added to each well. After 4 h at 37  $^{\circ}\text{C}$ , 100  $\mu\text{L}$  of each solution were transferred to a new micro titer plate and the optical density (OD) was measured photometrically. The control was standardized as 0% of metabolism inhibition and referred as 100% viability. Cell viability below 70% was considered indicative of cytotoxicity. Data are expressed as mean  $\pm$  SD of six determinations.

### Photometrical and microscopical methods

For the photometric absorbance measurements, a TECAN Infinite M200 PRO plate reader (TECAN, Crailsheim, Germany) was used to measure the absorption of samples from the XTT cytotoxicity assay (570 nm with a background correction of the optical density (OD) at 690 nm). Each well containing the sample was measured in four different spots each with 25 flashes per scan.

The evaluation of micelles/vesicles uptake was performed by flow cytometry (FC) measured on a Beckmann Coulter Cytomics FC-500 equipped with Uniphase Argon ion laser, 488 nm, 20 mW output and analyzed with the Cytomics CXP software. For time dependent uptake, cells (L929) were incubated between 30 min and 24 h with micelles (**13**)/vesicles (**15**) at a concentration of 0.5 mg  $\text{mL}^{-1}$ , whereas the concentration dependent uptake was investigated over an incubation time of 24 h using micelle/vesicle concentrations in the range between 0.05 and 0.5 mg  $\text{mL}^{-1}$ . Cells incubated with culture medium only served as control. Data are expressed as mean  $\pm$  SD of three determinations. To visualize the viability of cells after incubation with the micelles/vesicles as well as for the time/concentration dependent kinetic studies on cellular uptake, the blue/red/green fluorescence signal of cells cultured in a 96 well plate and stained with Hoechst 33342 and propidium iodide (PI) was

observed on a Cell Observer Z1 fluorescence microscope (Carl Zeiss, Jena, Germany) equipped with a mercury arc UV lamp and the appropriate filter combinations for excitation and detection of emission. Images of a series were captured with a 40 $\times$  objective using identical instrument settings (e.g. UV lamp power, integration time, camera gain) and cell-spots in the 96 well plate were addressed using an automated XY table.

For CLSM analysis of uptake and co-localization with cell organelle, the nuclei, late endosomes/lysosomes and cell membranes were either stained with SYTO@Red 59, LysoTracker Red or Cell Mask Orange. CLSM images were acquired using a Zeiss LSM 510 META (Carl Zeiss) with excitation wavelengths/emission filters of 633 nm/LP 650 nm for SYTO@Red and 543 nm/BP 585 to 615 nm for LysoTracker Red and Cell Mask Orange respectively.

Images were captured with a Plan-Apochromat 63 $\times$  objective and in multitrack mode, enabling single excitation and emission of fluorescence dyes. Co-localization was visualized in overlay images of the multiple channels.

**Microscopic evaluation of cell viability.** In addition to the above described measurement of the metabolic cell activity by the XTT assay, viability of the cells after exposure to the micelles and vesicles was examined microscopically using a propidium iodide (PI)/Hoechst staining assay. After incubation with the test substances, the cells were washed once with PBS, submerged with medium containing PI (10  $\mu\text{g mL}^{-1}$ ) and Hoechst 33342 (10  $\mu\text{g mL}^{-1}$ ) and incubated for 10 min at 37  $^{\circ}\text{C}$ . During that time, PI enters into the nuclei of dead cells *via* the leaky cell membrane, whereas the dye is kept outside of viable cells. Hoechst dye is capable of fluorescently labeling nuclei of dead and viable cells and was used to tag the entire cell collective. The blue (Hoechst), red (PI), and green (6AF labeled vesicles and micelles) fluorescence signals of cells were captured on a fluorescence microscope.

#### Fluorescence microscopy for kinetic studies on cellular uptake of micelles (13)/vesicles (15)

For kinetic investigations concerning a concentration dependent uptake, the cells, growing as a semiconfluent cell layer in 6 well plates, were incubated separately with different concentrations (0.05, 0.1, 0.25 and 0.5  $\text{mg mL}^{-1}$ ) of micelles and vesicles for 24 h at 37  $^{\circ}\text{C}$  under 5%  $\text{CO}_2$  atmosphere. Control cells were incubated with fresh culture medium. After incubation, the solutions were aspirated from the wells and any excess materials were removed by washing the cell layer three times with PBS. For flow cytometry, the adherent cells were detached by trypsin treatment and 10,000 cells were analyzed using gates of forward and side scatters to exclude debris and cell aggregates. For microscopic analysis, the adherent cells were additionally stained with Hoechst 33342 (10  $\mu\text{g mL}^{-1}$ ) and immediately subjected to fluorescence imaging.

For kinetic investigation concerning a time dependent uptake, cells were treated with 0.5  $\text{mg mL}^{-1}$  of micelles or vesicles for 0.5 h, 1 h, 3 h, 12 h and 24 h at 37  $^{\circ}\text{C}$  under 5%  $\text{CO}_2$  atmosphere. Subsequent analysis was performed as mentioned above.

#### Co-localization study

In order to analyze the micelle/vesicle uptake and co-localization with cell organelle, adherent cells were treated with 0.1  $\text{mg mL}^{-1}$  of micelles/vesicles for 24 h at 37  $^{\circ}\text{C}$  under 5%  $\text{CO}_2$  atmosphere. Subsequently, the nuclei, late endosomes/lysosomes and cell membranes were stained with Hoechst 33342 and LysoTracker Red or Cell Mask Orange according to manufactures instructions (all dyes from Life Technologies, Darmstadt, Germany) and the adherent cell populations were, subsequently, subjected to microscopic investigation immediately using an epifluorescence microscope. In order to prove an effective internalization of the fluorescent micelles (13)/vesicles (15) and to exclude a false positive fluorescence signal by a simple adsorption on the extracellular leaflet of the cell membrane, CLSM was utilized to perform an optical z-sectioning through the cells. For that purpose, adherent cells were enzymatically detached after the above mentioned incubation with the micelles/vesicles. The nuclei, late endosomes/lysosomes and cell membranes were stained with SYTO@Red 59, LysoTracker Red or Cell Mask Orange according to manufactures instructions and, subsequently, fixed with 4% paraformaldehyde dissolved in PBS. Aliquots of the cell suspensions were then transferred onto microscopic slides, decorated with coverslips and subjected to CLSM analysis.

#### Acknowledgements

Cryo-TEM investigations were performed at the cryo-TEM facilities of the Jena Center for Soft Matter (JCSM). The TEM facilities were funded by a grant of the DFG (German Research Foundation) and the EFRE (European Fund for Regional Development). The Leibniz Institute for Age Research – Fritz Lipmann Institute (FLI) is a member of the Leibniz Society and is financially supported by the State of Thuringia and the Federal Government of Germany.

#### Notes and references

- 1 G. Liu and Z. An, *Polym. Chem.*, 2014, **5**, 1559–1565.
- 2 R. Tong, L. Tang, L. Ma, C. Tu, R. Baumgartner and J. Cheng, *Chem. Soc. Rev.*, 2014, **43**, 6982–7012.
- 3 H. Wei, R.-X. Zhuo and X.-Z. Zhang, *Prog. Polym. Sci.*, 2013, **38**, 503–535.
- 4 W. Xu, P. Ling and T. Zhang, *J. Drug Delivery*, 2013, **2013**, 15.
- 5 H. Ding, X. Wang, S. Zhang and X. Liu, *J. Nanopart. Res.*, 2012, **14**, 1–13.
- 6 M. Talelli, C. J. F. Rijcken, W. E. Hennink and T. Lammers, *Curr. Opin. Solid State Mater. Sci.*, 2012, **16**, 302–309.
- 7 S. E. Averick, E. Paredes, A. Irastorza, A. R. Shrivats, A. Srinivasan, D. J. Siegwart, A. J. Magenau, H. Y. Cho, E. Hsu, A. A. Averick, J. Kim, S. Liu, J. O. Hollinger, S. R. Das and K. Matyjaszewski, *Biomacromolecules*, 2012, **13**, 3445–3449.
- 8 W. Chen, M. Zheng, F. Meng, R. Cheng, C. Deng, J. Feijen and Z. Zhong, *Biomacromolecules*, 2013, **14**, 1214–1222.

- 9 R. Luxenhofer, G. Sahay, A. Schulz, D. Alakhova, T. K. Bronich, R. Jordan and A. V. Kabanov, *J. Controlled Release*, 2011, **153**, 73–82.
- 10 M. Bauer, S. Schroeder, L. Tauhardt, K. Kempe, U. S. Schubert and D. Fischer, *J. Polym. Sci., Part A: Polym. Chem.*, 2013, **51**, 1816–1821.
- 11 M. C. Woodle, C. M. Engbers and S. Zalipsky, *Bioconjugate Chem.*, 1994, **5**, 493–496.
- 12 S. Zalipsky, C. B. Hansen, J. M. Oaks and T. M. Allen, *J. Pharm. Sci.*, 1996, **85**, 133–137.
- 13 B. Guillermin, S. Monge, V. Lapinte and J.-J. Robin, *Macromol. Rapid Commun.*, 2012, **33**, 6000–6016.
- 14 O. Sedlacek, B. D. Monnery, S. K. Filippov, R. Hoogenboom and M. Hruby, *Macromol. Rapid Commun.*, 2012, **33**, 1648–1662.
- 15 P. Persigehl, R. Jordan and O. Nuyken, *Macromolecules*, 2000, **33**, 6977–6981.
- 16 R. Hoogenboom, M. M. Leenen, H. Huang, C.-A. Fustin, J.-F. Gohy and U. S. Schubert, *Colloid Polym. Sci.*, 2006, **284**, 1313–1318.
- 17 U. Mansfeld, S. Hoepfner, K. Kempe, J.-M. Schumers, J.-F. Gohy and U. S. Schubert, *Soft Matter*, 2013, **9**, 5966–5974.
- 18 R. Takahashi, T. Sato, K. Terao, X.-P. Qiu and F. M. Winnik, *Macromolecules*, 2012, **45**, 6111–6119.
- 19 R. Obeid, E. Maltseva, A. F. Thünemann, F. Tanaka and F. M. Winnik, *Macromolecules*, 2009, **42**, 2204–2214.
- 20 T. B. Bonn , K. L dtke, R. Jordan and C. M. Papadakis, *Macromol. Chem. Phys.*, 2007, **208**, 1402–1408.
- 21 R. Ivanova, T. Komenda, T. B. Bonn , K. L dtke, K. Mortensen, P. K. Pranzas, R. Jordan and C. M. Papadakis, *Macromol. Chem. Phys.*, 2008, **209**, 2248–2258.
- 22 R. Luxenhofer, A. Schulz, C. Roques, S. Li, T. K. Bronich, E. V. Batrakova, R. Jordan and A. V. Kabanov, *Biomaterials*, 2010, **31**, 4972–4979.
- 23 Y. Han, Z. He, A. Schulz, T. K. Bronich, R. Jordan, R. Luxenhofer and A. V. Kabanov, *Mol. Pharm.*, 2012, **9**, 2302–2313.
- 24 A. Schulz, S. Jaksch, R. Schubel, E. Wegener, Z. Di, Y. Han, A. Meister, J. Kressler, A. V. Kabanov, R. Luxenhofer, C. M. Papadakis and R. Jordan, *ACS Nano*, 2014, **8**, 2686–2696.
- 25 R. K. O'Reilly, C. J. Hawker and K. L. Wooley, *Chem. Soc. Rev.*, 2006, **35**, 1068–1083.
- 26 N. t. Brummelhuis and H. Schlaad, *Polym. Chem.*, 2011, **2**, 1180–1184.
- 27 N. Engelhardt, A. Ernst, A.-L. Kampmann and R. Weberskirch, *Macromol. Chem. Phys.*, 2013, **214**, 2783–2791.
- 28 C. Legros, A.-L. Wirotius, M.-C. De Pauw-Gillet, K. C. Tam, D. Taton and S. Lecommandoux, *Biomacromolecules*, 2014, **16**, 183–191.
- 29 H. Huang, R. Hoogenboom, M. A. M. Leenen, P. Guillet, A. M. Jonas, U. S. Schubert and J.-F. Gohy, *J. Am. Chem. Soc.*, 2006, **128**, 3784–3788.
- 30 Y. Liu, Y. Wang, Y. Wang, J. Lu, V. Pi n n and M. Weck, *J. Am. Chem. Soc.*, 2011, **133**, 14260–14263.
- 31 S. Zschoche, J. C. Rueda, M. Binner, H. Komber, A. Janke, K.-F. Arndt, S. Lehmann and B. Voit, *Macromol. Chem. Phys.*, 2012, **213**, 215–226.
- 32 S. Zschoche, J. Rueda, V. Boyko, F. Krahl, K.-F. Arndt and B. Voit, *Macromol. Chem. Phys.*, 2010, **211**, 1035–1042.
- 33 C. Legros, M.-C. De Pauw-Gillet, K. C. Tam, S. Lecommandoux and D. Taton, *Polym. Chem.*, 2013, **4**, 4801–4808.
- 34 S. Cesana, J. Auernheimer, R. Jordan, H. Kessler and O. Nuyken, *Macromol. Chem. Phys.*, 2006, **207**, 183–192.
- 35 M. Hartlieb, D. Pretzel, K. Kempe, C. Fritzsche, R. M. Paulus, M. Gottschaldt and U. S. Schubert, *Soft Matter*, 2013, **9**, 4693–4704.
- 36 C. Legros, M.-C. De Pauw-Gillet, K. C. Tam, S. Lecommandoux and D. Taton, *Eur. Polym. J.*, 2015, **62**, 322–330.
- 37 J. Kronek, Z. Kronekov , J. Lusto n, E. Paulovi ov , L. Paulovi ov  and B. Mendrek, *J. Mater. Sci.: Mater. Med.*, 2011, **22**, 1725–1734.
- 38 J. Kronek, E. Paulovi ov , L. Paulovi ov , Z. Kronekov  and J. Lusto n, *J. Mater. Sci.: Mater. Med.*, 2012, **23**, 1457–1464.
- 39 F. Wiesbrock, R. Hoogenboom, C. H. Abeln and U. S. Schubert, *Macromol. Rapid Commun.*, 2004, **25**, 1895–1899.
- 40 J. Rodr guez-Hern ndez, J. Babin, B. Zappone and S. Lecommandoux, *Biomacromolecules*, 2005, **6**, 2213–2220.
- 41 M. Wagner, S. Holzschuh, A. Traeger, A. Fahr and U. S. Schubert, *Anal. Chem.*, 2014, **86**, 5201–5210.
- 42 W. Burchard, in *Branched Polymers II*, ed. J. Roovers, Springer Berlin Heidelberg, 1999, vol. 143, pp. 113–194.
- 43 J. N. Israelachvili, D. J. Mitchell and B. W. Ninham, *J. Chem. Soc., Faraday Trans. 2*, 1976, **72**, 1525–1568.
- 44 R. Sj back, J. Nygren and M. Kubista, *Spectrochim. Acta, Part A*, 1995, **51**, L7–L21.
- 45 T. Tsuchiya, *J. Biomater. Appl.*, 1994, **9**, 138–157.
- 46 S. Xiang, H. Tong, Q. Shi, J. C. Fernandes, T. Jin, K. Dai and X. Zhang, *J. Controlled Release*, 2012, **158**, 371–378.
- 47 S. Lerch, M. Dass, A. Musyanovych, K. Landfester and V. Mail nder, *Eur. J. Pharm. Biopharm.*, 2013, **84**, 265–274.



## Supporting information

### Core cross-linked micelles and vesicles based on the self-assembly of double hydrophilic poly(2-oxazoline) block copolymers

Matthias Hartlieb,<sup>1,2</sup> David Pretzel,<sup>1,2</sup> Michael Wagner,<sup>1,2</sup> Stephanie Hoepfener,<sup>1,2</sup> Peter Bellstedt,<sup>3</sup> Matthias Görlach,<sup>3</sup> Christoph Englert,<sup>1,2</sup> Kristian Kempe,<sup>1,2,†</sup> Ulrich S. Schubert<sup>1,2,\*</sup>

<sup>1</sup> Laboratory of Organic and Macromolecular Chemistry (IOMC), Friedrich Schiller University Jena, Humboldtstrasse 10, 07743, Jena, Germany

<sup>2</sup> Jena Center for Soft Matter (JCSM), Friedrich Schiller University Jena, Philosophenweg 7, 07743, Jena, Germany

<sup>3</sup> Biomolecular NMR Spectroscopy, Leibniz Institute for Age Research – Fritz Lipmann Institute, Beutenbergstr. 11, 07745 Jena, Germany

† Current address: Department of Chemistry, University of Warwick, Gibbet Hill Road, Coventry, CV4 7AL, U.K.

\* Address correspondence to [ulrich.schubert@uni-jena.de](mailto:ulrich.schubert@uni-jena.de)

#### I Materials and instrumentation

Chemicals and solvents were purchased from Sigma-Aldrich, Merck, Fluka, and Acros. 2-Ethyl-2-oxazoline (EtOx) and methyl tosylate (MeOTos) were distilled to dryness prior to use. EtOx was dried using barium oxide before distillation. 2-(4-((*tert*-Butoxycarbonyl)amino)butyl)-2-oxazoline (BocOx) was synthesized as described in a previous publication.<sup>1</sup>

The Initiator Sixty single-mode microwave synthesizer from Biotage, equipped with a non-invasive IR sensor (accuracy: 2%), was used for polymerizations under microwave irradiation.



Microwave vials were heated overnight to 110 °C and allowed to cool to room temperature under argon atmosphere before use. All polymerizations were carried out under temperature control. Size-exclusion chromatography (SEC) of protected polymers was performed on a Shimadzu system equipped with a SCL-10A system controller, a LC-10AD pump, a RID-10A refractive index detector and a PSS SDV column with chloroform/triethylamine (NEt<sub>3</sub>)/*iso*-propanol (94:4:2) as eluent. The column oven was set to 50 °C. SEC of the deprotected statistical copolymers was performed on a Shimadzu system with a LC-10AD pump, a RID-10A refractive index detector, a system controller SCL-10A, a degasser DGU-14A, and a CTO-10A column oven using *N,N*-dimethyl acetamide (DMAc) with 2.1 g L<sup>-1</sup> LiCl as the eluent and the column oven set to 50 °C. Poly(styrene) (PS) samples were used as calibration standards for both solvent systems. Proton NMR spectroscopy (<sup>1</sup>H NMR) measurements were performed at room temperature on a Bruker AC 300 and 400 MHz spectrometer, using CDCl<sub>3</sub> or *N,N* dimethyl formamide (DMF)-D<sub>7</sub> as solvents. The chemical shifts are given in ppm relative to the signal of the residual non-deuterated solvent.

Batch dynamic light scattering (DLS) was performed on a Zetasizer Nano ZS (Malvern Instruments, Herrenberg, Germany). All measurements were performed in folded capillary cells (DTS1071, Malvern Instruments, Herrenberg, Germany). After an equilibration time of 180 s, 3 × 30 s runs were carried out at 25 °C ( $\lambda = 633$  nm). The counts were detected at an angle of 173°. Each measurement was performed in triplicate. Apparent hydrodynamic radii, R<sub>h</sub>, were calculated according to the Stokes–Einstein equation.

Laser Doppler velocimetry was used to measure the electrokinetic potential, also known as zeta potential. The measurements were performed on a Zetasizer Nano ZS (Malvern Instruments, Herrenberg, Germany) in folded capillary cells (DTS1071). For each measurement, 15 runs were

carried out using the fast-field and slow-field reversal mode at 150 V. Each experiment was performed in triplicate at 25 °C. The zeta potential ( $\zeta$ ) was calculated from the electrophoretic mobility ( $\mu$ ) according to the Henry Equation.<sup>2</sup> The Henry coefficient,  $f(ka)$ , was calculated according to Ohshima.<sup>3</sup>

Cryo-TEM investigations were conducted with a FEI Tecnai G<sup>2</sup> 20 at 200 kV acceleration voltage. Specimens were vitrified by a Vitrobot Mark V system on Quantifoil grids (R2/2). The blotting time was 1 s with blotting force offset of 0. The amount of solution was 7  $\mu$ L. Samples were plunge frozen in liquid ethane and stored under liquid nitrogen until transferred to the Gatan cryo-holder and brought into the microscope. Images were acquired with a 4k  $\times$  4k CCD Eagle camera.

#### *Solid state (ss) NMR spectroscopy*

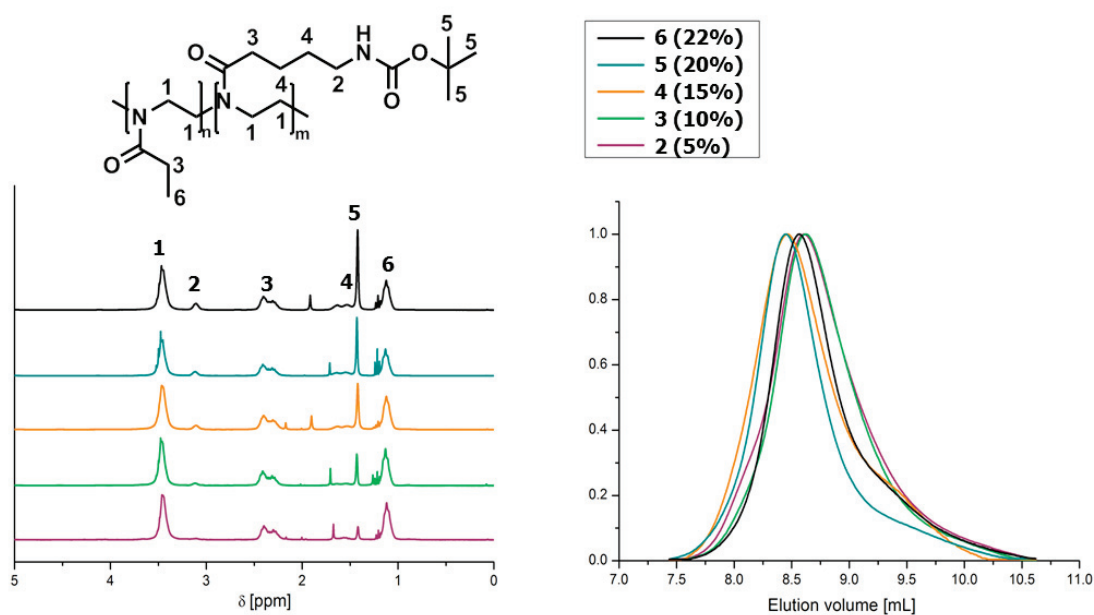
One-dimensional (1D) natural abundance <sup>13</sup>C cross polarization magic angle spinning ssNMR spectroscopy was carried out using a Bruker Avance II spectrometer operating at <sup>1</sup>H (<sup>13</sup>C) frequencies of 500 (125) MHz and using a 3.2 mm triple resonance probe. Sample temperature was 293 K at 20 kHz spinning frequency. Cross polarization (CP) contact time was 1.5 ms, and <sup>1</sup>H decoupling was performed using 90 kHz decoupling field strength. Final spectra were collected with 295006 scans and a 2 s recycle time, processed (exponential window function; line broadening 20 Hz) and evaluated with Bruker Topspin. Referencing was relative to Adamantan, setting the methine line to 29.46 ppm relative to neat trimethylsilane.<sup>4</sup>

#### *Asymmetric flow field-flow fractionation (AF4)*

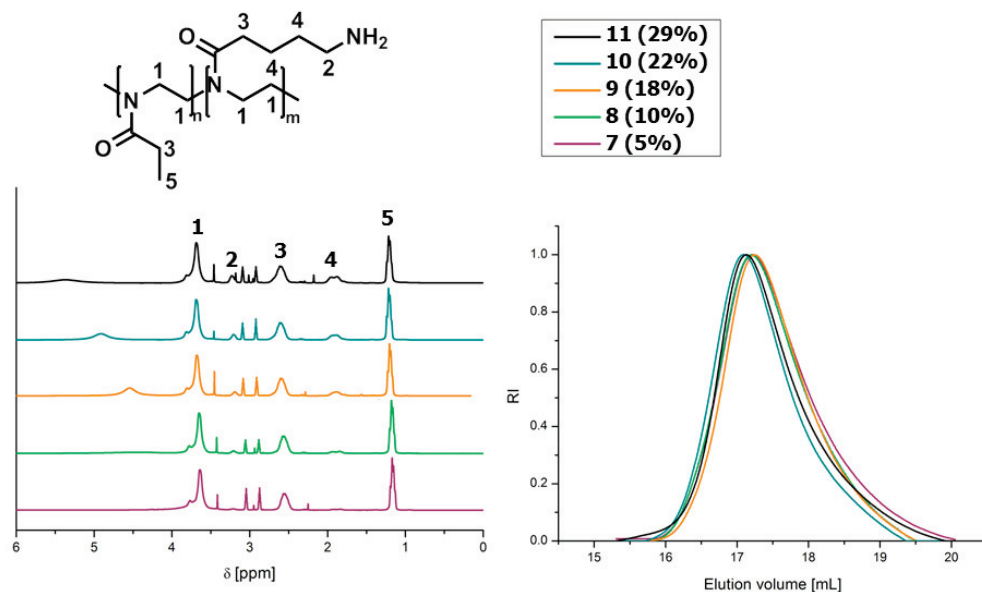
Asymmetric flow field-flow fractionation (AF4) was performed on an AF2000 MT System (Postnova Analytics, Landsberg, Germany) coupled to an UV (PN3211, 260 nm), RI (PN3150), MALLS (PN3070, 633 nm) and DLS (ZetaSizerNano ZS, 633 nm) detector. The eluent is delivered by two different pumps (tip and focus-flow) and the sample is injected by an auto-sampler (PN5300) into the channel. The channel has a trapezoidal geometry and an overall area of 31.6 cm<sup>2</sup>. The nominal height of the spacer was 500 μm and a regenerated cellulose membrane with a molar mass cut-off of 10,000 g mol<sup>-1</sup> was used as accumulation wall. All experiments were carried out at 25 °C. For molar mass determination of the polymers, the eluent was composed of 25 mM acetate buffer at a pH value of 3.5 and 20 mM NaCl. The detector flow rate was set to 0.5 mL min<sup>-1</sup> for all samples and 50 μL (5 mg mL<sup>-1</sup>) were injected with an injection flow rate of 0.2 mL min<sup>-1</sup> for 7 min. For all samples the cross-flow was set to 1.8 mL min<sup>-1</sup>. After the focusing period and a transition time of 1 min, the cross flow was kept constant for 3 min and then decreased under a power function gradient (0.4) to 0 within 15 min. Afterwards, the cross-flow was kept constant at zero for at least 20 min to ensure complete elution. For characterization of the colloidal structures, the eluent was 0.025% NovaChem Surfactant 100 detergents mix. The detector flow rate was set to 0.5 mL min<sup>-1</sup> for all samples and 20 μL (5 mg mL<sup>-1</sup>) were injected with an injection flow rate of 0.2 mL min<sup>-1</sup> for 7 min. For all samples the cross-flow was set to 1.0 mL min<sup>-1</sup>. After the focusing period and a transition time of 1 min, the cross flow was kept constant for 2 min and then decreased under a power function gradient (0.4) to 0 within 18 min. Afterwards, the cross-flow was kept constant at zero for at least 25 min to ensure complete elution. For calculation of the molar mass and the radius of gyration, a Zimm plot was used. All measurements were repeated three times. The refractive

index increment ( $dn/dc$ ) of all samples was measured by manual injection of a known concentration directly into the channel without any focusing or cross-flow. The  $dn/dc$  was calculated as the average of at least three injections from the area under the RI curve ( $AUC_{RI}$ ).

## II Analytcs of P(EtOx)-*b*-(BocOx) and P(EtOx)-*b*-(AmOx)



**Figure S1.**  $^1\text{H}$  NMR spectra (300 MHz,  $\text{CDCl}_3$ ) and size exclusion chromatograms (chloroform/ $\text{NEt}_3$ /*iso*-propanol) of the protected block copolymers (P(EtOx)-*b*-BocOx, **2-6**) with BocOx-contents between 5 and 22%.

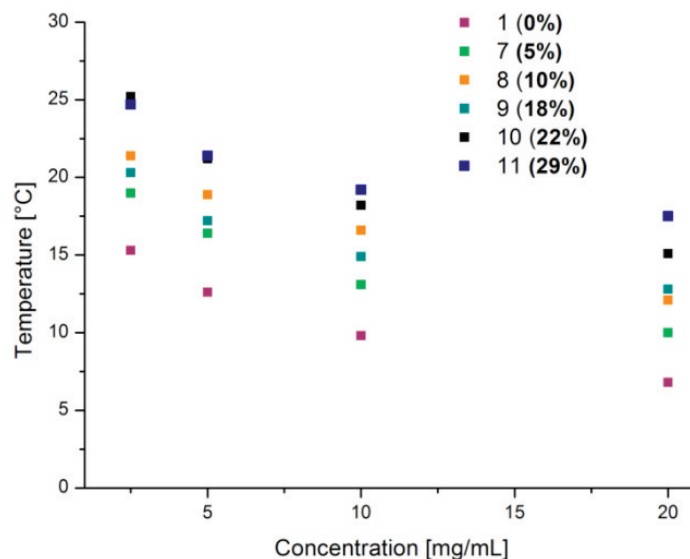


**Figure S2.**  $^1\text{H}$  NMR spectra (300 MHz,  $\text{DMF-D}_7$ ) and size exclusion chromatograms ( $N,N$ -dimethyl acetamide) of the deprotected block copolymers (P(EtOx-*b*-AmOx, **7-11**) with AmOx-contents between 5 and 29%.

**Table S1.** Asymmetric flow field flow fractionation (AF4) data of the deprotected block copolymers.

Sample	$\frac{dn}{dc}$ [ $\text{mL g}^{-1}$ ]	$M_n$ [ $\text{g mol}^{-1}$ ]	Error [ $\text{g mol}^{-1}$ ]	$M_w$ [ $\text{g mol}^{-1}$ ]	Error [ $\text{g mol}^{-1}$ ]	$M_z$ [ $\text{g mol}^{-1}$ ]	Error [ $\text{g mol}^{-1}$ ]	$\bar{D}$	Error	Rec [%]	Error [%]
<b>7</b>	0.153	11,700	670	12,900	530	14,000	560	1.10	0.024	73.7	0.1
<b>8</b>	0.160	9,200	360	10,500	840	11,300	860	1.14	0.065	74.9	0.9
<b>9</b>	0.153	13,300	340	14,600	270	15,900	260	1.10	0.008	77.6	0.3
<b>10</b>	0.156	13,600	430	14,900	450	16,600	820	1.09	0.003	77.1	0.5
<b>11</b>	0.139	12,500	500	15,700	180	18,100	380	1.26	0.039	75.9	0.9

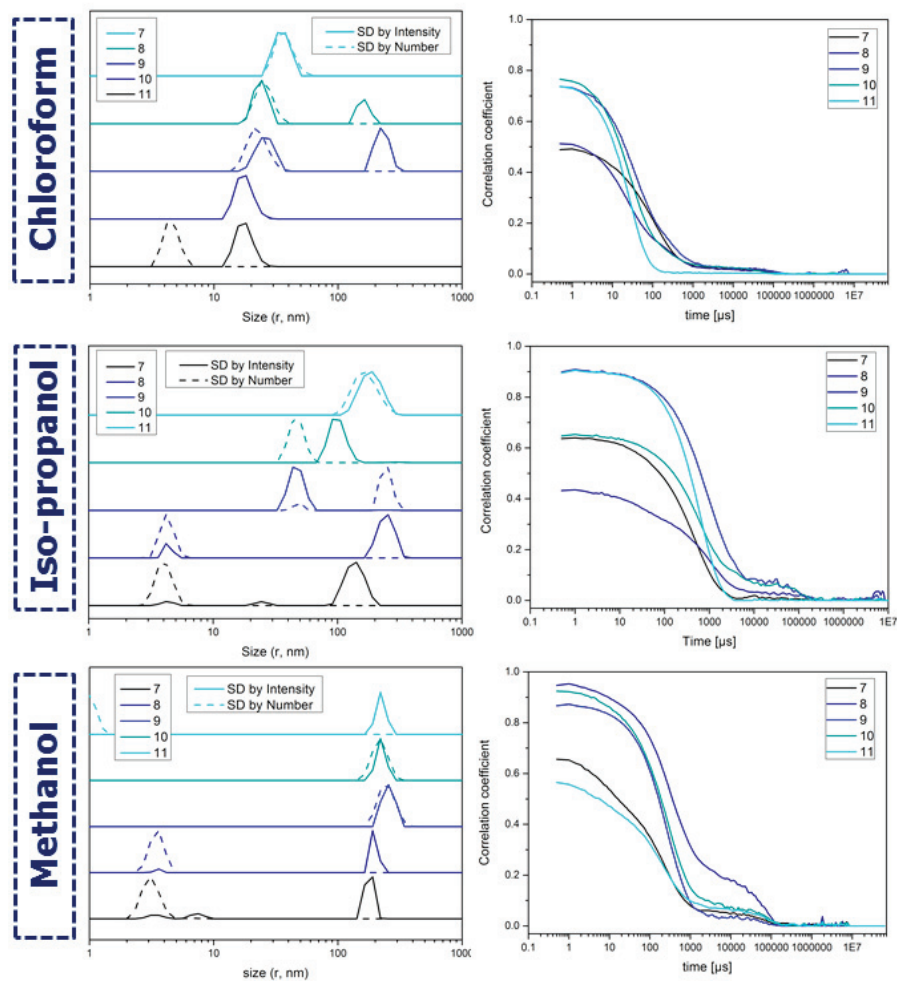




**Figure S3.** Cloud-points of P(EtOx-*b*-AmOx) in dependency of the concentration.

In a recent publication we described the formation of cationic hydrogels, originating from statistical copolymers P(EtOx-*stat*-AmOx) with comparable compositions, which were formed due to phase separation during the gelation leading to micron-sized hydrogel beads.<sup>5</sup> Such a behavior was observed under strong alkaline conditions (5 wt% aqueous NaOH) at elevated temperatures (50 °C). As a consequence, the prepared P(EtOx-*b*-AmOx) block copolymers were investigated regarding their LCST behavior at the conditions described earlier, revealing a similar phase transition (Figure S3). However, also a PEtOx homopolymer was included into the study and exhibited a lower  $T_{cp}$  than any of the copolymers. This prompted us to conclude that PEtOx is the segment which undergoes phase separation upon heating. This can be explained by a chaotropic influence of the high hydroxyl ion concentration in solution.<sup>6, 7</sup> Therefore, the phase separation at these conditions cannot be exploited to create micellar systems with the cationic building block in the core since PEtOx collapses at increasing temperatures.

### III Analytics of cross-linked and non-cross-linked self-assembled structures.



**Figure S4.** DLS size distributions and correlation functions of P(EtOx-*b*-AmOx) in organic solvents ( $1 \text{ mg mL}^{-1}$ ).

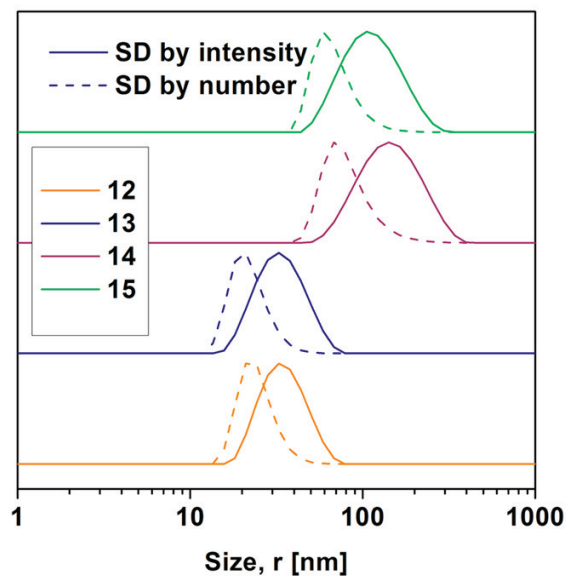


Figure S5. DLS size distributions of cross-linked nanostructures in water.

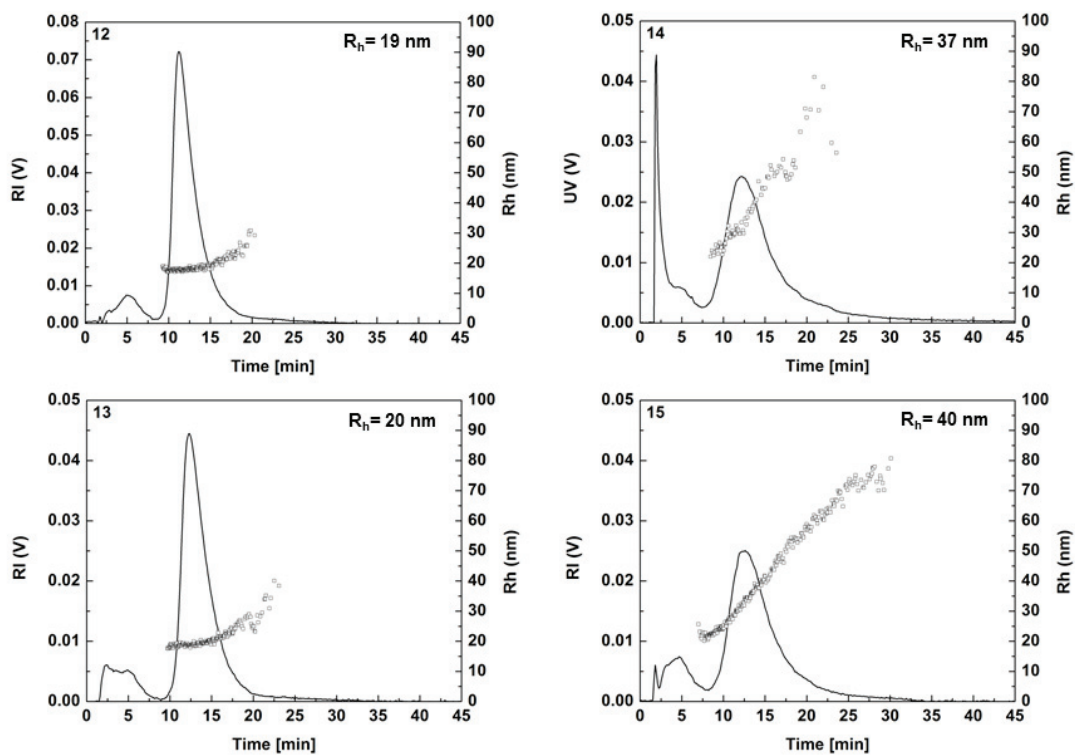
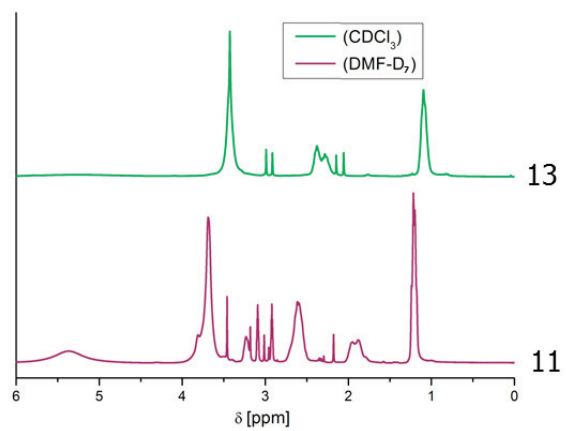
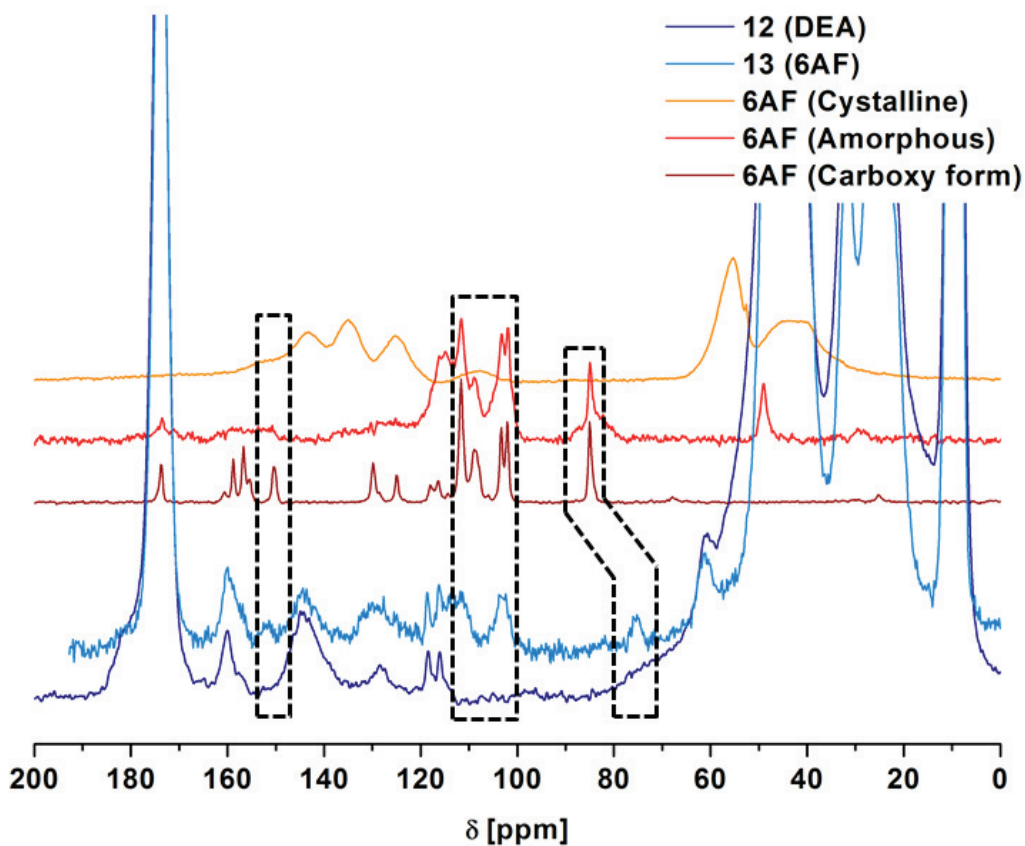


Figure S6. AF4 elugrams of cross-linked nanostructures (in 0.025% NovaChem Surfactant 100 detergents mix).



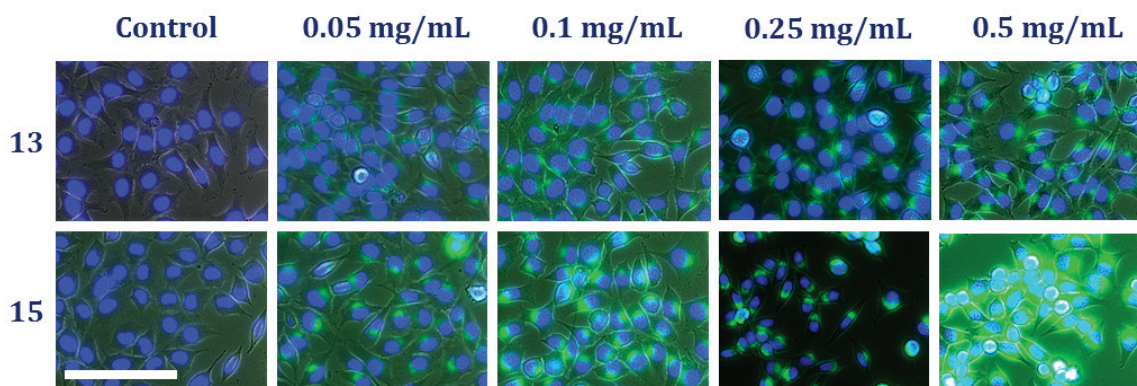
**Figure S7.** Comparison of the <sup>1</sup>H NMR spectra of polymer **11** in CDCl<sub>3</sub> (self-assembly) and DMF-D<sub>7</sub> (no assembly).



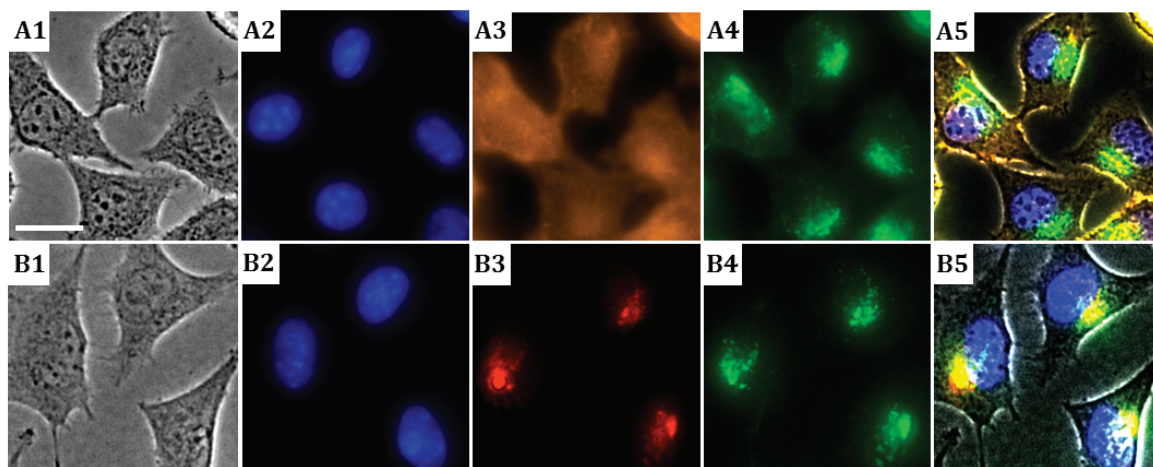
**Figure S8.** Solid state  $^{13}\text{C}$  NMR spectra of different 6AF forms and micelles with (**13**) and without (**12**) 6AF. Commercial, microcrystalline 6AF, amorphous 6AF and KOH-induced ring-opened 6AF were analyzed by natural abundance  $^{13}\text{C}$  CP MAS ssNMR. All MAS ssNMR spectra were acquired at 293 K, with 295006 scans, 2 s recycle time and a CP contact time of 1.5 ms. Microcrystalline 6AF was used as commercially supplied, amorphous 6AF was produced by dissolving commercial 6AF in MeOH, flash-freezing in liquid  $\text{N}_2$  and subsequent lyophilisation; ring-open 6AF was derived from microcrystalline material by dissolving it in 1 M KOH, subsequent flash-freezing and lyophilisation.



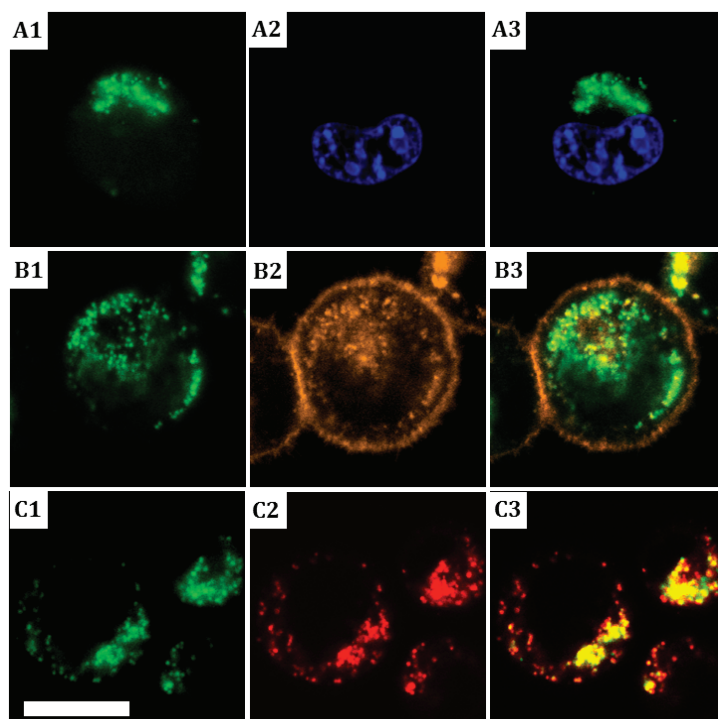
IV Cellular uptake and co-localization studies of nano-assemblies.



**Figure S9.** Fluorescence microscopy images on the concentration dependent uptake of dye containing micelles (**13**)/vesicles (**15**) by L929 mouse fibroblasts. Cells were incubated for 24 h using micelle/vesicle concentrations in the range between 0.05 and 0.5 mg mL<sup>-1</sup>. Cells incubated with culture medium only served as control. The cell nuclei were stained with blue fluorescent Hoechst 33342. Shown are fluorescence images resulting from superimposing the blue and green channels. Increasing green fluorescence emitted by the dye-containing micelles/vesicles indicates a concentration dependent internalization of both structures with an elevated uptake of vesicles vs. micelles. Scale bar 50  $\mu$ m.



**Figure S10.** Representative bright field (A1 and B1) and epifluorescence images of adherent L929 cells after 24 h incubation at 37 °C in the presence of micelles (**13**) at a concentration of 0.1 mg mL<sup>-1</sup>. Cell nuclei (A2 and B2), cell membranes (A3) or late endosomes/lysosomes (B3) were specifically stained and their fluorescence signal was captured in addition to the fluorescence signal originating from the internalized 6AF labeled vesicles (A4 and B4). Superimposition of all four channels (A5 and B5). Scale bar: 20 μm.



**Figure S11.** Representative CLSM images of detached L929 cells after 24 h incubation at 37 °C in the presence of micelles (**13**) at a concentration of 0.1 mg mL<sup>-1</sup>. Cell membranes (A2), cell nuclei (B2), or late endosomes/lysosomes (C2) were specifically stained and correlated with the fluorescence signal of 6AF labeled micelles (A1, B1, and C1). Superimposition of both channels (A3, B3 and C3) proves intracellular (A3) but extra-nuclear (B3) localization of the vesicles and their apparent co-localization with lysosomal structures (C3). Scale bar: 10 μm.

## References

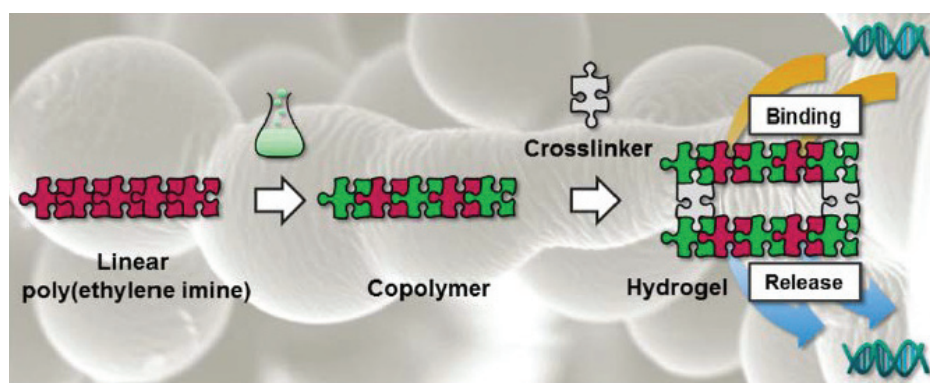
1. M. Hartlieb, D. Pretzel, K. Kempe, C. Fritzsche, R. M. Paulus, M. Gottschaldt and U. S. Schubert, *Soft Matter*, 2013, **9**, 4693-4704.
2. A. V. Delgado, F. Gonzalez-Caballero, R. J. Hunter, L. K. Koopal and J. Lyklema, *J. Colloid Interface Sci.*, 2007, **309**, 194-224.
3. H. Ohshima, *Journal of Colloid and Interface Science*, 1994, **168**, 269-271.
4. C. R. Morcombe and K. W. Zilm, *J. Magn. Reson.*, 2003, **162**, 479-486.
5. M. Hartlieb, D. Pretzel, C. Englert, M. Hentschel, K. Kempe, M. Gottschaldt and U. S. Schubert, *Biomacromolecules*, 2014, **15**, 1970-1978.
6. M. M. Bloksma, D. J. Bakker, C. Weber, R. Hoogenboom and U. S. Schubert, *Macromol. Rapid Commun.*, 2010, **31**, 724-728.
7. F. E. Bailey and R. W. Callard, *J. Appl. Polym. Sci.*, 1959, **1**, 56-62.

## Publication 5

### „Linear poly(ethylene imine)-based hydrogels for effective binding and release of DNA“

C. Englert, L. Tauhardt, M. Hartlieb, K. Kempe, M. Gottschaldt, U. S. Schubert

*Biomacromolecules* **2014**, *15*, 1124-1131.





# Linear Poly(ethylene imine)-Based Hydrogels for Effective Binding and Release of DNA

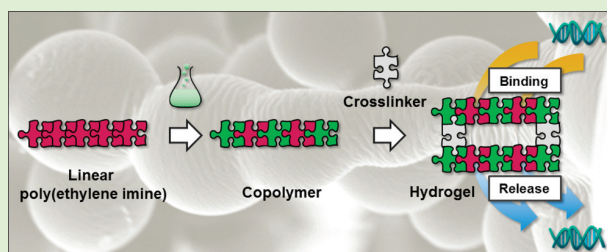
Christoph Englert,<sup>†,‡</sup> Lutz Tauhardt,<sup>†,‡</sup> Matthias Hartlieb,<sup>†,‡</sup> Kristian Kempe,<sup>†,‡,§</sup> Michael Gottschaldt,<sup>†,‡</sup> and Ulrich S. Schubert<sup>\*,†,‡</sup>

<sup>†</sup>Laboratory of Organic and Macromolecular Chemistry (IOMC), Friedrich Schiller University Jena, Humboldtstr. 10, 07743 Jena, Germany

<sup>‡</sup>Jena Center for Soft Matter (JCSM), Friedrich Schiller University Jena, Philosophenweg 7, 07743, Jena, Germany

## Supporting Information

**ABSTRACT:** A series of copolymers containing both amine groups of linear poly(ethylene imine) (LPEI) and double bonds of poly(2-(3-butenyl)-2-oxazoline) (PButEnOx) was prepared. To this end, a poly(2-ethyl-2-oxazoline) (PEtOx) precursor was hydrolyzed to the respective LPEI and functionalized in an amidation reaction with butenyl groups resulting in the double bond containing poly(2-(3-butenyl-2-oxazoline)-*co*-ethylene imine) (P(ButEnOx-*co*-EI)). Hydrogels were obtained by cross-linking with dithiols under UV-irradiation resulting in networks with different properties in dependence of the content of double bonds. The developed method allows the exact control of the amount of ethylene imine units within the copolymer and, thus, within the resulting hydrogels. The gel structures were characterized by solid state NMR and infrared spectroscopy. In addition the water uptake behavior from the liquid and the gas phase was investigated. It was shown by an ethidium bromide assay (EBA) that the copolymers and the respective hydrogels were able to bind and release DNA. Furthermore, the influence of the ethylene imine content on this interaction was investigated.



## INTRODUCTION

The fast and efficient detection of pathogens is of tremendous interest nowadays, ranging from applications in agriculture to medicine. Each species of pathogen carries a unique set of DNA and RNA sequences, which can be potentially detected by hybridization with another DNA strand containing complementary nucleic acid sequences. This approach is exploited by DNA biochips that consist of DNA sequences covalently bound/attached to solid substrates like glass,<sup>1,2</sup> silicon, gold,<sup>3</sup> or polymers such as poly(methyl methacrylate).<sup>4</sup> However, an essential prerequisite for a successful detection is the isolation and purification of nucleic acids from highly complex samples, such as blood and feces.<sup>5</sup> For this purpose, materials that can specifically and reversibly bind genetic materials are of significant interest. In this context, the interaction between DNA and cationic polymers has been investigated intensely. In particular, poly(ethylene imine) (PEI) has been widely studied, since its amine groups interact effectively with the DNA/RNA phosphate groups, forming a so-called polyplex.<sup>6–11</sup>

The major drawbacks of two-dimensional DNA chips are the limited loading capacity of surface materials and the restricted hybridization efficiency.<sup>12,13</sup> An alternative approach, overcoming these issues, is the reversible binding of genetic materials within a three-dimensional network. In this way a considerable increase of the loading capacity compared to a two-dimensional system can be achieved.<sup>14,15</sup> A special class of three-dimensional networks are the so-called hydrogels.

Although insoluble in any solvents, they can incorporate water up to a multitude of their own mass. This property allows the encapsulation and rapid diffusion of DNA molecules inside the network. The immobilization of DNA and other biomolecules within hydrogel-like structures has been recently the topic of intensive research.<sup>16–19</sup>

In this contribution we focus on the synthesis of three-dimensional networks based on linear poly(ethylene imine) (LPEI). The most common method for the formation of PEI-based hydrogels is the cross-linking of the amine groups using difunctional compounds like diglycidyl ethers or diisocyanates.<sup>20–26</sup> However, due to the insolubility of the network, it is not possible to determine the amount of amine groups that remain after the cross-linking process. For the binding and release of genetic material, it is essential to know the exact amount of amine groups. Hence, it is desirable to perform the cross-linking without decreasing the amine binding sites. To this end, a second functionality needs to be incorporated into the hydrogel precursor, which can be exploited for cross-linking. Possible candidates could be partially hydrolyzed double bond bearing poly(2-oxazoline)-based homo- and copolymers.<sup>27</sup> However, the double bonds of poly(2-(3-butenyl)-2-oxazoline) (PButEnOx)<sup>28–30</sup> and poly(2-(9-decen-

**Received:** October 7, 2013

**Revised:** January 20, 2014

**Published:** January 26, 2014

yl)-2-oxazoline) (PDecEnOx)<sup>31–33</sup> based polymers do not stand the harsh hydrolysis conditions required to cleave of the oxazoline side chains. To overcome this problem, the alkene functionalities have to be introduced subsequently to hydrolysis.

This report introduces a new route to obtain LPEI-hydrogels with an adjustable amount of amine groups. To this end, we have synthesized an eight-membered library of poly(2-(3-butenyl)-2-oxazoline-co-ethylene imine) (P(ButEnOx-co-EI) copolymers by reaction of LPEI with *N*-succinimidyl-4-pentenat. Subsequent cross-linking via thiol-ene photo-addition leads to the formation of LPEI-containing hydrogels with a predetermined amount of amine groups.

Both the copolymers and the hydrogels are characterized by means of NMR and IR spectroscopies. The synthesized systems are investigated regarding their structure and swelling ability. The DNA interaction of the copolymers and the hydrogels is studied using the ethidium bromide assay (EBA; DNA binding) and a heparin assay (DNA release).

## EXPERIMENTAL SECTION

**Materials.** PEtOx (50,000 g/mol), pyridine, 4-*N,N*-dimethylamino-pyridine (DMAP), ethanol, 3,6-dioxaoctane-1,8-dithiol, and 2,2-dimethoxy-2-phenylacetophenone (DMPA), and genomic DNA sodium salt from herring testes (gDNA) were obtained from Sigma Aldrich. Ethidium bromide solution (1%) was purchased from Carl Roth (Karlsruhe, Germany). *N*-Succinimidyl-4-pentenat was prepared according to literature procedures.<sup>28</sup>

**General Methods and Instrumentation.** The hydrolysis of PEtOx was performed under microwave irradiation in an Initiator Sixty single-mode microwave synthesizer from Biotage, equipped with a noninvasive IR sensor (accuracy 2%). <sup>1</sup>H NMR spectra were recorded at room temperature using a Bruker AC 300 MHz spectrometer or a Bruker AC 250 MHz spectrometer, respectively. <sup>13</sup>C NMR was recorded at 100 MHz. Chemical shifts are reported in parts per million (ppm,  $\delta$  scale) relative to the residual signal of the deuterated methanol. Solid state NMR measurements were performed on a Bruker Avance 400 spectrometer. The dry hydrogels were measured with 4 mm zircon-oxid rotors at 12.5 kHz. Swollen samples (12 h in D<sub>2</sub>O) were measured using Kel-F rotors from Bruker-Biospin at 6.5 kHz. Tetrakis-trimethylsilylsilan (<sup>1</sup>H) and adamantan (<sup>13</sup>C) were used as standards. <sup>1</sup>H NMR was measured for 6 s, for <sup>13</sup>C NMR 70000 scans were carried out. Size exclusion chromatographies (SEC) were performed on an Agilent Technologies 1200 Series gel permeation chromatography system equipped with a G1329A autosampler, a G131A isocratic pump, a G1362A refractive index detector, and both a PSS Gram 30 and a PSS Gram 1000 column placed in series. As eluent a 0.21% LiCl solution in *N,N*-dimethylacetamide (DMAc) was used at 1 mL min<sup>-1</sup> flow rate and a column oven temperature of 40 °C. Molar masses were calculated using poly(styrene) as standard. Fourier transform infrared (FT-IR) spectra were recorded on a FT-IR spectrometer IRAffinity-1 (Shimadzu) using the reflection method.

The water uptake measurements from the gas phase were performed using a TGA Q5000 SA thermogravimetric analyzer from TA Instruments Eschborn, Germany. For the data evaluation the "Universal Analysis" software was used. The water uptake of the hydrogels from the liquid state was measured gravimetrically. The used filter tubes were centrifuged with a Multifuge 1S-R from Thermo Scientific, and the swelling values ( $Q_{eq}$ ) were calculated according to literature.<sup>34</sup> The fluorescence measurements were recorded on the microplate reader Infinite M200 PRO. The samples were excited at 525 nm and the emission was measured at a wavelength of 605 nm in a temperature range between 25 and 30 °C. Well plates were obtained from Sigma-Aldrich (NunclonTM Surface, 96 well, F-bottom) and centrifuge filter tubes from Costar (Spin-X, cellulose acetate membrane, 0.45  $\mu$ m).

Microscopic detection of the DNA binding of hydrogels was performed using a fluorescence microscope (Cell Observer Z1, Carl Zeiss, Jena, Germany) equipped with a mercury arc UV lamp and the appropriate filter combinations for excitation and detection of emission. The fluorescence signal was captured directly in the wells. Images of a series (11  $\times$  11 pictures per well) were captured with a 10 $\times$  objective using identical instrument settings (e.g., UV lamp power, integration time, and camera gain) and spots of the 12-well plate were addressed using an automated XY table.

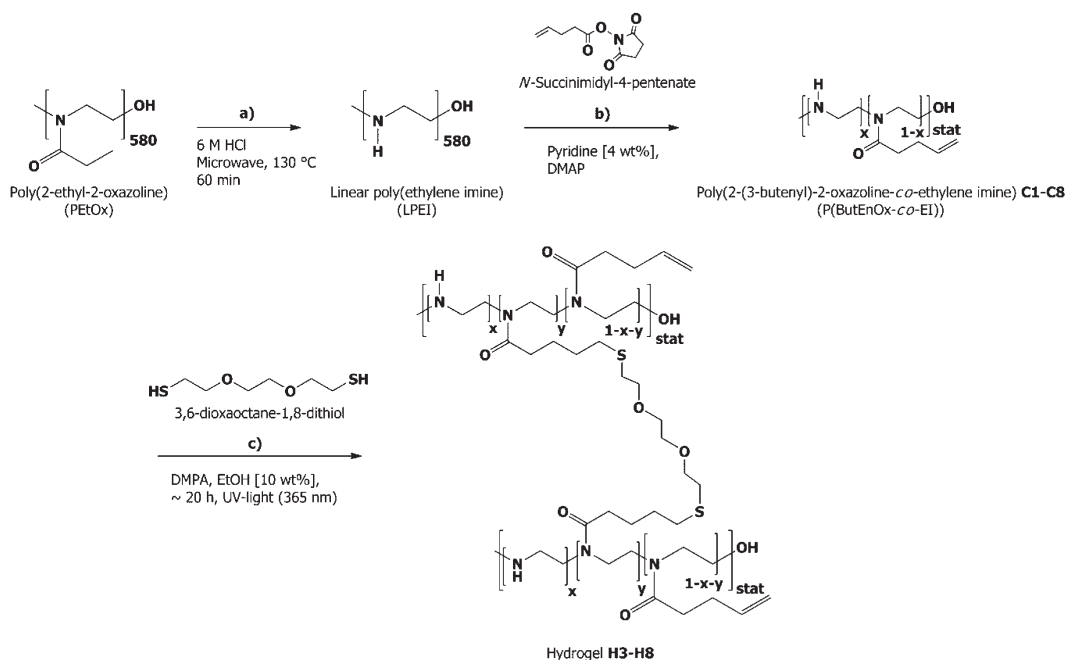
**Linear Poly(ethylene imine).** Poly(2-ethyl-2-oxazoline) (50,000 g/mol, PDI = 2.0; 5.0 g) was treated with an excess of 6 M aqueous hydrochloric acid (30 mL) for 1 h at 130 °C in a microwave synthesizer.<sup>35</sup> The excess of HCl and the resulting propionic acid were removed under reduced pressure and the obtained LPEI hydrochloride was dissolved in water. After addition of 3 M NaOH up to a pH value of 9, precipitation occurred. The LPEI was filtered off, recrystallized from water, dissolved in methanol, and precipitated into 650 mL of ice-cold diethyl ether. The white solid was dried at 85 °C under high vacuum and the degree of hydrolysis was determined by <sup>1</sup>H NMR by correlating the integrals of the PEI backbone and the remaining methyl group of the PEtOx side chain (yield: 3.0 g). <sup>1</sup>H NMR (250 MHz, MeOD):  $\delta$  2.95–2.52 (N-CH<sub>2</sub>), 1.45–0.81 (CH<sub>3</sub> EtOx) ppm. FT-IR (ATR): 3175 (OH, NH), 2866 (CH asym/sym str), 1485 (C–H def), 1281, 1134 (C–N str), 1045 (C–N) cm<sup>-1</sup>.

***N*-Succinimidyl-4-pentenat.** The synthesis of *N*-succinimidyl-4-pentenat was performed with minor changes according to a procedure described earlier by Gress et al.<sup>28</sup> 4-Pentenoic acid (30.738 g, 307 mmol) and *N*-hydroxysuccinimide (56.401 g, 490 mmol) were dissolved in 800 mL of dichloromethane. To the solution, *N,N'*-dicyclohexylcarbodiimide (74.334 g, 360 mmol) was added. After stirring for 23 h at room temperature, the white precipitate was filtered off and the filtrate was evaporated to dryness under reduced pressure. The residue was dissolved in 450 mL of diethyl ether and 150 mL of water. After separation, the organic phase was washed five times with water. The organic layer was dried over sodium sulfate and the solvent was removed. The high viscous product was dried in high vacuum ( $5 \times 10^{-2}$  mbar) at room temperature for three days and crystallized in the freezer at –18 °C for two days. The activated acid, *N*-succinimidyl-4-pentenat, was obtained as a white solid (yield: 54.9 g, 91%). <sup>1</sup>H NMR (250 MHz, CDCl<sub>3</sub>):  $\delta$  5.82 (HC=CH<sub>2</sub>), 5.03 (HC=CH<sub>2</sub>), 2.82 (CH<sub>2</sub> NHS), 2.70 (CH<sub>2</sub>-CH<sub>2</sub>-CO), 2.48 (CH<sub>2</sub>-CH<sub>2</sub>-CO) ppm. FT-IR (ATR): 2932 (CH asym/sym str), 1802 (CH=CH), 1728 (C=O), 1643, 1528 (C–H def), 1369, 1204 (C–N str), 1065 (C–N str) cm<sup>-1</sup>.

**Poly(2-(3-butenyl)-2-oxazoline-co-ethylene imine).** The synthesis is exemplified by the copolymer with a 50% PEI content. LPEI (0.475 g) and the catalyst 4-*N,N*-dimethylamino-pyridine (DMAP, 0.117 g, 1.0 mmol) were dissolved in a microwave vial in pyridine at 80 °C. In a second vial, a defined quantity of *N*-succinimidyl-4-pentenat (1 equiv per EI unit, 1.015 g, 5.2 mmol for 50% PEI) was dissolved in the same solvent. The two solutions were combined to a 4 wt % mixture of LPEI and stirred for 20 h at 80 °C. Afterward, the mixture was added dropwise into 500 mL of cold diethyl ether. The precipitated copolymer was filtered off and washed with 40 mL of diethyl ether. The residue was dried under reduced pressure to constant weight. The side product *N*-hydroxysuccinimide (NHS) was removed by dialysis in a regenerated cellulose membrane (Spectra/Por, Rancho Dominguez, CA, molar mass cutoff 3500 g/mol) against water. <sup>1</sup>H NMR (250 MHz, MeOD):  $\delta$  6.00–5.74 (HC=CH<sub>2</sub>), 5.18–4.93 (HC=CH<sub>2</sub>), 3.79–3.36 (NR-CH<sub>2</sub>-CH<sub>2</sub>), 3.12–2.61 (NH-CH<sub>2</sub>-CH<sub>2</sub>), 2.63–2.59 (NHS), 2.60–2.17 (CH<sub>2</sub> ButEnOx), 1.41–0.80 (CH<sub>3</sub> EtOx) ppm, PEI = 50%. SEC (DMAc, LiCl):  $M_n$  = 10700 g mol<sup>-1</sup>, PDI = 1.44. FT-IR (ATR): 3280 (OH, NH), 2870 (CH asym/sym str), 1640 (C=O), 1420 (C–H def), 1240 (C–N str), 1080 (C–N str) cm<sup>-1</sup>.

**Poly(2-(3-butenyl)-2-oxazoline-co-ethylene imine)-Based Hydrogel.** The synthesis is exemplified by the gel starting from the 50% PEI containing copolymer described above. In a microwave vial, poly(2-(3-butenyl)-2-oxazoline-co-ethylene imine) with 50% PEI content (0.103 g) was dissolved in ethanol. In a second vial, the

**Scheme 1. Schematic Representation of the Synthesis of (a) Linear Poly(ethylene imine) by Acidic Hydrolysis of Poly(2-ethyl-2-oxazoline); (b) Copolymer Poly(2-(3-butenyl)-2-oxazoline-*co*-ethylene imine) Starting from Linear Poly(ethylene imine); and (c) Hydrogel by Cross-Linking the Copolymer via Thiol–Ene Photoaddition**



photoinitiator 2,2-dimethoxy-2-phenylacetophenone (0.013 g, 0.05 mmol) and the *bis*-functional thiol, 3,6-dioxaoctane-1,8-dithiol (45  $\mu\text{L}$ , 0.28 mmol), were dissolved in ethanol (0.9:1.0 thiol/double bond). The combined solutions (10 wt %) were degassed with nitrogen for 30 min. Afterward, the clear solution was exposed to UV light (365 nm) for 24 h. The occurring gelation announced the successful synthesis of a three-dimensional network. Subsequently, the obtained gel was washed several times with ethanol (150 mL) and water (150 mL) for 20 min, respectively, and dried by lyophilization.<sup>27,32</sup>

**Swelling Value.**  $Q_{\text{eq}}$  74%. Solid state  $^{13}\text{C}$  NMR (100 MHz):  $\delta$  173.5, 138.6, 116.4, 71.1, 47.7, 39.4, 32.3 ppm. Solid state  $^1\text{H}$  NMR (400 MHz, swollen state):  $\delta$  5.94 ( $\text{HC}=\text{CH}_2$ ), 5.12 ( $\text{HC}=\text{CH}_2$ ), 4.37–3.25 ( $\text{N}-\text{CH}_2$ ,  $\text{CH}_2$  EDDET), 3.30–2.07 ( $\text{CH}_2$  ButEnOx,  $\text{CH}_2$ -S- $\text{CH}_2$ ), 2.02–1.22 ( $\text{RS}-\text{CH}_2-\text{CH}_2-\text{CH}_2$ ) ppm. FT-IR (ATR): 3294 (OH, NH), 2886 (CH asym/sym str), 1636 (C=O), 1421 (C-H def), 1367, 1292, 1234, 1103 (C–N str), 1038 (C–N str)  $\text{cm}^{-1}$ .

**Ethidium Bromide Assay (EBA) of P(ButEnOx-*co*-EI) and Release Studies.** The interaction between genomic DNA (gDNA) and cationic copolymers was detected by fluorescence measurements. The EBA was carried out by a procedure adapted from literature.<sup>19</sup> gDNA (7.5  $\text{mg mL}^{-1}$ ) and EB (0.4  $\text{mg mL}^{-1}$ ) were dissolved in HBG-buffer (HEPES buffered glucose, pH 7) and incubated for 10 min at room temperature. A total of 100  $\mu\text{L}$  of the gDNA-EB solution were transferred to the wells of a black 96-well plate containing copolymers at defined concentrations (N/P ratios) with different PEI contents. Fluorescence was measured after 15 min of incubation in a repeat determination. A mixture containing only gDNA, EB, and HBG buffer served as calibration standard.

For release studies, 100  $\mu\text{L}$  of the gDNA-EB solution were transferred to a well-plate as described above and the copolymers (3.6  $\mu\text{L}$  of a 1  $\text{mg mL}^{-1}$  stock solution, respectively) were added. After incubation, the fluorescence was measured and defined as start value. Subsequently, 10  $\mu\text{L}$  of a heparin stock solution (3  $\text{mg mL}^{-1}$ ) was added to each of the samples and the fluorescence was measured at defined times.

**EBA of P(ButEnOx-*co*-EI)-Based Hydrogels and Release Studies.** The hydrogels (1.7 to 2.0 mg) were swollen for 19 h in 250 mL of HBG buffer (pH 7). Subsequently, 1 mL of gDNA-EB solution (containing 7.5 mg gDNA per mL and 0.4 mg EB per mL)

was added. The sample aliquot of 50  $\mu\text{L}$  was taken at defined times and returned after fluorescence measurement. Microscopic detection of the resulting fluorescence signal was performed at different time points (0, 1.5, and 18 h).

The release studies were performed by adding 1 mL of a mixture of heparin (6  $\text{mg mL}^{-1}$ ) and EB (0.4  $\text{mg mL}^{-1}$ ), dissolved in HBG buffer, to the swollen and loaded hydrogel samples. In addition, the temperature was increased up to 90 °C. Aliquots of 50  $\mu\text{L}$  were taken at defined times and returned after fluorescence measurement.

## RESULTS AND DISCUSSION

**Synthesis and Characterization of a Copolymer Library of P(ButEnOx-*co*-EI)s.** Starting from commercially available poly(2-ethyl-2-oxazoline) (PEtOx, 50,000 g/mol), LPEI was prepared by acidic hydrolysis (degree of hydrolysis > 99%) using a microwave synthesizer (Scheme 1a).<sup>35</sup> Subsequently, LPEI was reacted in an amidation reaction with *N*-succinimidyl-4-pentenate to introduce alkenyl functionalities into the polymer (Scheme 1b). To this end, LPEI and the catalyst 4-(dimethylamino)-pyridine (DMAP) were dissolved in pyridine at 80 °C and mixed with the activated acid. Due to the negligible effect of the side product *N*-hydroxysuccinimide on the formation of hydrogels, the step of dialysis (performed for 71% PEI containing copolymer) was skipped for further reactions.

Using this method, an eight-membered library of P(ButEnOx-*co*-EI)s (C1–C8) with varying amounts of secondary amine groups was synthesized (Table 1).

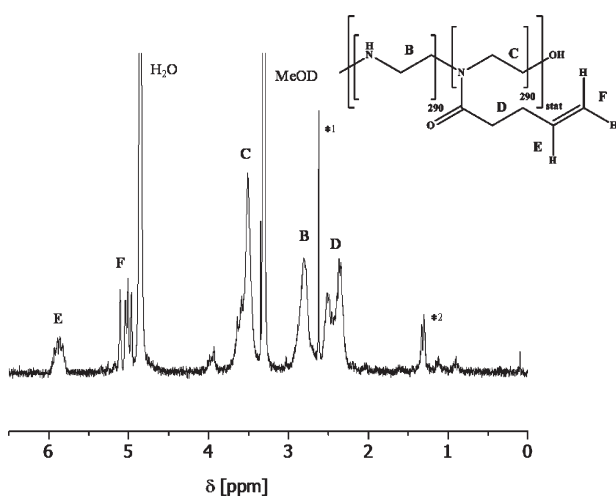
$^1\text{H}$  NMR spectroscopy showed the successful conversion of LPEI to the copolymers. The percentage of remaining LPEI units in the copolymer was determined by correlating the integrals of the single proton signal of the double bond ( $\delta = 5.9$  ppm,  $\text{HC}=\text{CH}_2$ , E) to the ones of the LPEI backbone ( $\delta = 3.0$  to 2.6 ppm,  $\text{HN}-\text{CH}_2-\text{CH}_2$ , B; Figure 1). Moreover, the appearance of the signals of the 4-pentenate protons ( $\delta = 2.6$  to



**Table 1. Summary of the Characterization Data for the P(ButEnOx-co-EI)s (C1–C8): PEI Content and SEC Data**

	C1	C2	C3	C4	C5	C6	C7	C8
PEI [%] <sup>a</sup>	85	82	71	62	50	44	36	5
$M_n'$ (NMR) [g·mol <sup>-1</sup> ] <sup>b</sup>	32,100	33,500	38,700	43,000	48,700	51,600	55,400	70,100
PDI <sup>b</sup>	–*	–*	1.35	1.37	1.44	1.38	1.64	1.48
$M_n$ (SEC) [g·mol <sup>-1</sup> ] <sup>c</sup>	–*	–*	9,400	9,900	10,700	13,700	14,800	14,400

<sup>a</sup>Percentage of remaining LPEI units determined by <sup>1</sup>H NMR spectroscopy. <sup>b</sup>Determined by <sup>1</sup>H NMR (calculated from LPEI: 25,000 g/mol, PEI content). <sup>c</sup>Determined by SEC (eluent: DMAc + 0.21% LiCl, calibration against polystyrene). \*Not soluble in SEC eluent DMAc.



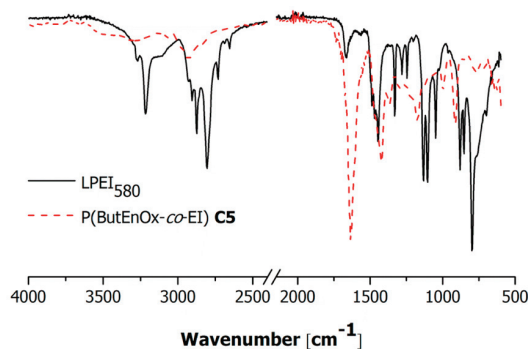
**Figure 1.** <sup>1</sup>H NMR spectrum (MeOD, 250 MHz) of C5 (50% PEI) produced from linear poly(ethylene imine) (580 units); \*<sup>1</sup> side-product *N*-hydroxysuccinimide, \*<sup>2</sup> remaining 2-ethyl-2-oxazoline side chains (~1%).

2.2 ppm, CH<sub>2</sub> ButEnOx, D), the protons of the double bond ( $\delta = 5.0$  ppm, HC=CH<sub>2</sub>, F) and the oxazoline backbone ( $\delta = 3.8$  to 3.4 ppm, RN-CH<sub>2</sub>-CH<sub>2</sub>, C) prove the proposed structure of the synthesized polymers. The successful conversion was also shown by infrared spectroscopy (IR). After the reaction, a carbonyl vibration of the oxazoline units appears at 1,636 cm<sup>-1</sup> ( $\nu_{C=O}$ ; Figure 2).

Mass spectrometry (MS) of the copolymers is not possible due to the high molar masses (>32,000 g/mol), which are difficult to transfer to the gas phase. However, using MALDI-TOF-MS, we could obtain a complex isotopic pattern of a low molar mass copolymer (45% PEI content,  $M_n \sim 1,650$  g/mol, <sup>1</sup>H NMR:  $M_n' = 1,800$  g/mol). The results are shown in the Supporting Information (Figure S1). Clearly the repeating units of the copolymer can be seen, but due to the complexity of the spectrum, a further assignment is nearly impossible.

Up to a content of 82% PEI, the copolymers are soluble in water. It is known that above a PEI content of 85% the copolymers only dissolve at elevated temperatures.<sup>36</sup> However, all the copolymers showed good solubility in organic solvents such as alcohols (e.g. methanol).

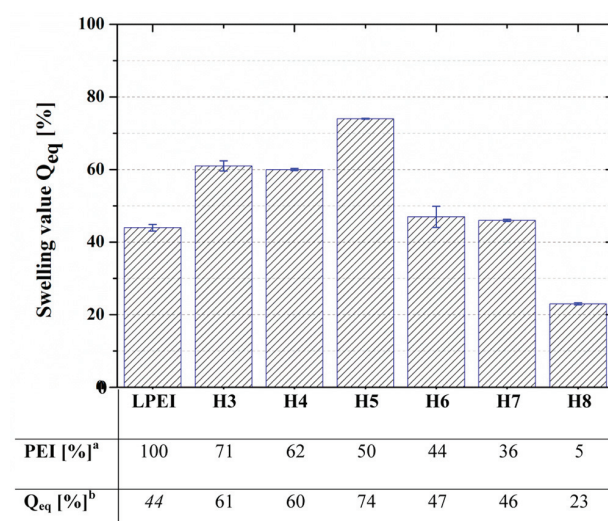
Characterization by size exclusion chromatography (SEC) revealed the formation of polymers with polydispersity indices



**Figure 2.** IR spectra of the starting linear poly(ethylene imine) homopolymer and the synthesized copolymer C5 (50% PEI; determined by <sup>1</sup>H NMR spectroscopy of the precursor copolymers).

(PDI values) between 1.35 and 1.64 (Table 1). The molar masses obtained by SEC differ from the molar masses calculated from <sup>1</sup>H NMR ( $M_n'$ ), which are based on the molar mass data of the poly(2-ethyl-2-oxazoline) precursor provided by the supplier. Possible cross-linking or other side reactions are not taken into account. The low molar mass values measured by SEC can be explained considering the different physicochemical properties, that is, the different hydrodynamic volumes of the copolymers and the used PS calibration standard.

**Hydrogel Synthesis and Characterization.** LPEI-based hydrogels were formed by the reaction of the precursor copolymers P(ButEnOx-co-EI)s (C3–C8) with 3,6-dioxaoctane-1,8-dithiol (EDDET; Scheme 1c) in a thiol-ene photo-addition reaction. It was performed under UV light using 2,2-dimethoxy-2-phenylacetophenone (DMPA) as initiator. In this way, a library of six hydrogels (H3–H8) was synthesized (Figure 3). Due to an insufficient amount of double bonds for cross-linking, copolymers with a PEI content above 82% (C1, C2) did not form hydrogels at a polymer concentration of 10 wt %, which was adapted from literature.<sup>27</sup> Gelation occurred



**Figure 3.** Swelling values  $Q_{eq}$  depending on the amount of poly(ethylene imine) units in formed hydrogels H3–H8 ( $T = 25.5$  °C). Linear poly(ethylene imine) was added as reference (repeated determination).

after an irradiation time between 150 min for **H3** and 5 min for **H8**. Moreover, an effect of concentration of the prepolymer could be observed. Further information can be found in the Supporting Information (Table S1).

When the reaction was performed under the same conditions but without the dithiol, neither cross-linking nor gelation was observed.

The swelling behavior of the synthesized hydrogels was investigated gravimetrically using centrifuge filter tubes.<sup>19</sup> The filter tubes were saturated with water and the excess water was removed by centrifugation (3,000 rpm, 10 min). The determined mass of the tube was set to  $m_0$ . After addition of the hydrogel ( $m_{0, \text{gel}}$ ), the sample weight could be determined by eq 1.

$$m_{\text{gel}} = m_{0, \text{gel}} - m_0 \quad (1)$$

Subsequently, the hydrogel sample was swollen in water for 24 h. The filter tube was centrifuged again (3,000 rpm, 10 min) and weighted ( $m_{\text{wet}}$ ) to determine the mass of the swollen gel ( $m_{\text{sw}}$ ) using eq 2.

$$m_{\text{sw}} = m_{\text{wet}} - m_0 \quad (2)$$

The swelling value  $Q_{\text{eq}}$  was calculated according to literature (eq 3).<sup>34</sup>

$$Q_{\text{eq}} = \frac{m_{\text{sw}} - m_{\text{gel}}}{m_{\text{sw}}} \times 100\% \quad (3)$$

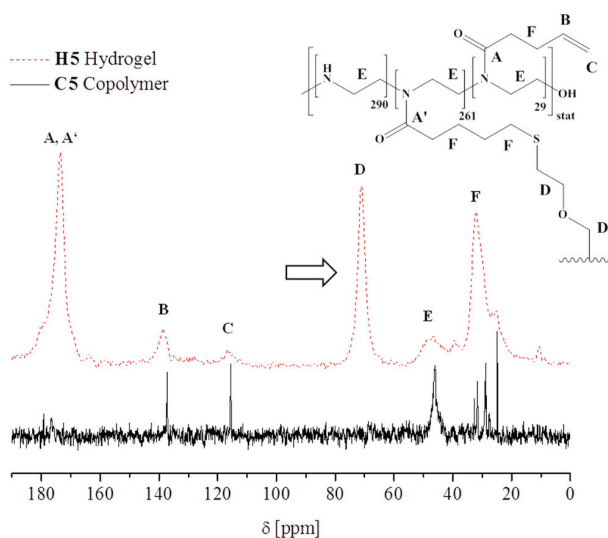
The formed hydrogels revealed a water uptake up to a multitude of their own mass ( $Q_{\text{eq}} = 23\text{--}74\%$ ) from the liquid phase. The ability of the formed networks to absorb water is ascribed to the hydrophilic parts of the cross-linker and the oxazoline units. But also the LPEI segments have hygroscopic properties and can exhibit different hydrated states.<sup>37–39</sup> As a reference, pure LPEI (which is insoluble in cold water) was investigated regarding its swelling value ( $Q_{\text{eq}} = 44\%$ ).

A maximum of the swelling values of the investigated hydrogels was reached for a PEI content of 50% (**H5**, Figure 3) with 74%. This behavior can be explained with two competing trends. Starting from pure LPEI as reference, a decreasing PEI content, accompanied with an increasing amount of water-soluble gel components, leads to higher swelling values. The decreasing swelling values at LPEI contents lower than 50% can be ascribed to a higher network density, caused by a higher degree of cross-linking for these polymers. The increased linking density and the associated decrease of the degrees of freedom of the polymer chains limit the amount of water, which can be incorporated within the polymer network. This causes the low swelling of the 5% PEI containing gel. Compared to PEtOx-containing hydrogels with similar degrees of cross-linking ( $Q_{\text{eq}} = 97\text{--}98\%$ <sup>19</sup>), the swelling values are significantly decreased, which is caused by the lower hydrophilicity of the LPEI systems.

The water uptake behavior from the gas phase was analyzed for **H5** (50% PEI content) at varying humidity levels using a thermogravimetric analysis (TGA) setup, which was already described for the investigation of hydrophilic polymers.<sup>40</sup> The TGA diagram showed the adsorption of water molecules to the hydrogel network as a function of the weight change (%) and the relative humidity (%) at a constant temperature (25 °C). Before starting the measurement, the sample was heated to 60 °C at 0% humidity to completely dry the sample. After the weight of the gel was constant, its mass was set as  $m_{\text{gel}}$  (compare to eq 1). Subsequently, the relative humidity was

gradually increased to 90%, whereupon a weight change of up to 30% ( $m_{\text{sw}}$ , eq 2) could be observed (equates to  $Q_{\text{eq}} = 23\%$ ), with an exponential increase. This value is identical to the swelling behavior of the 5% PEI containing hydrogel determined from the liquid phase. By decreasing the relative humidity in the same way, the desorption curve showed an identical trend, stating a reversibility of the swelling process. In comparison to the swelling studies from the liquid phase (for PEI content >5%), water uptake from the gas phase is much less efficient (about 10×), as depicted in Figure 3.

To confirm the structure of hydrogel **H5** (50% PEI content), solid state NMR measurements were performed. In Figure 4, a



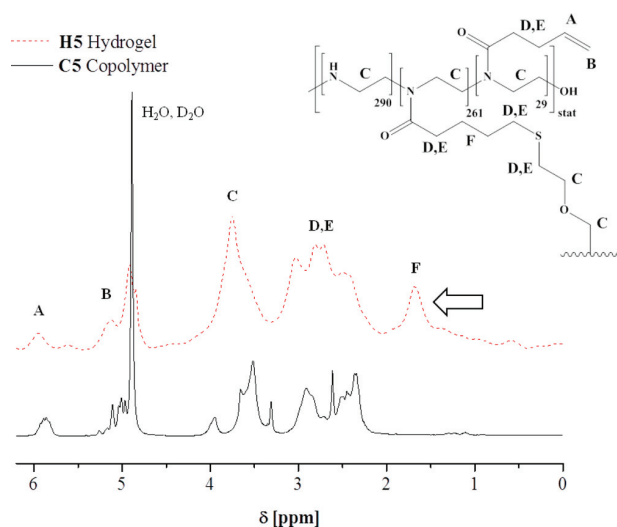
**Figure 4.** Solid state  $^{13}\text{C}$  NMR spectrum of the 50% PEI containing copolymer **C5** ( $\text{D}_2\text{O}$ , 63 MHz) and the resulting hydrogel **H5** (100 MHz).

comparison of the  $^{13}\text{C}$  NMR spectrum of the copolymer **C5** and the solid state  $^{13}\text{C}$  NMR spectrum of the resulting purified hydrogel **H5** is depicted. An important evidence for a successful synthesis is the appearance of the signal of the cross-linker (**D**) at 71.0 ppm. In addition, a solid state  $^1\text{H}$  NMR spectrum was recorded (Figure 5). To improve the resolution, a special method for the sample preparation was used. The gel was swollen for 16 h inside a Kel-F rotor in  $\text{D}_2\text{O}$  to increase the degrees of freedom of the polymer chains, which was placed into the spinning tube. Signals between 2.0 and 1.2 ppm ( $\text{RS-CH}_2\text{-CH}_2\text{-CH}_2$ ) belonging to the EDDET cross-linker further demonstrated the success of the reaction. Both  $^{13}\text{C}$  and  $^1\text{H}$  NMR spectra revealed an incomplete conversion of the double bonds that, hence, can be used for further functionalization.

**DNA Binding Studies.** After the successful synthesis of copolymers and hydrogels with well-defined LPEI contents, their ability to bind and release DNA was investigated using an ethidium bromide assay (EBA). Genomic herring DNA was treated with ethidium bromide (EB) resulting in a fluorescent DNA-EB complex, which could be detected using a fluorescence microscope. The assay allowed to monitor the interaction between DNA and polymer/hydrogel by a displacement of EB resulting in a decrease of the fluorescence intensity.<sup>41</sup>

The results of the EBA for the chosen copolymers P(ButEnOx-co-EI)s (**C3–C5**, **C7**) are depicted in Figure 6a.





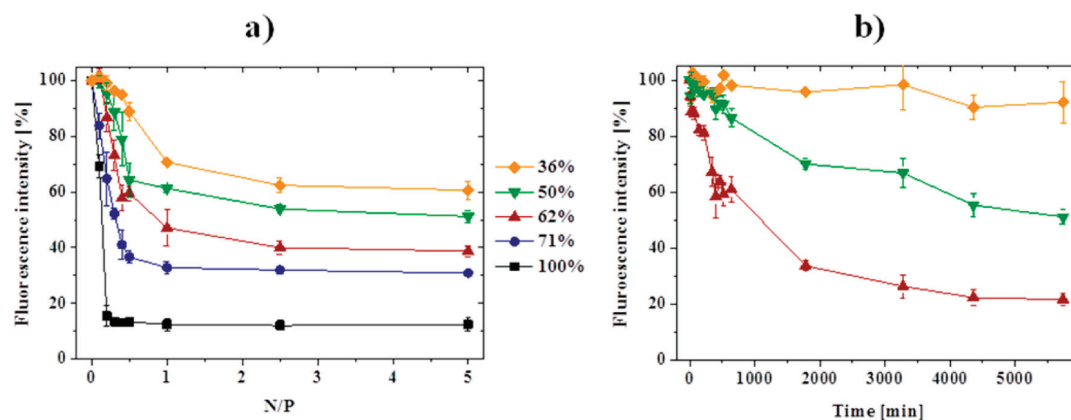
**Figure 5.** Comparison of the  $^1\text{H}$  NMR spectrum of the 50% PEI containing copolymer **C5** (MeOD, 250 MHz) and the solid state  $^1\text{H}$  NMR of the resulting hydrogel **H5** (swollen in  $\text{D}_2\text{O}$ , 400 MHz).

As expected, the system with a high content of LPEI showed an increased binding capacity and, hence, a decreased fluorescence intensity. At a nitrogen<sub>polymer</sub> to phosphate<sub>DNA</sub> (N/P) ratio higher than 2, a constant fluorescence level was reached, meaning that further excess of positively charged copolymers was not able to replace more EB. The copolymer with the highest charge density (71% PEI content) showed the highest complexation efficiency of all investigated copolymers, with a decrease in fluorescence intensity of 70%. As reference the LPEI precursor was used, which led to a fluorescence intensity decrease of about 90%.

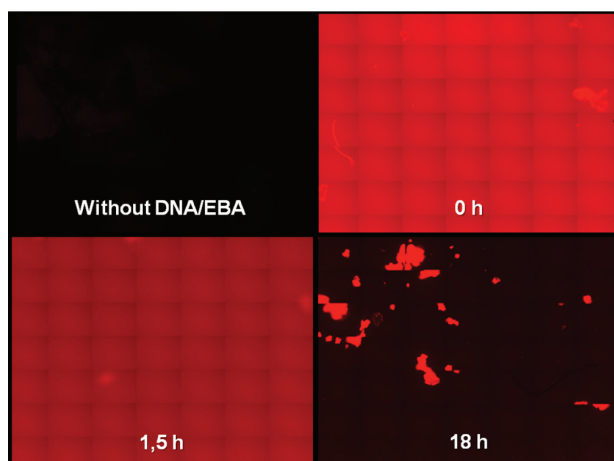
Three hydrogels with different PEI contents, namely, **H4** (62%), **H5** (50%), and **H7** (36%), were chosen to study their DNA binding and release capability. Due to the high molar masses and the large network structures, low N/P ratios, as used for the copolymers, were not suitable. Hence, the EBA procedure had to be adjusted and N/P ratios between 250 and 500 were investigated (Figure 6b). To obtain comparable results for hydrogels, similar masses were used (1.7–2.0 mg). Prior to the EBA measurements, the hydrogel samples were

swollen for 19 h in a 96-well plate in 250  $\mu\text{L}$  of HBG buffer solution, respectively. The large excess of buffer allowed a complete swelling of the hydrogels independent of the PEI content and swelling value. Moreover, the concentration after the addition of 1 mL stock solution to each swollen sample was nearly identical. For each measurement an aliquot of 50  $\mu\text{L}$  of each sample was taken at defined times and returned afterward. A mixture of 250  $\mu\text{L}$  of HBG buffer and 1 mL of stock solution served as reference for each measuring point. To exclude the decrease of fluorescence intensity due to the degradation of the DNA-EB complex, the reference sample was treated and stored exactly as the other samples.

A similar behavior was observed for the copolymers for the corresponding hydrogels. Besides the decrease in fluorescence intensity over time, a trend dependent on the PEI content was observed. The gel **H4** with the highest amount of PEI units (62%) showed the highest binding capacity with a fluorescence level of 20%, which was significantly lower than the value of the corresponding copolymer. For the 50% PEI containing gel, similar results to the corresponding copolymer were obtained. The hydrogel **H7** with 36% of LPEI showed no DNA binding. A possible explanation is the dense structure of the hydrogel due to the high amount of cross-linking sites hindering the access of DNA to the hydrogel network. This fact also causes the long time required for a complete DNA binding (95 h). Furthermore, the low swelling values and, thus, the inflexibility of the network, led to a time-consuming complexation process. These long adsorption periods might indicate a diffusion controlled process. To sum up, a high PEI content seems to be the predominant factor for high binding capacities of the hydrogels studied as demonstrated by the remarkable value of **H4**. However, the amount of amine groups is limited by the number of functional sides (here alkene groups) necessary for the formation of stable hydrogels. In addition, the DNA binding of the hydrogel sample **H4** was monitored using a fluorescence microscope (Figure 7). The photometric measurements showed the decrease of the fluorescence intensity of the DNA-EB complex over time after the addition of the hydrogel. A DNA-EB solution of the same concentration served as reference and showed no indications of degradation of the dye. In contrast to the DNA investigations of the supernatant of the P(ButEnOx-co-EI) copolymers and the corresponding hydrogels, the microscopic study was performed with the complete



**Figure 6.** Binding of DNA (ethidium bromide assay)<sup>41</sup> to (a) copolymers **C3**–**C5** and **C7** at increasing nitrogen/phosphate ratios (triple determination) and (b) hydrogel samples **H4**, **H5**, and **H7** at nitrogen/phosphate ratios above 250 (repeated determination) with different PEI content via fluorescence measurements.



**Figure 7.** Microscopic pictures of DNA binding to hydrogel H4 (62% PEI) measured by fluorescence microscopy without DNA/EBA and after addition of DNA/EBA at defined times.

sample including the hydrogel. Since the bound DNA still has free coordination sides for EB, a fluorescence signal is detectable in the area of the hydrogel.

Besides an effective DNA binding, its release from the hydrogel and the copolymer, respectively, represents an essential step for further applications. The DNA release was studied using a heparin assay. Heparin is a polyanion with multiple negative charges per repeating unit, which can effectively bind to the positively charged hydrogel or copolymer, causing the release of the DNA. Thus, the latter can intercalate again with free EB, which was added in the same concentrations as before. The formation of the DNA-EB complex led to an increase of the fluorescence intensity. For the copolymers, the DNA was released very fast. Within 4 min, the fluorescence intensity increased rapidly up to a constant level of nearly 90% (Figure 8a). As reference, a mixture of 250  $\mu\text{L}$  of HBG buffer and 1 mL of DNA-EB stock solution was chosen. It was treated with heparin in the same way as the copolymers, and the resulting fluorescence intensity was set to 100%.

The hydrogels showed a different behavior. Here, neither the addition of heparin (5% release) nor an increase of temperature

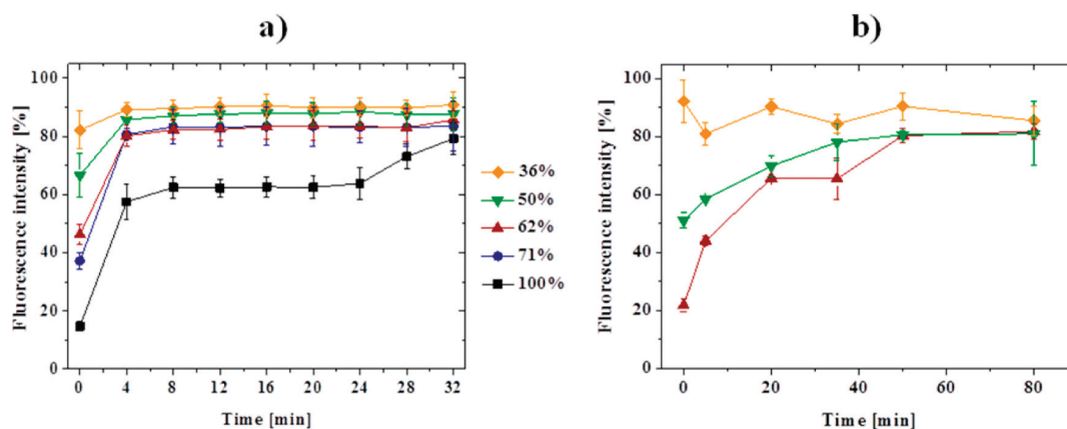
(up to 90  $^{\circ}\text{C}$ , 10%) resulted in an efficient release. However, a combination of both led to a detachment of nearly 50% of the bound DNA within 80 min (Figure 8b). This behavior could be associated with the PEI segments of the synthesized hydrogels. LPEI is not soluble in cold water and the PEI components of the hydrogels could form clusters within the network that inhibit an efficient release due to sterical reasons. At higher temperatures, the PEI segments melt and a replacement of DNA with heparin becomes possible.

## CONCLUSION

In summary, a new and efficient method to obtain hydrogels for the binding and release of DNA with a controlled amount of amine binding sides was developed. To this end, a new class of copolymer containing 2-butenyl-2-oxazoline and ethylene imine units was synthesized by partial functionalization of LPEI with *N*-succinimidyl-4-pentenate. An eight-membered library of P(ButEnOx-co-EI)s was prepared, and subsequently, the double bonds were exploited for cross-linking via thiol-ene photo-addition using *bis*-functional 3,6-dioxaoctane-1,8-dithiol. Compared to the formation of PEI hydrogels by cross-linking the free amines, the presented approach allows the exact adjustment of the amount of free amines in the copolymer and, thus, within the hydrogel. Both copolymers and hydrogels were characterized by means of NMR spectroscopy and FT-IR spectroscopy. Furthermore, the swelling and deswelling behavior of the hydrogels from liquid and gas phase was investigated, showing that the water uptake from the liquid phase is 10 $\times$  more efficient. Swelling values up to 74% were observed.

The DNA studies showed that copolymers and hydrogels are able to bind and release DNA reversibly via the secondary amine groups with binding capacities strongly depending on the PEI content. The copolymers bound up to 70% of the initial DNA. Because of their large three-dimensional networks, the hydrogels exhibited a much higher binding capacity for the appropriate PEI contents. However, due to the low swelling values compared to POx-based hydrogels and, thus, the inflexibility of the network, the DNA uptake was rather slow, probably indicating a diffusion-controlled process.

The DNA release studies were performed using a heparin assay. While the copolymers at room temperature rapidly



**Figure 8.** Time-dependent release of DNA from (a) copolymers C3–C5 and C7 (heparin, triple determination) at a nitrogen/phosphate ratio of 2 and (b) hydrogel samples H4, H5, and H7 at nitrogen/phosphate ratios above 250 (heparin, 90  $^{\circ}\text{C}$ , repeat determination) with different PEI content via fluorescence measurements.

released up to 90% of the initial DNA quantity after heparin addition, the hydrogels released 50% at elevated temperatures.

To accelerate the binding and release of genetic material, further studies, dealing with the improvement of the swelling behavior of the hydrogels, have to be performed. Hence, hydrogels starting from a precursor poly(2-ethyl-2-oxazoline-co-ethylene imine) instead of linear poly(ethylene imine) should be investigated. This will be part of a follow-up study.

In addition, solid NMR spectroscopy revealed the presence of unreacted alkene groups, which could be used for further functionalizations like surface attachment. The treated surfaces are available for DNA binding and release studies in terms of chip-based point-of-care diagnostics.

Besides its use in hydrogel synthesis, the copolymer P(ButEnOx-co-EI) represents an interesting molecule for other applications, such as gene delivery or gene silencing.

## ■ ASSOCIATED CONTENT

### Supporting Information

Supporting Figure S1 and Table S1. This material is available free of charge via the Internet at <http://pubs.acs.org>.

## ■ AUTHOR INFORMATION

### Corresponding Author

\*Fax: +49 3641 948 202. E-mail: [ulrich.schubert@uni-jena.de](mailto:ulrich.schubert@uni-jena.de).

### Present Address

<sup>§</sup>Department of Chemical and Biomolecular Engineering, The University of Melbourne, Victoria 3010, Australia (K.K.).

### Notes

The authors declare no competing financial interest.

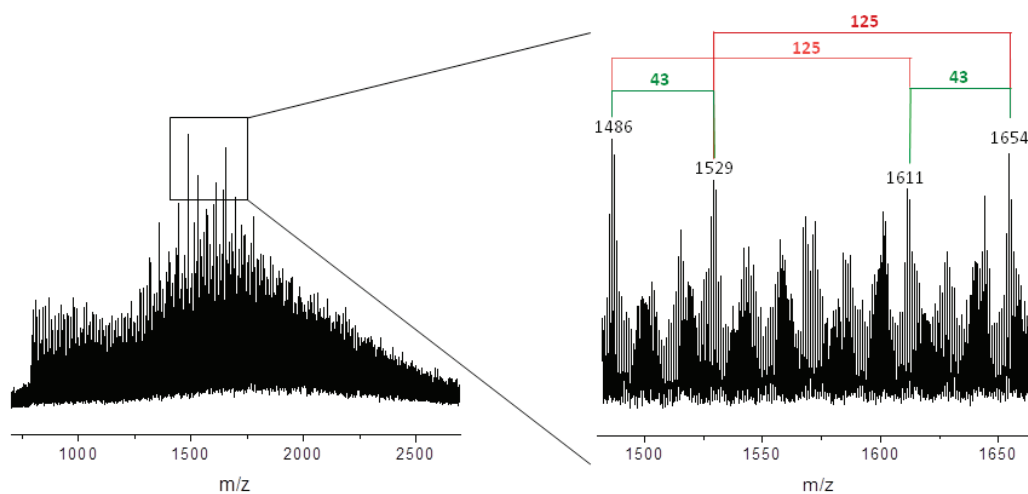
## ■ ACKNOWLEDGMENTS

C.E. is grateful to the Stiftung Industrieforschung for financial support. We thank Dr. Andreas Seifert from TU Chemnitz for the solid NMR measurements. Grateful thanks to Dr. Jürgen Vitz for water uptake measurements from the gas phase and Dr. David Pretzel for the fluorescence microscopy investigations.

## ■ REFERENCES

- Joos, B.; Kuster, H.; Cone, R. *Anal. Biochem.* **1997**, *247*, 96–101.
- Rogers, Y.-H.; Jiang-Baucom, P.; Huang, Z.-J.; Bogdanov, V.; Anderson, S.; Boyce-Jacino, M. T. *Anal. Biochem.* **1999**, *266*, 23–30.
- Steel, A. B.; Levicky, R. L.; Herne, T. M.; Tarlov, M. J. *Biophys. J.* **2000**, *79*, 975–981.
- Fixe, F.; Dufva, M.; Telleman, P.; Christensen, C. B. V. *Nucleic Acids Res.* **2004**, *32*, e9.
- Wink, M. *An Introduction to Molecular Biotechnology: Molecular Fundamentals, Methods and Applications in Modern Biotechnology*; Wiley-VCH: Weinheim, Germany, 2006.
- Brissault, B.; Kichler, A.; Guis, C.; Leborgne, C.; Danos, O.; Cheradame, H. *Bioconjugate Chem.* **2003**, *14*, 581–587.
- Boussif, O.; Lezoualch, F.; Zanta, M. A.; Mergny, M. D.; Scherman, D.; Demeneix, B.; Behr, J. P. *Proc. Natl. Acad. Sci. U.S.A.* **1995**, *92*, 7297–7301.
- Zhou, Y.-L.; Li, Y.-z. *Spectrochim. Acta, Part A* **2004**, *60*, 377–384.
- Hellweg, T.; Henry-Toulmé, N.; Chambon, M.; Roux, D. *Colloids Surf., A* **2000**, *163*, 71–80.
- Sharma, V. K.; Thomas, M.; Klivanov, A. M. *Biotechnol. Bioeng.* **2005**, *90*, 614–620.
- Godbey, W. T.; Wu, K. K.; Mikos, A. G. *J. Controlled Release* **1999**, *60*, 149–160.
- Peterson, A. W.; Heaton, R. J.; Georgiadis, R. M. *Nucleic Acids Res.* **2001**, *29*, 5163–5168.
- Rampal, J. B. *Microarrays: Synthesis Methods*; Humana Press: Totowa, NJ, 2001.
- Anzenbacher, P.; Liu, Y.-L.; Kozelkova, M. E. *Curr. Opin. Chem. Biol.* **2010**, *14*, 693–704.
- Guschin, D.; Yershov, G.; Zaslavsky, A.; Gemmel, A.; Shick, V.; Proudnikov, D.; Arenkov, P.; Mirzabekov, A. *Anal. Biochem.* **1997**, *250*, 203–211.
- Okay, O. *J. Polym. Sci., Part B: Polym. Phys.* **2011**, *49*, 551–556.
- Kivlehan, F.; Paolucci, M.; Brennan, D.; Ragoussis, I.; Galvin, P. *Anal. Biochem.* **2012**, *421*, 1–8.
- Liu, J. *Soft Matter* **2011**, *7*, 6757–6767.
- Hartlieb, M.; Pretzel, D.; Kempe, K.; Fritzsche, C.; Paulus, R. M.; Gottschaldt, M.; Schubert, U. S. *Soft Matter* **2013**, *9*, 4693–4704.
- Chujo, Y.; Sada, K.; Saegusa, T. *Polym. J.* **1993**, *25*, 599–608.
- Chujo, Y.; Sada, K.; Saegusa, T. *Macromolecules* **1993**, *26*, 6315–6319.
- Chujo, Y.; Sada, K.; Saegusa, T. *Macromolecules* **1993**, *26*, 6320–6323.
- Chujo, Y.; Yoshifuji, Y.; Sada, K.; Saegusa, T. *Macromolecules* **1989**, *22*, 1074–1077.
- Chujo, Y.; Sada, K.; Saegusa, T. *Macromolecules* **1990**, *23*, 2636–2641.
- Wiesbrock, F.; Hoogenboom, R.; Leenen, M.; van Nispen, S. F. G. M.; van der Loop, M.; Abeln, C. H.; van den Berg, A. M. J.; Schubert, U. S. *Macromolecules* **2005**, *38*, 7957–7966.
- Goyal, R.; Tripathi, S. K.; Tyagi, S.; Sharma, A.; Ram, K. R.; Chowdhuri, D. K.; Shukla, Y.; Kumar, P.; Gupta, K. C. *Nanomed. Nanotechnol. Biol. Med.* **2012**, *8*, 167–175.
- Dargaville, T. R.; Forster, R.; Farrugia, B. L.; Kempe, K.; Voorhaar, L.; Schubert, U. S.; Hoogenboom, R. *Macromol. Rapid Commun.* **2012**, *33*, 1695–1700.
- Gress, A.; Volkel, A.; Schlaad, H. *Macromolecules* **2007**, *40*, 7928–7933.
- Diehl, C.; Schlaad, H. *Macromol. Biosci.* **2009**, *9*, 157–161.
- Diehl, C.; Schlaad, H. *Chem.—Eur. J.* **2009**, *15*, 11469–11472.
- Kempe, K.; Vollrath, A.; Schaefer, H. W.; Poehlmann, T. G.; Biskup, C.; Hoogenboom, R.; Hornig, S.; Schubert, U. S. *Macromol. Rapid Commun.* **2010**, *31*, 1869–1873.
- Kempe, K.; Hoogenboom, R.; Jaeger, M.; Schubert, U. S. *Macromolecules* **2011**, *44*, 6424–6432.
- Kempe, K.; Hoogenboom, R.; Schubert, U. S. *Macromol. Rapid Commun.* **2011**, *32*, 1484–1489.
- Koschella, A.; Hartlieb, M.; Heinze, T. *Carbohydr. Polym.* **2011**, *86*, 154–161.
- Tauhardt, L.; Kempe, K.; Knop, K.; Altuntas, E.; Jäger, M.; Schubert, S.; Fischer, D.; Schubert, U. S. *Macromol. Chem. Phys.* **2011**, *212*, 1918–1924.
- Lambermont-Thijs, H. M. L.; van der Woerd, F. S.; Baumgaertel, A.; Bonami, L.; Du Prez, F. E.; Schubert, U. S.; Hoogenboom, R. *Macromolecules* **2010**, *43*, 927–933.
- Chatani, Y.; Tadokoro, H.; Saegusa, T.; Ikeda, H. *Macromolecules* **1981**, *14*, 315–321.
- Chatani, Y.; Kobatake, T.; Tadokoro, H.; Tanaka, R. *Macromolecules* **1982**, *15*, 170–176.
- Chatani, Y.; Kobatake, T.; Tadokoro, H. *Macromolecules* **1983**, *16*, 199–204.
- Thijs, H. M. L.; Becer, C. R.; Guerrero-Sanchez, C.; Fournier, D.; Hoogenboom, R.; Schubert, U. S. *J. Mater. Chem.* **2007**, *17*, 4864–4871.
- Wagner, M.; Rinkenauer, A. C.; Schallon, A.; Schubert, U. S. *RSC Adv.* **2013**, *3*, 12774–12785.

SUPPORTING INFORMATION



**Figure S1.** MALDI-TOF-MS spectrum (matrix: DHB, solvent: methanol) of a 45% PEI containing copolymer (20 units,  $M_n \sim 1,650$  g/mol,  $^1\text{H NMR}$ :  $M_n' = 1,800$  g/mol) with a detailed analysis of a selected part of the spectrum.

**Table S1.** Effect of concentration of the prepolymer for sample C5 (50% PEI content) and C3 (71% PEI content).

	<b>P(ButEnOx-co-EI<sub>71%</sub>)</b>			<b>P(ButEnOx-co-EI<sub>50%</sub>)</b>		
Polymer concentration [wt%]	5.8	9.4	16.9	5.0	9.7	14.8
Swelling value $Q_{eq}$ [%]	-*	62	64	68	74	70

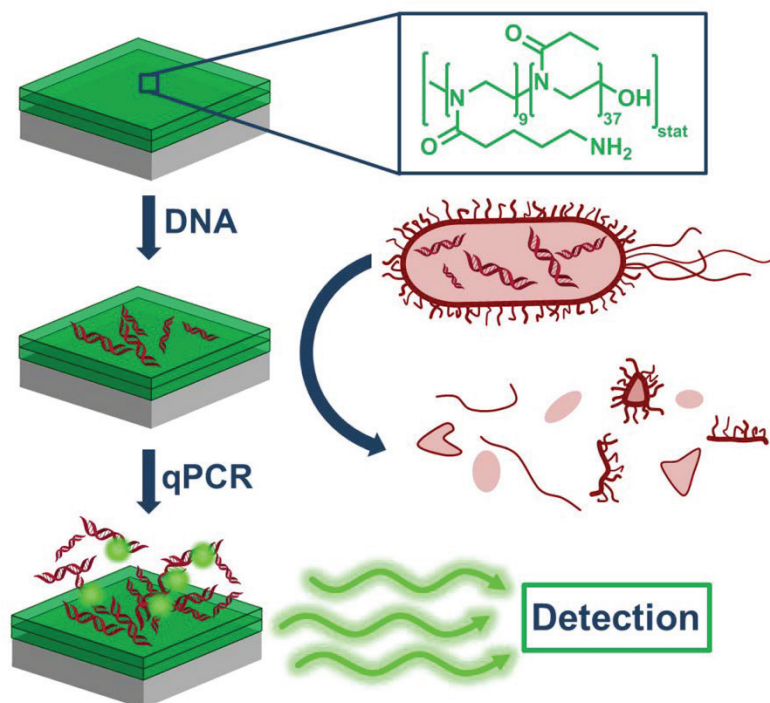
\* No hydrogel was obtained.

## Publication 6

### „Lab in a tube: Purification, amplification and detection of DNA using poly(2-oxazoline) multilayers“

M. N. Leiske,<sup>‡</sup> M. Hartlieb,<sup>‡</sup> C. Paulenz, D. Pretzel, M. Hentschel, C. Englert, M. Gottschaldt, U. S. Schubert

*Adv. Funct. Mater.*, in press.



<sup>‡</sup> Equal contribution



DOI: 10.1002/ ((please add manuscript number))

Article type: Full Paper

**Lab in a tube: Purification, amplification and detection of DNA using poly(2-oxazoline) multilayers**

*Meike N. Leiske,<sup>‡</sup> Matthias Hartlieb,<sup>‡</sup> Christian Paulenz, David Pretzel, Martin Hentschel, C. Englert, Michael Gottschaldt, Ulrich S. Schubert,\**

M. N. Leiske, M. Hartlieb, Dr. D. Pretzel, C. Englert, Dr. M. Gottschaldt, Prof U. S. Schubert  
Laboratory of Organic and Macromolecular Chemistry (IOMC), Friedrich Schiller University  
Jena, Humboldtstrasse 10, 07743 Jena, Germany

M. N. Leiske, M. Hartlieb, Dr. D. Pretzel, C. Englert, Dr. M. Gottschaldt, Prof U. S. Schubert  
Jena Center for Soft Matter (JCSM), Friedrich Schiller University Jena, Philosophenweg 7,  
07743 Jena, Germany

C. Paulenz, M. Hentschel  
Analytik Jena AG, Konrad-Zuse-Straße 1, 07745 Jena, German

C. Paulenz,  
Institute of Pharmacy, Friedrich-Schiller-University, Philosophenweg 14, 07743 Jena,  
Germany

E-mail: ulrich.schubert@uni-jena.de

Keywords: bioanalytics, DNA, lab in a tube, layer-by-layer, poly(2-oxazoline),

Fast and easy purification and amplification of DNA are prerequisites for the development of point-of-care diagnostics. For this reason covalent coatings of amine containing poly(2-oxazoline)s (POx) on glass and poly(propylene) surfaces were prepared to reversibly bind genetic material directly from biological samples. The polymer was deposited in a layer-by-layer process, whereas initial immobilization of macromolecules on the surface was accomplished by the use of an epoxy functionalized siloxane monolayer. Alternating treatment with polymer and cross-linker leads to the construction of amine containing POx multi layers on the substrates. Successful deposition was investigated by confocal laser scanning microscopy (using labeled polymers), contact angle measurements, as well as reflectometric interference spectroscopy. The interaction of these layer systems with DNA regarding binding and temperature dependent release was studied using labeled genetic

material. Finally, PCR reaction vessels were coated with POx layers on the inside and used for qPCR experiments. It was possible to bind genetic material directly from cell lysates to perform qPCR assays from surface adsorbed DNA within the same tube including amplification, as well as detection. The presented system displays an easy to use device for a point of care diagnostic.

## 1. Introduction

A reliable and time saving point-of-care diagnostic is one of the most important targets in bioanalytical science.<sup>[1]</sup> The optimal method would comprise an analysis of sample material directly on the spot, however, operating with the same accuracy as laboratory tests.<sup>[2]</sup> Moreover, cost efficiency is a major requirement in this context, rendering the design of new bioanalytical devices a highly challenging task.<sup>[3]</sup> The detection of diseases based on bacterial, fungal or viral infections can be accomplished by the investigation of the pathogens nucleic acid profiles,<sup>[4]</sup> providing the opportunity of a fast determination and a targeted medication.<sup>[5]</sup> The recognition of the genetic material can be accomplished *via* specialized DNA assays,<sup>[6]</sup> *e.g.* based on microchip systems.<sup>[7]</sup> However, this presents only the last step in bioanalytics. The isolation of nucleic acids from whole tissue and cell samples and, in particular, the separation from proteins is still a prerequisite for downstream analytical processes. The general steps of nucleic acid purification include 1) tissue and/or cell lysis, 2) inactivation of cellular nucleases and, 3) separation of the desired nucleic acids from the cell debris.<sup>[8]</sup> To separate proteins from genetic material, phenol-chloroform extraction and density gradient centrifugation displayed the method of choice for many years.<sup>[8a, 9]</sup> Besides the use of toxic substances,<sup>[9]</sup> these liquid phase based methods had the drawback of very time consuming and laborious working steps.<sup>[10]</sup> An enormous improvement was achieved in 1989, when the first solid phase extraction (SPE) system for DNA purification was described by McCormick *et al.*<sup>[8b]</sup> It has the advantage to separate nucleic acids from proteins more effectively, and

without the generation of toxic by-products. Since its introduction, the SPE system evolved to the most common and easily adaptable purification method for genetic material.<sup>[11]</sup> Still, there are remaining disadvantages, such as the labor-intensive multiple washing procedures, the limited loading capacity of the silica matrix, as well as limitations in the extraction efficiency.<sup>[8a]</sup>

To overcome these restrictions, a challenging alternative approach is the binding of DNA within polymer matrices. Such scaffolds can be considered as a potential alternative for DNA immobilization, based on the fact that they have the potential of low cost production at large scales and mostly exhibit a biocompatible character.<sup>[12]</sup> Furthermore, they can be functionalized easily,<sup>[13]</sup> e.g. with positively charged groups, able to interact with the negatively charged phosphate backbone of polynucleotides.<sup>[14]</sup>

However, these polymers are mostly water soluble and, therefore, an assignment in biological, water based systems is not possible, since a separation from solution is difficult. For this reason, polymer-based hydrogels offer a great opportunity for a reversible DNA binding and release.<sup>[15]</sup> Because of their high water content and the resulting permeability of the three-dimensional matrix, as well as the adjustable functionalities and a high surface to volume ratio, hydrogels represent attractive candidates for DNA immobilization. The suitability of poly(2-oxazoline) (POx) based hydrogels<sup>[16]</sup> and networks composed of POx-poly(ethylenimine) (PEI) copolymers<sup>[17]</sup> was already investigated. The amine content and, therefore, the affinity to DNA are adjustable in both systems, resulting in a tunable DNA binding behavior. The combination of charged moieties with hydrophilic monomers such as 2-ethyl-2-oxazoline (EtOx) results in water swellable networks able to interact with genetic material. Furthermore, a release can be induced by the addition of heparin which replaces the DNA, generating eluates compatible with subsequent polymerase chain reaction (PCR) based DNA amplification.<sup>[16]</sup> However, the diffusion of genetic material within the gel is the limiting factor preventing fast purification procedures. Additionally, also non- or low-charged residues

from cell lysis could be entrapped within the pores of the gel and, hence, interfere with downstream processes.

Surface bound polymer coatings are a potential way to overcome the drawbacks discussed above and combine the advantages of hydrogels with diffusion independent, surface mediated processes. The covalent immobilization of POx on glass substrates was already demonstrated in the context of low-fouling coatings,<sup>[18]</sup> however, to the best of our knowledge, no investigations regarding their bioanalytical potential are reported. A major requirement for DNA purification systems is their compatibility with subsequent PCR processes which are indispensable for a later detection. The PCR was invented by Kary B. Mullis in 1983 and enveloped to one of the most important methods in bioanalytical science.<sup>[19]</sup> *Via* PCR, a few copies of a specific sequence of genetic material can be amplified by the naturally thermostable enzyme polymerase,<sup>[20]</sup> using specifically, synthesized oligonucleotides (primers) for the gene-of-interest.<sup>[19]</sup> The process itself consists of three steps:<sup>[21]</sup> 1) The denaturation (melting), 2) the primer annealing to the specific gene sequences, and, 3) the elongation at a polymerase-specific temperature. Without PCR, DNA detection would be impossible due the low amounts of genetic material in biological samples.<sup>[22]</sup> However, the PCR process is limited by the purity of the bioanalytical samples, as well as by the template DNA amount.<sup>[23]</sup> Cellular components, remaining from cell lysis or other impurities, can interfere with the process and lead to non-exponential amplification or even a complete inhibition of the process. Therefore, pure polynucleotide solutions with a high concentration are preferable.

In this contribution we describe the synthesis of POx based surface coatings, containing a defined amount of amine groups for DNA binding and release. The polymers are covalently immobilized in a layer-by-layer (LbL) approach, generating films of defined thicknesses and DNA binding/release profiles. The coating procedure is established on glass and, subsequently, transferred to poly(propylene) (PP), being one of the most common and important materials in bioanalytics. After investigation of the DNA interaction on plain

substrates, PCR tubes are coated on the inside, creating a system able to separate DNA from impurities and, moreover, amplify and detect specific sequences by quantitative real-time PCR (qPCR). Exploiting the temperature dependent DNA binding behavior of POx multilayers it is possible to extract and detect DNA directly from cell lysate rendering this “lab in a tube” system a highly versatile and likewise easy to use tool for pathogen detection.

## 2. Results and Discussion

### 2.1. Polymerization and fluorescent labeling

The synthesis of amine containing POx was reported previously by our group.<sup>[15]</sup> Briefly, a 2-oxazoline bearing a Boc protected amine group (BocOx) was used in a copolymerization with EtOx to yield a statistical copolymer having 24% of functional comonomer incorporated (P(EtOx<sub>35</sub>-*stat*-BocOx<sub>11</sub>, **1**). Deprotection using trifluoroacetic acid (TFA) was applied to obtain amine containing POx (P(EtOx<sub>37</sub>-*stat*-AmOx<sub>9</sub>, **2**) with a molar mass ( $M_n$ ) of 4,600 and a narrow size distribution. Recalculation of the composition by NMR measurements after deprotection resulted in a final AmOx content of 20% (**Table 1**). Since this polymer should be used as a surface coating material, labeling was conducted using fluorescent dyes (fluorescein-5-*N*-hydroxysuccinimide ester for polymer **3** or rhodamine B *iso*-thiocyanate for polymer **4**) which are able to react with amine groups to enable a later detection of deposits. The coupling reaction was performed using one equivalent of dye per polymer chain, leaving a sufficient amount of free amine groups for surface attachment and DNA interaction. The success of the dye functionalization was verified by SEC measurements, comparing the signal from the refractive index (RI) detector with the UV/VIS signals. Purification (precipitation, and in the case of polymer **4** preparative size exclusion chromatography) was conducted until no trace of unbound dye was detected in the SEC traces. Overlapping RI and UV/VIS traces prove a homogeneous functionalization of the polymeric material (**SI: Figure S1**). The efficiency of the labeling reaction was quantified by NMR spectroscopy (Table 1).

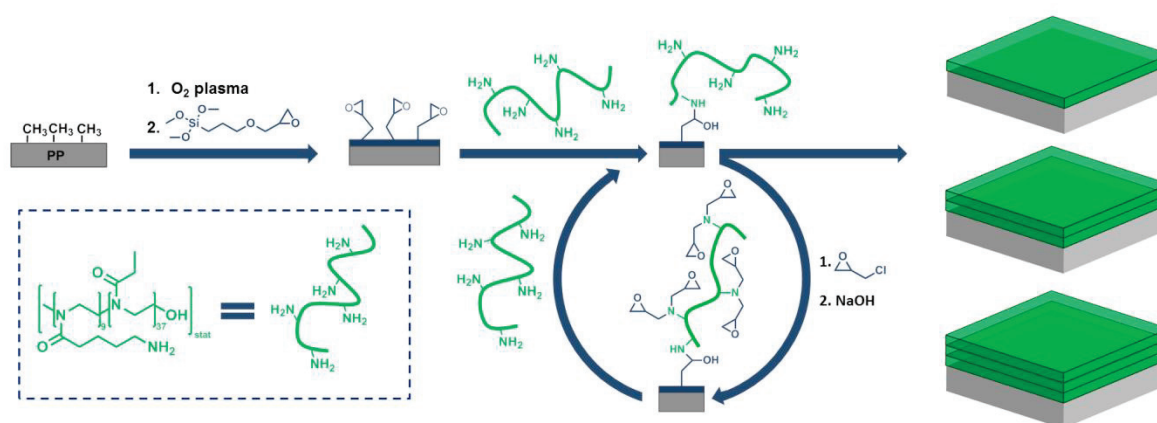


**Table 1:** Selected characteristics of the synthesized polymers (\*SEC measurements in chloroform; \*\*SEC measurements in DMAc).

Polymer	Compound	Dye	M <sub>n</sub> (g mol <sup>-1</sup> )	Đ	Degree of func. (%)	Abs. Max. (nm)	Em. Max. (nm)
1	P(EtOx <sub>35</sub> -stat-BocOX <sub>11</sub> )	-	4,600*	1.30	-	-	-
2	P(EtOx <sub>37</sub> -stat-AmOX <sub>9</sub> )	-	9,300**	1.13	-	-	-
3	P(EtOx <sub>37</sub> -stat-AmOX <sub>9</sub> -stat-FAmOX <sub>1</sub> )	Fluorescein	11,000**	1.16	78	485	530
4	P(EtOx <sub>37</sub> -stat-AmOX <sub>9</sub> -stat-RAmOX <sub>1</sub> )	Rhodamine B	12,000**	1.19	5	555	590

## 2.2 Surface functionalization

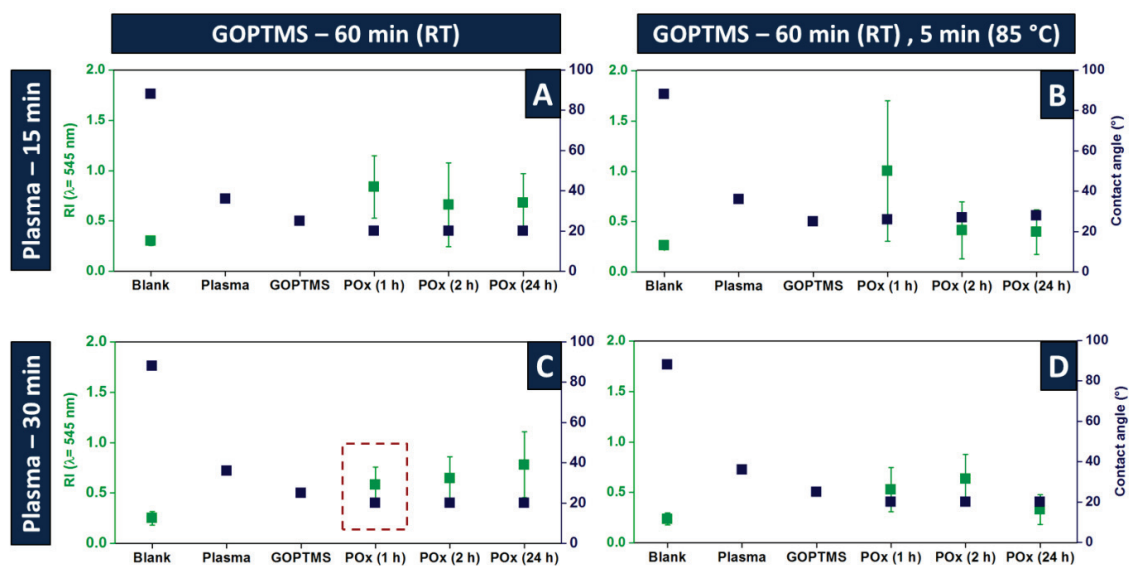
The covalent attachment of amine functionalized POx to (activated) glass substrates was already reported by our group.<sup>[24]</sup> The method comprises the cleaning and activation by plasma and the subsequent deposition of a siloxane monolayer using 3-glycidyloxypropyl trimethoxysilane (GOPTMS). The epoxide groups of the siloxane layer react readily with the amine groups of the POx material to form a polymeric monolayer on the surface. While glass is a substrate frequently used for functionalization by silanization, also PP was utilized as a support material in this study since it is cheap, flexible and relatively inert regarding biological processes. For this reason, the surface chemistry described before was transferred to PP. An overview over the performed coating procedures is depicted in **Scheme 1**.



**Scheme 1:** Schematic representation of the deposition of P(EtOx<sub>37</sub>-stat-AmOX<sub>9</sub>) on substrates by LbL immobilization.

To generate oxygen based functionalities on the highly inert substrate, O<sub>2</sub>-Plasma was applied. The oxidative conditions lead to the formation of OH groups and other oxygen based functionalities on the surface.<sup>[25]</sup> These functional groups can be used to attach a siloxane monolayer of GOPTMS. The present epoxide groups were subsequently quenched by the reaction with the amine groups of polymers **2**, **3** or **4**. The success of the reaction could be verified by contact angle (CA) measurements determining the surface energy, as well as by fluorescence using confocal laser scanning microscopy (CLSM).

To optimize the amount and homogeneity of the deposited POx, the O<sub>2</sub>-plasma treatment time, as well as the GOPTMS incubation temperature was altered since coating experiments with conditions described for glass resulted in heterogeneous coated surfaces. Additionally, the incubation time of the polymer was varied between 1, 2 and 24 hours. The success of coating experiments was analyzed *via* CA and CLSM measurements (**Figure 1**). The CA measurements revealed that the hydrophobic character of untreated PP (CA = 88 °) decreases after activation with O<sub>2</sub> plasma (CA = 36 °), most probably due to the formation of hydroxyl groups. These oxygen functionalities react with GOPTMS to form a monolayer on the surface (CA = 25). After coating with polymer **4**, the hydrophilicity increases (CA < 20 °) as a result of the covalently bound macromolecules. According to the CA results, there are no differences in the coating efficiencies for varying incubation times. CLSM measurements at  $\lambda_{\text{ex}} = 543 \text{ nm}$  ( $\lambda_{\text{em}}$ : 560 to 615 nm) were performed for all coated slides, as well as for the blank substrates measuring an increase of fluorescence after coating with fluorescently labeled POx (**4**). The fluorescence intensity does not change significantly by varying either coating conditions or POx incubation time, however, the film homogeneity does, which is indicated by the standard deviation of the signal. 30 min O<sub>2</sub> plasma treatment and 1 h GOPTMS incubation at room temperature (RT) were chosen as the best activation and functionalization conditions, because of a high mean fluorescence in combination with the most homogenous distribution of polymer on the surface within a reasonable time (Figure 1C).



**Figure 1:** Optimization of the coating conditions for POx (3) on PP. The plasma incubation time was investigated using 15 min (A, B) or 30 min (C, D) of treatment. GOPTMS incubation was performed for 60 min at RT (A, C) or with an additional heat treatment for 5 min at 85 °C (B, D). POx coating was performed for 1, 2 or 24 h at 50 °C. Success and homogeneity of the coating procedure was verified by CA and CLSM.

### 2.3 LbL assembly

The aim of this work is the production of POx coatings having a defined thickness to tailor the strength of interaction with the genetic material. To this end, an LbL deposition method was conducted to produce multilayers of amine containing POx on PP. The general procedure is shown in Scheme 1, starting with the already described deposition of a POx coating on a GOPTMS monolayer. Subsequently, the remaining amine groups were activated by the use of an excess of epichlorohydrin (ECH). The epoxide groups of this cross-linker molecule react with primary and secondary amines present in the first POx layer resulting in tertiary amine groups. In a second step, basic conditions are applied, leading to a re-formation of an epoxide ring, based on the elimination of hydrochloric acid. The generated epoxide groups can be used to attach a second layer of POx as described before. This cycle can be repeated to immobilize a defined amount of POx layers on the substrate. Within this study films composed of up to three layers were produced. A first indication of a successful layer deposition was generated by CA measurements (**Table 2**). The blank PP substrate produced high CA values due to the hydrophobicity of the material.

**Table 2:** Analytical data of the multilayer POx coatings.

Coating step	CA (°)	POx amount by TGA (wt%)	Layer thickness (on glass, nm)
Blank	100	-	0.0
O <sub>2</sub> plasma	80	-	0.6
GOPTMS	48	-	0.8
1st POx layer	< 20	0.7	3.5
ECH-XL	57	n. d.	n. d.
2nd POx layer	< 20	1.3	28.4
ECH-XL	72	n. d.	n. d.
3rd POx layer	< 20	1.8	109.4

Plasma activation, as well as GOTMS deposition reduces the CA significantly, indicating an effective functionalization. Upon the attachment of POx, the CA decreases below 20 ° which displays the minimum measurable CA. The activation using ECH cross-linker yields CA values above 50° which is decreased again below 20° upon the addition of another POx layer. This behavior of surface energy changes is in perfect agreement with the successful deposition of POx in an LbL approach.

To gain further insights into the system, thermo gravimetric analysis (TGA) experiments were conducted. Pure PP substrates, as well as POx (**2**) were subjected to thermal combustion. The weight loss as a function of temperature was recorded revealing different decomposition temperatures (**SI Figure S2**).

Using this information it is possible to calculate the amount of deposited POx on PP from the TGA measurements of the coated samples (Table 2). The relatively linear mass increase per POx layer indicates a homogeneous LbL deposition.

Further analysis of the POx coating was conducted using reflectometric interference spectroscopy (RIFS) measurements. The method determines the thickness of layers on glass substrates having a reflective Ta<sub>2</sub>O<sub>5</sub> layer on the opposite site of the coating by measuring the peak shift of light reflected by the polymer layers.<sup>[26]</sup> For this purpose, glass slides were coated applying the conditions used for PP and analyzed accordingly (**SI Table S1**). During

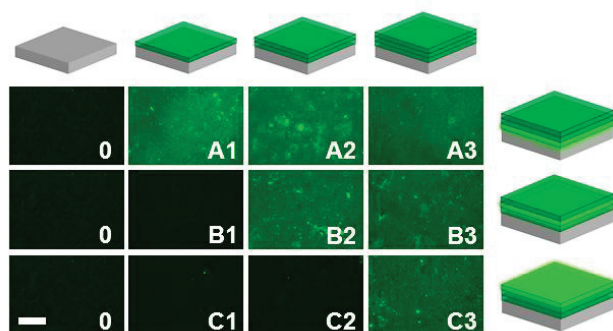
the measurements, a water flow was channeled over the POx surface continuously to generate information about the swollen layers. The exponential increase of the layer thickness is, at first sight, inconsistent with the information obtained from TGA. A varying cross-linking density of individual layers could be an explanation for this discrepancy. The first layer is attached to the substrate *via* the reaction with epoxide groups directly on the surface, generating a flat film of polymer chains. With every additional layer the mobility of the epoxide binding sites increases generating more loosely bound and mobile POx layers able to incorporate more water into the polymeric matrix, describing the transition from a surface coating to an immobilized hydrogel (**Figure 2**).



**Figure 2:** Schematically representation of water-swollen POx multi-layers.

As a final proof of the LbL deposition, fluorescence analyses were performed using polymer **3**. All investigated PP slides were coated with three POx layers; however, fluorescently labeled POx was only used in the first, second or third coating step, respectively. For the other two layers, polymer **2** was used. In this way samples with one fluorescently labeled POx layer and two unlabeled layers are obtained. Every coating step was investigated using CLSM measurements (**Figure 3**). The pictures illustrate the control over the layer deposition by the applied method. A significant increase in fluorescence upon coating with polymer **3** shows the successful immobilization of the material (*e.g.* A1). The fluorescence signal remains relatively constant upon the addition of further layers (*e.g.* A2 and A4) proving the existence of LbL structures on the surfaces.

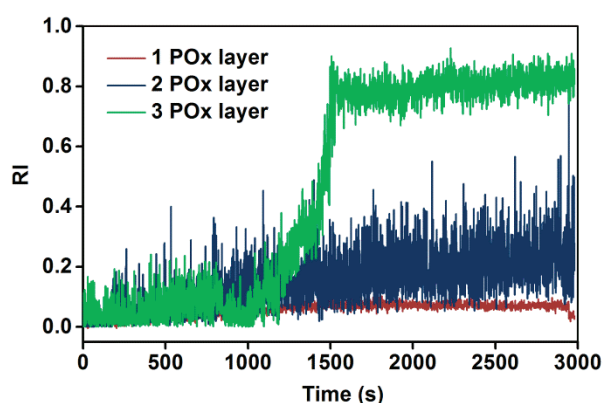




**Figure 3:** CLSM pictures of fluorescently labeled POx multilayers. Polymer **3** was used for the first (A), second (B) or third (C) polymer layer. Pictures were captured of blank PP (0), and after the first (1), second (2), as well as third (3) coating step at a wavelength between 505 and 530 nm. Scale bar: 200  $\mu\text{m}$ .

## 2.4 DNA binding and release

The ability of the presented POx films to adsorb genetic material in a reversible manner is a prerequisite for the aimed application. First tests were conducted using the RIFS method (BIAffinity®) as described before, however, using DNA solutions instead of pure water to swell the POx layers. Differences at the peak minimum (500 nm) enable information about the layer thickness which, in the end, allows a conclusion about the relative amount of bound DNA (Figure 4).



**Figure 4:** RIFS measurements using a DNA solution of  $100 \text{ ng } \mu\text{L}^{-1}$  to swell POx multilayers.

Slides containing a POx monolayer do not show a significant swelling upon addition of DNA while the thickness of coatings with two, as well as three polymer layers increases. This trend correlates well with the increase of the hydrogel character per deposited layer. A weaker

interconnection between the polymer chains of a film leads to a higher DNA adsorption due to the incorporation of DNA molecules within the layer and an increased interaction between amine groups and the DNA backbone. However, the presence of DNA as a polyanion could also lead to an alteration of the swelling behavior without a distinct binding.

To track the fate of the genetic material in the presence of POx multilayers directly by CLSM investigations, Cy5-labeled DNA strands were used. These measurements allow a quantification of the amount of bound DNA on the substrate assuming that the fluorescence emission increases proportional to the amount of immobilized genetic material. Cy5-labeled DNA lacZ segments were synthesized *via* PCR using Cy5-labeled primers. After amplification, the PCR products were purified and analyzed *via* gel electrophoresis. The DNA amount was determined using UV/VIS spectroscopy (ScanDrop®250).

The time required to establish an equilibrium between bound and unbound DNA is crucial for a later application since it determines the velocity of the first step of *e.g.* pathogen detection. To this end, the immobilization of labeled DNA on POx multilayers was investigated (**Figure 5A**). PP chips with a defined surface (78 mm<sup>2</sup>) were covered with a water droplet (15  $\mu$ L) containing 1.5  $\mu$ g of DNA for a defined time. To exclude an unspecific interaction, the chips were subsequently washed with water at RT.

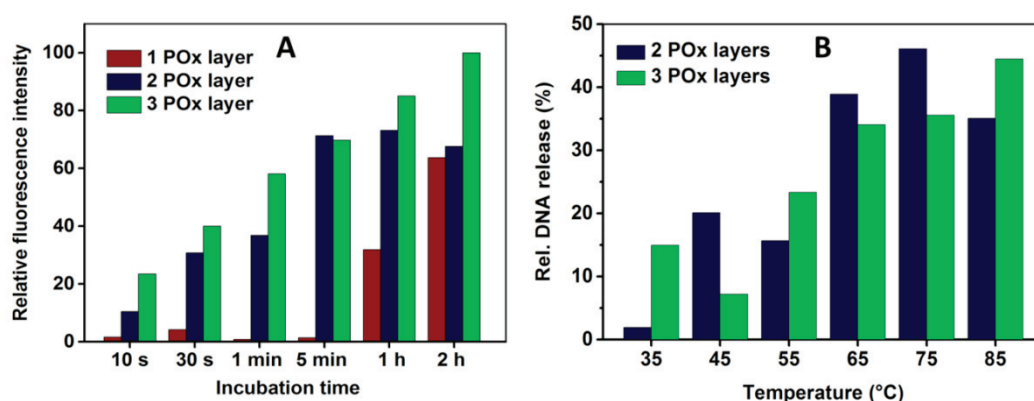


Figure 5: Adsorption and release of Cy5 labeled DNA by POx multilayers. A: Time dependent uptake of labeled genetic material determined by mean fluorescence of POx multilayers after treatment. B: Temperature dependent release of POx multilayers loaded with DNA for 1 h displayed as percentage of the initially bound DNA amount.

The CLSM measurements show an increase of fluorescence emission that is proportional to the incubation time of Cy5-labeled DNA strands. Chips containing one POx layer do not show a pronounced uptake behavior which is assumedly a result of the diminished swelling of this monolayer preventing an efficient uptake of the oppositely charged species. In contrast, PP chips with two POx layers reveal an increase in fluorescence up to 5 minutes incubation time. PP chips with three POx layers show a constant increase in emission up to two hours. Those results indicate a correlation between the amount of polymer layers and the total DNA adsorption. It is assumable that the hydrogel-like character of chips coated with three layers of POx results in an increasing impact of diffusion processes on the DNA adsorption which is not pronounced for the two-layered systems.

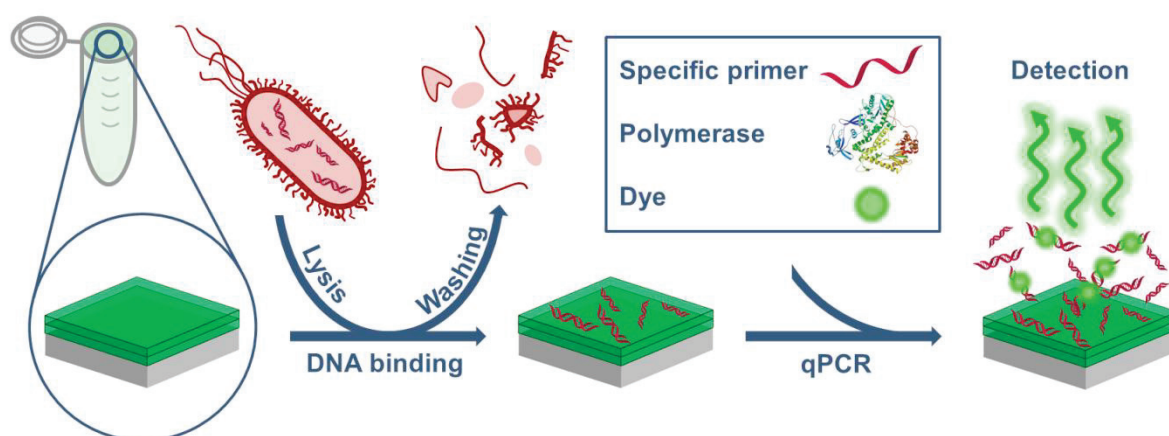
As the polymer associated DNA will be used for surface mediated PCR experiments, the ability of a controllable DNA release behavior is likewise important. Since the genetic material must be available for the polymerase to be amplified, a quantitative release is preferable.

For these experiments, chips loaded for one hour with the above described procedure were subjected to a temperature dependent washing process (Figure 5B). DNA release studies were not performed for chips containing one polymer layer, due to the fact that the long incubation times necessary for binding makes them unfavorable for further studies. All samples were investigated regarding Cy5 fluorescence before and after the release was accomplished resulting in a percentage amount of released genetic material. The measurements show a release of around 40% of the initially bound DNA at a temperature of 65 °C or above representing ideal conditions for PCR experiments, since the temperature in the amplification cycles varies between 57 and 95 °C. Since no significant improvement regarding DNA binding and release is achieved by the deposition of three instead of two POx layers, further experiments were conducted using a POx double layer.

## PCR experiments

One major advantage of the presented method is the possibility of coating PP substrates enabling a larger variety in the design of analytical systems. Up to now, only two dimensional PP slides were used for polymer immobilization. For detection applications, however, it would be favorable to apply POx layers on the inside of PCR reaction vessels. For this reason, PP-tubes (RoboStrip® PP white 8 –well strips low profile) were coated using the already described procedure. The success of the coating was verified using CLSM measurements of layers deposited using polymer **3** (SI: Figure S3). However, for qPCR experiments, unlabeled polymers (**2**) were used to avoid interference with fluorescence based detection process. To demonstrate the convenience of the “Lab in a tube“-approach, qPCR assays were performed using coated PCR tubes.

In first experiments, DNA from Escherichia coli BL21 (*E. coli*) was extracted with innuPREP DNA Mini Kit (AJ Innuscreen GmbH, Berlin), bound within POx coatings for 1 h at room temperature and washed thoroughly. The DNA loaded tubes were filled with 10  $\mu$ L of qPCR master mix and subjected to qPCR. The assay detects specific gene sequences, like the LacZ- Gene as *E. coli* specific target, by the use of specific primer sequences which only bind to the desired gene. A schematic representation of the whole process is displayed in **Scheme 2**.



**Scheme 2:** Working principle of the “Lab in a tube” approach. Cells are lysed by heat treatment and genetic material is adsorbed in POx surface coatings. After addition of a specific primer, and a PCR master mix, amplification and detection is accomplished in a qPCR process.

The cycle threshold ( $c_t$ ) value of the qPCR assay shows at which cycle the DNA has reached a defined concentration providing an indication about the efficiency of the process and the amount of available template. After amplification, a positive result is reported by the melting peak of the PCR product, as detected by the use of intercalating dyes. In the case of LacZ, the melting curve of the product should exhibit a peak around 87.5 °C. This melting-point is equivalent to the expected product of 224 base pairs (GenBank sequence accession number: AM946981.2). The results of the detection of extracted *E. coli* samples are shown in **Table 3** and the amplification curves as well as melting points are depicted in the supporting information (**Figure S4**). Uncoated tubes with additional template served as a positive control, whereas, a PCR experiment without sample DNA was used as a negative control.

**Table 3:** Results of *E. coli* detection from extracted DNA using the LacZ-Gene as target. The amount of bound DNA within the POx coatings could not be determined.

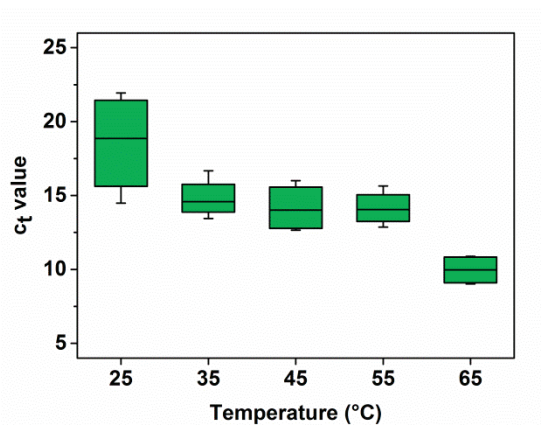
Template	Sample	Amount of DNA (ng)	Melting point (°C)	Mean $c_t$ value	Sample count
<i>E. coli</i>	Positive control	0.6	87.3	16.4	3
	Negative control	0	-	-	3
	Surface bound	n. d.	87.5	20.5	4
<i>E. coli</i> + Herring testes	Positive control	1	87.5	13.7	3
	Negative control	0	-	-	4
	Surface bound	n. d.	87.2	20	4

The qPCR result of surface bound DNA is positive for the specific *E. coli*-target and the amplicon shows the same characteristic melting point as the positive control. Also the assay is able to detect *E. coli* DNA in the presence of a background of Herring testes DNA, proving the working principle in the presence of undesired genetic material.

However, for an easy and cost-effective sample analysis it is necessary to bind DNA directly from a cell lysate instead of using already purified genetic material. Consequently, the



presence of other (charged) cellular components has to be tolerated. Therefore, an *E. coli* suspension ( $1.36 \times 10^9$  cfu mL<sup>-1</sup>) was incubated for 10 min at 95 °C to lyse the cells by heat induction. Each 50 µL of this cell lysate were filled in POx modified tubes and incubated for 1 h. To investigate the influence of temperature to the binding behavior during the incubation, the tubes were incubated at 25, 35, 45, 55 and 65 °C (incubation performed on BioShake iQ with adapter for 96 × 0.2 mL tubes) and the supernatant solution was removed at the specific temperature. Every incubation temperature step was tested positive for *E. coli* DNA with a melting point around 87.3 °C with no detectable melting point on negative control (**Figure 6**).



**Figure 6:** Box-plot of qPCR experiments, performed in POx coated reaction vessels. The tubes were loaded with genetic material from cell lysates at different temperatures and the  $c_t$  value of the amplification was recorded.

As shown in the box-plot the  $c_t$  values of the qPCR decrease with increasing temperature which indicates a faster amplification process. Generally, the  $c_t$  value is dependent on the amount of accessible template (a higher initial DNA concentrations leads to lower values) and the presence of inhibitors which increase the  $c_t$  value by lowering the efficiency of the reaction. Since the amount of bound DNA is not increasing at higher temperatures (Figure 5B) the latter reason is presumably responsible for the faster amplification. A further indication is given by a narrowing of the value distribution at higher temperatures.

To explain this behavior, the complex composition of the cell lysate can be accounted. While DNA has a high density of negative charge, also other former cell components have potentially negative charges and can interact with the POx layers. The presence of these

compounds leads to a disturbance or inhibition of the PCR process, resulting in high  $c_t$  values. However, the binding affinity of negatively charged material decreases with increasing temperature, as already demonstrated by temperature dependent release studies (Figure 5B). It is likely that these compounds are released from the POx layers at lower temperatures than the DNA with its multiple negative charges. At 65 °C, the majority of contaminants are present unbound in solution and can be washed away while a considerable amount of genetic material is still adsorbed to the polymer layers, accessible for a subsequent amplification. The performed experiments demonstrate the suitability of POx modified surfaces for a qPCR detection of DNA. Due to the compatibility of the modified PP surface with the qPCR process a combination of sample purification and detection in a single tube or cavity is possible.

### 3. Conclusion

We demonstrated the production of a poly(2-oxazoline) (POx)-based separation and detection system for pathogen analysis without prior purification steps. Covalent amine containing POx multilayers were deposited on PP substrates in a layer-by-layer process. The affinity of DNA to the surface coatings was studied in detail and the binding and release was found to be temperature dependent. PCR tubes, coated with POx were used to bind and purify DNA directly from cell lysates and the amplification of genetic material can be accomplished directly from the adsorbed DNA templates. Moreover, detection can be performed using a qPCR assay. The presented system displays an easy and elegant way to collect sample DNA from biological materials, as well as to perform purification, amplification and detection within just one coated PCR tube. The method is likewise effective and easy-to-use while requiring only low amounts of functional polymer coating. The straight forward preparation of the layer system and the cost efficiency of the support material should enable for large scale production and automation of detection processes. For this reason, this “lab-in-a-tube” displays a promising tool for bioanalytics. Further studies have to show how reliable the

method is concerning varying samples sources, primers and in which concentration ranges a successful detection is possible.

#### 4. Experimental Section

##### *Material and instrumentation*

All chemicals were purchased from Sigma-Aldrich and Merck. 2-Ethyl-2-oxazoline (EtOx) and methyl tosylate (MeTos) were distilled to dryness under argon atmosphere prior to usage. PCR ingredients, as well as polypropylene (PP) substrates were provided by Analytik Jena. PP slides (1 × 3 cm) were used for optimization of the coating procedure and verification of the LbL deposition (CA and CLSM measurements). Round PP-chips with a diameter of 0.5 cm were utilized for TGA investigations as well as DNA binding and release studies. For PCR experiments, PCR-tubes (RoboStrip® PP white 8-well strips low profile) were coated on the inside. 2-(4-((*tert*-Butoxycarbonyl)amino)butyl)-2-oxazoline (BocOx) was synthesized according to a published procedure.<sup>[15]</sup>

The polymerization was performed under microwave irradiation, using an Initiator Sixty single-mode microwave synthesizer from Biotage, equipped with a noninvasive IR sensor (accuracy: 2%). Microwave vials were heated overnight to 100 °C under vacuum and allowed to cool to RT under argon before usage. Polymerizations were performed under temperature control.

Size-exclusion chromatography (SEC) of the protected statistic copolymers was performed on a Shimadzu system equipped with a SCL-10A system controller, a LC-10AD pump, a RID-10A refractive index detector and a PSS SDV column with chloroform-triethylamine(TEA)-2-propanol (94:4:2) as eluent. The column oven was set to 50 °C.

SEC measurements of the deprotected statistic copolymers and the fluorescently labeled macromolecules were accomplished on a Shimadzu system equipped with a LC-10AD pump, a RID-10A refractive index detector, a degasser DGU-14A, and a CTO-10A column oven

utilizing *N,N*-dimethylacetamide with  $2.1 \text{ g L}^{-1}$  LiCl as eluent. The column oven was set to  $50 \text{ }^{\circ}\text{C}$ . Poly(styrene) (PS) samples were used as calibration standards for both solvent systems. Proton NMR spectroscopy ( $^1\text{H-NMR}$ ) measurements were performed at RT on a Bruker AC 300 MHz spectrometer, using  $\text{CDCl}_3$  or  $\text{D}_2\text{O}$  as solvents. The chemical shifts are given in ppm relative to the signal from the residual non-deuterated solvent.

Absorption and emission spectra of the fluorescently labeled POxs were recorded using the Tecan M200 Pro fluorescence microplate reader (Crailsheim, Germany) at wavelengths from  $\lambda = 350$  to  $800 \text{ nm}$ .

Fluorescence images were obtained using a confocal laser-scanning microscope (CLSM 510 Meta, Zeiss, Jena, Germany), equipped with a  $10 \times$  objective. Fluorescein-labeled polymers were excited with the  $488 \text{ nm}$  line of the argon laser. The emitted fluorescence was collected using a  $505$  to  $530 \text{ nm}$  band-pass filter. Scans for the rhodamine-labeled polymers were accomplished using the  $543 \text{ nm}$  line of the He/Ne laser. The fluorescent emission was recorded with a  $560$  to  $615 \text{ nm}$  band-pass filter. To excite the Cy5-labeled DNA, the He/Ne  $633 \text{ nm}$  laser was used. Fluorescence was recorded using a  $650 \text{ nm}$  long-pass filter. To allow a comparison, all images were captured under identical conditions and instrument settings (laser power, pinhole diameter and detector gain). Quantitative image analysis was performed on grayscale converted images using the ImageJ software.

The hydrophilicity of the substrate surfaces was determined using a contact angle measuring system (OCA 30, Dataphysics, Germany) with droplets of distilled water having a volume of about  $10 \text{ }\mu\text{L}$ . The measurements were performed in triplicates on different positions of the surface area of the substrates at RT.

Thermo-gravimetric analysis (TGA) was performed under a nitrogen atmosphere on a Netzsch TG 209 F1 Iris in the range from RT to  $800 \text{ }^{\circ}\text{C}$  with a heating rate of  $10 \text{ K min}^{-1}$ . The amount of surface bound POx was calculated at a temperature of  $280 \text{ }^{\circ}\text{C}$  comparing uncoated and coated samples.

The Reflectometric interference spectroscopy (BIAffinity®) the swelling and DNA binding measurements were accomplished in a new set up, the parallel flow device (Analytik Jena AG), using a flow rate for polymer swelling of  $20 \mu\text{L min}^{-1}$  and for the gDNA binding a flow rate of  $5 \mu\text{L min}^{-1}$  at room temperature. During DNA binding experiments  $100 \mu\text{L}$  of a gDNA *Escherichia coli* BL21 solution ( $100 \text{ ng } \mu\text{L}^{-1}$ ) was injected and channeled in Channel 1 over the coated chip surface and in Channel 2 over the coated chip surface parallel with pure water. The residual DNA content was determined by UV/VIS spectroscopy (ScanDrop®250).

#### *Synthesis of P(EtOx<sub>35</sub>-stat-BocOx<sub>11</sub>) (1)*

In a microwave vial EtOx ( $35.3 \mu\text{L}$ ,  $0.35 \text{ mmol}$ ), MeTos ( $17.7 \mu\text{L}$ ,  $0.12 \text{ mmol}$ ), and acetonitrile ( $2.6 \text{ mL}$ ) were mixed under inert conditions. After heating in the microwave synthesizer at  $140 \text{ }^\circ\text{C}$  for  $19 \text{ min}$  EtOx ( $530 \mu\text{L}$ ,  $5.95 \text{ mmol}$ ) and BocOx ( $350 \mu\text{L}$ ,  $0.70 \text{ mmol}$ ) were added under inert conditions and the reaction mixture was heated to  $140 \text{ }^\circ\text{C}$  for another  $13 \text{ min}$ . The solution was diluted in  $\text{CH}_2\text{Cl}_2$  ( $10 \text{ mL}$ ) and precipitated in cold diethyl ether ( $300 \text{ mL}$ ). The white solid was filtered off and dried in high vacuum to obtain the product as a white powder ( $810 \text{ mg}$ ,  $88\%$ ).

$^1\text{H NMR}$  ( $\text{CDCl}_3$ ,  $300 \text{ MHz}$ ):  $\delta = 4.99$  (s,  $0.2 \text{ H}$ , NH),  $3.45$  (s,  $4 \text{ H}$ , backbone),  $3.11$  (s,  $0.3 \text{ H}$ ,  $\text{CH}_2\text{-CH}_2\text{-NH}$  (BocOx)),  $2.40$  (s,  $1.9 \text{ H}$ ,  $\text{CH}_2$  (EtOx)),  $1.92$  (s,  $0.3 \text{ H}$ ,  $\text{CH}_2\text{-CH}_2\text{-CO}$  (BocOx)),  $1.64$  (s,  $0.3 \text{ H}$ ,  $\text{CH}_2\text{-CH}_2\text{-CH}_2$  (BocOx)),  $1.53$  (s,  $0.3 \text{ H}$ ,  $\text{CH}_2\text{-CH}_2\text{-CH}_2$  (BocOx)),  $1.42$  (s,  $\text{CH}_3$  (BocOx)),  $1.21$  (s,  $1.3 \text{ H}$ ,  $\text{CH}_3$  (EtOx)) ppm.

SEC (eluent:  $\text{CHCl}_3$ -*i*-propanol-TEA, PS-standard):  $M_n = 4,600 \text{ g mol}^{-1}$ ,  $M_w = 6,000 \text{ g mol}^{-1}$ ,  $\text{Đ} = 1.30$ .

#### *Synthesis of P(EtOx<sub>37</sub>-stat-AmOx<sub>9</sub>) (2)*

$10 \text{ mL}$  of Trifluoro acetic acid (TFA) were added to solid P(EtOx<sub>37</sub>-stat-BocOx<sub>11</sub>) ( $810 \text{ mg}$ ), heated to  $60 \text{ }^\circ\text{C}$  and stirred for  $1 \text{ h}$ . Subsequently, the solution was cooled to RT, stirred for



another 12 h and was diluted by the addition of 10 mL methanol (MeOH) followed by precipitation in cold diethyl ether (500 mL). The white solid was filtered and re-dissolved in MeOH (50 mL). Amberlyst© A21 free base was added and the mixture was stirred at RT for 24 h. The solid phase was filtered off and the solvent was evaporated under reduced pressure. The product was obtained as a slightly yellow powder (450 mg, 60%).

$^1\text{H-NMR}$  ( $\text{D}_2\text{O}$ , 300 MHz):  $\delta = 3.48$  (s, 4 H, backbone), 2.98 (0.23 H, s,  $\text{CH}_2\text{-CH}_2\text{-NH}_2$ ), 2.23 (2 H, s,  $\text{CH}_2$  (EtOx) +  $\text{CH}_2\text{-CH}_2\text{-CO}$  (AmOx)), 1.53 (0.41 H, s,  $\text{CH}_2\text{-CH}_2\text{-CH}_2\text{-CH}_2$  (AmOx)) 1.11 (2.8 H, s,  $\text{CH}_3$  (EtOx)) ppm.

SEC (eluent: DMAc-LiCl, PS-standard):  $M_n = 9,300 \text{ g mol}^{-1}$ ,  $M_w = 12,000 \text{ g mol}^{-1}$ ,  $\text{Đ} = 1.13$ .

*Fluorescent labeling of P(EtOx<sub>37</sub>-stat-AmOx<sub>9</sub>) (2) with fluorescein-5-N-hydroxysuccinimide ester (Fluorescein-NHS-ester) (3)*

P(EtOx<sub>37</sub>-stat-AmOx<sub>9</sub>) (**2**, 1.35 g, 0.24 mmol) was dissolved in DMF (50 mL) followed by the addition of the fluorescein-NHS-ester (112 mg, 0.24 mmol) and TEA (2.5 mL, 18 mmol). The reaction mixture was stirred at RT for 3 h. Subsequently, the solvent was evaporated and the crude product was re-dissolved in MeOH (10 mL). The polymer was precipitated in cold diethyl ether (800 mL), filtered and re-dissolved in MeOH (50 mL). The solvent was evaporated and the product was obtained as yellow powder (1.17 g, 80%).

$^1\text{H-NMR}$  ( $\text{D}_2\text{O}$ , 300 MHz):  $\delta = 6.60 - 6.78$  (m, 4.7 H, dye), 3.48 (s, 4 H, backbone), 2.98 (0.23 H, s,  $\text{CH}_2\text{-CH}_2\text{-NH}_2$ ), 2.23 (2 H, s,  $\text{CH}_2$  (EtOx) +  $\text{CH}_2\text{-CH}_2\text{-CO}$  (AmOx)), 1.53 (0.41 H, s,  $\text{CH}_2\text{-CH}_2\text{-CH}_2\text{-CH}_2$  (AmOx)) 1.11 (2.8 H, s,  $\text{CH}_3$  (EtOx)) ppm..

SEC (eluent: DMAc-LiCl, PS-standard):  $M_n = 11,000 \text{ g mol}^{-1}$ ,  $M_w = 13,000 \text{ g mol}^{-1}$ ,  $\text{Đ} = 1.16$

*Fluorescent labeling of P(EtOx<sub>37</sub>-stat-AmOx<sub>9</sub>) (2) with Rhodamine B iso-thiocyanate (4)*

P(EtOx<sub>37</sub>-stat-AmOx<sub>9</sub>) (**2**, 300 mg, 0.05 mmol) was dissolved in DMF (20 mL). After addition of rhodamine B iso-thiocyanate (26.1 mg, 0.05 mmol), the reaction was stirred at RT

for 48 h. Subsequently, the solvent was evaporated and the crude product was re-dissolved in MeOH (10 mL). The polymer was precipitated in cold diethyl ether (800 mL), filtered and re-dissolved in MeOH (50 mL). After evaporation of the solvent, the crude product was purified *via* preparative size exclusion chromatography (SEC) using bio beads SX-1 and DMF used as eluent. The product was obtained as a pink powder (280 mg, 86%).

$^1\text{H-NMR}$  ( $\text{D}_2\text{O}$ , 300 MHz):  $\delta = 6.70 - 6.88$  (m, 0.3 H, aromatic peaks), 3.48 (s, 133.2 H, backbone), 1.56 (s, 37.7 H,  $\text{CH}_2$  (AmOx)), 1.11 (s, 111.0 H,  $\text{CH}_3$  (EtOx)) ppm.

SEC (eluent: DMAc-LiCl, PS-standard):  $M_n = 12,000 \text{ g mol}^{-1}$ ,  $M_w = 14,000 \text{ g mol}^{-1}$ ,  $\text{Đ} = 1.19$ .

### *Surface coating*

PP slides ( $3 \times 1 \text{ cm}$ ), PP Chips (diameter = 0.5 cm) and PCR tubes were washed in a water/ethanol (EtOH) mixture (1:1) for 24 h. The dried material was treated with  $\text{O}_2$  plasma for 30 min. Subsequently, the slides were incubated in an excess of 3-glycidoxypropyltrimethoxysilane (GOPTMS) molten on the substrates at RT for 1 h and cleaned by washing with DMF repeatedly.

The epoxide functionalized PP was coated in a layer-by-layer (LbL) approach. First, the substrates were incubated in a POx solution (10 wt%, DMF) at  $50 \text{ }^\circ\text{C}$  for 1 h and washed with DMF to create the first polymer. Subsequently, the material was incubated in an ECH solution (1 wt%, DMF) at  $50 \text{ }^\circ\text{C}$  for 1 h and washed with DMF as well as water. Afterwards, the slides were incubated in an aqueous sodium hydroxide solution (5 wt%) at  $50 \text{ }^\circ\text{C}$  for 1 h and washed with water and DMF. This cycle was repeated, until the desired amount of POx layers were deposited on the glass slides.

The same procedure was used for BIAffinity® glass slides (10 mm  $\times$  10 mm; thickness: 1.1 mm; single-sided coated with  $\text{Ta}_2\text{O}_5$ ).

### *DNA binding and release*

DNA binding and release experiments were performed using Cy5-labeled lacZ amplicates that were synthesized by standardized PCR experiments from lacZ transfected *Escherichia coli* BL21 using Cy5-labeled primers (SI). All experiments were conducted using PP chips coated with one, two or three POx layers. In each case the first polymer layer was fluorescein labeled (polymer 3). 15  $\mu\text{L}$  of a DNA solution containing 100  $\text{ng } \mu\text{L}^{-1}$  Cy5 labeled lacZ DNA was added to the POx coated PP chips and incubated at RT for different times (10 s, 30 s, 2 min, 5 min, 1 h, 2 h). Afterwards, the chips were washed with water ( $5 \times 500 \mu\text{L}$ ) and dried using compressed air. Subsequently, the mean fluorescence was determined by LSM measurements ( $\lambda_{\text{ex}} = 633 \text{ nm}$ ,  $\lambda_{\text{em}} \geq 650 \text{ nm}$ ).

For release, the PP chips were loaded with DNA as described above for 1 h and, subsequently, incubated in water for 1 h at different temperatures. After separation from the solution and drying using compressed air, the mean fluorescence was determined *via* CLSM ( $\lambda_{\text{ex}} = 633 \text{ nm}$ ,  $\lambda_{\text{em}} \geq 650 \text{ nm}$ ) before and after treatment and the relative DNA release was determined by comparison of the two values.

### *PCR experiments*

The qPCR assay was designed to detect DNA of *E. coli* in a POx coated and uncoated cavities. Therefore, every qPCR experiment had a minimum three PP POx modified tubes with qPCR master mix and no template as negative control and 1  $\mu\text{L}$  of DNA extract out of  $10^7 \text{ cfu mL}^{-1}$  *E. coli* as positive control. The qPCR master mix contains: 3 mmol of  $\text{MgCl}_2$ , 1  $\times$  Hot Start Buffer w/o  $\text{MgCl}_2$  pH 8.5, 0.1 mmol dNTPs each, 0.025  $\text{U } \mu\text{L}^{-1}$  InnuTaq HOT-A DNA Polymerase (provided by AJ Innuscreen GmbH, Berlin, 1  $\times$  EvaGreen (Jena BioScience GmbH, Jena), 1  $\mu\text{mol}$  Primer each (Eurofins Genomics, Ebersberg), 3% DMSO (Carl Roth GmbH + Co. KG, Karlsruhe). The qPCR protocol was optimized for sensitivity and specificity up to  $<10^1 \text{ cfu}$  (data not shown). For amplification an initial denaturation for 2 min

at 95 °C was followed by 10 cycles 95 °C for 5 s, 72 °C for 15s and 30 cycles 95 °C for 5 s, 67 °C for 5 s, 72 °C for 10 s with one final amplification of 2 min at 72 °C. The qPCR products were analyzed by melting curve measurements with a temperature range from 60 to 95 °C. The whole qPCR was performed using a TOptical Gradient Thermocycler (Biometra GmbH, Göttingen)

**Table 4:** Used primer sequences.

Label	Target	Sequence	nt	GC (%)	T <sub>m</sub> (°C)
SekuL ZF	LacZ	5'-cgcagcctgaatggcgaatg-3'	20	60	61.4
SekuL ZR	LacZ	5'-gtgagcgagtaacaaccgctcg-3'	22	59.1	64.0

### Supporting Information

Supporting Information is available from the Wiley Online Library or from the author.

Figure S1: SEC traces of labeled polymers, Figure S2: TGA graphs of coated and uncoated substrates, Table S1: CA values for coatings on glass, Figure S3: CLSM pictures of coated PCR tubes, Experimental detail for the synthesis of Cy5 labeled DNA strands. Figure S4: Amplification curves and melting points of qPCR assays using *E. Coli* + Herring testes.

### Acknowledgements

The authors gratefully acknowledge the Bundesministerium für Bildung und Forschung (Germany) for funding (project: BASIS, 03WKCB01C). We thank to Renzo Paulus for TGA measurements and Stephanie Höppener for helpful discussions. ‡M. N. Leiske and M. Hartlieb contributed equally to this work.

Received: ((will be filled in by the editorial staff))

Revised: ((will be filled in by the editorial staff))

Published online: ((will be filled in by the editorial staff))

### References

- [1] a) A. Moody, *Clin. Microbiol. Rev.* **2002**, *15*, 66; b) B. C. Ross, L. Marino, F. Oppedisano, R. Edwards, R. M. Robins-Browne, P. D. Johnson, *J. Clin. Microbiol.* **1997**, *35*, 1696; c) A. J. Herring, N. F. Inglis, C. K. Ojeh, D. R. Snodgrass, J. D. Menzies, *J. Clin. Microbiol.* **1982**, *16*, 473.
- [2] M. Bally, M. Graule, F. Parra, G. Larson, F. Hook, *Biointerphases* **2013**, *8*, 4.
- [3] P. L. Kole, G. Venkatesh, J. Kotecha, R. Sheshala, *Biomed. Chromatogr.* **2011**, *25*, 199.
- [4] a) K. Zro, S. Azelmat, Y. Bendouro, J. H. Kuhn, E. El Fahime, M. M. Ennaji, *J. Virol. Methods* **2014**, *204*, 38; b) N. C. Engleberg, B. I. Eisenstein, *Annu. Rev. Med.* **1992**, *43*, 147.

- [5] A. T. Press, A. Traeger, C. Pietsch, A. Mosig, M. Wagner, M. G. Clemens, N. Jbeily, N. Koch, M. Gottschaldt, N. Bézière, V. Ermolayev, V. Ntziachristos, J. Popp, M. M. Kessels, B. Qualmann, U. S. Schubert, M. Bauer, *Nat Commun* **2014**, *5*.
- [6] A. Sassolas, B. D. Leca-Bouvier, L. J. Blum, *Chem. Rev.* **2007**, *108*, 109.
- [7] L. Schwenkbier, S. König, S. Wagner, S. Pollok, J. Weber, M. Hentschel, J. Popp, S. Werres, K. Weber, *Microchim. Acta* **2014**, *181*, 1669.
- [8] a) C. W. Price, D. C. Leslie, J. P. Landers, *Lab Chip* **2009**, *9*, 2484; b) R. M. McCormick, *Anal. Biochem.* **1989**, *181*, 66.
- [9] A. Paterson, C. Brubaker, J. Wendel, *Plant Mol. Biol. Rep.* **1993**, *11*, 122.
- [10] P. Chomczynski, N. Sacchi, *Anal. Biochem.* **1987**, *162*, 156.
- [11] J. M. Bienvenue, N. Duncalf, D. Marchiarullo, J. P. Ferrance, J. P. Landers, *J. Forensic Sci.* **2006**, *51*, 266.
- [12] a) C. R. Reedy, C. W. Price, J. Sniegowski, J. P. Ferrance, M. Begley, J. P. Landers, *Lab Chip* **2011**, *11*, 1603; b) J. Lunt, *Polym. Degrad. Stab.* **1998**, *59*, 145.
- [13] J. M. Pollino, M. Weck, *Chem. Soc. Rev.* **2005**, *34*, 193.
- [14] L. Zhai, R. L. Pilston, K. L. Zaiger, K. K. Stokes, R. D. McCullough, *Macromolecules* **2002**, *36*, 61.
- [15] M. Hartlieb, D. Pretzel, K. Kempe, C. Fritzsche, R. M. Paulus, M. Gottschaldt, U. S. Schubert, *Soft Matter* **2013**, *9*, 4693.
- [16] M. Hartlieb, D. Pretzel, C. Englert, M. Hentschel, K. Kempe, M. Gottschaldt, U. S. Schubert, *Biomacromolecules* **2014**, *15*, 1970.
- [17] C. Englert, L. Tauhardt, M. Hartlieb, K. Kempe, M. Gottschaldt, U. S. Schubert, *Biomacromolecules* **2014**, *15*, 1124.
- [18] L. Tauhardt, K. Kempe, M. Gottschaldt, U. S. Schubert, *Chem. Soc. Rev.* **2013**, *42*, 7998.
- [19] K. B. Mullis, H. A. Erlich, N. Arnheim, G. T. Horn, R. K. Saiki, S. J. Scharf, *US4683195 A*, 1987.
- [20] a) M. A. Innis, K. B. Myambo, D. H. Gelfand, M. A. Brow, *Proc. Natl. Acad. Sci.* **1988**, *85*, 9436; b) R. Saiki, D. Gelfand, S. Stoffel, S. Scharf, R. Higuchi, G. Horn, K. Mullis, H. Erlich, *Science* **1988**, *239*, 487; c) A. M. Wang, M. V. Doyle, D. F. Mark, *Proc. Natl. Acad. Sci.* **1989**, *86*, 9717.
- [21] B. I. Eisenstein, *N. Engl. J. Med.* **1990**, *322*, 178.
- [22] N. Wellinghausen, C. Frost, R. Marre, *Appl. Environ. Microbiol.* **2001**, *67*, 3985.
- [23] J. Ning, J. Liebich, M. Kästner, J. Zhou, A. Schäffer, P. Burauel, *Appl. Microbiol. Biotechnol.* **2009**, *82*, 983.
- [24] L. Tauhardt, M. Frant, D. Pretzel, M. Hartlieb, C. Bucher, G. Hildebrand, B. Schroter, C. Weber, K. Kempe, M. Gottschaldt, K. Liefelth, U. S. Schubert, *J. Mater. Chem. B* **2014**, *2*, 4883.
- [25] K. T. Lee, J. M. Goddard, J. H. Hotchkiss, *Packag. Technol. Sci.* **2009**, *22*, 139.
- [26] O. Birkert, G. Gauglitz, *Anal. Bioanal. Chem.* **2002**, *372*, 141.





## Supporting Information

**Lab in a tube: Purification, amplification and detection of DNA using poly(2-oxazoline) multilayers**

Meike N. Leiske,<sup>‡</sup> Matthias Hartlieb,<sup>‡</sup> Christian Paulenz, David Pretzel, Martin Hentschel, C. Englert, Michael Gottschaldt, Ulrich S. Schubert,\*

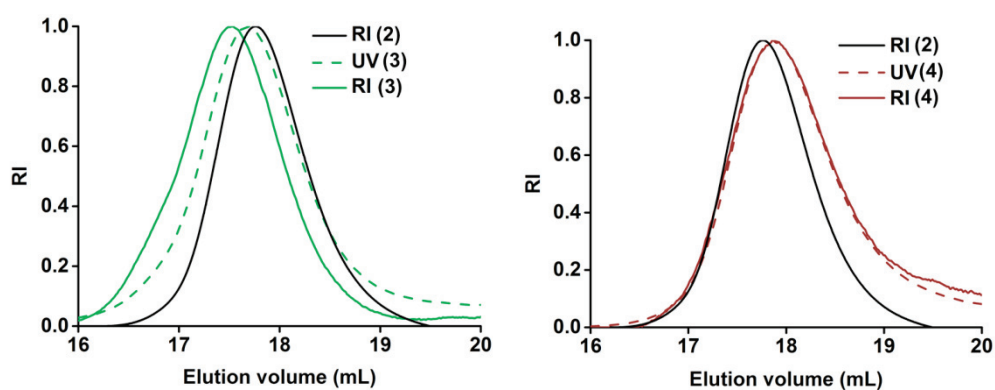


Figure S1: SEC elugrams of labeled polymers (3 and 4) in comparison to the unlabeled starting material (2).

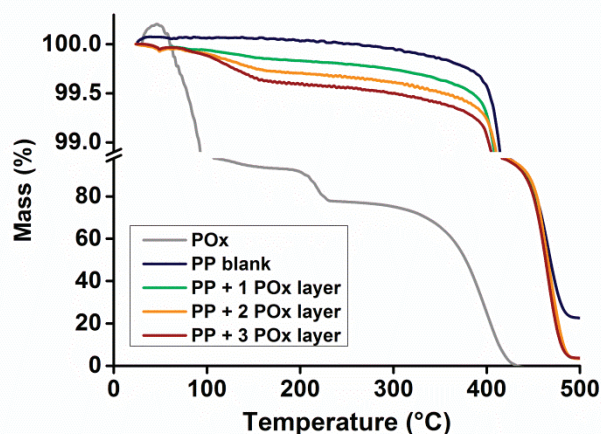


Figure S2: TGA graphs of uncoated PP, pure POx, as well as substrates coated with one, two or three layers of POx.

Table S1: CA values for POx deposition on biaffinity glass. \* CA values below 20 ° cannot be measured and are, therefore, specified as < 20 °.

Coating step	CA (°)
Blank	59
O <sub>2</sub> plasma	< 20*
GOPTMS	43
1 <sup>st</sup> POx layer	< 20*
ECH-XL	43
2 <sup>nd</sup> POx layer	< 20*
ECH-XL	44
3 <sup>rd</sup> POx-layer	< 20*

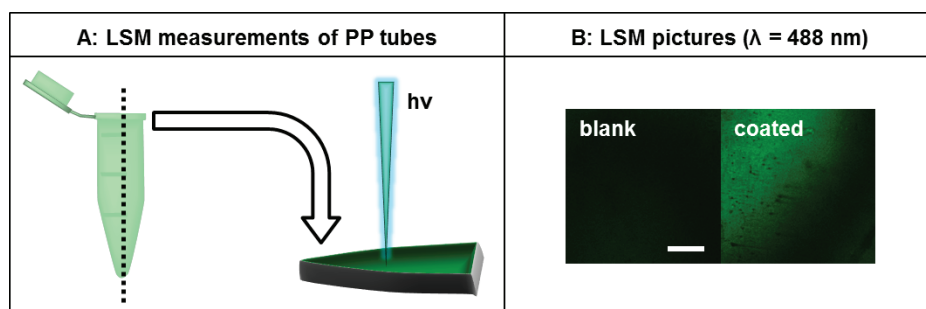


Figure S3: CLSM measurements ( $\lambda_{\text{ex}} = 488 \text{ nm}$ ,  $\lambda_{\text{em}}: 505 \text{ to } 530 \text{ nm}$ ) of coated PCR Tubes. A) Scheme of the bisection of PP PCR tubes and measurement on the inner wall; B) comparison of emission between blank value and POx coated tube (scale bar: 200  $\mu\text{m}$ ).

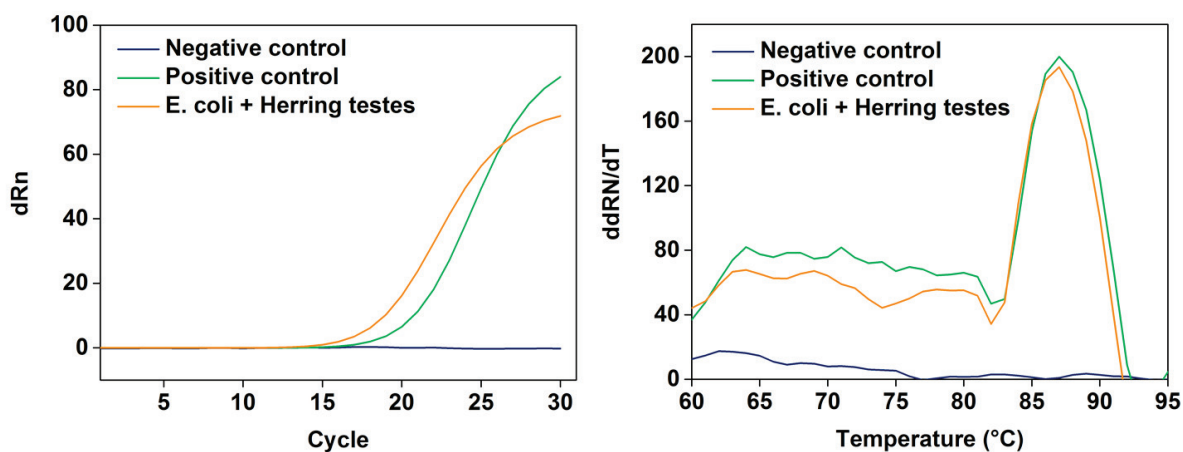


Figure S4: Amplification curves and melting points of qPCR assays using *E. Coli* + Herring testes.

*PCR of DNA from lacZ transfected Escherichia coli BL21*

Target	Sequence	Product size (base pairs)	Label
LacZ	5'-Cy5-GGA TTG ACC GTA ATG GGA TAG-3'	228	Cy5
LacZ	5'-biotin-CTG GCG TAA TAG CGA AGA GG-3'	228	Biotin

DNA was isolated using the innuPREP DNA/RNA Mini Kit, according to the manufacturer's instructions (Analytik Jena AG). An *E. coli* BL21 pellet was re-suspended in 100  $\mu$ L TE-buffer to induce cell lysis. Subsequently, 450  $\mu$ L lysis buffer RL were added and the mixture was incubated at room temperature for 3 min. The mixture was centrifuged at 14,000 rpm for 1 min to separate the lysed from the unlysed parts. A spin filter D was placed on a receiver tube, the supernatant was added and centrifuged at 12,000 rpm for 2 min. 500  $\mu$ L HS washing solution was added and the mixture was centrifuged for at 12,000 rpm for 1 min. Afterwards, 700  $\mu$ L lysis buffer were added and the combined solution was centrifuged at 12,000 rpm for 1 min. The filtrate was discarded and the spin filter D containing the extract was added to another receiver tube and centrifuged at 14,000 rpm for another 2 min. Subsequently, a spin filter D was added to an elution tube and, after addition of 100  $\mu$ L elution buffer, it was incubated at room temperature for 1 min. The mixture was centrifuged at 8,000 rpm for 1 min to obtain the DNA extract into the elution tube. Finally, the DNA concentration was determined via UV/VIS spectroscopy (ScanDrop<sup>®</sup>250) ( $\lambda_{1,ex} = 260$  nm,  $\lambda_{2,ex} = 280$  nm).

The PCR assay was carried out in a 50  $\mu$ L reaction mixture containing the following compounds: DNA extract (0.5  $\mu$ L of  $\sim 10$  ng  $\mu$ L<sup>-1</sup>), 1.00 units Taq DNA polymerase (AJ innuTaq DNA polymerase), 0.25 mM desoxy-nucleotriphosphates (dNTPs), 0.5  $\mu$ M of each primer. The PCR was started with an initial denaturation for 3 min at 95 °C followed by 45 cycles with 95 °C for 30 s (denaturation), 57 °C for 30 s (annealing) and 72 °C for 30 s (amplification). At the end of the repeated PCR cycles, the mixture was heated to 72 °C for another 5 min to ensure the completion of the amplicates elongation. The purity of the crude PCR product was controlled by gel electrophoresis, which was performed

using a 2% agarose gel containing GelRed (1:25,000). The gels were run for 30 min at 100 V with TAE-buffer, which consists of Tris acetate ( $2 \text{ mol L}^{-1}$ ) and EDTA ( $0.05 \text{ mol L}^{-1}$ ), dissolved in deionized water and has a pH value of 8.2 to 8.4 at RT. The gels were imaged on a UV transilluminator (AJ Biometra UVsolo TS).

All PCR and qPCR products were purified using the innuPREP PCRpure Kit, according to the manufacturer's instructions (Analytik Jena). 500  $\mu\text{L}$  binding buffer were added to a spin filter positioned on an elution tube and then spin coated at 12,000 rpm for 2 min. Subsequently, the spin filter was placed into a receiver tube, 10  $\mu\text{L}$  of elution buffer were added and incubated at RT for 1 min, before spin coating at 8,000 rpm for 1 min. Finally, the DNA concentration was determined *via* UV/VIS spectroscopy (ScanDrop<sup>®</sup> 250) ( $\lambda_{1, \text{ex}} = 260 \text{ nm}$ ,  $\lambda_{2, \text{ex}} = 280 \text{ nm}$ ). Since the generated PCR products contained both, biotin- and Cy5-labeled DNA, the biotin-labeled DNA amplicates could be used for the horseradish peroxidase assay and the Cy5-labeled DNA sequences for DNA binding and release determinations based on the DNA derived fluorescence emission intensity.

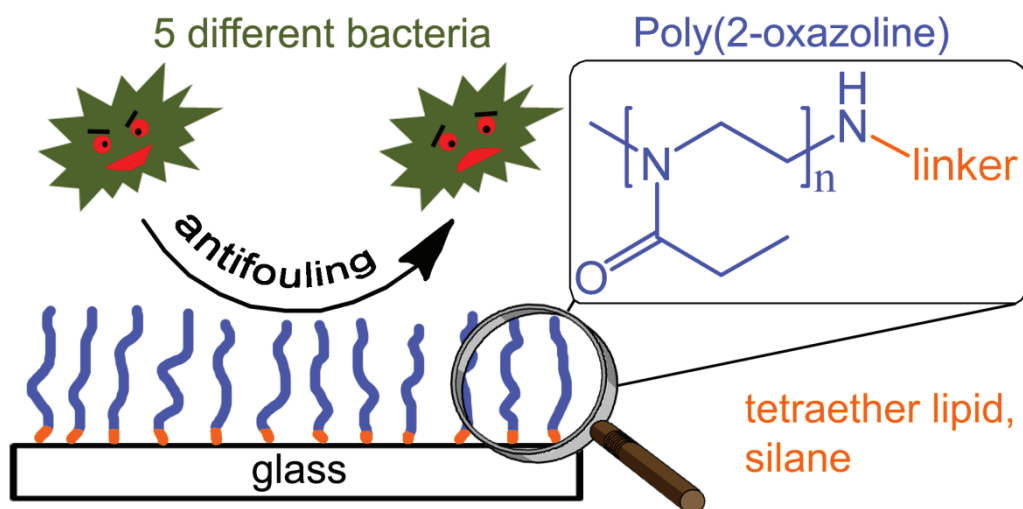


## Publication 7

“Amine end-functionalized poly(2-ethyl-2-oxazoline) as promising coating material for antifouling applications”

L. Tauhardt, M. Frant, D. Pretzel, M. Hartlieb, C. Bucher, G. Hildebrand, B. Schröter, C. Weber, K. Kempe, M. Gottschaldt, K. Liefeth, U. S. Schubert

*J. Mater. Chem. B* **2014**, *2*, 4883-4893.



## Amine end-functionalized poly(2-ethyl-2-oxazoline) as promising coating material for antifouling applications†

Cite this: *J. Mater. Chem. B*, 2014, 2, 4883

Lutz Tauhardt,<sup>ab</sup> Marion Frant,<sup>c</sup> David Pretzel,<sup>ab</sup> Matthias Hartlieb,<sup>ab</sup> Christian Bücher,<sup>c</sup> Gerhard Hildebrand,<sup>c</sup> Bernd Schröter,<sup>d</sup> Christine Weber,<sup>ab</sup> Kristian Kempe,<sup>‡ab</sup> Michael Gottschaldt,<sup>ab</sup> Klaus Liefeth<sup>c</sup> and Ulrich S. Schubert<sup>\*abe</sup>

The antifouling behavior of different poly(2-ethyl-2-oxazoline) (PEtOx) coatings was investigated under "real live" conditions. Amine end-functionalized PEtOx of different molar masses have been prepared using a new and straightforward, two step synthesis method. Subsequently, the PEtOx were attached to glass surfaces via a tetraether lipid and a common silane, respectively. The polymers and coatings were characterized using techniques such as <sup>1</sup>H NMR spectroscopy and MALDI-TOF-MS as well as XPS and contact angle measurements. In a next step, the coatings were exposed to the simultaneous attack of five different bacteria in synthetic river water. A clear reduction of the biofilm formation was observed. In addition, the stability of the coatings against thermal, mechanical, and chemical stress was studied.

Received 5th February 2014  
Accepted 27th May 2014

DOI: 10.1039/c4tb00193a

www.rsc.org/MaterialsB

### Introduction

Preventing the uncontrolled adhesion and adsorption of proteins, cells, bacteria, and other microorganisms onto surfaces, the so called fouling process, represents a major challenge for a wide range of applications such as medicine (*e.g.* medical devices, implants, drug delivery systems),<sup>1,2</sup> mobility (*e.g.* ship hull coatings),<sup>3,4</sup> food industry (*e.g.* packaging),<sup>5</sup> but also for membranes (*e.g.* in water purification systems),<sup>6</sup> microarrays, and (bio)sensors.<sup>7</sup>

In principle one can distinguish between two types of antifouling coatings: (1) bioactive coatings that cause a direct or indirect inactivation of adherent microorganisms or biofilms by either releasing an antifouling agent (*e.g.* biocides), or by killing the cells, bacteria, or microorganisms on contact using specific molecules (*e.g.* quarternized polymers), and (2) biopassive

coatings, which reduce fouling due their protein and cell repellent character without interfering with the proliferation cycle or the cell metabolism.<sup>8–10</sup> However, coatings that are bioactive or release antifouling agents suffer from a loss of activity over time. In case of bioactive coatings self-deactivation occurs due to the fact that dead cells or microorganisms adhere to the active layer, cover it and, therefore, allow the adhesion and proliferation of new cells on the cell debris.<sup>10</sup> Coatings that release antifouling agents lose their activity when all antifouling agent (*e.g.* biocide) is consumed. Moreover, they are harmful to the environment, since the released antifouling agents are not only active on the surface that should be protected and, hence, can kill in a nonselective way or accumulate in microorganisms, animals (*e.g.* fish), and plants.<sup>11,12</sup> An approach to overcome these issues is the covalent binding of the antifouling coatings onto the surface. In particular biopassive coatings are promising, since they are not self-deactivating and do not release toxic and polluting compounds. Recently published studies have led to the conclusion that materials for biopassive coating have to meet the following criteria: (1) the presence of hydrogen bond accepting and hydrophilic (polar) groups, and (2) the absence of hydrogen bond donating groups and net charges.<sup>8,13</sup> If we otherwise accept, that the formation of a hydration layer (water barrier) is a vital prerequisite to build up anti-adhesive surfaces with non-fouling properties hydrogen bond accepting groups are of the same importance as hydrogen bond donating groups.<sup>14</sup> Based on the possibility to tune their properties, polymers can be adapted to a wide range of requirements and, thus, represent an interesting class of compounds for such surface tethered antifouling coatings. A widely used polymer for biopassive and repellent coatings is poly(ethylene glycol)

<sup>a</sup>Laboratory of Organic and Macromolecular Chemistry (IOMC), Friedrich Schiller University Jena, Humboldtstr. 10, 07743 Jena, Germany. E-mail: ulrich.schubert@uni-jena.de; Fax: +49 3641 948 202

<sup>b</sup>Jena Center for Soft Matter (JCSM), Friedrich Schiller University Jena, Philosophenweg 7, 07743 Jena, Germany

<sup>c</sup>Institute for Bioprocessing and Analytical Measurement Techniques e.V. (IBA), Rosenhof, 37308 Heilbad Heiligenstadt, Germany

<sup>d</sup>Institute for Solid State Physics, Friedrich Schiller University Jena, Helmholtzweg 5, 07743 Jena, Germany

<sup>e</sup>Dutch Polymer Institute (DPI), John F. Kennedylaan 2, 5612 AB Eindhoven, The Netherlands

† Electronic supplementary information (ESI) available. See DOI: 10.1039/c4tb00193a

‡ Current address: Department of Chemical and Biomolecular Engineering, The University of Melbourne, Victoria 3010, Australia.

(PEG).<sup>8,15–18</sup> However, PEG is known to undergo degradation by (auto-)oxidation to form ethers and aldehydes, hampering its long-term application.<sup>13,19–22</sup> On this account, poly(2-oxazoline)s (POx), in particular the water soluble poly(2-methyl-2-oxazoline)s (PMeOx) and poly(2-ethyl-2-oxazoline)s (PEtOx), are investigated as alternative coating materials.<sup>13,19,23–31</sup> Compared to the synthesis of PEG by anionic polymerization, the preparation of POx by cationic ring-opening polymerization (CROP) is less labor demanding, but also yields well-defined polymers with controlled molar masses and low polydispersity index (PDI) values. Moreover, a broad variety of functional electrophilic initiators, nucleophilic terminating agents, and 2-oxazoline monomers allows the synthesis of well-defined (co)polymers and the tuning of the polymer properties.<sup>32</sup> It was shown that POx coatings have similar antifouling properties as PEG, but are stable in an oxidizing environment.<sup>13,19</sup> However, up to now all antifouling investigations on POx surfaces were performed under laboratory conditions using only a single type of protein (*e.g.* fibronectin,<sup>29,30</sup> bovine serum albumin<sup>27,28</sup>), cell (*e.g.* fibroblasts<sup>24</sup>), or bacterium (*e.g.* *E. coli*<sup>13,25,26</sup>). A review on methods to attach POx to surfaces as well the properties and applications of POx functionalized surfaces was published recently.<sup>33</sup>

The chemical long-term stability of antifouling coatings is mandatory and can be greatly improved by covalent tethering of the polymers to the surface *via* linker molecules. Recently, tetraether lipids (TEL), *i.e.* bipolar membrane spanning lipids from thermoacidophilic archaea, were presented as an interesting new class of linker molecules.<sup>34–39</sup> By a simple self-assembling process, a stable, highly ordered impermeable TEL monolayer (~4 nm) with biomembrane-like properties is formed. The covalent immobilization of this thin lipid layer on surfaces can be achieved easily when the lipid headgroups are functionalized with cyanuric chloride.<sup>35–37,39</sup> An outstanding property of TELs is their excellent stability against oxidation, acidic and basic hydrolysis as well as biodegradation, which is based on the fully saturated character of the methyl branched alkyl chains.<sup>34</sup> Moreover, biocompatibility analyses revealed that TELs are both nontoxic and immunologically inert and, additionally, exhibit antifouling activity.<sup>35–38</sup> Hence, the usage of TEL linkers to attach POx to surfaces is highly interesting.

Here, we report the antifouling behavior of amine end-functionalized PEtOx, covalently bound to glass substrates using two different methods: (1) attachment *via* epoxide ring-opening reaction of a common glycidyl ether silane tethered to the surface as described in literature, *e.g.* for PEG,<sup>15,40</sup> and (2) immobilization *via* the cyanuric chloride functionalized headgroups of a TEL linker. To this end, a new approach to synthesize amine end-functionalized POx was developed. PEtOx of different chain lengths were prepared and characterized by <sup>1</sup>H NMR spectroscopy, matrix-assisted laser desorption/ionization time of flight laser mass spectrometry (MALDI-TOF-MS), and size exclusion chromatography (SEC). The PEtOx coatings were analyzed by contact angle measurements and X-ray photoelectron spectroscopy (XPS). The subsequent antifouling investigations were performed in synthetic river water using a microbiological mixed culture consisting of five different types

of bacteria. Biofilm formation and the stability of the coatings were studied using confocal laser scanning microscopy.

## Methods and materials

### General methods and surface characterization

Used chemicals, instruments, and characterization methods are described in the ESI.†

### Synthesis of phthalimide end-capped PEtOx (1)

A solution of initiator (MeOTs), monomer (EtOx), and solvent (acetonitrile) was prepared with a total monomer to initiator ratio of  $[M]/[I] = 20, 40, 60,$  and  $80,$  respectively. The total monomer concentration was adjusted to 4 M. The solution was heated at 140 °C in a microwave synthesizer for a predetermined time. After cooling to room temperature a 2-fold excess of potassium phthalimide was added and the reaction mixture was stirred overnight at 70 °C. The reaction mixture was filtered and the solvent removed. The residue was dissolved in chloroform and washed twice with a saturated aqueous solution of NaHCO<sub>3</sub> and once with brine. The organic phase was dried over sodium sulfate. After filtration, the polymer was concentrated under reduced pressure, precipitated into ice-cold diethyl ether, and dried at 40 °C under reduced pressure.

### Synthesis of amine end-capped PEtOx (2)

Phthalimide end-capped PEtOx was dissolved in ethanol and a 10-fold excess of hydrazine monohydrate was added. The reaction mixture was heated under reflux overnight. After cooling to room temperature, a concentrated hydrochloric acid was added to adjust the pH value to 2–3. The precipitate was removed by filtration and the ethanol was evaporated. The residue was dissolved in water and aqueous sodium hydroxide solution until the pH value reached 9–10. The aqueous solution was extracted thrice with chloroform. The organic phase was dried over sodium sulfate, concentrated, and precipitated into ice-cold diethyl ether. The white precipitate was filtered off and dried at 40 °C under reduced pressure.

### Synthesis of fluorescein labeled P(EtOx-*stat*-AmOx) (Fluo-PEtOx) (5)

The starting material P(EtOx<sub>36</sub>-*stat*-AmOx<sub>4</sub>) (4) was synthesized as reported earlier.<sup>41</sup>

P(EtOx<sub>36</sub>-*stat*-AmOx<sub>4</sub>) (1 g, 242 mmol) was dissolved in DMSO (50 mL). 5(6)-Carboxyfluorescein *N*-hydroxysuccin-imide ester (114.5 mg, 242 mmol, 1 eq. per polymer chain) and TEA (2.5 mL) were added to the solution and the reaction was stirred for 3 h. Subsequently, the product was precipitated in cold diethyl ether (700 mL), filtered off, dissolved in methanol (20 mL) and precipitated again into diethyl ether (200 mL). The polymer was obtained as orange solid (1.039 g, 95%).

### Coating procedure for silane on borofloat® 33 glass slides

Prior to use, each side of the glass slides was cleaned in oxygen plasma for 15 min. In a glove box, the glass slides were treated

with (3-glycidyloxypropyl)trimethoxysilane for 1 h and subsequently rinsed with dry DMF. One side of the glass slide was covered with the respective polymer solution in DMF (200 mg mL<sup>-1</sup>) at a concentration of 3 mL cm<sup>-2</sup> (64 mg cm<sup>-2</sup>). Then, a second glass slide was put on top (face-to-face assembly). After 2 days at room temperature, the slides were separated, intensely rinsed with deionized water and air-dried.

#### Coating procedure for tetraether lipid on borofloat® 33 glass slides

**Preparation of TEL vesicle emulsion.** The main phospholipid included in dried biomass of *Sulfolobus acidocaldarius* was isolated and purified as described earlier.<sup>39</sup> The head-groups of the extracted tetraether lipid were activated by refluxing with cyanuric chloride over 1 week in dry chloroform/methanol (1 : 1).

The activated lipids were dissolved in dry chloroform/methanol 1 : 1, sodium bicarbonate (1.5 g per 100 mg lipid) was added and a thin lipid layer at the sides of the flask was formed. Subsequently, the solvents were removed completely under reduced pressure. The lipid film was hydrated with pure water at a final lipid concentration of about 2 mg mL<sup>-1</sup>. Further treatment in an ultrasonic bath at 50 °C for 15 minutes yielded a cloudy lipid emulsion consisting of large multilamellar vesicles. Afterwards, the emulsion was extruded through a polycarbonate membrane (pore diameter 100 nm).

**Coating.** The glass substrates were purified as follows: (1) sonication in diluted detergent solution (Blanchipon®, Optical II), (2) incubation in ethanol and 35% nitric acid, and (3) storing in de-ionised water. Subsequently, the surfaces were activated with nitric acid and by exposure to UV irradiation. After amino silanization using 3-(ethoxydimethylsilyl)propylamine the substrates were cleaned with chloroform, methanol, and water. TEL coating was performed *via* liposome spreading in a PTFE reaction chamber by incubation with a freshly prepared lipid emulsion at 70 °C overnight.<sup>39</sup> Finally, the coated substrates were sonicated in chloroform for 10 minutes and dried with pressurized air. In a next step, the PETox were immobilized on the TEL-coated glass by coupling the amine end group of the polymer with the cyanuric chloride moiety of the TEL. The reaction was performed in borate buffer solution (10 mg PETox per mL, pH = 8.5) at 60 °C overnight. Subsequently, the glass slides were extensively rinsed with distilled water and dried under ambient conditions.

#### Preparation of synthetic river water medium

The synthetic river water was prepared by dissolving calcium chloride dihydrate (34.6 mg L<sup>-1</sup>), magnesium sulfate heptahydrate (112.3 mg L<sup>-1</sup>), sodium bicarbonate (126.0 mg L<sup>-1</sup>), monopotassium phosphate (4.35 mg L<sup>-1</sup>), sodium nitrate (85.0 mg L<sup>-1</sup>), glucose (6.6 mg L<sup>-1</sup>), and pepton (2.0 mg L<sup>-1</sup>) in distilled water.

Five typical microorganisms with a high potential of biofilm formation were isolated from the river Ruhr near Mühlheim (Germany): *Aeromonas hydrophila/caviae*, *Sphingomonas paucimobilis*, *Pasteurella* spp., *Aeromonas salmonicida*, and

*Leuconostoc* spp. The microorganisms were precultivated at 30 °C overnight on a shaker (100 rpm) in a special water medium (pH 7) consisting of: yeast extract (0.5 g mL<sup>-1</sup>), peptone (0.5 mg mL<sup>-1</sup>), casein hydrolysate (0.5 mg mL<sup>-1</sup>), glucose (0.5 mg mL<sup>-1</sup>), sodium pyruvate (0.3 mg mL<sup>-1</sup>), starch (0.5 mg mL<sup>-1</sup>), dipotassium hydrogenphosphate (0.3 mg mL<sup>-1</sup>), and monopotassium phosphate (0.05 mg mL<sup>-1</sup>). Bacteria were harvested by centrifugation at 4000g for 15 min. The pellet was washed twice with synthetic river medium to remove other particle-like components that may have an impact on the kinetic process. A constant cell concentration of 2 × 10<sup>6</sup> cells per mL synthetic river water was adjusted.

#### Investigation of the biofilm formation

Polymer coated sterilized glass slides were incubated in flow chambers. Prior to use, all probes were sterilized using ethanol (70%). Subsequently, the coated glass slides were placed in a flow chamber running with bacteria containing synthetic river water at a flow rate of 0.3 mL min<sup>-1</sup> at room temperature. After incubating for 15 hours, a rinsing cycle with pure cultivation medium was performed to remove non-adhered microorganisms from the surface. The bioadhesion was evaluated by means of confocal laser scanning microscopy. To this end, the adherent microorganisms were stained using a LIVE/DEAD® BacLight™ Bacterial Viability Kit (MoBiTec, Germany). At each sample ten images of biofilms were taken at different positions in the flow channel by confocal laser scanning microscopy (LSM710, Zeiss microscopy, Germany, Plan Apochromat 5×/0.16). The surface area covered by microorganisms was quantified by software supported analysis of the microscopy images (Volocity improvisation®). Bioadhesion experiments were performed in triplicate.

#### Stability tests

Stability tests were performed on Fluo-PETox coated glass slides attached *via* TEL and silane linker, respectively.

**Investigation of the resistance against chemical stress.** Samples were incubated at room temperature over 12 weeks in an upright position in closed boxes on a shaker (75 rpm) filled with sterile filtrated water of a drinking water dam (Neustadt/Ilm, Germany) and salt water from the North sea, respectively. Media were changed weekly.

**Investigation of the resistance against mechanical stress.** Resistance against mechanical stress was investigated using aluminum oxide and silicon carbide particles in distilled water, based on environmental data. The test solution comprised 150 mg particles per liter. The particle size was distributed as follows: Ø 320 µm = 0.4%, Ø 120 µm = 41%, Ø 20 µm = 31.8%, Ø 9 µm = 26.8%. Samples were incubated at room temperature in a closed beaker glass with stirring (750 rpm) corresponding to a streaming of 2 m s<sup>-1</sup>. Over 1 week a permanent change between 8 h rotation time and 16 h resting time without rotation was realized.

**Investigation of the resistance against thermal stress.** In order to investigate thermal stability the samples were placed in distilled water and exposed to a defined temperature protocol



with 25 cycles between 2 and 38 °C and an incubation period of 14 days. Dwell time at each temperature was 1 h.

**Image analysis.** After each stress procedure fluorescence image data of the Fluo-PEtOx coated samples were recorded by confocal laser scanning microscopic method (LSM710, Zeiss microscopy, Germany, Plan Apochromat 5×/0.16). The recordings were made with uniform measurement parameters (gain, offset, pinhole, average, *etc.*) to allow a comparison of results among each other but also to untreated coatings as a proof of the layer stability.

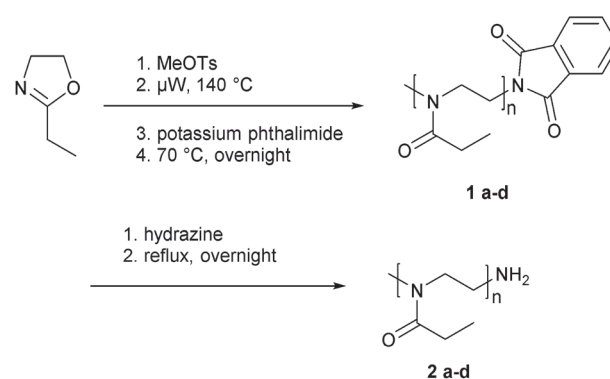
## Results and discussion

### Synthesis and characterization of amine end-capped poly(2-ethyl-2-oxazoline)s

PEtOx of different molar masses were synthesized with the aim to covalently bind the polymer to the surface *via* an epoxide bearing silane and a cyanuric chloride functionalized tetraether lipid (TEL), respectively. Since it is known that both epoxides and cyanuric chloride can react quite easily with amines, PEtOx bearing an amine end group were prepared using a new synthesis route.

The synthesis of an amine end-functionalized poly(2-oxazoline) (POx) was already described in literature. Lin *et al.* terminated the living oxazolium species directly with ammonia in acetonitrile.<sup>42</sup> However, the authors only obtained a degree of functionalization of about 80%. As an alternative three step method, Park *et al.* quenched the reaction mixture with a methanolic NaOH solution.<sup>43</sup> The resulting hydroxyl end group was then reacted with phthalimide in the presence of triphenylphosphine and diethyl azodicarboxylate to yield a POx with a phthalimide end group. In a final step, the amine end group was obtained by treatment with hydrazine monohydrate. However, this procedure led only to an amine end group functionalization efficiency of 62%. An additional problem, reducing the efficiency of this method, is the possible formation of ester end groups instead of hydroxyl end groups, when the reaction is quenched.<sup>44–46</sup> These esters need to be hydrolyzed to hydroxyl groups before the polymer can be further functionalized. To overcome the drawbacks of these methods, a new synthesis route to synthesize amine end-functionalized PEtOx was developed (Scheme 1). In this approach the living cationic species is quenched directly with an excess of potassium phthalimide, saving one step compared to the method described by Park *et al.* Moreover, the end-capping efficiency is quantitative according to <sup>1</sup>H NMR spectroscopy and MALDI-TOF-MS.

The <sup>1</sup>H NMR spectrum of **1** (Fig. 1 top) shows a broad signal around 7.76 ppm deriving from the aromatic protons of the phthalimide unit (4 protons). By correlation with the signals at about 3 ppm, which are associated with the CH<sub>2</sub>  $\alpha$ -end group (3 protons), the quantitative functionalization with the desired  $\omega$ -end group is confirmed. The broad peak at 3.44 ppm derives from the polymer backbone. The side chain signals can be found at 1.11 ppm (CH<sub>3</sub>) and 2.32 ppm (CH<sub>2</sub>), respectively. Due to a different chemical environment, the backbone CH<sub>2</sub> group adjacent to the phthalimide is shifted to 3.83 ppm.



Scheme 1 Schematic representation of the synthesis of amine end-functionalized PEtOx.

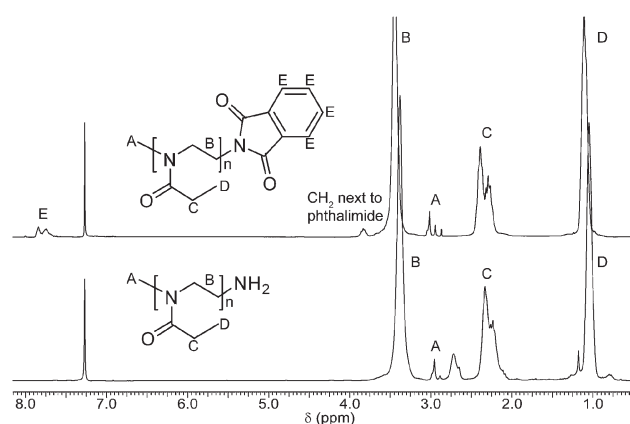


Fig. 1 <sup>1</sup>H NMR spectra of phthalimide (**1a**, top) and amine (**2a**, bottom) end-functionalized PEtOx (300 MHz, solvent CDCl<sub>3</sub>).

The MALDI-TOF mass spectrum of **1** shows two distributions that can be assigned to the sodium adduct of phthalimide end-capped PEtOx (Fig. 2). The methyl-initiated species derives from the initiation of the polymerization with methyl tosylate. The proton-initiated species is formed by chain transfer reactions occurring during the polymerization.<sup>47,48</sup> A hydroxyl end group bearing species could not be observed. This fact further underlines the complete functionalization and is in accordance with the results from <sup>1</sup>H NMR analysis. Moreover, the measured isotopic patterns match with the calculated isotopic patterns of the assigned species.

The phthalimide end-capped PEtOx **1** were subsequently treated with hydrazine monohydrate to obtain the amine functionalized polymers (**2**).<sup>43,49</sup> Characterization of the product by <sup>1</sup>H NMR spectrometry revealed the success of the reaction (Fig. 1 bottom). After the hydrazinolysis, the signals of the aromatic phthalimide end group and the CH<sub>2</sub> group adjacent to the phthalimide disappeared quantitatively.

The MALDI-TOF mass spectrum of **2** shows two major distributions which belong to the sodium adducts of methyl and proton initiated PEtOx bearing an amine end group (Fig. 3). The initial phthalimide-bearing species could not be detected



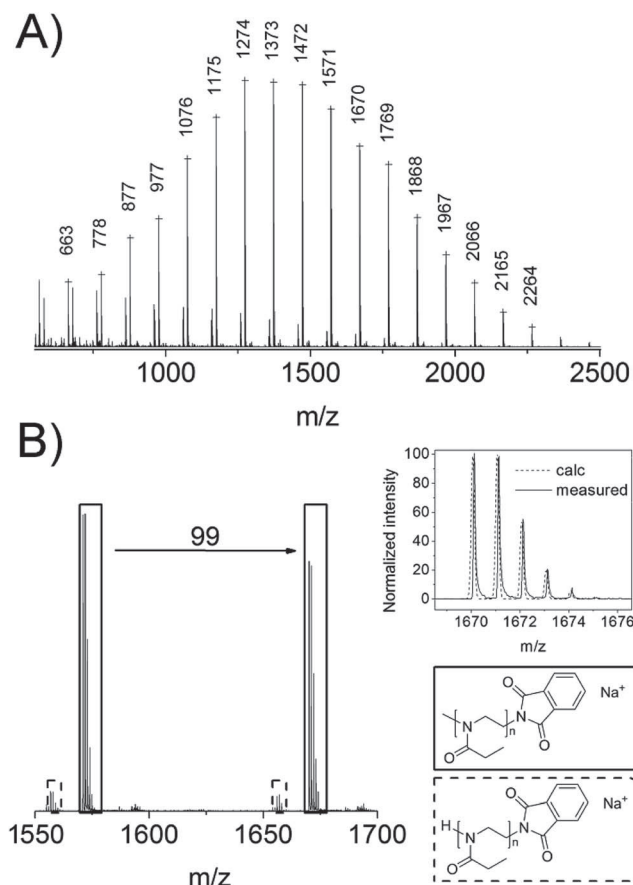


Fig. 2 (A) MALDI-TOF mass spectrum of phthalimide end-capped PEtOx. (B) An expanded region of the spectrum (right), the structural assignments for the different distributions as well as the calculated and measured isotopic pattern of the peak at  $m/z = 1670$  (left).

anymore. In addition, the measured and the calculated isotopic pattern coincide.

The presented synthesis route was used to prepare amine functionalized PEtOx (2) with different molar masses, namely 2000, 4000, 6000, and 8000  $\text{g mol}^{-1}$  ( $n = 20, 40, 60,$  and  $80$ ), which can be achieved simply by variation of the  $[M]/[I]$  ratio applied for the CROP. Characterization by size exclusion chromatography (SEC) revealed PDI values between 1.12 and 1.19 (Table 1).

### Fluorescein labeled PEtOx

To prove the suitability of the attachment methods and to investigate the stability of the obtained PEtOx layers against different types of stress, a fluorescein labeled PEtOx (Fluo-PEtOx, 5) was used. To this end, a copolymer with an amine monomer content of 10% and an overall degree of polymerization (DP) of 40 ( $\text{P}(\text{EtOx}_{36}\text{-stat-AmOx}_4)$ , 4) was synthesized by copolymerization of EtOx and a *tert*-butyloxycarbonyl (Boc)-protected amine group containing 2-oxazoline followed by deprotection (Scheme 2).<sup>41</sup> In a next step one amine group was labeled using a fluorescein-NHS ester derivative. The reaction of this activated acid with amine groups is highly efficient under

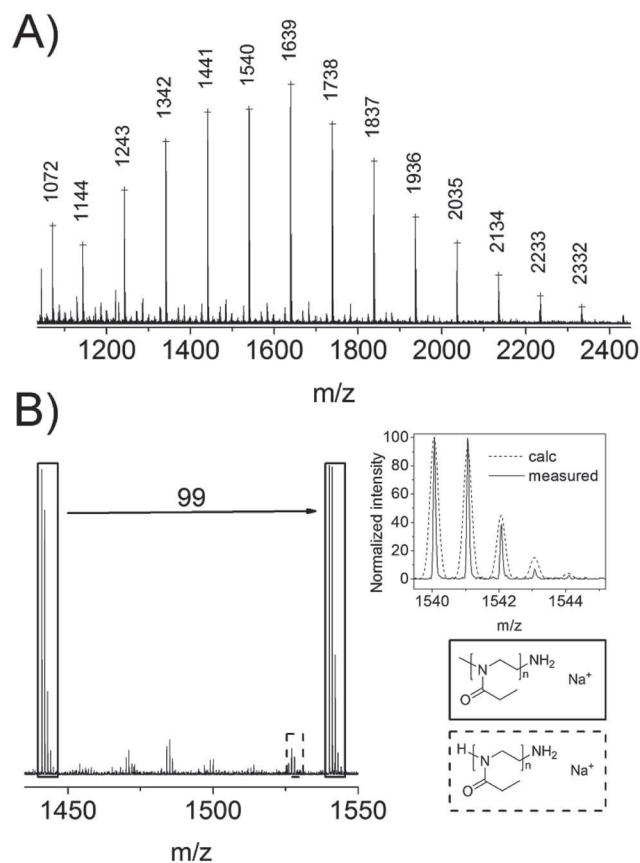


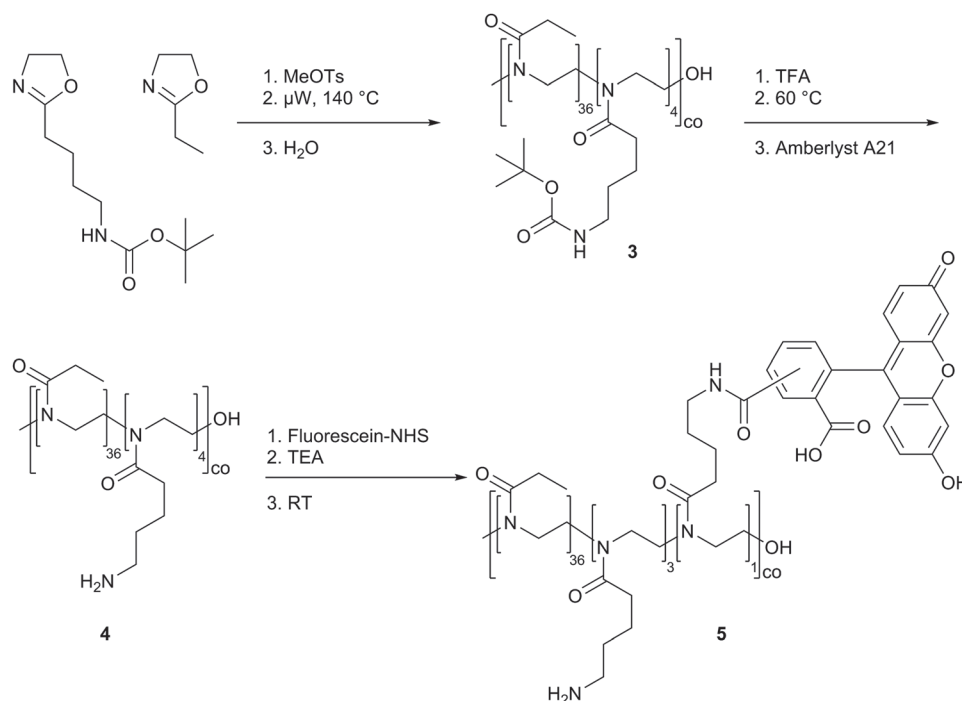
Fig. 3 (A) MALDI-TOF mass spectrum of amine functionalized PEtOx. (B) An expanded region of the spectrum (right), the structural assignments for the different distributions as well as the calculated and measured isotopic pattern of the peak at  $m/z = 1540$  (left).

Table 1 SEC-data of the different POx

Sample	EtOx : BocOx : AmOx : F	$M_n^a$ ( $\text{g mol}^{-1}$ )	PDI <sup>a</sup>
2a	20 : 0 : 0 : 0	2460	1.12
2b	40 : 0 : 0 : 0	3790	1.15
2c	60 : 0 : 0 : 0	5175	1.14
2d	80 : 0 : 0 : 0	5990	1.19
3	36 : 4 : 0 : 0	5300	1.08
4	36 : 0 : 4 : 0	5400	1.12
5	36 : 0 : 3 : 1	5500	1.18

<sup>a</sup> Determined by SEC (eluent:  $\text{CHCl}_3/2\text{-propanol/TEA}$ , calibration with a PS standard).

basic conditions and was, therefore, performed with triethylamine (TEA) as a base. Purification was accomplished by repeated precipitation into diethyl ether to eliminate traces of unreacted fluorescein. The successful labeling of the copolymer was confirmed by SEC, which provided congruent UV (485 nm) and RI-detector traces (Table 1 and Fig. S1†). Moreover, no signal of unreacted fluorescein was detected. In addition, <sup>1</sup>H NMR spectroscopy shows the characteristic peaks of fluorescein with broadening attributed to the attachment to the polymer chain (Fig. S2†).



Scheme 2 Schematic representation of the synthesis of amine containing POx and labeling of the polymer with fluorescein.

### Coating of glass slides with PEtOx of different molar masses using different spacers

To investigate their suitability for the prevention of bioadhesion, the PEtOx polymers (2a–d) were immobilized on borofloat<sup>®</sup> 33 glass employing either (1) a silane based linker or (2) a TEL linker (Scheme 3). In case of coupling *via* a silane based linker, the glass slides were first treated with (3-glycidyloxypropyl)trimethoxysilane (GOPTMS). Subsequently, PEtOx of different molar masses were attached by reaction of the epoxide unit of GOPTMS with the end group of the polymer (Scheme 3A route 1). For the coupling *via* a TEL linker (Scheme 3B) the terminal hydroxyl groups of the lipid were modified with cyanuric chloride to enable the covalent coupling to the glass surfaces as well as the covalent binding of PEtOx on top of the lipid membrane (Scheme 3A route 2). The TEL functionalized glass slides were coated with PEtOx with the same molar masses as for route 1.

### Characterization of the polymer thin films

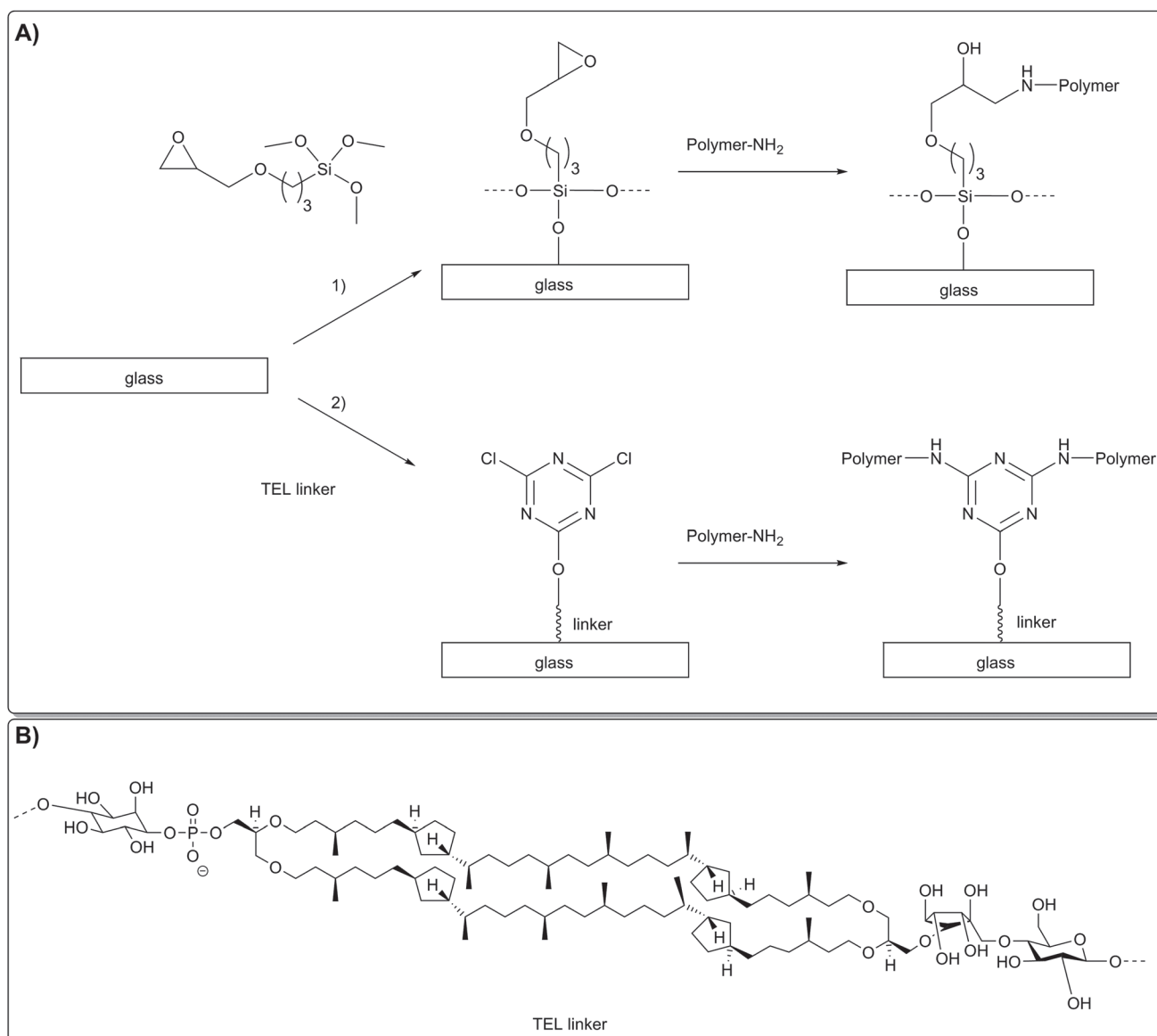
In order to examine the suitability of the attachment methods and the quality of the PEtOx coatings, fluorescein labeled PEtOx was grafted to the different linker molecules in the same way as the PEtOx homopolymers. By means of laser scanning microscopy it could be shown that homogenous Fluo-PEtOx films are obtained for both the GOPTMS and the TEL linker (Fig. 4).

The coating process with the PEtOx homopolymers was further monitored by means of X-ray photoelectron spectroscopy (XPS). Using this method information on the chemical composition of surface layers, which are only a couple of nanometers thick, can be obtained. A comparison of the

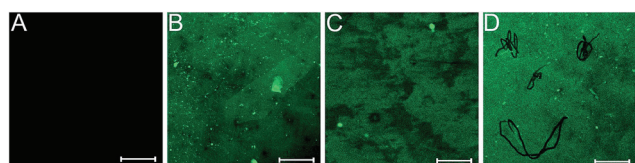
nitrogen 1s signal of pure borofloat glass, the different linkers, and the different PEtOx films showed the successful coating (Fig. 5). While on pure glass and GOPTMS treated substrate, no nitrogen was found, the TEL coated glass shows a nitrogen signal due to the cyanuric chloride moieties. Moreover, the nitrogen signal intensity increased significantly after attaching the PEtOx.

Water contact angle measurements on air-dried and hydrated polymer coatings were performed with the aim to investigate the wetting behavior of the surface tethered PEtOx films (Fig. 6). Both, samples that were coated with GOPTMS and TEL linker, respectively, displayed an increased water contact angle compared to the reference borosilicate glass (after treatment with argon plasma). Subsequent PEtOx grafting further increased the water contact angles for GOPTMS attached samples. In case of TEL linked PEtOx only for a DP of 20, referred to as 20(TEL), an increased contact angle could be observed when compared to pure TEL. For all other chain lengths the contact angle is in the same range as for pure TEL or even decreased. These changes in wettability indicate a successful coating of the substrates with the linkers and PEtOx, respectively.

In the air-dried state, surfaces that were coated with PEtOx *via* a GOPTMS linker display water contact angles in a rather wide range between 57° and 85°. The variations for surfaces that were coated with PEtOx *via* TEL linkers are narrower, ranging from 53° to 70°. While for coatings attached through TEL decreasing contact angles with increasing chain lengths could be observed, no trend could be found for GOPTMS attached PEtOx.



**Scheme 3** (A) Schematic representation of the PETox coating process using GOPTMS (route 1) and a TEL (route 2) linker, respectively, and (B) of the TEL linker structure.



**Fig. 4** Confocal laser scanning microscopy images of (A) uncoated glass, (B) Fluo-PETox attached via GOPTMS, (C) Fluo-PETox attached via TEL, and (D) scratched sample of Fluo-PETox attached via GOPTMS (scale bar: 100  $\mu\text{m}$ ).

After swelling in water, the coatings display reduced contact angles. This finding is ascribed to the hydration of the hygroscopic, hydrophilic PETox. Again a clear trend to reduced contact angles for longer polymer chains can be found for TEL

attached coatings. Moreover, the difference in contact angles between air-dried and hydrated state ( $\Delta\theta$ ) increases with the chain length from  $0.7^\circ$  for  $n = 20(\text{TEL})$  to  $18.1^\circ$  for  $n = 80(\text{TEL})$ . This observation indicates that longer polymers can bind/absorb more water molecules and, thus, should have a higher antifouling potential. This is in accordance with theoretical calculation for PEG.<sup>8</sup> For GOPTMS tethered films such tendency could not be observed. Here, a constant  $\Delta\theta$  of  $\sim 10^\circ$  was determined.

An important parameter with regard to the antifouling properties is the grafting density,<sup>33</sup> which is in general calculated either from the film thickness<sup>28,50</sup> or the weight loss of the sample upon heating.<sup>51,52</sup> However, due to technical reasons (*e.g.* monolayer, glass substrate) the determination of these parameters was not possible. To ensure the highest possible grafting density an excess of polymer was used.

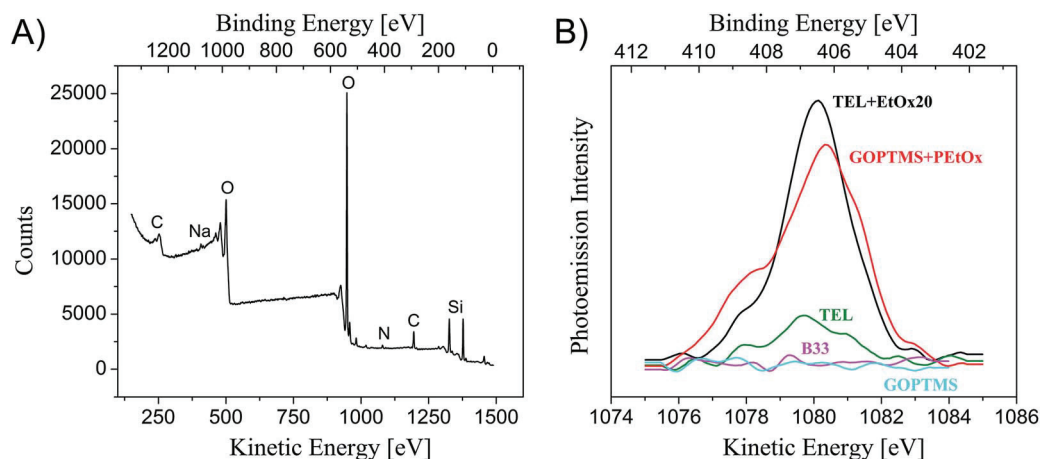


Fig. 5 (A) Typical XPS spectrum of a TEL-PETox coating. (B) Overlay of the nitrogen 1s signals of bare borofloat glass as well as the different linkers and coatings.

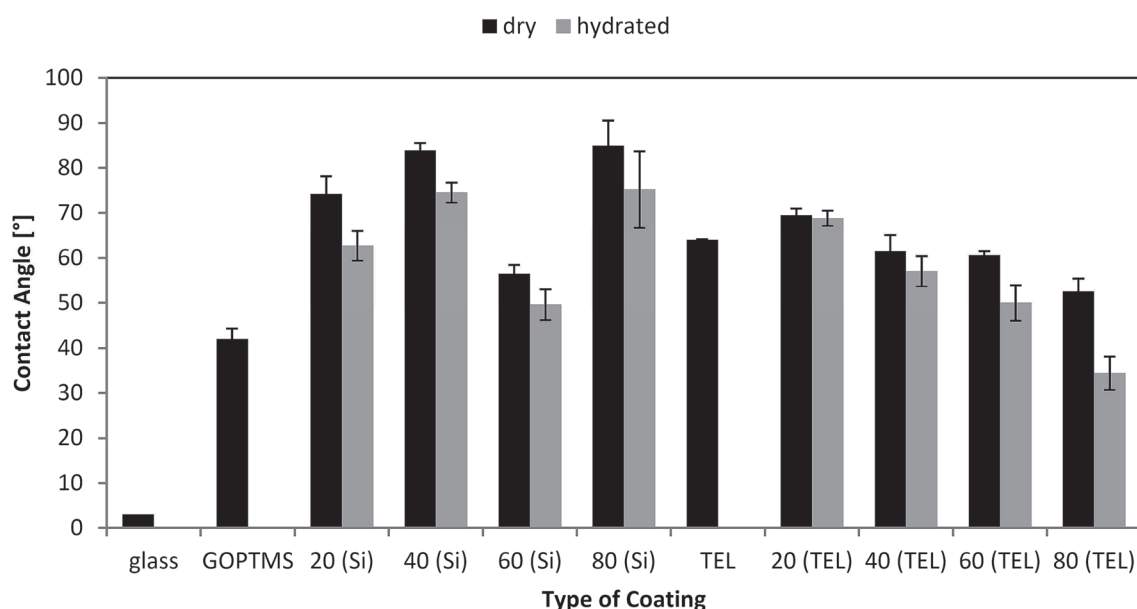


Fig. 6 Water contact angles of the different PETox-coatings in dry and hydrated state (data are presented as mean  $\pm$  standard deviation for  $n = 45$ ). The numbers indicate the different DPs of PETox (20, 40, 60 and 80), linkers are given in brackets.

### Antifouling properties of the different PETox coatings

The antifouling properties of the different PETox-coated glass slides were investigated in flow-through chambers that allow a continuous cross flow of synthetic river water under reproducible conditions over an arbitrary period of time. Based on the water composition of the river Ruhr near Mühlheim (Germany), five different microorganisms with a high potential of biofilm formation were chosen, namely: *Aeromonas hydrophila/caviae*, *Sphingomonas paucimobilis*, *Pasteurella* spp., *Aeromonas salmonicida*, and *Leuconostoc* spp. After 15 hours incubation the adherent microorganisms were stained using a LIVE/DEAD<sup>®</sup> BacLight<sup>™</sup> Bacterial Viability Kit and investigated by means of confocal laser scanning microscopy. A clear reduction of the bioadhesion, induced by

the PETox coatings, was detected (up to 66% compared to uncoated glass), with no significant differences between films attached *via* GOPTMS and TEL, respectively, suggesting that similar grafting efficiencies are reached (Fig. 7). Although in case of TEL linkers the hydrophilicity of swollen PETox samples increased with the chain length and longer chains should, therefore, have a higher antifouling potential, an influence of the molar mass on the cell adhesion could not be observed. Also the bacterial viability rate was hardly affected. Only the samples 40(Si) and 20(TEL) showed higher deviations. While on 40(Si) nearly no dead cells could be found, the 20(TEL) coating showed a reduced cell viability. In addition, 20(TEL) shows the lowest overall bioadhesion, making it the best coating produced within this study. However, from an

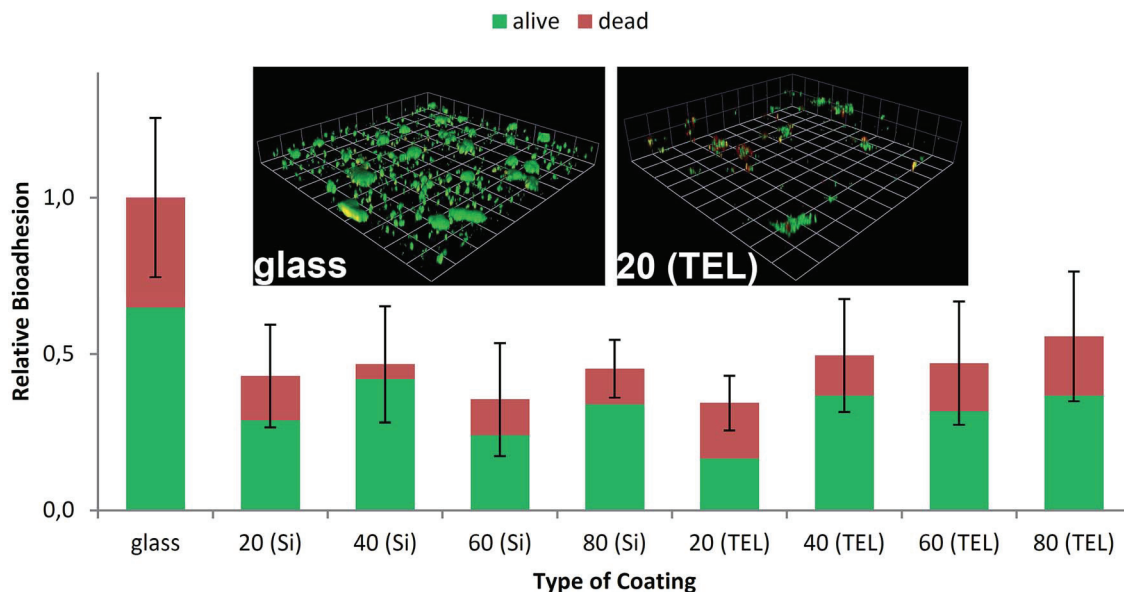


Fig. 7 Bioadhesion on PEtOx coatings of different DP (20, 40, 60, and 80) to the glass slides *via* a silane (Si) and a tetraether lipid (TEL) linker (standard deviation is related to the total bioadhesion (sum of dead and vital bacteria)) as well as confocal laser scanning microscopy images of the stained biofilms on glass and 20 (TEL).

use-oriented point of view, *i.e.* for large scale applications, the attachment *via* GOPTMS is favored, since similar results are obtained and the coating process is easier. Moreover, GOPTMS, in contrast to TEL, is easily available in large amounts.

Antifouling properties of immobilized PEG- and POx-based coatings have been widely reported in the literature.<sup>8,14–20</sup> Due to the different, more real life test conditions, *e.g.* attack of multiple bacteria and synthetic river water medium, a comparison of the obtained results to other POx or PEG coatings, reported in literature, is difficult.

### Stability of the PEtOx coatings

An important parameter with regard to their application, *e.g.* as sensor coatings, is the stability of the PEtOx films. To this end, Fluo-PEtOx coated glass slides, attached through GOPTS and TEL spacer, respectively, were exposed to three different types of stress: (1) chemical stress, (2) mechanical stress and (3) thermal stress. The resistance against chemical stress, caused *e.g.* by fresh and salt water, was investigated over 12 weeks using dam and North Sea water, respectively. The durability of the coatings against abrasion in particle containing water is essential in the field of environmental monitoring. Based on environmental data a corresponding test solution containing aluminum oxide and silicon carbide particles was prepared. Mechanical stress was simulated by placing the glass slides into this solution and stirring for 8 hours a day over 1 week. In order to verify their thermal stability, the samples were exposed to a defined heating profile for 14 days with temperatures between 2 and 38 °C. Subsequent analysis by means of confocal laser scanning microscopy showed that the coatings withstood the different types of stress (Fig. 8).

## Conclusion

The potential of PEtOx coatings to prevent bioadhesion under “real life” conditions was investigated. To this end, amine end-functionalized PEtOx of four different molar masses have been prepared applying a new and straightforward synthesis method. The polymers obtained were characterized by MALDI-TOF mass spectrometry, <sup>1</sup>H NMR spectroscopy, and size exclusion chromatography, which showed the successful introduction of ω-amine groups. PEtOx were attached to glass surfaces through silane and tetraether lipid based linkers. The surface immobilization of PEtOx was investigated by fluorescence microscopy measurements of surfaces modified with fluorescently labeled PEtOx as well as by XPS investigations, which showed the presence of nitrogen signals after the PEtOx coating process. Contact angle measurements of air-dried and swollen coatings revealed a higher hydrophilicity of the swollen samples, ascribed to the formation of PEtOx hydrates. Fouling studies were performed in a flow-through chamber under “real-life” relevant conditions using a synthetic river water model containing five different bacteria. PEtOx modified glass samples exposed to the synthetic river water for 15 h showed a bioadhesion reduction of up to 66% with no significant differences between the two different linkers. The best results were obtained by PEtOx with 20 repeating units attached *via* a tetraether lipid linker, which revealed the lowest biofilm formation and the highest amount of dead bacteria. In addition, the stability of the PEtOx coatings towards chemical, mechanical, and thermal stress was investigated. No significant destruction of the polymer layer was observed, demonstrating the capability of the films for long term applications.

The present study underlines the potential of POx for anti-fouling coatings and is in agreement with other studies.<sup>33</sup>



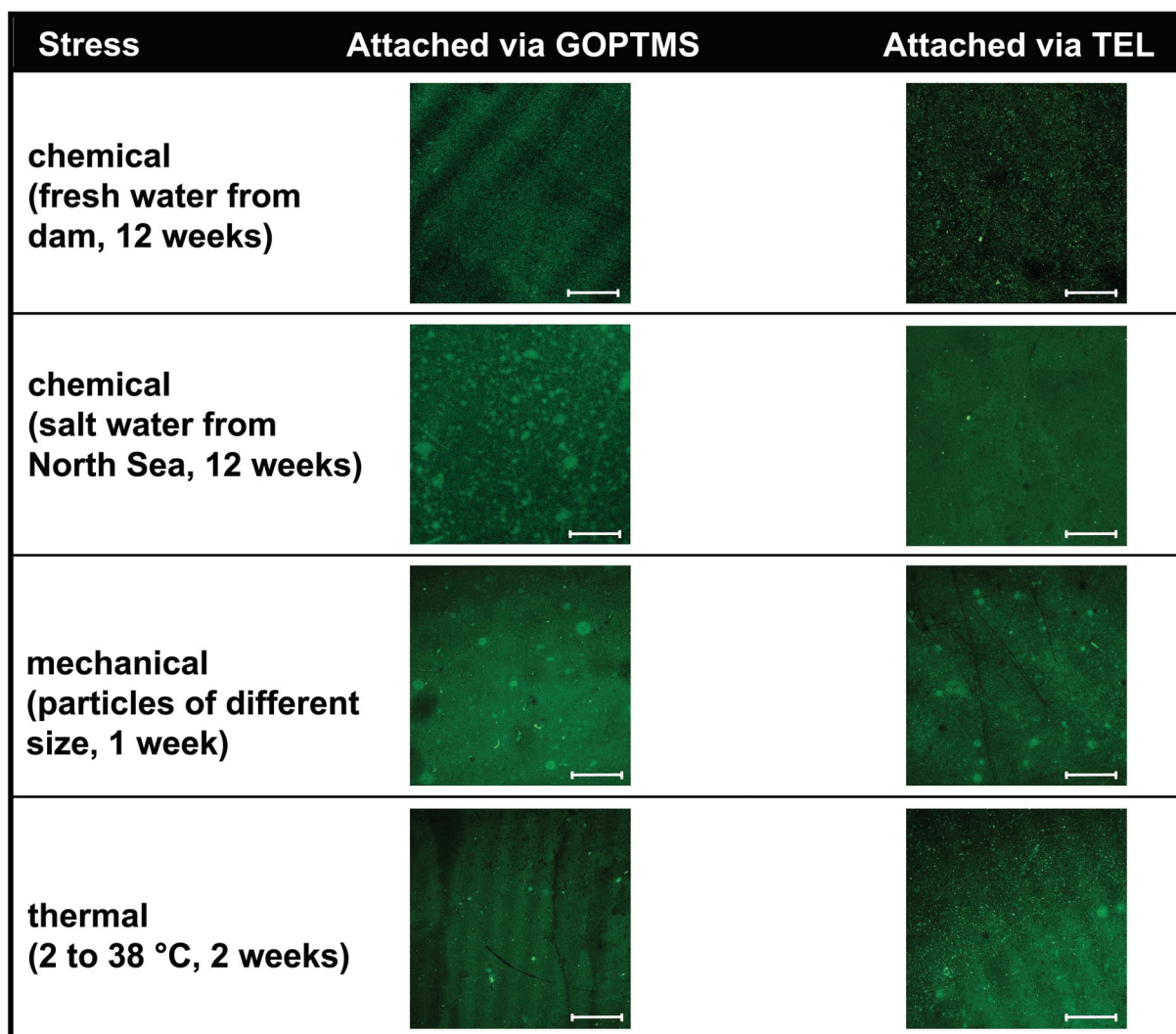


Fig. 8 Confocal laser scanning microscopy images of the Fluo-PEtOx coatings after stress tests (scale bar: 100  $\mu\text{m}$ ).

However, at the chosen, more realistic conditions, a complete reduction of biofilm formation could not be observed. Further investigations have to be performed and will aim at the application of mixtures of PEtOx with different molar masses as well as PEtOx of different architectures to result in a denser packing of the polymer chains on the surface. Another interesting aspect is probably the grafting of polyhydrophilic and polyzwitterionic entities to form a stable superficial water barrier. Future tests will have to show whether the presented coatings are able to maintain their antifouling behavior under real life conditions, *i.e.* the simultaneous acting of bacteria and stresses.

## Acknowledgements

The authors would like to thank the Bundesministerium für Bildung und Forschung (Germany) funding (project: BASIS, 03WKCB01C) and 4H Jena Engineering for the stability tests. CW acknowledges the Carl-Zeiss foundation. KK is grateful to the Alexander von Humboldt-foundation for financial support.

We also thank the Dutch Polymer Institute (DPI, technology area HTE).

## Notes and references

- 1 V. K. Vendra, L. Wu and S. Krishnan, in *Nanotechnologies for the Life Sciences*, Wiley-VCH Verlag GmbH & Co. KGaA, 2007.
- 2 C. Blaszykowski, S. Sheikh and M. Thompson, *Chem. Soc. Rev.*, 2012, **41**, 5599–5612.
- 3 S. Cao, J. Wang, H. Chen and D. Chen, *Chin. Sci. Bull.*, 2011, **56**, 598–612.
- 4 P. Buskens, M. Wouters, C. Rentrop and Z. Vroon, *J. Coat. Technol. Res.*, 2013, **10**, 29–36.
- 5 T. Mérian and J. M. Goddard, *J. Agric. Food Chem.*, 2012, **60**, 2943–2957.
- 6 D. Rana and T. Matsuura, *Chem. Rev.*, 2010, **110**, 2448–2471.
- 7 C. Zhao, L.-Y. Li, M.-M. Guo and J. Zheng, *Chem. Pap.*, 2012, **66**, 323–339.
- 8 I. Banerjee, R. C. Pangule and R. S. Kane, *Adv. Mater.*, 2011, **23**, 690–718.

- 9 M. Charnley, M. Textor and C. Acikgoz, *React. Funct. Polym.*, 2011, **71**, 329–334.
- 10 F. Siedenbiedel and J. C. Tiller, *Polymers*, 2012, **4**, 46–71.
- 11 F. A. Guardiola, A. Cuesta, J. Meseguer and M. A. Esteban, *Int. J. Mol. Sci.*, 2012, **13**, 1541–1560.
- 12 J.-P. Maréchal and C. Hellio, *Int. J. Mol. Sci.*, 2009, **10**, 4623–4637.
- 13 R. Konradi, C. Acikgoz and M. Textor, *Macromol. Rapid Commun.*, 2012, **33**, 1663–1676.
- 14 K. Liefeth, H. Rothe, M. Frant and R. Schade, in *Biofunctional Surface Engineering*, ed. M. Scholz, Pan Stanford Publishing Pte. Ltd, Singapore, 2014, pp. 71–120.
- 15 J. Blümmel, N. Perschmann, D. Aydin, J. Drinjakovic, T. Surrey, M. Lopez-Garcia, H. Kessler and J. P. Spatz, *Biomaterials*, 2007, **28**, 4739–4747.
- 16 A. Rosenhahn, S. Schilp, H. J. Kreuzer and M. Grunze, *Phys. Chem. Chem. Phys.*, 2010, **12**, 4275–4286.
- 17 A. Roosjen, H. C. van der Mei, H. J. Busscher and W. Norde, *Langmuir*, 2004, **20**, 10949–10955.
- 18 E. Ostuni, R. G. Chapman, R. E. Holmlin, S. Takayama and G. M. Whitesides, *Langmuir*, 2001, **17**, 5605–5620.
- 19 B. Pidhatika, M. Rodenstein, Y. Chen, E. Rakhmatullina, A. Muhlebach, C. Acikgoz, M. Textor and R. Konradi, *Biointerphases*, 2012, **7**, 1–15.
- 20 C. Crouzet, C. Decker and J. Marchal, *Makromol. Chem.*, 1976, **177**, 145–157.
- 21 F. Kawai, T. Kimura, M. Fukaya, Y. Tani, K. Ogata, T. Ueno and H. Fukami, *Appl. Environ. Microbiol.*, 1978, **35**, 679–684.
- 22 C. F. Gonzalez, W. A. Taber and M. A. Zeitoun, *Appl. Microbiol.*, 1972, **24**, 911–919.
- 23 R. Konradi, B. Pidhatika, A. Muhlebach and M. Textor, *Langmuir*, 2008, **24**, 613–616.
- 24 J. U. Lind, C. Acikgöz, A. E. Daugaard, T. L. Andresen, S. Hvilsted, M. Textor and N. B. Larsen, *Langmuir*, 2012, **28**, 6502–6511.
- 25 B. Pidhatika, J. Iler, V. Vogel and R. Konradi, *Chimia*, 2008, **62**, 264–269.
- 26 B. Pidhatika, J. Möller, E. M. Benetti, R. Konradi, E. Rakhmatullina, A. Mühlebach, R. Zimmermann, C. Werner, V. Vogel and M. Textor, *Biomaterials*, 2010, **31**, 9462–9472.
- 27 H. Wang, L. Li, Q. Tong and M. Yan, *ACS Appl. Mater. Interfaces*, 2011, **3**, 3463–3471.
- 28 H. Wang, J. Ren, A. Hlaing and M. Yan, *J. Colloid Interface Sci.*, 2011, **354**, 160–167.
- 29 N. Zhang, T. Pompe, I. Amin, R. Luxenhofer, C. Werner and R. Jordan, *Macromol. Biosci.*, 2012, **12**, 926–936.
- 30 N. Zhang, T. Pompe, R. Luxenhofer, C. Werner and R. Jordan, *Polym. Prepr. (Am. Chem. Soc., Div. Polym. Chem.)*, 2012, **53**, 301–302.
- 31 N. Zhang, M. Steenackers, R. Luxenhofer and R. Jordan, *Macromolecules*, 2009, **42**, 5345–5351.
- 32 B. Guillermin, S. Monge, V. Lapinte and J.-J. Robin, *Macromol. Rapid Commun.*, 2012, **33**, 1600–1612.
- 33 L. Tauhardt, K. Kempe, M. Gottschaldt and U. S. Schubert, *Chem. Soc. Rev.*, 2013, **42**, 7998–8011.
- 34 M. Hanford and T. Peeples, *Appl. Biochem. Biotechnol.*, 2002, **97**, 45–62.
- 35 M. Frant, in *Zentrum für Ingenieurwissenschaften Martin-Luther-Universität Halle-Wittenberg*, Halle, 2008.
- 36 M. Frant, P. Stenstad, H. Johnsen, K. Dölling, U. Rothe, R. Schmid and K. Liefeth, *Materialwiss. Werkstofftech.*, 2006, **37**, 538–545.
- 37 A. Sateesh, J. Vogel, E. Dayss, B. Fricke, K. Dölling and U. Rothe, *J. Biomed. Mater. Res., Part A*, 2008, **84A**, 672–681.
- 38 S. Vidawati, J. Sitterberg, U. Bakowsky and U. Rothe, *Colloids Surf., B*, 2010, **78**, 303–309.
- 39 C. Bücher, X. Grosse, H. Rothe, A. Fiethen, H. Kuhn and K. Liefeth, *Biointerphases*, 2014, **9**, 011002.
- 40 J. Piehler, A. Brecht, R. Valiokas, B. Liedberg and G. Gauglitz, *Biosens. Bioelectron.*, 2000, **15**, 473–481.
- 41 M. Hartlieb, D. Pretzel, K. Kempe, C. Fritzsche, R. M. Paulus, M. Gottschaldt and U. S. Schubert, *Soft Matter*, 2013, **9**, 4693–4704.
- 42 C. P. Lin, Y. C. Sung and G. H. Hsiue, *J. Med. Biol. Eng.*, 2012, **32**, 365–372.
- 43 J.-S. Park, Y. Akiyama, F. M. Winnik and K. Kataoka, *Macromolecules*, 2004, **37**, 6786–6792.
- 44 A. Baumgaertel, E. Altuntaş, K. Kempe, A. Crecelius and U. S. Schubert, *J. Polym. Sci., Part A: Polym. Chem.*, 2010, **48**, 5533–5540.
- 45 A. Baumgaertel, C. Weber, N. Fritz, G. Festag, E. Altuntaş, K. Kempe, R. Hoogenboom and U. S. Schubert, *J. Chromatogr. A*, 2011, **1218**, 8370–8378.
- 46 S. Kobayashi, E. Masuda, S. Shoda and Y. Shimano, *Macromolecules*, 1989, **22**, 2878–2884.
- 47 M. Litt, A. Levy and J. Herz, *J. Macromol. Sci., Part A: Pure Appl. Chem.*, 1975, **9**, 703–727.
- 48 A. Levy and M. Litt, *J. Polym. Sci., Part A-1: Polym. Chem.*, 1968, **6**, 1883–1894.
- 49 P. Mongondry, C. Bonnans-Plaisance, M. Jean and J. F. Tassin, *Macromol. Rapid Commun.*, 2003, **24**, 681–685.
- 50 M. Agrawal, J. C. Rueda, P. Uhlmann, M. Müller, F. Simon and M. Stamm, *ACS Appl. Mater. Interfaces*, 2012, **4**, 1357–1364.
- 51 C. Bartholome, E. Beyou, E. Bourgeat-Lami, P. Chaumont and N. Zydowicz, *Macromolecules*, 2003, **36**, 7946–7952.
- 52 J. P. Gann and M. Yan, *Langmuir*, 2008, **24**, 5319–5323.

## Supporting Information

### **Amine end-functionalized poly(2-ethyl-2-oxazoline) as promising coating material for antifouling applications**

Lutz Tauhardt,<sup>1,2</sup> Marion Frant,<sup>3</sup> David Pretzel,<sup>1,2</sup> Matthias Hartlieb,<sup>1,2</sup> Christian Bücher,<sup>3</sup> Gerhard Hildebrand,<sup>3</sup> Bernd Schröter,<sup>4</sup> Christine Weber,<sup>1,2</sup> Kristian Kempe,<sup>1,2,6</sup> Michael Gottschaldt,<sup>1,2</sup> Klaus Liefeth,<sup>3</sup> Ulrich S. Schubert\*<sup>1,2,5</sup>

<sup>1</sup>Laboratory of Organic and Macromolecular Chemistry (IOMC), Friedrich Schiller University Jena, Humboldtstr. 10, 07743 Jena, Germany.

<sup>2</sup>Jena Center for Soft Matter (JCSM), Friedrich Schiller University Jena, Philosophenweg 7, 07743 Jena, Germany.

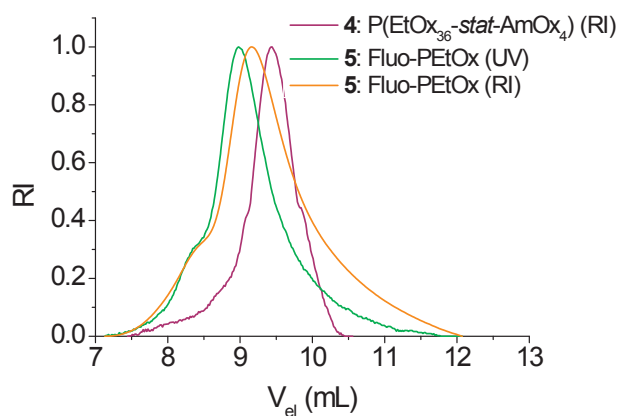
<sup>3</sup>Institute for Bioprocessing and Analytical Measurement Techniques e.V. (IBA), Rosenhof, 37308 Heilbad Heiligenstadt, Germany.

<sup>4</sup>Institute for Solid State Physics, Friedrich Schiller University Jena, Helmholtzweg 5, 07743 Jena.

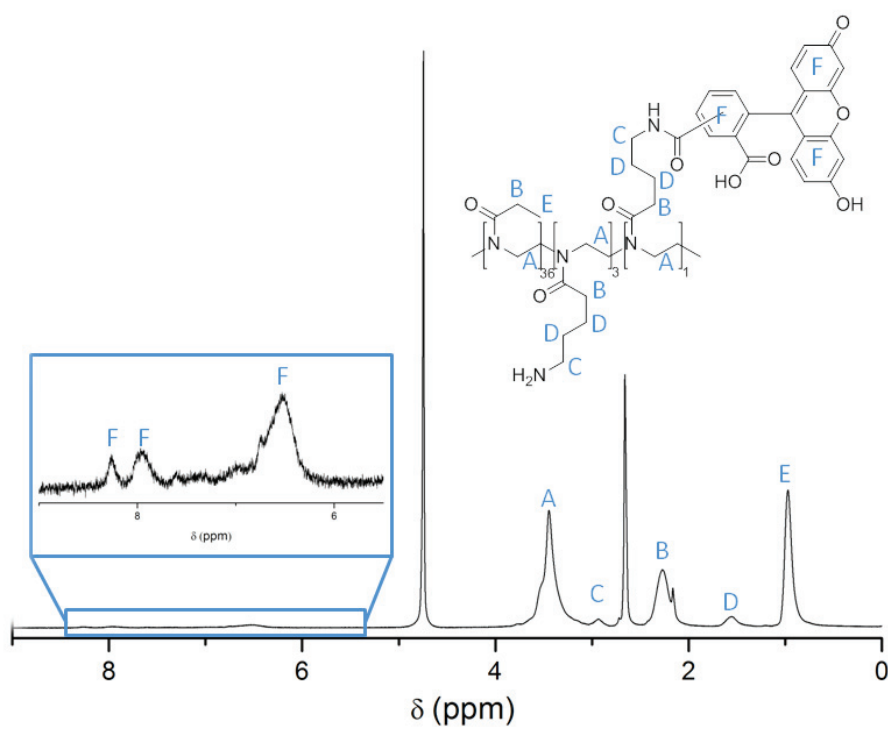
<sup>5</sup>Dutch Polymer Institute (DPI), John F. Kennedylaan 2, 5612 AB Eindhoven, The Netherlands.

Corresponding author footnote: Fax. +49 3641 948 202; Email: [ulrich.schubert@uni-jena.de](mailto:ulrich.schubert@uni-jena.de)

<sup>6</sup>Current address: Department of Chemical and Biomolecular Engineering, The University of Melbourne, Victoria 3010, Australia.



**Fig. S1.** SEC curves of amine containing POx **4** and Fluo-PEtOx **5** (eluent: CHCl<sub>3</sub>/2-propanol/TEA).



**Fig. S2** <sup>1</sup>H NMR spectrum of PEtOx-FITC (300 MHz, solvent CD<sub>3</sub>OD).

## Methods and materials

### General

Dry acetonitrile, MeOx and methyl tosylate (MeOTs) were obtained from Acros Organics, distilled to dryness over barium oxide (BaO), and stored under nitrogen. Dry *N,N*-dimethylformamide (DMF) was purchased from Acros Organics, (3-glycidyoxypropyl)-trimethoxysilane from ABCR, hydrazine monohydrate and potassium phthalimide from Fluka. Triethylamine was distilled over calcium hydride prior use.

Borofloat 33 glass slides were purchased from Schott (Jena, Germany) and cleaned using a low-pressure oxygen plasma instrument from Diener Electronic (Nagold, Germany). The Initiator Sixty single-mode microwave synthesizer from Biotage, equipped with a noninvasive IR sensor (accuracy:  $\pm 2\%$ ), was used for polymerizations under microwave irradiation. Prior to use, the microwave vials were heated at 110 °C overnight and allowed to cool to room temperature under a nitrogen atmosphere. Proton ( $^1\text{H}$ ) nuclear magnetic resonance (NMR) spectra were recorded on a Bruker AC 300 MHz at 298 K. Chemical shifts are reported in parts per million (ppm,  $\delta$  scale) relative to the residual signal of the deuterated solvent. Size exclusion chromatographies (SEC) of the PEtOx were measured on a Shimadzu system equipped with a SCL-10A VP system controller, a DGU-14A degasser, a LC-10AD VP pump, a RID-10A refractive index detector and a PSS SDV column running with chloroform, triethylamine (TEA), and 2-propanol (94:4:2) as eluent. The Techlab column oven was set to 50 °C. Molar masses were calculated using a polystyrene (PS) standard. The MALDI-TOF-MS spectra were recorded utilizing an Ultraflex III TOF/TOF (Bruker Daltonics GmbH, Bremen, Germany), equipped with a frequency-tripled Nd:YAG laser, operating at a wavelength of 355 nm. All spectra were measured in the positive reflector mode using *trans*-2-[3-(4-*tert*-butylphenyl)-2-methyl-2-propenylidene]malononitrile (DCTB) with sodium iodide as matrix. XPS measurements were performed on an EA200-ESCA-system (SPECS Surface Nano Analysis GmbH, Berlin, Germany).

### X-ray photoelectron spectroscopy (XPS)

XPS investigations were carried out with an EA200-ESCA-system (SPECS) using nonmonochromatic Al  $K\alpha$  radiation ( $h\nu = 1486$  eV). The samples have been measured as received under constant conditions ( $\theta = 0^\circ$ ). The nitrogen 1s photoemission signals have been background subtracted and smoothed.

### Contact angle measurements

Determination of water contact angles has been carried out with a computer controlled contact angle measuring system (DCA20, dataphysics, Germany) using the sessile drop technique (drops of 3  $\mu\text{L}$ ). In order to evaluate expected hydration effects of the PEtOx-layers, both dry and swollen samples were characterized. To obtain the latter, the coated glass slides were swollen in distilled water for 30 min. Prior to the determination, excess of water on the surface was removed with pressurized air. The presented contact angles are an average from 15 measurements at 5 different surface points ( $n = 45$ ).

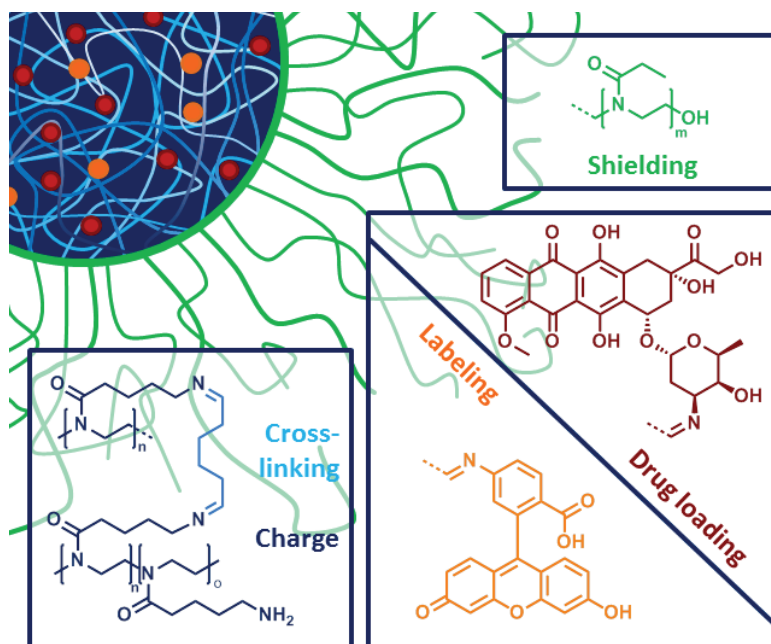


## Publication 8

### “Poly(2-oxazoline) based nanogels for doxorubicin delivery”

M. Hartlieb, T. Bús, J. Kübel, D. Pretzel, S. Hoepfner, K. Kempe, B. Dietzek, U. S. Schubert

in preparation.



# Nanogels based on double hydrophilic poly(2-oxazoline) for doxorubicin delivery

Matthias Hartlieb,<sup>a,b</sup> Tanja Buś,<sup>a,b</sup> David Pretzel,<sup>a,b</sup> Joachim Kübel,<sup>c,d</sup> Stephanie Hoeppener,<sup>a,b</sup> Kristian Kempe,<sup>a,b,†</sup> Benjamin Dietzek,<sup>c,d</sup> Ulrich S. Schubert<sup>a,b,\*</sup>

<sup>a</sup> Laboratory of Organic and Macromolecular Chemistry (IOMC), Friedrich Schiller University Jena, Humboldtstrasse 10, 07743, Jena, Germany

<sup>b</sup> Jena Center for Soft Matter (JCSM), Friedrich Schiller University Jena, Philosophenweg 7, 07743, Jena, Germany

<sup>c</sup> Institute of Physical Chemistry (IPC) and Abbe Center of Photonics, Friedrich Schiller University Jena, Helmholtzweg 4, 07743 Jena, Germany

<sup>d</sup> Leibniz Institute of Photonic Technology (IPHT), Albert-Einstein-Str. 9, 07745 Jena, Germany

<sup>†</sup> Current address: Department of Chemistry, University of Warwick, Gibbet Hill Road, Coventry, CV4 7AL, U.K.

\* Address correspondence to [ulrich.schubert@uni-jena.de](mailto:ulrich.schubert@uni-jena.de)

## Introduction

The treatment of cancer remains a challenging task in modern medicine. Nanomedicine displays a promising tool to improve the performance of common anti-cancer drugs such as Doxorubicin (Dox) which have severe side effects due to a lack of tissue specificity.<sup>[1-3]</sup> The association of Dox to drug delivery systems such as polymeric micelles can lead to a passive targeting for cancerous tissue as a result of the enhanced permeability and retention (EPR) effect, based on the accumulation of nanoscopic objects in leaky tumor tissue.<sup>[4]</sup> Polymeric micelles are the result of the self-aggregation of block copolymers in a suitable solvent and, are usually composed of a hydrophilic segment, which constitutes the shell, as well as a hydrophobic core able to incorporate hydrophobic (drug) molecules. One major limitation of this approach is the equilibrium behind the self-assembly process. At concentrations below the critical micelle concentration (CMC) the system dissociated into unimers, however, also above this point, a component exchange and an escape of the cargo is possible.<sup>[5]</sup> When administered intravenously, the drug carrier has to face high dilution and a resulting premature disassembly leads to the accumulation of the drug in non-cancerous tissue.<sup>[6]</sup> To overcome these restrictions (reversible) covalent cross-linking and a covalent attachment of the drug molecule are promising approaches.<sup>[7]</sup> The cross-linking of micelles leading to the formation of nanogels has attracted considerable attention by researchers in the recent years.<sup>[8-10]</sup> There are several examples of

either core [11-12] or shell [13-14] cross-linking of micelles forming reversible<sup>[15-16]</sup> and non-reversible<sup>[17-18]</sup> nanogels for the delivery of Dox. The suitability of these covalently cross-linked systems in this context was proven by various *in vivo* studies.<sup>[14-15, 19-22]</sup> It was shown that cross-linking results in a tremendous improvement regarding the reduction of tumor growth in mice.<sup>[20]</sup> However, only a few reports deal with nanogels having covalently attached Dox.<sup>[15, 20]</sup> Also, most research focuses on the nanogel formation of systems which were assembled in water having the disadvantage that the micellar form could persist even after cleavage of the linker.

We herein present core cross-linked nanogels from double hydrophilic poly(2-oxazoline)s (POx) containing covalently attached Dox. Poly(2-ethyl-2-oxazoline) (PEtOx), which constitutes the shell of the system, is known to be biocompatible<sup>[23-25]</sup> and possess a stealth effect similar to poly(ethylenglycole).<sup>[26-27]</sup> The core forming block bears amine groups which can be used to lock the structure and, attach a cargo, as well as a labeling unit. The cross-linking was performed by the formation of (pH) reversible imines, generating nanogels. Only a few examples of nanogels based on POx are described so far<sup>[28]</sup> and even fewer are cross-linked reversibly.<sup>[29]</sup>

## Results and Discussion

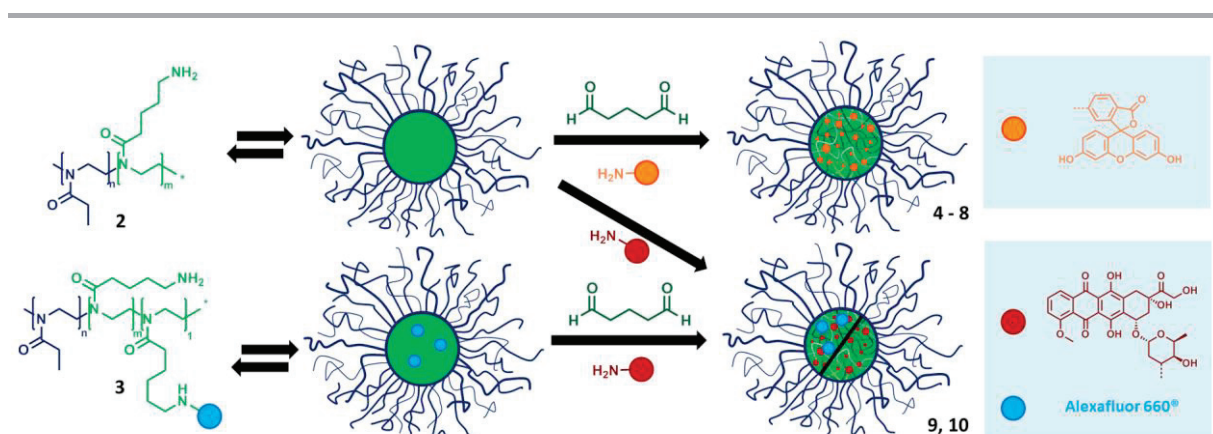
Recently, we reported the synthesis of nanogels based on the self-assembly of poly(2-oxazoline) (POx) block copolymers consisting of an amine containing, cationic block (PAmOx) and a hydrophilic poly(2-ethyl-2-oxazoline) (PEtOx) segment.<sup>[30]</sup> To produce polymeric systems with a reduced dispersity, the synthesis was conducted in a glove-box in order to obtain highly defined diblock copolymers (Table 1). In order to track the fate of this polymeric material within a biological system, labeling using Alexafluor 660<sup>®</sup> was performed. The dye possesses a NHS ester function, able to react with the amine groups of the PAmOx block. One equivalent of dye per polymer chain was applied to retain a sufficient amount of free amine groups for further self-assembly processes, and cross-linking reactions. To separate the polymer from unreacted dye molecules, precipitation, as well as dialysis was performed. The success of the attachment was confirmed by size exclusion chromatography (SEC) measurements comparing the RI and UV traces of the polymer (SI: Figure 1A). The lack of an UV signal at high elution volumes indicates the absence of unbound dye. The fluorescence maximum of the dye coupled to the polymer was found to be identical to the free chromophore (SI: Figure 1B). The coupling efficiency as determined by the emission of the polymer was found to be 30%.

**Table 1:** Composition and analytical data of the POx block copolymers.

Sample	Composition (NMR)	NMR		SEC
		$M_n$ (g mol <sup>-1</sup> )	$M_n$ (g mol <sup>-1</sup> )	$\bar{D}$
1 <sup>a</sup>	P(EtOx <sub>98</sub> - <i>b</i> -BocOx <sub>32</sub> )	17,500	8,200	1.07
2 <sup>b</sup>	P(EtOx <sub>98</sub> - <i>b</i> -AmOx <sub>32</sub> )	14,200	13,900	1.11
3 <sup>b</sup>	P(EtOx <sub>98</sub> - <i>b</i> -[AmOx <sub>31</sub> - <i>stat</i> -FOx <sub>1</sub> ])	15,300	14,100	1.12

<sup>a</sup> SEC measurement in CHCl<sub>3</sub>; <sup>b</sup> SEC Measurement in DMAc.

The self-assembly behavior of these systems was conducted as reported previously.<sup>[30]</sup> Briefly, the polymers were dissolved in chloroform which leads to the formation of micellar structures comprising an PAmOx core. Cross-linking was applied using glutar aldehyde (GA) resulting in the formation of nanogels. To quench the gelation and the obtain water stable systems, 6-amino fluorescein and Doxorubicin (Dox) were used, respectively. The free amine groups of these molecules react with supernumerous aldehyde groups of the cross-linker resulting in a covalent attachment to the nanogel (Scheme 1).



**Scheme 1:** Self-assembly of P(EtOx-*b*-AmOx) to micelles and subsequent cross-linking to dye or Dox loaded nanogels.

Dox quenched nanogels were also produced including 10% of Alexafluor 660<sup>®</sup> labeled polymer (3) to obtain covalently labeled drug carriers (10). The fluorescence of the cross-linked system shows a pronounced shoulder at high wavelengths compared to nanogels containing only Dox (SI: Figure 2A). By increasing the excitation wavelength from 470 to 600 nm, the fluorescence of Alexafluor 660<sup>®</sup> could be isolated to prove the incorporation of the dye into the nanogel (SI: Figure S2B and C).

In order to exploit the EPR effect, the interaction of the produced nanogels with cells is of outstanding importance. To that end, the content of cross-linker was varied to alter the charge of the resulting nanogels. A higher degree of cross-linking and, consequently, a lower amount of free amine groups should result in a reduced zeta potential and, henceforth, in a reduction of the

cellular uptake. The content of GA was varied between 1 and 3 equivalence (per 2 amine groups).

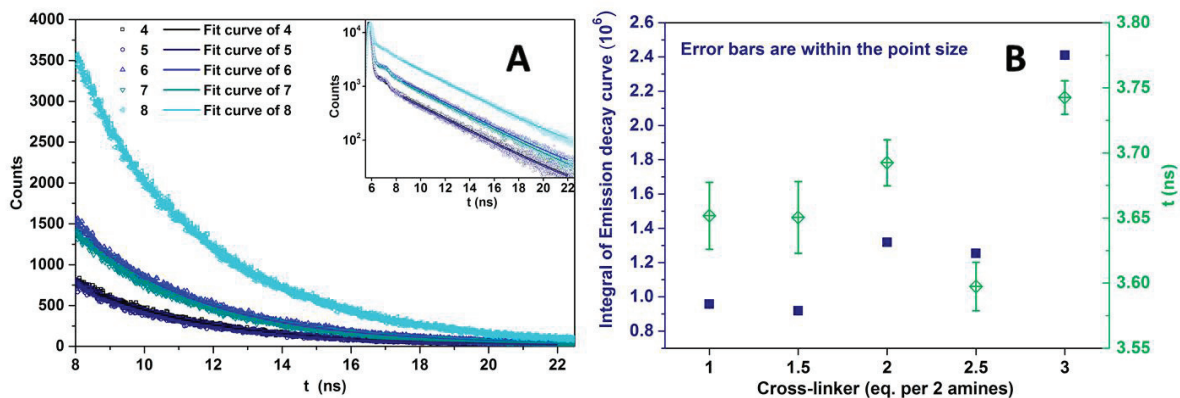
As displayed in Table 2, an increase of the content of GA leads to a reduction of the charge density of the resulting nanogels from 28 mV for equimolar cross-linking to 7 mV for a threefold excess of GA. Moreover, an increase in size, as detected by DLS, can be observed for compounds **4** to **8**. These findings seem best explained by an increased amounts water present during gelation. GA was applied in a 70 wt% aqueous solution and during the cross-linking reaction water is produced as a side product. The additional water will accumulate within the hydrophilic core compartment of the micelle and swell the nanostructure prior or during cross-linking resulting in larger nanogel sizes. This trend is supported by cryoTEM measurements showing an increase in size with an increasing amount of cross-linking. (SI: Figure S3) The absolute values determined by the evaluation of cryoTEM images are, however, significantly smaller indicating a falsification of the DLS derived data by the presence of a small fraction of agglomerates.

**Table 2:** Analytical data of nanogels formed by the self-assembly of polymers **2** and **3**. DLS and zeta potential values are determined in water. Sizes determined by DLS are derived from the number distribution.

Sample	Precursor polymer	Cross-linker (eq. per 2 amines)	Capping agent	Size (DLS, nm, r)	$\zeta$ (mV)	Content of capping agent (wt%)	Size (cryoTEM, r, nm)
4	2	1	6AF	13	28	17	12
5	2	1.5	6AF	17	13	27	13
6	2	2	6AF	20	10	20	14
7	2	2.5	6AF	22	8	24	n.d
8	2	3	6AF	24	7	17	n.d
9	2	3	Dox	13	18	5	n.d
10	3	3	Dox	5	25	6	n.d

A third parameter, which was investigated in dependence on the cross-linking density, was the dye-loading of the resulting systems by evaluating their absorption and fluorescence. Based on absorbance the amount of 6AF dye bound in the micelles can be estimated to values between 17 and 27 wt%. Those numbers are consistent with the experimental procedure and a constant relative amount of dye in the micelles. If, however, measured by the fluorescence of 6AF, a steady increase in dye amount was monitored up to values above 100% indicating a boost in fluorescence intensity by varying the core composition (SI: Figure 4). To study this effect in detail fluorescence lifetime measurements were conducted (Figure 1).



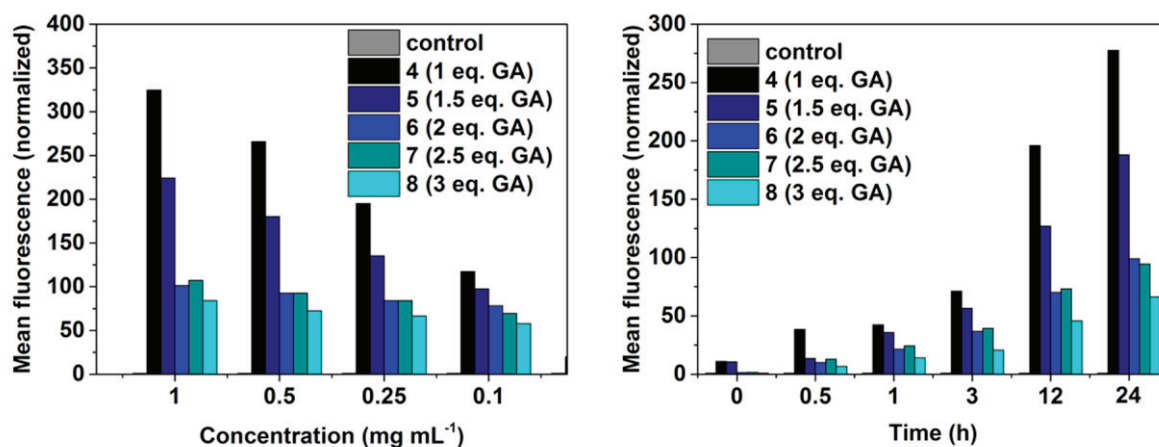


**Figure 1:** Fluorescence lifetime measurements of micelles with varying degree of cross-linking.

The investigation shows an increase in fluorescence lifetime with increasing degree of cross-linking except for 2.5 equivalents of GA used. Also the integrals of the decay curves, which serve as a measure of the fluorescence quantum yield, increase within the series. It is described for fluorescein and its derivatives that electrostatic interactions between the dye and a cationic (surfactant) micelle are able to stabilize the anionic form of the molecule which leads to an increase in fluorescence lifetime and quantum yield.<sup>[31]</sup> However, the cationic character decreases with a higher degree of cross-linking and can, therefore, be held responsible for a general boost of fluorescence compared to pure 6AF, but not for the increasing lifetimes within the series. As an increasing micelle volume is observed upon increasing the amount of cross-linker, it can be estimated that the concentration determining the dye-dye distance also stays roughly constant. Therefore dye-dye interactions such as excimer formation are unlikely to be responsible for the increase in emission intensity and the increase in emission lifetime. Presumably increasing the amount of cross-linker will make the core of the micelles stiffer. Thus the increases in quantum yield and emission lifetime in the stiffer micelles can be due to frozen degrees of freedom, which means that the rate-constant for non-radiative decay ( $k_{nr}$ ) processes is reduced.<sup>[32-33]</sup>

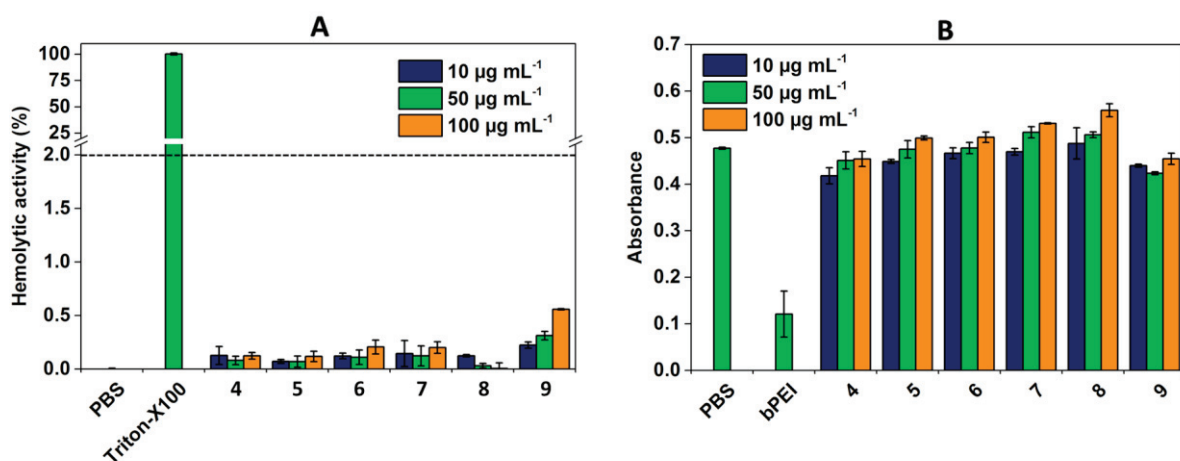
In order to determine the influence of the varying cross-linking density on the cellular uptake, flow cytometry investigations were performed using L929 mouse fibroblasts (Figure 2). The decrease in mean fluorescence with increasing cross-linking degree within the series of micelles clearly shows the influence of the zeta potential on the internalization. This effect can be observed for all concentrations investigated. Also the time dependent uptake study visualizes this behavior of the nanoscopic structures. The difference in the fluorescence intensity of the different micelles was already considered for the calculation of the values. This finding is in agreement with literature reports where objects having an positive net charge are described to be taken up more efficiently as compared to neutral or anionic structures.<sup>[34]</sup> The reported investigation shows that the uptake, which displays a crucial factor for the utilization of the EPR

effect, can be fine-tuned for the presented nanogel systems. The internalization *via* endocytosis is an energy-dependent mechanism, which is usually observed for structures with sizes between 50 to 500 nm. [35] Due to the small size of the micelles the nature of cellular internalization was investigated by uptake studies at 4 °C (SI: Figure S4). The diminished uptake at low temperatures suggest an energy (and temperature) dependent internalization of the micelles as for instance by endocytosis instead of a passive diffusion through the cell membrane.



**Figure 2:** Flow cytometry investigation on the time and concentration dependent uptake of 6AF containing micelles (**61** to **65**) by L929 mouse fibroblasts. Cellular internalization of micelles **4** to **8** in dependency of the concentration after 24 h at 37 °C of incubation or at varying incubation times with a concentration of 0.5 mg mL<sup>-1</sup> at 37 °C.

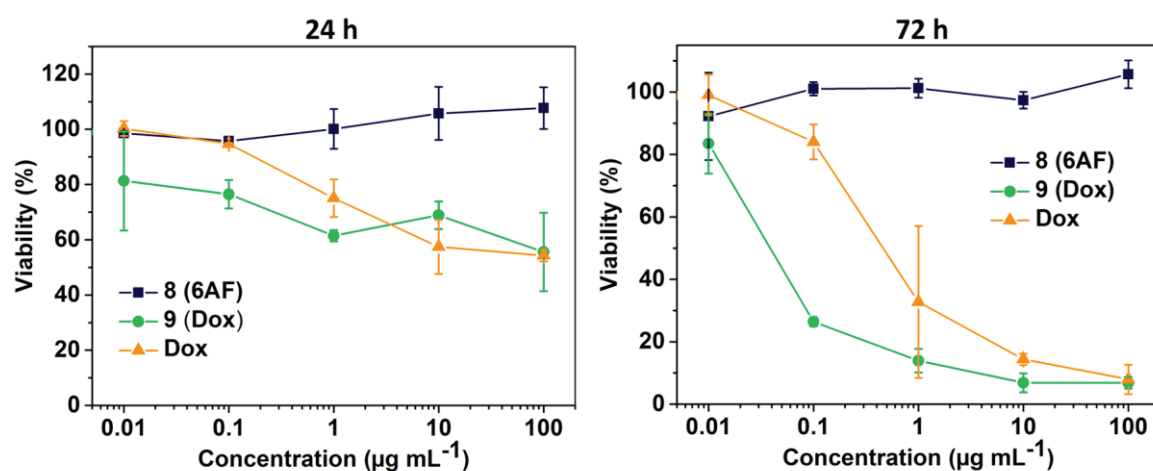
Besides cellular uptake, the blood compatibility of the drug carriers displays an important parameter for the suitability of the drug delivery system. To exploit the EPR effect, long blood circulation times of the nanoscopic carrier are a basic requirement. An interaction with erythrocytes resulting in clotting or disruption is highly undesired. In order to investigate this interaction, the haemolytic activity of 6AF, as well as of the Dox loaded micelles was studied in dependence of the applied concentration (Figure 3A). Triton-X100, which destroys the cellular membranes of red blood cells served as a positive control and pure phosphate buffered saline (PBS) buffer was used as non-hemolytic reference. All micellar structures in a concentration range between 10 and 100 µg mL<sup>-1</sup> resulted in hemolytic activity values well below 2%, which is defined as the minimum value for a hemolysis (according to the ASTM F756-00 standard).



**Figure 3:** A) Hemolysis assay (hemolytic activity) of 6AF loaded micelles (4 to 8) and of the Dox loaded micelle (9) in a concentration range between 10 and 100  $\mu\text{g mL}^{-1}$  of drug carrier as well as B) erythrocyte aggregation of micellar drug carriers using blood of three different donors.

Furthermore, the erythrocyte aggregation was investigated using branched poly(ethylenimine) (bPEI, 25,000  $\text{g mol}^{-1}$ , 50  $\mu\text{g mL}^{-1}$ ) as a positive control and found to be negligible in the given concentration range (Figure 3B, SI Figure S6). The absorbance level of the blood samples, treated with micellar compound, all lie in the region of the PBS negative control.

To act as an efficient drug carrier, the synthesized nanogels have to possess the ability to release their cargo after cellular uptake. The toxicity of Dox is based on the intercalation of the drug within the base pairs of DNA<sup>[36]</sup> which results in an inhibition of the transcription and, consequently, cell death.<sup>[37]</sup> Henceforth, the drug has to be released from the nanogels and migrate into the nucleus of the cell to have a negative effect on the cell viability. For this reason, the concentration dependent toxicity of Dox loaded nanogels (9) was investigated by the XTT assay and compared to the free drug and 6AF loaded nanogels (Figure 4).



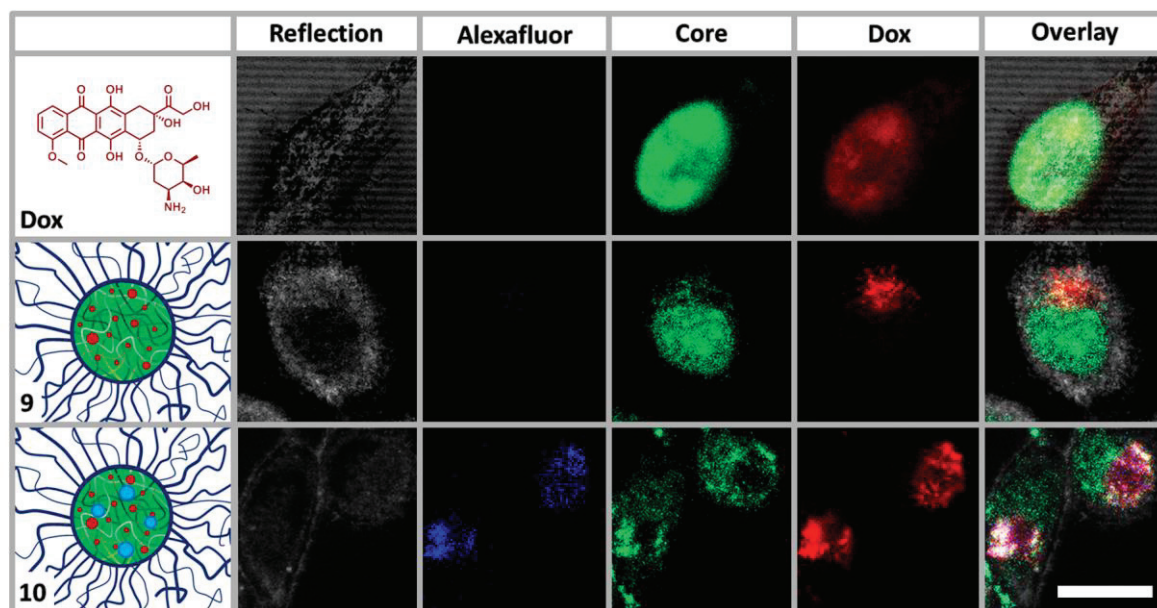
**Figure 4:** Cytotoxicity investigation of 6AF loaded micelles (8), Dox associated micelles (9) and free Dox in dependence on the concentration after 1 or 3 d of incubation at 37 °C. Cell viability

was investigated on L929 mouse fibroblasts using the XTT assay. Data are expressed as mean  $\pm$  SD of three determinations.

---

The indicated concentration refers to the free Dox. Since only 5% of the drug is incorporated into nanogel **9**, the 20 fold concentration of this nanocarrier was used to reach equal Dox concentrations for each measuring point. The 6AF loaded micelle (**8**) was applied in equal concentrations as the Dox loaded nanostructure. As expected, the 6AF loaded nanogel has no negative effect on the cell viability. PEOx, which constitutes the shell of the micellar nanogels, is reported to be biocompatible<sup>[25]</sup> and prevents the nanostructure from harmful interactions with cellular compartments. In contrast, Dox as well as the Dox loaded nanogel show a significant decrease in cell viability, already at very low concentrations for both incubation times investigated. It is noteworthy that the toxicity of compound **9** is significantly higher at low concentrations (0.1 and 1  $\mu\text{g mL}^{-1}$ ) as the respective free drug. This suggests an efficient transport of Dox to the nucleus once taken up by cells.

To investigate this effect in more detail, the colocalization of Dox and Dox loaded nanogels was studied by confocal laser scanning microscopy (CLSM). To visualize the fate of drug and carrier separately, non-labeled (**9**) as well as labeled nanogels (**10**) were utilized. The fluorescence spectrum of nanogel **10** possesses a shoulder at high wavelength as a result of the presence of Alexafluor 660<sup>®</sup> (SI: Figure 2). By using higher excitation wavelength, the emission of the dye can be isolated which enables a separate detection by CLSM. The colocalization was investigated in L929 mouse fibroblasts after 12 h of incubation with either Dox or Dox-containing nanogels (Figure 5). The free drug is clearly associated with the nucleus of the cells which is a result of the intercalation with DNA. For both nanogels, however, the fluorescence of Dox is visible at an additional nuclear intracellular location. Our recent studies on this type of nanogel suggests a endosomal or lysosomal localization of the drug carrier.<sup>[30]</sup> As evident by the fluorescence signal of Alexafluor 660<sup>®</sup> at the same location of the Dox fluorescence this signal is attributed to intact nanocarriers. This result can be explained by the high dependency of the Dox emission on its environment. It is reported that the fluorescence signal of the drug strongly decreases upon intercalation with genetic material<sup>[38]</sup> and can be increased by incorporation in membranes or micelles.<sup>[39]</sup> Consequently, in the case of Dox associated nanogels, the fluorescence of the drug carrier in the cytosol is likely to outshine the intercalated drug. The similar toxicity of both, the free drug and the nanogel, however, suggests an efficient uptake and release of Dox within the cell.



**Figure 5:** CLSM images of L292 mouse fibroblasts treated with either Dox, Dox conjugated micelle (**9**) or Dox conjugated micelle labeled with Alexafluor 660® (**10**) for 12 h at 37 °C using a Dox concentration of 1  $\mu\text{g mL}^{-1}$ . Cell nuclei were stained using SYTO®Green 13:  $\lambda_{\text{ex}} = 488 \text{ nm}$ ,  $\lambda_{\text{em}} = 505 \text{ to } 530$ ; Dox:  $\lambda_{\text{ex}} = 488 \text{ nm}$ ,  $\lambda_{\text{em}} = 585 \text{ to } 615 \text{ nm}$ ; Dox:  $\lambda_{\text{ex}} = 633 \text{ nm}$ ,  $\lambda_{\text{em}} = 724 \text{ to } 777 \text{ nm}$ . Scale bar: 10  $\mu\text{m}$ .

A likely scenario is the combination of a superior cellular uptake of Dox associated nanogels (compared to free Dox at similar concentrations) and an incomplete release of the payload. The total amount of Dox taken up by the cells in the presence of nanogel **8** is higher as for the free drug. However, the drug partially remains in the lysosome resulting in similar toxicities. Further investigations of the cellular uptake and the toxicity of Dox associated nanogels have to be conducted in order to fully understand the mechanism behind the toxicity of Dox loaded POx nanogels.

## Conclusion

In summary we were able to show that a variation of the cross-linking density of cationic POx nanogels is able to influence the zeta potential of the nanoscopic assemblies and that this alteration directly affects the cellular uptake *in vitro*. The changed microenvironment within the nanostructures influences the fluorescence of covalently bound amino-fluorescein in a positive way, increasing the fluorescence lifetimes. In order to investigate the ability of POx nanogels to serve as a potential drug carrier in cancer therapy, Dox was covalently bound and the cytotoxicity of the resulting nanogel was found to be similar to the free drug while nanocarriers without the Dox did not interfere with the cell viability. The blood compatibility of the produced systems was evaluated and erythrocyte aggregation, as well as hemolysis investigations revealed no harmful effects of either dye or Dox associated structures. The intracellular



localization of Dox associated POx drug carriers were studied by the use of labeled nanogels indicating a lysosomal localization of the nanostructures.

Further studies will focus on the elucidation of the intracellular drug release and toxicity mechanism of Dox conjugated nanogels and their performance in *in vivo* studies.

## Experimental

### *Material and Instrumentation*

Chemicals and solvents were purchased from Sigma-Aldrich, Merck, Fluka, and Acros. 2-Ethyl-2-oxazoline (EtOx) and methyl tosylate (MeOTos) were distilled to dryness prior to use. EtOx was dried using barium oxide before distillation. 2-(4-((*tert*-Butoxycarbonyl)amino)butyl)-2-oxazoline (BocOx) was synthesized as described in a previous publication.<sup>[40]</sup>

The Initiator Sixty single-mode microwave synthesizer from Biotage, equipped with a non-invasive IR sensor (accuracy: 2%), was used for polymerizations under microwave irradiation. Microwave vials were heated overnight to 110 °C and allowed to cool to room temperature under an argon atmosphere before use. All polymerizations were carried out under temperature control. Size-exclusion chromatography (SEC) measurements of the protected polymers were performed on a Shimadzu system equipped with a SCL-10A system controller, a LC-10AD pump, a RID-10A refractive index detector and a PSS SDV column with chloroform/triethylamine (NEt<sub>3</sub>)/*iso*-propanol (94:4:2) as eluent. The column oven was set to 50 °C. SEC of the deprotected statistical copolymers was performed on a Shimadzu system with a LC-10AD pump, a RID-10A refractive index detector, a system controller SCL-10A, a degasser DGU-14A, and a CTO-10A column oven using *N,N*-dimethyl acetamide (DMAc) with 2.1 g L<sup>-1</sup> LiCl as the eluent and the column oven set to 50 °C. Poly(styrene) (PS) samples were used as calibration standards for both solvent systems. Proton NMR spectroscopy (<sup>1</sup>H NMR) measurements were performed at room temperature on a Bruker AC 300 and 400 MHz spectrometer, using CDCl<sub>3</sub> or *N,N*-dimethyl formamide (DMF)-D<sub>7</sub> as solvents. The chemical shifts are given in ppm relative to the signal of the residual non-deuterated solvent.

Batch dynamic light scattering (DLS) was performed on a Zetasizer Nano ZS (Malvern Instruments, Herrenberg, Germany). All measurements were performed in folded capillary cells (DTS1071, Malvern Instruments, Herrenberg, Germany). After an equilibration time of 180 s, 3 × 30 s runs were carried out at 25 °C ( $\lambda = 633$  nm). The counts were detected at an angle of 173°. Each measurement was performed in triplicate. Apparent hydrodynamic radii, R<sub>h</sub>, were calculated according to the Stokes–Einstein equation.

Laser Doppler velocimetry was used to measure the electrokinetic potential, also known as zeta potential. The measurements were performed on a Zetasizer Nano ZS (Malvern Instruments, Herrenberg, Germany) in folded capillary cells (DTS1071). For each measurement, 15 runs were carried out using the fast-field and slow-field reversal mode at 150 V. Each experiment was performed in triplicate at 25 °C. The zeta potential ( $\zeta$ ) was calculated from the electrophoretic mobility ( $\mu$ ) according to the Henry Equation.<sup>[41]</sup> The Henry coefficient,  $f(\kappa a)$ , was calculated according to Ohshima.<sup>[42]</sup>

cryoTEM investigations were conducted with a FEI Tecnai G<sup>2</sup> 20 at 200 kV acceleration voltage. Specimens were vitrified by a Vitrobot Mark V system on Quantifoil grids (R2/2). The blotting time was 1 s with blotting force offset of 0. The amount of solution was 7  $\mu$ L. Samples were plunge frozen in liquid ethane and stored under liquid nitrogen until transferred to the Gatan cryo-holder and brought into the microscope. Images were acquired with a 4k  $\times$  4k CCD Eagle camera.

Absorbance and fluorescence spectra were recorded using a Tecan M200 Pro fluorescence micro plate reader (Crailsheim, Germany) by the use of black well plates with a flat and transparent bottom.

*Block copolymer of 2-ethyl-2-oxazoline (EtOx) and 2-(4-((tert-butoxycarbonyl)amino)butyl)-2-oxazoline (BocOx) (P(EtOx-b-BocOx)), (1)*

In a microwave vial, EtOx (757  $\mu$ L, 7.5 mmol), MeOTos (16.2  $\mu$ L, 0.107 mmol) and acetonitrile (3.4 mL) were mixed under inert conditions. After heating in the microwave synthesizer at 140 °C for 25 min the vial was introduced into a glove box with nitrogen atmosphere and BocOx (803  $\mu$ L, 3.2 mmol) was added. The closed vial was heated again in the microwave synthesizer (140 °C, 20 min). The solution was precipitated in cold (–80 °C, 300 mL) diethyl ether. The white precipitate was filtered and dried in high vacuum (1.4 g, 92%).

<sup>1</sup>H NMR (CDCl<sub>3</sub>, 300 MHz) (**6**):  $\delta$  = 7.66, (d, 8.1 Hz, 0.019 H, tosylate), 7.14 (d, 8.21 Hz, 0.019 H, tosylate), 3.45 (s, 4 H, backbone), 3.10 (s, 0.58 H, CH<sub>2</sub>-CH<sub>2</sub>-NH (BocOx)), 2.50-2.15 (m, 1.96 H, CH<sub>2</sub> (EtOx)/CH<sub>2</sub>-CH<sub>2</sub>-NHBoc), 1.62 (s, 0.52 H, CH<sub>2</sub>-CH<sub>2</sub>-CH<sub>2</sub> (BocOx)), 1.52 (s, 0.52 H, CH<sub>2</sub>-CH<sub>2</sub>-CH<sub>2</sub> (BocOx)), 1.42 (s, 2.3 H, CH<sub>3</sub> (BocOx)), 1.21 (s, 2.1 H, CH<sub>3</sub> (EtOx)) ppm.

SEC (eluent: CHCl<sub>3</sub>/iso-propanol/NEt<sub>3</sub>, PS-standard): M<sub>n</sub> = 8,200 g mol<sup>-1</sup>, M<sub>w</sub> = 9,900 g mol<sup>-1</sup>, Đ = 1.07.

#### *Deprotection of P(EtOx-b-BocOx) (1) to yield P(EtOx-b-AmOx), (2)*

P(EtOx-b-BocOx) (**1**, 1.3 g) was dissolved in TFA (5 mL) and heated to 60 °C for 1 h. After stirring for 12 h at room temperature, the mixture was diluted with 10 mL methanol and precipitated in 400 mL of cold (−80 °C) diethyl ether. The precipitate was re-dissolved in methanol (100 mL) and stirred with Amberlyst A21 for 48 h. Subsequently, the solvent was removed, the polymer was dissolved in de-ionized water and freeze dried (−80 °C, 0.003 mbar). The polymer was obtained as white powder (1.2 g, 92%).

<sup>1</sup>H NMR (DMF-D<sub>7</sub>, 300 MHz) (**2**): δ = 4.9 (s, 2.3 H, NH<sub>2</sub>), 3.51 (s, 4 H, backbone), 3.07 (s, 0.49 H, CH<sub>2</sub>-CH<sub>2</sub>-NH<sub>2</sub>), 2.44 (m, 2.1 H, CH<sub>2</sub> (EtOx)/CH<sub>2</sub>-CH<sub>2</sub>-CO (AmOx)), 1.9-1.54 (m, 0.96 H, CH<sub>2</sub>-CH<sub>2</sub>-CH<sub>2</sub>-CH<sub>2</sub> (AmOx)), 1.2 (s, 2,3 H, CH<sub>3</sub> (EtOx)) ppm.

SEC (eluent: DMAc/LiCl, PS-standard): M<sub>n</sub> = 13,900 g mol<sup>-1</sup>, Đ = 1.11.

#### *Labeling of P(EtOx-b-AmOx)(2) using Alexafluor 660®, (3)*

P(EtOx-b-AmOx) (**2**, 14 mg) was dissolved in DMF (5 mL) and Alexafluor 660® (1 mg, ~1 eq. per macromolecule) as well as triethyl amine (1 μL) were added under stirring. The solution was stirred at room temperature overnight and subsequently precipitated in cold diethyl ether, (300 mL, -80 °C). The precipitated was filtered off, dissolved in water and transferred to a dialysis tube (6,000 to 8,000 g mol<sup>-1</sup> cut off, Spectra/Por®). The polymer was dialysed against water until the solution outside the tube stayed colorless. After freeze drying, the product was obtained as deep blue powder (8 mg, 53%, degree of functionalization = 30%).

SEC (eluent: DMAc/LiCl, PS-standard): M<sub>n</sub> = 14,600 g mol<sup>-1</sup>, Đ = 1.11.

UV/Vis: λ<sub>Abs</sub> = 660 nm, λ<sub>Em</sub> (excitation at 600 nm) = 690 nm.

#### *Self-assembly and cross-linking (4 -10)*

To create nanostructures, the unlabeled block copolymer (**2**, 90 mg, 0.006 mmol) or a mixture of the polymers **2** and **3** (9:1, 90 mg, 0.006 mmol) were dissolved in CHCl<sub>3</sub>, (5 mg mL<sup>-1</sup>) and stirred for 3 h. Subsequently, glutaraldehyde (30 mg, 0.3 mmol, 1.5 eq. per amine) was added and the solution was stirred another 3 h. With proceeding reaction time the color of the solution changed from colorless to yellow. To quench the excess of aldehyde functionalities, 6-amino fluorescein (50 mg) or Doxorubicin (50 mg) were added, respectively, and stirred for 12 h. Subsequently, the amount of solvent was reduced under an argon stream and the residual was precipitated in 100 mL cold diethyl ether (−80 °C). To purify the self-assembled structures from residual capping agent and cross-linker, dialysis in MeOH/water (1:4) was applied using a membrane with a molar mass cut off of 3,500 g mol<sup>-1</sup> (Roth Zellutrans). After the extraction was finished, the

dialysis medium was changed to pure water and the aqueous solution was freeze dried to yield an orange or, in the case of Dox, a red powder.

#### *Determination of dye loading content by absorbance/fluorescence*

The absorbance/fluorescence of 6AF loaded nanostructures was investigated under alkaline conditions ( $1 \text{ mol L}^{-1}$  NaOH in water) in diluted solution ( $0.1 \text{ mg mL}^{-1}$ ). The absorbance was determined at a wavelength of 490 nm and compared to a dilution series of 6AF in the same aqueous NaOH solution. To the 6AF stock solution a 100 fold excess of glutaraldehyde was added to ensure that only the imine species of 6AF is present. Emission was detected at an excitation wavelength of 450 nm. Micellar samples as well as 6AF calibration exhibit an emission maximum at 510 nm.

Dox conjugated samples were measured in water ( $0.1 \text{ mg mL}^{-1}$ ) and compared to a dilution series of Dox in water. All measurements were carried out in a 96 well-plate format with  $200 \mu\text{L}$  per well and double determination for each measuring point. The read out was accomplished using a Tecan M200 Pro fluorescence micro plate reader (Crailsheim, Germany).

#### *Fluorescence lifetime measurements*

The emission decay curves were obtained by time-correlated-single-photon-counting. After excitation with a frequency-doubled Ti-sapphire laser adjusted to 870 nm (Tsunami, Newport Spectra-Physics GmbH, pulse-to-pulse repetition rate 400 kHz after passing a pulse selector, model 3980, Newport Spectra-Physics GmbH), *i.e.* at  $\lambda_{\text{ex}} = 435 \text{ nm}$ , the luminescence of the sample was collected in a  $90^\circ$ -geometry and detected with a Becker & Hickl PMC-100-4 photon-counting module. A long-pass filter (455 nm) is inserted in the detection beam path. The samples were adjusted to yield optical densities  $< 0.03$  at the excitation wavelength in aqueous NaOH ( $0.1 \text{ mol L}^{-1}$ ). The measurements were accumulated at count rates  $< 3\%$  of the rep.-rate until 15000 counts in the maximum were reached.

#### *Determination of the cytotoxicity by XTT assay*

Cytotoxicity studies were performed with the sensitive mouse fibroblast cell line L929, which is recommended by DIN ISO10993-5. The cells were routinely cultured in Dulbecco's modified eagle's medium (DMEM) supplemented with 10% fetal calf serum (FCS),  $100 \text{ U mL}^{-1}$  penicillin and  $100 \mu\text{g mL}^{-1}$  streptomycin at  $37^\circ\text{C}$  in a humidified 5% (v/v)  $\text{CO}_2$  atmosphere.

In detail, the cells were seeded at  $10^4$  cells per well in a 96-well plate and incubated for 24 h, whereas no cells were seeded in the outer wells. Afterwards, the testing substances (nanogels or doxorubicin) at indicated end concentrations were added to the cells and the plates were incubated for further 24 h. Subsequently, a XTT assay (Cell Proliferation

Kit II, Roche Diagnostics) was performed as recommended by supplier's information. After a further incubation of 4 h, the absorbance was measured at a wavelength of 450 nm and 630 nm as reference wavelength, with untreated cells on the same well plate serving as negative controls. The negative control was standardized as 0% of metabolism inhibition and referred as 100% viability. Cell viability below 70% was considered indicative of cytotoxicity. Data are expressed as mean  $\pm$  SD of three determinations.

#### *Blood compatibility measurements*

To assess the hemolytic activity of the polymer solutions, blood from sheep, collected in heparinized-tubes (Institut für Versuchstierkunde und Tierschutz, Friedrich Schiller University Jena), was centrifuged at 4500 g for 5 min, and the pellet was washed three times with cold 1.5 mmol L<sup>-1</sup> phosphate buffered saline (PBS, pH 7.4). After dilution with PBS in a ratio of 1:7, aliquots of erythrocyte suspension were mixed 1:1 with the polymer solution and incubated in a water bath at 37 °C for 60 min. After centrifugation at 2400 g for 5 min the hemoglobin release into the supernatant was determined spectrophotometrically using a microplate reader (TECAN Infinite M200 PRO plate reader, Crailsheim, Germany) at 544 nm wavelength. Complete hemolysis (100%) was achieved using 1% Triton X-100 serving as positive control. Thereby, PBS served as negative control (0%). A value less than 2% hemolysis rate was taken as non-hemolytic. Experiments were run in triplicates and were performed with three different blood donors.

For the examination of the erythrocyte aggregation, erythrocytes were isolated as described above. An erythrocytes suspension was mixed with the same volume of polymer solution in a clear flat bottomed 96-well plate. The cells were incubated at 37 °C for 2 h, and the absorbance was measured at 645 nm in a microplate reader (TECAN, Crailsheim, Germany). 25 kDa bPEI (50  $\mu$ g mL<sup>-1</sup>) was used as positive control and as negative control, cells were treated with PBS. Absorbance values of the test solutions lower than negative control were regarded as aggregation. Experiments are the result of triplicates and were performed with three different donor blood batches.

#### *Photometrical and microscopical methods*

For the photometric absorbance measurements, a TECAN Infinite M200 PRO plate reader (TECAN, Crailsheim, Germany) was used to measure the absorption of samples from the XTT cytotoxicity assay (570 nm with a background correction of the optical density (OD) at 690 nm). Each well containing the sample was measured in four different spots each with 25 flashes per scan. For CLSM analysis of uptake and co-localization with cell organelle, a Dox concentration of 1  $\mu$ g mL<sup>-1</sup> was used and the nuclei were stained using SYTO®Green 13. CLSM images were acquired using a Zeiss LSM 510 META (Carl Zeiss) with excitation wavelengths/emission filters of 633 nm/BP 724 to 777 nm for Alexafluor



660®, 488 nm/BP 505 to 530 nm for SYTO®Green 13 and 488 nm/BP 585 to 615 nm for Dox. Images were captured with a Plan-Apochromat 63 × objective and in multitrack mode, enabling single excitation and emission of fluorescence dyes. Co-localization was visualized in overlay images of the multiple channels.

#### *Investigation of the cellular uptake*

The evaluation of the micellar uptake was performed by flow cytometry (FC) measured on a Beckmann Coulter Cytomics FC-500 equipped with an Uniphase Argon ion laser (488 nm, 20 mW output) and analyzed with the Cytomics CXP software. For the time dependent uptake investigations, cells (L929) were incubated between 30 min and 24 h with micelles at a concentration of 0.5 mg mL<sup>-1</sup>, whereas the concentration dependent uptake was investigated over an incubation time of 24 h using micelle concentrations in the range between 0.1 and 1 mg mL<sup>-1</sup>. Cells incubated with culture medium only served as control. Data are expressed as mean ± SD of three determinations. For uptake studies at low temperature, the cells were incubated with micelles (0.5 mg mL<sup>-1</sup>) for 4 h at 4 and 37 °C respectively and the internalization was monitored using FC analysis as described above.

#### **Acknowledgements**

cryoTEM investigations were performed at the cryoTEM facilities of the Jena Center for Soft Matter (JCSM). TEM facilities were funded by a grant of the DFG (German Research Foundation) and the EFRE (European Fund for Regional Development).

#### **References**

- [1] R. Tong, L. Tang, L. Ma, C. Tu, R. Baumgartner, J. Cheng, *Chem. Soc. Rev.* **2014**, *43*, 6982-7012.
- [2] M. Narvekar, H. Xue, J. Eoh, H. Wong, *AAPS PharmSciTech* **2014**, *15*, 822-833.
- [3] V. Delplace, P. Couvreur, J. Nicolas, *Polym. Chem.* **2014**, *5*, 1529-1544.
- [4] H. Maeda, K. Greish, J. Fang, in *Polymer Therapeutics II, Vol. 193* (Eds.: R. Satchi-Fainaro, R. Duncan), Springer Berlin Heidelberg, **2006**, pp. 103-121.
- [5] G. Riess, *Prog. Polym. Sci.* **2003**, *28*, 1107-1170.
- [6] H. Ding, X. Wang, S. Zhang, X. Liu, *Journal of Nanoparticle Research* **2012**, *14*, 1-13.
- [7] M. Talelli, C. J. F. Rijcken, W. E. Hennink, T. Lammers, *Curr. Opin. Solid State Mater. Sci.* **2012**, *16*, 302-309.
- [8] R. T. Chacko, J. Ventura, J. Zhuang, S. Thayumanavan, *Adv. Drug Deliv. Rev.* **2012**, *64*, 836-851.
- [9] C. F. van Nostrum, *Soft Matter* **2011**, *7*, 3246-3259.
- [10] O. Jung Kwon, D. Ray, J. S. Daniel, M. Krzysztow, *Prog. Polym. Sci.* **2008**, *33*, 448-477.
- [11] J. Ding, F. Shi, D. Li, L. Chen, X. Zhuang, X. Chen, *Biomater. Sci.* **2013**, *1*, 633-646.
- [12] J. O. Kim, G. Sahay, A. V. Kabanov, T. K. Bronich, *Biomacromolecules* **2010**, *11*, 919-926.
- [13] K. Wang, G.-F. Luo, Y. Liu, C. Li, S.-X. Cheng, R.-X. Zhuo, X.-Z. Zhang, *Polym. Chem.* **2012**, *3*, 1084-1090.
- [14] J. Dai, S. Lin, D. Cheng, S. Zou, X. Shuai, *Angew. Chem. Int. Ed.* **2011**, *50*, 9404-9408.
- [15] T. C. Lai, H. Cho, G. S. Kwon, *Polym. Chem.* **2014**, *5*, 1650-1661.

- [16] Y. Xu, F. Meng, R. Cheng, Z. Zhong, *Macromol. Biosci.* **2009**, *9*, 1254-1261.
- [17] M. Talelli, M. Iman, A. K. Varkouhi, C. J. F. Rijcken, R. M. Schiffelers, T. Etrych, K. Ulbrich, C. F. van Nostrum, T. Lammers, G. Storm, W. E. Hennink, *Biomaterials* **2010**, *31*, 7797-7804.
- [18] Y. Wu, Q. Lai, S. Lai, J. Wu, W. Wang, Z. Yuan, *Colloids. Surf. B: Biointerfaces* **2014**, *118*, 298-305.
- [19] H.-z. Jia, J.-y. Zhu, X.-l. Wang, H. Cheng, G. Chen, Y.-f. Zhao, X. Zeng, J. Feng, X.-z. Zhang, R.-x. Zhuo, *Biomaterials* **2014**, *35*, 5240-5249.
- [20] Z. Zhou, L. Li, Y. Yang, X. Xu, Y. Huang, *Biomaterials* **2014**, *35*, 6622-6635.
- [21] Y. Li, K. Xiao, J. Luo, W. Xiao, J. S. Lee, A. M. Gonik, J. Kato, T. A. Dong, K. S. Lam, *Biomaterials* **2011**, *32*, 6633-6645.
- [22] S. Yu, J. Ding, C. He, Y. Cao, W. Xu, X. Chen, *Adv. Healthcare Mater.* **2014**, *3*, 752-760.
- [23] J. Kronek, Z. Kroneková, J. Lustoň, E. Paulovičová, L. Paulovičová, B. Mendrek, *J. Mater. Sci.: Mater. Med.* **2011**, *22*, 1725-1734.
- [24] J. Kronek, E. Paulovičová, L. Paulovičová, Z. Kroneková, J. Lustoň, *J. Mater. Sci.: Mater. Med.* **2012**, *23*, 1457-1464.
- [25] R. Luxenhofer, G. Sahay, A. Schulz, D. Alakhova, T. K. Bronich, R. Jordan, A. V. Kabanov, *J. Control. Release* **2011**, *153*, 73-82.
- [26] M. C. Woodle, C. M. Engbers, S. Zalipsky, *Bioconjugate Chem.* **1994**, *5*, 493-496.
- [27] S. Zalipsky, C. B. Hansen, J. M. Oaks, T. M. Allen, *J. Pharm. Sci.* **1996**, *85*, 133-137.
- [28] M. Hartlieb, K. Kempe, U. S. Schubert, *J. Mater. Chem. B* **2015**, *3*, 526-538.
- [29] C. Legros, M.-C. De Pauw-Gillet, K. C. Tam, S. Lecommandoux, D. Taton, *Polym. Chem.* **2013**, *4*, 4801-4808.
- [30] M. Hartlieb, D. Pretzel, M. Wagner, S. Hoepfener, P. Bellstedt, M. Görlach, C. Englert, K. Kempe, U. S. Schubert, *J. Mater. Chem. B* **2015**, DOI: 10.1039/C1034TB02069C
- [31] A. Song, J. Zhang, M. Zhang, T. Shen, J. a. Tang, *Colloids Surf., A* **2000**, *167*, 253-262.
- [32] R. Humphry-Baker, M. Graetzel, R. Steiger, *J. Am. Chem. Soc.* **1980**, *102*, 847-848.
- [33] W.-C. Wu, C.-Y. Chen, Y. Tian, S.-H. Jang, Y. Hong, Y. Liu, R. Hu, B. Z. Tang, Y.-T. Lee, C.-T. Chen, W.-C. Chen, A. K. Y. Jen, *Adv. Funct. Mater.* **2010**, *20*, 1413-1423.
- [34] A. Verma, F. Stellacci, *Small* **2010**, *6*, 12-21.
- [35] A. Albanese, P. S. Tang, W. C. W. Chan, *Annu. Rev. Biomed. Eng.* **2012**, *14*, 1-16.
- [36] C. A. Frederick, L. D. Williams, G. Ughetto, G. A. Van der Marel, J. H. Van Boom, A. Rich, A. H. J. Wang, *Biochemistry* **1990**, *29*, 2538-2549.
- [37] J. Cummings, J. F. Smyth, *Ann. Oncol.* **1993**, *4*, 533-543.
- [38] M. Fiallo, A. Laigle, M.-N. Borrel, A. Garnier-Suillerot, *Biochem. Pharmacol.* **1993**, *45*, 659-665.
- [39] P. Mohan, N. Rapoport, *Mol. Pharm.* **2010**, *7*, 1959-1973.
- [40] M. Hartlieb, D. Pretzel, K. Kempe, C. Fritzsche, R. M. Paulus, M. Gottschaldt, U. S. Schubert, *Soft Matter* **2013**, *9*, 4693-4704.
- [41] A. V. Delgado, F. Gonzalez-Caballero, R. J. Hunter, L. K. Koopal, J. Lyklema, *J. Colloid Interface Sci.* **2007**, *309*, 194-224.
- [42] H. Ohshima, *J. Colloid Interface Sci.* **1994**, *168*, 269-271.

## Supporting information

### Nanogels based on double hydrophilic poly(2-oxazoline) for doxorubicin delivery

Matthias Hartlieb,<sup>a,b</sup> Tanja Buš,<sup>a,b</sup> David Pretzel,<sup>a,b</sup> Joachim Kübel,<sup>c,d</sup> Stephanie Hoeppener,<sup>a,b</sup> Kristian Kempe,<sup>a,b,†</sup> Benjamin Dietzek,<sup>c,d</sup> Ulrich S. Schubert<sup>a,b,\*</sup>

<sup>a</sup> Laboratory of Organic and Macromolecular Chemistry (IOMC), Friedrich Schiller University Jena, Humboldtstrasse 10, 07743, Jena, Germany

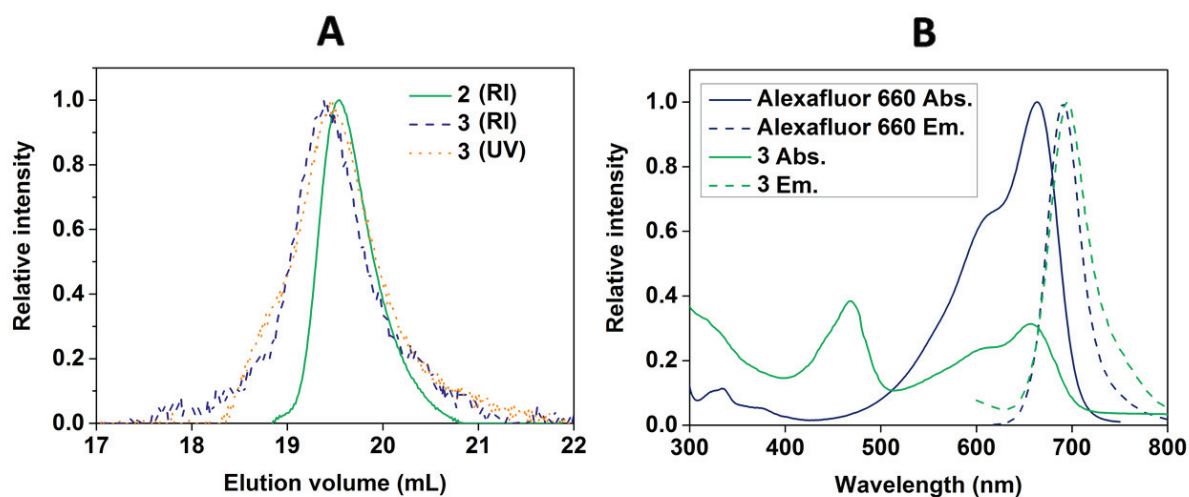
<sup>b</sup> Jena Center for Soft Matter (JCSM), Friedrich Schiller University Jena, Philosophenweg 7, 07743, Jena, Germany

<sup>c</sup> Institute of Physical Chemistry (IPC) and Abbe Center of Photonics, Friedrich Schiller University Jena, Helmholtzweg 4, 07743 Jena, Germany

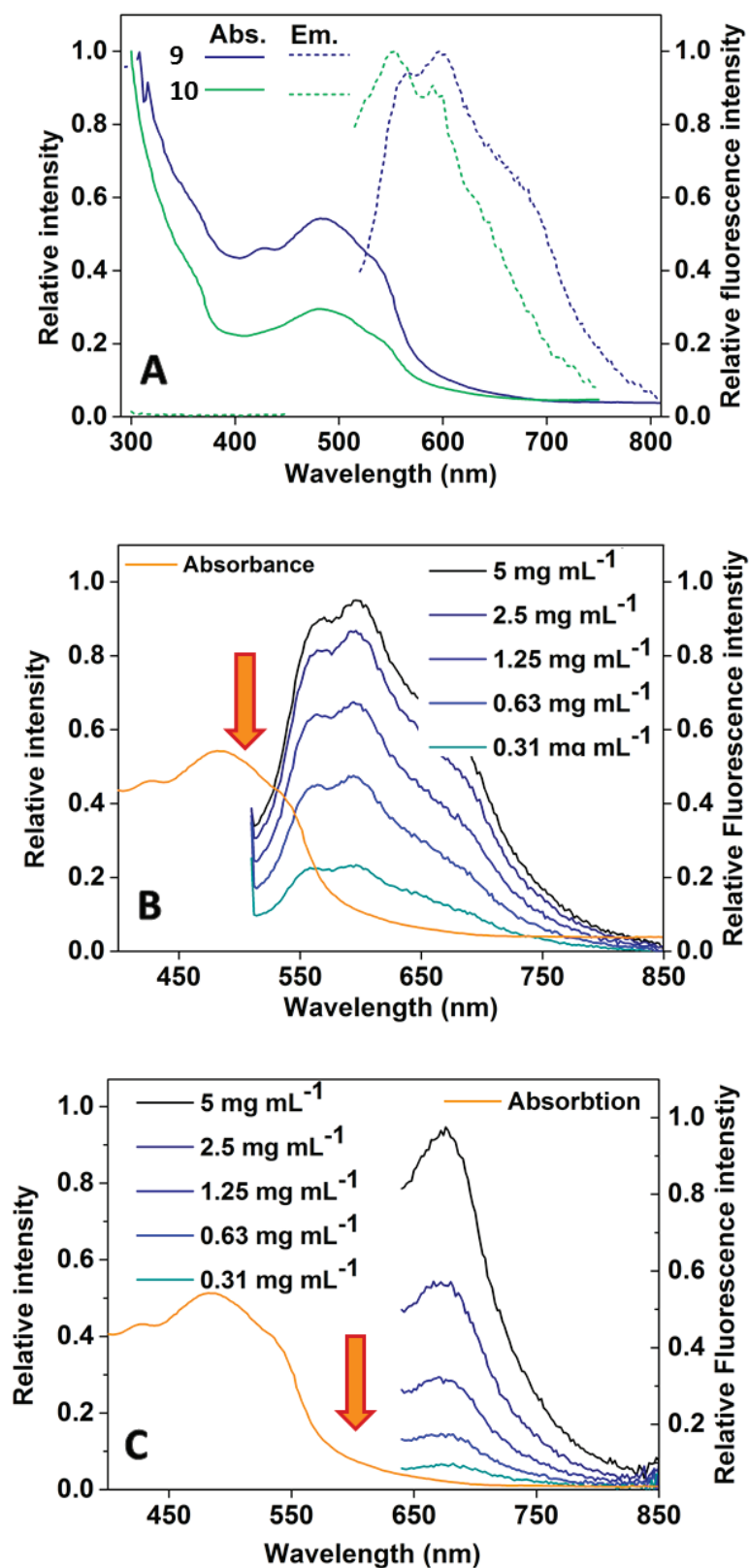
<sup>d</sup> Leibniz Institute of Photonic Technology (IPHT), Albert-Einstein-Str. 9, 07745 Jena, Germany

<sup>†</sup> Current address: Department of Chemistry, University of Warwick, Gibbet Hill Road, Coventry, CV4 7AL, U.K.

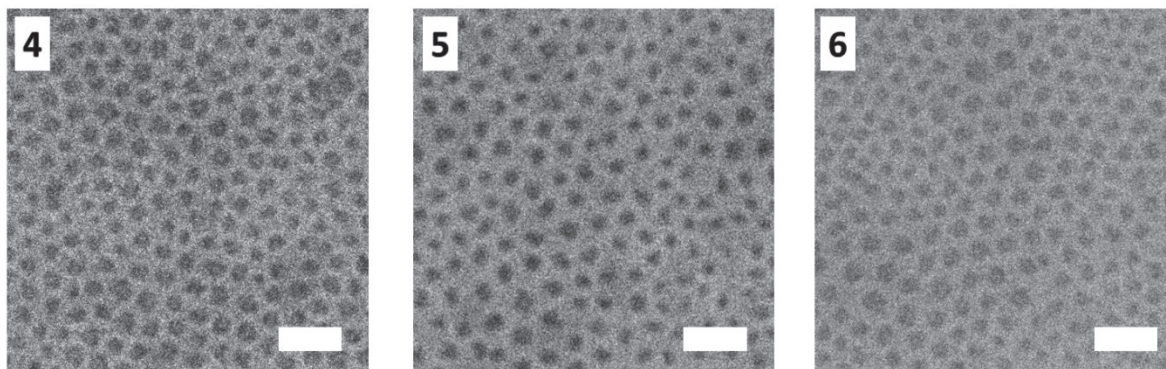
\* Address correspondence to [ulrich.schubert@uni-jena.de](mailto:ulrich.schubert@uni-jena.de)



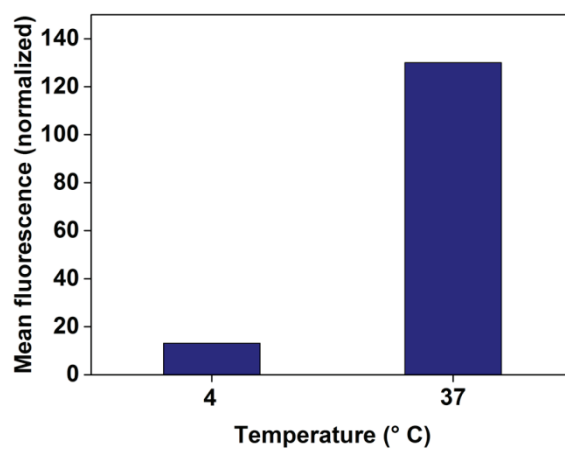
**Figure S1:** A) SEC traces of polymers 2 and 3 in DMAc; B) Absorbance and fluorescence spectra of Alexafluor 660<sup>®</sup> and polymer 3.



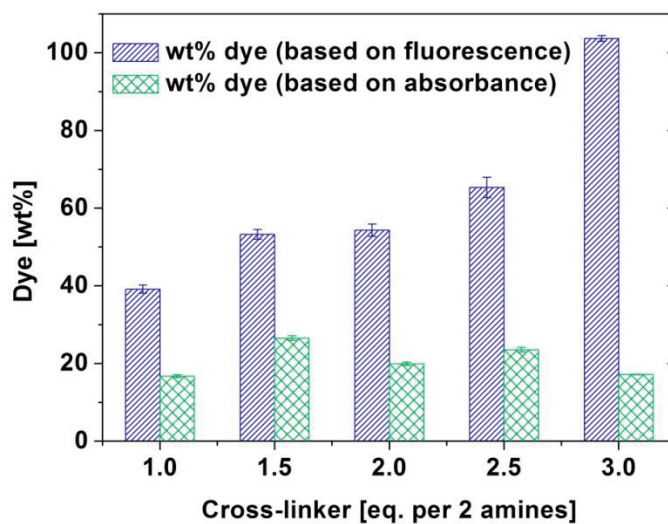
**Figure S2:** Absorbance and fluorescence of Alexafluor 660<sup>®</sup> labelled micelles (10). A) Comparison of absorbance and fluorescence spectra of compounds 9 and 10; B) concentration dependent emission spectra of compound 10 excited at 460 nm; C) concentration dependent emission spectra of compound 10 excited at 600 nm.



**Figure S3:** cryoTEM images of selected nanostructures. Scale bars: 50 nm.



**Figure S4:** Temperature dependence of the cellular uptake of compound 4 measured by FC analysis.



**Figure S5:** 6AF content of micelles with different degrees of cross-linking as determined by absorbance or fluorescence.





**Figure S6:** Erythrocyte aggregation of full blood treated with 6AF loaded micelles (4 to 8) and Dox loaded micelle (9) in a concentration range between 10 and 100  $\mu\text{g mL}^{-1}$  of drug carrier.

---